



**HAL**  
open science

# Development of multi-modal and multi-level molecular systems

Youssef Aidibi

► **To cite this version:**

Youssef Aidibi. Development of multi-modal and multi-level molecular systems. Organic chemistry. Université d'Angers, 2019. English. NNT : 2019ANGE0026 . tel-02873694

**HAL Id: tel-02873694**

**<https://theses.hal.science/tel-02873694v1>**

Submitted on 18 Jun 2020

**HAL** is a multi-disciplinary open access archive for the deposit and dissemination of scientific research documents, whether they are published or not. The documents may come from teaching and research institutions in France or abroad, or from public or private research centers.

L'archive ouverte pluridisciplinaire **HAL**, est destinée au dépôt et à la diffusion de documents scientifiques de niveau recherche, publiés ou non, émanant des établissements d'enseignement et de recherche français ou étrangers, des laboratoires publics ou privés.

# THESE DE DOCTORAT

DE L'UNIVERSITE D'ANGERS  
COMUE UNIVERSITE BRETAGNE LOIRE

ECOLE DOCTORALE N° 596  
*Matière, Molécules, Matériaux*  
Spécialité : Chimie Organique

**Youssef AIDIBI**

## **Development of Multi-Modal and Multi-Level Molecular systems**

Thèse présentée et soutenue à Angers, le 17 octobre 2019  
Unité de recherche : Laboratoire MOLTECH-Anjou – CNRS UMR 6200  
Thèse N° :

### **Composition du Jury :**

Rapporteurs :	<b>Chantal Andraud</b> , Directeur de Recherches CNRS, ENS Lyon <b>Frédéric Fagès</b> , Professeur des Universités, Université Aix-Marseille
Examineurs :	<b>Stéphanie Delbaere</b> , Professeur des Universités, Université de Lille <b>Ghassan Ibrahim</b> , Professeur des Universités, Université Libanaise
Invité :	<b>Rémi Dessapt</b> , Maître de Conférences, Université de Nantes <b>Abdelkrim El Ghayoury</b> , Maître de Conférences, Université d'Angers
Directeur :	<b>Lionel Sanguinet</b> , Maître de Conférences, Université d'Angers
Co- Directeur :	<b>Philippe Leriche</b> , Professeur des Universités, Université d'Angers



*"Fall in love with some activity, and do it! Nobody ever figures out what life is all about, and it doesn't matter. Explore the world. Nearly everything is really interesting if you go into it deeply enough. Work as hard and as much as you want to on the things you like to do the best."*

*Richard Feynman*



# Acknowledgment

This dissertation would not have been possible without the guidance and the help of several individuals who in one way or another contributed in the preparation and completion of my Ph.D. study.

My deepest gratitude goes first and foremost to my supervisors Dr. **Lionel Sanguinet** and Prof. **Philippe Leriche** who welcomed me in their laboratory and had provided all possible resources to carry out my work under the best conditions. Their guidance was a good help through all the time of research and writing of this thesis. I could have never imagined having better supervisors and mentors for my Ph.D. than them. Thank you very much for your time, your advice, your ideas, and for your encouragement throughout my thesis. I learned a lot from you.

I would also like to thank and express my deepest respect to all the members of the jury who were kind enough to do me the honor of attending my doctoral thesis defense in order to judge the quality of this work and to make their constructive remarks. The reviewers, Dr. **Chantal Andraud** (Directeur de Recherches CNRS, ENS Lyon) and Prof. **Frédéric Fagès** (Professeur des Universités, Université Aix-Marseille). The examiners, Prof. **Stéphanie Delbaere** (Professeur des Universités, Université de Lille) and Prof. **Ghassan Ibrahim** (Professeur des Universités, Université Libanaise). The invited members, Dr. **Rémi Dessapt** (Maître de Conférences, Université de Nantes) and Dr. **Abdelkrim El Ghayoury** (Maître de Conférences, Université d'Angers).

I am also particularly grateful to **Philippe Blanchard** (Directeur de Recherches CNRS, Université d'Angers) for welcoming me to the team of Linear Conjugated Systems (SCL), as well as all the members of this group: **Pierre Frère**, **Jean Roncali**, **Frédéric Gohier**, **Clement Cabanetos**, **Maïténa Oçafrain**, and **Olivier Segut**. Thank you for your kindness, availability and for making me benefit from your scientific expertise. Thank you!

Big thank to Dr. **Abdelkrim El Ghayoury** and Dr. **Nicolas Zigon** my lab colleagues for their support and Dr. **Olivier Alévêque** for the spectroelectrochemistry measurements at MOLTECH-Anjou laboratory.

A big thank to all the people that I had the chance to meet and work with in the group during my PhD: **Pablo Simon**, **Amir Habibi**, **Jose Maria**, **Yohan Cheret**, **Nataliya Plyuta** and Dr. **Jérémie Grolleau**. Thank you for the nice working environment and for all the fun we have had in the last three years at MOLTECH -Anjou laboratory.

I am very grateful to all our collaborators Prof. **Stéphanie Delbaere** and Dr. **Clement Guerrin** for the NMR titrations at University of Lille. Prof. **Benoit Champagne**, **Jean Quertinmont** and **Julien Stiennon** for the theoretical calculations at University of Namur-Belgium. Prof. **Vincent Rodriguez** for SHG measurements and Dr. **Mireille Blanchard-Desce** for the Two photon absorption measurements at University of Bordeaux. Dr. **Jean-Luc Fillaut** and Dr. **Huriye Akdas-Kiliç** for the luminescent measurements at University of Rennes 1.

This work could not have been completed without many people to whom I would like to thank: Dr. **Ingrid FREUZE** and Dr. **Sonia Ouledkram** from the University of Angers for mass spectrometry measurements; **Benjamin ZIEGLER** for NMR spectroscopy measurements. Finally, I would like to thank **Magali ALLAIN** in particular for solving the structures obtained by X-ray diffraction.

Special thank from the deep of my heart to Dr. **Ali Abbas** and Dr. **Bachar Moughayt** that I have met in Angers. It is a great blessing to have you in so many moments in my life inciting me toward my goals.

Finally, I especially thank my parents, my brothers (**Ahmad, Wehbe & Ali**) and my sisters (**Seham, Rawya & Jojo**) for their love and support throughout my life. It has been bumpy at times, but your confidence in me has enhanced my ability to get through it all and to succeed in the end. Thank you for giving me strength to reach the stars and fulfill my dreams.

*Youssef AIDIBI*

*TO MY FAMILY*



# Summary

LIST OF ABBREVIATIONS AND SYMBOLS: .....	1
<b>GENERAL INTRODUCTION .....</b>	<b>3</b>
<b>CHAPTER 1: INTRODUCTION TO MULTI-LEVEL AND MULTI-MODAL MOLECULAR SWITCHES .....</b>	<b>9</b>
I). MOLECULAR SWITCHES: GENERALITIES AND APPLICATION FIELDS .....	11
A. <i>Acidochromic molecular switches.</i> .....	13
B. <i>Photochromic molecular switches.</i> .....	14
B.1. <i>Azobenzene photochromic unit.</i> .....	17
B.2. <i>Diarylethenes.</i> .....	19
B.3. <i>Spiroyrans.</i> .....	22
C. <i>Electrochromic molecular switches.</i> .....	25
II). IMPROVEMENT OF METASTABLE STATE NUMBER (MULTI-CHROMOPHORIC SYSTEM) .....	28
III). DIFFERENT TYPES OF MULTI-ADDRESSABLE UNITS .....	34
A. <i>Multi-level system based on diarylethene and imidazo [4,5-f][1,10] phenanthroline.</i> .....	35
B. <i>Multi-mode molecular switches based on Spiroyrans.</i> .....	37
IV). THE DAE AS A MULTIMODE SWITCHABLE UNITS .....	41
V). INTRODUCTION TO INDOLINOXAZOLIDINE (BOX) AS A NICE MULTIMODE SWITCH .....	44
VI). COMMUTATION BEHAVIOR OF INDOLINOXAZOLIDINE (BOX) .....	50
A. <i>Solvatochromic and acidochromic properties of Indolinoxazolidine.</i> .....	51
B. <i>Photochromic properties of Indolinoxazolidine.</i> .....	53
C. <i>Electrochromic properties of Indolinoxazolidine.</i> .....	54
VII). MULTICHROMOPHORIC SYSTEMS RELATED TO INDOLINOXAZOLIDINE .....	57
VIII). SCOPE OF THIS THESIS. ....	62
IX). REFERENCES: .....	63
<b>CHAPTER 2: BIBOX DIMER THROUGH A LINEAR AROMATIC PLATFORM .....</b>	<b>69</b>
I). INTRODUCTION.....	71
II). ASSOCIATION OF BIBOX TO BITHIOPHENE PI-CONJUGATED SYSTEM.....	72
A. <i>Synthesis and characterization of BiBOX-bithiophene molecular systems under their closed-</i> <i>closed forms.</i> .....	72
B. <i>Commutation and abilities.</i> .....	79
B.1. <i>Acidochromic properties.</i> .....	80
B.2. <i>Photochromic properties.</i> .....	90
B.3. <i>Electrochromic properties.</i> .....	93
C. <i>BiBOX-bithiophene as multilevel molecular system to modulate the first hyperpolarizability.</i> 104	
C.1. <i>NLO and molecular switches.</i> .....	104
C.2. <i>Determination of the first hyperpolarizability of compound 20.</i> .....	109

III). ASSOCIATION OF TWO BOX WITH A EDOT-T-EDOT PI- CONJUGATED SYSTEM .....	115
A. <i>Synthesis and characterization of compound 23</i> .....	116
B. <i>Acidochromic properties</i> .....	119
C. <i>Photochromic properties</i> .....	124
D. <i>Electrochromic properties</i> .....	126
E. <i>BiBOX-ETE as multilevel molecular system to modulate the two photon absorption</i> .....	132
E.1. <i>One-photon absorption (1PA) and luminescence properties</i> .....	133
E.2. <i>Two-photon absorption properties</i> .....	135
IV). CONCLUSION .....	138
V). REFERENCES .....	141

### **CHAPTER 3: SYNTHESIS AND CHARACTERIZATION OF NEW MULTI-LEVEL SYSTEMS..... 145**

I). INTRODUCTION.....	147
II). ASSOCIATION OF THREE BOX UNITS TO A BENZENE CORE .....	149
A. <i>Synthesis</i> .....	149
B. <i>Commutation and abilities</i> .....	151
III). ASSOCIATION OF THREE BOX UNITS TO A SYMMETRICAL TRIPHENYLAMINE SYSTEM .....	153
A. <i>Synthesis</i> .....	153
B. <i>Commutation and abilities</i> .....	158
B.1. <i>Acidochromic properties</i> .....	158
B.2. <i>Photochromic properties</i> .....	165
B.3. <i>Electrochromic properties</i> .....	167
IV). ASSOCIATION OF THREE BOX UNITS TO AN UNSYMMETRICAL TRIPHENYLAMINE SYSTEMS.....	177
A. <i>Synthesis</i> .....	178
B. <i>Commutation and abilities</i> .....	180
B.1. <i>Acidochromic properties</i> .....	180
C.2. <i>Photochromic properties</i> .....	185
C.3. <i>Electrochromic properties</i> .....	186
V). CONCLUSION .....	191
VI). REFERENCES .....	193

### **CHAPTER 4: SYNTHESIS AND CHARACTERIZATIONS OF LIGANDS INCORPORATING BOX UNITS. .... 195**

I). INTRODUCTION.....	197
II). SYNTHESIS.....	200
A. <i>Synthesis and characterization of pyridine ligand with one BOX unit</i> .....	200
B. <i>Synthesis and characterization of bidentate ligands</i> .....	203
B.1. <i>Synthesis of bidentate ligands with one BOX unit</i> .....	203
B.2. <i>Synthesis of bidentate ligands with two BOX units</i> .....	205
B.3. <i>Synthesis and characterization of Pyridyl-imine ligands</i> .....	207

III). INFLUENCE OF THE PRESENCE OF A METAL BINDING FUNCTIONALITY ON COMMUTATION ABILITIES OF BOX	
DERIVATIVES .....	210
A. <i>Acidochromic properties</i> .....	211
B. <i>Photochromic properties</i> .....	219
C. <i>Electrochromic properties</i> .....	221
IV). CONCLUSION .....	225
V). REFERENCES .....	227
<b>CHAPTER 5: ELABORATION OF MULTI-LEVEL MOLECULAR SYSTEMS BASED ON COORDINATION</b>	
<b>CHEMISTRY</b> .....	<b>229</b>
I). INTRODUCTION.....	231
II). ELABORATION AND CHARACTERIZATION OF MULTI-LEVEL MOLECULAR SYSTEMS BY COORDINATION CHEMISTRY OF	
Zn(II).....	232
A. <i>Synthesis of Zinc complexes based on pyridine ligands</i> .....	233
B. <i>Synthesis of Zinc complex 57 based on pyrilyl-imide ligand</i> .....	240
C. <i>Commutation and abilities of Zinc complexes</i> .....	242
C.1. <i>Acidochromic properties</i> .....	242
C.2. <i>Release of Zinc ion under photo- or electro-stimulation</i> .....	251
III). ELABORATION AND CHARACTERIZATIONS OF MULTI-LEVEL MOLECULAR SYSTEMS BY COORDINATION CHEMISTRY OF	
Ru(II).....	255
A. <i>Synthesis of ruthenium complexes incorporating BOX unit(s)</i> .....	256
B. <i>Commutation and abilities of ruthenium complexes</i> .....	260
B.1. <i>Acidochromic properties</i> .....	263
B.2. <i>Photochromic properties</i> .....	266
B.3. <i>Electrochromic properties</i> .....	267
C. <i>Potential application of BOX complexes as multimodal switching luminophores</i> .....	270
IV). CONCLUSION .....	274
II). REFERENCES .....	277
<b>GENERAL CONCLUSION</b> .....	<b>279</b>
<b>APPENDIX 1: CRYSTALLOGRAPHIC STRUCTURES</b> .....	<b>287</b>
<b>APPENDIX 2: EXPERIMENTAL PARTS</b> .....	<b>299</b>



## List of abbreviations and symbols:

<b>A</b>	Electron acceptor material
<b>Abs</b>	Absorbance
<b>AcOH</b>	Acetic acid
<b>AcOEt</b>	Ethyl acetate
<b>ACN</b>	Acetonitrile
<b>Ar</b>	Argon
<b>BOX</b>	Indolino-[2,1,b]-oxazolidine
<b>BT</b>	Bithiophene
<b>CB</b>	Chlorobenzene
<b>CV</b>	Cyclic voltammetry
<b>d</b>	doublet
<b>dd</b>	doublet of doublet
<b>D</b>	Electron donor material
<b>DAE</b>	Diarylethenes
<b>DCE</b>	1,2-Dichloroethane
<b>DCM</b>	Dichloromethane
<b>DMF</b>	Dimethylformamide
<b>DMSO</b>	Dimethylsulfoxide
<b>DR1</b>	Disperse Red 1
<b>DTE</b>	Dithienylethene
<b>EDOT</b>	3,4-Ethylenedioxythiophene
<b>EFISH</b>	Electric field induced Second harmonic generation
<b>E<sub>pa</sub></b>	Potential of anodic peak (V)
<b>E<sub>pc</sub></b>	Potential of cathodic peak (V)
<b>ESI</b>	Electrospray Ionization
<b>esu</b>	Electrostatic unit
<b>EtOH</b>	Ethanol
<b>Et<sub>2</sub>O</b>	Diethyl ether
<b>Et<sub>3</sub>N</b>	Triethylamine
<b>Fc<sup>+</sup>/Fc</b>	ferrocenium/ferrocene Couple
<b>g</b>	gram
<b>h</b>	Planck's constant
<b>Hz</b>	Hertz
<b>KOH</b>	Potassium hydroxide
<b>HOMO</b>	Highest occupied molecular orbital
<b>HRMS</b>	High resolution mass spectrometry
<b>I</b>	Current
<b>IR</b>	Infrared
<b>KJ</b>	Kilo joule
<b>L</b>	Liter
<b>LUMO</b>	Lowest unoccupied molecular orbital
<b>m</b>	Multiplet

<b>MALDI</b>	Matrix-Assisted Laser Desorption/Ionisation
<b>MeOH</b>	Methanol
<b>MgSO<sub>4</sub></b>	Magnesium sulfate
<b>MHz</b>	Mega hertz
<b>min</b>	minute
<b>mL</b>	Milliliter
<b>mmol</b>	Millimole
<b>MS</b>	Mass Spectrometry
<b>NaOH</b>	Sodium hydroxide
<b>Na<sub>2</sub>SO<sub>4</sub></b>	Sodium sulfate
<b>NBS</b>	N-bromosuccinimide
<b>NaCl</b>	Sodium chloride
<b><i>n</i>-BuLi</b>	<i>n</i> -butyllithium
<b>NLO</b>	Nonlinear optics
<b>nm</b>	Nanometer
<b>NMR</b>	Nuclear Magnetic Resonance
<b>PE</b>	Petroleum ether
<b>ppm</b>	Part per million
<b>q</b>	Quartet
<b>s</b>	Singlet
<b>SHG</b>	Second harmonic generation
<b>SP</b>	Spiropyran
<b>t</b>	Triplet
<b>T</b>	Thiophene
<b>TBAPF<sub>6</sub></b>	Tetrabutylammonium hexafluorophosphate
<b>THF</b>	Tetrahydrofuran
<b>TLC</b>	Thin layer chromatography
<b>TLCV</b>	Thin layer cyclic voltammetry
<b>TPA</b>	Triphenylamine
<b>UV</b>	Ultraviolet
<b>V</b>	Tension (V)
<b>°C</b>	Degree Celsius
<b>ε</b>	Molar extinction coefficient (L.mol <sup>-1</sup> .cm <sup>-1</sup> )
<b>λ</b>	Wavelength (nm)
<b>Φ</b>	Fluorescence quantum yield
<b>1PA</b>	One photon absorption
<b>2PA</b>	Two photon absorption

---

# **General Introduction**

---



Since several years, many efforts have been focused on the synthesis and modification of multi-responsive molecular systems due to their large involvement in numerous applications fields as molecular logic gates or high-density optical memories.<sup>[1]</sup> In fact, the use of one switchable unit on a chemical compound can lead to two different states upon exposure to stimuli. Moreover, the use of multi-component molecular systems (two or more switches) can enhance the number of metastable states.

The common strategy for developing such systems consists in connecting different type of molecular (electro, photo or acido) switches through covalent links. However, two challenging issues have been identified as *(i)* synthesis difficulties to achieve these systems in order to obtain a synergetic effect between constitutive units and *(ii)* the difficulty to address selectively and in a controlled way the individual units, especially when the stimulus is light.

Complementary to this first approach, the use of a unique multimodal switchable unit that can be interconverted from one state to another by using indifferently several kinds of stimulations can participate to circumvent some of these difficulties. Within context, indolinoxazolidine moieties (generally referenced as BOX) represent a recent and still confidential class of promising switches. Indeed, those units appear acido, photo and, as more recently demonstrated, electro-stimulables when associated to a pi-conjugated system.

Moreover, in addition to their interest as multimodal molecular switches, the structural changes, upon stimulation of BOX derivatives, also allow NLO-phores properties potentially interesting for various applications such as optical communication, biomedical applications and material science to name a few.<sup>[2]</sup>

Unfortunately, most of the molecular systems based on BOX unit can present only two different levels due to the opening/closure of the oxazolidine ring. Following the classical approach, in order to increase the number of metastable states, the unit have already been connected with other photochromics such a DTE. Following this strategy, even if up to 13

different states have been characterized, the difficulty to obtain an efficient and selective addressability of all constitutive units has been underlined.

In this context, the objective of this thesis is to design multi-responsive molecular systems incorporating at least two BOX units and to study the possibility to address selectively one of these switchable units upon stimulation by light, acid or electron. Thus, this research work consists in assembling, by covalent linkage or coordination chemistry around a central platform, several identical BOX units in order to obtain a multi-level molecular system allowing to modulate a molecular property over more than two discrete levels. Besides an easier synthetic access to the molecular systems (first issue), the "all-in" and "step-wise" commutation modes will be obtained by playing on the nature of the stimulation (second issue).

As a consequence, this thesis manuscript is organized as follow.

After an introduction dealing with the general principle of molecular switches, the first chapter is dedicated to an overview of the reported multiaddressable molecular systems especially these based on BOX unit. The two following chapters report our efforts in the design, elaboration and switching abilities of BOX multimer beared by a common organic platform in order to increase the number of metastable states. These research works were organized following two main strategies.

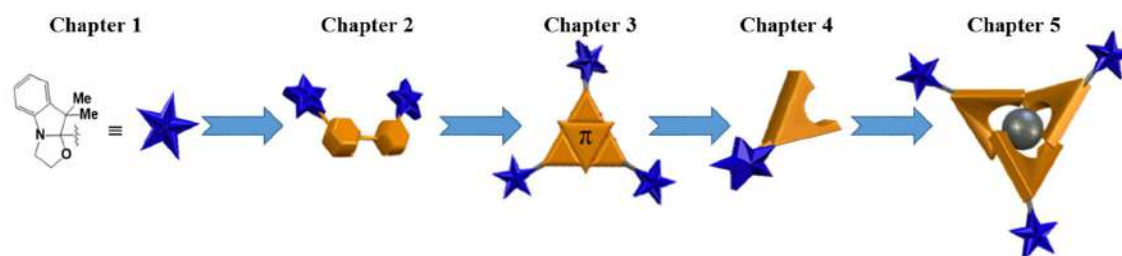
The first one concerns the elaboration of pure organic systems incorporating only two BOX units connected by a linear aromatic spacer, such as bithiophene and EDOT-Thiophene-EDOT systems. The work done to study the commutation ability of the systems upon stimulation, and the influence of the nature of the aromatic linker are reported. In addition, the modulations of their nonlinear optical (NLO) properties upon stimulation are reported as well in chapter 2.

Considering these BOX-dimers as a proof of concept, this idea has been extended to more elaborated systems bearing three BOX units. These compounds use as central organic cores phenyl, triphenylamine and tris (4-(thiophen-2-yl) phenyl) amine as  $C_{3v}$  symmetry systems. In addition, as a first try to promote the opening of each BOX system in a controlled way, a triphenylamine node has been connected to three BOX through 3 different conjugated systems. All syntheses and characterizations are presented in chapter 3.

Beside this pure organic approach, the connection of several BOX units using a central metal ion thanks to coordination chemistry has been explored. As consequence, the fourth chapter relies on the synthesis and characterization of several nitrogen ligands such as classical pyridine, bipyridine, phenanthroline and imino pyridine moieties functionalized by at least one BOX unit.

Finally, chapter five is dedicated to the syntheses and preliminary characterizations of various complexes involving zinc and ruthenium metals and ligands synthesized in chapter 4. Noteworthy, the chapter ends with the luminescent measurements of one ruthenium complex what paves the way to possible new experiments.

For better clarity, the organization of the studies undergone during this thesis and reported in this manuscript can be resumed by the following figure.



[1] J. Andréasson and U. Pischel, *Chemical Society Reviews* **2010**, 39, 174-188.

[2] S. R. Marder, *Chemical communications* **2006**, 131-134.



---

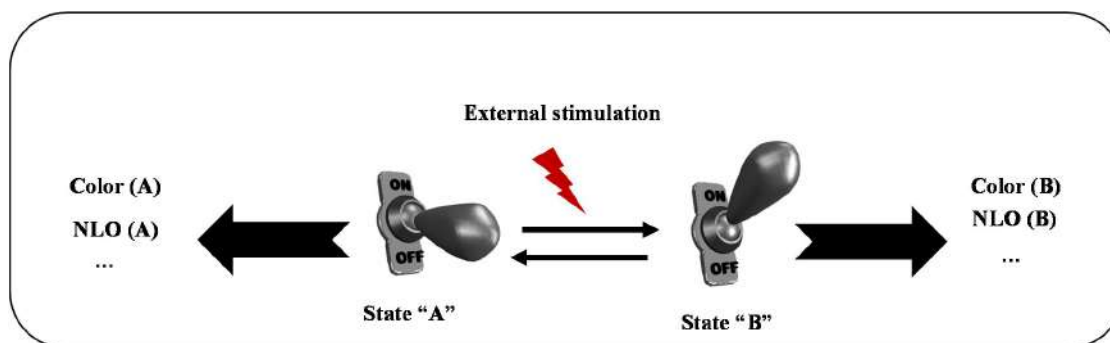
# **Chapter 1: Introduction to multi-level and multi-modal molecular switches**

---



## D). Molecular switches: Generalities and application fields

Molecular switches are compounds that are able to convert between one distinguishable form and another one on exposure to an external stimulations such as: light,<sup>[1, 2, 3]</sup> electricity,<sup>[4]</sup> pH,<sup>[5]</sup> temperature,<sup>[6]</sup> electrochemical stimulation<sup>[7]</sup> to name a few. Such kind of switching molecules, in which each meta stable state displays different physico-chemical properties, have gained a lot of interest.<sup>[8]</sup> In particular, they have generated a large degree of interest in material science due to their potential applications in the field of optical memory devices, photoswitches and future use in molecular electronics and nanomachinery (highlighted by the 2016 Nobel Prize in Chemistry awarded to Jean-Pierre Sauvage, Sir J. Fraser Stoddart and Ben L. Feringa).<sup>[9]</sup> The working principle of such a simple switch is illustrated in figure 1, where “A” and “B” represent the two different states of a bistable system. Among this context, a lot of molecules were designed and studied. In particular, the evolution of their optical,<sup>[10]</sup> photophysical<sup>[11]</sup> or redox behaviors<sup>[12]</sup> were studied upon reversible stimulation between the **A** and **B** states.

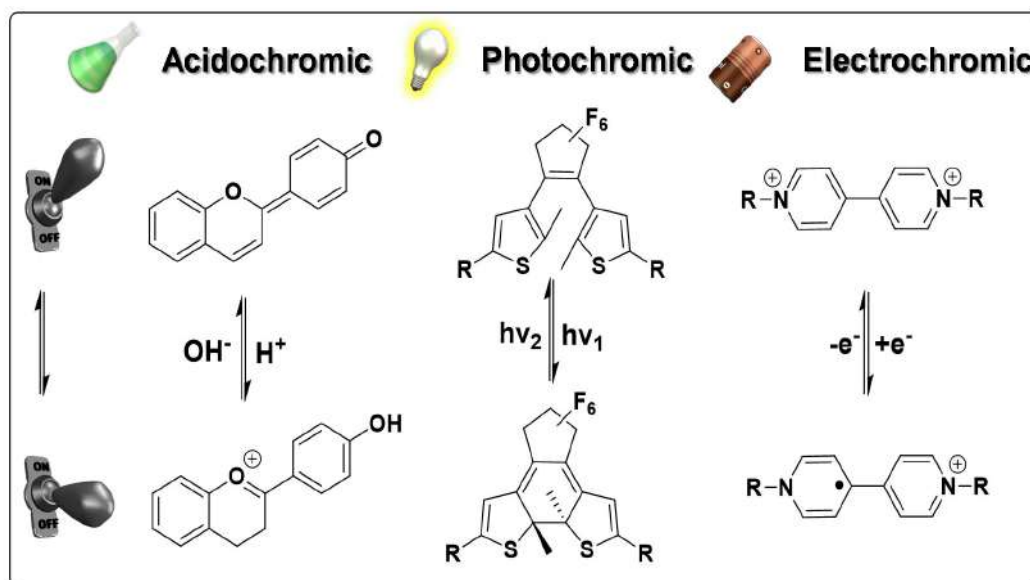


*Figure 1. Schematic representation of a switchable bi-stable system by responding to an external stimulation.*

Moreover, molecular switches offer a very advantageous avenue for a wide-range of interconnected fields. Faster data processing and high-density data storage technologies are in development. In fact, these switching systems are analogous to the bits of information which are currently used for data storage, the isomers ground states “on” and “off” can be often interpreted in terms of 1’s and 0’s. Indeed, as classical technologies read bits of information in

transistors as 1's or 0's *via* voltage measurements, molecular switches may allow (for example) UV-Visible light as a non-destructive readout method. Then, the processing of “reading” the data occurs *via* evaluation of spectral changes near the absorption bands corresponding to the two isomer states.

Depending on the nature of the stimulation generating optical changes, corresponding molecules/materials are considered as: thermochromic,<sup>[13]</sup> heliochromic,<sup>[14]</sup> tribochromic,<sup>[15]</sup> piezochromic,<sup>[16]</sup> acidochromic,<sup>[17]</sup> photochromic, electrochromic<sup>[18]</sup> (...) systems. In our concern, we have mainly focused our interest on acido-, photo and electrochromic systems in which the reversible transformation of a chemical species between **A** and **B** state is induced through an acidic treatment, a light irradiation and an electrochemical stimulation respectively (Figure 2).

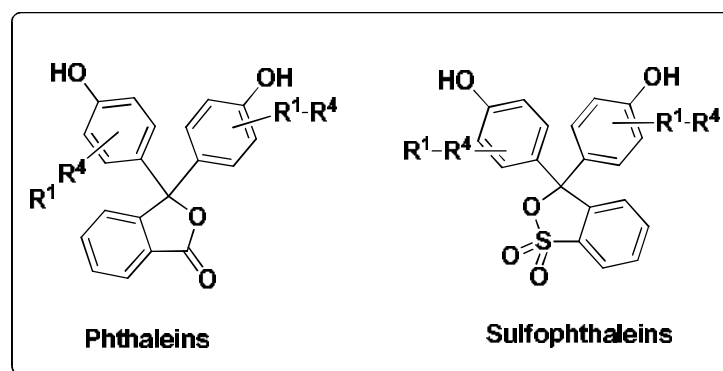


**Figure 2.** Chemical structures of 4'-hydroxyflavylium ion,<sup>[19]</sup> diarylethenes (DAE)<sup>[20]</sup> and viologens<sup>[21]</sup> acting respectively as examples of acidochromic, photochromic and electrochromic systems respectively.

As an uncountable number of structures capable of operating as molecular switches are identified, the next sections provide a rough summary of the most well spread acidochromic, electrochromic and photochromic units.

### A. Acidochromic molecular switches.

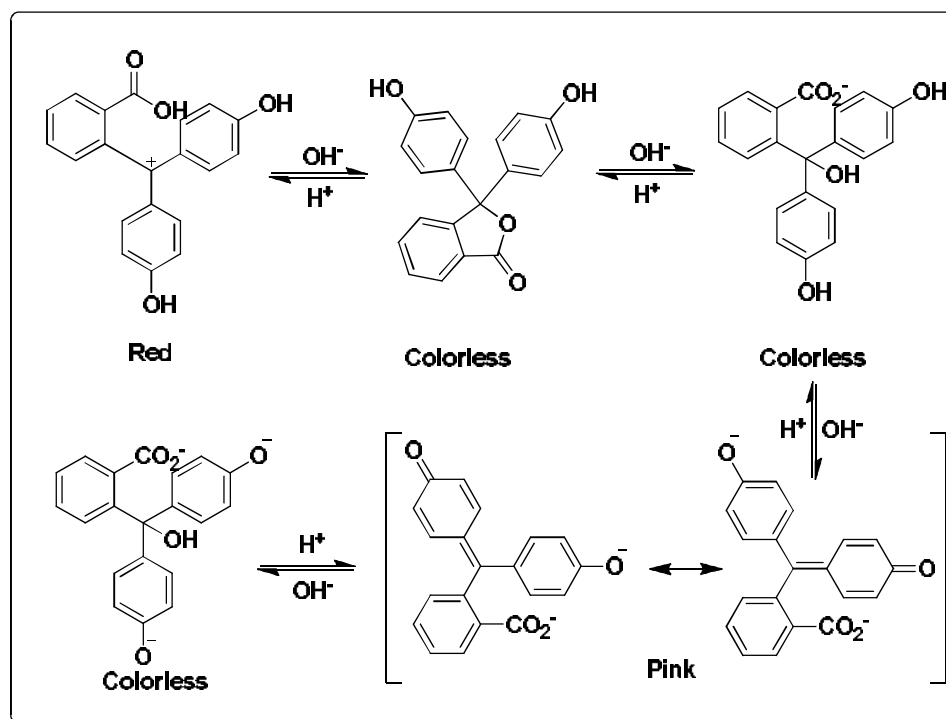
Acidochromism characterizes the propensity of a compound to change color during a pH variation. This modification in the position and intensity of the UV-Vis absorption band is due to a structural change upon acid/base stimulation. Among that, a lot of species can be considered as acidochromic molecular switches. As examples, pH-indicators, which color change depending on the pH, due to proton catching/release, are probably amongst the older and most known switches. Phthalides (subdivided in the two different types, such as phthaleins and sulfophthaleins in scheme 1) can certainly be considered as the main chemical class of technically important pH-sensitive dyes with the triarylmethines and fluoranes.<sup>[22]</sup> Nevertheless, several other major chromophores can undergo useful color changes on protonation such as neutral examples azo and styryl dyes.<sup>[23]</sup>



*Scheme 1. Two types of Phthalides dyes used as pH-indicator.*

However, phenolphthalein is a typical organic pH indicator that can be found in different states as shown in scheme 2. More specifically, in highly acidic solutions (pH < 0), phenolphthalein is present as a red carbocation. In a pH range from 0 to 8.2, Phenolphthalein transforms to a colorless lactone. By adding a base, the lactone ring opens, a water molecule splits and a quinone ring is formed inducing an enhancement of the size of the pi- conjugated system. Due to a bathochromic shift, the generated compound appears then pink. For this state two mesomeric isomers describe the bonding situation. Finally, in high alkaline media

phenolphthalein forms a colorless trianion. This special case where the protonated form and the conjugated base present different colors is called acidochromism<sup>[24]</sup>. Moreover, as shown in scheme 2, the commutation among the different states are almost quantitative and reversible. These barely decompositions of the compound during the processes have participate to the its commonly uses as indicator in laboratories during acid-base titrations until it was classified as a carcinogenic substance.<sup>[25]</sup>



Scheme 2. Different states of phenolphthalein.

Following acidochromic systems, a lot of other molecules can be considered as photochromic switches due to the mechanism involved in the commutation process.

### B. Photochromic molecular switches.

Molecular switches that interconvert between metastable states **A** and **B** under the influence of light are said to be photochromic. These systems, in solution or even in condensed phase, undergo rapid and reversible transformations or generate differentiated isomers when irradiated with light of a suitable wavelength.<sup>[20, 26]</sup>

If photochromic materials are known since antiquity (one say that Alexander the great armies coordinate their troops with photochromic bracelets),<sup>[27]</sup> the scientific story of molecular photo-switches only starts on the nineteenth century. In fact in 1867, Fritzsche has reported the bleaching of an orange solution of tetracene under sunlight and the regeneration of its initial color in the dark.<sup>[28]</sup> A few time later, in 1876,<sup>[29]</sup> Ter Meer observed a change of color of potassium salt of dinitroethane in the solid state from yellow in dark to red in daylight. Following this, other examples were investigated by Phipson and Markwald,<sup>[30, 31]</sup> as the first daylight/night depending observations of the change of color from white to black of a gate post painted with a zinc pigment (mixture of ZnS and BaSO<sub>4</sub>). Also interested, as others, by these phenomena, Hishberg suggested in 1950 the term of “photochromism” which comes from the Greek words: *Phos* (light) and *chroma* (color) to describe his observations.<sup>[32, 33, 34]</sup>

Among all kinds of stimulation, light is also particularly effective in its ability to spatially and temporally induce structural and functional changes in molecules and materials while at the same time having the potential to be non-destructive.<sup>[35]</sup> Photochromism, as mentioned before, denotes the light activated reversible transformation between two chemical species, which can display absorption spectra that are not only different but also readily distinguishable (Figure 3).<sup>[36, 37]</sup> Thus, the molecular structure and function of these molecules changes upon irradiation and, if incorporated into functional systems such as polymers, can cause drastic changes in the bulk properties of the compound by responding almost instantaneously to external stimuli at a molecular level.<sup>[26]</sup>

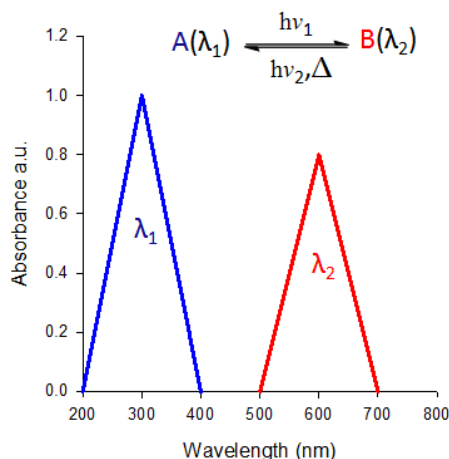


Figure 3. General representation of a reversible transformation from species A into B.

In general, photochromism can take place in both inorganic and organic compounds, as well as in biological systems.<sup>[38]</sup> Among that, many inorganic compounds can be cited, as metal oxides, alkaline earth sulfides, metal halides and some transition metal compounds known to exhibit photochromic properties.<sup>[39]</sup> As example, we can cite the silver halides which represent a well-known photo-responsive inorganic family used for the fabrication of photochromic lenses.<sup>[38, 40]</sup> Furthermore, some natural minerals exhibit photochromic properties such as hackmanite as shown in figure 4.



Figure 4. Photochromic behavior of hackmanite mineral.<sup>[38]</sup>

This kind of mineral is a well-known variety of sodalite ( $\text{Na}_8\text{Al}_6\text{Si}_6\text{O}_{24}\text{Cl}_2$ ) that undergoes a quick fade away initially from violet to colorless upon exposure to visible light. The original color can then be regenerated by two different ways, slowly in dark or quickly upon exposure to ultraviolet light.<sup>[38]</sup>

In this context of this thesis, these inorganic systems are out of the scope of this manuscript. For this reason, we have focused this general presentation of photochromic system on organic switches which represent the most part of the reported studies. Indeed, impressive number of various organic systems was reported in numerous application fields.

Due to this, several classifications have been proposed based on the mechanism involved during their photo-commutation.

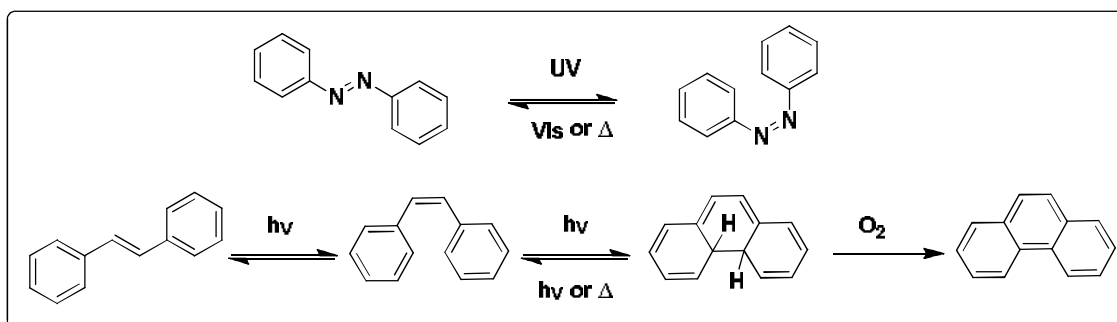
In first one, two categories were defined depending on the thermal stability of the photo-generated meta-stable state. When the reversible back reaction can be thermally induced, one speaks about T-type photochromic compound. Alternatively, if the meta-stable state appears thermally stable and the back reaction can only be photo-chemically induced, the derivative is considered as a P-type photochromic compound.

Beside this later, a second classification based on the nature of the involved photochemical process is generally adopted. Following that, several photochromic unit families were listed such as cis-trans isomerization, photocyclization, heteroleptic bond cleavage and cycloaddition to name few.<sup>[41]</sup> If countless structures were reported, it can be noticed that the large majority of the studies are focused on azobenzenes,<sup>[42]</sup> diarylethenes<sup>[43]</sup> and spiropyrans<sup>[44, 45]</sup> which are detailed below.

### B.1. Azobenzene photochromic unit.

The first azo-dye was synthesized by Martius in 1863. Only one year later, Griess described the coupling reaction of diazonium compounds.<sup>[46]</sup> This important discovery opened the way to the azo-dyes development, the most important and versatile group of colored organic compounds used as dyes and pigments<sup>[47]</sup>. Generally referenced as azobenzene, the general structure of these compounds can be resumed to two phenyl units (or aryl substituents) linked

by N=N double bond. Considered as structural analogs of stilbenes,<sup>[48, 49]</sup> these compounds differ by their photophysical behaviors (scheme 3).



*Scheme 3. Photoswitching of azobenzene (top) and of stilbene (bottom).*

At the opposite to stilbenes, the observation of the Trans/Cis, or E/Z, photoconversion on azobenzene firstly reported by Hartley in 1937,<sup>[50]</sup> doesn't require the presence of some substituent on the phenyl ring in order to avoid undesired subsequent 6  $\pi$  electrocyclization.<sup>[51]</sup> Indeed, the stilbene irradiation, leads to dihydrophenanthrene which, in presence of oxygen or some oxidant, is irreversibly and quickly transformed in phenanthrene (scheme 3).

Generally carried out by a UV light irradiation (340–380 nm),<sup>[52]</sup> the reversible E-Z isomerization of azobenzene induces a large change in spatial geometry (3Å) and dipole moment.<sup>[53]</sup> It represents one of the simplest ways of converting photon-energy into mechanical motion.<sup>[54]</sup>

Concerning the back conversion from Z to E-isomer, it can be carried out by irradiation using visible light (scheme 3) or by a thermal isomerization process. Within this context, the thermal stability of the Z-isomer of azobenzene switches can be regarded as both a disadvantage and an advantage depending on the chosen application.

The switching characteristics such as irradiation wavelength, quantum yield and thermal stability can be controlled through the substituents grafted on the azobenzene<sup>[39, 55, 56, 57]</sup>. As example the introduction of fluorine atoms on the ortho positions allows to strongly displace

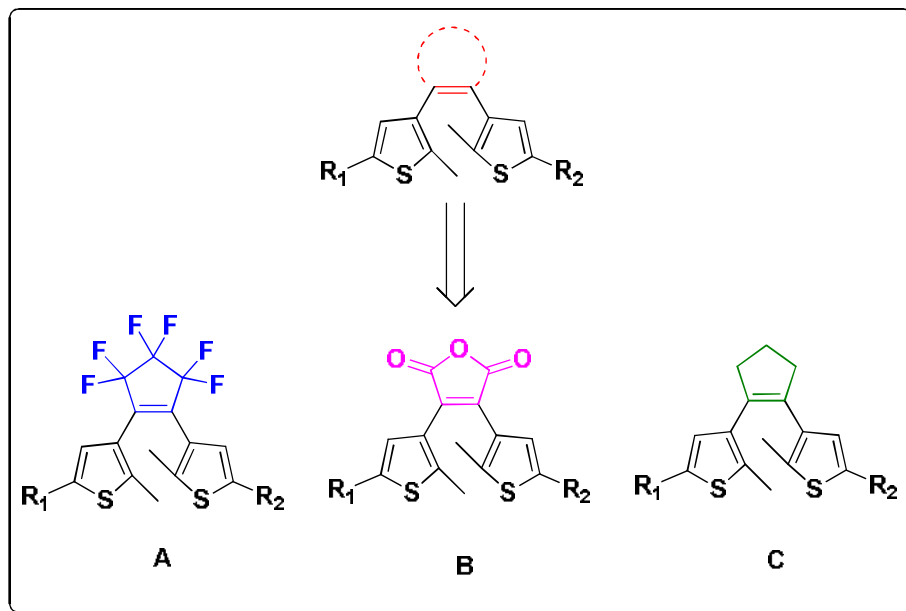
irradiation wavelength to visible range ( $\lambda > 500$  nm) and increases the thermal stability of the Z isomer. With a half-life of *ca.* 700 days at 25 °C, this system can be now considered as a P type photochromic system where the back conversion (Z→E) is induced by light irradiation at 410 nm.<sup>[58]</sup> More generally, the introduction of electron withdrawing groups (EWGs) at the para-position such as an ester function results in an enhancement of the ratio in photostationary states (PSS<sub>(E→Z)</sub> 90% with  $\lambda > 500$  nm and PSS<sub>(Z→E)</sub> 97% at 410 nm).<sup>[58]</sup> These differences of switching characteristics are related to the variation in terms of energy of the  $n \rightarrow \pi^*$  bands for isomer. Indeed, Hecht and coworkers have demonstrated that the introduction of EWGs on the ortho and para positions decreases repulsive interactions between nitrogen lone pairs in Z-isomer and, as consequence, increases its thermal stability.<sup>[58]</sup>

As mentioned above, the photo-isomerization leads to important geometrical changes such as length, angle, volume and polarity. As a consequence, both isomers of azobenzene exhibit very distinct physico-chemical properties.<sup>[59]</sup> This large modulation of its molecular properties associated with its easy tunable and high fatigue resistance<sup>[56]</sup> make azobenzene a candidate of primer choice for the development of photo-responsive molecular materials and devices. As consequence, numerous reviews were dedicated to the chemistry of azobenzene derivatives and to their various application fields.<sup>[60, 61, 62, 63, 64, 65, 66, 67]</sup>

### B.2. Diarylethenes.

Among the numerous photochromic units reported so far, diarylethene (DAE) represents another well-studied family in which the first example of a reversible photochromic reaction was described by Irie and Mohri in 1988.<sup>[51]</sup> The design of this system was inspired by the photo-reactivity of the cis-isomer of stilbene leading to the phenanthrene (see scheme 3). By substituting positions 2 and 6 of each aryl substituent, the non-reversible elimination step is avoided and the photoinduced  $6\pi$  electrocyclization becomes reversible even in presence of

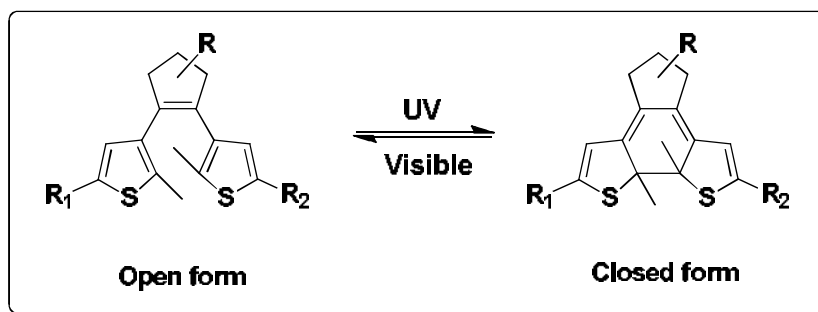
oxygen. In general, DAE are constituted on two aryl groups (generally thiophene rings) connected through a C=C bond. More important, to avoid the competition between C=C cis-trans isomerization and the  $6\pi$  cyclization process, the cis isomer is maintained by incorporating the double bond into a cycle such as: perfluorocyclopentene (A), maleic anhydride (B) or cyclopentene (C) (scheme 4).



*Scheme 4. General structures of dithienylethenes.*

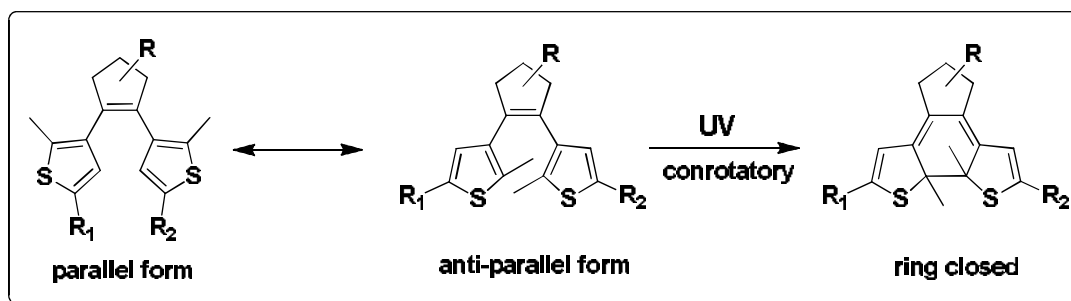
At the opposite to azobenzene derivatives, the geometrical changes between both metastable states are quite limited here, allowing observing the photocyclization even in the solid state.<sup>[68]</sup> In general, all diarylethenes exhibit in their open form a 1,3,5-hexatriene chain. According to the Woodward-Hoffman rules<sup>[36]</sup> based on the symmetry of  $\pi$  orbitals, the electrocyclization reaction is conrotatory if photoinduced. Upon irradiation with UV-light,<sup>[43]</sup> the colorless open structure undergoes a cyclisation leading to a corresponding 1,3-cyclohexadiene generally referenced as closed form. Due to the increase of the conjugation of the  $\pi$  system over the molecule, this cyclization leads to an impressive bathochromic shift of the maximum absorption wavelength. Indeed, as the structure of the open form appears non-planar (steric hindrances between the aryl groups and free rotation between ethylene bridge and

aryl terminations), which leads to two isolated conjugated systems on each side of the ethylene bridge. On the other hand, the closed state resulting from the photo-cyclization leads to a planar central diarylethene moiety *via* the formation of a central carbon carbon bond which allows the formation of a  $\pi$  conjugated system that covers the entire system. Furthermore, the closed form is usually thermally stable and can be converted back to the open one by irradiation with visible light (scheme 5).



*Scheme 5. Photoswitching of dithienylethene switches with a ring closing upon UV irradiation and ring opening by irradiation with visible light.*

Irie and co-workers proposed that the thermal stability is dependent on aromatic stabilization in the ring open form.<sup>[69]</sup> Noteworthy, compared to stilbene systems, which contain phenyl rings, most DAE switches, which exhibit two thiophene rings, present spectroscopic signatures generally red shifted. Beside the electronic effects mentioned above, it is important to notice that the efficiency of the photocyclisation is also strongly influenced by the geometrical organization of the open form. Indeed, absorption spectroscopy studies<sup>[70]</sup> and NMR analyses<sup>[71]</sup> have shown that two different conformers have to be considered for DAE under their open form. In fact, the latter can present a parallel (scheme 6, left) or an anti-parallel conformation (scheme 6, right). Nevertheless, only this second conformer can undergoes in photo-cyclization process due geometrical restrictions (scheme 6).



*Scheme 6. Mechanism of ring closing and opening of DAE.*

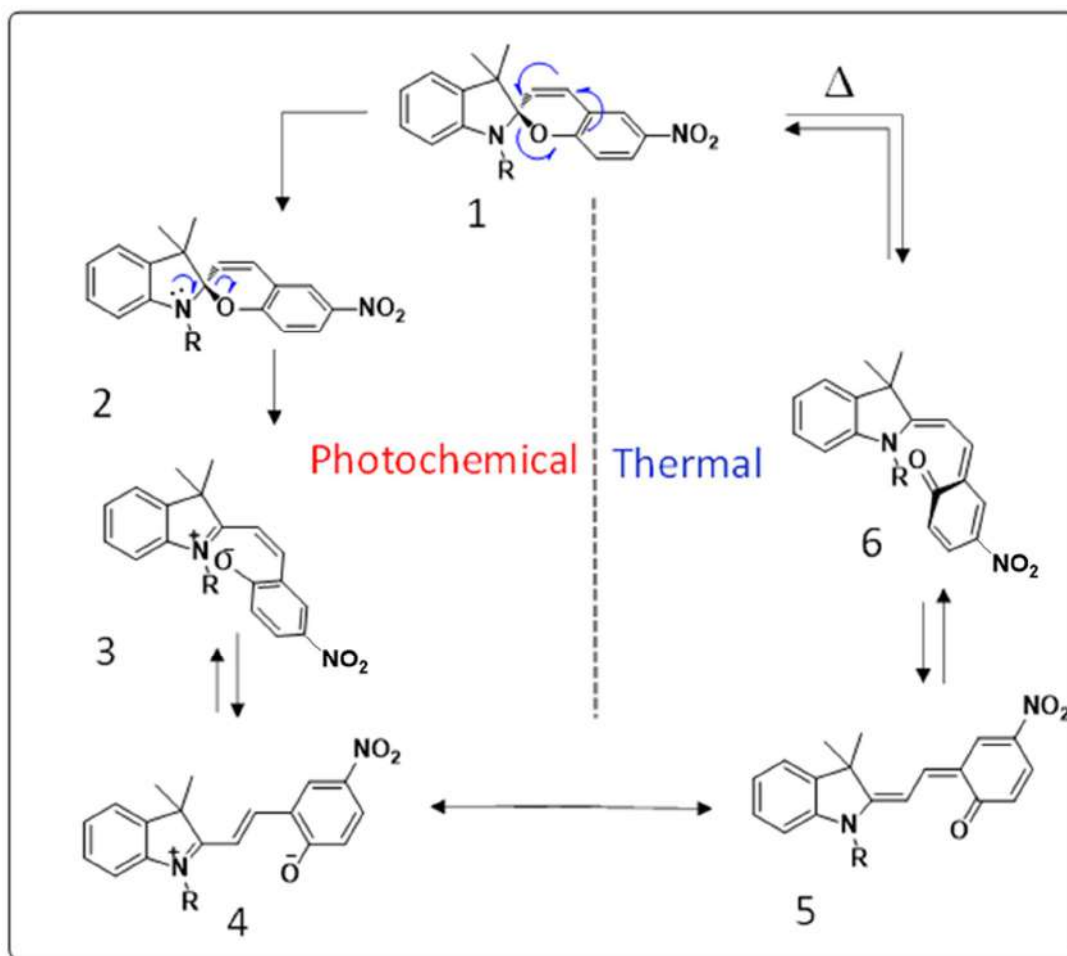
As DAE derivatives present high optical contrasts between their opened and closed forms whether in solution and in the solid state, associated, in most cases, with thermal stability, a lot of systems valorizing also the variation of physico-chemical properties of this motif have been designed and studied. Indeed, DAE have been used to sense photo-chemically the pKa,<sup>[72]</sup> to elaborate photo-commutable super hydrophobic surface,<sup>[73]</sup> as biological probe<sup>[74]</sup> or as molecular mechanical machine.<sup>[75]</sup> On the other hand, as DAE, some other molecules (switches) can be subject to bond change upon exposure to light as those described below.

### B.3. Spiroyrans.

The spiroyrans family also represents a prominent class of photochromic switches which undergo a heteroleptic bond cleavage upon exposure to light stimulation.

The first spiroyrans derivative was reported by Decker et al.<sup>[76]</sup> at the beginning of the last century and its thermochromic properties were discovered in 1926.<sup>[77, 78]</sup> The photochromic properties of spiroyrans were first demonstrated by Fischer and Hirshberg in 1952.<sup>[79]</sup> Spiroyrans system, as shown by its name, presents a spiro character due to the common sp<sup>3</sup> carbon atom which links its two heterocyclic units: an indoline and a 2H-benzopyran moieties. Upon UV-light irradiation, the colorless non-planar closed form of spiroyrans switches to the planar open metastable state generally referenced as merocyanine (MC) form. More precisely, the photoisomerization of the spiroyrans family involves an heteroleptic cleavage of the C-O

bond between the pyran-oxygen and the spiro-carbon.<sup>[80]</sup> Consequently, the carbon hybridization is changing from  $sp^3$  to  $sp^2$ , and the conjugation is extended to the whole molecule. This extension of the pi-conjugated system under MC form leads to a strong bathochromic shift that changes the absorption wavelength from the UV to the visible region.<sup>[41]</sup> Generally, the introduction of a strong withdrawing group (such as  $\text{NO}_2$ ) on the benzene ring increases the photoreactivity by providing a stabilization of the open merocyanine form since it enhances the delocalization of the negative charge on the oxygen. If the photo-generated zwitterionic MC form can exist in either one or both of two conformations (cis or trans), only trans isomer (**4**) is generally observed due to an higher stability (less steric hindrance than in cis isomer).<sup>[81]</sup> Noteworthy, this merocyanine form can be also described by two mesomeric forms: a zwitterionic form and a quinoidal one. Interestingly, Rafal et al have demonstrated/proposed that only this last one was involved in the thermal back-conversion from MC to SP state through a  $6\pi$  electro-cyclisation process (Scheme 7).



**Scheme 7.** Photochromic switching of spiropyrans (SP) showing the zwitterionic and quinoid forms.<sup>[82]</sup>

Generally, spiropyrans have a moderate to large quantum yield for the coloration process ( $\Phi_{\text{col}}$ ). As example, the nitro substituted spiropyrans, exhibit an  $\Phi_{\text{col}}$  oscillating between 0.40 to 0.85 in methylcyclohexane.<sup>[83]</sup> The switching of spiropyrans is, however solvent dependent. Increasing polarity results in a lower  $\Phi_{\text{col}}$  and higher activation barriers to the reverse process.

As observed with azobenzene derivatives, the photo-commutation of the spiropyran leads to important geometrical changes such as length, angle, volume, but in their cases it induces a much more important variation of the polarity due to the formation of a zwitterionic form and an impressive variation of their absorption spectrum. If the observed bathochromic

shift of the absorption wavelength is on the same range as obtained with DAE units, the poor thermal stability of the merocyanine form can represent a potential drawback.

Anyway, spiropyrans are largely used for the development of photo-sensitive materials and continue to rise interest as demonstrated by the numerous reviews dedicated to this photochromic family and its applications.<sup>[84]</sup> Among those, one can find the classical ones such as filters, sensors, biomolecules activity regulations and lenses.<sup>[44]</sup> However, the specificity of spiropyran resides on its ability to photogenerate a high polar and hydrophilic zwitterionic MC form <sup>[85]</sup> from an SP hydrophobic “closed” isomer. As consequence, spiropyrans appear as candidates of choice for the development of specific application fields especially in the surface wettability modulation.<sup>[86]</sup>

As mentioned above, light is particularly effective in its ability to spatially and temporally induce structural and functional changes in molecules and materials. However, other kinds of stimulations have attracted a large interest in order to induce a modulation of molecular properties. After the stimulation by chemical and light, the application of an electrochemical potential is certainly the stimulus which has raised the most of interest especially in molecular electronics due to fast response time. As consequence, we cannot finish this quick overview of molecular switches without presenting some details about the electrochromic units.

### C. Electrochromic molecular switches.

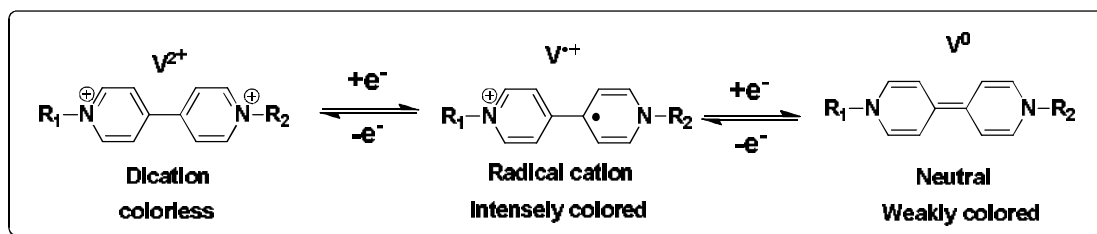
The term electrochromism was first assigned in 1961 by Platt in analogy to thermochromism and photochromism.<sup>[87]</sup> Furthermore, the first electrochemical change of color dates back to 1930, when Kobosew and Nekrassow observed the electrochemical reduction of a bulk tungsten oxide.<sup>[88]</sup> In general, electrochromic molecular switches are molecules that undergo a change in oxidation state, which may be accompanied by a change in their molecular structure.<sup>[89]</sup>

In fact, there are vast amount of organic materials, commercially available, and also many that can be synthesized in laboratory, with relative efficiency. As, obviously, all these derivatives are redox active, their various oxidized/reduced states also present different electronic absorption spectra.<sup>[90]</sup> As consequence, most of the redox active organic compounds that exhibit electronic transitions within the visible wavelength region are candidates for electrochromic materials. However, most of them are strongly limited by the poor stability of generated oxidized/reduced species which is the major drawback of this kind of molecular switch. If we can cite ferrocene/ferrocinium derivatives,<sup>[91]</sup> or poly- and oligo-thiophenes<sup>[92]</sup> we would detail the viologen as example since it constitutes one of the most widely studied class of organic electrochromic compounds.

Bipyridylum species, and particularly “viologen” systems, represent a major group of organic electrochromes.<sup>[93]</sup> These systems were discovered by Michaelis who observed that 1,1'-dimethyl-4,4'-bipyridilium,<sup>[94]</sup> upon reduction, turns to violet and who named it “methyl viologen” (MV).

Generally, their synthesis is resumed as the diquaternization reaction of 4,4'-bipyridine by various substituents yielding corresponding 1,1'-disubstituted-4,4'-bipyridylum salts. In the continuity of the seminal observation of Michaelis, many of these derivatives hold trivial non-IUPAC names often based on the “viologen” root. Noteworthy, viologen derivatives are also developed by Imperial Chemical Industries (ICI) for herbicidal use.<sup>[95]</sup>

Viologen (V) exhibits three well defined redox states: A dication ( $V^{2+}$ ), a radical cation ( $V^{\bullet+}$ ) and a di-reduced neutral form ( $V^0$ ), as shown in scheme 8. The dication salt is the most stable one and is colorless in its pure form. Reductive electron transfer to the dication produces a radical cation ( $V^{\bullet+}$ ) which is intensely colored and highly stable among organic radicals. The strong color in  $V^{\bullet+}$  is owing to the intramolecular optical charge transfer process.



*Scheme 8. Redox states of viologen.*

Indeed, most of the viologen compounds exhibit electrochromism due to their ability to form a highly colored radical cation. As discussed before, such coloration is arising from the delocalization of positive charge in the radical cation accompanied by an optical charge transfer process. Hence, the origin of the color is perhaps better viewed as an intramolecular photo-effected electronic excitation.<sup>[88]</sup> Desired color can be tuned by choosing suitable nitrogen substituents, thereby attaining the appropriate molecular orbital energy levels. Simple, alkyl groups offer a blue violet coloration to the radicals.<sup>[96]</sup> As the chain length increases, color transforms into crimson due to the increased dimerization, as the dimer is generally red colored. On the other hand, aryl groups such as 4-cyanophenyl usually imparts a green hue to the viologen radical cation.<sup>[96]</sup> Finally, the color properties of the radical cation is also strongly dependent on nature of the counter ion and the solvent used.<sup>[88]</sup>

Unfortunately, the viologen radical cation is very sensitive to oxidizing agents or molecular oxygen.<sup>[93]</sup> The stability of the radical cation is governed by the delocalization of the radical electron along the  $\pi$ -framework of the bipyridyl nucleus, part of the charge being weakly carried by the 1 and 1' substituents.<sup>[97]</sup> Further reduction of  $V^{\bullet+}$  gives neutral di-reduced viologens ( $V^0$ ), decaying the intense color of radicals. The neutral form of viologen is extremely reactive, hence often termed as bi-radical.<sup>[88]</sup> Studies have shown that bi-radicals are diamagnetic in the solid state and that the spins are paired.  $V^0$  is often weakly colored as there is no optically assisted charge transfer or any accessible internal transition corresponding to the visible wavelength.<sup>[18]</sup>

The major advantage of viologen electrochromes lies in their ease in molecular design, relatively high charge efficiency, and quick response time. Unlike inorganic materials, viologen absorption spectrum is sharp and can be located anywhere in the visible wavelength region. Poor consistency and unexpected side reactions leading to further degradation represent the major problems of the viologen electrochromic system. Besides all the mentioned liabilities, viologens are by far the most intensively studied organic electrochromes for research and commercialization purposes.<sup>[88]</sup>

Concerning what we have presented before and what we have seen, we conclude that using only one switch on a chemical compound can lead at least to two different states upon exposure to a single stimulus. In order to obtain more complex systems, an obvious solution consists in combining several bistable switches in the same molecular system. Designed as multichromophoric systems, several examples reported in the literature are presented below.

### **II). Improvement of metastable state number (multi-chromophoric system)**

To enhance the number of metastable states, numerous attempts to combine several switchable units in the same molecular system have been generally undertaken. Indeed, such strategy may allow synergetic effects between the properties of each constitutive unit and, as consequence, lead to increase the functionality of the resulting molecular architecture. As straightforward examples, a multi-chromophoric system which is elaborated by the combination of  $n$  switches, is potentially able to exhibit up to  $2^n$  different states (figure 5). This strong enhancement of the metastable states number brings new perspectives to the design of molecular-scale high-density optical memory or multinary logic devices.<sup>[98, 99]</sup>

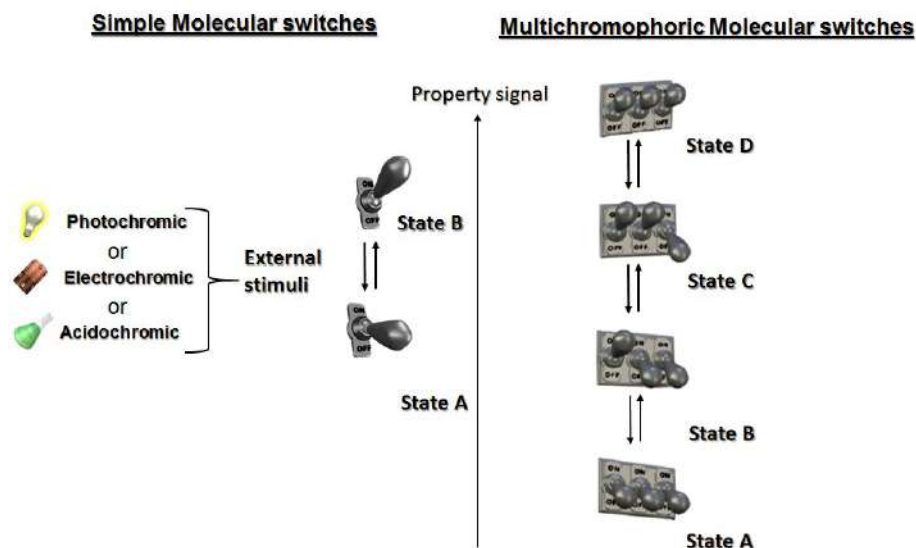
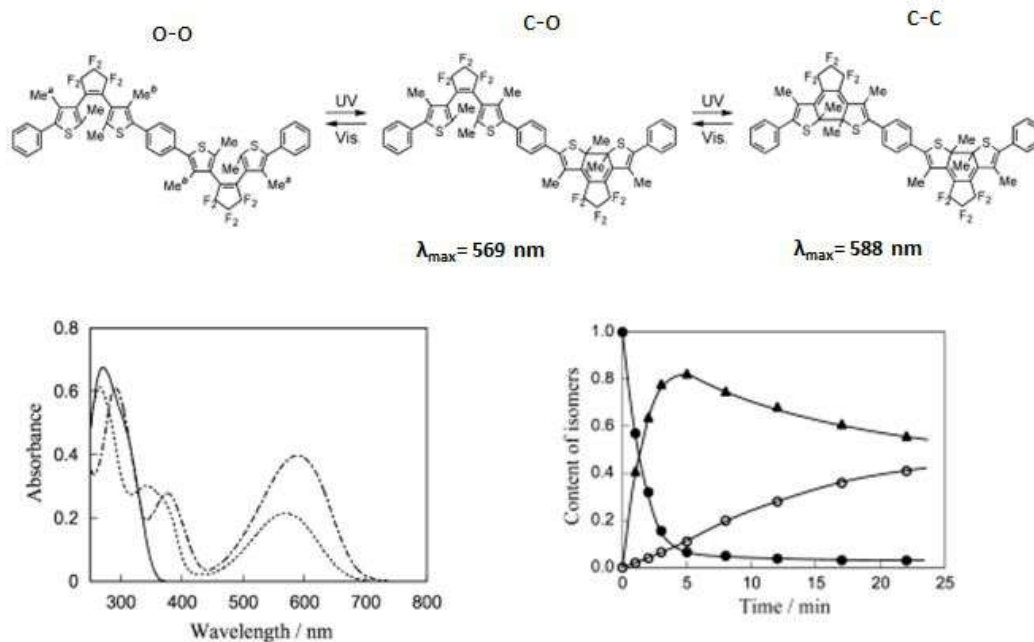


Figure 5. Representation of Multi-state systems (right 4 states chosen among 8 possible).

A first approach for obtaining a multi-chromophoric system consists in connecting two or more acido-, electro- or photochromic units through covalent links.<sup>[100]</sup> A second approach consisting to merge several kind of switches could appear at first sight more promising due to a predictable better addressability of motifs by using orthogonal stimulations. However, corresponding syntheses are more challenging. Thus, even if their selective addressability poses more question, due to synthetic purposes, biphotochromic systems exhibiting two identical switches have been intensively studied. In this context, several systems based on various photochromic unit were reported such as example DHP-DHP<sup>[101, 102]</sup> and bisnaphthopyrans,<sup>[103]</sup> etc... but the dimers and, by extension, the multimers of DAE unit are undoubtedly the most abundant.<sup>[104, 105, 106, 107, 108]</sup>

Concerning these later, it may be assumed that the photochromic state of one photochromic unit would influence the reactivity of the other when a conjugated pathway is used to link two DAE units. The closing of the second unit will be more difficult than the first one. As example, Figure 6 sums up the multichromophoric properties of the system developed by Masahiro Irie in which two diarylethene moieties are associated through a phenyl spacer.<sup>[109]</sup>

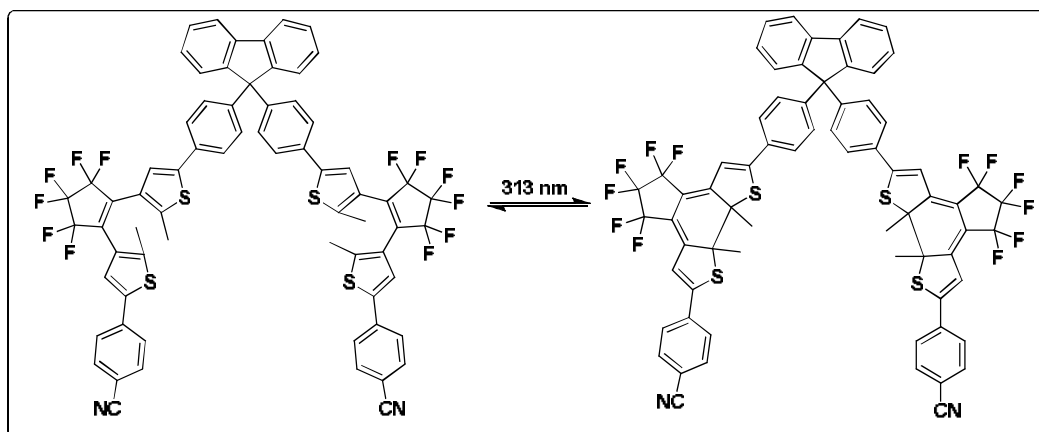


**Figure 6.** Structures of diarylethene dimer linked by a phenyl spacer (top). Absorption spectra of *o-o* (—), *c-o* (....), *c-c* (-.-.-) (bottom left) and change in the mole fraction of the isomers *o-o* (●), *c-o* (▲), and *c-c* (○) in the photocyclization reaction upon irradiation at 313 nm (bottom right)<sup>[109]</sup>.

Starting from the **o-o** form, irradiation at 313nm allows observing the typical spectroscopic signatures of **c-o** (596nm,  $\epsilon=13,500 \text{ M}^{-1}\text{cm}^{-1}$ ) and **c-c** forms (588nm,  $\epsilon=25,000 \text{ M}^{-1}\text{cm}^{-1}$ ). Quantification of the relative quantities by HPLC/UV-vis technique (figure 6) shows that the **o-o** isomer completely disappeared but PSS analysis characterizes only the partial formation of **c-c** one. This study represents a nice example where a through bond interaction involving  $\pi$ -conjugation between several DTE units leads to a partial annihilation of photochromic conversion and the difficulty to obtain the full commutation of the molecular system.

In contrary, two diarylethene photochromic units behave independently when they are connected by a non-conjugated bridge. As a result, the full ring-closing commutation can be reached.<sup>[110]</sup> As example, two diarylethene photochromic units combined through a linker (fluorene derivative) logically behave independently (scheme 9). In this case, stimulation leads

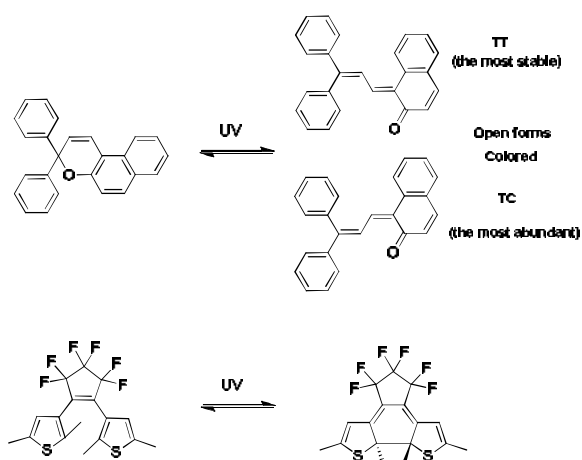
to the full conversion of the system and at the photostationary state, the ratio of (o-o), (o-c), and (c-c) was 0.1:3.5:96.4 respectively.<sup>[110]</sup>



Scheme 9. Diarylethene dimer linked by a fluorene unit.<sup>[110]</sup>

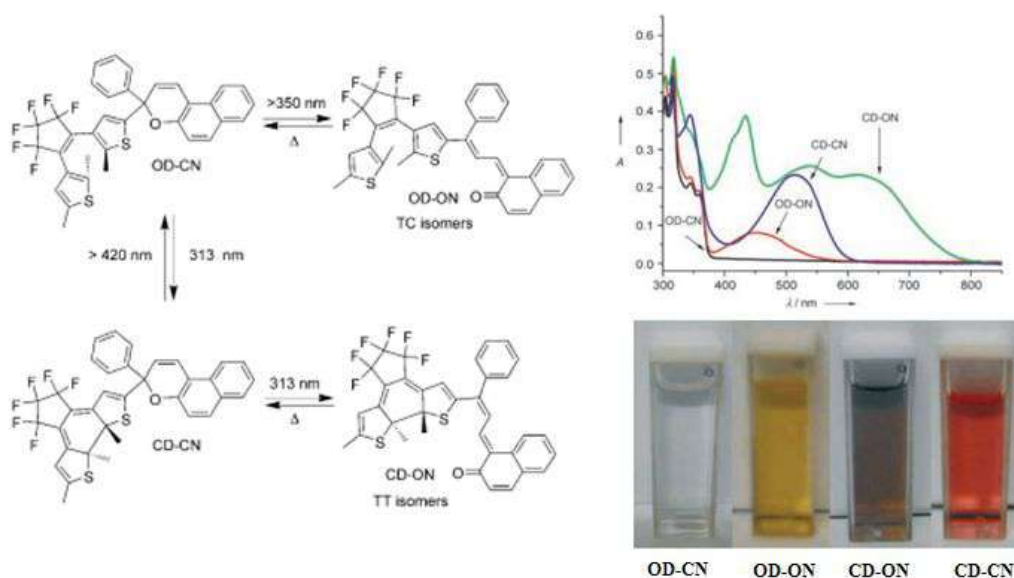
Due to the difficulty of addressing selectively one of the two identical switchable units, several examples of multi-chromophoric switching systems, incorporating two different photochromic units, have been described in the literature.

Among various examples, Michel Frigoli and Georg H. Mehl have described in 2005 a biphotochromic system based on the combination of naphthopyrans and photochemically bistable and very fatigue resistant diarylethene groups.<sup>[111]</sup> The photochromic properties of isolated naphthopyrans can be described as follow: upon irradiation (UV light) the closed colorless form in which the phenyl groups at the 3,3'-positions are linked to the photochromic core by a C-sp<sup>3</sup>, transforms in two isomeric open colored forms, transoid-trans (TT) which is the most stable isomer and transoid-cis (TC) the most abundant isomer<sup>[112, 113, 114]</sup>. As a reminder, as mentioned before, the photochemical interconversion of diarylethene takes place between two different states the open colorless form and closed colored one (scheme 10).



*Scheme 10. Photochromic interconversion of naphthopyran and diarylethene.*

In this context, the association of naphthopyran and diarylethene leads to a compound allowing four photochromic states (presented in figure 7) [111] where OD/CD and ON/CN refers to the open/closed status of the DTE unit and naphthopyran moiety respectively. As expected, each of four metastable states of this system presents a unique and specific UV-visible signature. Indeed, the colorless solution of OD-CN form can be converted successively to orange, pink and brown solutions upon irradiation with a wavelength suitable to induce the commutation of each photochromic unit (366 or 313 nm).



*Figure 7. UV/Vis absorption spectra of the four photochromic states based on the association of naphthopyran and diarylethene followed by the colors obtained at each stationary state.[111]*

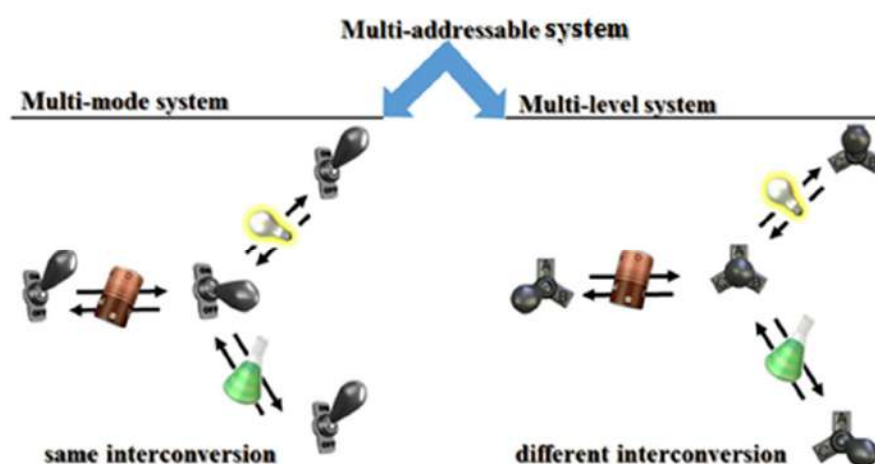
The irradiation at 366 nm induces selectively the opening of the naphthopyran allowing the commutation from OD-CN to OD-ON form translated by an orange coloration of the solution. At the opposite, the irradiation at 313nm does not induce selectively the DTE unit commutation. In fact, such UV light irradiation triggers both the ring-opening reaction of the naphthopyran but also the ring-closing of DTE which conducts to a mixture of OD-ON and CD-CN forms. The rapid thermal back conversion from OD-ON to OD-CN states should conduct to an enrichment of CD-CN in the mixture under prolonged irradiation time. Unfortunately, the photo-induced opening of naphthopyran unit of CD-CN is also effective at this wavelength. As consequence, OD-CN state is directly converted to CD-ON under prolonged irradiation time at 313 nm (20 min) and the intermediate CD-CN can be only isolated after a subsequent thermal bleaching of the fully commutated system.

As demonstrated by this example, the association of several different photochromic units can be reached out by overcoming synthesis difficulties. If a large variety of all-photon mode multichromic systems are reported, effective multi-addressable and multi-active compounds remain a minority.<sup>[100]</sup> Indeed, most of the photochromic units are addressed under UV light irradiation but they are not exhibiting sufficient absorption properties differences in this range to assure their selective photo-addressability.

This problem of selectivity between similar switchable units have drawn the research toward the elaboration of multi-responsive systems. In place of one unique mode of stimulation as for previous examples, these systems can be fully addressed by using a combination of orthogonal stimuli (photon, electron and proton). Some nice examples of this strategy are detailed below.

### III). Different types of multi-addressable units

The construction of functional molecular devices requires access to molecular components with physical properties that can be reversibly modified by applying one or more external stimuli. In this context, multi-addressable organic materials are currently an active area of research. Able to respond to several kind of stimulation, these systems will appear useful in optical computing as logic gates.<sup>[98]</sup> Among the multi-addressable molecular systems reported so far, two different kinds can be defined (Figure 8).



*Figure 8. Comparison between the two different types of Multi-addressable unit.*

The first category (figure 8 right) gathers multi-responsive molecular systems in which each different kind of stimulation leads to its own and distinct metastable state. Each of these states exhibiting specific physico-chemical properties, these compounds are referenced as multi-state systems and exhibit as much metastable states as stimulations.

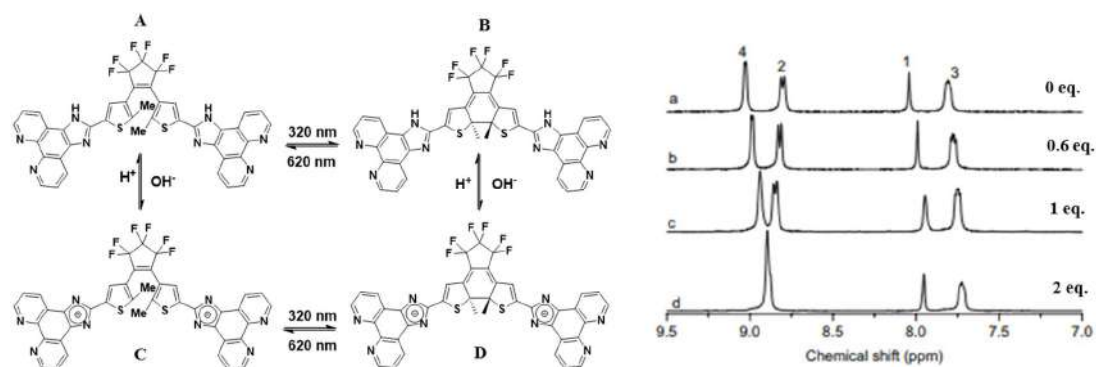
The second category of multi-addressable systems (figure 8 left) is generally referenced as multi-mode molecular systems. Exhibiting only two different metastable states, the intercommutation between states can be carried out by using indifferently at least two different stimuli.

Multi-level molecular systems are generally elaborated by connecting different types of molecular switches through covalent links<sup>[100]</sup> or by mixing them within supramolecular

assemblies<sup>[115]</sup> to obtain multi-responsiveness through the combination of various stimulations (*i.e.*, photon, electron, proton, magnetic field, etc...). As mentioned above, due to synthesis difficulties, their preparation continue to be a challenging task.<sup>[100]</sup> As example of this approach, we can cite nice examples reported by Xiao et al. in 2006 which are based on the association of diarylethene, a photochromic unit, and two imidazo [4,5-f] [1,10] phenanthroline as acidochromic ones.<sup>[116]</sup>

### A. Multi-level system based on diarylethene and imidazo [4,5-f][1,10] phenanthroline.

Xiao et al. in 2006<sup>[116]</sup> described two multi-state systems composed on a dithienylethene linked to two imidazo [4,5-f] [1,10] phenanthroline units directly through the thiophene groups. Clearly, imidazo-phenanthrolines are not photochromic molecules: their physico-chemical properties change according to the pH of the solution. Incorporating three switchable units, these systems should lead to  $2^3$  different metastable states but the 8 possible states are reduced to 4 due to symmetry considerations and the impossibility to stimulate selectively only one of both acidochromic units (*vide infra*). All observed metastable states are presented in Figure 9.



**Figure 9.** Multi-state systems generated upon photochromism and deprotonation (left). <sup>1</sup>H NMR spectral changes of state A upon titration by NaOD (30%) at the equivalence of 0 (a), 0.6 (b), 1.0 (c), and 2.0 (d) of A (400 MHz, DMSO-*d*<sub>6</sub> at 298 K).<sup>[116]</sup>

Obviously, the system exhibits a sensitivity to light and pH changes. The photoreactivity of the DTE is not affected by the presence of the phenanthroline units, and the irradiation of the

initial state **A** at 320 nm causes its photocyclisation which leads to the coloration of the solution. Due to the good thermal stability of the photogenerated form **B**, the reverse reaction is carried out by irradiation with visible light (620 nm). Sensitive to pH changes, the imidazo [4,5-f] [1,10] phenanthroline can be addressed by addition of base aliquots. From that, the addition of two equivalents of sodium hydroxide from the initial state **A** and photo-generated **B** state causes the deprotonation of NH leading to state **C** and **D** respectively. With the help of  $^1\text{H}$  NMR studies, it is possible to observe that the deprotonation is not occurring in a stepwise manner. In fact, a quick proton exchange occurs between protonated and unprotonated substituents of the DTE.

On the other hand, the absorption spectra of the closed forms of dithienylene (**B** and **D**), appear analogous whatever the protonated and deprotonated status of imidazo-phenanthrolines moieties, which translates that the increase of the electron density of the deprotonated imidazole has no influence on the closed dithienylenes.

If the absorption properties of the closed DTE are not strongly influenced by the status of phenanthroline, the interest of this system lies in the photochemical and chemical control of the fluorescence of the four different states. Indeed; the initial state **A** is the most fluorescent one. Upon the addition of base to give the **C** state or by irradiation at 320 nm to form the **B** state, the luminescence properties decrease by half. Similarly, the interconversion of the **B** state to **D** by adding sodium hydroxide leads to a further decrease in the intensity of the fluorescence.

Finally, such kind of system displays four different states where each state can be distinguished by a unique stimulation and differentiated by proton NMR. Furthermore, the phenanthroline units on this molecular system can also act as a suitable ligand to coordinate and form metal complexes with various metal ions.

Beside this classical approach consisting in the association of several kind of simple switchable units, the elaboration of multi-level molecular system can be also obtained in a more

elegant manner from single unit exhibiting multi-responsiveness. Among the different photochromic families, only few of them are able to generate two different metastable states when stimulated with different stimuli. To the best of our knowledge, they are limited to some flavylum derivatives and in more general manner to spiropyran, spiroxazine and chromene whose acido- and electrochromic behaviors are detailed below.

### B. Multi-mode molecular switches based on Spiroprans.

As mentioned before, spiropyran is a photochromic motif but, as introduced by Raymo and co-workers in 2001,<sup>[117]</sup> they present also acidochromic properties. Indeed, the treatment of spiropyran in acidic conditions undergoes through the protonation of the spiro-oxygen the cycle opening and generates the corresponding protonated MC motif ( $MCH^+$ ) that can be detected by a change in the absorption spectrum: protonated MC ( $MCH^+$ ) typically absorbs around 400-450 nm while MC isomer absorbs around 500-600 nm. The process is then accompanied by a variation in color. When the MC binds protons, the solution turns yellow.<sup>[79, 117, 118, 119, 120]</sup> Addition of base to the yellowish solution of protonated MC leads to the formation of MC isomer (Figure 10). Moreover, the transformation of MC form to SP form can only be done under visible light exposure.

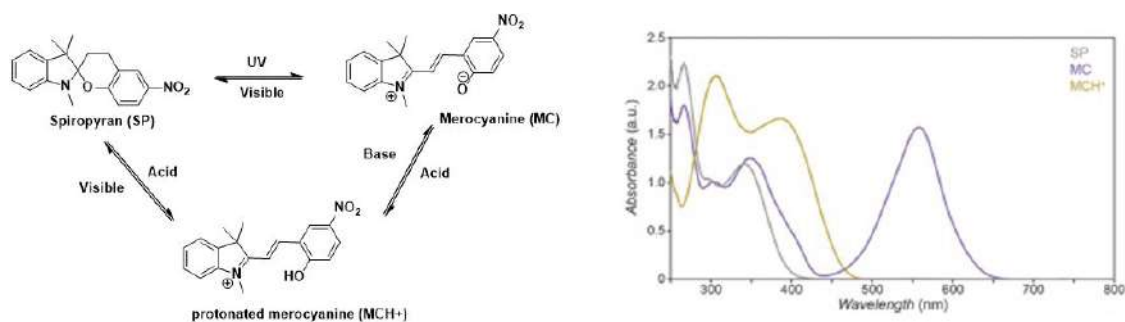


Figure 10. UV Absorption spectra of each form of Spiropyran.

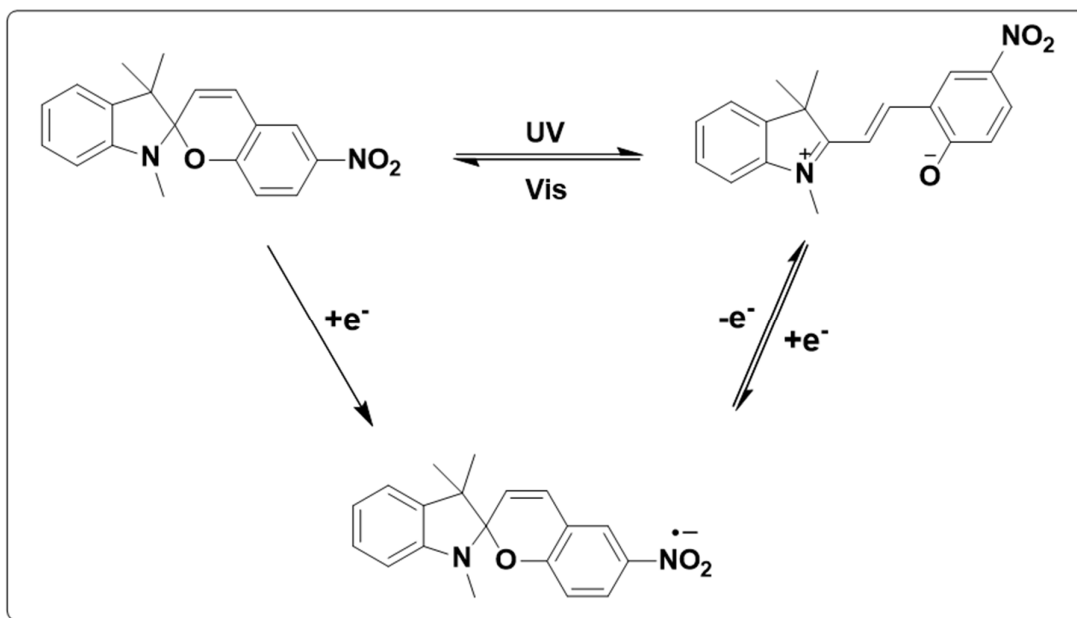
In addition to these interesting properties, spiropyran derivatives exhibit also electrochromic property only scantily studied. Campredon *et al.*, in 1993,<sup>[121]</sup> first described the

electrochemical study on a series of spiropyran derivatives (nitrospiropyrans). Cyclic voltammetry of compounds presented in Scheme 11 shows that these molecules can be electrochemically reversibly reduced, but undergo non reversible oxidation processes.



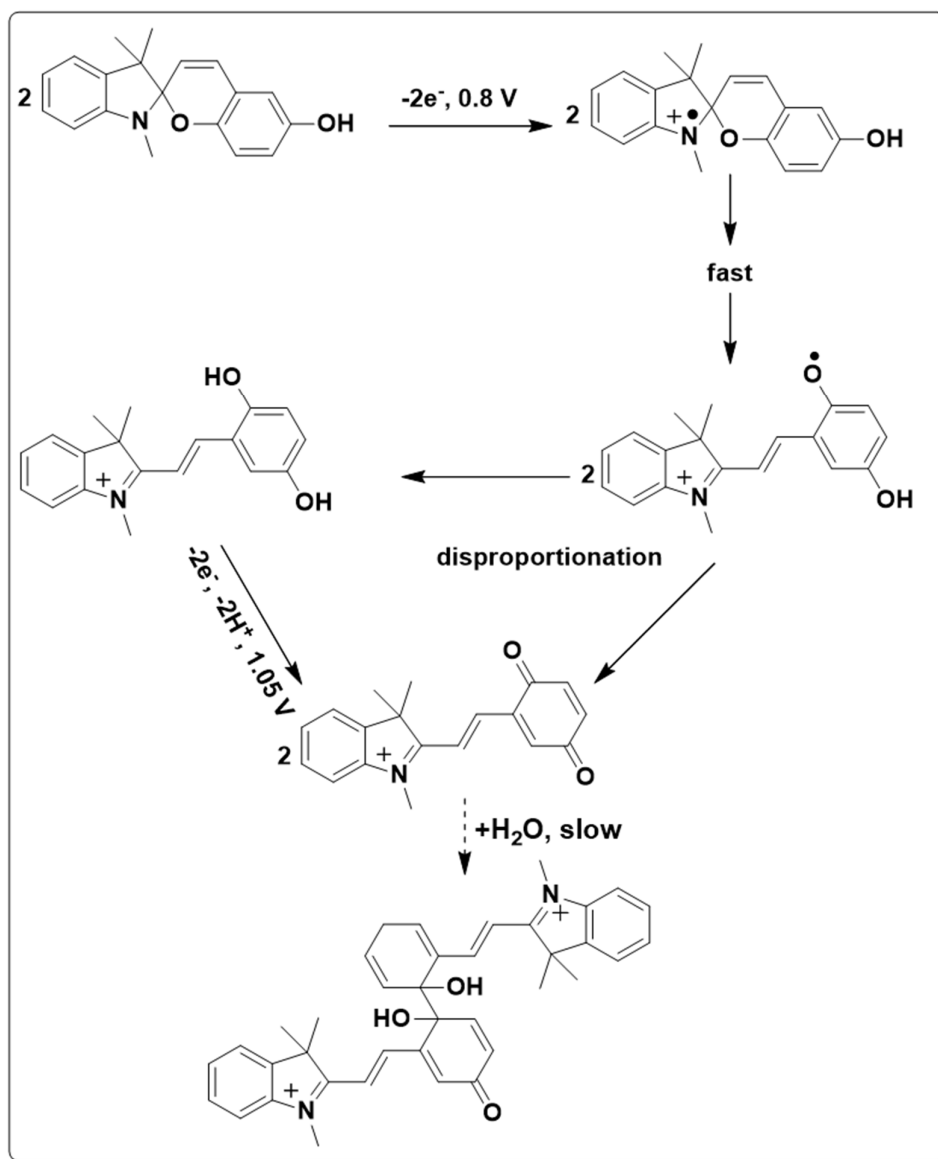
*Scheme 11. Structure of the spiropyran derivatives studied by Campredon et al. [121]*

In 1995, Zhi *et al* have suggested the possibility to induce the reversible ring opening of nitrospiropyran through a reduction pathway.<sup>[122]</sup> Indeed, upon reduction, the nitrospiropyran leads to a radical anion which shows, as demonstrated by spectroelectrochemistry, an absorption band centered at 455 nm and probably mainly localized on the pyrene moiety. More interestingly, its subsequent oxidation suggests the formation of merocyanine (MC) characterized by an absorption band at 556 nm. From that, authors concluded that this new redox reversible process indicates that closed/open ring isomerization can be induced through an electrochemical process. In addition, the initial ring-closed form is regenerated by irradiation with visible light (scheme 12). Thus, the photo- and electro-commutabilities of this system could find applications in multifunctional electro-optical devices.<sup>[122]</sup>



**Scheme 12.** Suggested mechanism of the generation of merocyanine under the influence of electrochemistry.<sup>[122]</sup>

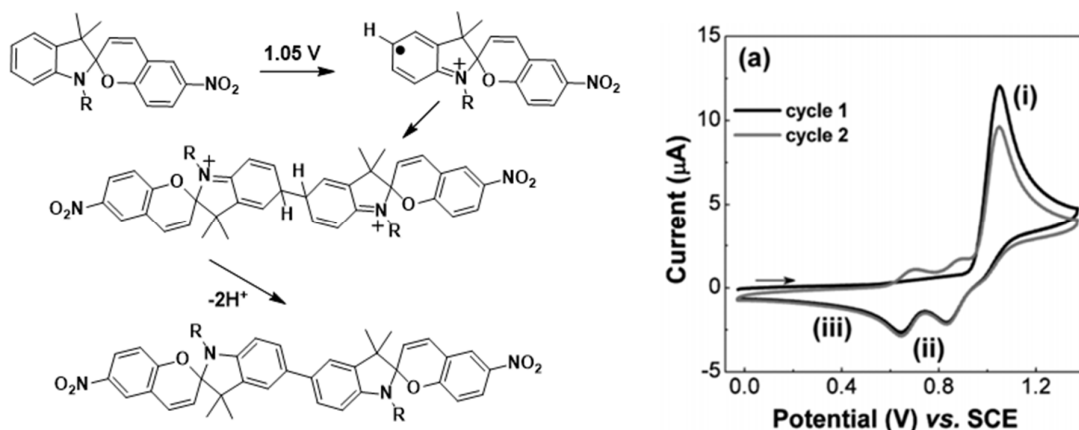
Later new electrochemistry studies on spiropyran were performed by Preigh *et al.* they have explored the mechanism of oxidative process of hydroxyspiropyran and of indoline and chromene model compounds.<sup>[123]</sup> From bulk electrolysis, cyclic voltammetry and NMR spectroscopy of the oxidation product, the authors concluded that the oxidation of hydroxyspiropyran involves the transfer of two electrons to produce a radical cation (centered on the indoline moiety of the SP), which rapidly undergoes ring-opening and disproportionates to hydroquinone and quinone. In addition, the potential of the second oxidation wave at 1.05V was explained by the two-electron oxidation of the protonated compound which leads to the quinone form. This quinone undergoes a slow, water-mediated dimerization (C-O-C) as shown in scheme 13.



**Scheme 13.** Suggested mechanism of the oxidation of hydroxyspiropyran and the resulting dimerization obtained.<sup>[123]</sup>

In recent studies, it has been demonstrated that the oxidation of nitrospiropyran (one electron electrochemical oxidation) can lead to oxidative C-C coupling at the para position of the indoline moieties to form the SP-SP dimer (figure 11). More precisely, in cyclic voltammetry, a non-reversible oxidation of nitrospiropyran at 1.05 V vs. SCE is attributed to fast ring-opening of the formed radical cation.<sup>[124]</sup> During the second cycle of the cyclic voltammetry two new reversible oxidation waves, attributable to the dimer generated by C-C coupling, are observed at lower potentials, namely at 0.65 and 0.83 V vs. SCE. Moreover,

Feringa *et al*, have observed that the substitution of the position 5 by methyl group blocks the dimerization and leads to a reversible oxidation process (no opening).<sup>[125]</sup>



**Figure 11.** Cyclic voltammetry of nitrospiropyran at a glassy carbon (GC) electrode in 1,2-dichloroethane (0.1 M TBAPF<sub>6</sub>) with the corresponding mechanism of dimerization process.<sup>[125]</sup>

As we can see, a single switchable unit can present multi-responsiveness. In the case of spiropyran and spiroxazine, their stimulation by different stimuli (photon, electron and proton) leads to different metastable states and paves the ways for the elaboration of simple multi-level molecular systems.

At the opposite, the elaboration of multi-mode systems requires some switchable unit which can undergo the same commutation between two forms by applying different stimulations. Among all photochromic families, few systems are known to exhibit such switching ability. To the best of our knowledge only DTE and indolino-oxazolidine units are able to commute between two identical forms by using indifferently at least two different kinds of stimulations such as example light or electrochemical potential. As consequence, these multi-modal switchable units are presented in the next section.

#### IV). The DAE as a multimode switchable units

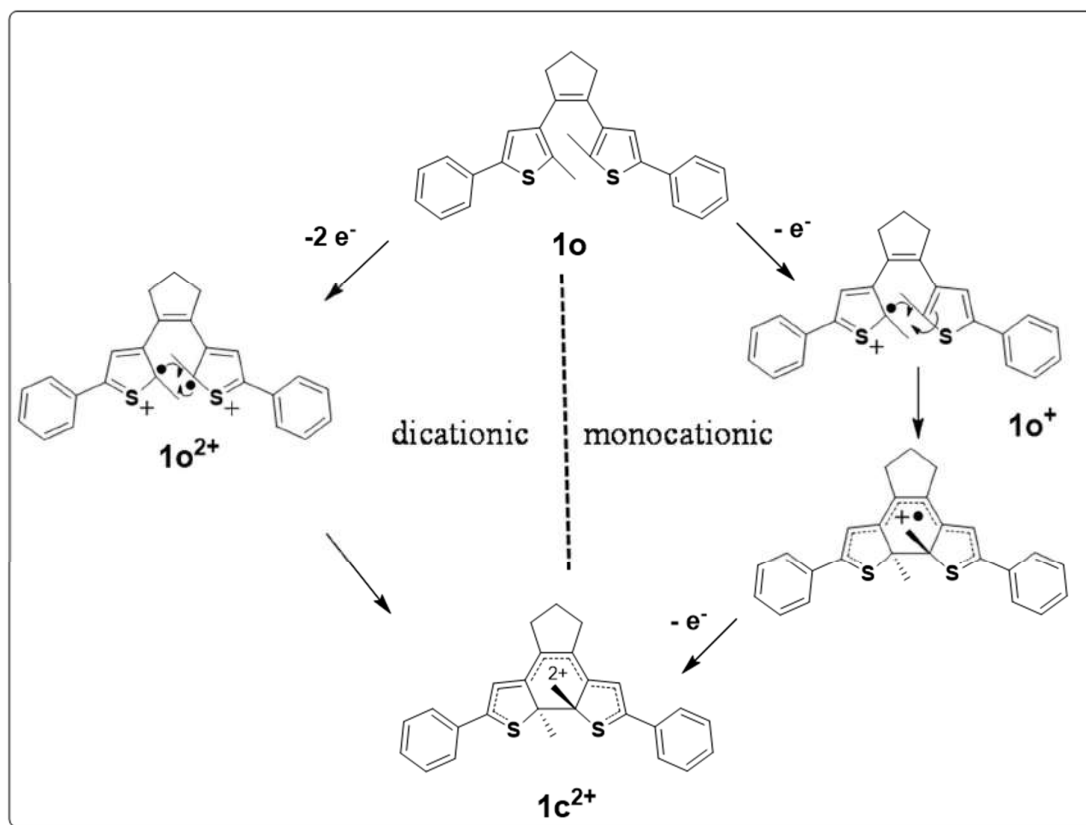
The DTE derivative represents a very well-known switchable unit recognized to exhibit very interesting photochromic performances (see section I.B.2). Moreover, the opening/closure

of the DTE can be also induced by the application of an electrochemical potential. Less studied than their photophysical properties, their electrochromic behavior is summarized here in order to highlight their multimodal switching abilities.

In addition to their photochromic properties and as mentioned before (*vide supra*), diarylethene derivatives exhibit also electrochromic properties. Within this context, the redox switching of dithienylethene was first described by Kawai<sup>[126]</sup> in 1995 and later by Branda and co-workers.<sup>[127]</sup>

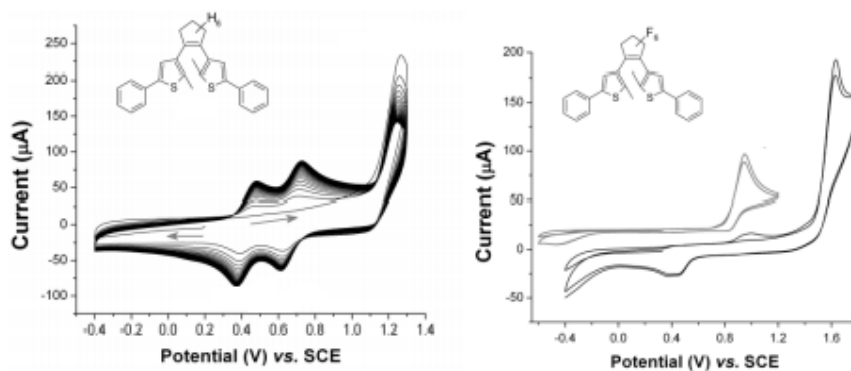
According to literature and early studies, the nature (opening or closure) of the electrochemical switching of dithienylethene appears highly dependent on both substituents on the thienyl rings and on the nature of the central alkene. Following this idea, Feringa and Browne have written a series of publications reporting the influence of the nature of the bridge as well as the effect of thienyl substituents.<sup>[128, 129, 130]</sup>

Indeed, cyclic voltammetry of symmetrical dithienylethene connected by different cyclopentene units (perhydrocyclopentene (**1o**) and perfluorocyclopentene (**2o**)) reveals “opposite” electrochromic behaviors. More precisely, in the case of the perhydro DTE (**1o**), when cycling towards positive potentials, an irreversible two-electron oxidation wave is observed at 1.2 V *vs* SCE (figure 12). On the return sweep two well resolved reductions are observed at 0.7 and 0.4 V. These two new and reversible redox processes were assigned to the two oxidation states of the closed form leading to **1c**<sup>+</sup> radical cation and **1c**<sup>2+</sup> dicationic species. As consequence, the authors conclude that oxidation of the open form **1o** leads immediately to the ring closing of the DTE (from **1o** to **1c**) which undergoes at this potential two successive oxidation processes to form corresponding dicationic closing form **1c**<sup>2+</sup>. However, the authors mentioned that the formation of **1c** state can reasonably follow two different mechanisms through a monocationic state or via a dicationic state (scheme 14) depending on the experimental conditions.



*Scheme 14. Electrochemical ring closing of  $1o$  via a dicationic and monocationic state.*

In fact, strongly affected on one hand by the nature of the bridge and substituent beard by the thienyl moiety, and on the other hand by the solvent employed, the driving force for ring closure appears to be the stabilization achieved from the mono- and/or dication of the open form by the ring-closure.



*Figure 12. Cyclic voltammetry of diarylethene with hydrogenated cyclopentene (left) and fluorinated cyclopentene (right) in dichloromethane at a scan rate of  $0.1 \text{ V} \cdot \text{s}^{-1}$  at glassy carbon electrode (GCE).<sup>[128]</sup>*

In contrary, using perfluorocyclopentene (an electron withdrawing group) as linker, results in loss of the electro-induced (by reduction) ring closure process translated on a CV by the absence of new signal at lower potential (figure 12). To restore it, donor or electroactive substituent have to be introduced on the thienyl position 5 such as example chloro, methoxy-phenyl,<sup>[128, 129]</sup> N-methyl- pyridinium<sup>[131]</sup> to name few.

On the other hand, the substitution of perhydro- by perfluorocyclopentene bridge can also change the direction of the electrochemical switching. As mentioned above, the oxidation of **1o** will lead to the closure of the DTE. At the opposite, the oxidation of **2c** leads to the ring opening and leads after immediate reduction to **2o** due to the higher oxidation potential of this later.

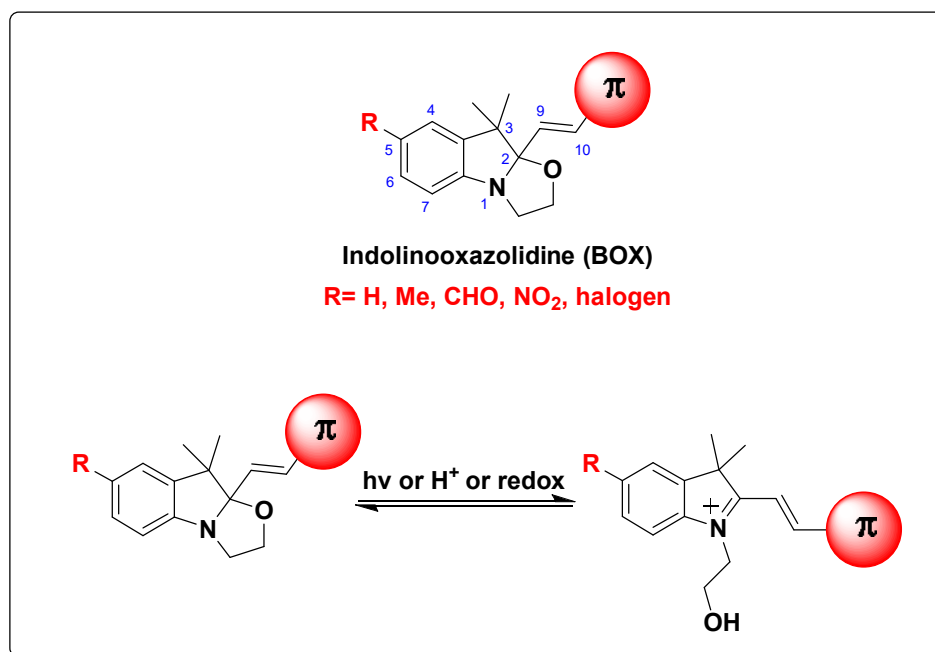
Thus, at the opposite to their almost universal photochromic behavior, the electrochemical switching of the DTE is strongly affected by the nature of the central core and by the thienyl substituent. However, the possibility to induce the opening and/or the closure of the DTE under electrochemical stimulation stays up to now less explored than their photochemical switching. Nevertheless, the versatility of DTE as multi-modal switchable unit shows considerable promise for the development of future applications such as novel modified electrode surfaces in which both light and electrochemical potential can be used as triggers.

Compared with DTE, indolino[2,1-b]oxazolidine derivatives are a relatively confidential sub-class of multi-modal addressable units known to display photo-, acido- and electrochromic performances.<sup>[132, 133, 134, 135]</sup>

### **V). Introduction to Indolinoxazolidine (BOX) as a nice multimode switch**

Among the huge number of molecular switches, indolinoxazolidine is a recent and still confidential class of promising switches which have been firstly reported in a patent in the

1970s by the Japanese company Matsushita Electric Industrial by introducing the first example based on styryl compounds.<sup>[136]</sup> Structurally, indolinooxazolidine (referenced as BOX) is characterized by the fusion of a 2,3,3'-trimethylindoline group with an oxazolidine heterocycle (scheme 15). In fact, the success of such kind of molecular switch doesn't lie only on its easy synthetic accessibility, but is also due to its interconversion from one state to another under the influence of different stimulations.



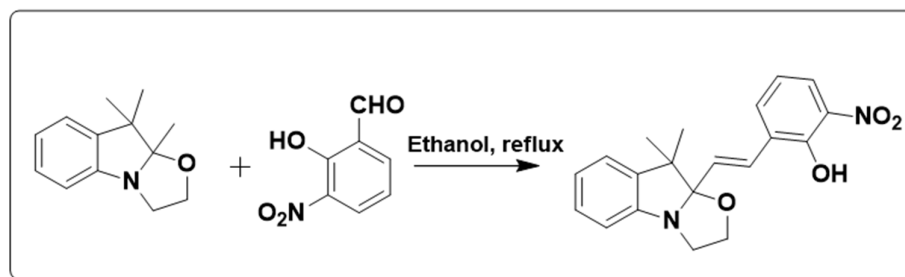
*Scheme 15. General structure of indolinooxazolidine derivatives.*

Interestingly, the reversible opening of oxazolidine ring of indolinooxazolidine (BOX) can be induced under external stimulation and leads to structural modifications and drastic change of their physico-chemical properties. Under their closed form, the indoline and its olefinic or styrylic substituent are almost orthogonal and not conjugated together due to the  $sp^3$  hybridization of the carbon 2. Without any communication between them, the absorption bands are then limited to UV- near visible range. With the opening of the oxazolidine ring and the generation of the corresponding indoleninium moiety which acts as a strong electron withdrawing group (EWG), the hybridization of the carbon 2 changes from  $sp^3$  to  $sp^2$  and the pi-

conjugation is now extended to the whole molecule. As consequence, a bathochromic shift of the absorption band is observed especially when the associated pi-conjugated system bears a donor group. In this case, the open form of the system behaves as a classical push-pull system characterized by a large and intense charge transfer absorption band in the visible range. These chromogenic properties of the open form were first noticed by Hayami and Torikoshi in 1976,<sup>[137]</sup> who have patented 83 members of functionalized indolino-oxazolidine.

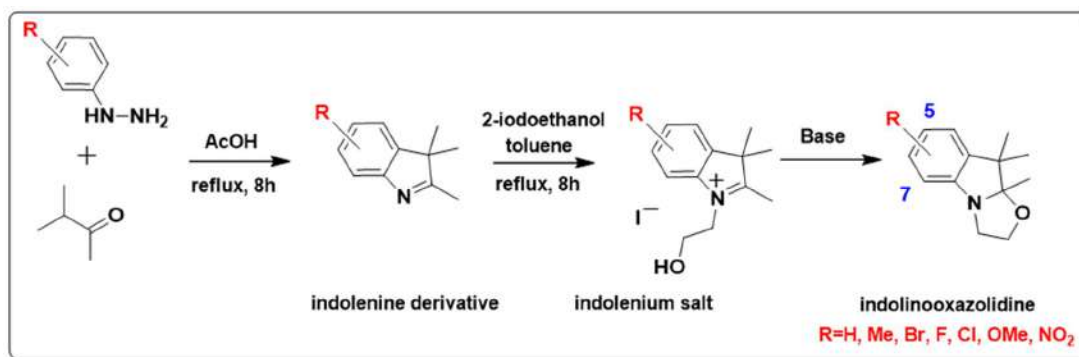
The acidochromic properties of indolinoxazolidine derivatives are known for a long time and are certainly their most known properties. Photochromic ones have been described in the late 90's by Petkov and collaborators<sup>[135]</sup> as electrochromic behavior of BOX derivatives were only more recently characterized. Within this context, indolinoxazolidines (BOX) can be considered as an almost confidential subfamily of molecular switches exhibiting photo-, electro- and acidochromic properties. Their interesting commutation properties will be described in the following part after a quick overview concerning their preparation and functionalization.

If all first patents published in early 1970s concern exclusively the indoleninium form of BOX, the first detailed synthesis and characterization of one of them under its closed form was described by Krongauz et al. in 1973 from 2,3,3-trimethylindolino[2,1-b]oxazolidine (scheme 16).



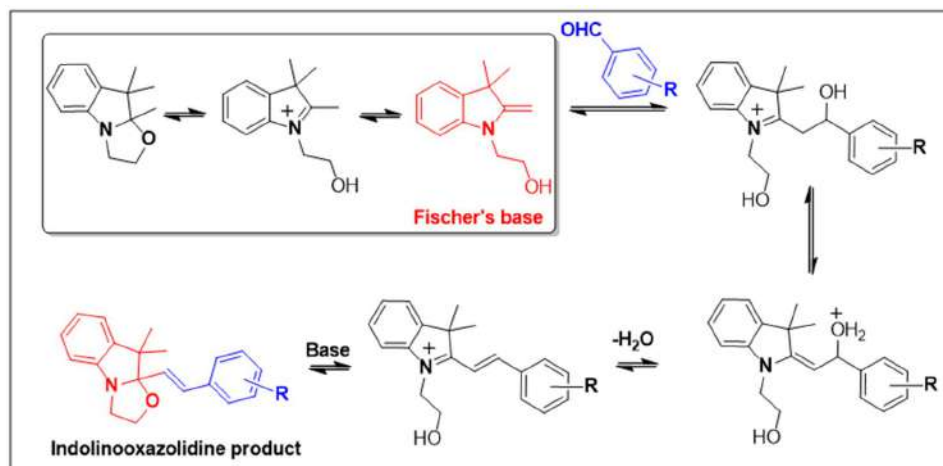
*Scheme 16. Synthesis of the first indolinoxazolidine derivative.*

Used generally to prepare spiropyran with pendant alcohol function,<sup>[138]</sup> this synthon is still the corner stone of all described BOX syntheses. It can be prepared at multigram scale in two successive steps by alkylation of the corresponding indoline derivative with 2-iodo or 2-bromoethanol and subsequent treatment of the resulting indoleninium salt by a base. The functionalization of the BOX derivative in position 5 and 7 requires then to prepare corresponding substituted synthon which can be carried out easily (Scheme 17) thanks to the Fischer indole synthesis<sup>[139]</sup> and the commercial availability of numerous substituted phenylhydrazines.



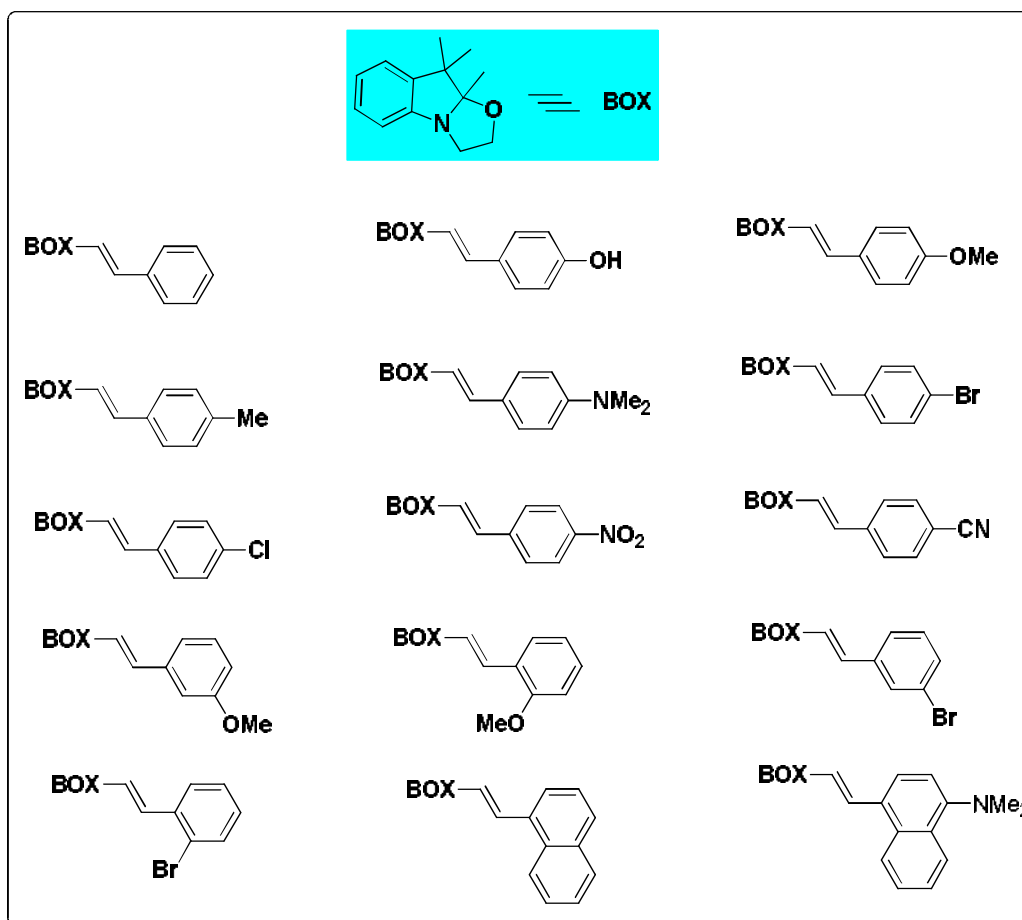
*Scheme 17. Synthesis of indolinoxazolidine derivatives.*

As mentioned above, all BOX derivatives are prepared from 2,3,3-trimethylindolino[2,1-b]oxazolidine derivatives due to their efficient condensation on a large variety of aromatic aldehyde and nitroso derivatives. However, this latter is not considered as the reactive species. In place, the proposed mechanism<sup>[41]</sup> refers to the nucleophilic attack of aldehyde and nitroso by the corresponding Fisher's base arising from successive tautomeric equilibria as resumed below (scheme 18).



*Scheme 18.* Reaction mechanism between indolinoxazolidine and aromatic aldehydes.

As consequence, numerous structural modifications can be envisioned either on the indoline heterocycle or on the associated pi-conjugated system. The introduction of substituents on the indoline heterocycle have opened the way for further structural modifications by post-functionalization such as example a palladiated C-C coupling after introduction of a bromine atom.<sup>[134]</sup> However, most of the structural modifications reported so far concern the variation of the aromatic pi-conjugated aldehydes condensed onto the trimethylindolino-oxazolidine on its position 2(scheme 19).<sup>[137]</sup>

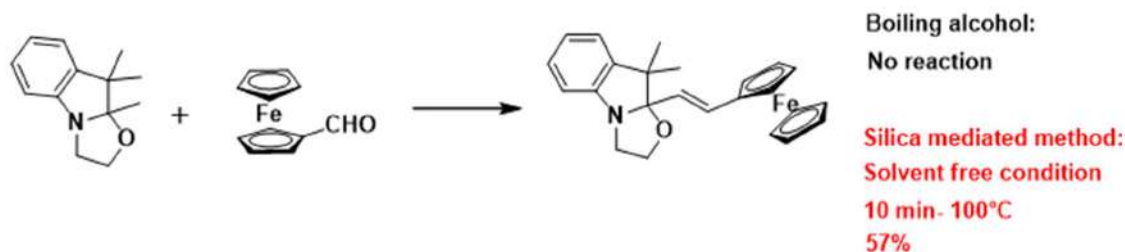


*Scheme 19. Example of reported indolinoxazolidine derivatives.*<sup>[140, 141]</sup>

If the reaction is identical, different set of experimental conditions are reported (protic and aprotic solvents, acid or basic catalysis). However, most examples report the use of boiling alcoholic solvents without any additives and give satisfactory yields.<sup>[142]</sup> Recently, a more efficient procedure was reported in our group at MOLTECH-Anjou. Performing the reaction in solvent-free conditions in the presence of commercial silica gel, allowed reducing drastically the reaction time from several days in classical conditions (boiling ethanol) to only 10-15 minutes.<sup>[141]</sup>

Obviously, this new synthetic procedure allowed the quick preparation of large panel of BOX derivatives, but more important, the later permits the preparation of some BOX derivatives unreachable with other routes by an enhancement of the reactivity of both reactants.

For example, ferrocenecarboxaldehyde does not react in solution with trimethylindolinoxazolidine, and no trace of the compound issue from their condensation is observed after several days even under more forcing conditions (100°C, tert-butanol, sealed tube). At the opposite, the silica mediated synthesis provides the targeted dyad in 57% isolated yield after 10 minutes (scheme 20).



*Scheme 20.* Reaction of Ferrocenecarboxaldehyde and indolinoxazolidine in two different conditions.

Concerning what we have seen, indolinoxazolidine (BOX) can be easily prepared in four steps without the need of any additives (inert atmosphere and distilled solvents) from commercially available phenyl hydrazine. Moreover, a lot of structural modifications can be envisioned by playing on the substitution of the BOX and of the aromatic part. After this overview concerning the limitation and outlook on BOX synthesis, their interesting commutation properties will be described in the following part.

### VI). Commutation behavior of Indolinoxazolidine (BOX)

As mentioned earlier, the opening/closure of the oxazolidine ring of BOX derivatives can be induced under stimulation of the system by using indifferently protons, photons and even electrons. The modification of the hybridation of carbon in position 2 and the generation of an indoleninium moiety acting as strong withdrawing group confers to the open and the closed forms of BOX drastic different physico-chemical properties especially optical properties. As consequence, BOX represents an interesting multi-mode molecular switch exhibiting acido-, photo- and electrochromic properties. Their switching abilities and some of their direct application are presented below.

### A. Solvatochromic and acidochromic properties of Indolinooxazolidine.

As previously reminded, acidochromic and solvatochromic properties of indolinooxazolidine are demonstrated and described for years. Indeed, the strong difference of physico-chemical properties such as the polarity between open and close forms of BOX have attracted a lot of attention. In fact, the colored open form (**OP**) or open protonated form (**POF**) presents a high dipolar moment and as a consequence will be more stabilized by strong solvation, especially in polar solvents compared to the closed form (**CF**), which is destabilized in such solvents.

In 1976,<sup>[137]</sup> Hayami and coworkers reported the strong solvatochromism of a BOX derivative incorporating in position 2 a phenyl group substituted by a dimethylamino termination. Noteworthy, its maximum wavelength is not varying continuously between 298 and 550 nm depending on the nature of the solvent as clarified and shown in figure 13. This behavior is explained by the existence of an equilibrium between **CF** and **OP**. In polar or protic solvent, the later is strongly displaced where the colored open form is preponderant leading to corresponding coloration of the solution. At the opposite, apolar solvent displace the equilibrium to **CF** leading to corresponding colorless solution. It was confirmed by Zhang and collaborators in 2013 who have demonstrated the importance of the microenvironment onto the BOX status. They have in particular shown that the presence in the hydrogen bond-donor or receptor such as water and dimethylsulfoxide can strongly stabilize the energy of the open colored form and then favor the switch from the close to the open form of BOX derivatives.

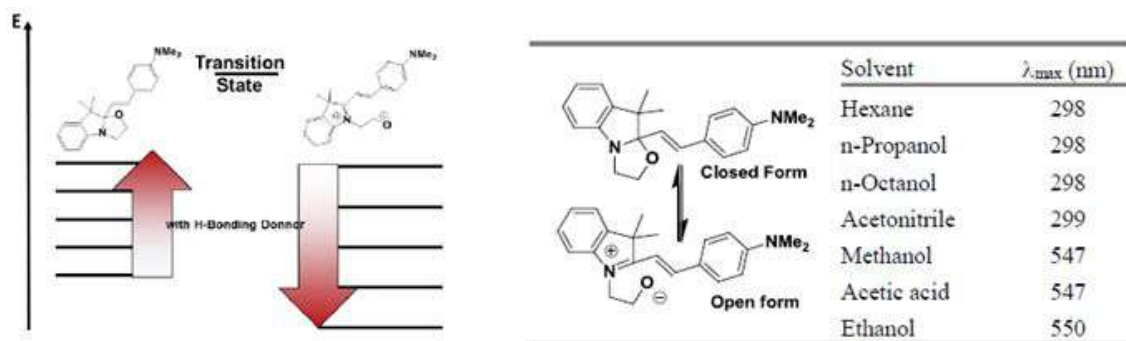
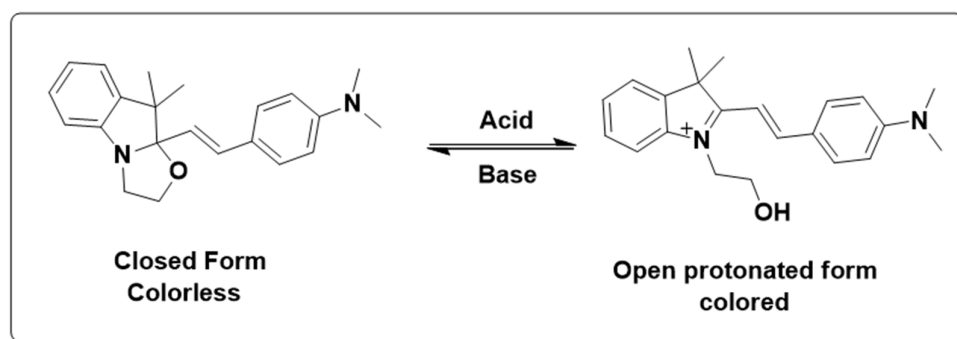


Figure 13. Influence of the nature of solvents on BOX.

Concerning the BOX acidochromic properties, they have been reported at the end of the last century. Indeed, the possibility to displace the equilibrium between the colored and colorless forms by modification of the environment acidity (pH) was reported by Bartnik et al. in 1990.<sup>[143]</sup> Among that, the addition of acid from the initial colorless or weakly colored closed form leads to the protonated and colored open form. Unlike the zwitterionic form (**OP** form), the cationic (**POF** form) is thermally stable and can be kept for several days without significant degradation. On the other hand, the discoloration of the solution and return to the original form are ensured by the addition of base (scheme 21).



Scheme 21. Acidochromic example of an indolinoxazolidine derivative.

Zhang *et al.*<sup>[144]</sup> have described in 2013 a new multi-responsive system based on the association of an indolino-oxazolidine motif as switchable unit with a tetraphenylethylene (TPE) moiety known to display remarkable aggregation-induced emission (AIE) effect.<sup>[145]</sup> Depending on the open/close status of the BOX, this system shows a tunable multi-emission in

both solution and solid state. In this context, the reversible interconversion (**CF** vs **POF**) of this system was controlled under the use of acid and base. As a consequence, the addition of hydrochloric acid on the **CF** form leads to the decrease of its absorption peak at 323 nm and to the generation of a new internal charge transfer (ICT between TPE and indoleninium units) absorption band centered at 453 nm corresponding to the open protonated form (**POF**). Strictly, the reverse back process was realized by treating the system with a sodium hydroxide solution (figure 14).

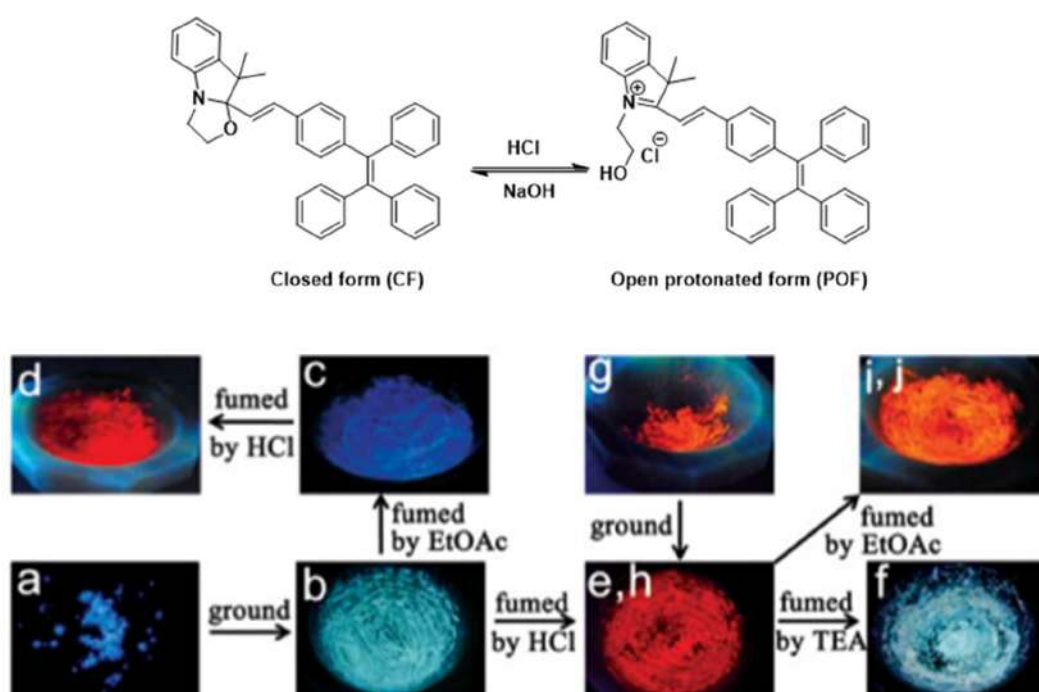


Figure 14. Chemical transformation of TPE-OX from CF to POF (top), with the fluorescent images (bottom).<sup>[144]</sup>

### B. Photochromic properties of Indolinoxazolidine.

Few years later after the demonstration of their acidochromic properties, Petkov *et al.* were the firsts, in 1998, to highlight the photochromic properties of two BOX derivatives (A and B (figure 15)).<sup>[135]</sup> In both cases, the irradiation at 254 nm of corresponding closed forms in solution leads to coloration translating the formation of the zwitterionic form due to the oxazolidine ring opening.

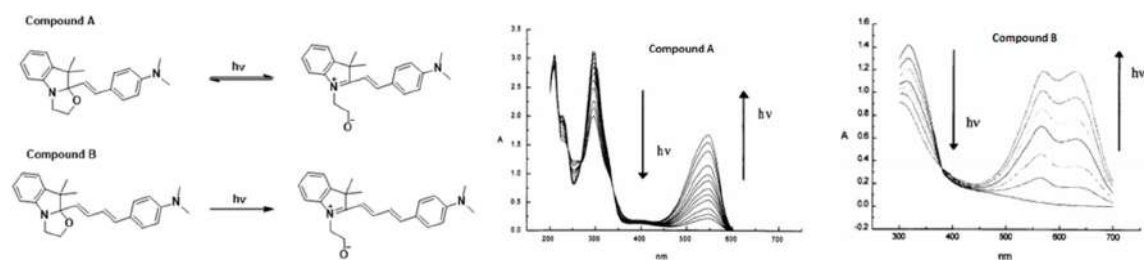


Figure 15. UV-vis absorbance spectra of compounds A and B after photo irradiation. <sup>[135]</sup>

Unfortunately, the closure of the system could only be promoted by visible light in the case of compound B. Otherwise the closed form can be restored by the treatment of basic media or heating of the irradiated sample in all cases.<sup>[146]</sup> Unfortunately, they also report that a photodegradation of the open form was observed after a long time of irradiation that prevents the full reversibility of the system.

More important, the efficiency of the photoinduced oxazolidine ring opening is strongly affected by the nature of the solvent employed and can be greatly improved by the presence of photosensitizer. Indeed, this study demonstrated that the opening through the C-O heterolytic bond cleavage of the close form occurs more efficiently in ethanol (stabilization by hydrogen bonding) and in chlorobenzene (used as photosensitizer) than in acetonitrile.

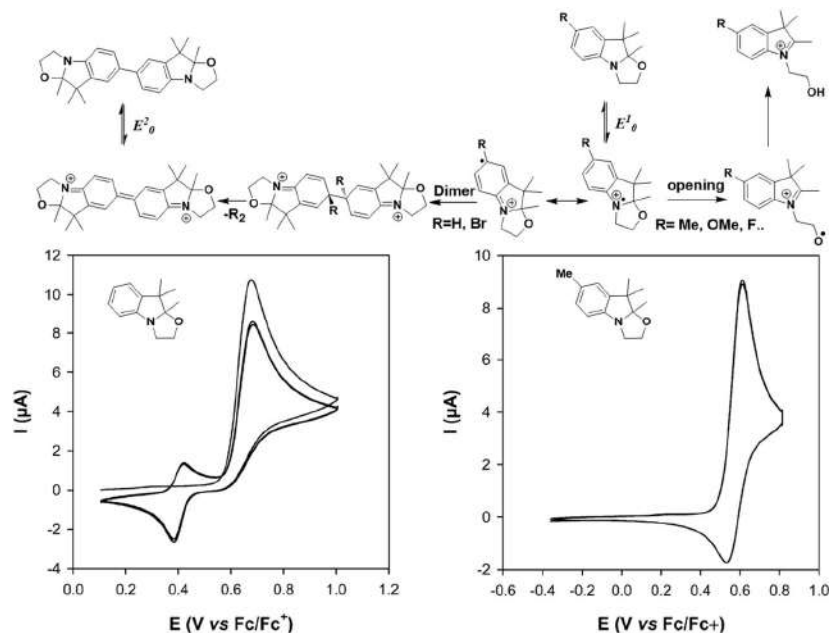
### C. Electrochromic properties of Indolinoxazolidine.

Recently, in 2015, a detailed study, focused on the electrochemical behavior of indolinoxazolidine units, has been published by Alévêque and coworkers.<sup>[134]</sup> By studying a small library of 2,3,3-trimethylindolino-oxazolidine derivatives differently substituted, they have highlighted the strong influence of the nature of the substituent in position 5 on their electrochemical behavior. Properly, as in all cases a monoelectronic oxidation process was observed, standard potentials (a 600mV shift is observed from R=CHO to R=OMe) and stabilities of the corresponding radical cations were strongly affected by the nature of substituent. In fact, radical cation bearing a MeO or F are stable while substituted ones by Me or CHO undergo an irreversible oxidation process (figure 16).<sup>[134]</sup> The authors demonstrated

that the instability of the generated radical cation is related to the oxazolidine ring opening which leads after a H-atom transfer from the media to the corresponding indoleninium form. Nevertheless, no clear trend of the inductive or mesomeric effects of substituents in position 5 on the kinetic constant of this chemical process was observed.

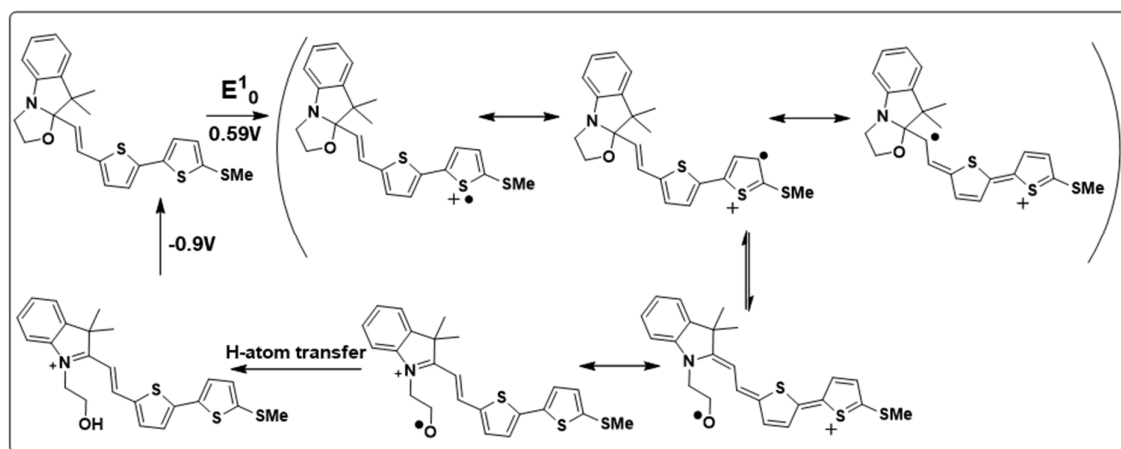
Surprisingly, the electrochemical behaviors of naked compound or one bearing a Br atom differ strongly from others. If their cyclic voltammogram reveals also a non-reversible oxidation peak, on the return sweep a new quasi-reversible wave is observed at 0.39V. The emergence of this new redox system is explained by the involvement of the radical cation in a C-C oxidative coupling in place of oxazolidine ring opening process (figure 16).

To summarize, the radical cation generated upon the oxidation of the 2,3,3-trimethylindolino-oxazolidine can be involved into two different pathways depending on the nature of the substituent in position 5 as represented on figure 16. First route leads to the opening of the oxazolidine as the second leads towards an oxidative C-C coupling to the dimerization.



**Figure 16.** Electrochemical mechanisms undergone by indolino-oxazolidine derivatives with the observed CV of H-BOX (left) and Me-BOX (right) in acetonitrile (1 mM) with TBAPF6 (0.1 M) on Pt working electrode at  $100 \text{ mV}\cdot\text{s}^{-1}$ .

The direct oxidation of the indolino-oxazolidines bearing suitable substituent in position 5 to avoid the dimerization process is not the only manner to electro-induce the oxazolidine ring opening. Indeed, it can be also achieved through an electromediated process when the BOX is functionalized in position 2 by an electroactive unit exhibiting a lower oxidation potential. The first example of such system was developed in the laboratory MOLTECH-Anjou by the association between a BOX unit and a bithiophene moiety.<sup>[147]</sup> Not conjugated under its closed form (*vide infra*), BOX and bithiophene units act independently. Exhibiting a lower oxidation potential, the oxidation is then mainly localized on the bithiophene and leads to the generation of the corresponding radical cation. The delocalization of this later in the close vicinity of the indoline then induces the oxazolidine ring opening followed by an H-atom transfer from the media to lead to the open form of the system (scheme 22).



Scheme 22. Electrochemical mechanism of BOX bithiophene dyad.

In these conditions, as oxidized form appears stabilized by the conjugated pendant system, the dimerization process is not observed whatever the nature of the substituent in position 5 of the indoline heterocycle. The opening of the oxazolidine ring and as consequence the generation of the indoleninium part induce a shift of the oxidation potential to more positive value.<sup>[147]</sup> More important, it also conducts surprisingly to the emergence of a new non reversible reduction wave at -0.9V. If the nature of the process stays for the moment unclear,

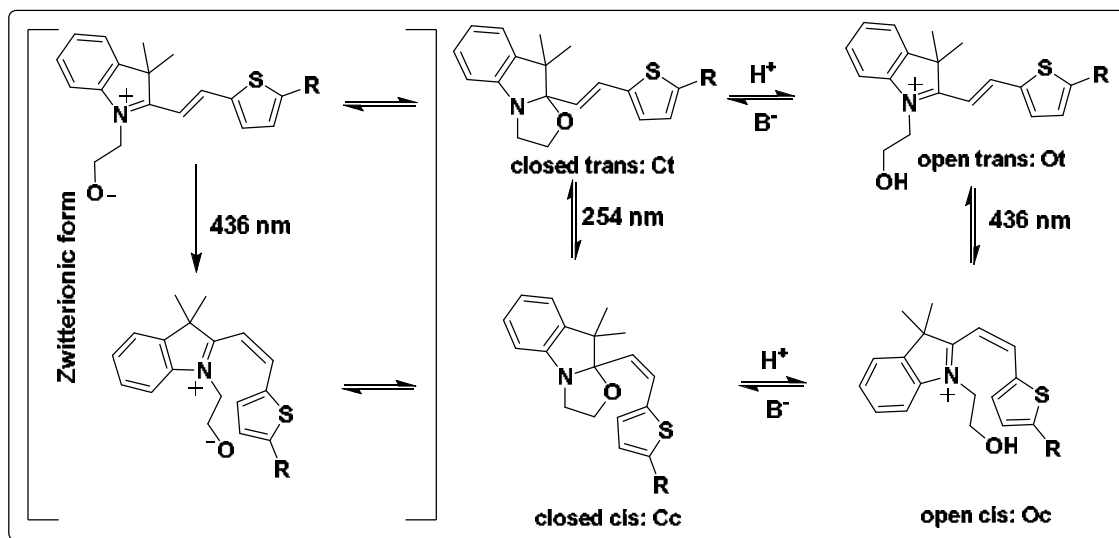
the application of a negative potential leads to the restoration of the system under its closed form.

By resuming, the reversible opening of the oxazolidine ring can be achieved by either acido, photo or electrochemical stimulation. Here again, closed low polar and open colored polar forms exhibit contrasted physico-chemical properties. Noteworthy, when substituted in position 2 with a system bearing an electron donor, the open form presents a strong push-pull character suitable for NLO applications.

### VII). Multichromophoric systems related to indolinoxazolidine

As shown before in part II, the association of several switches on the same system enhances the number of metastable states and as a consequence the possible data storage capacity.<sup>[98]</sup> Nevertheless, the selective, efficient and sequential addressability of switches represent a challenging task. As mentioned above, the association of several switchable units sensitive to different stimulations is a manner to circumvent these issues. Within this context, some indolino[2,1-b]oxazolidine moieties which act as multi-modal switch (pH, oxidation and irradiation), were combined with other photochromic units. Obviously, famous DAE unit comes first in mind (*vide supra*).

However, it is important to consider that the possible photo-isomerization (Z to E) of ethylenic junction generated during the functionalization of simple pi- conjugated system by a BOX unit. As consequence, the system can present up  $2^2$  different metastable states. Indeed, Delbaere *et al.* have recently studied the switching abilities of one of the simplest multi-addressable systems constituted by the association of a BOX unit with a simple thiophene moiety bearing different substituents.<sup>[148]</sup> They have demonstrated that the system can be selectively commutated between the four possible states regarding the status open/closed (**O/C**) of the BOX and the Z/E (or cis/trans named **c** and **t** below) isomerization of the ethylenic bridge.

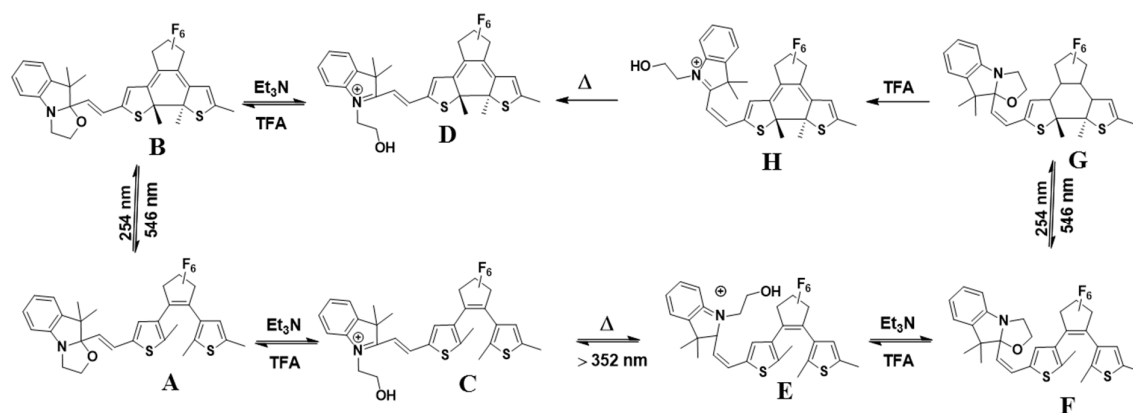


*Scheme 23. Structural transformation of BOX thiophene derivative in acetonitrile.*

Thanks to their acidochromic properties, the selective opening/closing of BOX moiety in these systems is easily and efficiently obtained by addition of TFA and  $Et_3N$  respectively. At the opposite, a loss of selectivity was observed when light is used as stimulation. Indeed, the irradiation of a solution of **Ct** in chloroform at 254 nm leads to mixture of both **Ot** and **Cc** forms. Nevertheless, the authors described two possibilities to obtain the selective photo-addressability of the ethylenic bridge. First, changing the nature of solvent from chloroform to acetonitrile induces a destabilization of the open form and as consequence reduces the photochromic properties of the BOX. The second solution consists surprisingly in shifting the irradiation wavelength to visible range (436nm) to convert **Ct** to **Cc** while no absorption was detected. In agreement with the work of Zhang and collaborators,<sup>[149]</sup> the authors refer to the equilibrium between zwitterionic open and closed forms to explain this unexpected behavior. In fact, irradiation at 436nm seems to induce a displacement of the equilibrium from **Ct** to **Ot** form by its subsequent isomerization to **Oc** which is itself in equilibrium with **Cc** (scheme 23).

As mentioned earlier, the number of metastable states and then the complexity of the system can be enhanced by adding an additional photochromic unit. In this context, the association between BOX and DAE units linked together by an ethylenic junction has attracted

a lot of attention. Firstly reported in 2010,<sup>[150]</sup> the functionalization of DAE by one indolinoxazolidine was considered at this time as a biphotochromic system allowing four different states. Once again, the BOX acidochromic properties represent an efficient and convenient manner to assure their selective addressability in all cases.<sup>[151]</sup> When stimulated by light, the switching abilities of the system are, once again, strongly dependent of the environment. Using some chlorobenzene, a BOX photosensitizer, as solvent allows enhancing drastically their photochromic properties. As consequence changing the irradiation wavelength between 254 and 313nm has allowed the author to observe selectively the addressability of the BOX or the DAE moiety respectively. Few years after, the same system was investigated in more details by NMR spectroscopy.<sup>[151]</sup> In this study, the system reveals the impressive possibility to commute between 8 different states. In such purpose, the study was carried out in pure acetonitrile to annihilate the photochromic properties of the BOX and promote the Cis/Trans photoisomerization of the ethylenic bridge. In place, acidochromic properties were used to induce the oxazolidine ring opening /closing.



**Scheme 24.** Photo and acidochromic transformation of compound A.<sup>[151]</sup>

In addition to this interesting result, DTE bearing a BOX on one side and a phenyl group substituted by a donating termination on other one allowed modifying the photochemical and electrochemical behaviors of the system.<sup>[152]</sup> With regard to this, the DTE photocyclization efficiency is greatly influenced by the state of the BOX and the substitution pattern. The authors

have noticed that the selective opening of the oxazolidine ring induced through a direct stimulation process (first oxidation happens on BOX) or through acidic treatment, results in the complete annihilation of the DTE photochromic properties.

One year after, in 2017, a new system, based on the covalent association of two BOX units to DTE moiety, was designed and studied.<sup>[153]</sup> Such kind of system has the ability to enhance the number of potential metastable states from 8 to 18 (due to symmetrical consideration) (figure 17).

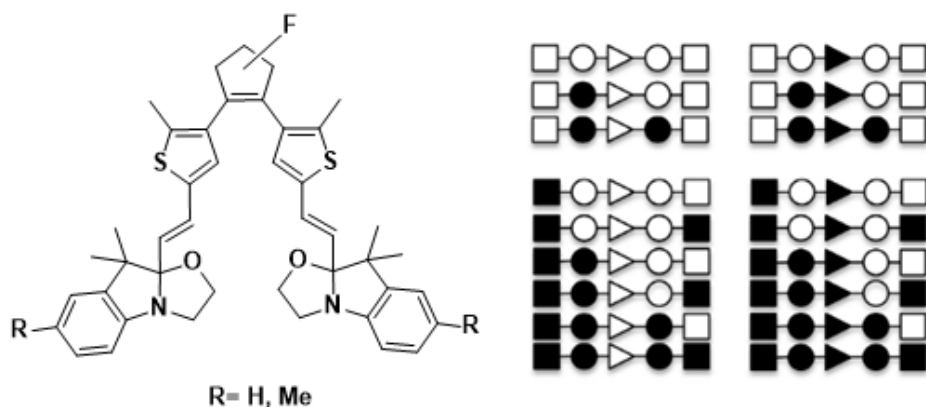
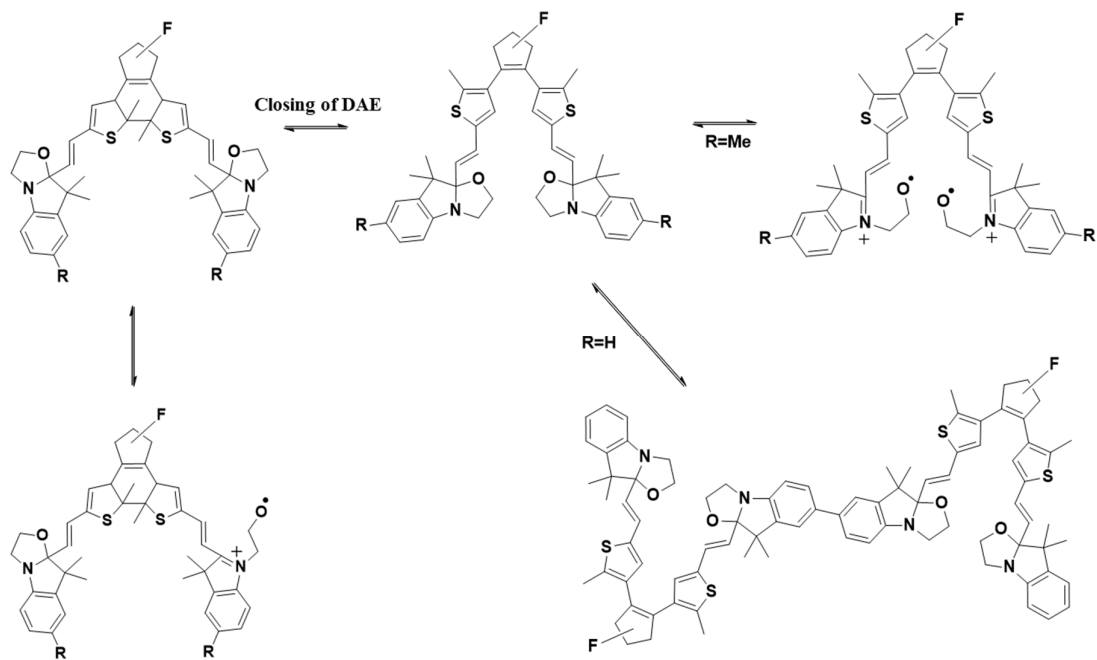


Figure 17. Target molecule with the 18 potential possible states

However, in this case only 13 states have been produced and detected by playing on the nature of the stimulation (light and pH changes). Specifically, the photochromic properties of the system (BOX-DTE-BOX) are highly affected by the nature of the solvent. First, in pure acetonitrile only DTE unit is affected selectively upon UV irradiation. At the opposite, the presence of chlorobenzene leads to observe under irradiation at 254nm the successive opening of both oxazolidine rings. As mentioned before, once one BOX is opened the photochromic properties of DTE are completely blocked and no photocyclization of DTE is observed. On the other hand, DTE has no influence on the acidochromic properties of BOX that can be achieved selectively and quantitatively. Moreover, the investigations based on the Z/E isomerization shows that each state having at least one ethylenic junction in cis isomery presents a thermal reversibility with no photoreaction on fully opened BOX (DTE closed or open).

Concerning the electrochromic properties, the authors noticed the strong influence central DTE status on the electrochemical behaviors of both BOX units. When DTE is opened, the oxidation leads to observe a C-C oxidative coupling when no substituent is present on the 5-position of BOX ( $R=H$ ). In contrary, if the 5-position is blocked by a Me group, the simultaneously opening of both oxazolidine rings are observed (scheme 25). When the central DTE is cyclized, the electrochemical stimulation of the system induces the opening of only one BOX unit. To explain it, the authors hypothesize that the oxidation happens on the closed DTE and leads to the selective opening of 1 BOX by an electromediated process (Scheme 25). Unfortunately, subsequent oxidation of the system leads to the opening of the central DTE.



*Scheme 25. Electrochromic transformations of compound **BOX-DAE-BOX**.*

Concerning what we have seen, the selective addressability is still quite challenging when several switching units are present. In this case, each change of state is controlled by different stimulations (photon, electron, acid) in order to achieve the selectivity.

### **VIII). Scope of This Thesis.**

The work presented in this manuscript deals with the design, elaboration and study of multi-level molecular systems. Built by covalent or coordination chemistry association of several BOX subunits, they are expected to allow the modulation of a molecular property over more than two discrete levels. It implies that constitutive switchable subunits can be addressed in global fashion, referenced as the "all-in" mode, but also selectively, referenced as the "step-wise" mode, on demand. From the examples of the literature described previously, we have developed a new family of multi-level molecular systems composed of, at least, two identical indolinooxazolidine units through a  $\pi$ -conjugated system and by synthesizing some ligands possessing indolinooxazolidine in order to perform some complexes by using zinc and ruthenium metals.

## IX). References:

- [1] B. Feringa, N. Koumura, R. Van Delden and M. Ter Wiel, *Applied Physics A* **2002**, 75, 301-308.
- [2] K. Matsuda and M. Irie, *Journal of Photochemistry and Photobiology C: Photochemistry Reviews* **2004**, 5, 169-182.
- [3] C. Yun, J. You, J. Kim, J. Huh and E. Kim, *Journal of Photochemistry and Photobiology C: Photochemistry Reviews* **2009**, 10, 111-129.
- [4] T. J. Huang, A. H. Flood, B. Brough, Y. Liu, P. A. Bonvallet, S. Kang, C.-W. Chu, T.-F. Guo, W. Lu and Y. Yang, *IEEE transactions on automation science and engineering* **2006**, 3, 254-259.
- [5] H.-h. Liu, X. Zhang, Z. Gao and Y. Chen, *The Journal of Physical Chemistry A* **2012**, 116, 9900-9903.
- [6] G. Mehta and S. Sen, *Chemical Communications* **2009**, 5981-5983.
- [7] E. Zahedi, S. Emamian and A. Shiroudi, *结构化学* **2012**, 31, 240-244.
- [8] B. L. Feringa, R. A. van Delden, N. Koumura and E. M. Geertsema, *Chemical Reviews* **2000**, 100, 1789-1816.
- [9] N. Sakai and S. Matile, *Beilstein journal of organic chemistry* **2012**, 8, 897-904.
- [10] A. W. Czarnik, *Fluorescent chemosensors for ion and molecule recognition*, American Chemical Society, **1993**, p.
- [11] D. Canevet, M. Sallé, G. Zhang, D. Zhang and D. Zhu, *Chemical Communications* **2009**, 2245-2269.
- [12] C. Tock, J. Frey and J. P. Sauvage, *Molecular Switches* **2011**, 1, 97-119.
- [13] A. Ault, R. Kopet and A. Serianz, *Journal of Chemical Education* **1971**, 48, 410.
- [14] H. G. Heller and J. LS Miller in *Photochromics for the Future Electronic Materials*, Vol. Plenum, Oxford, **1991**.
- [15] H. Heller and A. Asiri, *PCT, Int. Appl* **1994**.
- [16] A. Schönberg, M. Elkaschef, M. Nosseir and M. M. Sidky, *Journal of the American Chemical Society* **1958**, 80, 6312-6315.
- [17] X. Sun, M. Fan, X. Meng and E. Knobbe, *Journal of Photochemistry and Photobiology A: Chemistry* **1997**, 102, 213-216.
- [18] P. M. Monk, R. J. Mortimer and D. R. Rosseinsky, *Electrochromism: fundamentals and applications*, John Wiley & Sons, **2008**, p.
- [19] F. Castet, B. Champagne, F. Pina and V. Rodriguez, *ChemPhysChem* **2014**, 15, 2221-2224.
- [20] B. L. Feringa, W. F. Jager and B. de Lange, *Tetrahedron* **1993**, 49, 8267-8310.
- [21] Y. Zeng, S. Liao, J. Dai and Z. Fu, *Chemical Communications* **2012**, 48, 11641-11643.
- [22] R. Christie, *Advances in the dyeing and finishing of technical textiles: 1. Chromic materials for technical textile applications*, Elsevier Inc. Chapters, **2013**, p.
- [23] P. Bamfield, *Chromic phenomena: technological applications of colour chemistry*, Royal Society of Chemistry, **2010**, p.
- [24] H. Bouas-Laurent and H. Dürr, *Pure and Applied Chemistry* **2001**, 73, 639-665.
- [25] J. K. Dunnick and J. R. Hailey, *Cancer research* **1996**, 56, 4922-4926.
- [26] S. AnithaáNagamani, D. ShankaráRao and S. KrishnaáPrasad, *Journal of materials chemistry* **2001**, 11, 1818-1822.
- [27] H. Tian and J. Zhang, *Photochromic materials: Preparation, properties and applications*, John Wiley & Sons, **2016**, p.
- [28] O. Fritzsche, *J Prakt Chem* **1867**, 101, 333-343.
- [29] E. ter Meer, *Justus Liebigs Annalen der Chemie* **1876**, 181, 1-22.
- [30] W. Marckwald, *Zeitschrift für Physikalische Chemie* **1899**, 30, 140-145.
- [31] T. Phipson, *News* **1881**, 43, 283.
- [32] R. Bertelson, *Ed. GH Brown, Wiley Interscience, New York* **1971**, 3, 45.
- [33] J. C. Crano and R. J. Guglielmetti, *Organic Photochromic and Thermochromic Compounds: Volume 2: Physicochemical Studies, Biological Applications, and Thermochromism*, Springer Science & Business Media, **1999**, p.
- [34] M. Photochromism in Systems; Dürr, H.; Bouas-Laurent, H., Eds, Vol. Elsevier: Amsterdam, **1990**.

- [35] Y. Yokoyama, *Chemical Reviews* **2000**, *100*, 1717-1740.
- [36] R. B. Woodward and R. Hoffmann, *Journal of the American Chemical Society* **1965**, *87*, 395-397.
- [37] P. Zacharias, M. C. Gather, A. Köhnen, N. Rehmman and K. Meerholz, *Angewandte Chemie International Edition* **2009**, *48*, 4038-4041.
- [38] R. Pardo, M. Zayat and D. Levy, *Chemical Society Reviews* **2011**, *40*, 672-687.
- [39] G. H. Brown, *Techniques of Chemistry* **1971**, 853.
- [40] H. Dürr, *Molecules and Systems*, Elsevier, Amsterdam **1990**.
- [41] H. Dürr and H. Bouas-Laurent, *Photochromism: molecules and systems*, Elsevier, **2003**, p.
- [42] H. A. Wegner, *Angewandte Chemie International Edition* **2012**, *51*, 4787-4788.
- [43] M. Irie, *Chemical Reviews* **2000**, *100*, 1685-1716.
- [44] G. Berkovic, V. Krongauz and V. Weiss, *Chemical reviews* **2000**, *100*, 1741-1754.
- [45] B. Seefeldt, R. Kasper, M. Beining, J. Mattay, J. Arden-Jacob, N. Kemnitzer, K. H. Drexhage, M. Heilemann and M. Sauer, *Photochemical & Photobiological Sciences* **2010**, *9*, 213-220.
- [46] E. Yates and A. Yates, *Notes and Records: the Royal Society Journal of the History of Science* **2015**, *70*, 65-81.
- [47] J. Griffiths, *Chemical Society Reviews* **1972**, *1*, 481-493.
- [48] C. Dugave and L. Demange, *Chemical reviews* **2003**, *103*, 2475-2532.
- [49] D. H. Waldeck, *Chemical Reviews* **1991**, *91*, 415-436.
- [50] G. S. Hartley, *Nature* **1937**, *140*, 281.
- [51] M. Irie and M. Mohri, *The Journal of Organic Chemistry* **1988**, *53*, 803-808.
- [52] M. Ogawa, T. Ishii, N. Miyamoto and K. Kuroda, *Applied Clay Science* **2003**, *22*, 179-185.
- [53] J. Auernheimer, C. Dahmen, U. Hersel, A. Bausch and H. Kessler, *Journal of the American Chemical Society* **2005**, *127*, 16107-16110.
- [54] B. G. Levine and T. J. Martinez, *Annu. Rev. Phys. Chem.* **2007**, *58*, 613-634.
- [55] T. Asano, T. Okada, S. Shinkai, K. Shigematsu, Y. Kusano and O. Manabe, *Journal of the American Chemical Society* **1981**, *103*, 5161-5165.
- [56] H. D. Bandara and S. C. Burdette, *Chemical Society Reviews* **2012**, *41*, 1809-1825.
- [57] Y. Kuriyama and S. Oishi, *Chemistry Letters* **1999**, *28*, 1045-1046.
- [58] D. Bléger, J. Schwarz, A. M. Brouwer and S. Hecht, *Journal of the American Chemical Society* **2012**, *134*, 20597-20600.
- [59] Z. Sekkat in *Photoisomerization effects in organic nonlinear optics: photo-assisted poling and depoling and polarizability switching*, Elsevier, **2002**, pp. 271-287.
- [60] N. Basílio and L. García-Río, *Current opinion in colloid & interface science* **2017**, *32*, 29-38.
- [61] S. Crespi, N. A. Simeth and B. König, *Nature Reviews Chemistry* **2019**, *1*.
- [62] L. Dong, Y. Feng, L. Wang and W. Feng, *Chemical Society Reviews* **2018**, *47*, 7339-7368.
- [63] P. Leippe and J. A. Frank, *Current opinion in structural biology* **2019**, *57*, 23-30.
- [64] N. K. Mishra, J. Park, H. Oh, S. H. Han and I. S. Kim, *Tetrahedron* **2018**.
- [65] T. L. Nguyen, N. Gigant and D. Joseph, *ACS Catalysis* **2018**, *8*, 1546-1579.
- [66] B. Tylkowski, A. Trojanowska, V. Marturano, M. Nowak, L. Marciniak, M. Giamberini, V. Ambroggi and P. Cerruti, *Coordination Chemistry Reviews* **2017**, *351*, 205-217.
- [67] P. Weis, W. Tian and S. Wu, *Chemistry—A European Journal* **2018**, *24*, 6494-6505.
- [68] S. Kobatake, K. Uchida, E. Tsuchida and M. Irie, *Chemical Communications* **2002**, 2804-2805.
- [69] S. Nakamura and M. Irie, *The Journal of Organic Chemistry* **1988**, *53*, 6136-6138.
- [70] S. Kawata and Y. Kawata, *Chemical reviews* **2000**, *100*, 1777-1788.
- [71] A. Goldberg, A. Murakami, K. Kanda, T. Kobayashi, S. Nakamura, K. Uchida, H. Sekiya, T. Fukaminato, T. Kawai and S. Kobatake, *The Journal of Physical Chemistry A* **2003**, *107*, 4982-4988.
- [72] Y. Odo, K. Matsuda and M. Irie, *Chemistry—A European Journal* **2006**, *12*, 4283-4288.
- [73] K. Uchida, N. Izumi, S. Sukata, Y. Kojima, S. Nakamura and M. Irie, *Angewandte Chemie International Edition* **2006**, *45*, 6470-6473.
- [74] N. Soh, K. Yoshida, H. Nakajima, K. Nakano, T. Imato, T. Fukaminato and M. Irie, *Chemical Communications* **2007**, 5206-5208.
- [75] S. Kobatake, S. Takami, H. Muto, T. Ishikawa and M. Irie, *Nature* **2007**, *446*, 778.
- [76] H. Decker and T. v. Fellenberg, *Justus Liebigs Annalen der Chemie* **1909**, *364*, 1-44.
- [77] W. Dilthey, C. Berres, E. Hölterhoff and H. Wübken, *Journal für Praktische Chemie* **1926**, *114*, 179-198.

- [78] A. Löwenbein and W. Katz, *Berichte der deutschen chemischen Gesellschaft (A and B Series)* **1926**, 59, 1377-1383.
- [79] E. Fischer and Y. Hirshberg in *Formation of coloured forms of spirans by low-temperature irradiation*, Vol. ROYAL SOC CHEMISTRY THOMAS GRAHAM HOUSE, SCIENCE PARK, MILTON RD, CAMBRIDGE ..., **1952**, pp. 4522-4524.
- [80] Y. Hirshberg and E. Fischer, *Journal of the Chemical Society (Resumed)* **1954**, 3129-3137.
- [81] F. M. Raymo, S. Giordani, A. J. White and D. J. Williams, *The Journal of organic chemistry* **2003**, 68, 4158-4169.
- [82] R. Klajn, *Chemical Society Reviews* **2014**, 43, 148-184.
- [83] H. Görner, *Physical Chemistry Chemical Physics* **2001**, 3, 416-423.
- [84] B. Lukyanov and M. Lukyanova, *Chemistry of Heterocyclic Compounds* **2005**, 41, 281-311.
- [85] N. Katsonis, M. Lubomska, M. M. Pollard, B. L. Feringa and P. Rudolf, *Progress in Surface Science* **2007**, 82, 407-434.
- [86] L. Florea, D. Diamond and F. Benito-Lopez, *Macromolecular Materials and Engineering* **2012**, 297, 1148-1159.
- [87] J. R. Platt, *The Journal of Chemical Physics* **1961**, 34, 862-863.
- [88] P. Monk, R. Mortimer and D. Rosseinsky, *Electrochromism and electrochromic devices*, Cambridge University Press, **2007**, p.
- [89] W. R. Browne and B. L. Feringa, *CHIMIA International Journal for Chemistry* **2010**, 64, 398-403.
- [90] R. J. Mortimer, *Electrochimica Acta* **1999**, 44, 2971-2981.
- [91] R. Pietschnig, *Chemical Society Reviews* **2016**, 45, 5216-5231.
- [92] P. Blanchard, A. Cravino and E. Levillain, *Handbook of Thiophene-Based Materials* **2009**, 419-453.
- [93] P. Monk, *Wiley: Chichester, UK* **1998**, 8, 926.
- [94] L. Michaelis and E. S. Hill, *The Journal of general physiology* **1933**, 16, 859.
- [95] R. Dinis-Oliveira, J. Duarte, A. Sanchez-Navarro, F. Remiao, M. Bastos and F. Carvalho, *Critical reviews in toxicology* **2008**, 38, 13-71.
- [96] R. J. Mortimer, D. R. Rosseinsky and P. M. Monk, *Electrochromic materials and devices*, John Wiley & Sons, **2015**, p.
- [97] R. J. Mortimer, *Chemical Society Reviews* **1997**, 26, 147-156.
- [98] J. Andréasson and U. Pischel, *Chemical Society Reviews* **2010**, 39, 174-188.
- [99] J. Andréasson and U. Pischel, *Chemical Society Reviews* **2015**, 44, 1053-1069.
- [100] A. Fihey, A. Perrier, W. R. Browne and D. Jacquemin, *Chemical Society Reviews* **2015**, 44, 3719-3759.
- [101] R. H. Mitchell and S. Bandyopadhyay, *Organic letters* **2004**, 6, 1729-1732.
- [102] R. H. Mitchell, T. R. Ward, Y. Wang and P. W. Dibble, *Journal of the American Chemical Society* **1999**, 121, 2601-2602.
- [103] W. Zhao and E. M. Carreira, *Chemistry—A European Journal* **2007**, 13, 2671-2685.
- [104] T. Kaieda, S. Kobatake, H. Miyasaka, M. Murakami, N. Iwai, Y. Nagata, A. Itaya and M. Irie, *Journal of the American Chemical Society* **2002**, 124, 2015-2024.
- [105] K. Matsuda and M. Irie, *Journal of the American Chemical Society* **2001**, 123, 9896-9897.
- [106] A. Peters and N. R. Branda, *Advanced Materials for Optics and Electronics* **2000**, 10, 245-249.
- [107] S. Saita, T. Yamaguchi, T. Kawai and M. Irie, *ChemPhysChem* **2005**, 6, 2300-2306.
- [108] K. Yagi and M. Irie, *Chemistry letters* **2003**, 32, 848-849.
- [109] S. Kobatake and M. Irie, *Tetrahedron* **2003**, 59, 8359-8364.
- [110] S. Kobatake, S. Kuma and M. Irie, *Bulletin of the Chemical Society of Japan* **2004**, 77, 945-951.
- [111] M. Frigoli and G. H. Mehl, *Angewandte Chemie International Edition* **2005**, 44, 5048-5052.
- [112] D. Clarke, B. Heron, C. Gabutt, J. Hepworth, S. Partington, S. Corns and P. WO, *Van Gemert, MB Bergomi, US Pat* **1998**.
- [113] M. Frigoli and G. H. Mehl, *Chemical Communications* **2004**, 2040-2041.
- [114] C. D. Gabbutt, J. D. Hepworth, B. M. Heron, S. M. Partington and D. A. Thomas, *Dyes and pigments* **2001**, 49, 65-74.
- [115] X. Yan, F. Wang, B. Zheng and F. Huang, *Chemical Society Reviews* **2012**, 41, 6042-6065.
- [116] S. Xiao, T. Yi, Y. Zhou, Q. Zhao, F. Li and C. Huang, *Tetrahedron* **2006**, 62, 10072-10078.
- [117] F. M. Raymo and S. Giordani, *Journal of the American Chemical Society* **2001**, 123, 4651-4652.

- [118] F. Liu and K. Morokuma, *Journal of the American Chemical Society* **2013**, *135*, 10693-10702.
- [119] A. Radu, R. Byrne, N. Alhashimy, M. Fusaro, S. Scarmagnani and D. Diamond, *Journal of Photochemistry and Photobiology A: Chemistry* **2009**, *206*, 109-115.
- [120] F. M. Raymo, *Advanced Materials* **2002**, *14*, 401-414.
- [121] M. Campredon, G. Giusti, R. Guglielmetti, A. Samat, G. Gronchi, A. Alberti and M. Benaglia, *Journal of the Chemical Society, Perkin Transactions 2* **1993**, 2089-2094.
- [122] J. F. Zhi, R. Baba, K. Hashimoto and A. Fujishima, *Berichte der Bunsengesellschaft für physikalische Chemie* **1995**, *99*, 32-39.
- [123] M. J. Preigh, M. T. Stauffer, F.-T. Lin and S. G. Weber, *Journal of the Chemical Society, Faraday Transactions* **1996**, *92*, 3991-3996.
- [124] K. Wagner, R. Byrne, M. Zaroni, S. Gambhir, L. Dennany, R. Breukers, M. Higgins, P. Wagner, D. Diamond and G. G. Wallace, *Journal of the American Chemical Society* **2011**, *133*, 5453-5462.
- [125] O. Ivashenko, J. T. van Herpt, P. Rudolf, B. L. Feringa and W. R. Browne, *Chemical Communications* **2013**, *49*, 6737-6739.
- [126] T. Koshido, T. Kawai and K. Yoshino, *The Journal of Physical Chemistry* **1995**, *99*, 6110-6114.
- [127] A. Peters and N. R. Branda, *Journal of the American Chemical Society* **2003**, *125*, 3404-3405.
- [128] W. R. Browne, J. J. de Jong, T. Kudernac, M. Walko, L. N. Lucas, K. Uchida, J. H. van Esch and B. L. Feringa, *Chemistry—A European Journal* **2005**, *11*, 6414-6429.
- [129] W. R. Browne, J. J. de Jong, T. Kudernac, M. Walko, L. N. Lucas, K. Uchida, J. H. van Esch and B. L. Feringa, *Chemistry—A European Journal* **2005**, *11*, 6430-6441.
- [130] G. Guirado, C. Coudret, M. Hliwa and J.-P. Launay, *The Journal of Physical Chemistry B* **2005**, *109*, 17445-17459.
- [131] B. Gorodetsky, H. D. Samachetty, R. L. Donkers, M. S. Workentin and N. R. Branda, *Angewandte Chemie International Edition* **2004**, *43*, 2812-2815.
- [132] R. Bartnik, S. Lesniak, G. Mloston, T. Zielinski and K. Gebicki, *Chem. Stosow* **1990**, *34*, 325-334.
- [133] R. Bartnik, G. Mloston and Z. Cebulska, *Chem. Stosow* **1990**, *34*, 343-352.
- [134] R. Hadji, G. Szalóki, O. Alévêque, E. Levillain and L. Sanguinet, *Journal of Electroanalytical Chemistry* **2015**, *749*, 1-9.
- [135] N. Sertova, J.-M. Nunzi, I. Petkov and T. Deligeorgiev, *Journal of Photochemistry and Photobiology A: Chemistry* **1998**, *112*, 187-190.
- [136] G. SEVEZ in *L'UNIVERSITÉ BORDEAUX, Vol. Université Bordeaux 1*, **2009**.
- [137] M. Hayami and S. Torikoshi in *Color-changing compounds, Vol. DE2541666A1*, **1976**.
- [138] E. Zaitseva, A. Prokhoda, L. Kurkovskaya, R. Shifrina, N. Kardash, D. Drapkina and V. Krongauz, *VI. Preparation of N-methacryloylhydroxyethyl derivatives of indoline spiropyrans. Khim Geterotsik l (10)* **1973**, 1362.
- [139] O. Photochromic and T. Compounds in *Crano, JC, Guglielmetti, RJ, Eds, Vol. Plenum Press: New York*, **1999**.
- [140] L. Sanguinet, J.-L. Pozzo, V. Rodriguez, F. Adamietz, F. Castet, L. Ducasse and B. Champagne, *The Journal of Physical Chemistry B* **2005**, *109*, 11139-11150.
- [141] G. r. Szalóki and L. Sanguinet, *The Journal of organic chemistry* **2015**, *80*, 3949-3956.
- [142] G. Sevez in *Conception, synthèse et étude de nouveaux switches multimodulables, Vol. Bordeaux 1*, **2009**.
- [143] R. Bartnik, S. Lesniak, G. Mloston, T. Zielinski and K. Gebicki, *Chemia Stosowana* **1990**, *34*, 325-334.
- [144] Q. Qi, X. Fang, Y. Liu, P. Zhou, Y. Zhang, B. Yang, W. Tian and S. X.-A. Zhang, *RSC Advances* **2013**, *3*, 16986-16989.
- [145] H.-T. Feng, Y.-X. Yuan, J.-B. Xiong, Y.-S. Zheng and B. Z. Tang, *Chemical Society Reviews* **2018**, *47*, 7452-7476.
- [146] I. Petkov, F. Charra, J. Nunzi and T. Deligeorgiev, *Open Chemistry* **2004**, *2*, 290-301.
- [147] G. r. Szalóki, O. Alévêque, J.-L. Pozzo, R. Hadji, E. Levillain and L. Sanguinet, *The Journal of Physical Chemistry B* **2014**, *119*, 307-315.
- [148] C. Guerrin, G. r. Szalóki, J. r. m. Berthet, L. Sanguinet, M. Orio and S. Delbaere, *The Journal of organic chemistry* **2018**, *83*, 10409-10419.
- [149] S. X.-A. Zhang, L. Sheng and M. Li in *Reusable water writing paper, preparation method thereof, and inkless printing device used for same, Vol. Google Patents*, **2016**.

- [150] G. Sevez, J. Gan, S. Delbaere, G. Vermeersch, L. Sanguinet, E. Levillain and J.-L. Pozzo, *Photochemical & Photobiological Sciences* **2010**, *9*, 131-135.
- [151] G. r. Szalóki, G. Sevez, J. m. Berthet, J.-L. Pozzo and S. p. Delbaere, *Journal of the American Chemical Society* **2014**, *136*, 13510-13513.
- [152] L. Sanguinet, S. Delbaere, J. Berthet, G. Szalóki, D. Jardel and J. L. Pozzo, *Advanced Optical Materials* **2016**, *4*, 1358-1362.
- [153] L. Sanguinet, J. Berthet, G. Szalóki, O. Alévêque, J.-L. Pozzo and S. Delbaere, *Dyes and Pigments* **2017**, *137*, 490-498.



---

## **Chapter 2: BiBOX dimer through a linear aromatic platform**

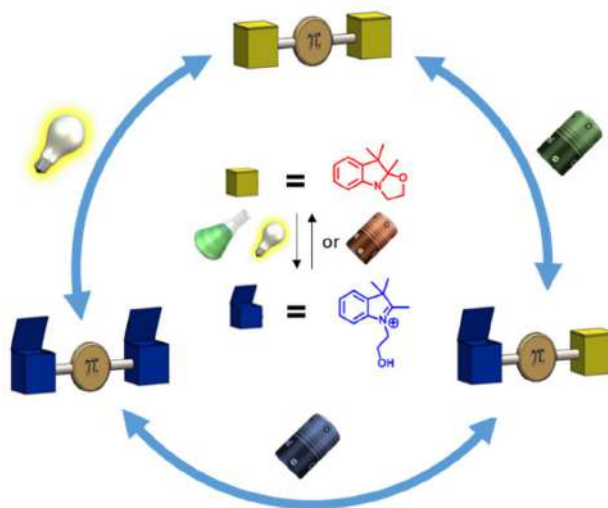
---



## I). Introduction

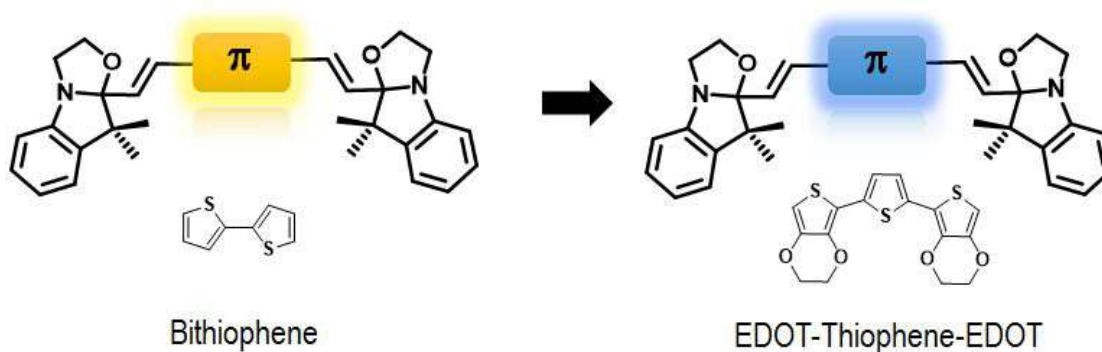
As previously mentioned, the elaboration of multi-level molecular switches still represents a challenging task. If introducing two different switches in the same molecular system seems logical, this approach presents synthetic and control difficulties. In contrary, if using a unique switching unit may allow simplified syntheses, it could lead to some difficulties to address selectively one of them. In order to circumvent issues, the use of multi-modal switching molecules that can be interconverted from one state to another by using indifferently several kinds of stimulation (*i.e.*, light, redox potential, pH) represents a promising approach. As consequence, this chapter describes the syntheses, properties and optimizations of simple models based on a linear conjugated system linking two indolinoxazolidine moieties (BOX). Indeed, such structures connecting two identical BOX units through a pi-conjugated system

- May allow upon direct stimulation of BOX units (by photon or proton) a global commutation,
- As an electro-mediated stimulation may allow a stepwise conversion (Figure 1).



**Figure 1.** Schematic representation of a multichromophoric system based on BOX responding to different stimulations.

As a consequence, we have firstly, due to its well-known redox behavior and easy synthetic access, selected bithiophene as pi-conjugated system to connect two BOX units. First results then prompt us to extend the study to linear conjugated systems exhibiting lower oxidation potential. Thus, the bithiophene unit was replaced by an EDOT-Thiophene-EDOT as spacer (Figure 2).



*Figure 2. Structure of chosen BiBOX dimers.*

After a description of their straightforward synthesis, their commutation abilities were investigated by different suitable measurements such as: UV-Vis absorption spectroscopy, NMR spectroscopy and electrochemistry as reported below.

## II). Association of BiBOX to bithiophene pi-conjugated system

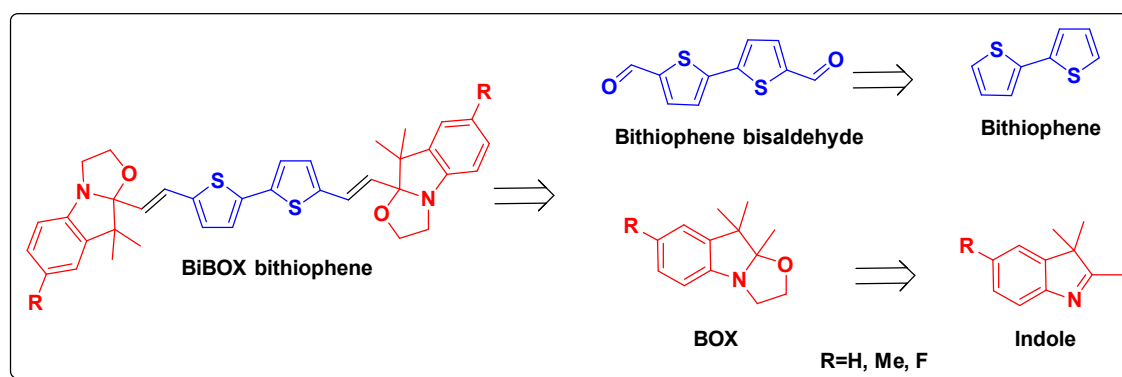
### A. Synthesis and characterization of BiBOX-bithiophene molecular systems under their closed-closed forms.

As shown on scheme 1, three different systems differentiated by the substituent nature in the position 5 (H, Me, F) of the indoline heterocycle were envisioned. These modifications may indeed, in different ways, facilitate the investigations of the commutation properties.

Firstly, the comparison of their electrochemical behavior could lead to determine the localization of the first oxidation process. As explained in chapter 1, when the oxidation is mainly localized on the BOX units, different electrochemical processes are observed as function

of the substituent in position 5. Nude derivative (R=H) is known to undergo dimerization, whereas a methyl group avoids it and promotes the oxazolidine ring opening, while, at the opposite, a fluorine atom stabilizes the corresponding radical cation.<sup>[1]</sup> As consequence, an identical electrochemical behavior whatever the nature of the substituent would represent an indirect manner to demonstrate that the oxidation is occurring on the associated pi-conjugated system and not directly on the BOX. If the UV-visible spectroscopy is certainly the simplest characterization technique to monitor the commutation of various molecular switches under various stimuli, NMR spectroscopy is generally used to structurally characterize the various metastable states. Nevertheless, the partial commutation of a molecular system including several identical switchable units could lead to some difficulties in the peaks assignment and the quantification of the different metastable states. In this context, the presence of a fluorine atom on the indoline heterocycle is an elegant manner to circumvent these difficulties thanks to <sup>19</sup>F NMR spectroscopy (*vide infra*).

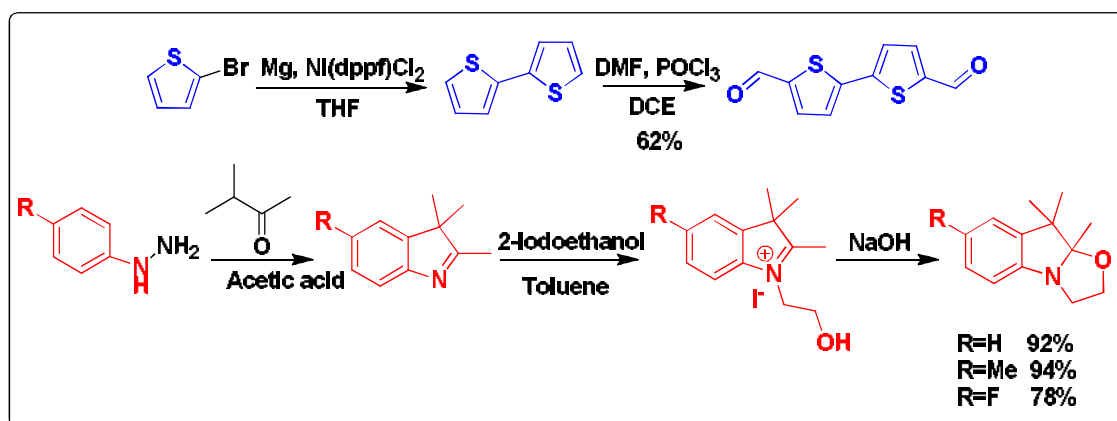
To prepare the targeted molecules, a convergent synthesis strategy, relying on condensation between an aromatic aldehyde and the corresponding trimethylindolino-oxazolidine derivative as final step (Scheme 1), was adopted.



*Scheme 1. Retrosynthesis of the designed BiBOX bithiophene system.*

More important, the preparations of target derivatives appear straightforward and do not require a lot of synthetic efforts. Indeed, the syntheses of both precursors were already reported in the literature (scheme 2). Thus, the three BOX precursors are prepared in two steps from

corresponding substituted phenylhydrazines (R=H, Me, F). After indole preparation by Fisher synthesis, a quaternization step using 2-iodoethanol<sup>[2, 3]</sup> leads to opened BOX which are closed in basic conditions. According to reported procedure,<sup>[4]</sup> the preparation of 2,2'-bithiophene-5,5'-dicarboxaldehyde is also conducted in two steps from 2-bromothiophene. After a 2,2'-bithiophene synthesis by Kumada coupling, a Vilsmeier-Haack reaction leads to the target in an overall 62% yield.

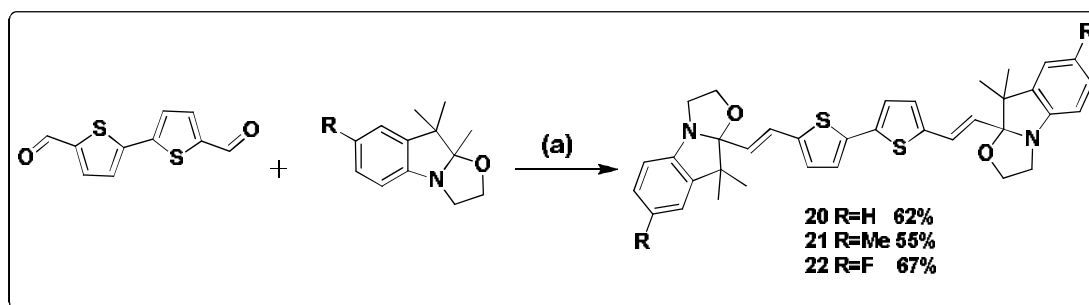


Scheme 2. Synthetic route to 2,2'-bithiophene-5,5'-dicarboxaldehyde and BOX derivatives.

Generally the functionalization of pi-conjugated core by several switchable units requires a lot of synthetic efforts and drastic experimental conditions such as classical palladiated cross coupling used for the elaboration of numerous DTE multimer.<sup>[5, 6]</sup> In this context, the trimethylindolino-oxazolidine unit presents certainly an incommensurable advantage as its grafting to aromatic aldehydes can be resumed to a simple condensation. The latter, well documented in the literature is, most of the time, carried out in boiling ethanol what can require extended reaction time sometimes as long as several days.

Recently, our group at MOLTECH-Anjou has reported an original synthesis methodology in solvent-free conditions with the help of commercial silica as support.<sup>[3]</sup> Allowing to reduce drastically the reaction time from several days to few minutes, these new experimental conditions can also assure good selectivity when several aldehyde functions are

present on the aromatic partner. By applying this methodology, our three targeted molecular systems (**20**, **21** and **22**) were quickly obtained in satisfactory yields ranging from 55 to 67% as shown in scheme 3.



*Scheme 3. Synthetic route to compounds 20, 21 and 22, (a) silica gel, 100°C, 10 minutes.*

If an influence of the nature of the substituent in position 5 of the BOX can be suspected in order to explain this variation of yield, the proton NMR characterization of the crude materials reveals in all three cases a complete consumption and conversion of the bisaldehyde starting material. As consequence, the difference of isolated yield between compounds **20**, **21** and **22** is certainly due to some issues in the purification steps especially for **21** which presents the lowest solubility (*vide supra*).

In order to confirm the isomery of both ethylenic junctions between the BOX and the bithiophene, the structure of all the compounds was confirmed by NMR spectroscopy (proton and carbon). The  $^1\text{H}$  NMR spectra of compounds **20**, **21** and **22** are shown in Figure 3.

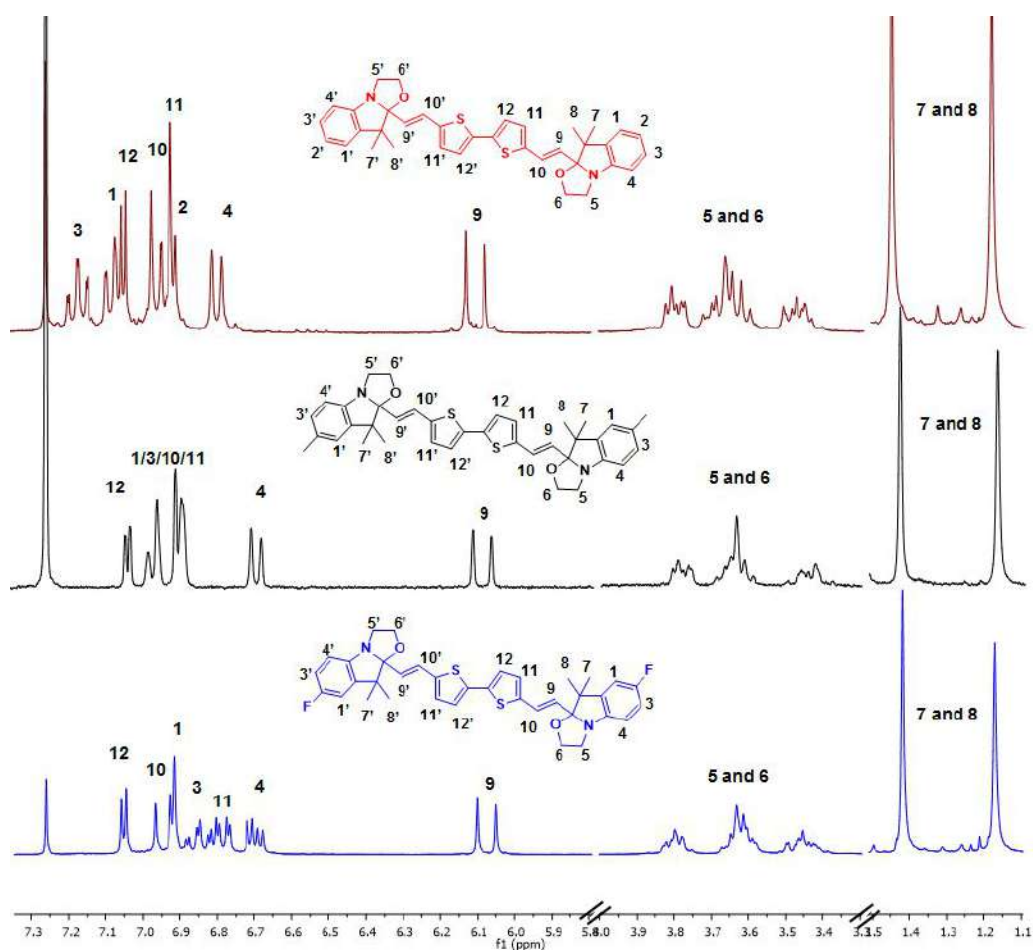


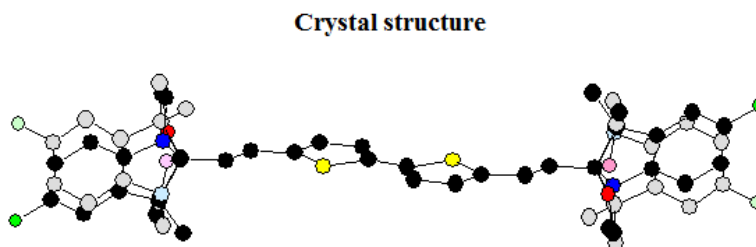
Figure 3.  $^1\text{H}$  NMR spectra of compounds **20**, **21**, **22** (from top to bottom) in chloroform ( $\text{CDCl}_3$ ) at rt.

The simplicity and symmetry of molecules allow a facile assignment of spectra (figure 3). For example, the doublets distinguishable at 6.11, 6.10 and 6.08 ppm for compounds **20**, **21** and **22** respectively all exhibit vicinal coupling of 16 Hz characterizing a C=C linkage (9 and 9') in trans-trans isomery of all the three derivatives under their closed form. Interestingly, no trace of corresponding cis-isomers were detected by NMR analysis.

Both aromatic, thienyl and phenyl protons appear at different chemical shifts in  $^1\text{H}$  NMR spectra, and so are readily distinguishable in the spectrum especially by paying attention of their vicinal coupling constant smaller for the bithiophene unit (3.8 Hz) than for the indoline heterocycle (7.7 Hz). The general characteristics of closed BOX unit are also well observed on the spectra such as the two singlets at 1.17 and 1.4 ppm assigned to both germinal methyl groups

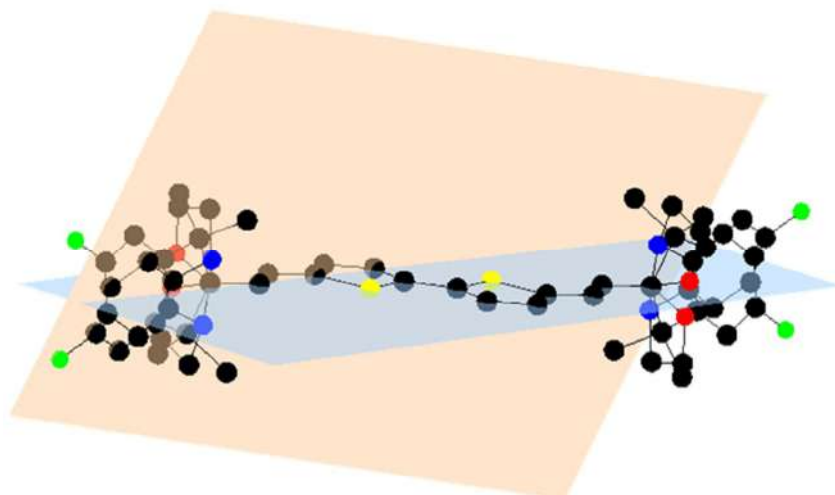
on the indoline part (referenced as 7 and 8) and series of multiplets centered at 3.6ppm (5 and 6) corresponding to the methylene groups adjacent to the nitrogen and oxygen atoms due to some geometrical constraint.

Under their closed form, each of these three molecular systems exhibit two asymmetric carbons which raise the question of the presence of only one diastereoisomer or a mixture of them. Knowing that the existence of a rapid equilibrium between close and open forms can be still considered at the NMR time scale,<sup>[7]</sup> leading to ponderated signals. In this context, crystal X-ray diffraction measurements appear as the most suitable technique to rise this assumption. Despite many attempts and efforts, only compound **22** (R=F) allowed formation of single crystals good enough for X-Ray diffraction (from a concentrated dimethylsulfoxide solution). Its crystal structure is represented in figure 4.



*Figure 4. Crystallographic structure of compound 22.*

Compound **22** crystallizes in the orthorhombic space group *Pbam* and the recorded data clearly corroborate the proposed structure in particular the *trans* conformational ethylenic junction between BOX and bithiophene units. In addition, it is important to note that the vinyl-bithiophene central core appears planar with the two thiophene rings in *anti*-conformation. Noteworthy, the presence of the two asymmetric carbons ( $sp^3$ -hybridized, R or S) in both sides of the molecule is characterized by the disorder observed on the indolinoxazolidine units.



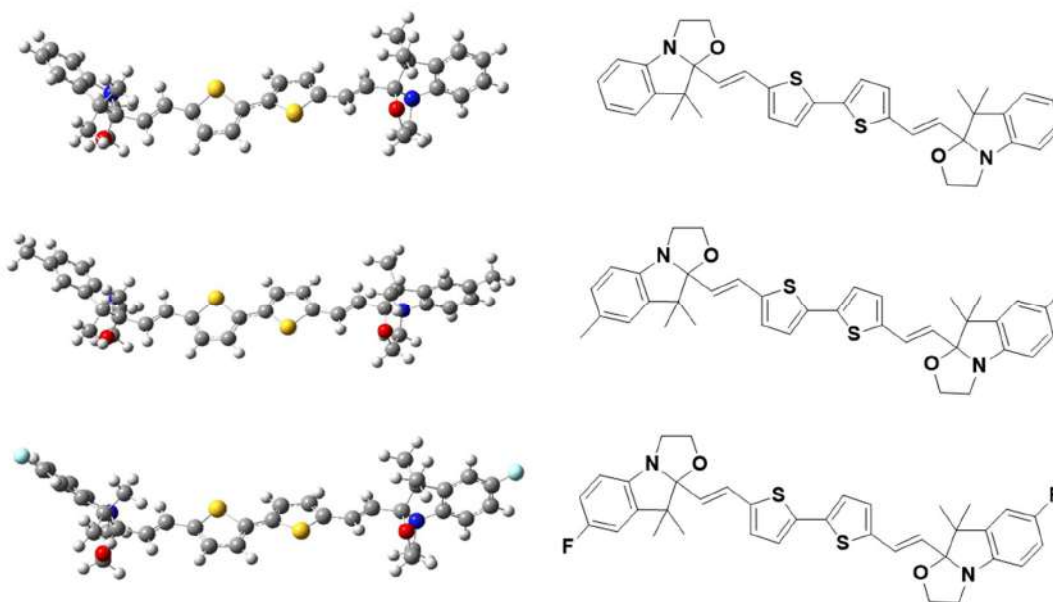
*Figure 5. The two main planes of crystallographic structure of compound 22.*

Finally, it is worth to note that the two main parts (indolinooxazolidine and bithiophene) of the molecule are located in two planes presenting an angle of  $75.2^\circ$  between them (figure 5), and can be then considered as non-conjugated. For better illustration, crystallographic data are listed in the crystallographic part.

In order to rationalize experimental observations made so far on the system, a full theoretical study, based on Density Functional Theory (DFT) and its time dependent extension (TD-DFT), has been performed. Acetonitrile was employed as solvent in the calculation. As energetic considerations are discussed later, it can here be pointed out that geometric optimizations of all compounds (**20**, **21** and **22**) (figure 6) appear in accordance with X-ray observations for compound 22:

- vinyl-bithiophene central core appears almost planar
- bithiophene moiety is in an anti-conformation
- indolinooxazolidine and bithiophene motifs are in two different plans and not conjugated (*vide supra*).

The symmetry and analogy of geometries demonstrate the lack of influence of the terminal substituent on the molecular geometry in accordance with  $^1\text{H}$  NMR results.



*Figure 6. Optimized structures of compounds 20, 21 and 22.*

### B. Commutation and abilities.

As mentioned above, indolino-oxazolidine moieties are a family of molecular switches known to display acido-, photo- and more recently electrochromic properties. In fact, the opening/closure of the oxazolidine ring can be carried out by applying indifferently different external stimulations. By connecting two BOX units through a central bithiophene bridge, the elaborated multi-responsive molecular system are expected to progressively generate up to 3 different states under stimulation referenced later in the text as **Closed-Closed (CC)**, **Open-Close (OC)**, and **Open-Open (OO)**, depending on closed (C) or open (O) status of each BOX unit. As other molecular systems incorporating two identical switchable units, two commutation modes can be envisioned: an "all-in" and a "step-wise" commutation depending on the ability to selectively address one of both BOX units (Figure 7).

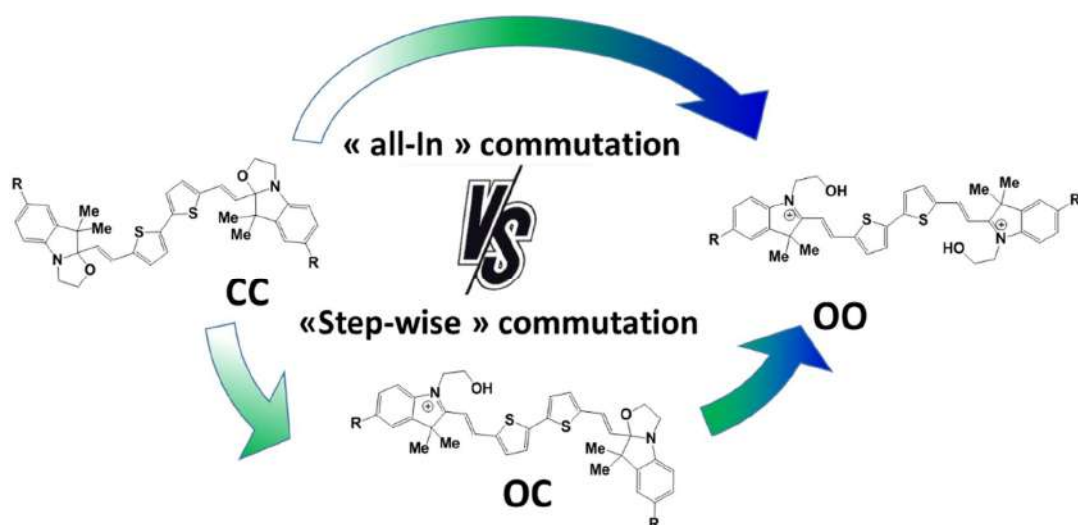
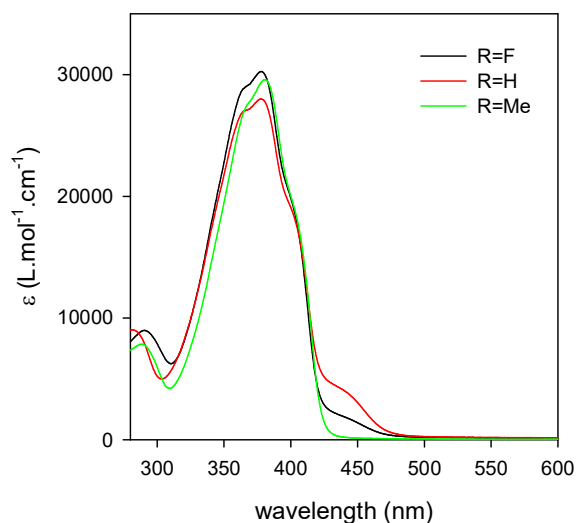


Figure 7. Schematic representation of the “all-in” and the “step-wise” commutation modes.

As the stimulation of the BOX involves very different processes depending on the nature of the external stimulation (photon, electron, proton), the preferential commutation mode should be strongly influenced by this later. As consequence, the commutation of the three different synthesized molecular systems, under acidic, photochemical and electrochemical stimulation, were investigated in details.

### B.1. Acidochromic properties.

Under their closed forms, all compounds present almost identical UV-visible spectra with a maximum absorption wavelength of 378-379 nm showing only a slight effect of the substituent on the epsilon value (figure 8).



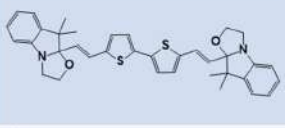
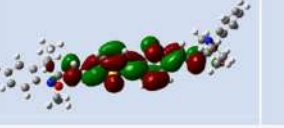
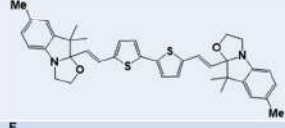
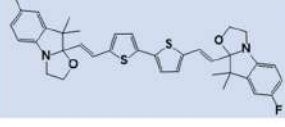
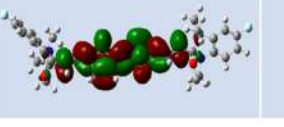
**Figure 8.** UV-Visible spectra of compound **20**, **21** and **22** under their CC form in ACN solution.

Associated to the slight peak structuration, this maximal absorption band is assigned to the central bithiophene moiety in agreement with the reported optical properties of various 5,5'-disubstitued-2,2-bithiophene derivatives.<sup>[8]</sup> Moreover, the  $sp^3$  hybridization of the carbons linking the BOX unit to the central vinyl-bithiophene node breaks the conjugation and leads to a central and two lateral independent pi-conjugated systems what explains the poor effect of the substituents on the absorption maxima wavelength of the three different systems under their CC (Closed-Closed) form.

Following the analysis of the structural results for the three compounds (**20**, **21** and **22**) and in order to support this assumption, DFT and TD-DFT theoretical calculations (B3LYP-6.311(d)) were performed on the three compounds (table 1) using IEFPCM (acetonitrile) model to consider solvation effect.

Under their closed forms, the independence of indolinoxazolidine and bithiophene motifs is well confirmed as demonstrated by the exclusive location of the HOMO and LUMO are on the central bithiophene core. Additionally, the lack of influence of the substituent on indoline position 5 is also well correlated by observation of the almost same values of HOMO-

LUMO gap for the three compounds **20**, **21** and **22** at 3.37, 3.33 and 3.33 eV respectively. Furthermore, the calculated UV-visible absorption spectra for all compounds confirm the assignment of main absorption band to a  $\pi$ - $\pi^*$  transition centered on the central bithiophene core as an HOMO-LUMO transition (table 1). The calculated wavelengths are found to be 36 to 40 nm above the experimental values, which can be explained by the choice of the basis set (B3LYP-6.311(d)). However, the general trends in terms of variation of absorption wavelength and extinction coefficient induced by the variation of the nature of the substituent in indoline position 5 are pretty well corroborated.

Compound	HOMO	LUMO	$\lambda_{\text{theo}}$ ( $\lambda_{\text{exp}}$ )	Oscillator strength
			414 (378)	1.5349
			419 (379)	1.5561
			418 (378)	1.5426

*Table 1. DFT (B3LYP-6.311 G(d)) visualization of compounds **20**, **21** and **22** molecular orbitals, displaying the HOMO and LUMO of the three different states, calculated  $\lambda$  and oscillator strength.*

To conclude, these computational results confirm the localization on the central pi-conjugated system of the HOMO, LUMO levels and lower energy transition what explain the similarity of their experimental absorption spectra.

The acido-chromic properties of compounds were studied by UV-vis spectroscopy upon HCl aliquots addition. Interestingly, despite the different nature of substituents (R=H, Me, F), the behaviors of compounds **20-22** appear analogous.

In all cases, the addition of HCl to compound solution under its CC form induces a deep pink coloration due to the appearance of an intense broad band in the visible 450-600 nm range

with a concomitant decrease of their characteristic UV absorption band around 378 nm as presented below for compound **20** (figure 9).

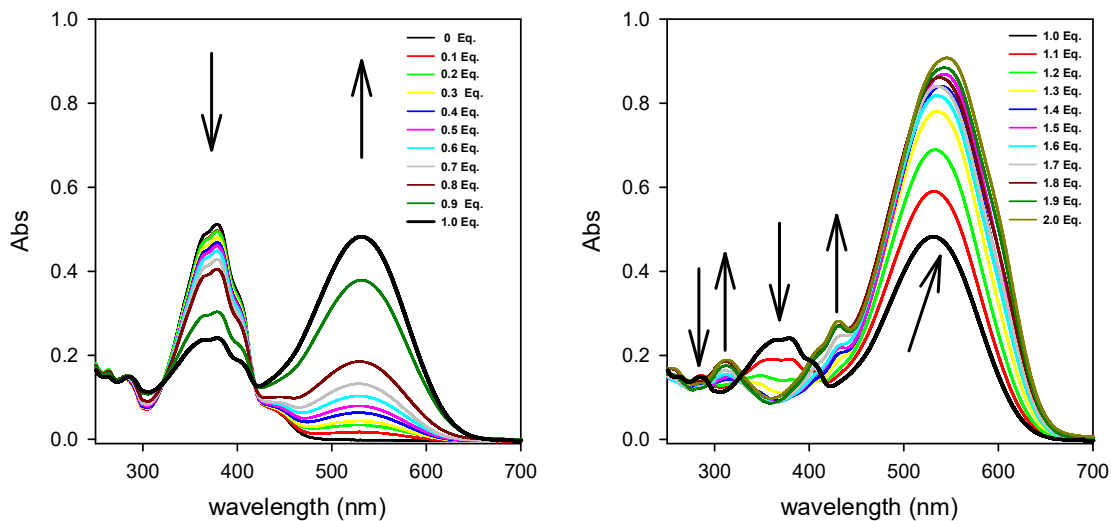
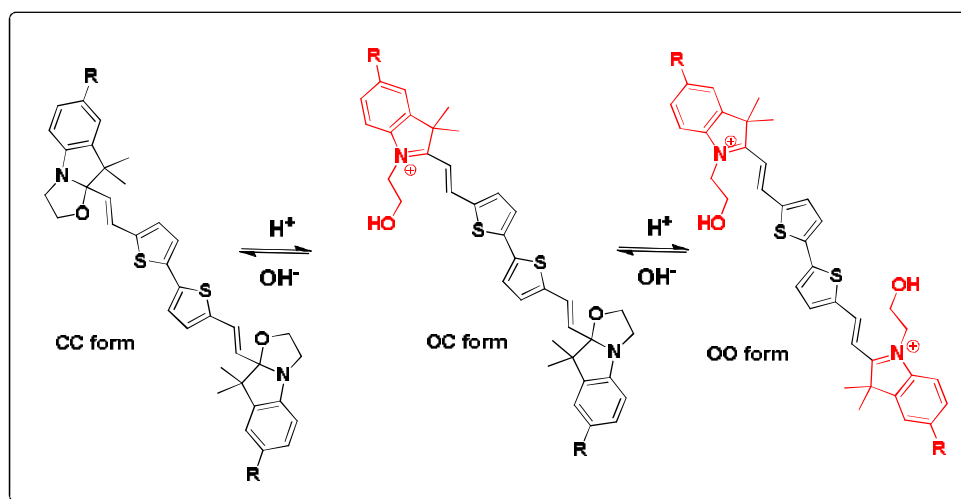


Figure 9. UV-Visible spectrum changes of a solution of **BOX-H (20)** in ACN (0.021mM) upon addition of HCl aliquots.

Based on previous studies on BOX derivatives,<sup>[9]</sup> such behavior can be easily explained by the commutation of BOX units. Indeed, such pH changes lead at the end to the opening of both oxazolidine rings. This opening results in the generation of an indoleninium terminal motif which acts as strong withdrawing group and allow extension of the pi-conjugation on the whole molecule what explains the strong bathochromic shift of the absorption wavelength experimentally observed.

If the presence of two switching units lets presume the possibility to progressively generate 3 different states under acidic stimulation, as previously mentioned, a such stepwise commutation was, up to now, to our knowledge, not reported. In fact, only one system incorporating several BOX units was described. Constituted by two identical BOX separated by a DAE moiety, this complex molecular system did not allow addressing selectively each BOX unit under acidic stimulation whatever the open/closed status of the DAE.<sup>[10]</sup>

In contrary, in the case of compounds **20**, **21** and **22**, the observation of an irregular evolution of the UV-Visible spectra along the titration with acid aliquots could translate a stepwise opening of the BOX units. Such as presented in Figure 9 for compound **20** as example, up to one equivalent, the UV spectra reveal the appearance of a unique band centered at 529 nm as well as a strong decrease of the band intensity at 378 nm. More important, below one equivalent the presence of two isosbestic points at 321 and 417 nm indicates that only two species are in equilibrium, then deduced to be **CC** and **OC**. To induce the ring-opening in the second BOX unit, the added quantity of HCl is pushed further than one equivalent. It leads to an enhancement of the solution coloration with the complete disappearance of the band at 378 nm. In addition, a bathochromic shift of the main absorption band from 529 nm to 546 nm is observed with the concomitant appearance of two small higher energy absorption bands at 311 and 431 nm respectively. More important, this increment of the acid quantity did not allow maintaining the observation of the previous isosbestic points at 321 and 417 nm which are replaced by a unique one at 326 nm possibly associated to equilibrium between **OC** and **OO** forms. As consequence, this experiment suggests the commutation of the connected BOX units in a stepwise manner (scheme 4).



*Scheme 4. Representation of the stepwise commutation of the elaborated molecular systems between the 3 different states (CC, OC and OO) under acidic stimulation.*

As previously mentioned, calculations indicate that the HOMO and LUMO levels of the CC form are mainly localized on the central core of the system and that the main band corresponds to a  $\pi$ - $\pi^*$  transition between these levels. Upon opening one BOX, the compound loses its symmetry and the resulting OC state presents a LUMO level delocalized on the generated electron-withdrawing indoleninium motif and the bithiophene system (as shown for **20** on table 2 as example). In contrary, the OC HOMO level appears localized on the conjugated central skeleton as well as on the opposite closed BOX.

Considering the Open-Open form (OO), the two carbons joining the two indoline and vinyl-bithiophene display now a  $sp^2$  hybridization, leading to a flat fully conjugated structure. Thus, the HOMO orbitals appear delocalized on the whole molecule while the LUMO orbitals present dominant localization on the central core including the vinylic bridge as well as a characteristic quinodimethanic structure.

Compound	HOMO	LUMO

Table 2. Frontier orbitals of each form of compound **20**.

Data presented in Table 3 show that TD-DFT calculations reproduce well the experimental main absorption bands variation of the three different forms (CC, OC and OO) for the three compounds. Thus, a first large bathochromic shift is observed when passing from

CC to OC systems as a less important one characterizes the passage from the OC to the OO form.

Compound Form	Experimental			Theoretical		
	$\lambda_{CC}$	$\lambda_{OC}$	$\lambda_{OO}$	$\lambda_{CC}(f)$	$\lambda_{OC}(f)$	$\lambda_{OO}(f)$
<b>20</b>	378	529	546	414 (1.54)	582 (1.48)	627 (2.52)
					551 (0.35)	432 (0.05)
					412 (0.13)	
<b>21</b>	379	533	561	419 (1.56)	600 (0.58)	640 (2.58)
					570 (1.33)	447 (0.04)
					422 (0.08)	
<b>22</b>	378	538	552	418 (1.54)	584 (1.46)	632 (2.53)
					554 (0.39)	436 (0.05)
					414 (0.11)	

*Table 3. Comparison between experimental (in acetonitrile) and calculated results for the prediction of the main absorption band for each form of the compounds (20, 21 and 22).*

The differences of absorption wavelength are extremely thin between the CC forms of **20**, **21** and **22**. Thus, the agreement of experimental and theoretical measurements is not so significant. Moreover, the relative impacts of these terminations on the spectroscopic behavior of OC and CC form are not so clear.

If the UV-Visible spectroscopy represents certainly the most convenient technique to monitor the commutation of elaborated systems under stimulation, it doesn't allow the clear structural identification of the different forms. For this reason, a monitoring of the commutation by NMR spectroscopy offers an unambiguous identification of the various structural organizations formed upon the stimulation of a molecular system but also allow their quantification. As consequence, it is a technique of choice to confirm the stepwise commutation of our systems under acidic stimulation.

For this reason, the evolution, presented below (figure 10), of the proton NMR spectrum of a solution of compound **22** under its CC form was recorded upon the addition of aliquots of hydrochloric acid.

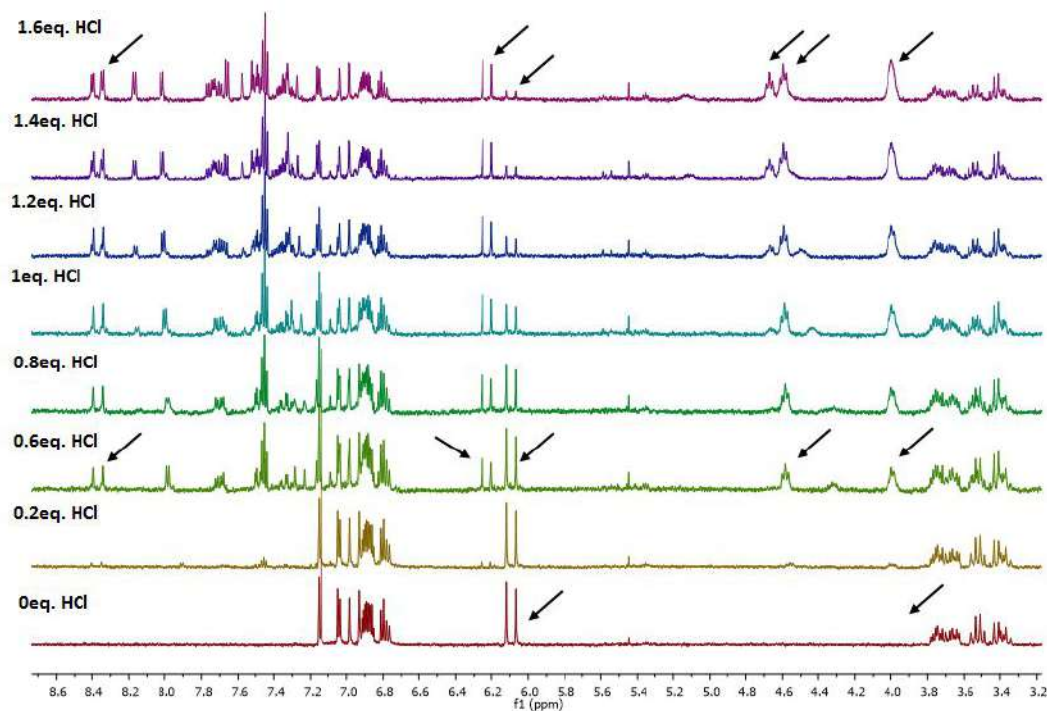


Figure 10.  $^1\text{H}$  NMR spectra upon titration of compound **22** (2.27 mM) by HCl in  $\text{ACN-d}^3$  at  $20^\circ\text{C}$ .

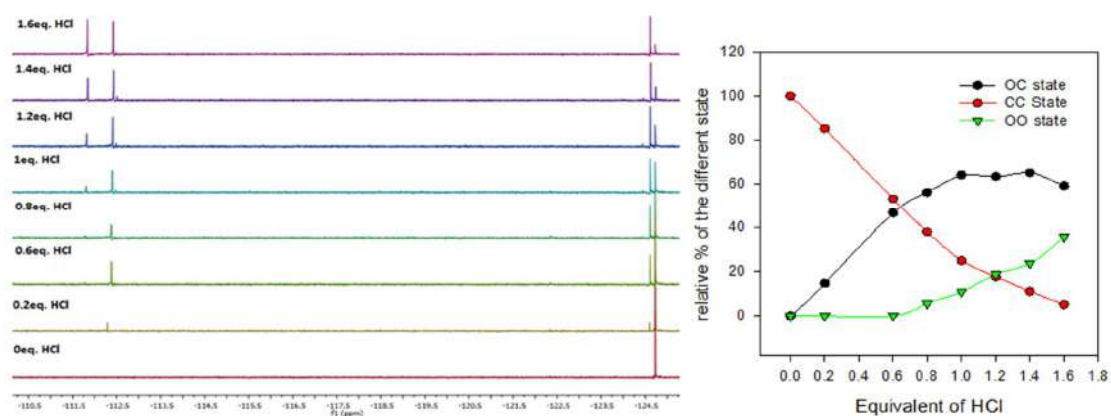
As mentioned above, the doublet assigned to one of the two ethylenic protons (9 and 9') is easily distinguishable at 6.08 ppm and represents a probe of choice to track the presence of the compound under its CC form. Adding acid (HCl) induces, as expected, a decrease of intensity of this doublet, with the concomitant appearance of new NMR signals especially two triplets around 4.6 and 4 ppm. Characteristic of the indoleninium moieties ( $\text{N-CH}_2\text{-CH}_2\text{-OH}$ ), they are confirming undoubtedly the opening of the oxazolidine ring under pH changes.

More important, one can easily notice that the variation of the NMR spectrum is not linear upon the addition of acid. Below one equivalent, the generation of both triplets is accompanied by the appearance of at least two doublets at higher chemical shifts (6.3 and 8.4 ppm respectively) exhibiting a vicinal coupling constant of 15.9 Hz. Characteristic of ethylenic proton in trans isomery, they can be explained by a loss of the symmetry due to the commutation of one of the two BOX units. When the addition of acid is pursued, these both doublets are replaced by a new doublet exhibiting similar vicinal coupling constant slightly more deshielded

(8.42ppm) and new signals characteristic of an indoleninium formation are observed around 4.65ppm. This behavior can be explained by the opening of the second BOX, and then the regeneration of the molecular symmetry of the whole system. The observation of the **OO** state formation only after the generation of the **OC** isomer confirms the stepwise commutation of the system under acidic stimulation.

In addition, it is good to note that the isomery of the ethylenic junctions is never affected by the acidic stimulation as assigned doublets exhibit similar vicinal coupling constant (16Hz) whatever the state of the system (**CC**, **OC** and **OO**).

While the identification of each metastable states (**CC**, **OC** and **OO** forms) was obtained by  $^1\text{H}$  NMR (see Figure 10), the introduction of the fluorine atom in position 5 (compound **22**) facilitates their quantification. Indeed, the signals assigned to ethylenic proton 10, useful for the quantification of the **OO** state, are overlapped with one of the **OC** form avoiding its specific integration. At the opposite, the evolution of  $^{19}\text{F}$  NMR spectrum of a solution of compound **22** under its **CC** form upon the addition of HCl aliquots is clearer than proton ones as shown below.



**Figure 11.**  $^{19}\text{F}$  NMR spectra upon titration of compound **22** (2.27 mM) by HCl in  $\text{ACN-d}_3$  at  $20^\circ\text{C}$  (left), percentage of each state according to number of equivalents of HCl added (right).

As expected, the  $^{19}\text{F}$  NMR spectrum of the compound **22** under its initial state (**CC**) exhibits only one signal at -124.73 ppm in agreement with the existence of an element of

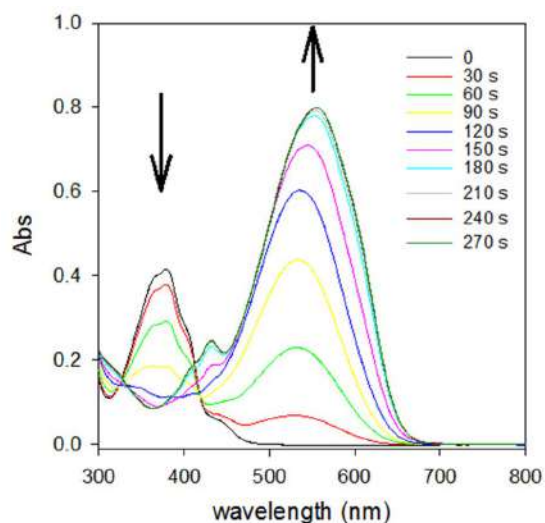
symmetry between both BOX units. As soon the addition of HCl aliquots starts, the appearance of two new peaks is observed at -124.60 and -112.29 ppm (Figure 11) what demonstrates the appearance of the **OC** form. Indeed, the breaking of the molecular symmetry due to the commutation of only one BOX unit leads to two peaks exhibiting a similar integration low-field shifted in comparison with the **CC** form. This assignment was confirmed by the clear appearance of only one new signal at -111.84 ppm when the amount of HCl was increased beyond 0.8 equivalent in agreement with the re-establishment of a molecular symmetry with the opening of the second BOX unit. If the lack of solubility of the **OO** form in acetonitrile leads to its precipitation when the addition of acid reaches 1.8 equivalent and avoid any quantification beyond this point, below, the integration of the different peaks can be used to determine the relative proportion of the three different states of the molecule as function of the added amount of acid (Figure 11).

As seen on Figure 11, the distribution between the three different states is not statistically driven and the stepwise opening of both BOX units is, once again, clearly confirmed. This behavior seems a difference of pKa between both species what allow stepwise protonation processes. Considering each BOX unit being independent under their closed form due to the  $sp^3$  hybridization of the carbon 2, such difference could be explained by a variation of the donor ability of the associated bithiophene which is involved in the stabilization of the corresponding open form. In fact, the first opening of an oxazolidine ring induces the generation of the corresponding indoleninium group which acts as a strong electron withdrawing group and decreases the donor character of the bithiophene moiety. As consequence, the bithiophene moiety is not able to stabilize the dicationic specie by internal charge transfer as efficiently as the monocationic one. It conducts to observe a more difficult second opening. In addition, it can be noticed that the presence of **CC** form is still detected after 1.6 equivalent of acid leading to an unsuitable coexistence of the three different forms over a large period of stimulation

incompatible with a sharp modulation of molecular properties over three discrete levels. Knowing the multi-modal commutation properties of the BOX, the other kind of stimuli were explored. Indeed, depending on the stimulus, the addressability selectivity between both connected BOX units could differ.<sup>[11, 12, 13, 14]</sup>

### B.2. Photochromic properties.

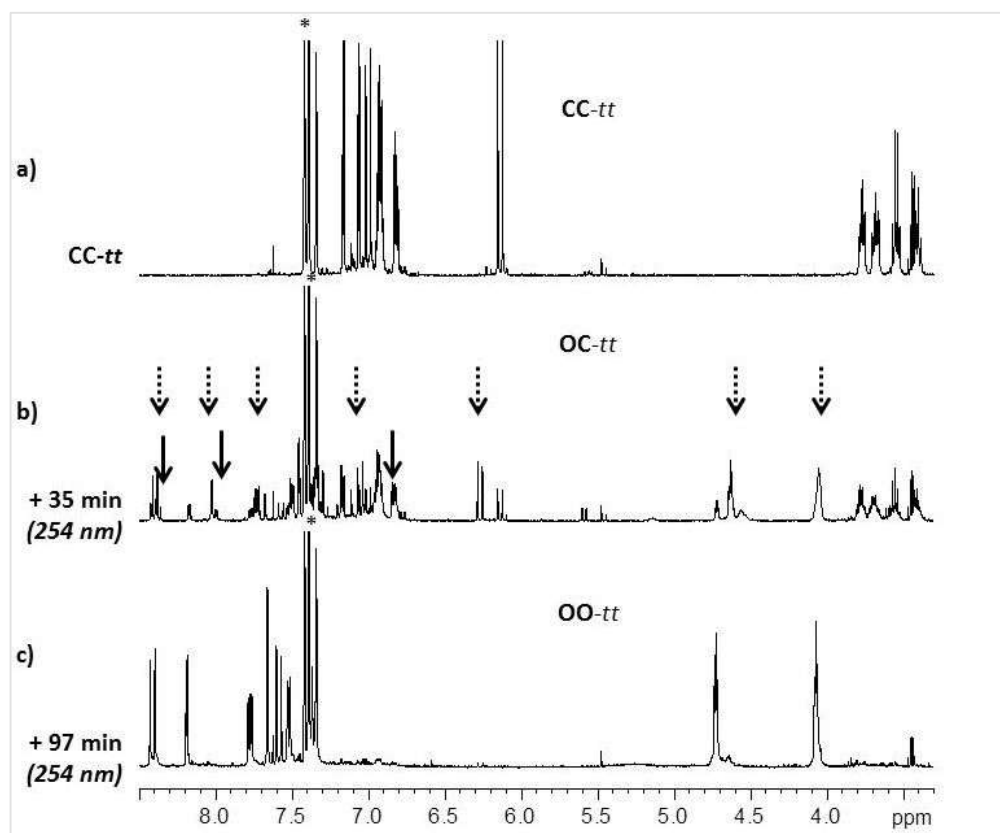
Among the different stimuli able to induce the BOX oxazolidine ring opening reported so far, light irradiation stays one of the most used due to its promising potential applications.<sup>[14]</sup> Based on our previous works on simple dyad bithiophene-BOX,<sup>[15]</sup> the compounds **20**, **21** and **22** dissolved in acetonitrile have been irradiated with 254 nm light in presence of chlorobenzene (10%) as photosensitizer. As expected, the UV irradiation leads quickly to the strong coloration of the solution reaching a photostationary state after 4 min. The evolution of the UV-Visible absorption spectra as function of the irradiation time lets clearly appear two stages such as example for compound **20** presented on Figure 12.



*Figure 12. UV-Visible spectrum changes of a solution of **20** in ACN:PhCl (90/10; 0.016mM) upon UV light irradiation (254 nm).*

Below 2 min of irradiation duration, the appearance of an absorption band centered at 529 nm is concomitant with the reduction of the absorption at 378 nm. The presence of two

isosbestic points at 321 and 417 nm are also observed. Upon longer irradiation time, the visible absorption band continues to increase but is also bathochromically shifted and associated with the generation of two weak bands at higher energy. By comparison with acidochromic properties (*vide supra*), we can here also suggest a stepwise commutation of the system under light stimulation, the second BOX unit opening requiring a longer irradiation time. More important, the overlapping of the UV-visible spectra obtained by either irradiation or acidic titration is noticed, and the addition of base to irradiated solution allows quantitatively the restoration of the initial state of the system. Both observations suggest then some multi-modal switching abilities of these molecular systems. In order to confirm the stepwise commutation and exclude other photochemical process than BOX opening such as the *cis/trans* isomerization of one ethylenic junction,<sup>[7]</sup> or a photooxidation process,<sup>[16]</sup> <sup>1</sup>H NMR has been used. In collaboration with Pr S. Delbaere and Dr J. Berthet (LASIR, Lille university), the photoconversion of the compound **22** was monitored by <sup>1</sup>H NMR in the same conditions of solvent (ACN-d<sup>3</sup> + 10% of chlorobenzene-d<sup>5</sup>) and irradiation (254 nm) (Figure 13).



**Figure 13.**  $^1\text{H}$  NMR spectra and assignment of compound **22** under its three states in acetonitrile- $d_3$  + chlorobenzene- $d_5$  after 254nm-light irradiation at rt.

Upon successive periods of irradiation at 254 nm, the decrease of signals assigned to the initial **CC** state such as the doublet at 6.08 ppm assigned to one ethylenic proton is clearly observed. This disappearance comes with the concomitant gradual appearance of new resonances. Thanks to the results obtained under acidic stimulation, these new signals reveal the predominant formation of **OC** and **OO** forms depending on the irradiation time. For short irradiation time, the generation of two well-resolved triplets at 4.0 and 4.6 ppm as well as the appearance of four doublets at 6.2, 7.1 ppm, 7.6 and 8.4 ppm indicate clearly the almost exclusive formation of the **OC** state. When irradiation time is increased, these signals disappear and finally, a simple spectrum is observed with more particularly, two triplets at 4.1 and 4.7 ppm and two doublets at 7.55 and 8.45 ppm previously assigned to the **OO** state of the molecular system, thus proving the opening of the second BOX entity.

Consequently, this experiment allows us to assume that UV light irradiation of our system leads also to the stepwise commutation of our system but with a relatively low efficiency and selectivity. Indeed, after 10 minutes of illumination, only 20% of **OC** is detected. Increasing the illumination time up to 40 minutes allows to produce 50% of **OC** but with also 10% of **OO**. Finally, the total conversion of **CC** and subsequently **OC** into **OO** is obtained after 97 minutes of irradiation.

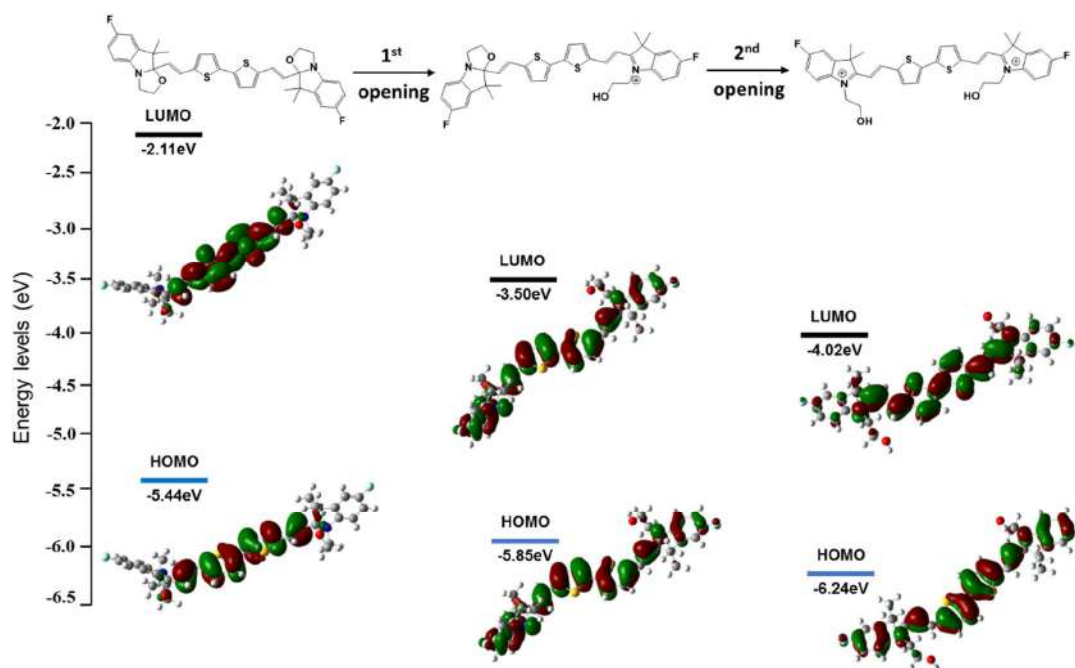
As observed with acidic stimulation, the photostimulation leads also to an unsuitable coexistence of the three different forms over a large period of stimulation incompatible with a sharp modulation of molecular properties over three discrete levels. BOX derivatives presenting also interesting electrochromic properties, their electrochemical behavior has been also studied.

### B.3. Electrochromic properties.

As early mentioned, the oxazolidine ring opening can be also electro-induced and can result from two different processes depending (*i*) on the substitution pattern of the BOX and (*ii*) on the nature of the pi-conjugated system associated in position 2 (see chapter 1). Indeed, both systems acting independently under the closed form, the first oxidation of the system could then occur either on the BOX moiety (direct electrostimulation) or on the associated aromatic system (mediated electrostimulation) depending on the relative position of their oxidation potentials.

Theoretical calculations performed on our three molecular systems under their **CC** and **OC** forms (*vide infra*) suggest that the electromediated ring opening process should be promoted. Indeed, for all three compounds, the HOMO is centered on the bithiophene moiety which should logically undergo the first oxidation.<sup>[15]</sup> Based on previous studies on similar BOX-bithiophene dyad, the generation of the corresponding radical during this first oxidation is expected to lead to only one oxazolidine ring opening and to the selective formation of the **OC** state. This commutation conducting to functionalization of the bithiophene by an

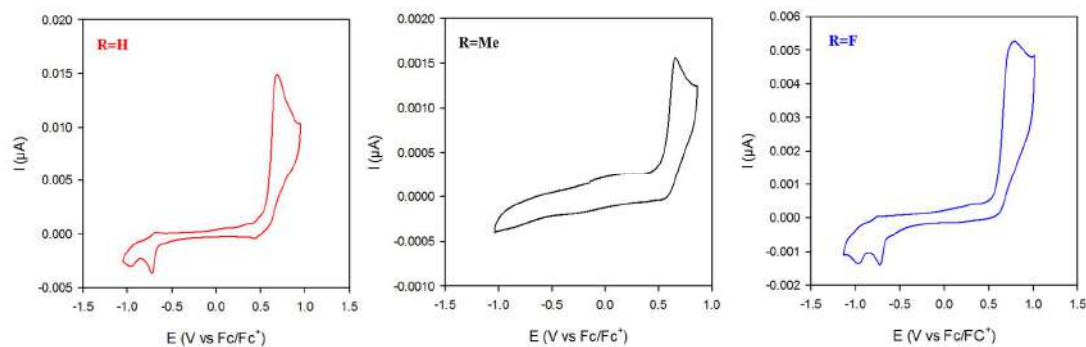
indoleninium moiety acting as a strong electron withdrawing group, its subsequent oxidation to induce a second BOX opening should occur at a higher potential.



*Figure 14. HOMO and LUMO Molecular Orbitals and energies obtained from DFT calculations at B3LYP-6.311(d) in the case of **22** CC (left), OC (middle) and OO (right).*

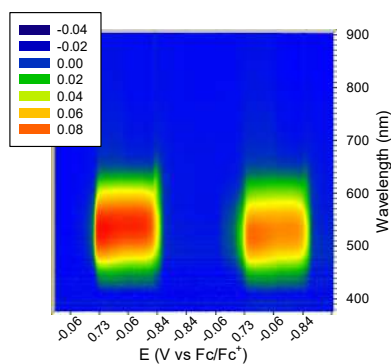
This difference of oxidation potential between CC and OC should conduct to a better discrimination between OC and OO states formation under electrochemical stimulation than with acid or light. This assumption is well supported by the evolution of HOMO energy level in function of the status of both BOX units. As example, this energy level decreases from successively -5.44, -5.85, to -6.24 eV for the compound **22** under its CC, OC and OO form respectively (figure 14).

In this context, the electrochemical behaviors of all molecular systems have been investigated by cyclic voltammetry (CV) in acetonitrile. As shown on Figure 15, all compounds exhibit similar behaviors with a broad non reversible oxidation process at 0.69, 0.66 and 0.78 V for compound **20**, **21** and **22** respectively.



**Figure 15.** Cyclic voltammetry of compound **20**, **21** and **22** in ACN (1.12; 0.53 and 0.68 mM) with  $TBAPF_6$  as electrolyte (0.1M) on Pt working electrode at  $100\text{mV}\cdot\text{s}^{-1}$ .

More important, almost all CV show the appearance of two new redox systems between  $-0.73\text{V}$  and  $-0.97\text{V}$  on the scan back when this first oxidation process is reached translating a strong transformation of the molecular structure at this potential. Based on our previous studies, this typical electrochemical behavior suggests the electro-induced opening of one or several oxazolidine ring(s) under electrochemical stimulation. To confirm this assumption, spectroelectrochemical experiments have been carried out. As expected, successive coloration/bleaching of the solution of all compounds can be obtained by varying the applied electrochemical potential. As example, the variation of the absorption spectra of a solution of compound **20** under its CC form as function of the applied electrochemical potential is presented in figure 16.

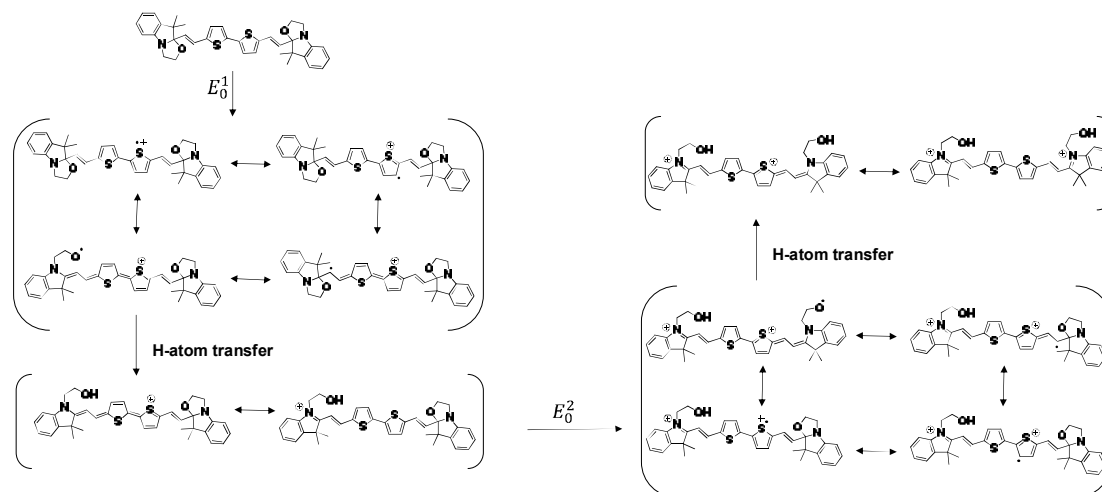


**Figure 16.** Spectroelectrochemistry in TLCV conditions ( $\sim 50\ \mu\text{m}$ ;  $20\ \text{mV}\cdot\text{s}^{-1}$ ) of **20** (0.53 mM) in acetonitrile with  $TBAPF_6$  as electrolyte (0.1M) on a platinum electrode.

As soon as the potential reaches 0.69V, we can notice the appearance of an intense absorption band in the 500-600 nm range. The perfect overlapping of absorption maxima observed under electrochemical stimulation with these recorded under other kind of stimulation (proton and photon) confirms as expected the opening of the two oxazolidine rings at this potential and the perfect commutation of the molecular system between **CC** and **OO** state. In addition, a complete bleaching is observed when -0.9V is applied restoring the initial state of the solution and demonstrating the possibility to induce a back conversion from **OO** to **CC** state under an electrochemical stimulation.

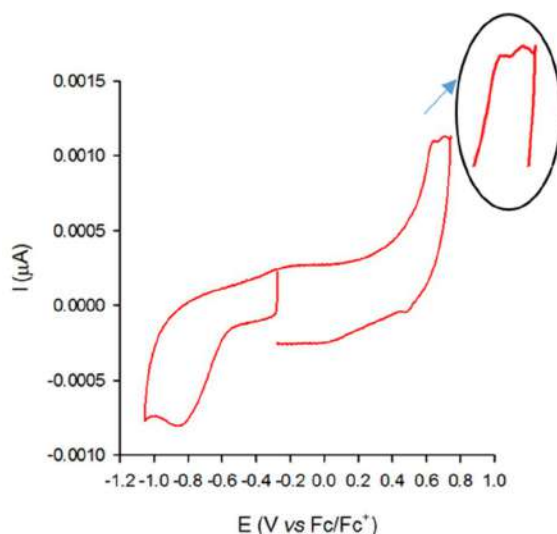
Except a slight bathochromic shift of the maximum absorption wavelength observed during the oxidation process, no evidence of a stepwise commutation and by consequence the intermediate formation of **OC** form, was detected during these experiments. Moreover, the observation of only one oxidation wave on the CV suggests that the oxidation occurred directly on both BOX units at the same time (direct electrostimulation) leading to an "all-in" commutation mode. However, this hypothesis is not in agreement with the poor effect of substituents in position 5 on the electrochemical behavior. Indeed, the direct oxidation of a BOX substituted by a bromine or an hydrogen (like in compound **20**) atom in position 5 is known to conduct to its dimerization by C-C oxidative coupling characterized on the CV by the emergence of a new redox system at lower potential (*c.a* 0.39V).<sup>[1, 10]</sup> At the opposite, the presence of a methyl group or a fluorine atom promotes the evolution of the generated radical cation toward the opening of the oxazolidine ring or assure its stability respectively.<sup>[1]</sup> Here, a non-reversible oxidation process without detection of dimerization product is observed for all three compounds whatever the nature of the substituent in position 5, and the variation of the substituent induces only a minor anodic shift of electrochemical potential (in example 30mV between compounds **20** and **21**). Thus, even if electrochemical and spectro-electrochemical experiments don't demonstrate a stepwise commutation and the intermediate formation of the

OC derivative, both calculations and experimental similarities suggest a redox mediated opening compatible with the step by step opening of the two BOX terminations. Indeed, as already exposed, the indolonium genesee in OC derivative should, due to delocalization of charges, deactivate the second BOX opening which should then occur at higher potential (figure 17).



**Figure 17.** Proposed mechanism for the stepwise opening of both oxazolidine rings of BOX-2-Bt under stimulation under an electrochemical potential.

For some reasons, this potential variation appears surprisingly limited here and only a broadening of the oxidation wave in place of two distinct peaks is observed on CV. Nevertheless, the position of the anodic peak potential is known to be strongly influenced by the chemical kinetic rate constant when a chemical reaction is coupled to an electron transfer. As consequence, a kinetic difference between the first and the second BOX opening can be also envisioned in order to explain the merging of both processes on the CV. To verify this assumption, cyclic voltammetry experiments were carried out in thin layer conditions, TLCV.



**Figure 18.** TLCV ( $<5\mu\text{m}$ ;  $20\text{ mV}\cdot\text{s}^{-1}$ ) of a solution of **20** in ACN with TBAPF<sub>6</sub> as electrolyte (0.1M) on a gold electrode.

As shown on figure 18 presenting the TLCV of a solution of **20** under its CC form, the reduction of the diffusion layer as well as the potential scan rate have allowed observing the splitting of the oxidation wave and finally evidenced a difference of oxidation potential between CC and OC forms and by consequence a stepwise commutation under electrochemical stimulation.

To confirm this point, the commutation of the system was investigated by using an oxidizing reagent such as NOSbF<sub>6</sub> (0.87 V vs Fc/Fc<sup>+</sup>)<sup>[17]</sup> which is largely used to evidence mixed valence in electroactive species by UV-Visible-NIR spectroscopy<sup>[18, 19]</sup> or generating oxidation of organic donors.<sup>[20]</sup>

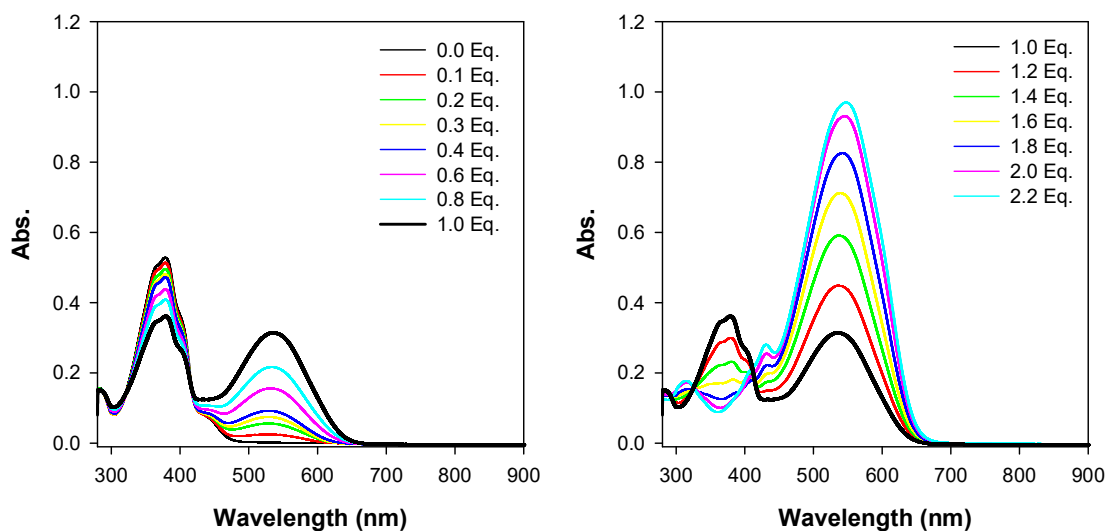


Figure 19. UV-Visible spectrum changes of a solution of **BOX-H 20** in ACN (0.086mM) upon addition of  $\text{NOSbF}_6$ .

As showed on figure 19 for compound **20**, a drastic change of the UV-Visible absorption properties upon addition of  $\text{NOSbF}_6$  aliquots is observed. At the end, we can notice that this addition of oxidizing reagent leads to an identical spectrum as the one obtained after stimulation with an excess of acid (see figure 9). In addition, initial spectrum can be recovered after treatment with an excess of base such as triethylamine demonstrating once again the multi-modal (proton, photon electron) switching ability of these molecular systems. If the UV-visible spectra obtained upon gradual chemical oxidation of compounds (Figure 7, compound **20**) present strong similarities with those chemically and optically induced, subtle differences appear. Indeed, this later shows upon addition of the first equivalent of  $\text{NOSbF}_6$  the appearance of a unique band centered at 529nm assigned to the **OC** form (*vide infra*) associated with the concomitant decrease of the **CC** characteristic band at 378nm. Pushing further the addition of oxidant to 2 equivalents leads to the disappearance of the characteristic band of **OC** toward a bathochromically shifted new band (546nm assigned to **OO** form) as well as the appearance of two weak bands at high energy around 300 and 430nm. Despite these strong similarities, a clear isosbestic point is observed from the beginning of the oxidant addition up to the last addition what could be a clue indicating selective successive processes.

As used earlier with acidic stimulation, the  $^{19}\text{F}$  NMR spectroscopy is a technique of choice to confirm the stepwise commutation of the system but also probes the selectivity of the addressability under chemical oxidation. The results of the titration of compound **22** by  $\text{NOSbF}_6$  are presented on Figure 20.

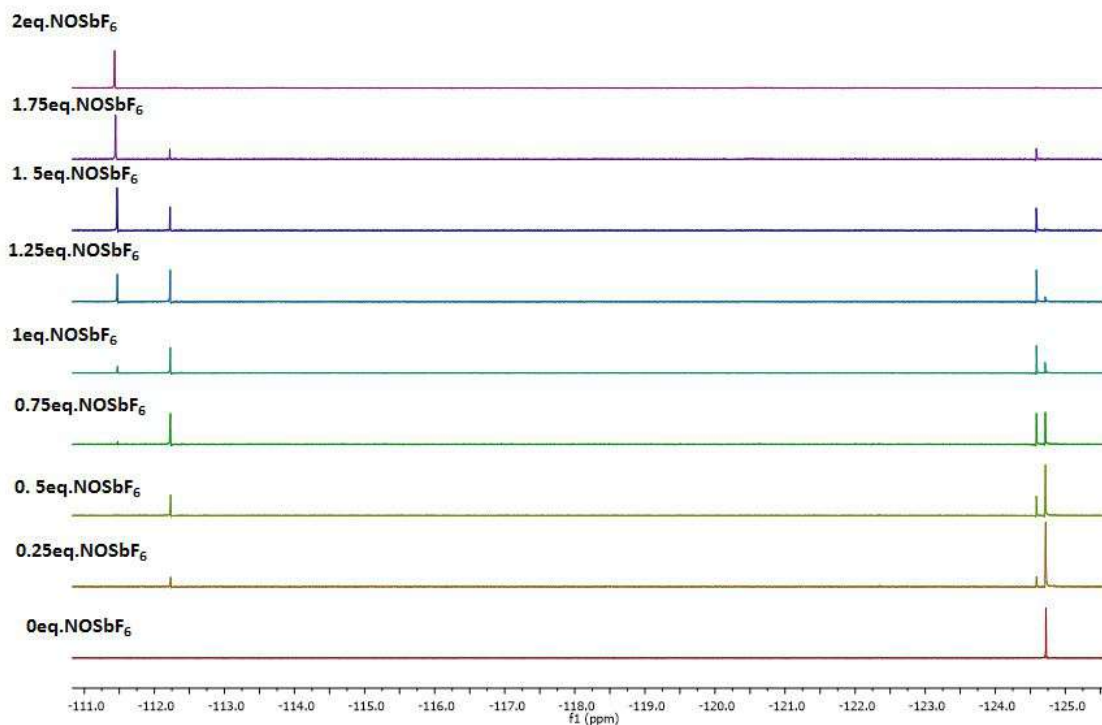


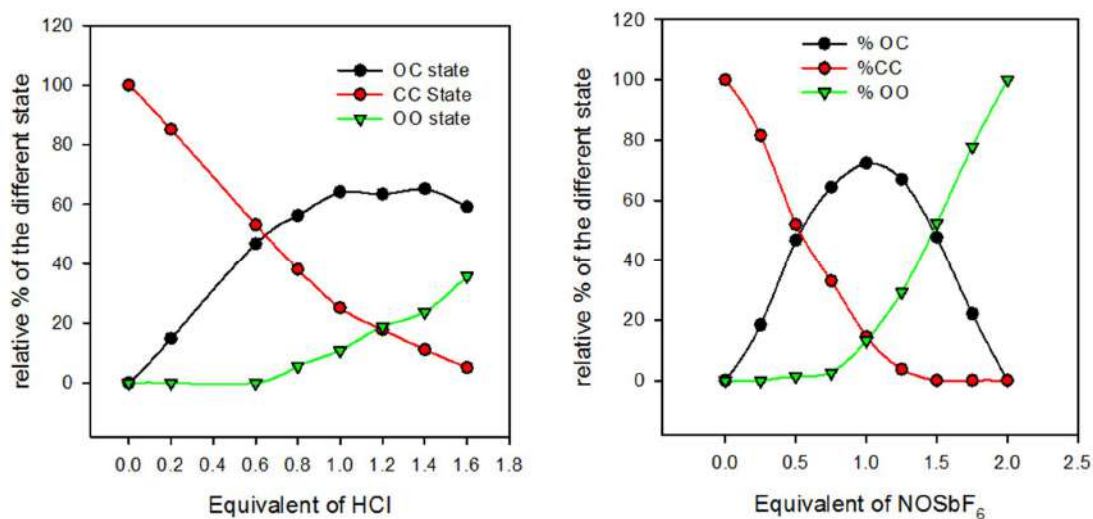
Figure 20.  $^{19}\text{F}$  NMR spectrum changes of a solution of **BOX-F 22** in  $\text{ACN-d}_3$  (2.27mM) upon addition of  $\text{NOSbF}_6$  aliquots.

As expected, the addition of chemical oxidant aliquots leads to almost identical peaks emergence as observed when the stimulation of the system was performed with HCl. Indeed, as soon as the addition starts, two new peaks, assigned to the **OC** form, are observed at -124.60 and -112.22 ppm. When the addition is pushed further, these latter are replaced by a unique signal at -111.49 ppm corresponding to the symmetric **OO** form. However, subtle differences are noticed between the acidic and oxidative stimulations.

First of all, the large formation of **OO** form by chemical oxidation doesn't lead to its precipitation in acetonitrile as previously observed with acid allowing to fully convert the system between **CC** and **OO** form. This can be easily explained by the change of counter ion

from a simple chloride to a hexafluoroantimonate anion which is considered as a weakly coordinating anion and leads generally to more lipophilic salt as generally reported for ionic liquid.<sup>[21, 22]</sup> This hypothesis is also in agreement with the slight variation of the chemical shift values observed between both stimulations, especially for the peak assigned to the fluoride borne by the open BOX unit (-112.29/-112.22 for **OC** form and -111.84/-111.49 for **OO** form).

As mentioned previously, the integration of the different peaks is an easy and convenient manner to determine the relative proportion of the three different states of compound **22** along its stimulation. If the evolution of their proportions upon the addition of  $\text{NOSbF}_6$  demonstrate unambiguously the stepwise commutation of the system under an electrochemical stimulation, the recorded results differ strongly from those obtained under acidic stimulation (figure 21).



**Figure 21.** Evolution of percentage of each state according to number of equivalents of HCl (left) and  $\text{NOSbF}_6$  (right) added to **22** under its **CC** form in  $\text{ACN-d}_3$  at  $20^\circ\text{C}$ .

As example, the **OC** is the predominant form as soon as the amount of  $\text{NOSbF}_6$  exceeds 0.5 equivalent while 0.8 equivalent was required with a stimulation by the acid. More generally, we can notice that the **CC** and **OC** forms are totally converted by electrochemical stimulation after 1 and 2 eq. respectively while they are still persistent with acid in the same conditions. As consequence, the narrowed coexistence region between the different **CC**, **OC** and **OO** species

highlights the higher selectivity and efficiency of the redox addressability compared with other kinds of stimulation. Noteworthy, the full conversion from **CC** to **OC** cannot be reached even through the oxidation process. Indeed, the addition of 1 equivalent of  $\text{NOSbF}_6$  led only to the generation of 72% of **OC** form, which is completed by almost an identical quantity of **OO** and **CC** forms (13 and 15% respectively).

To explain such behavior, we can suggest a possible disproportionation reaction where two molecules under their **OC** states lead to the formation of one molecule of each state **CC** and **OO**. Based on the Nernst law, the equilibrium constant of the reaction is directly correlated to the oxidation potential difference ( $\Delta E$ ) between **OC** and **CC** by the following relation (1):

$$\Delta E = (E_{(\text{CC}/\text{OC})}^0 - E_{(\text{OC}/\text{OO})}^0) = \frac{RT}{nF} \ln\left(\frac{[\text{CC}][\text{OO}]}{[\text{OC}]^2}\right) = \frac{0.059}{n} \log K \quad (1)$$

With  $R$  the molar gas constant,  $T$  the temperature,  $F$  the Faraday constant and the number of electrons transferred in each redox process. In this context, it was possible to estimate the oxidation potential difference between **OC** and **CC**, noted  $\Delta E$  around 0.08V by relation (1). This low value is in full agreement with the observation of only one broad oxidation wave in cyclic voltammetry and the slight splitting noticed when thin layer conditions are used.

In summary, we have elaborated three multi-modal molecular switches by the functionalization of a bithiophene unit used as a simple pi-conjugated system between two identical BOX moieties. As expected, all three systems exhibit multimodal switching ability under acid-, photo- and electrochemical stimulation. However, the efficiency and the selectivity of the commutation are strongly affected by the nature of the stimulation. Among the different possibilities, electrochemical stimulation exhibits the best results. Indeed, the addition of one and two equivalents of chemical oxidant to **CC** allows its full and selective conversion to **OC** and **OO** form respectively. Unfortunately, the **OC** species seems undergo a disproportionation

reaction due to a poor  $\Delta E$  between CC and OC redox processes. This later avoids getting pure OC but leads to a mixture with minor quantities of two others forms.

Nevertheless, we have demonstrated that the connection of two identical BOX units by a pi-conjugated bridge is a simple and convenient manner to elaborate a multi-level molecular system. Easily prepared through a condensation reaction, the system is able to commute between three metastable states exhibiting different physico-chemical properties. Indeed, the theoretical calculations have highlighted an important variation of the HOMO and LUMO energy levels with the successive opening of the oxazolidine rings. Unfortunately, these variations are only translated by an important bathochromic shift (150-160nm) of the absorption wavelength during the first BOX opening. The second opening conducts only to a thin color variation (14-28 nm) which does not allow clearly distinguishing both states. In this context, our first objective to elaborate a molecular system able to modulate a physico-chemical property over three distinct levels is then not perfectly fulfilled. However, the absorption properties are not the only ones which can be modulated by the opening/closure of the oxazolidine ring. Indeed, most of the recent researches on BOX derivatives deal with the modulation of the nonlinear optical (NLO) properties especially the first hyperpolarisability (see chapter I).<sup>[14]</sup> Concerning these systems, the successive BOX units commutation may lead to a strong structural variation transforming an almost apolar system when both BOX are closed, to a classical push-pull dipolar system (A-D) with the first opening, and finally, a quadrupolar structure (A-D-A) with the second one. Knowing that each of this kind of structures are known to present very distinct NLO properties, the first hyperpolarisabilities of these systems were investigated with the help of colleagues from Bordeaux university (team of Pr V. Rodriguez from Institut des Sciences Moléculaires).

### C. BiBOX-bithiophene as multilevel molecular system to modulate the first hyperpolarizability.

#### C.1. NLO and molecular switches.

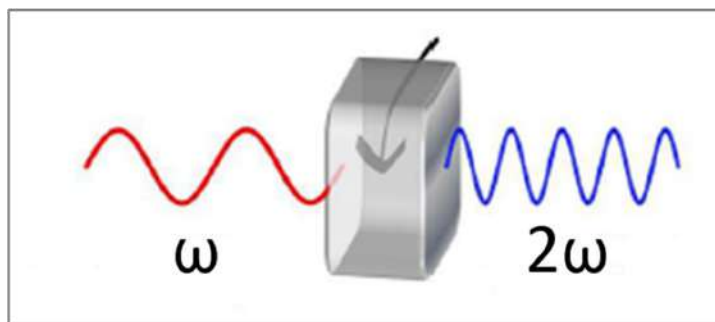
As suggested by its name, the field of the nonlinear optics deals with all phenomena resulting from the non-linear response of a material to an electromagnetic wave. In classical optic, the induced polarization in the media is proportional to the applied electric field of the light. When the intensity of the applied field is large, the induced dipole moment can be expressed as a Taylor series in the electric field strength: [23, 24]

$$\mu_i = \mu_i^0 + \alpha_{ij}E_j + \frac{1}{2}\beta_{ijk}E_jE_k + \frac{1}{3}\gamma_{ijkl}E_jE_kE_l + \dots$$

in which  $\mu$  is the dipole moment,  $\mu_i^0$  refers to the permanent electric dipole moment of the molecule in the Cartesian direction  $i$ ,  $E_j$  the optical field applied in direction  $j$ , and  $\alpha_{ij}$  the corresponding component of the linear electric polarizability tensor,  $\beta_{ijk}$  and  $\gamma_{ijkl}$  are the second- and third-order nonlinear polarizabilities, also referred as the first and second hyperpolarizabilities. In a similar manner to the linear response, the vectorial property of the electric field implies that the first- and second-order hyperpolarizabilities are third-rank and fourth-rank tensors, respectively.[25]

With the expansion of laser light uses, numerous nonlinear phenomena were reported and several of those led to interesting applications. Reporting a complete list of those is out of the scope of this manuscript as they concern optical signal processing (parametric amplification, modulators), transmission of optical signals (optical solitons, cross-phase modulation, fourwave mixing, phase conjugation, Raman scattering), sensing (temperature sensors, spectroscopy and imaging), lasers (pulse compression, and generation of super continuum) fields.[26] Nevertheless, the second harmonic generation (SHG) is certainly one of the most well-known of these phenomena. Reported by Franken and his collaborators in the study of a quartz

crystal,<sup>[27]</sup> one year after the invention of the laser in 1960,<sup>[28]</sup> it may be simply described as the doubling of the laboratory laser frequency (Figure 22).



*Figure 22. Representative diagram of the generation of the second harmonic.*

At the beginning, SHG signal was only observed with inorganic materials due to geometrical considerations. Indeed, it is essential to avoid an antiparallel dipole-dipole orientation: a noncentrosymmetrical material must be reached.<sup>[29]</sup> It was expanded later, in 1964, to organic materials with the case of benzopyrene<sup>[30]</sup> and hexamethylene tetraamine monocrystals.<sup>[31]</sup>

At the molecular level, the SHG efficiency is driven by the first hyperpolarizability of the molecule. The latter should then exhibit a strong polarizability associated with a good delocalization of electrons. As consequence, push-pull systems, constituted on an electron donor (D, EDG) and an electron acceptor (A, EWG), separated by a  $\pi$ -conjugated spacer (Figure 23), represent an important class of organic molecules capable of generating a second harmonic. Indeed, the latter allows intramolecular charge transfer from the donor to the acceptor propitious to high  $\beta$  values. Any examples can be provided to clarify more such as simple para-nitroaniline<sup>[32]</sup> which acts as a typical push-pull molecule and is largely used as standard with a  $\beta$  value  $28.8 \times 10^{-30}$  esu in DMSO.<sup>[33]</sup>



Figure 23. Schematic representation of a push-pull molecule composed of an EDG, a  $\pi$ -conjugated system and an EWG.

As mentioned before in the previous chapter, molecular switches are compounds, which upon stimulation (as pH, electrical current and light ...), shift between structures presenting different chemical and physical properties. Naturally, this ability was also investigated in NLO field in order to modulate a nonlinear optical phenomenon under an external stimulation. Generally referenced as NLO switches, numerous molecular switches exhibiting a strong variation of their first hyperpolarizability upon triggering were reported.<sup>[34, 35, 36, 37, 38, 39, 40, 41]</sup>

In this context, B. Coe has proposed a classifications of the different NLO switches in 1999.<sup>[42]</sup> Three different classes were defined based on the identification of the dipolar system constituent which is affected during the commutation process, leading to Type I, II and III NLO switches where the donor, acceptor and conjugated bridge ability are respectively modified upon triggering as resumed on figure 24.

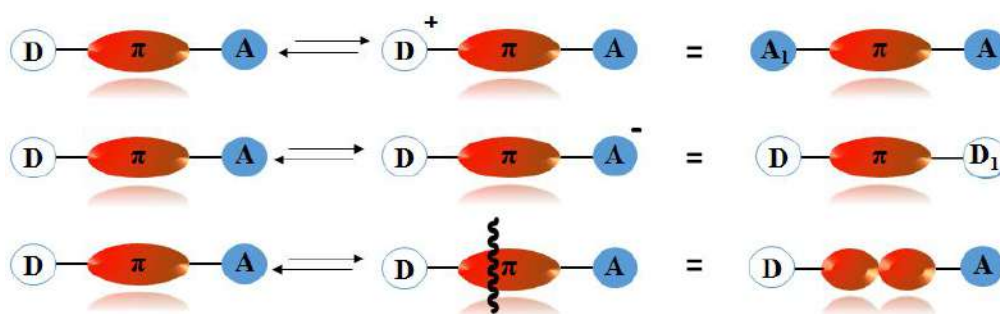


Figure 24: Schematic representation of different types of switching of NLO responses in dipolar  $D$ - $\pi$ - $A$  molecules: Type I = redox/proton transfer of  $D$ ; Type II = redox/proton transfer of  $A$ ; Type III = alteration of  $\pi$ -conjugation in bridge.

Disperse red one (DR1)<sup>[43]</sup> is certainly one of the first example of NLO switches which comes in mind due to its well-spread uses in NLO (Figure 25). As in other azo derivative

switches, a trans to cis photo-isomerization can be induced by light irradiation at 488 nm. Unfortunately, the cis isomer exhibits a poor thermal stability and the back isomerization occurs quickly at room temperature when the irradiation is stopped. As a type III NLO switch, this trans to cis photo-isomerization leads to a moderate reduction of DR1 first hyperpolarizability by a factor 5.

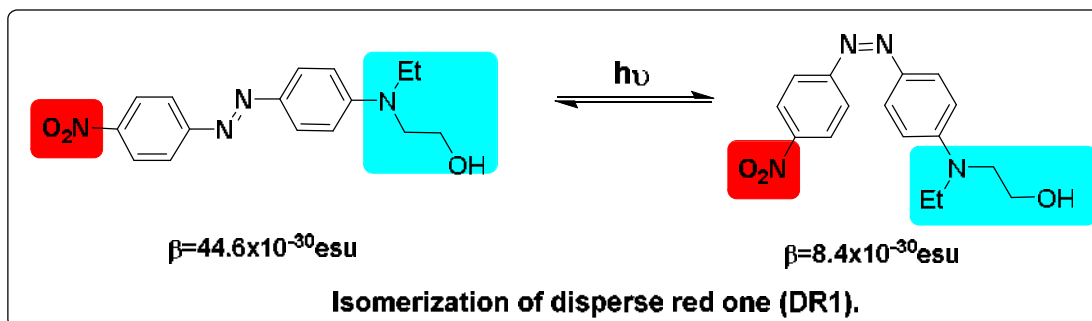


Figure 25. D- $\pi$ -A example of an organic chromophore.

Among molecular systems exhibiting multi-responsiveness, indolinooxazolidine based derivatives are known to display very large differences in their second-order NLO responses between closed colorless form and open  $\pi$ -conjugated colored one (figure 26). [44, 45, 46, 47]

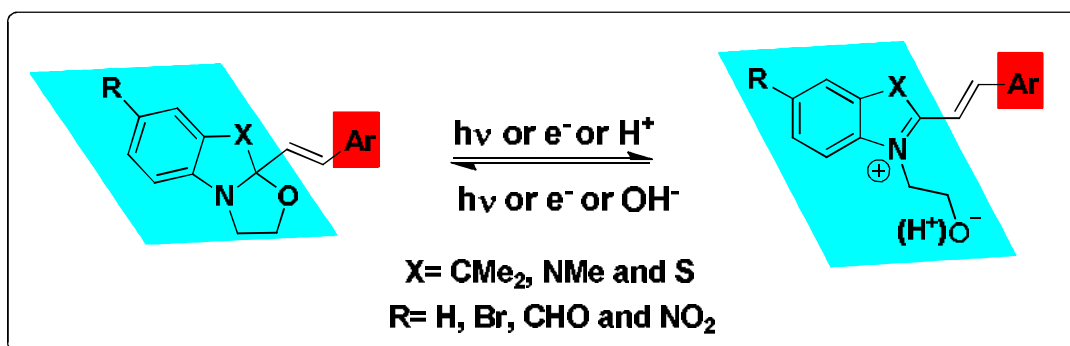


Figure 26. Photo-, acido- and electro-chromic properties for switches based on the indolinooxazolidine ( $X = \text{CMe}_2$ ), benzimidazolo-oxazolidine ( $X = \text{NMe}$ ), and benzothiazolo-oxazolidine ( $X = \text{S}$ ) moieties.

Indeed, the opening of the oxazolidine ring by indifferently light irradiation, electrochemical stimulation or pH variation leads to an indoleninium moiety acting as a strong electron withdrawing group. As consequence, their association to a pi-conjugated system

bearing a donor group conducts to very efficient Type II NLO multi-modal switches<sup>[47]</sup> exhibiting strong  $\beta$  contrasts. Such kind of system has been broadly studied through a multidisciplinary approach aiming at optimizing the contrasts between both forms.

As example, we can cite the elaboration of a tri-modal switch based on the association of one BOX unit to a bithiophene moiety as a redox center.<sup>[15]</sup> This system exhibits photo-, electro- and acidochromic properties in which the same interconversion could be performed by the different stimulations. In addition to these properties, upon stimulation, a modulation of the NLO properties of these systems of about a factor of 40-45 is observed what represents one the best contrast recorded so far (figure 27).<sup>[48]</sup>

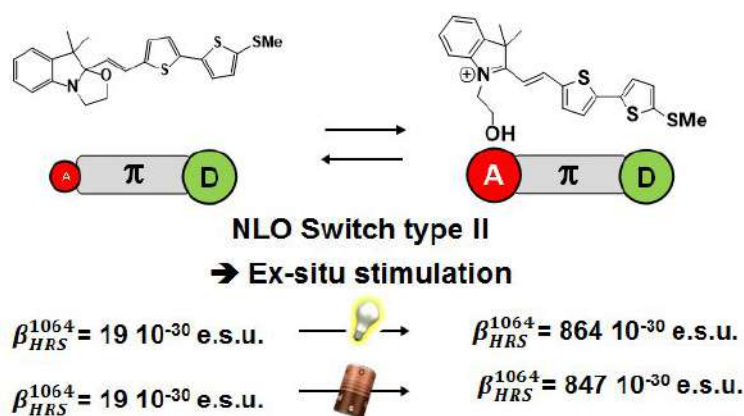


Figure 27. Difference of  $\beta$  between opened and closed form of BOX associated to bithiophene.<sup>[48]</sup>

Noteworthy, few Type II NLO switches are listed, indolinoxazolidine based derivatives appear then as an important family compounds regarding to the high  $\beta$  variations reaches by the opening/closure of the oxazolidine ring by applying indifferently one of three possible kinds of stimulation (proton, photon or electron). In this context, compounds **20-22** may represent a step forward as they allow a stepwise commutation between three states **CC**, **OC**, and **OO** where each of them is expected to present different 2<sup>nd</sup> order NLO properties.

### C.2. Determination of the first hyperpolarizability of compound 20.

To the best of our knowledge, only two experimental techniques allow to investigate directly the first hyperpolarizability: the electric field induced second harmonic generation (EFISHG) and the Hyper-Rayleigh scattering (HRS). Both techniques consist in measuring the scattering light emitted at double frequency by a molecular system placed in solution under a strong laser light illumination. Nevertheless, the EFISH technic uses a static electric field to orient the dipolar molecules in solution in order to generate the necessary macroscopic noncentrosymmetry. As consequence, octupolar and ionic molecules cannot be measured by EFISH since orientation in an electric field is not possible for these systems. At the opposite, HRS method implies pulsed lasers and tight focusing in order to observe nonlinear optical effects coming from the fluctuations, locally in time and space, away from centrosymmetric isotropic solution. As consequence, HRS is commonly considered as an almost universal experimental technique for molecular second-order nonlinear optics allowing determining molecular nonlinearities for a large variety of molecular or supramolecular assemblies.<sup>[25]</sup> Indeed, only non-centrosymmetric systems (dipolar or octupolar molecule) will give a response as an incoherent scattered light at optical frequency  $2\omega$  on incidence of an intense laser pulse at  $\omega$ .<sup>[49]</sup> From a practical point of view, the intensity of the scattered light is proportional to the square of the incident intensity, the mean value of the  $\beta$  tensor components, and naturally the chromophore concentration.

Thanks to our collaborators (Pr V. Rodriguez's team from Institut des Sciences Moléculaires) at Bordeaux University, we have carried out the measurements of the first hyperpolarisability of derivative **20** using the experimental set-up schematized in Figure 28.

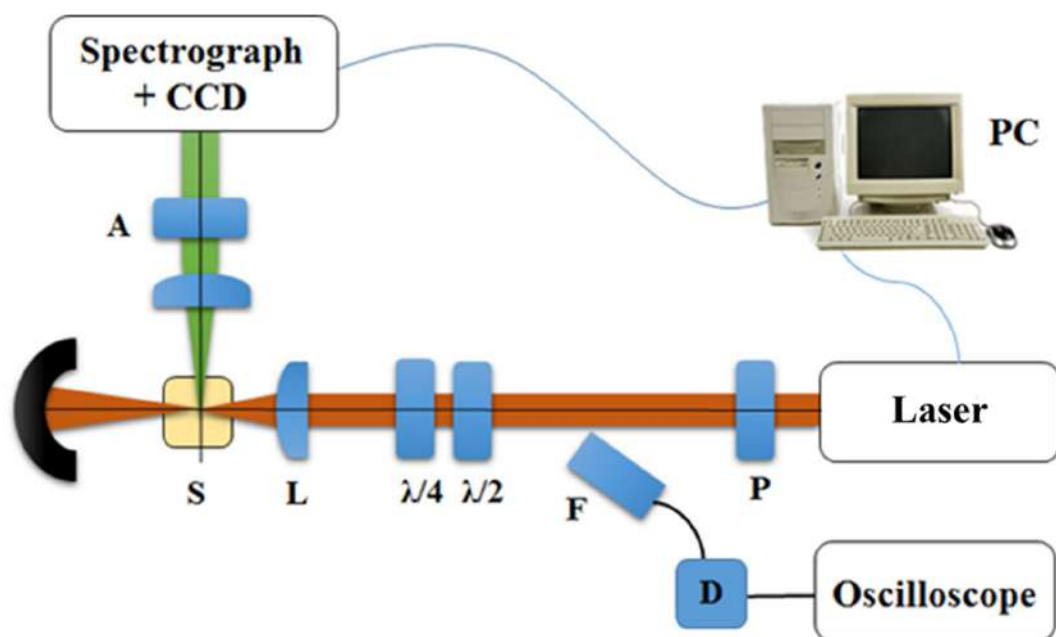


Figure 28. Experimental setup of the hyper Rayleigh scattering.

In this set-up, new OPG picosecond laser source (signal: 720-1000 nm, idler: 1150-2200 nm) at ISM (Bordeaux), it is possible to circumvent this issue by adjusting the incident energy ( $w$ ) to tune the SHS ( $2w$ ). The block power (P) is constituted on a half-wave plate and a polarizer, which provide linear vertical polarization. The fundamental relative intensity is precisely determined *via* the measurement of the scattered light intensity by the half-wave plate routed through an optical fiber (F) to a photodiode (D) connected at an oscilloscope. More important, the polarization of the incident beam can be continuously controlled (P, S, left/right circular polarization and all intermediate elliptic polarizations) thanks to the juxtaposition of a half-wave plate and a rotatable quarter-wave plate. This tunable of the incident beam polarization allows to probe different beta tensor components.<sup>[50]</sup>

By using this set up, the first hyperpolarizability of the closed-closed (CC), open-closed (OC) and open-open (OO) forms of compound **20** were investigated in solution by using the solvent (acetonitrile) as an internal reference.<sup>[51]</sup> The figure 29, gathers all results and shows the variations of the incoherent scattered light at optical frequency  $2\omega$  as function of the concentration of chromophore but also of the incident power (figure 29).

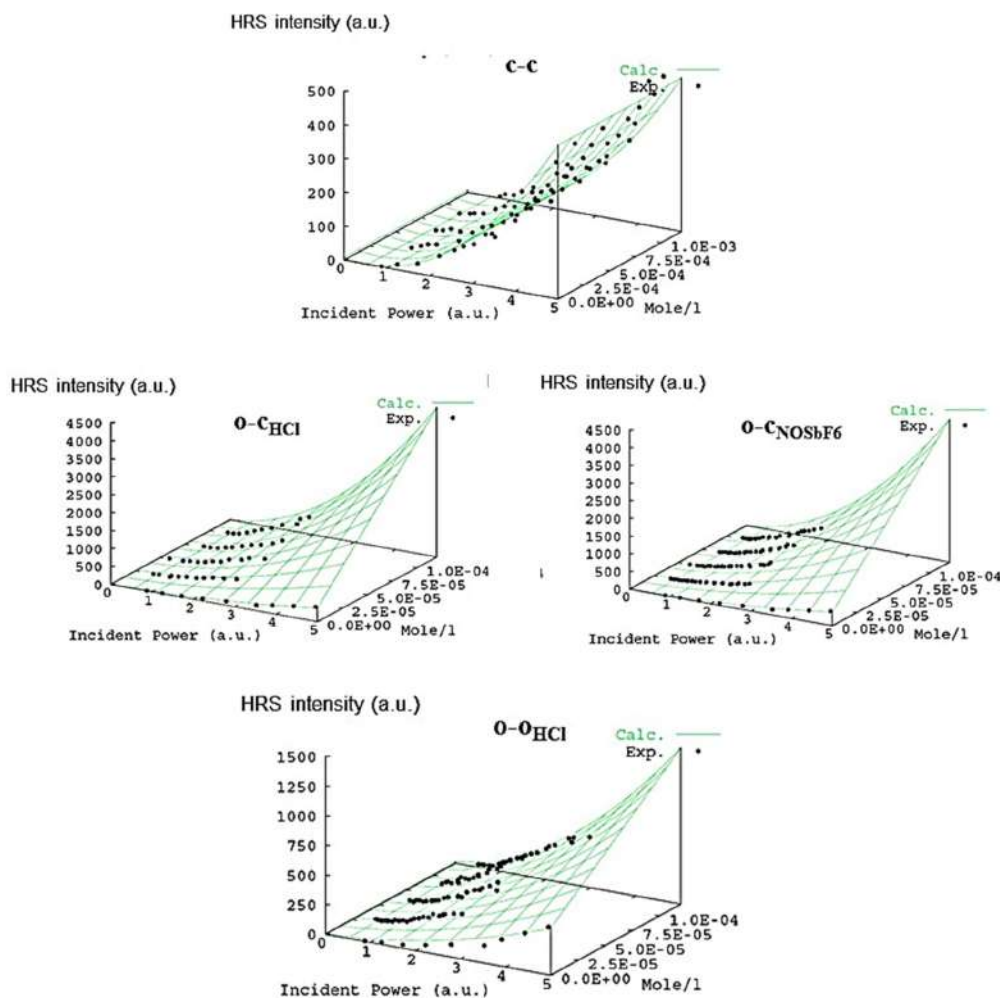


Figure 29. HRS responses of CC (top), OC by pH and NOSbF<sub>6</sub> (middle) and OO by pH (bottom) in solution using acetonitrile.

Commonly admitted, the variation of the scattered light as function of the concentration and the incident power follows expression (2):

$$I_{VV}^{2\omega} = F \cdot [(\Gamma_{Solv}) + (\Gamma_{Chr} \cdot C_{Chr})] 10^{-A(2\omega) \cdot C_{Chr}} \cdot I_{\omega}^2 \quad (2)$$

F is the common term,  $\Gamma_{Solv} (= c_{vv}^{Solv} \cdot \beta_{Solv}^2 \cdot C_{Solv})$  is the solvent-specific term, constant during all experiments,  $\Gamma_{Chr} (= c_{vv}^{Chr} \cdot \beta_{Chr}^2 \cdot C_{Chr})$  is the unknown to determine,  $C_{vv}$  is the average of the terms of the beta tensor expressed in the laboratory referential.

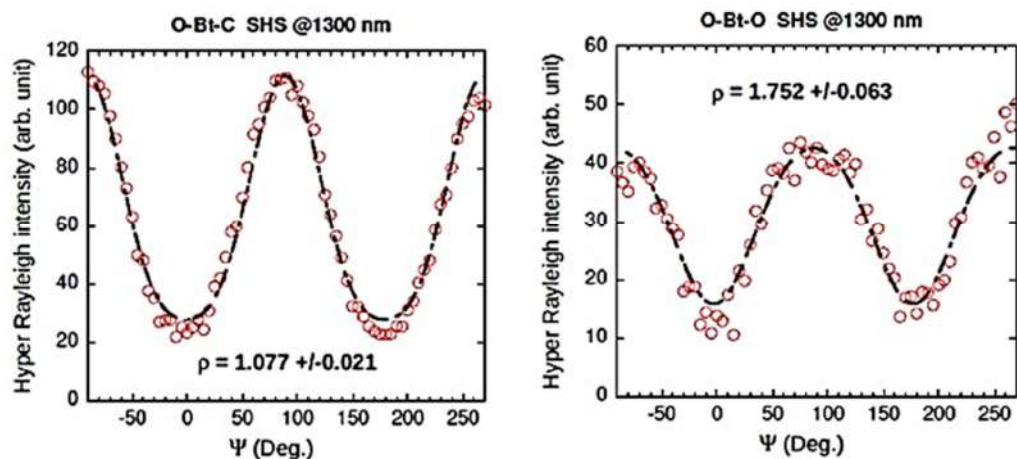


Figure 30. Extracted plot of the polarization curve of the solvated dye **20** in its **OC** (left) and **OO** (right) forms.

These experiments are completed by plotting the polarization curves of solvated dyes in the open and closed forms (figure 30) which allows estimating the global first hyperpolarizability for each form of compound **20**,  $\beta_{\text{HRS}}$ , but also the dipolar and octupolar contributions of this tensor noted  $\beta_{j=1}$  and  $\beta_{j=3}$  respectively. All results are gathered in table 4.

		$\beta_{\text{HRS}}$	DR	$\rho$	$\beta_{j=1}$	$\beta_{j=3}$	$\frac{\beta_{\text{HRS}}^{\text{o-c}}}{\beta_{\text{HRS}}^{\text{o-c}}}$
c-c		2064.59	2.38	2.1	2576.27	5410.17	-
o-c	pH	44148.16	4.01	1.077	76540.57	82434.19	0.53
o-c	NOSbF <sub>6</sub>	43146.29	4.01	1.077	74803.60	80563.48	0.55
o-o	pH	23659.29	2.74	1.718	33348.77	57293.18	-

Table 4. Data from HRS (in atomic unit) measurements on compound **20** at 1300 nm in Acetonitrile using pH and NOSbF<sub>6</sub>.

As expected, the fully closed form (**CC**) of this system exhibits only very weak NLO activity estimated below 4000 a.u. This can be easily explained by the poor dipolar moment of the molecule due to its symmetry.

As mentioned previously, the stimulation of the system by an acid or a chemical oxidant leads to the opening of the oxazolidine ring in a stepwise manner. In this context, it is not surprising to observe a strong enhancement of the NLO activity of the system with the first

opening. In fact, with the generation of an indoleninium moiety acting as strong EWG, the molecular system exhibits at this stage all the characteristics of a push pull system with the bithiophene as donor part. Knowing that the acid stimulation is less efficient and selective than chemical oxidation (*vide infra*), it is surprising to observe that both stimulations lead to almost similar results after one equivalent. Nevertheless, our previous NMR studies have demonstrated that the **OC** form is largely predominant at this stage (65% and 76% with HCl and  $\text{NOSBF}_6$  respectively). The slight variation of concentration of **OC** form associated with the largest beta value in comparison ( $\beta_{\text{HRS}}=44184$  a.u) to the two other forms can explain easily this poor variation of NLO activity as function of the stimulation.

At the opposite, the addition of an excess of acid in order to fully convert the **CC** form to **OO** one induces an important variation of the scattered light intensity. If an almost extinction of the signal was expected with the opening of the second oxazolidine ring and the restauration a centrosymmetric molecule, the **OO** form of compound **20** continues to exhibit a pretty decent beta value of  $23.7 \cdot 10^3$  a.u. To explain this interesting result, a preferential conformational change of the bithiophene moiety can, for example, be presumed from *anti* to *syn* (Figure 31) at this right moment.

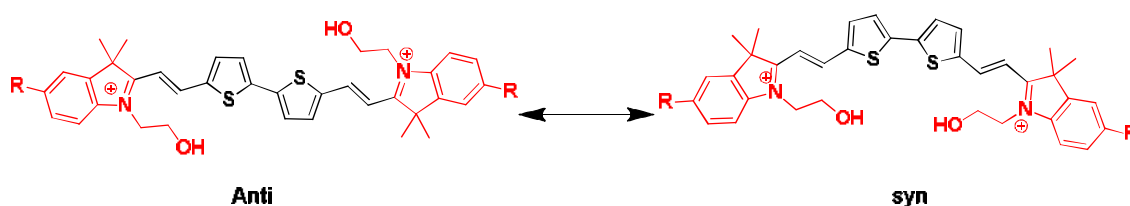


Figure 31. *Anti* and *syn* conformations of bithiophene moiety.

Indeed, the rotation along the central C-C bond of the bithiophene leads to pass from a centrosymmetric compound, which is by definition inactive in HRS, to a V shaped quadrupolar architecture (A-D-A). Generally confined to third order nonlinear optic, <sup>[52, 53, 54, 55]</sup> this kind of architecture has also demonstrated its ability to exhibit decent beta values whatever lower than

linear analogs.<sup>[56]</sup> If the predominance of octupolar component of the beta tensor represents a first clue, a theoretical study in order to support this assumption is necessary. The latter is still in progress (Pr B. Champagne's team from LCT UCPTS Département de Chimie at Université de Namur).

To conclude, the design, synthesis, analysis and physico-chemical properties of three new multi-modal systems based on the association of two indolinoxazolidine units to a bithiophene pi-conjugated core have been presented.

First, it has been shown that all of the three systems exhibit a multimodal switching ability under acid, photo- and electrochemical stimulation. Moreover, for the first time to our knowledge, both stimulations allow, a clear stepwise opening of two identical switches, namely the oxazolidine motif grafted through a simple pi-conjugated system.

If this never reported selectivity upon a unique stimulus with two identical switchable units is observed whatever the stimulation, it must be pointed out that its quality depends on the latter. Indeed, the direct stimulation of the BOX by acid leads to a large coexistence of the three different states of the system (**CC**, **OC** and **OO**) over a large range. At the opposite, the indirect stimulation of the BOX *via* an electromediated process thanks to the electroactivity of the bithiophene, allows to enhance the selective addressability between both identical BOX units.

In our objective to demonstrate the usefulness of these molecular systems to modulate a molecular property over three discrete levels by application of an external stimulation, we have seen that the variation of absorption wavelength maximum between one and two opening is not sufficient to obtain a clear differentiation between **OO** and **OC** forms. At the opposite, the elaborated molecular systems exhibit a pretty impressive variation of their NLO activity over three discrete levels with the successive BOX commutation. Indeed, the first hyperpolarizability of the system measured at 1300 nm is significantly improved by a factor 21

or a factor 11 in respect to the initial state **CC** with the first and second BOX opening respectively. At the opposite to UV-Visible absorption, both states **OC** and **OO** are now clearly distinguishable by HRS measurement with an NLO contrast value ( $\beta_{OC}/\beta_{OO}$ ) around 2. In addition to this strong variation of scattered light intensity, states are also undoubtedly identifiable through their depolarization ratio ( $I_{VV}/I_{HV}$ ). Indeed, this easily accessible experimental evidence varies from 4.01 for **OC** translating a main dipolar behavior to 2.74 for **OO** in agreement with its quadrupolar architecture.

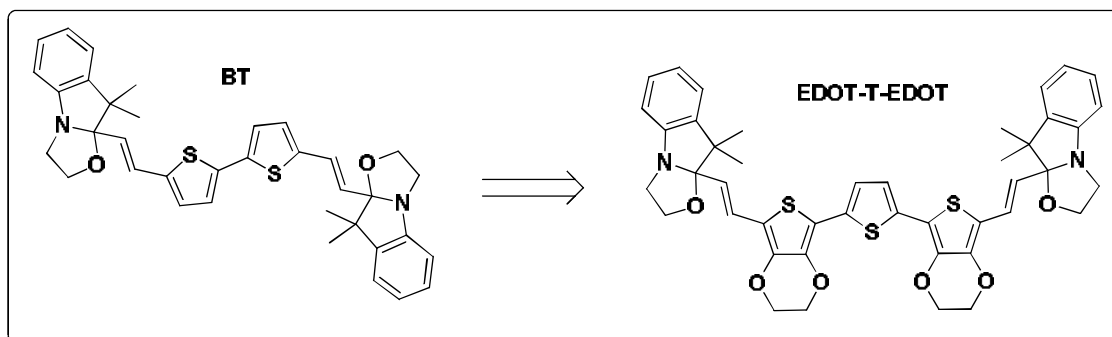
Considered as a proof of concept, these systems pave the way to more efficient ones. As a first example, in order to improve the electromediated stimulation, we have elaborated another system presenting, in place of the bithiophene bridge, another pi-conjugated spacer (linker) exhibiting a lower oxidation potential. By this structural modification, we expect inducing a higher variation of oxidation potential,  $\Delta E$ , between the first and second BOX opening. Preparation and characterization of targeted derivatives are detailed in the following section.

### **III). Association of two BOX with a EDOT-T-EDOT pi-conjugated system**

As discussed above, the association of two identical BOX units through a bithiophene as a pi-conjugated core leads to a very tiny difference between the two successive oxidation potentials leading to the stepwise commutation of the system. If each state can be addressed efficiently by using a chemical oxidant, this poor difference did not allow us to form specifically one of them by the direct application of an electrochemical potential as observed by cyclic voltammetry. To circumvent this issue, we have followed an approach consisting in changing the pi-conjugated bridge by another one exhibiting a lower oxidation potential in order to improve the electromediated stimulation process. In this context, we have chosen an EDOT-Thiophene-EDOT motif due to:

- its low oxidation potential explained by the strong electron donor effect of EDOT moieties,
- its improved conjugation allowed by S-O intramolecular interactions which rigidify the molecule,
- its facile and controlled reactivity in EDOT terminal positions

as demonstrated in numerous examples.<sup>[57]</sup>

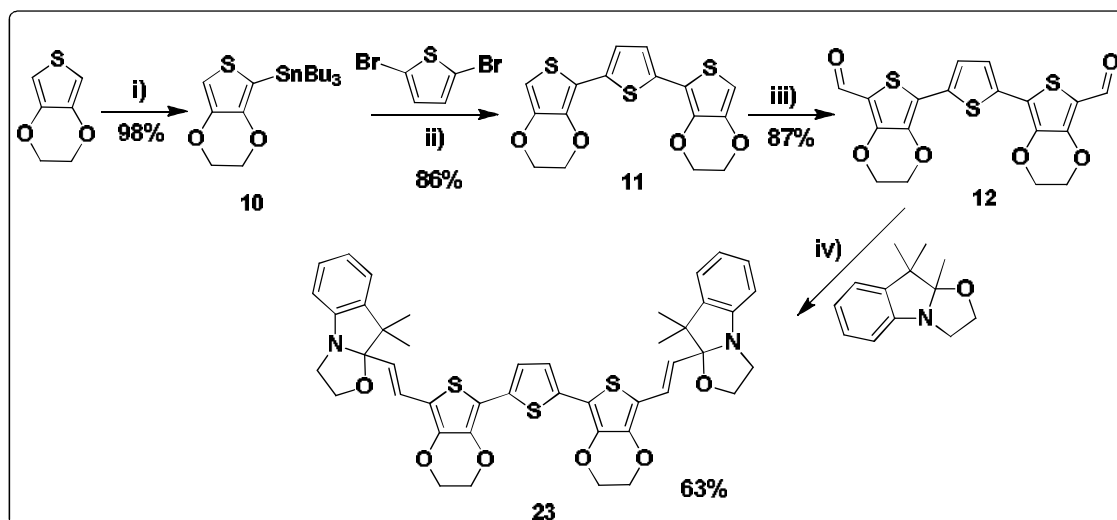


*Scheme 5. Chemical structure of the target molecules.*

Noteworthy, the lack of influence of the substituent on indoline position 5 observed in biBOX-Bithiophene series have conducted us to limit this study to only one triad where the EDOT-Thiophene-EDOT are substituted by two unsubstituted BOX moiety (Scheme 5).

### A. Synthesis and characterization of compound 23.

In order to prepare the targeted molecular system, a similar strategy as one used for the synthesis of the **20-22** biBOX-Bithiophene compounds was adopted. Based on the condensation between an aromatic aldehyde and the corresponding trimethylindolino-oxazolidine derivative as final step, this synthesis did not raise any particular problem and is depicted on scheme 6. In this context, as properties of compounds **20-22** only slightly differ, it was chosen here to focus our interest on the simplest derivative bearing “nude” (R=H) BOX terminations.



**Scheme 6.** Synthetic route to compound **23**. i)  $-78^{\circ}\text{C}$ ,  $n\text{-BuLi}$ ,  $\text{Bu}_3\text{SnCl}$ ,  $\text{THF}$ ; ii)  $\text{Pd}(\text{PPh}_3)_4$ ,  $\text{DMF}$ ; iii)  $\text{DMF}$ ,  $\text{POCl}_3$ , 1,2-dichloroethane; iv)  $\text{SiO}_2$ ,  $100^{\circ}\text{C}$ .

To prepare the bisaldehyde derivative, the 3,4-ethylenedioxythiophene stannic reagent **10** was first synthesized according to an already reported procedure.<sup>[58]</sup> Using  $n\text{-BuLi}$  as base, the EDOT is then deprotonated and subsequently treated with tin chloride to afford the compound **10** in 98% yield. This later is undertaken, without further purification, in a Stille cross-coupling reaction with 2,5-dibromothiophene in order to elaborate the pi-conjugated core **11** in 86% yield. Finally, the desired dicarbaldehyde compound **12** is obtained after a classical Vilsmeier-Haack reaction in decent yield (87%). As for bithiophene based systems (*vide supra*), the solvent-free experimental condition of silica mediated condensations<sup>[3]</sup> have been successfully applied here. Obtained in a satisfactory 63% yield, it can be noticed that the higher donor ability of this pi-conjugated core, compared with the bithiophene, impacts the reaction efficiency as the time of the reaction has to be increased of up to 7 hours.

As for our previous molecular systems, the *trans* isomerism of ethylenic junctions between the BOX and the EDOT-T-EDOT, as well as the structure were confirmed by NMR spectroscopy (proton and carbon).

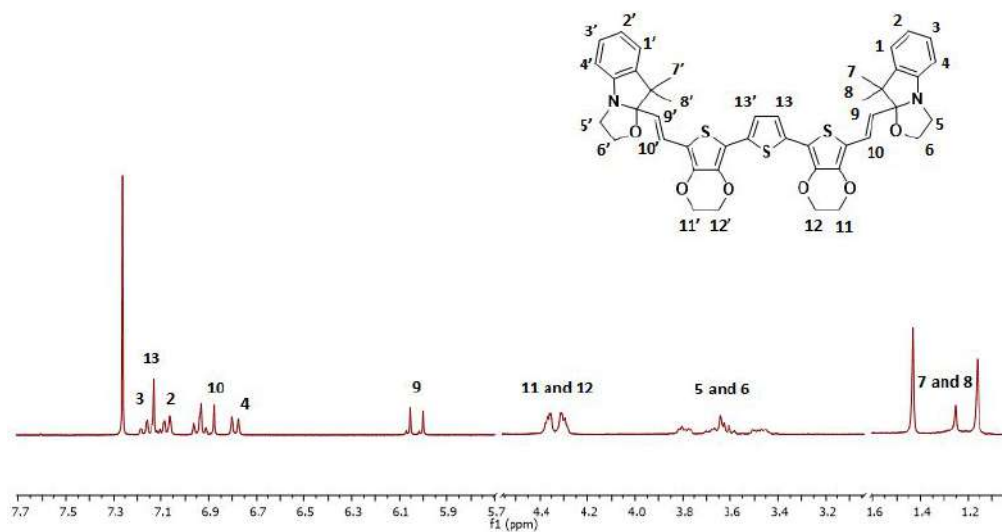


Figure 32.  $^1\text{H}$  NMR spectrum of compound **23** in chloroform ( $\text{CDCl}_3$ ) at rt.

As seen on figure 32, the  $^1\text{H}$  NMR spectrum of the compound exhibits the classical NMR signature of closed BOX derivatives such as:

- A doublet corresponding to one proton of the C=C linkage (9 and 9') easily distinguishable at 6.03 ppm exhibiting a vicinal coupling of 16 Hz confirming the full trans-trans isomery of the derivative. In this case, the simplicity of the aromatic part of the spectrum allows quickly to assign the second ethylenic proton (10 and 10') to the doublet at 6.9 ppm.
- A series of multiplets corresponding to the methylene groups adjacent to the nitrogen and oxygen atom centered at 3.65 ppm (5 and 6). As mentioned for the biBOX-Bithiophene compounds, these multiplets integrating for 4 protons reveal unambiguously the closed-closed status of the system.
- The presence of two singlets in aliphatic region at 1.43 and 1.16 ppm. Each of them integrating for 3 protons, they are assigned to geminal methyl groups on the indoline part (referenced as 7 and 8).

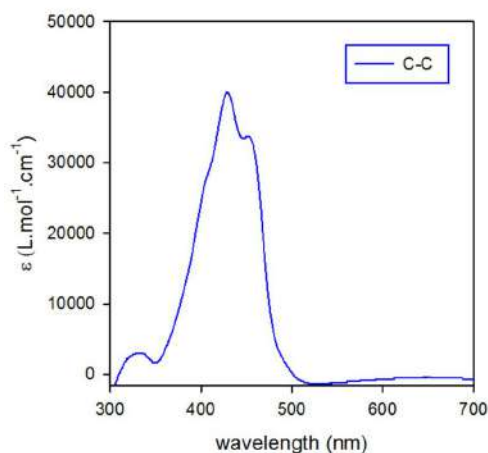
These typical signals of BOX derivatives are completed by the spectral signature of the pi-conjugated bridge with: *i*) two multiplets between 4.29 and 4.37 ppm integrating for 4

protons corresponding to both methylene group borne by the EDOT units; *ii*) one singlet at 7.13ppm assigned to the protons (13&13') of the central thiophene unit. One time again, the fact that the pi-conjugated bridge provides only these three signals confirms its symmetrical functionalization by two BOX units under their closed form.

Like previous molecular compounds, such kind of system should exhibit acido-, photo- and electrochromic properties due to the possible commutation between the three different possible states referenced later in the text as **Closed-Closed (CC)**, **Open-Close (OC)**, and **Open-Open (OO)**, depending on closed (C) or open (O) status of each BOX units. For this reason, the addressability of compound **23** under various stimulations is investigated and presented below.

### B. Acidochromic properties.

Under its closed-closed form (CC), compound **23** presents a UV-visible spectrum with a main absorption band centered at 428 nm exhibiting an epsilon value  $\epsilon=40000$  ( $\text{L}\cdot\text{mol}^{-1}\cdot\text{cm}^{-1}$ ) (figure 33).



**Figure 33.** UV-Visible spectrum of compound **23** under its CC form in ACN solution.

Due to the larger conjugated system, it is not surprising to observe a bathochromic shift of the maxima absorption wavelength ( $\lambda_{\text{max}} = 428\text{nm}$ ) of **23** in comparison to biBOX-Bithiophene analog **20** ( $\lambda_{\text{max}} = 378\text{nm}$ ). Similarly, the main transition is certainly centered on the central conjugated part of the molecule. This assumption is supported by, first, the presence of typical structuring observed in rigid based-EDOT conjugated systems, and second, by the similar value reported for Hex-ETE-Hex derivative ( $\lambda_{\text{max}} = 384\text{nm}$ ).<sup>[59]</sup>

In addition to the experimental studies, some theoretical calculations have been done using the density functional theory DFT (B3LYP-6.311 G(d) and IEFPCM model to consider solvation effect) for geometric and energetic optimization. As we can see on table 5, these calculations confirm that the HOMO and LUMO levels of compound **23** under its CC form appear both localized on the central EDOT-T-EDOT pi-conjugated core.

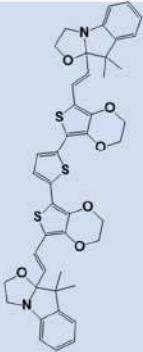
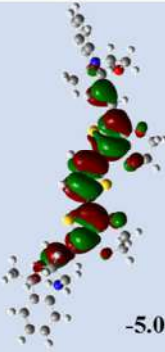
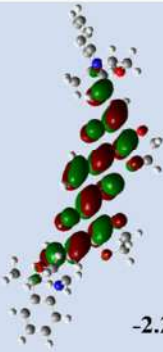
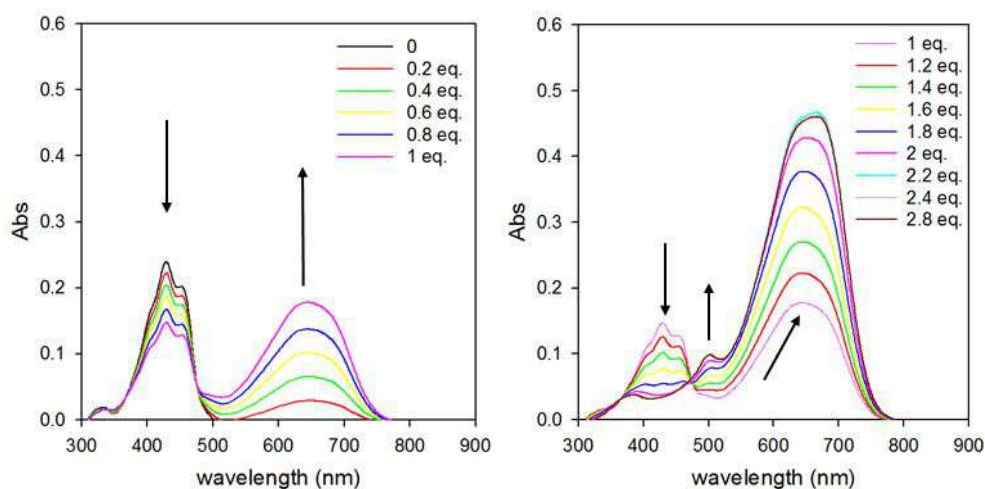
Compound	HOMO	LUMO	$\lambda_{\text{theo}}$ ( $\lambda_{\text{exp}}$ )	Oscillator strength
	 -5.00eV	 -2.21eV	505 (428)	1.7810

Table 5. Frontier orbitals and TD-DFT calculations of CC form of compound **23**.

As expected, the enhancement of the conjugation pathway leads to notice an important variation of the HOMO and LUMO levels of **23** (at -5.0 and -2.21eV) in comparison to bithiophene analog **20** (-5.44 and -2.07 eV respectively). It suggests a better donor character of the pi conjugated bridge and, as expected, a lower oxidation potential. Concerning TD-DFT calculations, they are confirming the assignment of the main absorption band to a  $\pi$ - $\pi^*$  transition centered on the EDOT-T-EDOT core as an HOMO-LUMO transition. Once again,

an important difference (77nm) between calculated and experimental maxima absorption wavelength is noticed which is not surprising when simple B3LYP hybrid functional is used for such highly polarizable compound.

As shown on the figure 34, the addition of HCl to compound **23** solution under its **CC** form induces a deep blue coloration due to the appearance of an intense broad band in the visible 500-710 nm range with the concomitant decrease of the absorption band centered at 428nm.

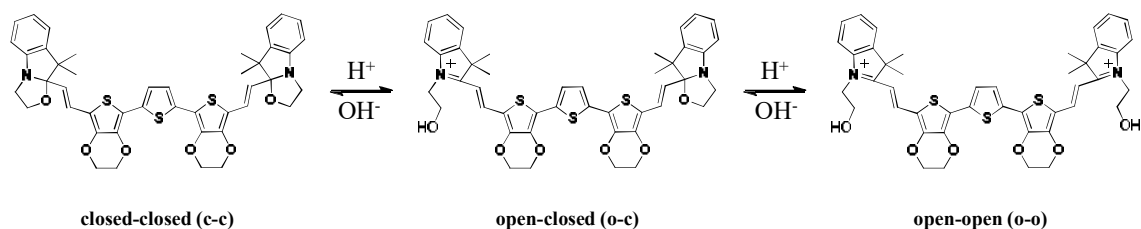


**Figure 34.** UV-Visible spectrum changes of a solution of compound **23** in ACN (0.006mM) upon addition of HCl aliquots.

As observed in the case of bithiophene series, a similar irregular evolution of the UV-Visible spectra along the titration with acid aliquots seems indicating a stepwise opening of the BOX units.

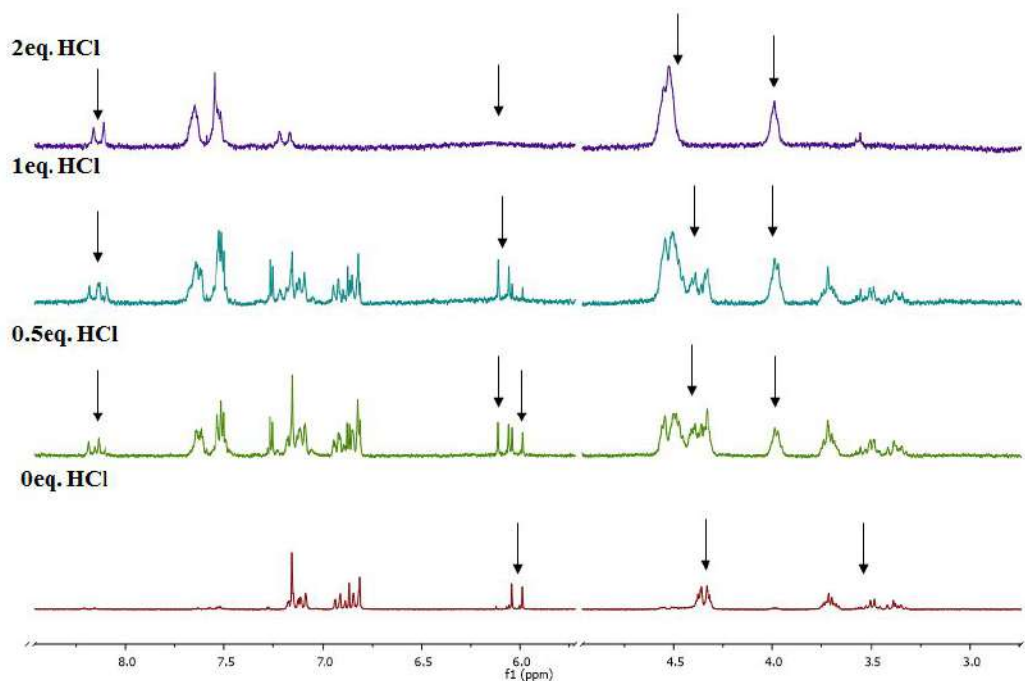
Up to one equivalent, the UV spectra reveal the appearance of a unique broad band centered at 642 nm as well as a strong decrease of the band intensity at 428 nm. More important, the presence of two isosbestic points at 368 and 476 nm is noted. Translating an equilibrium between two species, we can then deduce that, below one equivalent, the **CC** form is gradually converted into **OC** state. When the added quantity of HCl is pushed further than one equivalent, it leads to an enhancement of the solution coloration with the complete disappearance of the

band at 428 nm. In addition, a bathochromic shift of the main absorption band from 642 nm to 666 nm is observed with the concomitant appearance of a small higher energy absorption band at 503 nm. More important, this increment of the acid quantity did not allow maintaining the observation of the previous isosbestic points at 368 and 476 nm which can be translated to the shift of the equilibrium between **OC** and **OO** forms. As consequence, this experiment suggests the commutation of the connected BOX units in a stepwise manner (Scheme 7).



*Scheme 7.* Representation of the 3 different states of the molecular system **23**: **CC**, **OC** and **OO**, depending on closed (**C**) or open (**O**) status of BOX units.

As in biBOX-bithiophene series, NMR spectroscopy has been here used to unambiguously confirm the stepwise commutation of both BOX units. For this reason, the evolution of the proton NMR spectra of a solution of compound **23** under its **CC** form was recorded upon the addition of some aliquots of hydrochloric acid and is presented below (figure 35).



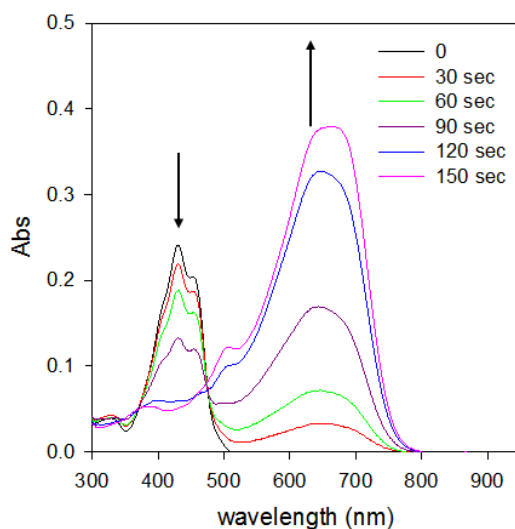
**Figure 35.**  $^1\text{H}$  NMR spectra upon titration of compound **23** (5.4 mM) by HCl in  $\text{ACN-d}_3$  at  $20^\circ\text{C}$ .

Here again, the doublet assigned to one ethylenic proton (9 and 9') is easily distinguishable at 6.03 ppm and a probe of choice to track the presence of the compound under its CC form. Adding acid (HCl) induces a decrease of intensity of this doublet and the appearance of two doublets at higher chemical shifts (6.1 and 8.15 ppm respectively) translating a loss of the symmetry and in agreement with the opening of only one BOX unit. This opening is well confirmed by the concomitant appearance of new NMR signals especially around 4 and 4.27 ppm characteristic of the pendant alkyl chain (N-CH<sub>2</sub>-CH<sub>2</sub>-OH) of the indoleninium. When the addition of acid is pursued, these both doublets are replaced by a new ones at a more shielded chemical shift, translating the regeneration of the molecular symmetry due to the opening of the second BOX. Once again, commutations induced by the acid stimulation didn't change the isomerism of ethylenic junctions. Indeed, a 16 Hz vicinal coupling constant for the doublets assigned to the ethylenic is observed in all state.

In a similar way as observed in previous series, the stepwise opening of both BOX units in compound **23** is well confirmed, but the selectivity and the efficiency of its commutation under an acid stimulation is not improved. Indeed, the formation of **OO** form is already detected after addition of 0.5 equivalent of acid and the **CC** form is still observed after one equivalent. We can then presume that the nature of the pi-conjugated core has unfortunately only a negligible influence on the selectivity of the addressability when the BOX are directly stimulated. In order to confirm this assumption, the photochromic properties of the system were investigated.

### C. Photochromic properties.

In this context, a solution of compound **23** under its **CC** form in acetonitrile has been irradiated with 254 nm light in presence of chlorobenzene (10%) as photosensitizer and the commutation of the system was monitored by UV-Visible spectroscopy. The evolution of the UV-Visible absorption spectra as function of the irradiation time is presented in Figure 36.



**Figure 36.** <sup>1</sup> UV-Visible spectrum changes of a solution of compound **23** in ACN/chlorobenzene 90/10 (0.006mM) upon irradiation at 254 nm.

As expected, the UV irradiation leads quickly to the strong coloration of the solution and the overlapping of the UV-visible spectra with ones obtained by addition of acid aliquots confirms the multi-modal switching abilities of compound **23**. Surprisingly, the photostationary state is reached after 2.5 min of irradiation duration, where 4 min were required in the case of compound **20** in the same conditions. As consequence it seems that the substitution of the bithiophene by a more electron donor bridge such as ETE, increases the photo-sensitivity of the compound. Beside this, both compounds behave in a similar way under irradiation as two stages can be noticed. Concerning compound **23**, below 1.5 min of irradiation duration, the appearance of an absorption band centered at 642 nm is concomitant with the reduction of the absorption at 428 nm and two isosbestic points at 368 and 476 nm are observed. Based on acidochromic studies, we can then assume that the initial **CC** state is gradually converted into **OC** one. Upon longer irradiation time, the visible absorption band continues to increase and is also bathochromically shifted and associated with the observation of a new weak band at higher energy suggesting that the second BOX opening occurs mainly at longer irradiation time and highlighting a stepwise commutation under light irradiation. Nevertheless, the behavior similarity with bithiophene analog **20** seems indicate that light induces a poor selectivity of the addressability and a large coexistence of the three different states.

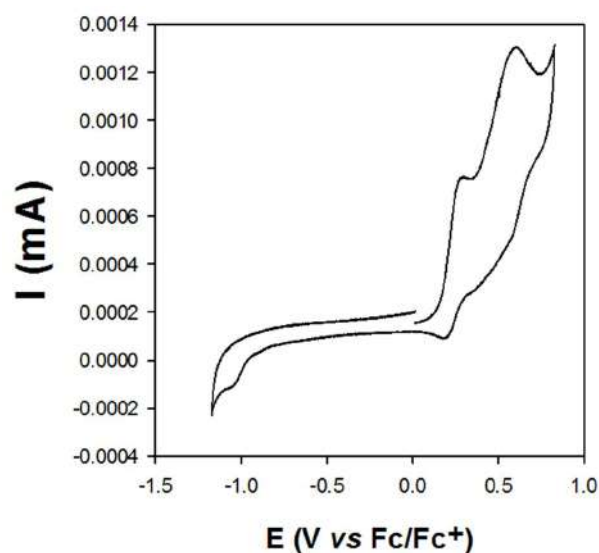
Based on these results it seems, as expected, that the nature of the pi-conjugated core used to connect two identical BOX units has negligible influence on the selectivity of the addressability when they are directly stimulated by light and/or acid. This behavior can be explained by the lack of conjugation of the BOX with the associated pi-conjugated system under their closed form. As consequence they are acting independently for each other and the stepwise commutation results from the decrease of the donor ability when one BOX is opened.

In this context, it appears interesting to check if the use of a better electron donor as pi-conjugated spacer has really an influence on the selectivity of the electromediated addressability process.

### D. Electrochromic properties.

In this case, playing on the nature of the pi-conjugated system can improve the electrochemical differentiation of the BiBOX dimer system. At the opposite of acid and light, stimulating the system by electron leads to an electromediated opening (indirect stimulation). Knowing that the first opening, leading to the **OC** form, conducts to the functionalization of the central EDOT-T-EDOT by an electron withdrawing group, its oxidation become more difficult than **CC** form and should occur at higher electrochemical potential. This difference of oxidation potential is then the corner stone to obtain a selective addressability between both identical BOX units under an electrochemical stimulation.

In this context, the electrochemical behavior of compound **23** has been investigated by cyclic voltammetry (CV).



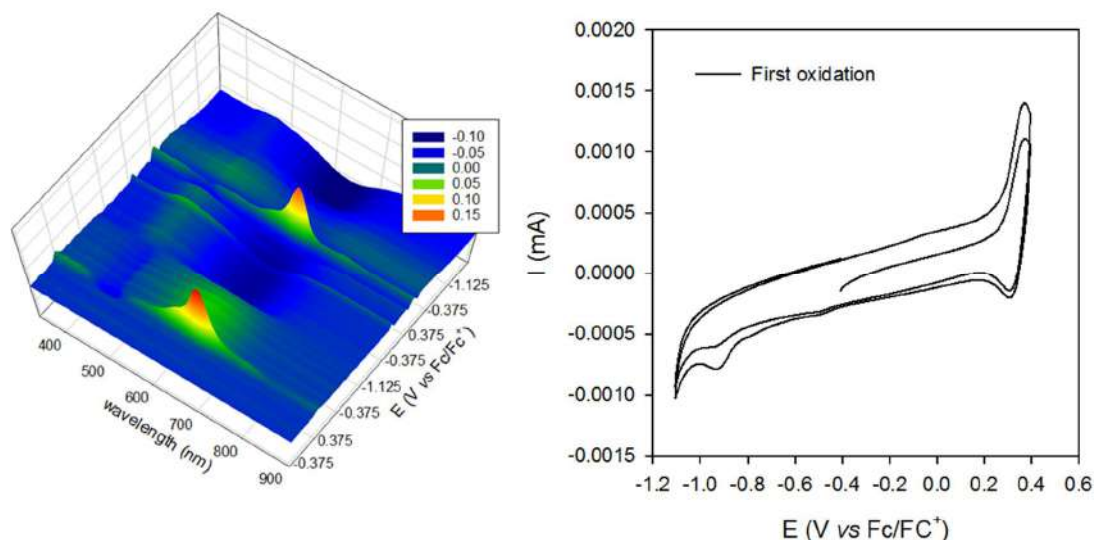
*Figure 37. Cyclic voltammetry of compound **23** in ACN (0.53 mM) with TBAPF<sub>6</sub> as electrolyte (0.1M) on Pt working electrode at 100mV.s<sup>-1</sup>.*

As shown on Figure 37, the CV of compound **23** shows two successive oxidation waves at 0.35 and 0.65V respectively. Surprisingly, perfectly reversible at high scan rate, the first oxidation process at 0.35 V becomes only quasi-reversible when the rate slows down. This first oxidation is assigned to the oxidation of the central ETE bridge. On one hand, this hypothesis is supported by the theoretical calculations (*vide supra*) which indicate a localization of the HOMO on this part of the system. On the other hand, the reported oxidation potential value for ETE (0.32V)<sup>[60]</sup> support this assumption. More important, we can conclude from the perfect reversibility of the peak at high scan rate that the generated radical cation during this first oxidation is stable enough despite the presence of both BOX units. At the opposite, the loss of signal reversibility at low scan rate translates the involvement of the radical cation into an irreversible chemical process which can be presumed as the opening of some BOX unit.

Concerning the second oxidation process occurring at 0.65V, several hypotheses can be envisioned for its assignation. First one consists to explain it by an oxidation mainly localized on the closed BOX unit, supported by the similar reported oxidation potential values of isolated BOX.<sup>[1]</sup> With any substituent present on position 5 of the indoline, this direct oxidation is known to conduct to some dimerization products by C-C oxidative coupling (see chapter 1).<sup>[1]</sup> Characterized by a peak around 0.4V, this hypothesis can then be discarded due to the absence of new signal on the scan back after reaching 0.65V. In addition, theoretical calculations (see above) suggest a HOMO of the **OC** form localized on the extended pi-conjugated system constituted by the ETE bridge and the opened BOX unit finishing to rebut this hypothesis.

As consequence, a second possible assignation for this oxidation process consists in the oxidation of the **OC** form leading to the second BOX unit opening by an electromediated process. In this context, the 0.3V positive shift of the anodic peak ( $E_{pa}$ ) will be due to the extension of the pi-conjugated system with the first oxazolidine ring opening and the generation of an indoleninium acting as strong withdrawing group. To confirm this assumption, spectro-

electrochemical experiments have been carried out from compound **23** under its CC form and are presented below (figure 38).

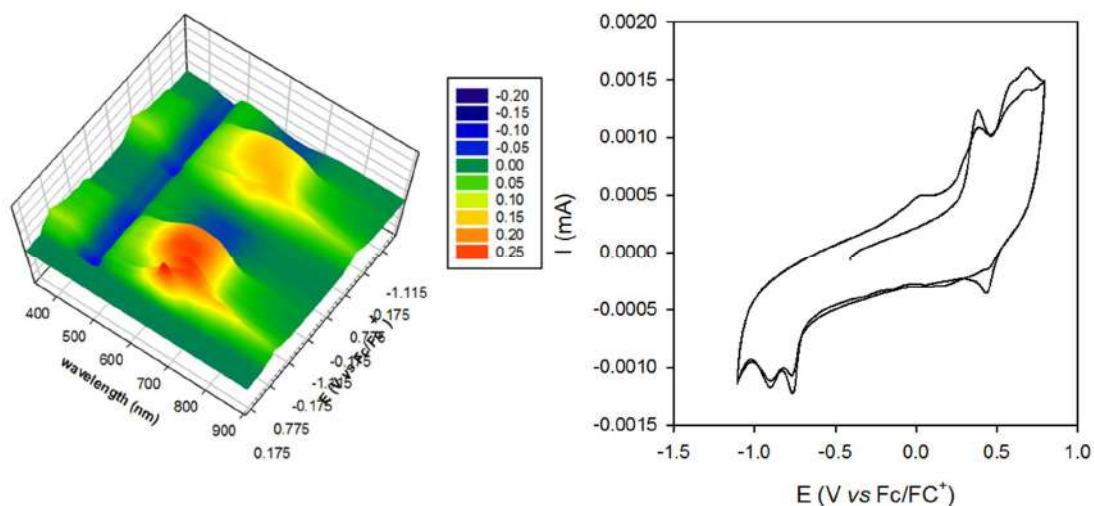


**Figure 38.** Spectroelectrochemistry in TLCV conditions ( $\sim 50 \mu\text{m}$ ;  $20 \text{ mV}\cdot\text{s}^{-1}$ ) of **23** (0.53 mM) in acetonitrile with  $\text{TBAPF}_6$  as electrolyte (0.1M) on a platinum electrode, vs  $\text{Fc}^+/\text{Fc}$ .

As soon as the potential reaches 0.35V, the UV-visible absorption spectrum of the solution is significantly impacted. First, we noticed the appearance of a broad absorption band in the 550-750 nm range and a decrease of the absorption band around 450nm which is characteristic for the **OO/OC** and the **CC** forms of compound **23** respectively. However, it is difficult to conclude to the opening of only one or both BOX units at this potential due to the slight bathochromic shift (24 nm) observed under acid stimulation between **OC** and **OO** states. More important, we can also notice the appearance of a sharp and intensive absorption band at 656nm and an increase of the absorption in the near UV range which were not detected under stimulation with HCl. Surprisingly; these last two modifications disappear as soon as the applied electrochemical potential is below 0.35V. At the opposite, to restore the initial stage of the solution with the disappearance of the broad absorption band in the 550-750 nm range as well as the restoration of the absorption around 450nm, we have to wait that the potential reaches -0.95 V. This restoration is translated on the CV by an irreversible reduction process.

To explain such behavior, we presume that the oxidation at 0.35V leads first to the formation of the radical cation of the central ETE core characterized by a higher absorbance in near UV range and more important by an intense and sharp absorption band centered at 656 nm. As the ETE motif appears more stable in its oxidized form than its bithiophene analogue, at the chosen scan rate, its signature is observed together with ones of the **OC** and/or **OO** species consecutive to the charge delocalization and some BOX opening. Indeed, as mentioned above, the slight bathochromic shift between both forms does not allow us to distinguish the opening of one or two oxazolidine rings at this potential. Upon reverse scan below 0.35V, the signature of this radical cation disappears and the **CC** form of **23** is fully recovered below -0.95V due to the BOX closure.

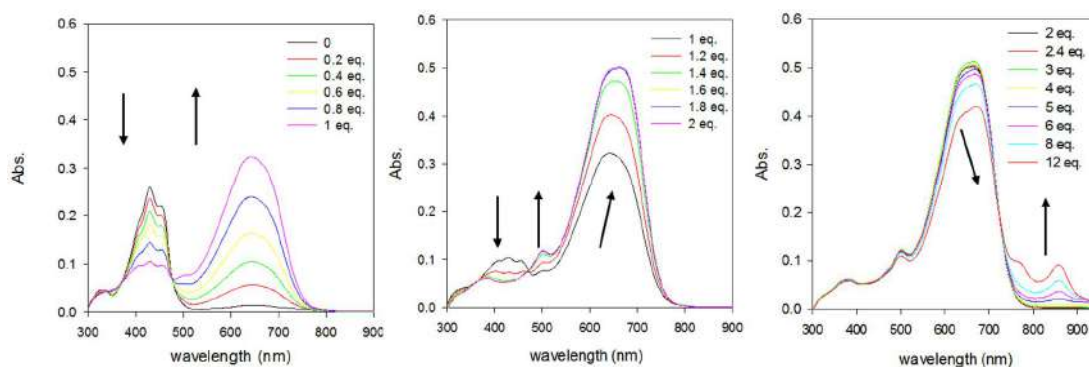
If only one BOX unit is open at 0.35V, the second opening should be open at higher potential. To verify this assumption, the explored oxidation potential range during the spectro-electrochemical experiment was increased.



**Figure 39.** Spectroelectrochemistry in TLCV conditions ( $\sim 50 \mu\text{m}$ ;  $20 \text{ mV}\cdot\text{s}^{-1}$ ) of **23** (0.53 mM) in acetonitrile with TBAPF<sub>6</sub> as electrolyte (0.1M) on a platinum electrode, vs Fc<sup>+</sup>/Fc.

As we can see on the figure 39, application of an oxidation potential around 0.65V to reach the second oxidation process observed on CV, induces a drastic change of the absorption

properties. At the first sight, we notice mainly an important bathochromic shift of the main absorption band and new ones at lower energy which was not observed during the stimulation of the system by HCl. Indeed, the conversion from **OC** to **OO** state under stimulation with acid is translated by a 24nm bathochromic shift of the main visible absorption band and important hyperchromic effect. As consequence, the assumption of the formation of **OO** form at 0.65 V is dismissed and, in place, the generation of a new oxidized state of the system have to be presumed. In order to check if this new state occurs before the second BOX unit opening which implies to consider the generation of the OC and OO during the first oxidation peak at close potential as observed for bithiophene analog **20**, the commutation of the system was investigated by using  $\text{NOSbF}_6$  (0.87 V vs  $\text{Fc}/\text{Fc}^+$ ) as an oxidizing reagent (figure 40).

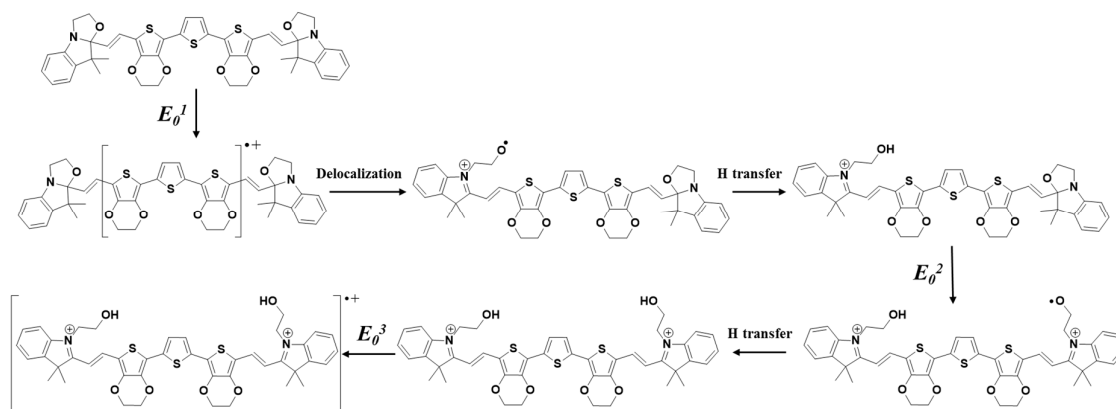


**Figure 40.** UV-Visible spectrum changes of a solution of compound **23** in ACN (0.006mM) upon addition of  $\text{NOSbF}_6$ .

As expected, a drastic change of the UV-Visible spectra upon the addition of  $\text{NOSbF}_6$  aliquots is observed. Up to 2 equivalents, we can notice that this addition of oxidizing reagent leads to an identical spectrum to those obtained after stimulation with an excess of acid (see figure 34). In addition, initial spectrum can be recovered after treatment with an excess of base such as triethylamine demonstrating the multi-modal switching ability of this molecular system. If the UV-visible spectra obtained upon gradual chemical oxidation of compounds (figure 40, compound **23**) present strong similarities with those chemically and optically induced, subtle differences appear. Indeed, this later shows upon addition of the first equivalent of  $\text{NOSbF}_6$  the

appearance of a unique band centered at 642 nm assigned to the **OC** form associated with the concomitant decrease of the **CC** characteristic band at 428 nm. The addition of the second equivalent of oxidant leads to the disappearance of the characteristic band of **OC** toward a bathochromically shifted new band (666 nm assigned to **OO** form) as well as the appearance of the weak band at high energy around 503 nm. Despite these strong similarities, a clear isosbestic point is observed from the beginning of the oxidant addition up to one equivalent (475nm) that could be a clue indicating selective successive processes. Furthermore, when the addition of  $\text{NOSbF}_6$  pursued up to 12 equivalents, a hypochromic effect with a bathochromic shift of the main absorption band from 666 to 674 nm is observed with the concomitant appearance of a small lower energy absorption band at 860nm, this can be also translated to the oxidation of the system under its **OO** form and in agreement with what we observed on the spectro-electrochemistry part.

We can conclude from these experiments that introducing a longer, rigid and efficient electrodonor spacer exhibiting a lower oxidation potential between BOX terminations did not fulfill our initial expectation. As expected, the cyclic voltammetry reveals well two distinct oxidation peaks. Unfortunately, it appears that the second one at 0.65V leads to the formation of a new oxidation states of the system which seems to lead to the radical cation of the **OO** form. Concerning the first oxidation peaks (0.35V), it is assigned to the oxidation of the central ETE bridge leading to the corresponding radical cation. Unluckily, the improved stability of this latter slow down the BOX opening through corresponding electromediated process. If the titration by the chemical oxidant have clearly demonstrated the stepwise commutation of the two BOX units suggesting a variation of oxidation potential between **CC** and **OC**, the spectro-electrochemistry and cyclic voltammetry experiments suggest that this difference is as limited as in bithiophene analog **20**. As consequence the electrochemical behavior of compound **23** can be summarized by the following figure:



**Figure 41.** Proposed mechanism for the stepwise opening of both oxazolidine rings of compound **23** by stimulating under an electrochemical potential.

### E. BiBOX-ETE as multilevel molecular system to modulate the two photon absorption.

As demonstrated before, the substitution of the bithiophene spacer by the ETE motif increases the donor ability of the system but, unfortunately, it did not allow to improve probably the discrimination of the potentials at which each BOX is opened. Nevertheless, this substitution is also expected to improve NLO properties of compounds:

- the better donor ability of EDOT-Thiophene-EDOT can enhance the dipole moment of the **OC** form and lead to higher  $\beta$ ,
- the rigidity of the central core (S-O interaction) may avoid the supposed anti/syn conformer formation of the bithiophene part in **OO** form.

In this context, the measurement the HRS ( $\beta$ ) has been logically undergone. If this experiment was not successful, it has demonstrated a strong two photon absorption fluorescence of the Open-Open form (**OO**) what can be considered as an interesting opportunity. Thus, linear and non-linear luminescence properties of compound **23** in its **CC** and **OO** states have been studied in Bordeaux in the team of Dr. Mireille Blanchard-Desce from Institut des Sciences Moléculaires.

E.1. One-photon absorption (1PA) and luminescence properties.

As mentioned in previous section, the open/close status of BOX unit have a strong impact on the UV-Visible absorption properties of compound **23** and the studies performed on its bithiophene analog have paved the way to use it as NLO switch. Beside these two classical uses of BOX derivative, we have chosen to explore some other potential applications especially the luminescence modulation under an external stimulation. Indeed, only few studies are dedicated to luminescence properties of BOX derivatives.<sup>[61]</sup>

In this context, the emission spectra of derivative **23** in acetonitrile under its **CC** and **OO** forms were recorded (Figure 42) and the luminescence quantum yields of each form were determined using fluorescein and indocyanine green respectively as standard. All corresponding data are gathered in Table 6.

**Table 6.** Photophysical properties of compound **23** in the two forms (**CC** and **OO**) in acetonitrile.

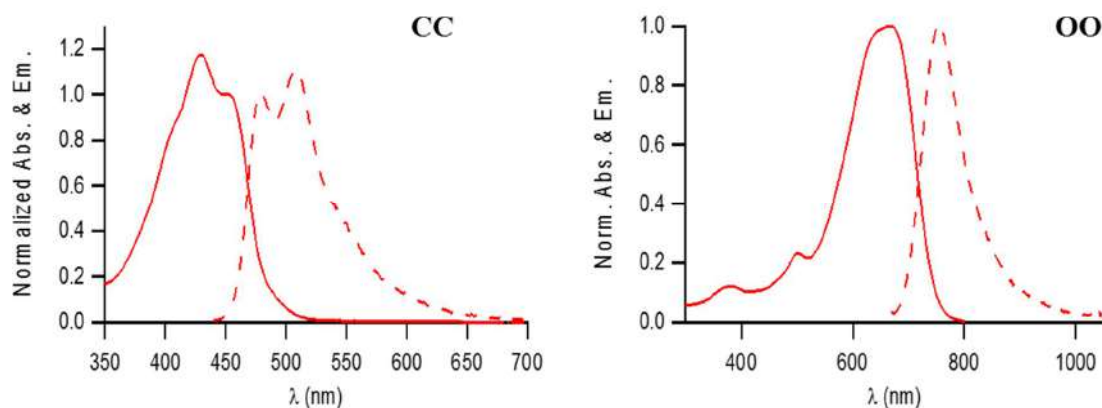
Compound <b>23</b>	$\lambda_{\text{abs}}^{\text{max}}$ (nm)	$\epsilon$ ( $10^4 \text{ M}^{-1} \cdot \text{cm}^{-1}$ )	$\lambda_{\text{em}}^{\text{max}}$ (nm)	Stoke'Shift ( $10^3 \text{ cm}^{-1}$ )	$\Phi$	$\tau$ (ns)
<b>CC</b>	429	5.0	478	2.4	0.34 <sup>b</sup>	0.9 <sup>d</sup>
<b>OO</b>	666	8.9	753	1.7	0.13 <sup>a</sup>	0.6 <sup>c</sup>

<sup>a)</sup> Standard: Indocyanine Green in DMSO ( $\Phi=0.11$ )

<sup>b)</sup> Standard: Fluorescein in NaOH 0.1M ( $\Phi=0.9$ )

<sup>c)</sup> Exc@670nm <sup>d)</sup> Exc@455nm.

As we can see on the figure 42, both forms exhibit luminescence into two different spectral range. When excited at 455 nm, the **CC** exhibit a structured emission band centered at 478nm. At the opposite, **OO** form presents a sharp emission band centered at 753nm when excited at 670 nm.



**Figure 42.** Absorption (solid line) and emission spectra (dashed line) of compound **23** under its **CC** (left, excited at 455nm) and **OO** (right, excited at 670nm) form.

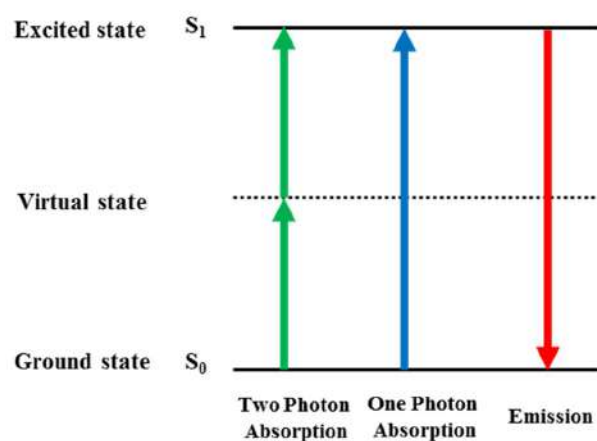
In addition to the strong bathochromic shift of the absorption and emission bands, the opening of both BOX unit induced an important decrease of the luminescence quantum yield which is reduced by an almost factor 3 (from 0.34 to 0.13). Concerning the **CC** state, we have highlighted that the  $\pi \rightarrow \pi^*$  electronic transition of the central ETE bridge is responsible of the main absorption band. As consequence, the luminescence properties of **CC** can be reasonably assigned to the ETE linker. More important, the luminescence of this long, rigid and efficient electrodonor spacer seems not affected by the presence of the BOX unit under their closed form and emission wavelength as well as quantum yield are similar to thus reported for similar compound.<sup>[62]</sup> The commutation of both BOX units induces a shift of the emission band towards the red region due to the extension of its conjugation to the whole molecule but also drop off the luminescence quantum yield. Several hypotheses could be envisioned to explain this decrease. As example, more degrees of freedom brought by the pendant alkyl chain of each indoleninium unit and the loss of rigidity by the system (no more band structuration are observed in **OO** form) have to be considered as they could allow a more efficient non radiative de-excitation in agreement with the observed luminescence lifetimes reduction. Nevertheless, the improvement of polar character as well as the possibility to observe exciplex formation

cannot be discarded for the moment more detailed photophysical studies have to be performed in order to obtain a clear explanation.

### E.2. Two-photon absorption properties.

If the strong variation of the polarity has been successfully applied to the modulation of the first hyperpolarizability other NLO phenomena can benefit of such features. Indeed, it is commonly admit that molecular design of compounds with large two-photon absorption (TPA) cross-section includes: a long conjugated  $\pi$ -backbone system with a planar conformation; the presence of electron-donor (**D**) and electron-acceptor (**A**) groups able to promote an intense displacement of charge during the transition.

Firstly predicted by Maria Göppert-Mayer in 1931,<sup>[63]</sup> TPA is by definition a third order non-linear optical (NLO) phenomenon involving the simultaneous absorption of two photons by a molecule resulting in an electronic excited state matching the combined energy of the photons. This excited state can then relax radiatively or non-radiatively *via* the same processes as linear absorption (see figure 43). However, due to the high incident power required to observe TPA, it was not experimentally demonstrated before the invention of pulsed lasers in 1961.<sup>[64]</sup>



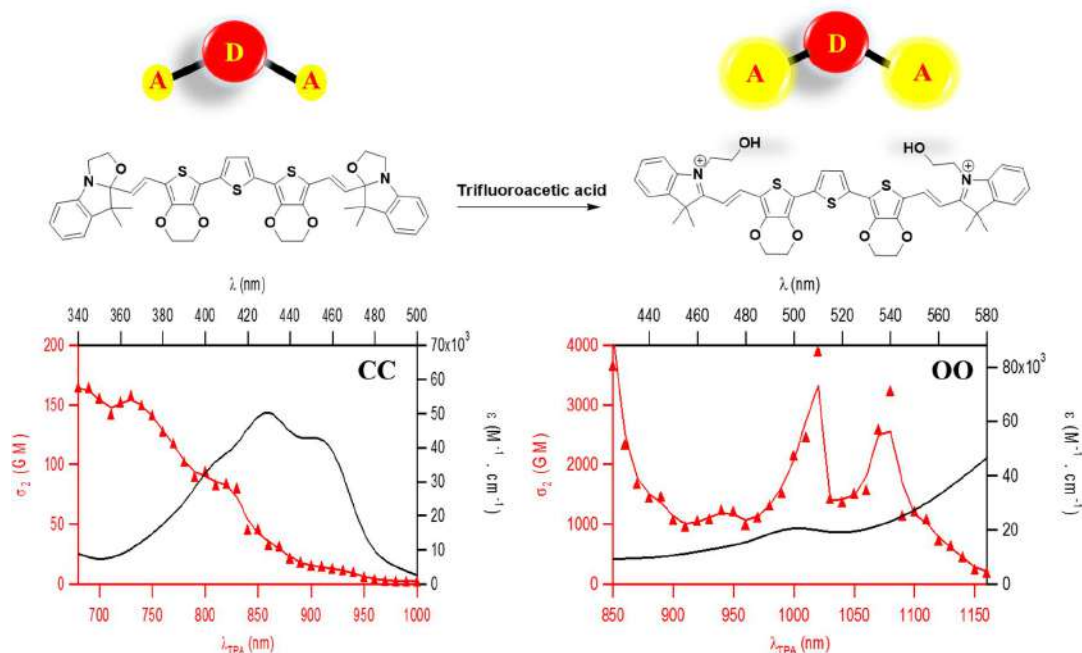
*Figure 43. Simplified diagram for IPA, TPA and emission.*

To obtain molecular system exhibiting efficient TPA cross section ( $\sigma_2$ ), several designs were investigated including classical dipolar push-pull system (**D- $\pi$ -A**) but also quadrupolar structures such as **D- $\pi$ -D**, **A- $\pi$ -A**, **D- $\pi$ -A- $\pi$ -D** and **A- $\pi$ -D- $\pi$ -A**.<sup>[53, 65, 66]</sup> As consequence, **CC** and **OO** forms of compound **23** exhibiting a quadrupolar structure can be considered as potential candidate for TPA.

Based on their fluorescence (*vide supra*), it was possible to determine the TPA characteristics of the two forms (**CC** and **OO**). Indeed, the TPA cross sections could be extracted from the two-photon excited fluorescence (TPEF) cross sections ( $\sigma_2\Phi$ ) when the fluorescence quantum yield is known.

Concerning compound **23**, Two-photon-excited fluorescence (TPEF) cross sections were measured using the method described by Xu and Webb<sup>[67, 68, 69, 70]</sup> and the appropriate solvent-related refractive index corrections.<sup>[69]</sup> To span the  $\lambda=680-980\text{nm}$  range, a Nd:YLF-pumped Ti:sapphire oscillator was used, generating 150 fs pulses at a 76 MHz rate. To span the  $\lambda=1000-1100\text{ nm}$  range, an OPO (PP-BBO) was added to the setup to collect and modulate the output signal of the Ti:sapphire oscillator. At each wavelength, the quadratic dependence of the fluorescence intensity on the excitation power was checked for the samples and the fluorescein reference.<sup>[67, 68, 69, 70]</sup>

The two-photon absorption spectra of the **CC** and **OO** forms of **23** are shown in Figure 44 along with their linear absorption spectra, whereas the corresponding data are listed in Table 7.



**Figure 44.** UV-absorption spectra (black) and two-photon absorption spectra (red) of compound **23** on its **CC** (left) and **OO** (right) forms.

As acceptor-donor-acceptor octupolar structure, it is not surprising to observe some TPA for both states of compound **23**. More interestingly, the TPA properties of **CC** and **OO** forms differ by their 2 photons cross section values but also by their spectral range. Indeed, the **CC** exhibits some TPA in a 680-900 nm excitation range where **OO** ones is logically bathochromically shifted to 850-1150 nm. In both cases, the one- and two-photon spectra are substantially different and degeneracy between one- and two-photon transitions are not observed suggesting a typical quadrupolar behavior. In this context, **CC** presents 3 main TPA peaks are observed at 680, 730, and 820nm exhibiting two photons cross section ranging between 82 and 165 GM (table 7). Surprisingly, the quadratic dependence of the fluorescence intensity of **OO** on the excitation power was not anymore observed below 850 nm while the  $\sigma_2$  is almost at its maximum at this wavelength (3656 GM). In fact, two other TPA peaks are observed at lower energy (1020 and 1080 nm) where the two photons cross rises more than 3000 GM (table 7).

Compound <b>23</b>	$2\lambda_{\text{abs}}^{\text{max}}$ (nm)	$\lambda_{\text{TPA}}$ (nm)	$\sigma_2\Phi$ (GM)	$\sigma_2$ (GM)
CC	858	820	28	82
		730	53	156
		680	56	165
OO	1332	1080	421	3240
		1020	506	3900
		<850	>475	>3656

*Table 7. Two-photon absorption properties of compound **23** on its CC and OO forms in acetonitrile.*

On this basis, both forms exhibit a short common spectral range (850-950 nm) where their respective TPA can be observed. In this range, the opening of both oxazolidine ring by using one of the three possible stimuli (photon, proton or electron) leads to strong variation of the two-photon-excited fluorescence color from 478 to 753 nm. The intensity of the phenomenon is also strongly affected but the important difference of luminescence quantum yield between both forms leads to only observe notwithstanding a contrast ratio around 17. As consequence, it seems that compound **23** is able to modulate its two photons cross section by at least an impressive factor 45 in this spectral range. This preliminary result represents one of the rare examples of modulation of TPA and certainly, to the best of our knowledge, one of the highest contrast ratio reported so far.

#### **IV). Conclusion**

In summary, this chapter describes the design, synthesis, analysis and theoretical approach of new multi-modal molecular switches based on the functionalization of bithiophene and EDOT-T-EDOT (simple pi-conjugated systems) by two identical BOX moieties (compounds **20**, **21**, **22** and **23**). As expected, all compounds exhibit multimodal switching abilities under acido-, photo- and electrochemical stimulation. While changing the bithiophene pi-conjugated core by EDOT-Thiophene-EDOT (better donor ability) motif still provides a

successive opening of oxazolidine rings (stepwise commutation) but without any improving on the difference of oxidation potential (very tiny difference) and its well demonstrated by spectroelectrochemistry.

Among that, the developments of such type of molecular systems possess the ability to modulate their nonlinear optical properties (second harmonic generation and two photon absorption). In this context, bithiophene series have demonstrated the feature to modulate the first hyperpolarisability of the systems between three different levels exhibiting important contrast ratios. The replacement of the bithiophene by the DOT-T-EDOT exhibiting a more important electron donor character have open new prospective for other three order NLO phenomenon. In fact, the measurement of TPA cross section of both extreme states of compound **23** (CC and OO) have revealed impressive variation in terms of efficiency but also in spectral range.



## V). References

- [1] R. Hadji, G. Szaloki, O. Aleveque, E. Levillain and L. Sanguinet, *J. Electroanal. Chem.* **2015**, 749, 1-9.
- [2] G. Sevez, J. Gan, S. Delbaere, G. Vermeersch, L. Sanguinet, E. Levillain and J. L. Pozzo, *Photochemical & Photobiological Sciences* **2010**, 9, 131-135.
- [3] G. Szaloki and L. Sanguinet, *Journal of Organic Chemistry* **2015**, 80, 3949-3956.
- [4] M. M. Bader, P.-T. T. Pham and E. H. Elandaloussi, *Crystal Growth & Design* **2010**, 10, 5027-5030.
- [5] I. Jung, H. Choi, E. Kim, C.-H. Lee, S. O. Kang and J. Ko, *Tetrahedron* **2005**, 61, 12256-12263.
- [6] B. Li, Y.-H. Wu, H.-M. Wen, L.-X. Shi and Z.-N. Chen, *Inorg. Chem.* **2012**, 51, 1933-1942.
- [7] C. Guerrin, G. Szalóki, J. Berthet, L. Sanguinet, M. Orio and S. Delbaere, *Journal of Organic Chemistry* **2018**, 83, 10409-10419.
- [8] A.-E. R. H. and A.-S. F. A., *Bulletin of the Chemical Society of Japan* **1985**, 58, 2126-2132.
- [9] L. Sanguinet, J. L. Pozzo, V. Rodriguez, F. Adamietz, F. Castet, L. Ducasse and B. Champagne, *Journal of Physical Chemistry B* **2005**, 109, 11139-11150.
- [10] L. Sanguinet, J. Berthet, G. Szalóki, O. Alévêque, J.-L. Pozzo and S. Delbaere, *Dyes and Pigments* **2017**, 137, 490-498.
- [11] N. Sertova, J. M. Nunzi, I. Petkov and T. Deligeorgiev, *Journal of Photochemistry and Photobiology A: Chemistry* **1998**, 112, 187-190.
- [12] R. Bartnik, S. Lesniak, G. Mloston, T. Zielinski and K. Gebicki, *Chem. Stosow.* **1990**, 34, 325-334.
- [13] R. Bartnik, G. Mloston and Z. Cebulska, *Chemia Stosowana* **1990**, 34, 343-352.
- [14] G. Szalóki and L. Sanguinet in *Properties and Applications of Indolinoxazolines as Photo-, Electro-, and Acidochromic Units*, Eds.: Y. Yokoyama and K. Nakatani), Springer Japan, Tokyo, **2017**, pp. 69-91.
- [15] G. r. Szalóki, O. Alévêque, J.-L. Pozzo, R. Hadji, E. Levillain and L. Sanguinet, *The Journal of Physical Chemistry B* **2014**, 119, 307-315.
- [16] Q. Chen, L. Sheng, J. Du, G. Xi and S. X.-A. Zhang, *Chemical Communications* **2018**, 54, 5094-5097.
- [17] J. K. Kochi, *Accounts of Chemical Research* **1992**, 25, 39-47.
- [18] Y. Cotelle, M. Hardouin-Lerouge, S. Legoupy, O. Alévêque, E. Levillain and P. Hudhomme, *Beilstein Journal of Organic Chemistry* **2015**, 11, 1023-1036.
- [19] Y. F. Ran, C. Blum, S. X. Liu, L. Sanguinet, E. Levillain and S. Decurtins, *Tetrahedron* **2011**, 67, 1623-1627.
- [20] T. Sasamori, N. Tokitoh; and R. Streubel in  *$\pi$ -Electron Redox Systems of Heavier Group 15 Elements*, (Ed. T. Nishinaga), John Wiley & Sons.
- [21] H. Olivier-Bourbigou and L. Magna, *Journal of Molecular Catalysis A: Chemical* **2002**, 182-183, 419-437.
- [22] L. S. Longo, E. F. Smith and P. Licence, *ACS Sustainable Chemistry & Engineering* **2016**, 4, 5953-5962.
- [23] J. Armstrong, N. Bloembergen, J. Ducuing and P. Pershan, *Physical review* **1962**, 127, 1918.
- [24] N. Bloembergen and P. Pershan, *Physical review* **1962**, 128, 606.
- [25] T. Verbiest, K. Clays and V. Rodriguez, *Second-order nonlinear optical characterization techniques: an introduction*, CRC press, **2009**, p.
- [26] K. Rottwitt and P. Tidemand-Lichtenberg, *Nonlinear optics: principles and applications*, CRC Press, **2014**, p.
- [27] e. P. Franken, A. E. Hill, C. Peters and G. Weinreich, *Physical Review Letters* **1961**, 7, 118.
- [28] T. H. Maiman, **1960**.
- [29] R. U. Khan, O. P. Kwon, A. Tapponnier, A. N. Rashid and P. Günter, *Advanced functional materials* **2006**, 16, 180-188.
- [30] P. Rentzepis and Y. H. Pao, *Applied Physics Letters* **1964**, 5, 156-158.
- [31] G. Heilmeyer, *Applied Optics* **1964**, 3, 1281-1287.
- [32] K. D. Singer, J. E. Sohn, L. King, H. Gordon, H. Katz and C. Dirk, *JOSA B* **1989**, 6, 1339-1350.
- [33] J. Woodford, M. A. Pauley and C. Wang, *The Journal of Physical Chemistry A* **1997**, 101, 1989-1992.

- [34] I. Asselberghs, K. Clays, A. Persoons, A. M. McDonagh, M. D. Ward and J. A. McCleverty, *Chemical physics letters* **2003**, 368, 408-411.
- [35] I. Asselberghs, G. Hennrich and K. Clays, *The Journal of Physical Chemistry A* **2006**, 110, 6271-6275.
- [36] E. Botek, M. Spassova, B. Champagne, I. Asselberghs, A. Persoons and K. Clays, *Chemical physics letters* **2005**, 412, 274-279.
- [37] E. Botek, M. Spassova, B. Champagne, I. Asselberghs, A. Persoons and K. Clays, *Chemical Physics Letters* **2006**, 417, 282-282.
- [38] B. J. Coe, S. Houbrechts, I. Asselberghs and A. Persoons, *Angewandte Chemie International Edition* **1999**, 38, 366-369.
- [39] J. F. Lamère, P. G. Lacroix, N. Farfán, J. M. Rivera, R. Santillan and K. Nakatani, *Journal of Materials Chemistry* **2006**, 16, 2913-2920.
- [40] M. Moreno Oliva, J. Casado, J. T. López Navarrete, G. Hennrich, M. C. Ruiz Delgado and J. Orduna, *The Journal of Physical Chemistry C* **2007**, 111, 18778-18784.
- [41] Y. Takimoto, C. Isborn, B. Eichinger, J. Rehr and B. Robinson, *The Journal of Physical Chemistry C* **2008**, 112, 8016-8021.
- [42] B. J. Coe, *Chemistry—A European Journal* **1999**, 5, 2464-2471.
- [43] R. Loucif-Saibi, K. Nakatani, J. Delaire, M. Dumont and Z. Sekkat, *Chemistry of materials* **1993**, 5, 229-236.
- [44] F. Mançois, J. L. Pozzo, J. Pan, F. Adamietz, V. Rodriguez, L. Ducasse, F. Castet, A. Plaquet and B. Champagne, *Chemistry—A European Journal* **2009**, 15, 2560-2571.
- [45] F. Mançois, L. Sanguinet, J.-L. Pozzo, M. Guillaume, B. Champagne, V. Rodriguez, F. Adamietz, L. Ducasse and F. Castet, *The Journal of Physical Chemistry B* **2007**, 111, 9795-9802.
- [46] L. Sanguinet, J.-L. Pozzo, M. Guillaume, B. Champagne, F. Castet, L. Ducasse, E. Maury, J. Soulié, F. Mançois and F. Adamietz, *The Journal of Physical Chemistry B* **2006**, 110, 10672-10682.
- [47] L. Sanguinet, J.-L. Pozzo, V. Rodriguez, F. Adamietz, F. Castet, L. Ducasse and B. Champagne, *The Journal of Physical Chemistry B* **2005**, 109, 11139-11150.
- [48] F. Bondu, R. Hadji, G. r. Szalóki, O. Alévêque, L. Sanguinet, J.-L. Pozzo, D. Cavagnat, T. Buffeteau and V. Rodriguez, *The Journal of Physical Chemistry B* **2015**, 119, 6758-6765.
- [49] R. Terhune, P. Maker and C. Savage, *Physical Review Letters* **1965**, 14, 681.
- [50] V. Rodriguez, J. Grondin, F. Adamietz and Y. Danten, *The Journal of Physical Chemistry B* **2010**, 114, 15057-15065.
- [51] F. Castet, E. Bogdan, A. Plaquet, L. Ducasse, B. Champagne and V. Rodriguez, *The Journal of chemical physics* **2012**, 136, 024506.
- [52] S.-J. Chung, M. Rumi, V. Alain, S. Barlow, J. W. Perry and S. R. Marder, *Journal of the American Chemical Society* **2005**, 127, 10844-10845.
- [53] C. Katan, F. Terenziani, O. Mongin, M. H. Werts, L. Porres, T. Pons, J. Mertz, S. Tretiak and M. Blanchard-Desce, *The Journal of Physical Chemistry A* **2005**, 109, 3024-3037.
- [54] C. Katan, S. Tretiak, M. H. Werts, A. J. Bain, R. J. Marsh, N. Leonczek, N. Nicolaou, E. Badaeva, O. Mongin and M. Blanchard-Desce, *The Journal of Physical Chemistry B* **2007**, 111, 9468-9483.
- [55] S. J. Pond, O. Tsutsumi, M. Rumi, O. Kwon, E. Zojer, J.-L. Brédas, S. R. Marder and J. W. Perry, *Journal of the American Chemical Society* **2004**, 126, 9291-9306.
- [56] F. Castet, T. Lerychard, K. Pielak, G. Szalóki, C. Dalinot, P. Leriche, L. Sanguinet, B. Champagne and V. Rodriguez, *ChemPhotoChem* **2017**, 1, 93-101.
- [57] J. Roncali, P. Blanchard and P. Frère, *Journal of Materials Chemistry* **2005**, 15, 1589-1610.
- [58] S. S. Zhu and T. M. Swager, *Journal of the American Chemical Society* **1997**, 119, 12568-12577.
- [59] M. Turbiez in *Nouveaux systèmes conjugués linéaires intégrant des motifs 3, 4-éthylènedioxythiophènes (EDOT): synthèse et étude des propriétés électroniques*, Vol. Angers, **2003**.
- [60] E. Pardieu, A. Saad, L. Dallery, F. Garnier, C. Vedrine, F. Hauquier, P. Dalko and C. Pernelle, *Synthetic Metals* **2013**, 171, 23-31.
- [61] Q. Qi, X. Fang, Y. Liu, P. Zhou, Y. Zhang, B. Yang, W. Tian and S. X.-A. Zhang, *RSC Advances* **2013**, 3, 16986-16989.
- [62] S. Zhen, J. Xu, B. Lu, S. Zhang, L. Zhao and J. Li, *Electrochimica Acta* **2014**, 146, 666-678.
- [63] M. Göppert-Mayer, *Annalen der Physik* **1931**, 401, 273-294.
- [64] W. Kaiser and C. Garrett, *Physical review letters* **1961**, 7, 229.

- [65] M. Drobizhev, A. Karotki, A. Rebane and C. W. Spangler, *Optics letters* **2001**, *26*, 1081-1083.
- [66] F. Terenziani, O. V. Przhonska, S. Webster, L. A. Padilha, Y. L. Slominsky, I. G. Davydenko, A. O. Gerasov, Y. P. Kovtun, M. P. Shandura and A. D. Kachkovski, *The Journal of Physical Chemistry Letters* **2010**, *1*, 1800-1804.
- [67] M. A. Albota, C. Xu and W. W. Webb, *Applied optics* **1998**, *37*, 7352-7356.
- [68] S. de Reguardati, J. Pahapill, A. Mikhailov, Y. Stepanenko and A. Rebane, *Optics express* **2016**, *24*, 9053-9066.
- [69] M. H. Werts, N. Nerambourg, D. Pélégry, Y. Le Grand and M. Blanchard-Desce, *Photochemical & Photobiological Sciences* **2005**, *4*, 531-538.
- [70] C. Xu and W. W. Webb, *JOSA B* **1996**, *13*, 481-491.



---

**Chapter 3: Synthesis and  
characterization of new multi-level  
systems.**

---



## **I). Introduction**

In the previous chapter, we have demonstrated that the functionalization of a linear pi-conjugated system by two BOX units is an elegant manner to elaborate some interesting multimodal molecular switches exhibiting acido-, electro- and photochromic properties. For all prepared systems we have noticed that:

- a stepwise opening of both indolinoxazolidine units linked by a conjugated motif is observed with a selectivity *ratio* which can depend on the nature of the stimulation,
- the use of a conjugated linker which exhibits a lower oxidation potential seems to any improvement of the selectivity under electrochemical stimulation. At the opposite, the greater stability of the generated radical cation impacts strongly the kinetic of the opening process by electromediated process,
- the successive oxazolidine ring opening induces a strong variation of the optical properties. As consequence the 3 different states (open-open, open-close, close-close) exhibit reproducible and specific properties, especially in NLO.

Considering these first systems as proof of concept, the next objective was to explore the possibility to extend this concept by increasing the number of BOX, and then of metastable states, on one single molecule. Indeed, as mentioned before, the enhancement of the number of metastable states brings new perspectives to the design of molecular-scale high-density optical memory or multinary logic devices.<sup>[1, 2]</sup> Within this context, some important questions have to be addressed such as:

- The requirement of an electroactive linker exhibiting some stability upon oxidation.
- The possibility to control the BOX opening sequence by playing on the nature of the conjugated bridge.

In order to answer to these questions, this chapter deals with the syntheses and characterizations of multi-level and multi-modal molecular switches bearing 3 BOX units. All these systems are potentially able to exhibit up to four discriminate metastable states. Based on two different central nodes, a simple phenyl ring or a triarylamine system, seven novel molecular switches were prepared and studied.

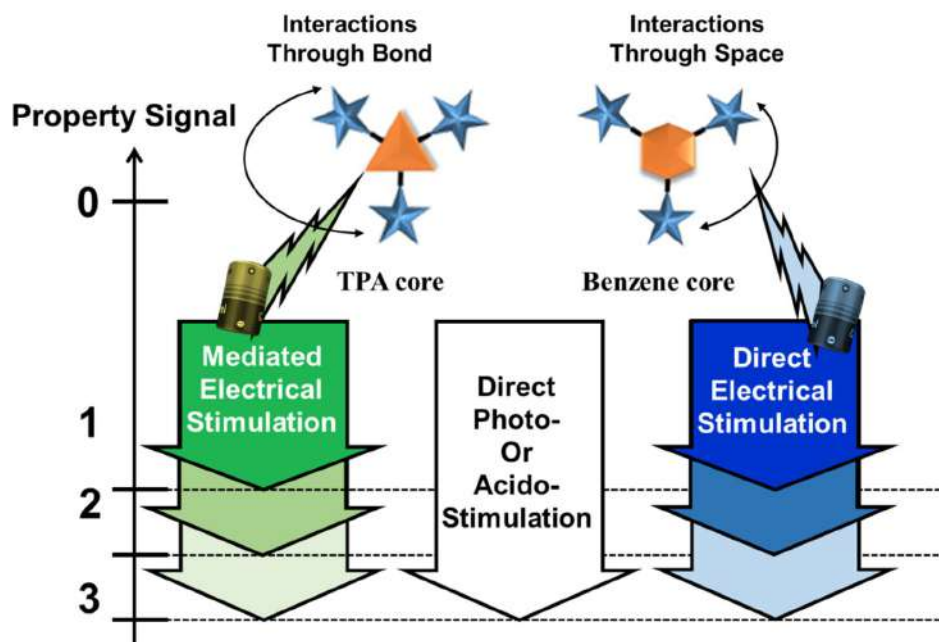


Figure 1. Switching features of tri-BOX conjugated system as multilevel molecular system.

If in all cases the opening of the oxazolidine ring should be induced either under UV irradiation, electrochemical stimulation or acidity changes,<sup>[3]</sup> the structural variation introduced here will allow investigating separately the influence of two types of interactions on the selectivity efficiency. To expect some selectivity, the BOX units have to be placed in a specific spatial arrangement in order to promote interaction between them either through bond when electrostimulation occurs on the central organic core or through space when the BOX are directly stimulated. On one hand, systems based on central phenyl core (figure 1) allows a straightforward access to compounds presenting BOX moieties close in the space and linked by a high oxidation potential aromatic linker. On the other hand, the series of molecules based

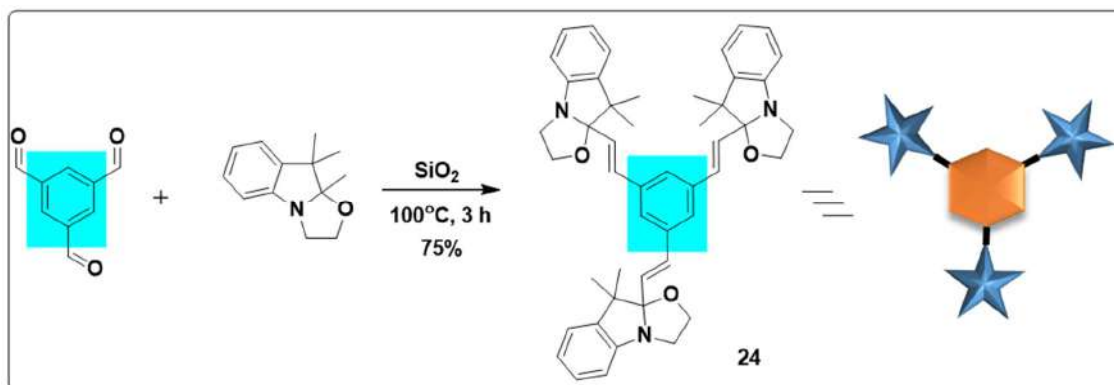
on a triarylamine node present linkers with lower, adjustable and dissymetrizable oxidation potentials (figure 1) allowing to modulate the interactions between BOX units.

The studies about both families are detailed in the next following sections.

## II). Association of three BOX units to a benzene core

### A. Synthesis.

According to previous results, the functionalization of an aromatic node by three BOX units could be simply resumed to a condensation between the corresponding aromatic system bearing three aldehyde functions and the trimethylindolino-oxazolidine using the already reported silica-mediated procedure under solvent free-conditions.<sup>[4]</sup> According to that, the compound **24**, chosen as model, was obtained starting from a commercially available benzene-1,3,5-tricarbaldehyde in a satisfactory yield of 75% as shown in scheme 1.



*Scheme 1. Synthetic route to compound 24.*

Obtained as a yellow powder, the <sup>1</sup>H NMR (presented on Figure 2) of compound **24** presents all characteristics of closed BOX derivatives.

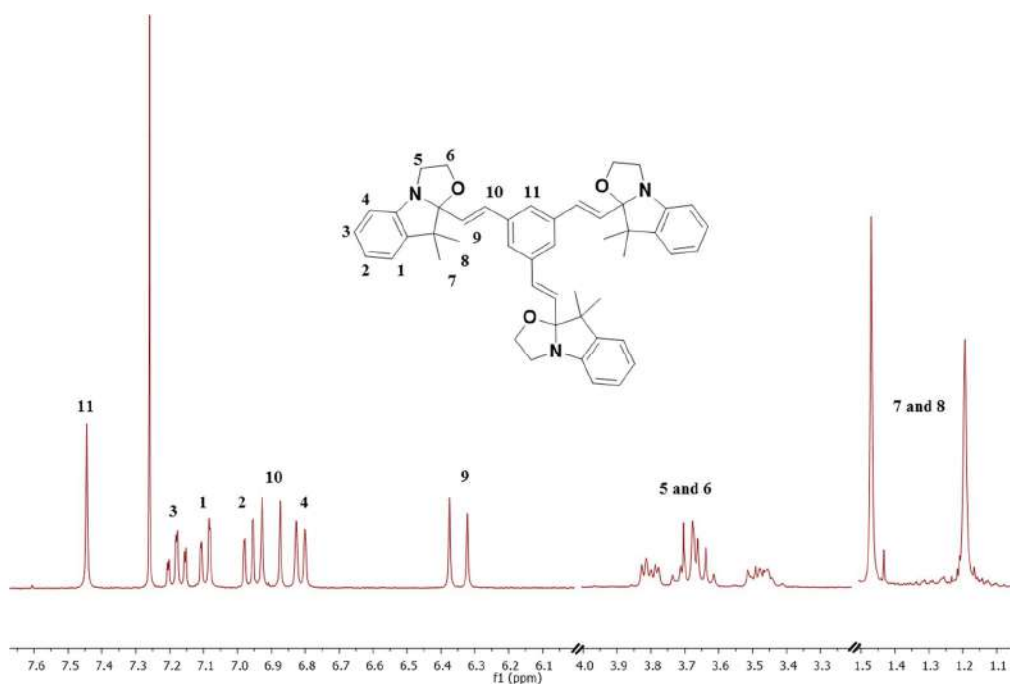


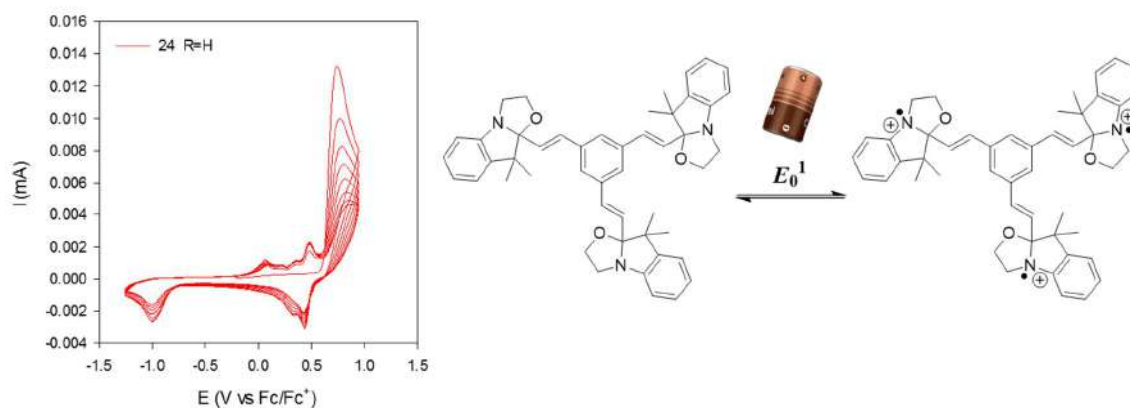
Figure 2.  $^1\text{H}$  NMR spectrum of compound 24 in chloroform ( $\text{CDCl}_3$ ) at rt.

Due to its  $\text{C}_3$  symmetry, the NMR spectrum is very simple, and, thanks to our previous studies, the complete assignment of different signals can be easily reached. As observed on previous BiBOX series, a doublet corresponding to one proton of the  $\text{C}=\text{C}$  linkage (9) is easily distinguishable at 6.35 ppm. Its  $J$  coupling constant of 15.9 Hz demonstrates unambiguously the all trans isomer form of the system (no trace of the cis-isomer was detected). Concerning the second ethylenic proton (10), it is down field shifted at 6.90 ppm. The closed status of all BOX units are confirmed by the observation of the two singlets at 1.47 and 1.19 ppm related to the germinal methyl groups (7 and 8) on the indoline and series of multiplets corresponding to the methylene groups adjacent to the nitrogen and oxygen atom (5 and 6) ranging from 3.46 to 3.83 ppm. Concerning the aromatic protons range, the global  $\text{C}_3$  symmetry of the molecular system is confirmed by the assignment of all protons of the central phenyl ring to only one singlet at 7.45 ppm. They are completed by the signals of the indolenine moieties which are constituted by two doublets at 6.81 and 7.09 ppm (1 and 4) and 2 triplets at 6.96 and 7.18 ppm (2 and 3) exhibiting a vicinal coupling constant of 7.7 Hz.

If this first model demonstrates the easy access to such derivatives, it does not represent an ideal platform for electrochromism studies.

#### B. Commutation and abilities.

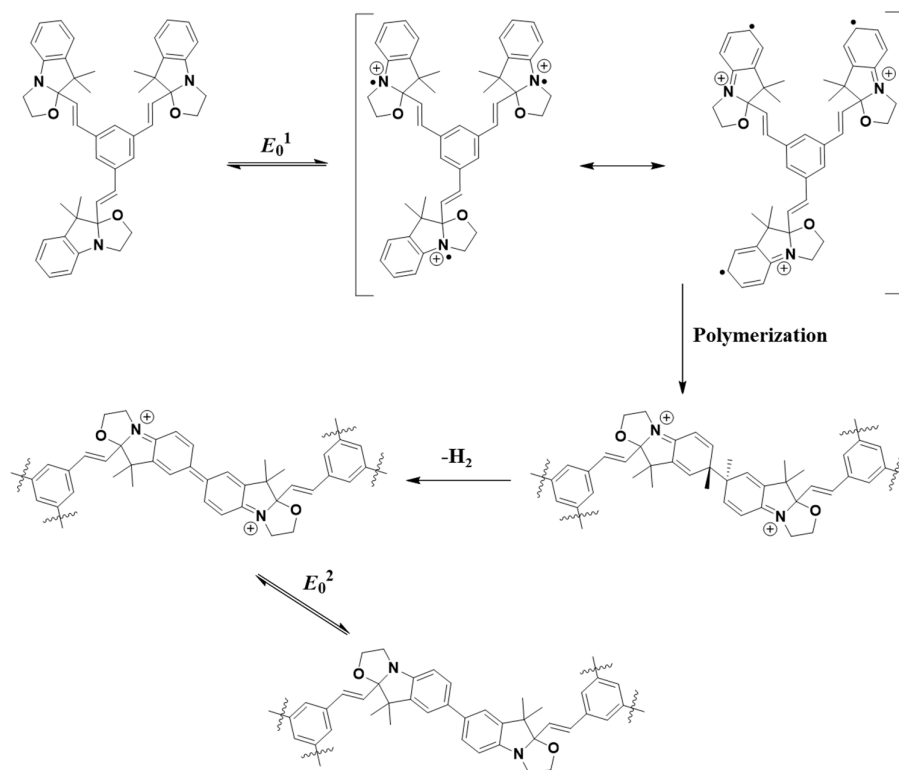
Indeed, as already shown and discussed,<sup>[5, 6, 7, 8, 9]</sup> it is important to notice that the association of BOX to a pi-conjugated system exhibiting a higher oxidation potential will probably lead to a direct stimulation not only by photon or proton, but also by electrochemical stimulation. In this case, it has already been demonstrated that, in absence of substituent on the position 5 of the BOX, dimerization (C-C oxidative coupling) can occur upon oxidation instead of opening.<sup>[10]</sup> In this context, the electrochemical behavior of compound **24** has been investigated by cyclic voltammetry (figure 3).



**Figure 3.** Cyclic voltammetry of compound **24** in ACN (1.28 mM) with TBAPF<sub>6</sub> as electrolyte (0.1M) on Pt working electrode at 100mV.s<sup>-1</sup>.

As expected, the cyclic voltammetry of compound **24** reveals one non reversible oxidation process at 0.74 V which is assigned to the concomitant oxidation of all three BOX units (direct stimulation). In fact, due to the absence of any substituent in position 5 of the indoline, this oxidation leads also to a C-C intermolecular oxidative coupling translated on the CV by the observation of a new redox reversible process at a lower potential (0.48 V) on the

scan back. As a consequence, we assume that the electro-stimulation of the target compound **24** conducts to an electropolymerization process as schematized on the scheme 2.



**Scheme 2.** Schematic representation of the mechanism generated upon stimulation compound **24** by an electron.

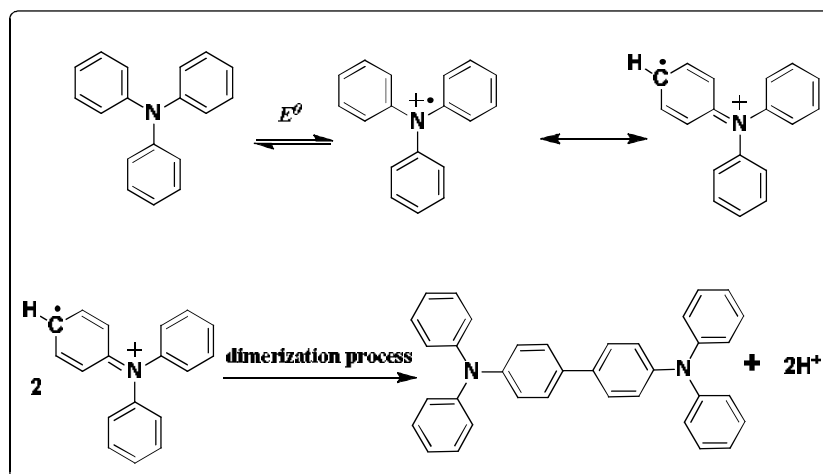
On one hand, this model appears very useful to investigate quickly the possibility to functionalize a central pi-conjugated core by three BOX units, and as consequence, explore the synthetic pathways to easily prepare a molecular system able to exhibit four different states under various stimulations. On the other hand, the electropolymerization observed on this system has convinced us to do not push further the investigations on their commutation abilities. Indeed, as observed in previous chapter, the acido- and photochromic properties of several BOX units connected to a central pi-conjugated bridge are less sensitive to the microenvironment of the molecule than electrochromic ones and should logically lead to a global mixture of the four different states. If this electro-polymerization could be avoided by the functionalization of the BOX in position 5, results of the chapter 2 convinced us to replace benzene with an electroactive core exhibiting lower oxidation potential than BOX ( $E_{\pi} < E_{BOX}$ ). Indeed, it should lead to an

electro-mediated stimulation favoring the opening of the BOX in a stepwise manner. With this objective, triphenylamine derivatives have been selected as a pi-conjugated cores.

### III). Association of three BOX units to a symmetrical

#### Triphenylamine system

Triphenylamine (TPA), an aromatic amine with a strong electron-donating nature, constitutes the basic node of an important group of modern electroactive functional materials showing semiconducting properties, sometimes used as organic electronics and optoelectronics. [11, 12, 13] Within the functional TPA moiety, the nitrogen center can be easily oxidized and unsubstituted TPA are known to undergo dimerization process leading to tetraphenylbenzidine (scheme 3).<sup>[13, 14]</sup>

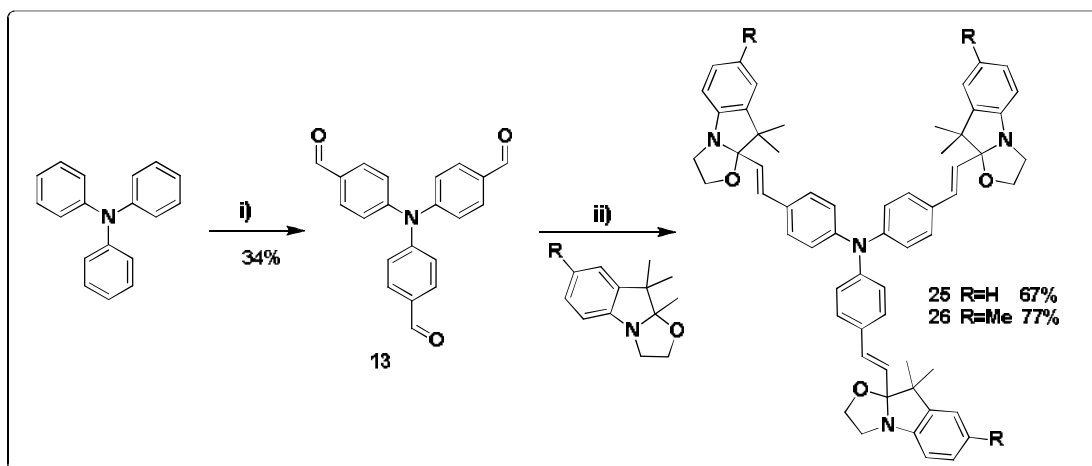


Scheme 3. Dimerization of TPA via the radical cation form.<sup>[13]</sup>

#### A. Synthesis.

On this basis, the first molecular system envisioned consists in a direct functionalization of the triphenyl amine by three BOX units. In such purpose, the convergent strategy successfully applied for the preparation of the different BiBOX systems was also adopted here. Based on the condensation between an aromatic aldehyde and the corresponding

trimethylindolino-oxazolidine derivative as final step, the syntheses of our first targeted compounds are resumed in scheme 4.

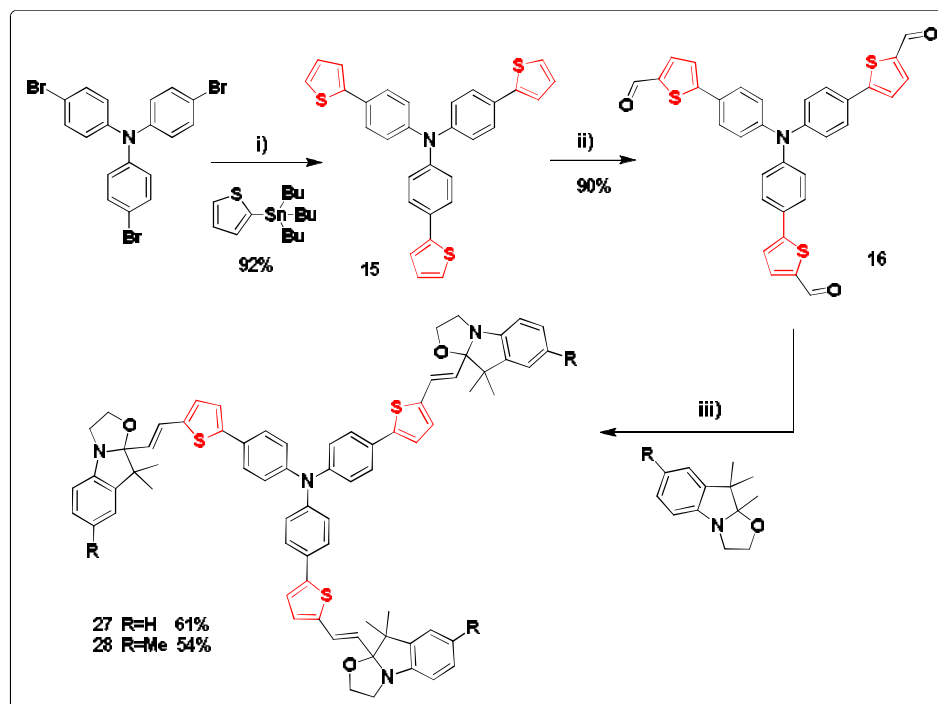


*Scheme 4. Synthetic route to compounds 25 and 26. i) DMF, POCl<sub>3</sub>; ii) silica gel, 100°C, 7 hours.*

Compounds **25** and **26** were efficiently prepared in two steps starting from triphenylamine. Already described,<sup>[16]</sup> the first step involves the synthesis of the 4,4',4''-nitrotribenzaldehyde compound **13** by Vilsmeier-Hack formylation with POCl<sub>3</sub> and DMF, in 34% yield. Concerning the condensation reaction with the different trimethylindolino-oxazolidine, it is important to note that we have to drastically increase the reaction time up to 7 hours in order to ensure the full conversion of the aldehyde derivative that can simplify the purification of the system. In these conditions, the two compounds **25** and **26** were obtained in satisfactory good yields of 67 and 77% respectively as shown in scheme 4.

As mentioned above, the TPA derivatives were largely used in molecular electronics especially as p-semiconductor material. In this context, numerous structural investigations were explored including the enhancement of the three pi-conjugated systems borne by the nitrogen atom. The latter is generally employed to tune the absorption properties as well as the electrochemical ones.<sup>[17]</sup> As a consequence, a second generation of molecular systems resulting

from the extension of the pi-conjugated system by a thiophene unit has been envisioned and prepared as depicted in scheme 5.



**Scheme 5.** Synthetic route to compounds **27** and **28**. i)  $\text{Pd}(\text{PPh}_3)_4$ , toluene; ii) DMF,  $\text{POCl}_3$ , 1,2-dichloroethane. iii) silica gel,  $100^\circ\text{C}$ , 7 hours.

A similar strategy as those already developed was applied for the preparation of compounds **27** and **28** in three steps starting from commercially available tris(4-bromophenyl)amine as resumed in scheme 5. The first step consists to extend the pi-conjugated system through a Stille cross-coupling reaction using tributyl(thiophen-2-yl)stannane and leads to compound **15** in 92% yield. Subsequently, a Vilsmeier-Haack formylation with  $\text{POCl}_3$  and DMF in 1,2-dichloroethane conducts to the trialdehyde compound **16** in 90% yield. Finally, its condensation with corresponding trimethylindolinooxazolidine derivatives under solvent-free conditions allows the obtainment of the targeted molecular systems **27** and **28** in descent yield (61 and 54 % respectively).

Obtained as yellow powders, the structures of all 4 compounds were confirmed by  $^1\text{H}$  NMR spectroscopy as presented in figure 4 and 5.

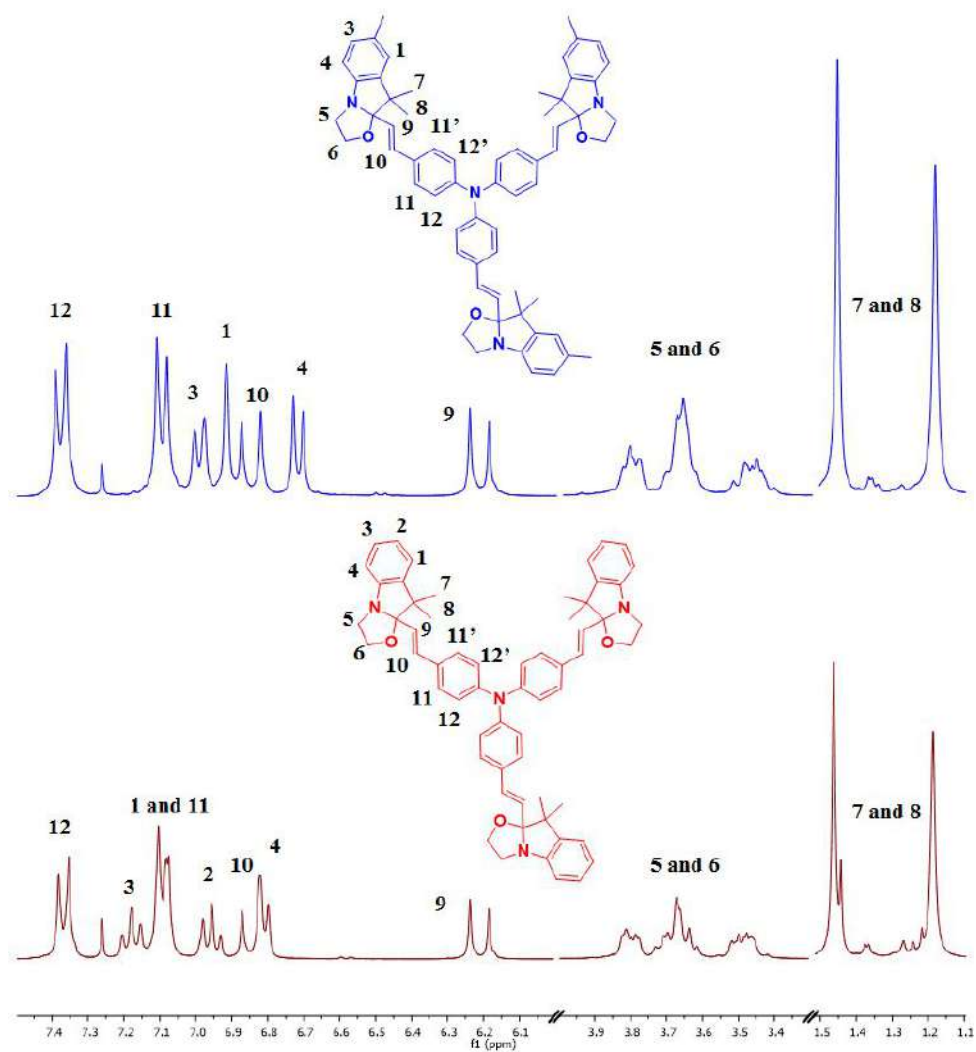


Figure 4. <sup>1</sup>H NMR spectra of compounds 25 and 26 in chloroform (CDCl<sub>3</sub>) at rt.

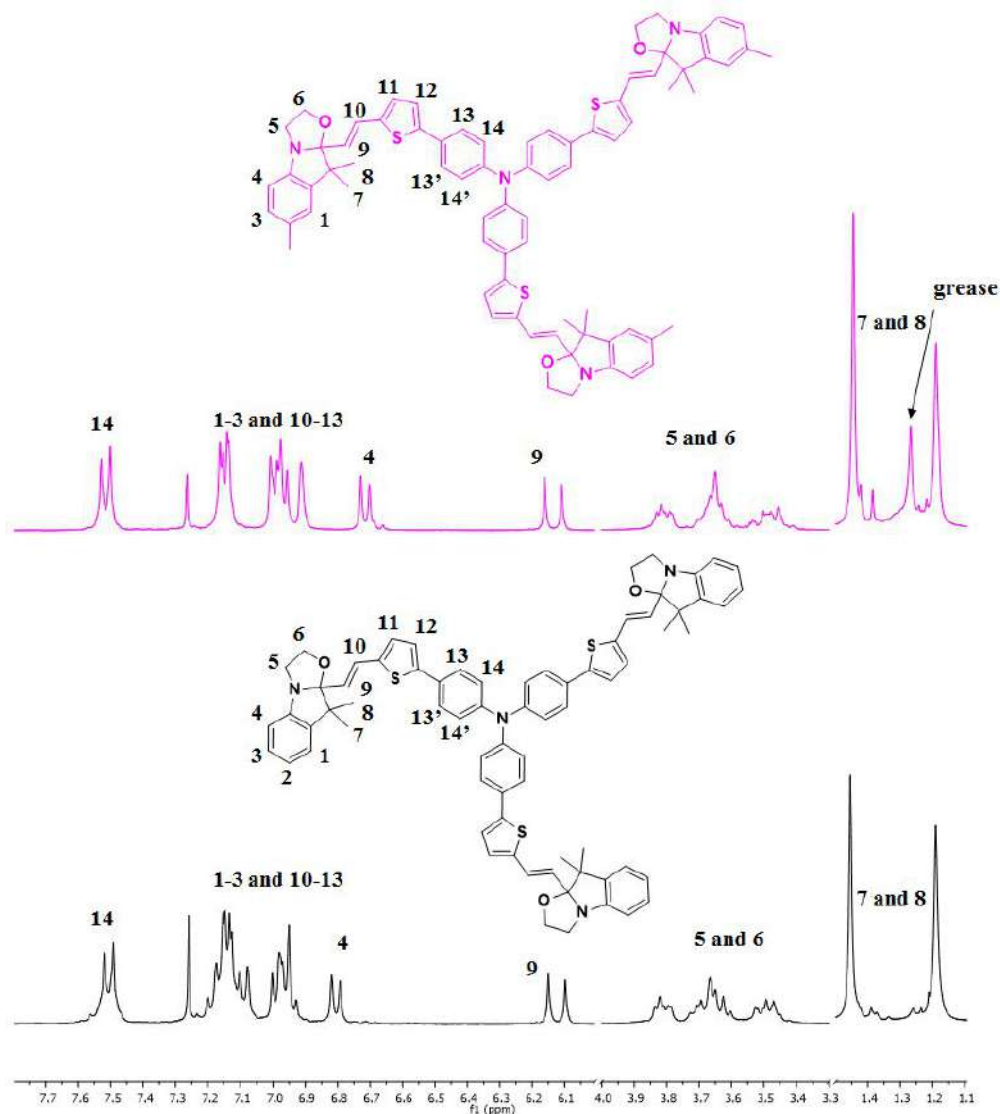


Figure 5. <sup>1</sup>H NMR spectra of compounds 27 and 28 in chloroform (CDCl<sub>3</sub>) at rt.

Here again, the C<sub>3</sub>-symmetry of compounds, allowed by the propeller shape geometry of the triphenylamine central core, leads to an easy lecture of spectra. As one can observe, all spectra exhibit the main characteristics indicating that all systems are in their closed-closed-closed form with ethylenic bridges in their trans isomery such as:

- An easily distinguishable doublet corresponding to one proton of the C=C linkage (9) with a J coupling constant around 16 Hz,

### Chapter 3: Synthesis and characterization of new multi-level systems.

- A series of multiplets corresponding to the methylene groups adjacent to the nitrogen and oxygen atom (5 and 6) ranging from 3.4 to 3.9 ppm,
- The two singlets around 1.5 and 1.2 ppm related to the methyl groups (7 and 8).

These easily accessible  $C_{3v}$ -symmetric molecular systems bearing 3 BOX moieties can be considered as multiresponsive molecular systems. Concerning the opening of the BOX units, it is important to note that their commutation can follow either "all-in" and/or "step-wise" route. More important, we have seen in previous BiBOX series that this commutation mode is strongly affected by the nature of the stimulation. As consequence the acido-, photo- and electro-chromic properties of this new TriBOX derivatives were investigated and are presented below.

#### B. Commutation and abilities.

##### B.1. Acidochromic properties.

All the "TriBOX" systems prepared exhibit relative low absorption properties in visible range under their closed-closed-closed (CCC) form. In fact, the spectra of compounds **25-28** are similar and reveal one simple absorption band with a maximum absorption wavelength in the near UV domain (table 1). Once again, we can notice the poor effect of the lateral substituents on the absorption maxima wavelength of the different systems under their CCC form. This behavior is explained by the break of the conjugation between the triarylamine moiety and the indoline due to the  $sp^3$  hybridization of the carbons in position 2. Thus **25-26** on one side and **27-28** on the other one present identical maximum absorption wavelengths at respectively 351 and 393 nm. This expected 42 nm bathochromic shift between both series can be easily explained by the extension of their pi-conjugated system.

Compound	$\lambda_{ccc}$ (nm)	$\lambda_{occ}$ (nm)	$\lambda_{ooc}$ (nm)	$\lambda_{ooo}$ (nm)
Triphenylamine	296			
13	369			
25	351	551	558	554
26	351	551	559	559
15	347			
16	414			
27	393	571	577	576
28	393	571	577	578

**Table 1.** UV-Visible spectra of compound **25**, **26**, **27** and **28** under their CCC form in ACN solution and the evolution of the maxima absorption wavelength (in nm) under their different metastable states.

To rationalize these experimental observations, simple theoretical calculations were performed using B3LYP hybrid functional and 6311G(d) basis set and IEFPCM model to take in account solvation effect. As behavior of **25-26** on one side and **27-28** on the other one are awaited similar, only one of those was studied. These calculations are completed by derivative **24** where the 3 BOX units are linked together by using a phenyl spacer and the resulted geometric optimizations are gathered in table 2.

On one hand for **24** and on the other hand for NPh-Box and N(PhT)-BOX derivatives the HOMO and the LUMO compound appear respectively pseudo-degenerated due to symmetry purposes. Beside this, important difference is noticed on triarylamine derivatives in comparison to compound **24**.

First of all, it must be underlined that, the HOMO of compound **24** is strictly localized on the BOX unit in agreement with the observation of some electro-polymerization in CV (*vide supra*) confirming its direct stimulation by redox media. In contrary, the HOMO energetic levels of triarylamine derivatives appear localized on the central node including the vinylene

bridge (table 2) which represents a prerequisite in order to obtain the stimulation of BOX units through an electromediated process. Logically the extension of the electron rich conjugated systems decreases the HOMO level. Thus, compound **28** which possesses the longer conjugated system presents the higher HOMO level as the lower one is exhibited by **24**. Similarly, compound **28** also presents the lower LUMO level (and thus the higher electron acceptor ability) as the two other compounds exhibit analogous levels.

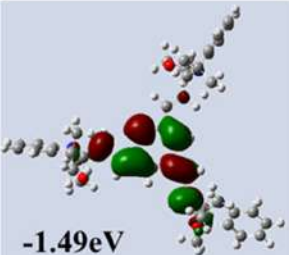
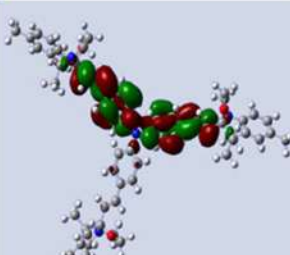
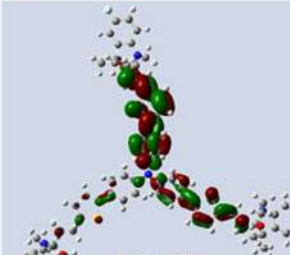
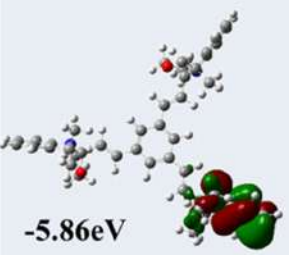
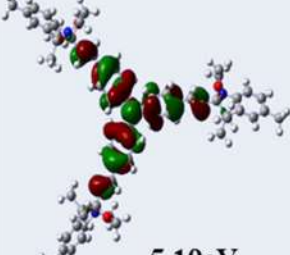
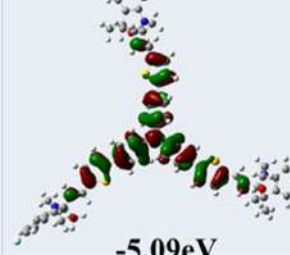
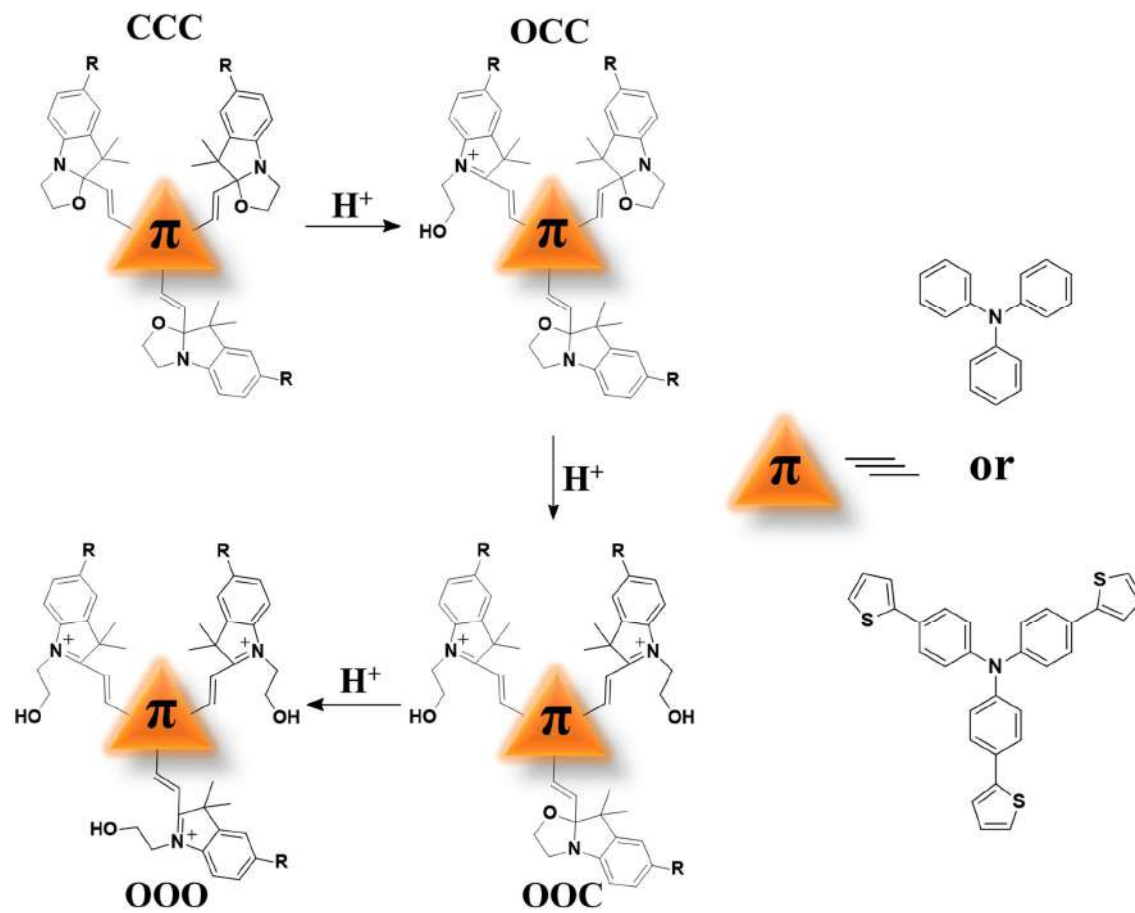
CCC form	Ph-BOX	NPh-BOX	N(Ph-T)BOX
LUMO	 -1.49eV	 -1.49eV	 -1.94eV
HOMO	 -5.86eV	 -5.19eV	 -5.09eV

Table 2. DFT visualization of compounds **24**, **26** and **28** displaying the HOMO and LUMO under their fully closed form.

More important, the TriBOX derivatives **26** and **28** exhibit a band gap value of 3.7 and 3.15 eV respectively which correspond roughly to their absorption maxima wavelengths (351 and 393nm respectively). As a consequence, the main absorption can reasonably be assigned to a  $\pi \rightarrow \pi^*$  transition mainly localized on the central triarylamine core.

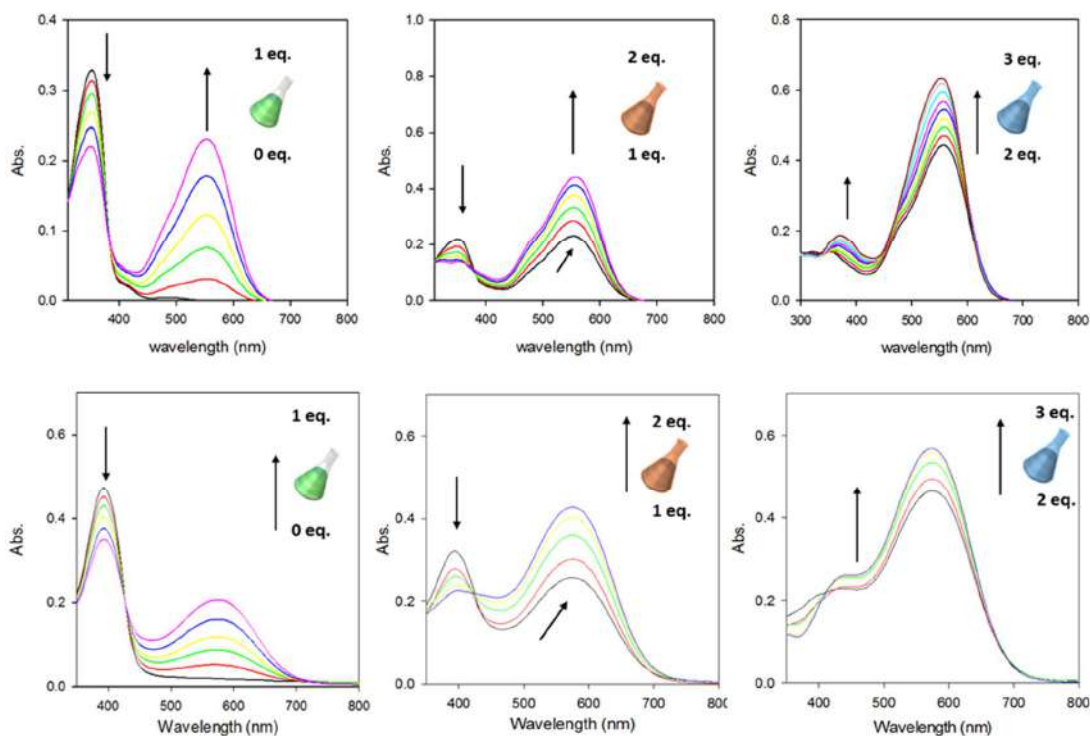
As already observed, the association of several indolinooxazolidine units with the organic core may not affect their acidochromic properties since acid acts directly onto BOX (direct stimulation). As a consequence, the presence of three switching units lets presume the

possibility to progressively generate four different states (due to geometrical restriction) under acidic stimulation, referenced later in the text as **CCC**, **OCC**, **OOC** and **OOO** depending on closed (**C**) or open (**O**) status of each BOX units (Scheme 6).



**Scheme 6.** Representation of the 4 different states of the molecular system: **CCC**, **OCC**, **OOC** and **OOO**, depending on closed (c) or open (o) status of BOX units.

As expected, the addition of some aliquots of acid (HCl) to a solution of the compound under its **CCC** form leads to the generation of a deep purple coloration due to the appearance of an intense broad band in the visible 450-650 nm and 590 to 690 nm range for compounds **25/ 26** and compounds **27/28** respectively (Figure 6). This strong variation of the absorption properties translates unambiguously the commutation of the different BOX units. More important, we can observe in all cases, an irregular evolution of the UV-Visible spectra along the titration with acid aliquots (Figure 6).



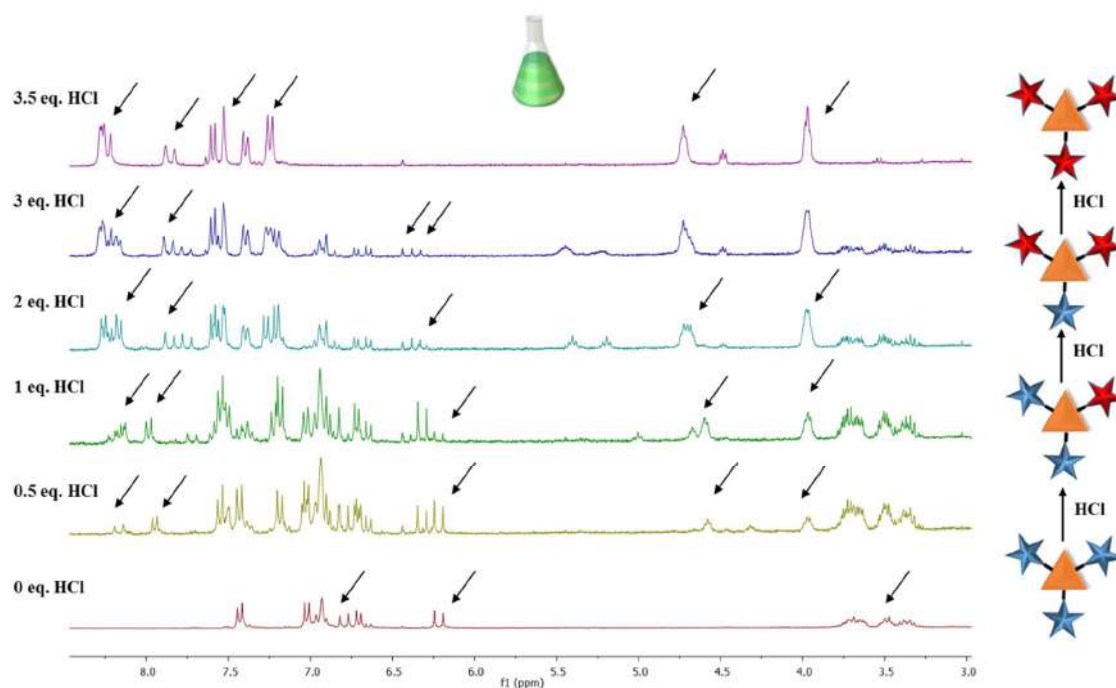
**Figure 6.** UV-Visible spectrum changes of a solution of compounds **26** (top) and **28** (bottom) in ACN (0.0086 and 0.0071mM respectively) upon addition of HCl aliquots.

As example for compound **26**, up to one equivalent, the UV spectra reveal the appearance of a unique band centered at 551 nm as well as a strong decrease of the band intensity at 351 nm assigned to the **CCC** form. The presence of one isosbestic point at 376 nm indicating an equilibrium between two species is also observed. Based on previous studies, we can then suggest that below one equivalent the **CCC** form is gradually transformed to the **OCC** form due the selective opening of only one BOX unit. When the addition of acid is pushed up to two equivalents, we notice an enhancement of the solution coloration with the complete disappearance of the band at 351 nm. In addition, a bathochromic shift of the main absorption band from 551 nm to 559 nm is observed with a generation of a new isosbestic point at 382 nm suggesting a new equilibrium which is assigned to the commutation from the **OCC** to the **OOC** form. In order to induce the commutation of the last closed BOX unit and reach the **OOO** form, the addition of HCl have to be continued beyond 2 equivalents. It results from this addition a

hyperchromic effect on the main visible absorption band. If the third BOX opening did not induce any variation of the maximum absorption wavelength, we can notice the appearance of a new higher energy band at 364 nm.

If the monitoring of the titration of our molecular systems by UV-Visible spectroscopy let us suggest a commutation of the connected BOX units in a stepwise manner, it didn't allow the clear structural identification of the different isomers. For this reason, a monitoring of the commutation by NMR spectroscopy offers an unambiguous identification of the various isomers formed upon the stimulation of a molecular system.

As mentioned many times in this manuscript, the specificity of some NMR signals of the BOX closed form, especially the proton of the ethylenic junction, represent a powerful and convenient manner to track the commutation of the molecular system. In this context, the evolution of NMR spectrum of compound **26** upon the addition of acid have been recorded (Figure 7) in order to follow the opening of the different BOX units.



**Figure 7.** Monitoring the titration of compound **26** (4.62 mM) in ACN-*d*<sub>3</sub> by HCl at 20°C.

Under its initial stage (the three BOX units are closed), the targeted molecules are perfectly symmetrical and only one doublet at 6.2 ppm with a coupling constant of 15.7 Hz is observed. Adding acid (HCl) induces a decrease of intensity of this doublet and an important complexification of the spectrum. More important, it is possible to notice the appearance of 3 new doublets at higher chemical shifts 6.3, 8.0 and 8.4 ppm respectively. Two of them (6.3 and 8.4 ppm) exhibit a vicinal constant coupling of 15.9 Hz and, as consequence, can be directly assigned to the ethylenic protons. Exhibiting an integration ratio close to 2, we can assume that the addition of the acid below one equivalent conducts specifically to the opening of only one BOX unit and the corresponding **OCC** form. Concerning the third doublet at 8.0 ppm, it is assigned to the protons of phenyl group. Indeed, the generated indoleninium moiety acting as strong electron withdrawing group, an important low field shift of the signal of the aromatic proton placed in ortho position is logically expected. An analogous behavior is noticed when the addition of acid is pursued up to two equivalents. Indeed, the three previous doublets (6.3, 8.0 and 8.4 ppm) disappear and are replaced by 3 new chemical shifts (6.4, 7.8 and 7.9 ppm) in agreement with the opening of a second oxazolidine ring. When the addition of acid is continued up to 3.5 equivalents, a simplification of the spectrum is noticed in agreement with the regeneration of the molecular symmetry due to the opening of the third BOX unit (figure 7). As consequence, all ethylenic protons of the compound **26** under its **OOO** form are represented by two doublets at 7.9 and 8.3 ppm exhibiting a scalar coupling constant of 15.7 Hz.

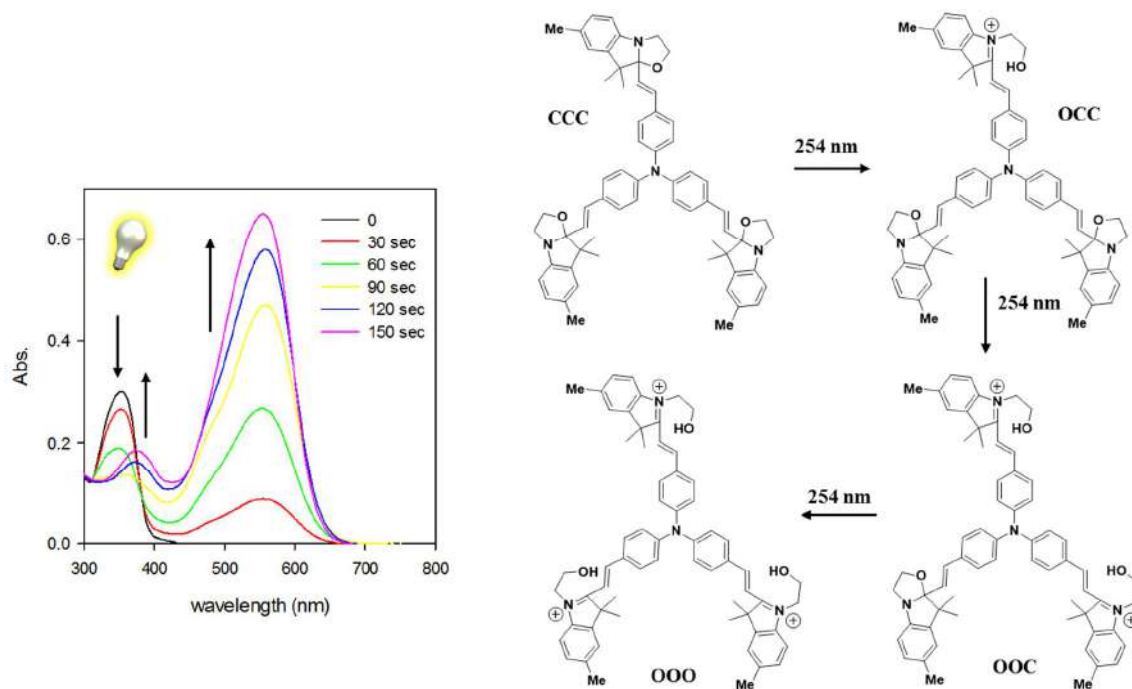
To conclude, the proton NMR spectroscopy confirms unambiguously the stepwise commutation of the three BOX units in triarylamine derivatives upon stimulation with acid. Moreover, the structure and the conservation of the full trans isomer of the compound whatever the state of the molecular system (**CCC**, **OCC**, **OOC** and **OOO**) is well corroborated especially by the value of scalar coupling constant around 16 Hz for all ethylenic protons. Unfortunately, it can be noticed that this selective addressability of each three BOX is not perfectly efficient

as in our previous BiBOX series. In fact, the CCC states is still easily observed after one equivalent as well as the OCC after 2 equivalents and at least 3.5 equivalent are required to fully displace these equilibrium to the OOO form. In this case, it was not possible to calculate the quantification of each form due to the very complicated system. In particular, the doublets of the ethylenic junction of the different states are too close to each other to assure their perfect integration. The substitution of the indoline position 5 by a fluor atom should circumvent this issue thanks to the  $^{19}\text{F}$  NMR. In this context, the syntheses of corresponding analogs were undertaken as well as NMR studies that are still under progress.

Knowing the influence of the nature of the stimulation on the addressability selectivity of system bearing several BOX units, the other kind of stimuli were explored starting by their photochromic behavior.

#### B.2. Photochromic properties.

According to previous work, it was proved that using light irradiation can also induce the opening of the oxazolidine ring. In this context, the photochromic properties of compounds **25-28** were investigated by performing the irradiation at 254 nm of a corresponding solution of CCC form in mixture of acetonitrile and chlorobenzene (90/10 in vol.). Starting from an almost colorless solution, a strong coloration is well observed in all cases. However, due to the strong similarities along this series, only the monitoring of the commutation of compound 26 by UV-Visible Spectroscopy is reported below (figure 8)



**Figure 8.** UV-Visible spectrum changes of a solution of compound **26** in ACN/PhCl (9/1) (0.0086mM) upon irradiation at 254 nm.

In this example, the UV irradiation leads quickly to the strong coloration of the solution before reaching a photostationary state after 2.5 min. More important, the overlapping of the UV-visible spectra obtained by either irradiation or acidic titration is noticed. The quantitative restoration of the initial state of the system can be obtained by adding some base to irradiated solution confirming the multi-modal switching abilities of these molecular systems.

Again, the evolution of the UV-Visible absorption spectra as a function of the irradiation time lets clearly appear different stages. Below 1.5 min of irradiation duration, the reduction of the absorption at 351 nm, assigned to the **CCC** state, concomitant with the appearance of an absorption band centered at 551 nm, corresponding to the **OCC** form, as well as the presence of one isosbestic point at 382 nm suggest an equilibrium between both species. Upon longer irradiation time, the visible absorption band continues to increase but is also bathochromically shifted (from 551 to 559 nm) and associated with the observation of a new weak band at higher energy (364nm) which are the spectral characteristic of **OOO** states. As in BiBOX series, it

appears that the first photoinduced opening of oxazolidine ring occurs quicker than the two others. Less efficient, these last require longer irradiation time.

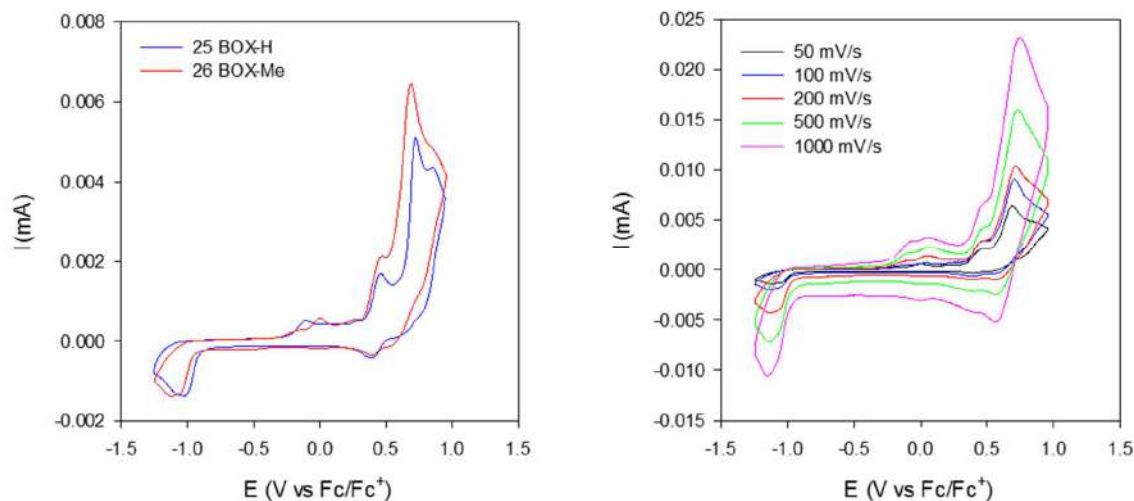
Unfortunately, the study of the photoconversion process of compound **26** by  $^1\text{H}$  NMR in the same conditions of solvent appears tedious due to the proximity of the ethylenic protons of the different forms **OCC**, **OOC** and **CCC**. In this context, we have chosen to focus our attention on the electrochromic properties of our system which should be more influenced by the nature of the pi-conjugated node.

#### B.3. Electrochromic properties.

As mentioned above, BOX opening can be also induced by an electromediated process when this unit is associated with an electroactive moiety such as bithiophene.<sup>[9]</sup> At the opposite of acid and light stimuli during which the processes are mainly localized on the BOX units, upon oxidation, a non-direct stimulation can occur. Consequently, such electrochemical process should lead to a better selectivity of commutations than other kinds of stimulations.

Indeed, after the first opening which leads to the **OCC** compound, the central pi-conjugated system becomes substituted by an open electron withdrawing BOX which decreases the global donor ability of the whole molecule what could then disadvantage further oxidation and consecutively the second and third oxazolidine ring opening.

In this context, the electrochemical behavior of all compounds has been investigated by cyclic voltammetry.



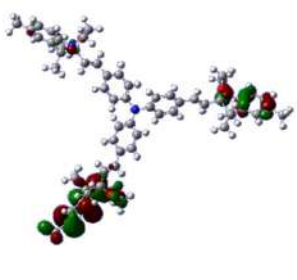
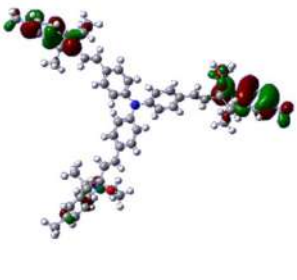
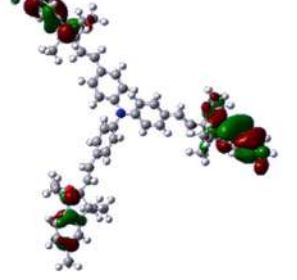
**Figure 9.** Cyclic voltammetry of compounds **25** and **26** in ACN (1.15 and 1.09 mM) with TBAPF<sub>6</sub> as electrolyte (0.1M) on Pt working electrode at 50mV.s<sup>-1</sup> (left), different scan rates of compound **25** (right).

As we can see on Figure 9, compounds **25** and **26** present similar behaviors and their voltamperograms exhibit several successive electrochemical processes (figure 9). Under their CCC form, BOX units and central triaryl amine moieties can be considered as 4 independent pi-conjugated systems. In this context, we presume that the first quasi-reversible oxidation process occurring at 0.47 V is mainly localized on the triarylamine part. This first oxidation leads to the generation of the corresponding radical cation which can be delocalize in the close vicinity of a BOX unit and can induce its opening through an electromediated process. Indeed, the supposed localization of the radical cation is corroborated by literature as oxidation potential values of many tri-para-substituted triphenylamine ranging from 0.1 to 0.84V vs Fc/Fc<sup>+</sup> (from OMe to COOMe substituent).<sup>[18]</sup> Moreover, no dimerization process was observed on the CV when any substituent is present on the indoline position 5.

As observed in the case of the BiBOX-ETE series, the triphenylamine localized radical cation appears relatively stable. As shown on figure 9, at high scan rate it appears pseudo-reversible and the scan rate has to be reduced below 100mV/s to notice the complete disappearance of its anodic peak. In these conditions, the radical cation has enough time to

undergo the chemical process leading presumably to the opening of one BOX unit (**OCC** state). The assignation of the second oxidation peak occurring at 0.72 and 0.69V for compounds **25** and **26** respectively is trickier. Indeed, we have to keep in mind that under their closed form each three BOX units and the central triarylamine core behave independently. Based on our results on BiBOX-ETE which exhibit also a relative stability of the radical cation generated during the first oxidation, we could presume that this second oxidation process is mainly localized on all remaining closed BOX units of the system (whatever the oxidation status of the central core and the open/close state of adjacent BOX units). This hypothesis is supported by four different factors:

- the oxidation potential values are in agreement with the oxidation potential of isolated BOX <sup>[7]</sup>
- the variation of the second oxidation potential by changing the nature of the substituent of the BOX (H or Me) <sup>[7]</sup>
- the high charge exchange by comparing the intensity of the first and second oxidation which can be due to the presence of 3 BOX on each triarylamine core
- theoretical data display that the HOMO-1/HOMO-2/HOMO-3 are all exhibiting almost the same energy level and symmetrical localizations (on the lateral BOX) as shown in the table 3 below.

HOMO-1	HOMO-2	HOMO-3
-5.72 eV	-5.73 eV	-5.73 eV
		

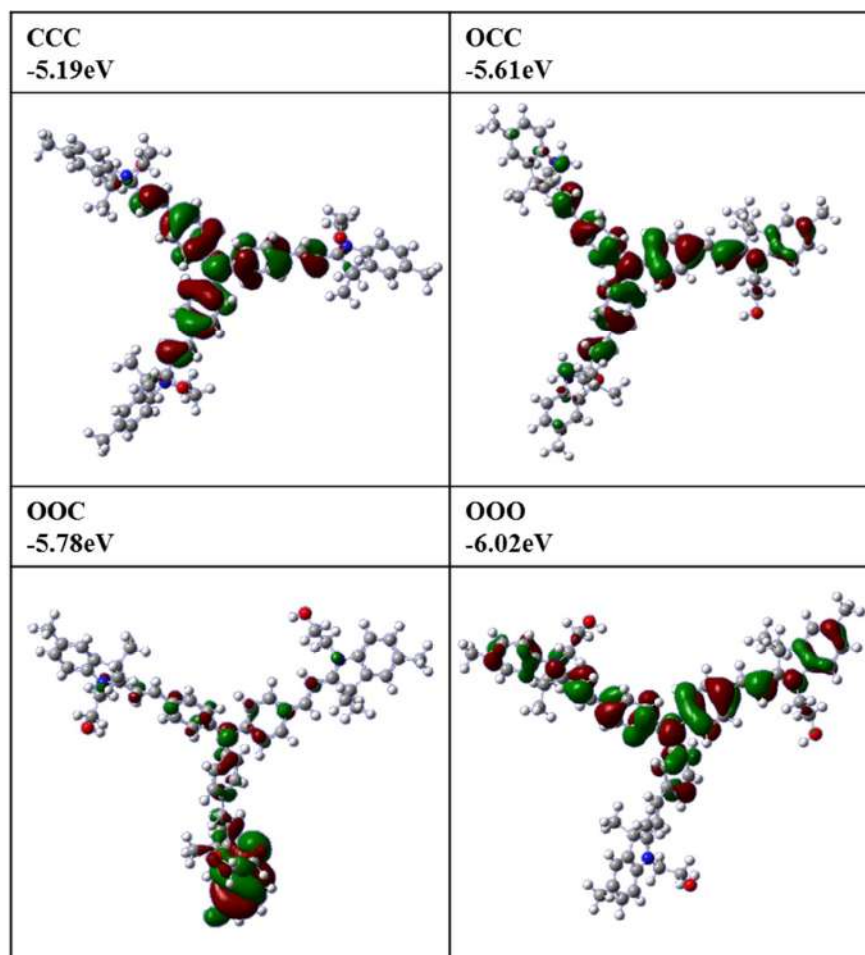
*Table 3. DFT visualization of the HOMO-1, HOMO-2 and HOMO-3 levels of compound 26 under its fully closed form.*

Based on our previous studies, the opening of some BOX units through an electromediated process at 0.47 V is perfectly sustained by the appearance of a new system on the scan back at -1.02V and -1.12V for compound **25** and **26** respectively. However, the counting of the opening BOX units at this potential is difficult. As in the case of BiBOX series (see chapter 2), the poor variation of absorption maxima between **OCC**, **OOC** and **OOO** states induce some difficulties to clarify it by spectroelectrochemistry experiments. In addition, the low reactivity of the generated radical cation exhibiting its own spectral characteristic will complicate seriously the identification of each species. Nevertheless, theoretical calculations suggest:

- the HOMO of the different states (**CCC**, **OCC** and **OOC**) are mainly localized on the central pi-conjugated node allowing an eventual opening of remained closed BOX unit(s) by an electromediated process (see Table 4).

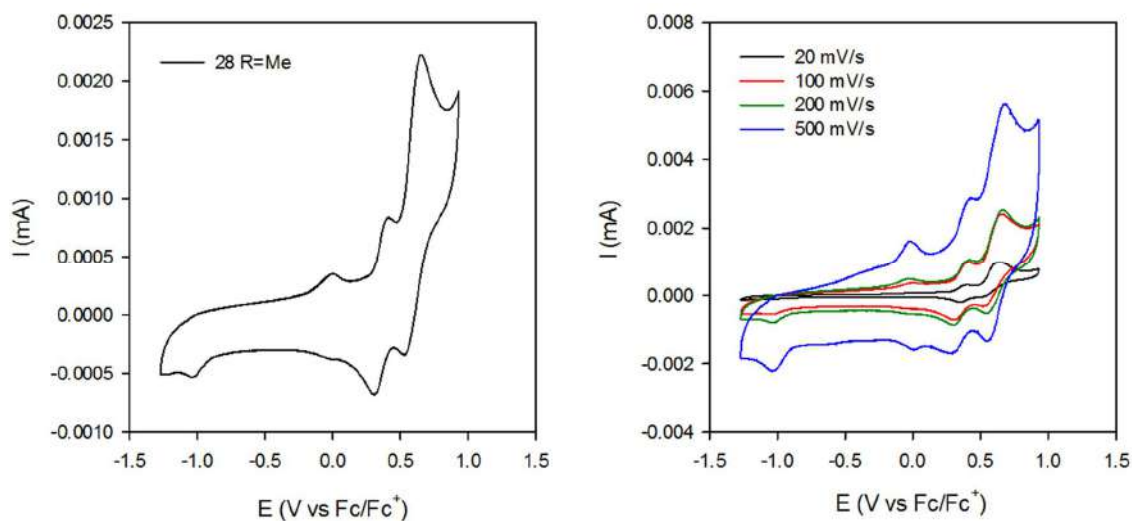
- as in the case of linear bridged (Bt and ETE) species, the successive BOX unit opening and generation of indoleninium EWG only lead to gradual and reasonable HOMO decreases. Indeed, the first opening induces only a decrease of the HOMO energy value of 0.34 and 0.36

eV when Bt and ETE were used as linker between two BOX units respectively. As we have observed this variation was not sufficient to observe in CV a clear differentiation of oxidation peaks between both states (**CC** and **OO**) of the molecule. In our present case, this calculated variation of energy between **CCC** and **OCC** is only slightly higher (0.42eV) and a clear separation of both oxidation process is not guaranteed. Moreover, the variation induced by the second opening, is largely reduced with only 0.18 eV between **OCC** and **OOC**. In this context, the unusual broadness of the first oxidation peak observed on the CV around 0.47 V is perfectly understandable and suggests the successive transformation from **CCC** to **OCC**, **OOC** and finally to **OOO** at very close oxidation potentials (see table 4).



*Table 4. DFT visualization of HOMO levels of compound 26 under its different forms.*

The extension of the pi-conjugated node by the replacement of the simple triphenylamine by a tris(4-(thiophen-2-yl)phenyl)amine motif (compounds **27-28**) conducts to a variation of the electrochemical behavior.



**Figure 10.** Cyclic voltammetry of compound **28** in ACN (0.69 mM) with TBAPF<sub>6</sub> as electrolyte (0.1M) on Pt working electrode at 100mV.s<sup>-1</sup> (left), different scan rates of compound **28** (right).

First, as shown on the figure 10, the CV of **28**, as its triphenyl analog (**26**), presents also two successive oxidation processes at 0.41 and 0.66V (vs 0.47 and 0.69V for **26**) assigned to the successive oxidations of the central triarylamine node and peripheral closed BOX units respectively. Logically, the introduction of three thiophene moieties to increase the conjugation, non only allows a moderate cathodic shift of the first oxidation process <sup>[19]</sup> but also, and more importantly, leads to a full reversibility whatever the scan rate (figure 10, right) of this first redox process. Thus, the radical cation is now enough stabilized to prevent its efficient delocalization in the close vicinity of the BOX and then its opening. This assumption is supported by DFT calculations which show that the HOMO level (Figure 11) of compound **28** presents a reduction of its electronic density on the ethylenic bridge.

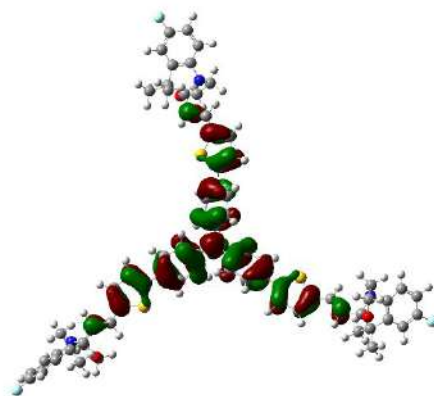


Figure 11. HOMO of *N*(Ph-T)BOX under its fully closed form.

As consequence, the radical cation should require a longer time to undergo the chemical steps leading to the opening of the BOX unit than in triphenylamine analogs.

To verify this assumption, the commutation of the systems **25-28** was investigated by using  $\text{NOSbF}_6$  ( $0.87 \text{ V vs Fc/Fc}^+$ )<sup>[20]</sup> as an oxidizing reagent and monitored by UV-Visible spectroscopy.

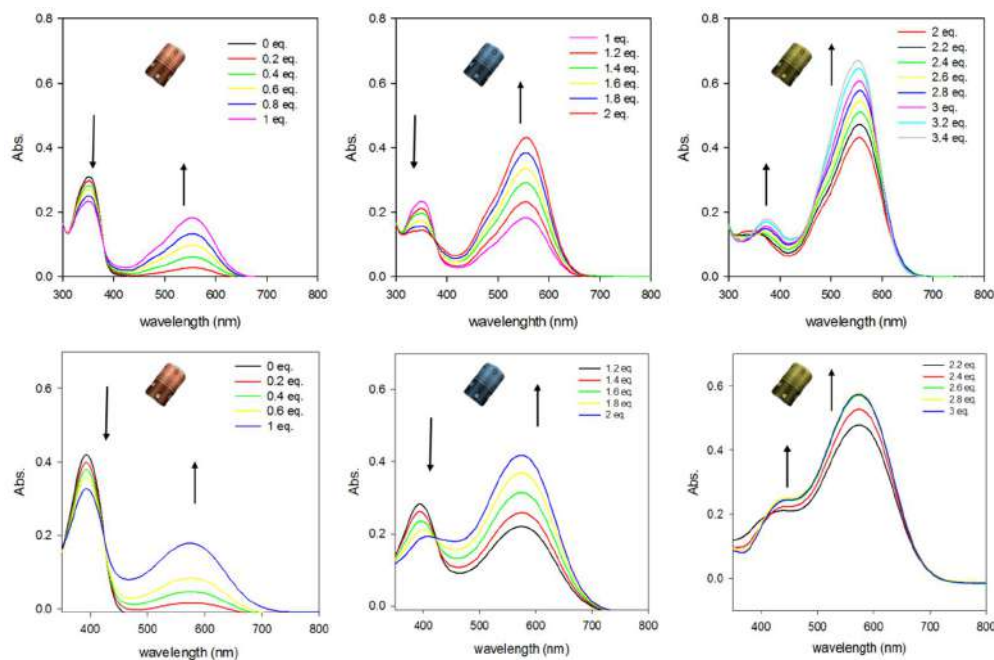


Figure 12. UV-Visible spectrum changes of a solution of compounds **26** (top) and **28** (bottom) in ACN (0.0086 and 0.0071mM respectively) upon addition of  $\text{NOSbF}_6$ .

In all cases, in chemical oxidation conditions, a drastic change of the UV-Visible spectra from the beginning of  $\text{NOSbF}_6$  addition is observed, demonstrating that the radical cation, stable in CV conditions, does allow delocalization and BOX opening in other conditions. After full oxidation, it can be noticed that the addition of oxidizing reagent leads to an identical spectrum as the one obtained after stimulation with an excess of acid and the treatment with an excess of base ( $\text{NEt}_3$ ) restore the initial spectrum as observed in previous BiBOX series.

If the UV-visible spectra obtained upon gradual chemical oxidation of compounds present strong similarities with those chemically and optically induced, subtle differences appear.

As example compound **26** shows upon addition of the first equivalent of  $\text{NOSbF}_6$  the appearance of a unique band centered at 551nm assigned to the **OCC** form (*vide supra*) associated with the concomitant decrease of the **CCC** characteristic band at 351nm. The addition of the second equivalent of oxidant leads to a bathochromic shift with a new band centered at 558nm assigned to **OOC** form as well as the disappearance of the band centered at 351nm. The opening of the third oxazolidine ring can be generated by adding more than two equivalents of  $\text{NOSbF}_6$  and induces an increased coloration of the solution due to the increase of the absorption band centered at 558 nm associated with the appearance of a new higher energy band at 364 nm. As consequence, this experiment suggests, again, the commutation of the connected BOX units in a stepwise manner in the two series of molecules despite their difference of electrochemical behavior.

To confirm the stepwise commutation of the system that also probes the selectivity of the addressability under chemical oxidation, as mentioned above, the  $^1\text{H}$  NMR spectroscopy represents an easy and convenient manner. The results of the titration of compound **25** by  $\text{NOSbF}_6$  are presented on Figure 13.

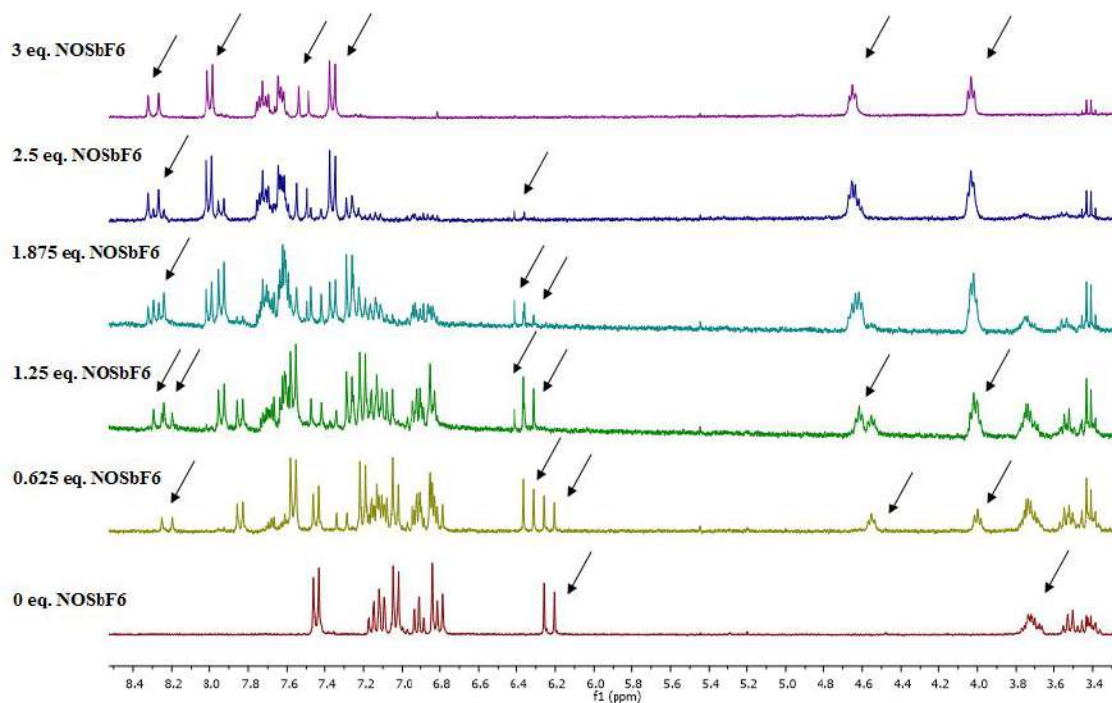
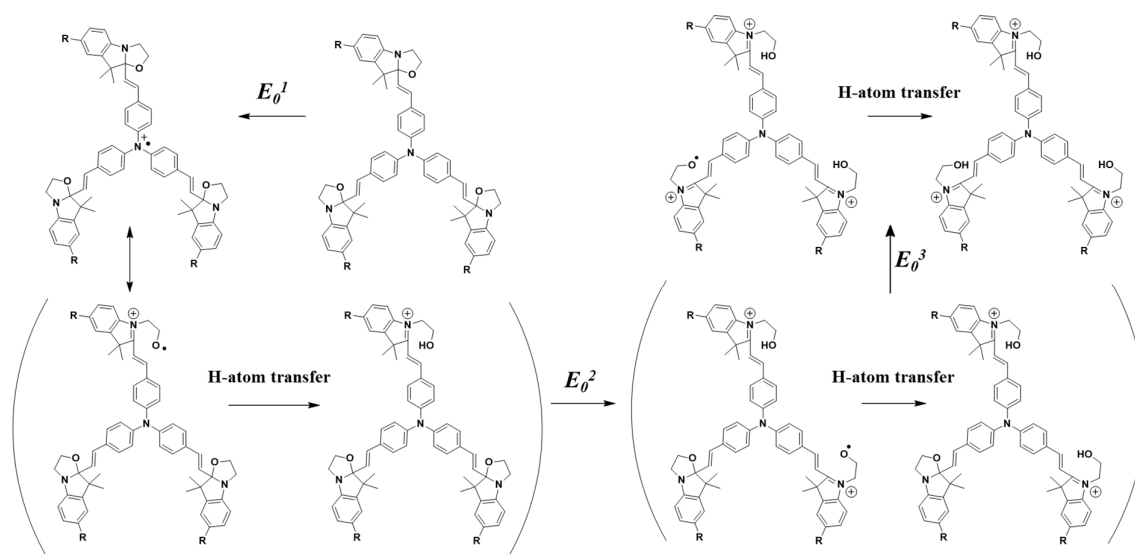


Figure 13.  $^1\text{H}$  NMR spectrum changes of a solution of compound **25** in ACN (1.54mM) upon addition of  $\text{NOSbF}_6$  aliquots.

As previously mentioned, the proton ethylenic junction NMR shift of the compound **25** is a powerful and convenient manner to track the opening of the different oxazolidine rings. Under its initial stage (the three BOX units are closed), the targeted molecules are perfectly symmetrical and only one doublet at 6.2 ppm with a scalar coupling constant of 15.7 Hz is observed. According to that, the addition of the oxidizing reagent ( $\text{NOSbF}_6$ ) below 1eq. induces the appearance of two new peaks (at 6.3 and 8.23 ppm respectively) translating a loss of the symmetry and in agreement with the opening of only one BOX unit leading to the **OCC** form. When the addition of  $\text{NOSbF}_6$  is pursued (between 1 and 2eq.), it induces a decrease of intensity of these doublets and the appearance of new doublets at higher chemical shifts (6.4 and 8.27 ppm respectively) attributable to the opening of the second oxazolidine ring. Finally, the further addition of  $\text{NOSbF}_6$  until 3 equivalents, leads to the replacement of these doublets by only two new doublets at a more shielded chemical shift 7.51 and 8.3 ppm respectively exhibiting a scalar coupling constant of 15.7 Hz, explained by the regeneration of the molecular symmetry due to

the opening of the third BOX (figure 13). Notably, it can be noted that in any state of the system (CCC, OCC, OOC and OOO), the trans isomer is observed (J coupling constant of the ethylenic junction is *c.a.* 16 Hz). Like in the cases discussed in previous chapter, the comparison of the proton NMR spectra obtained upon adding HCl or NOSbF<sub>6</sub>, as in the case of linear conjugated systems bearing only two BOX units, demonstrates the higher selectivity and efficiency of the redox addressability compared with other kind of stimulations. Thus, the electrochemical processes could be described as EC mechanisms as presented on Scheme 7.



**Scheme 7.** Proposed mechanism for the stepwise opening of three oxazolidine rings of compounds **25** and **26** under stimulation by an oxidant.

To conclude about this TriBOX series, we have demonstrated that the stepwise commutation can be obtained under acido-, photo- and electrostimulation. Nevertheless, only a strong modification of the optical properties can be observed between CCC and OCC form. Indeed, the second and third BOX opening induce only a poor bathochromic shift of the maxima absorption wavelength.

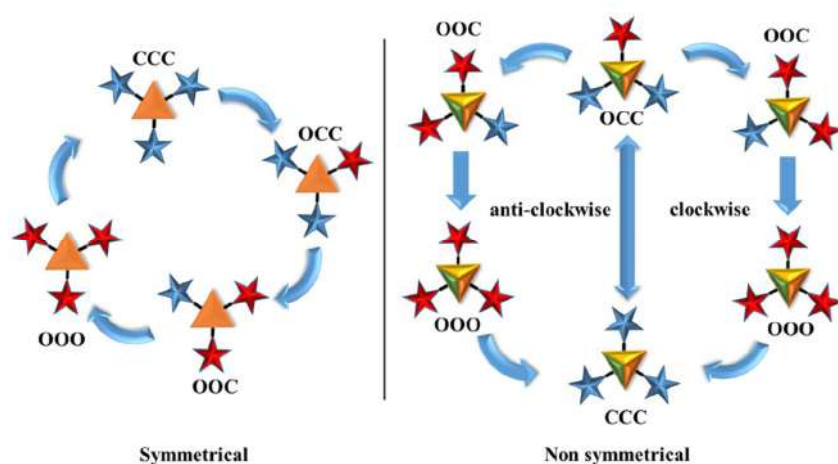
Noteworthy, despite their reversible first oxidation potentials, the behaviors of compounds **27-28**, upon chemical oxidation, are similar to those of **25-26**.

If the extension of the pi-conjugated system did not produce any drastic changes on the addressability selectivity, we have highlighted its strong influence on the opening kinetic rate under electrochemical stimulation. Indeed, the extension of the triphenylamine by a thiophene moiety in compounds **27** and **28** leads to longer pi-conjugated systems in which the delocalization to lateral ethylenic bridges of the radical cation is reduced. This limitation conducts to observe an important decrease of its reactivity and, as consequence, a slow-down of the BOX opening kinetics through an electro-mediated process. In this context, it paves the ways to elaborate new TriBOX derivatives where this difference of kinetic offers an opportunity to assure the addressability differentiation between three identical BOX units connected around an aromatic node.

#### **IV). Association of three BOX units to an unsymmetrical Triphenylamine systems**

To reach this objective, new systems based on a triphenylamine moiety were thus envisioned. To take advantage of the influence of the nature of the conjugated system on the opening kinetics, unsymmetrical compounds TriBOX molecular systems were designed. In such system, three identical BOX units were connected to a central triarylamine node by using three different pi-conjugated connectors. This dissymetrization of the compound should allow us to orient preferentially the delocalization of generated radical cation generated during the oxidation, and then the opening of the connected BOX moiety. If symmetrical TriBOX derivatives conduct to some molecular systems exhibiting a stepwise commutation between 4 different metastable states with potential applications in molecular-scale high-density optical memory or multinary logic devices,<sup>[2, 21]</sup> unsymmetrical ones offer new perspectives especially in the design of nano-molecular machines where the molecular switches involve a mechanical motion, and multicomponent add directionality control.<sup>[22]</sup> Impossible to differentiate in previous symmetrical compounds, the introduction of three different aromatic systems on the

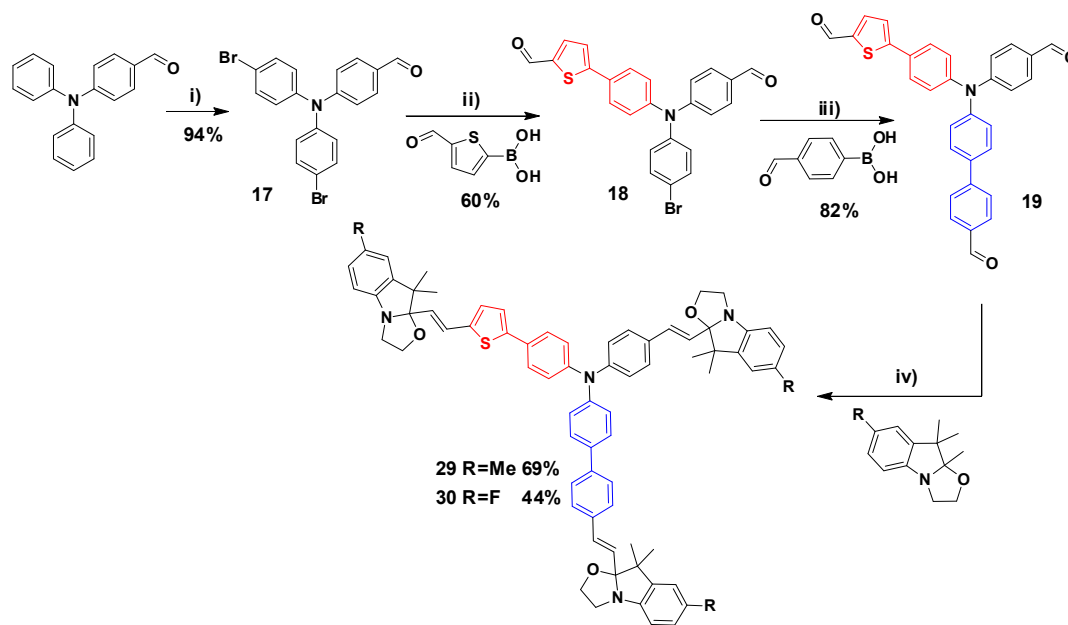
central nitrogen atom constrain us to envision two different sequences in the stepwise commutation of the system referenced later in the text as a clockwise and an anticlockwise one.



**Figure 14.** Does the dissymetrization allow the control not only of the number of BOX opened but also the prediction of which one opens first?

### A. Synthesis.

In this context, the targeted molecular systems **29** and **30** were prepared according to the convergent synthesis depicted in scheme 8.



**Scheme 8.** Synthetic route to compounds **29** and **30**. i) NBS, THF; ii) Pd(dppf)Cl<sub>2</sub>, K<sub>2</sub>CO<sub>3</sub>, Dioxane:H<sub>2</sub>O; iii) Pd(dppf)Cl<sub>2</sub>, K<sub>2</sub>CO<sub>3</sub>, Dioxane:H<sub>2</sub>O; iv) silica gel, 100°C, 7 hours.

### Chapter 3: Synthesis and characterization of new multi-level systems.

The synthetic sequence starts with the bromination of 4-(diphenylamino)benzaldehyde by NBS at 0 °C in THF affording the compound **17** in almost quantitative yield. This synthon undergoes two successive Suzuki-coupling reactions with (5-formylthiophen-2-yl)boronic acid, and then (4-formylphenyl)boronic acid to produce at the end the desired unsymmetrical tricarboxaldehyde **19** in three steps with an overall yield of 46%. As successfully used in other series, the final step, consisting in the condensation of the BOX unit on **19**, the silica mediated procedure,<sup>[23]</sup> permits to obtain targeted compounds **29** and **30** as yellow powders with satisfactory yields of 69 and 44% respectively due to some purification difficulties.

As expected, this dissymetrization have a huge impact on the complexity of the <sup>1</sup>H NMR spectrum especially in the aromatic proton range. Nevertheless, it can be noticed that the NMR spectra of compound **29** and **30** (figure 15) exhibit almost all specificities of BOX derivatives observed in previous series:

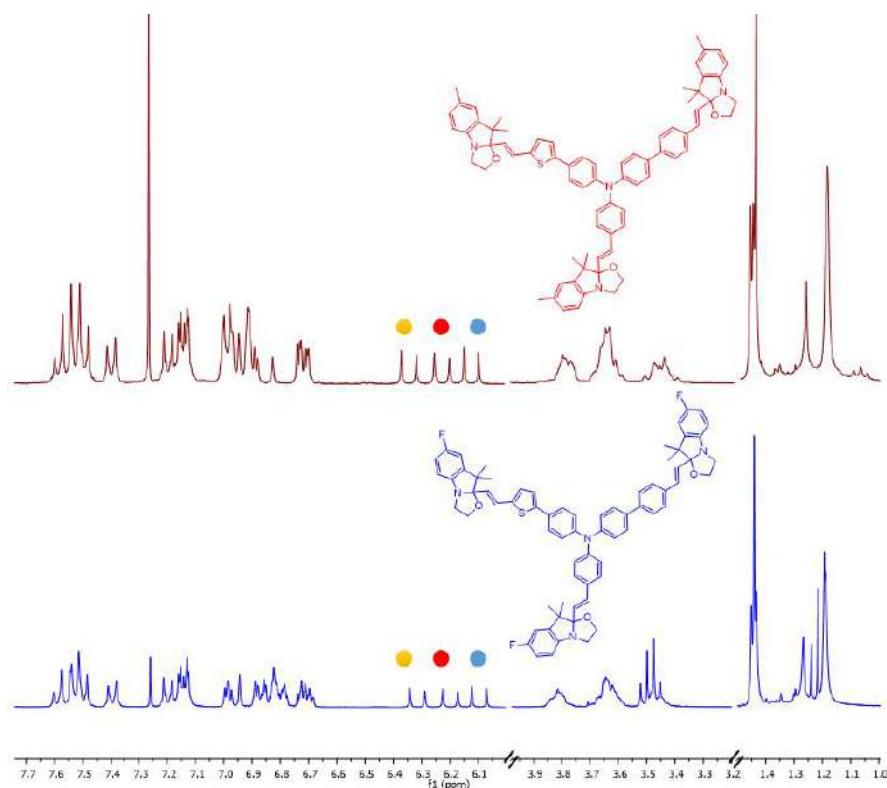


Figure 15. <sup>1</sup>H NMR spectra of compounds **29** and **30** in chloroform (CDCl<sub>3</sub>) at rt.

- The easy observation of vinylic protons around 6 ppm. Noticeably, the choice of a phenyl, a biphenyl and a phenylthiophene as pi-conjugated systems to decorate the nitrogen atom allows to observe three well discriminated doublets (at 6.12, 6.22 and 6.34 ppm) integrating for one proton each with a J coupling constant of 15.9 Hz.
- A series of multiplets corresponding to the methylene groups adjacent to the nitrogen and oxygen atom centered at 3.65 ppm.
- The presence in aliphatic region of intense peaks around 1.20 and 1.44 ppm each of them integrating for 9H and corresponding to both germinal methyl groups borne by the indoline moieties.

All these characteristics allow us to confirm undoubtedly the full closed status of the systems (CCC) as well as the full trans isomery of the three ethylenic junctions.

Naturally, the acido-, photo- and electrochromic properties of these molecular systems were studied in details and are reported in the next sections.

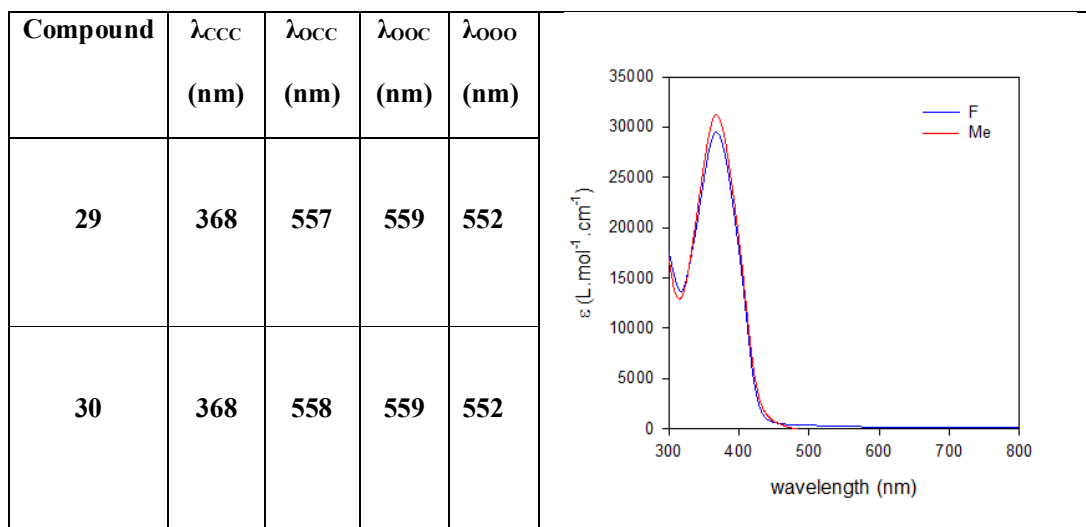
## B. Commutation and abilities.

### B.1. Acidochromic properties.

To investigate the acidochromic properties, the UV-Visible spectroscopy represents certainly the most convenient technique to monitor the commutation of elaborated systems under stimulation. Moreover, the dissymetrization of conjugated systems may also allow a better discrimination of absorbance UV-visible signatures between the four metastable systems.

As observed in other molecular systems, the substituent placed in the position 5 of the indolenine have negligible impact on the maximum absorption wavelength when the system is in its full closed form. As consequence, compounds **29** and **30** under their CCC form present almost identical UV-visible spectra with a maximum absorption wavelength of 368 nm (table 5). Interestingly, their absorption band appears 17nm bathochromically shifted compared to **25-**

26 TriBOX derivatives and in the contrary 25nm hypsochromically shifted compared to extended 27-28 ones.

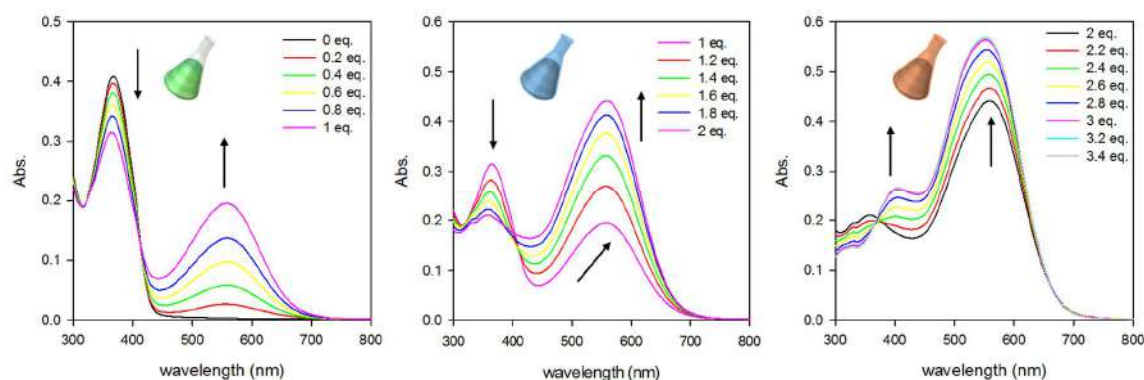


**Table 5.** UV-Visible spectra of compounds **29** and **30** under their CCC form in ACN solution and the evolution of the maxima absorption wavelength (in nm) under their different metastable states.

If one considers that the HOMO and LUMO levels of these derivatives, non-conjugated in their closed form with the pendant BOX, are probably strictly localized on the central triaryl system, it can be logical to observe an intermediate spectroscopic bandgap for **29-30**. This hypothesis can be supported by the experimental and theoretical studies of the  $C_{3V}$  symmetrical systems.

In both cases, a deep violet coloration of the solution is observed as soon as we start to add some acid aliquots (HCl) due to the appearance of an intense broad band in the visible 455-655 nm range. This expected coloration seems translating the opening of the oxazolidine rings under acidic stimulation leading to the establishment of a charge transfer band between the electron donor triarylamine moiety and the generated indoleninium acting as an electron withdrawing group. As we can see on figure 16 for compound **30** in example, we notice, as for

symmetrical analogs, an irregular evolution of the UV-Visible spectra along the titration with acid aliquots which seems translating a stepwise opening of the three BOX units.



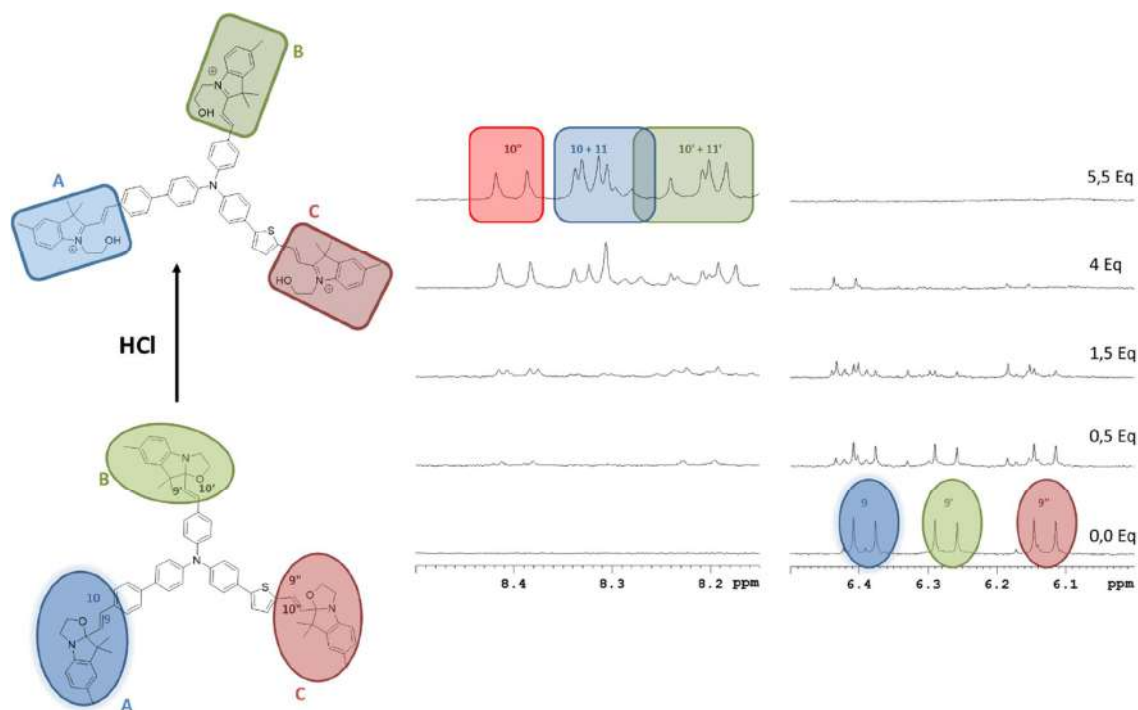
**Figure 16.** UV-Visible spectrum changes of a solution of compound **30** in ACN ( $1.38 \times 10^{-5} M$ ) upon addition of HCl.

Concerning compound **30**, up to one equivalent, the UV spectra reveal the concomitant appearance of a unique band centered at 559 nm with the strong decrease of the band intensity at 368 nm assigned to the CCC form. More important, the presence of an isosbestic point at 413 nm indicates that only two species are in equilibrium suggesting the opening of one BOX moiety in a regioselective manner. Pushing further the added quantity of HCl (until two equivalents) leads to an enhancement of the solution coloration. An increase of the main absorption band centered at 559 nm is noticed and the band intensity at higher energy continues to decrease and is hypsochromically shifted. As consequence, the previous isosbestic point at 413 nm is not anymore conserved suggesting the generation of a new species in agreement with the opening of a second BOX unit. Adding a more important quantity (up to 3 equivalents) continues to induce an hyperchromic effect. However, it is associated to a slight hypsochromic shift of the main visible absorption band (from 559 to 552 nm) as well as the generation of a new band at higher energy (404 nm) suggesting the commutation of last BOX moiety.

If this experiment suggests, again, a commutation of the connected BOX units in a stepwise manner, the dissymmetry of the conjugated systems did not induce a better discrimination of absorbance UV-visible signatures between the four metastable systems. More

important, it didn't allow the clear structural identification of the different isomers generated in acidic stimulation. For this reason, a monitoring of the commutation by NMR spectroscopy was performed by our colleagues in Lille (Pr Stephanie Delbaere and Dr. Jerome Berthet) allowing an unambiguous identification of the various isomers formed upon the stimulation of the molecular system but also their quantification.

As observed in other BOX derivatives, the NMR signals of the vinylic protons are a probe of choice to identify and monitor the commutation of the three BOX units. In fact, preliminary 2D NMR experiment have conducted to assign each doublet (6.13, 6.27 and 6.39 ppm) to one arm of the triarylamine (protons 9'', 9' and 9) and as consequence related to one closed BOX referenced later as **A**, **B** and **C** as depicted on the figure below.



**Figure 17.** NMR assignments of ethylenic junction protons of compound **29** on its CCC and OOO forms.

Adding some acid to compound **29** under its CCC form induces two antagonist effects on the NMR spectrum (Figure 18): the generation of new doublets at low field (ranging from 8.1 to 8.5 ppm) and the multiplication of signals for the vinylic protons (ranging from 6.0 to 6.5

ppm) suggesting the formation of several isomers upon this stimulation. In fact, depending on the position of the opening BOX 3 different isomers have to be considered for the **OCC** form and 3 others for the **OOC** one. Unfortunately, the close vicinity of the different signals did not allow quantifying individually each of them but only the relative proportion (Figure 18) of the three different BOX as function of their status (closed or open).

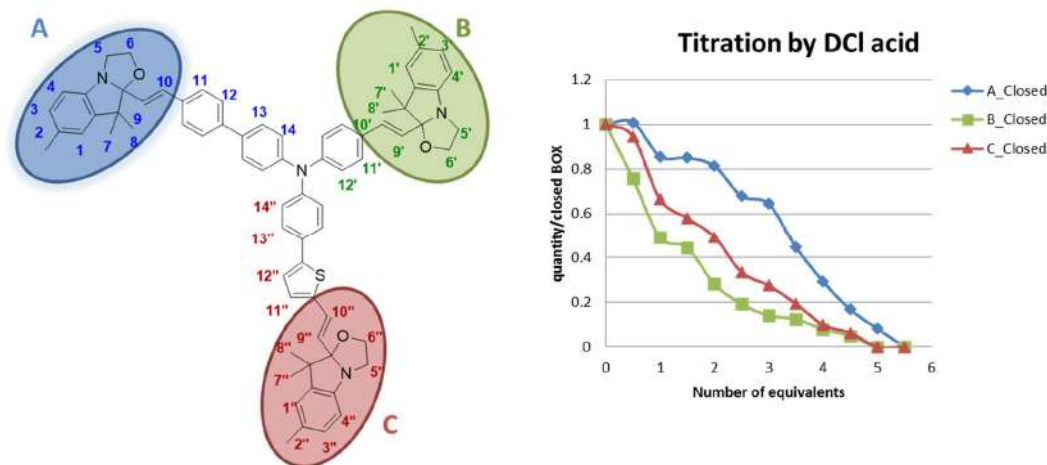


Figure 18. Quantity of closed BOX rest according to number of equivalents of DCl added in ACN-*d*3 at 20°C.

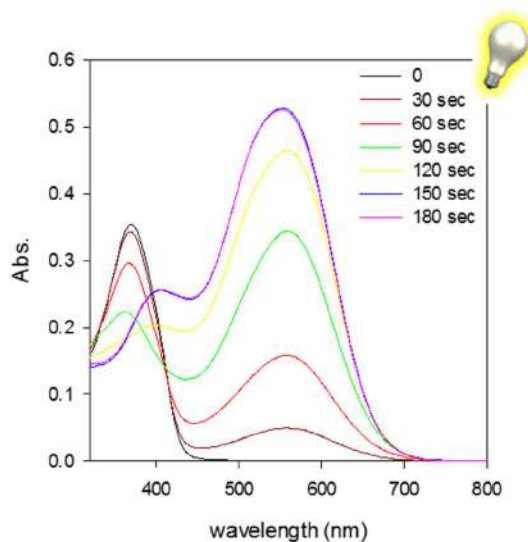
As we can see on the graph above, the addition of 0.5eq. of acid leads to observe predominantly the commutation of BOX **B** and **C** (24% and 5% of units respectively) while the BOX **A** is not impacted by a such stimulation. This discrimination is even more noticeable with further additions of acid. In fact, after addition of 2 eq. of acid, about 72% of BOX **B** appears converted vs about 51% and 19% for **C** and **A** respectively.

As a consequence, even if the observed selectivity of BOX opening appears weak, it can be here considered as a proof of concept. If one reminds that the full opening of BOX here necessitates a large excess of acid and that in this case, the stimulation is direct and not *via* the mediation of the conjugated system, one can envisage an improvement of the addressability selectivity between the BOX units with other stimulations, in particular by oxidative *media*.<sup>[3,</sup>

24, 25, 26]

#### C.2. Photochromic properties.

Compound **30** in acetonitrile has been irradiated with 254 nm light in presence of chlorobenzene (10%) as photosensitizer. As expected, the UV irradiation leads quickly to the strong coloration of the solution reaching a photostationary state after 2.5 min. The evolution of the UV-Visible absorption spectra as function of the irradiation time lets clearly appear stages presented on Figure 19.



**Figure 19.** UV-Visible spectrum changes of a solution of compound **30** in ACN/PhCl (9/1) ( $1.26 \times 10^{-5} \text{ mol.L}^{-1}$ ) upon irradiation at 254 nm.

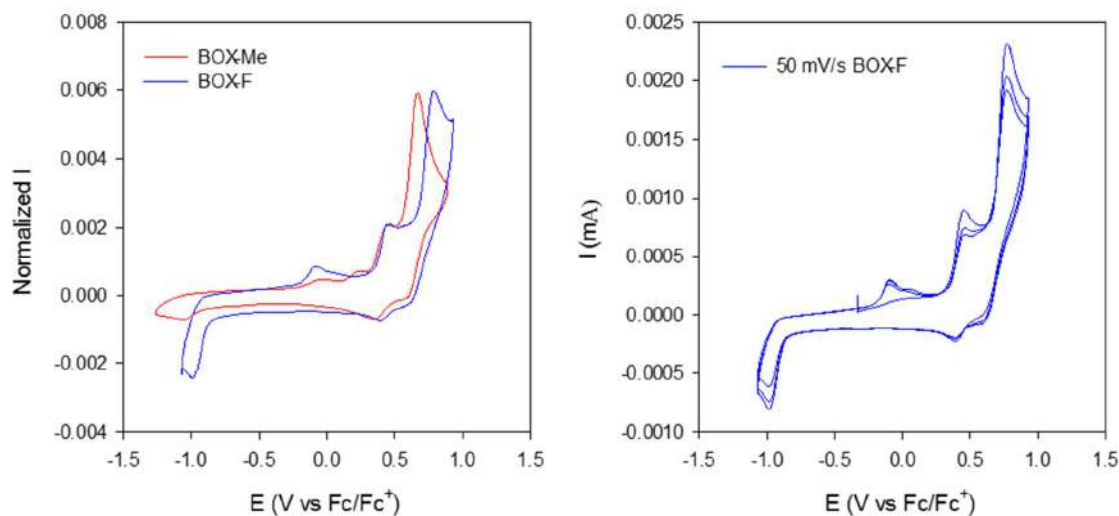
Below 1.5 min. of irradiation duration, the appearance of an absorption band centered at 559 nm is concomitant with the reduction of the absorption at 368 nm as well as the presence of one isosbestic point at 411 nm as under acid stimulation. Upon longer irradiation time, the visible absorption band continues to increase but is also bathochromically shifted and associated with the observation of a new weak band at higher energy (404nm). More important, the overlapping of the UV-visible spectra obtained by either irradiation or acidic titration is noticed, then translating that both stimulation lead to the same commutations, and then, confirming the multi-modal switching abilities of these molecular systems. At the opposite to acidochromic and photochromic properties, electrochromic properties of our systems may be

influenced by the nature of the pi-conjugated system. Corresponding experiments are described below.

### C.3. Electrochromic properties.

As redox stimulation, as demonstrated before, acts *via* the conjugated system media, a higher selectivity of BOX opening could be expected in this later case.

Before studying more deeply this point, the electrochemical behavior of compounds **29** and **30** has been investigated by cyclic voltammetry (CV). According to figure 20, the CV shows that the two compounds, which only differ from the substitution of the BOX termination (Me or F in position 5) exhibit similar behaviors with two successive oxidation waves. For both compounds the first quasi-reversible oxidation process occurs at 0.45 V. This latter can be reasonably assigned to the oxidation of the central core and leads to the generation of the corresponding radical cation in agreement with oxidation potential of symmetric TriBOX analogs **25/26** and **27/28** (0.47 and 0.41 V respectively). As them, the quasi-reversibility of the process suggests that the radical is able to be delocalized in the close vicinity of neighboring BOX units to induce its opening (figure 20 left). The second oxidation process occurring at 0.66 and 0.78 V for compounds **29** and **30** respectively can be assigned to an oxidation mainly localized on the closed BOX in agreement in agreement with the oxidation potential of isolated BOX.<sup>[7]</sup> On the return sweep, one resolved reduction wave appears at *c.a.* -1.07 and -0.99V for compounds **29** and **30** respectively translating a strong transformation of the molecular systems at this potential (closing of the oxazolidine ring) (figure 20 left). Based on our previous studies, this typical electrochemical behavior evidences the electro-induced opening of the oxazolidine rings under electrochemical stimulation. Since the first oxidation happened on the pi-conjugated core it can explain the stepwise commutation but unfortunately without displaying which BOX unit is opened first.

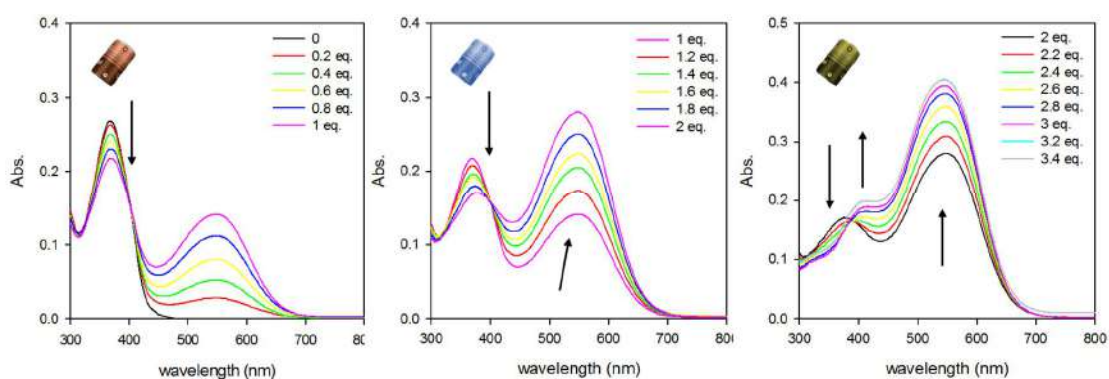


**Figure 20.** Cyclic voltammetry of compounds **29** and **30** in ACN (0.58 and 0.64 mM) with TBAPF<sub>6</sub> as electrolyte (0.1M) on Pt working electrode at 100mV.s<sup>-1</sup> (left), several cycles of compound **30** (right) at 50 mV.s<sup>-1</sup>.

To confirm the stepwise commutation of BOX in this new non symmetric system, its switching ability was investigated by using an oxidizing reagent such as NOSbF<sub>6</sub>.

As expected, a drastic change of the UV-Visible spectra upon the addition of NOSbF<sub>6</sub> aliquots is observed (figure 21). At the end, we can notice that this addition of oxidizing reagent leads to an identical spectrum as the one obtained after stimulation with an excess of acid as shown on figure 16 for compound **30**. In addition, initial spectrum can be recovered after treatment with an excess of base such as triethylamine demonstrating the multi-modal switching ability of these molecular systems. If the UV-visible spectra obtained upon gradual chemical oxidation of compounds (Figure 21, compound **30**) present strong similarities with those chemically and optically induced, subtle differences appear. Indeed, the later shows upon addition of the first equivalent of NOSbF<sub>6</sub> the appearance of a unique band centered at 558nm assigned to the **OCC** form (*vide infra*) associated with the concomitant decrease of the **CCC** characteristic band at 368nm. The addition of the second equivalent of oxidant leads to a bathochromic shift with a new band centered at 559nm assigned to **OOC** form as well as the disappearance of the band centered at 368nm. The opening of the third oxazolidine ring can be

generated by adding more than two equivalents of  $\text{NOSbF}_6$  that induces a more coloration of the solution lead to the increase of the absorption band centered at 552 nm with the appearance of a new higher energy band at 410 nm. As a consequence, this experiment suggests the commutation of the connected BOX units in a stepwise manner. Moreover, contrary to acidochromic experiments which needed 5.5 eq of acid to allow a stationary system, redox *media* appears more efficient as 3 eq. of oxidant is enough to attain the full commutation of the system.



**Figure 21.** UV-Visible spectrum changes of a solution of compound **29** in ACN ( $8.6 \times 10^{-6} \text{M}$ ) upon addition of  $\text{NOSbF}_6$ .

As mentioned earlier, the poor discrimination of the optical signature of the different metastable states did allow us to conclude about the selectivity of this addressability of the system. For this reason, we have monitored the commutation of this system by  $^1\text{H}$  NMR spectroscopy. The results of the titration of compound **29** by  $\text{NOSbF}_6$  are presented on Figure 22.

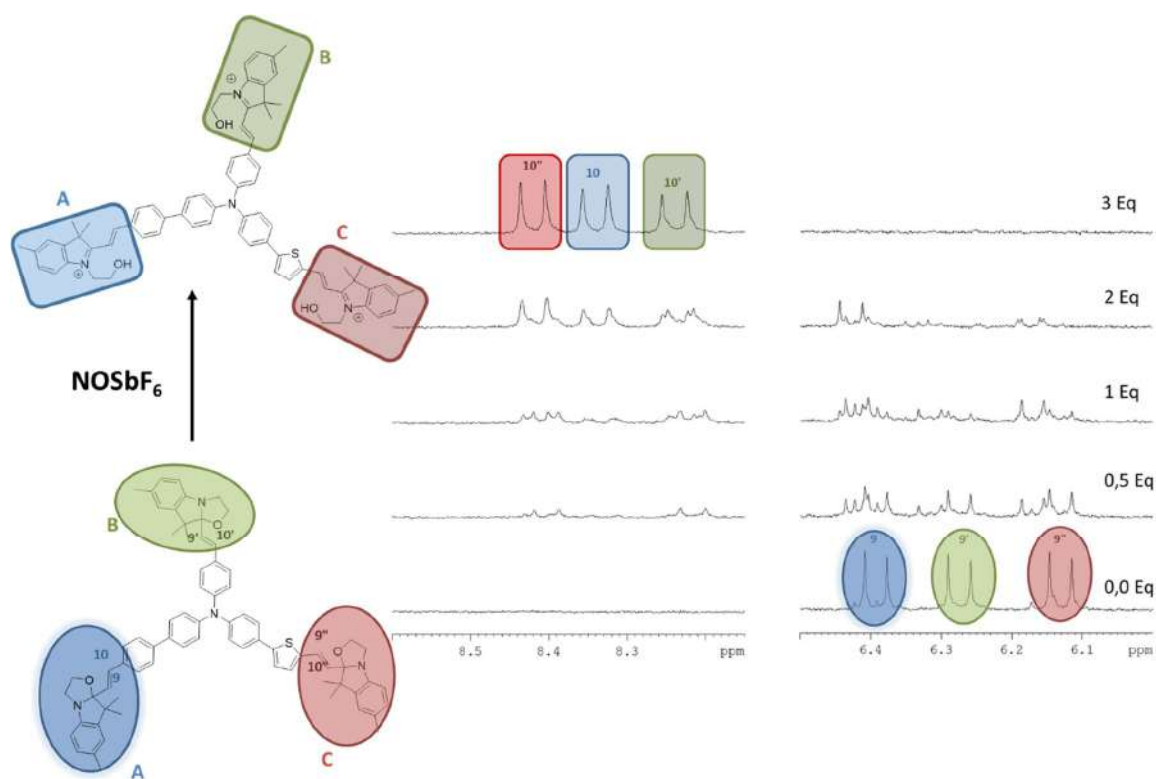
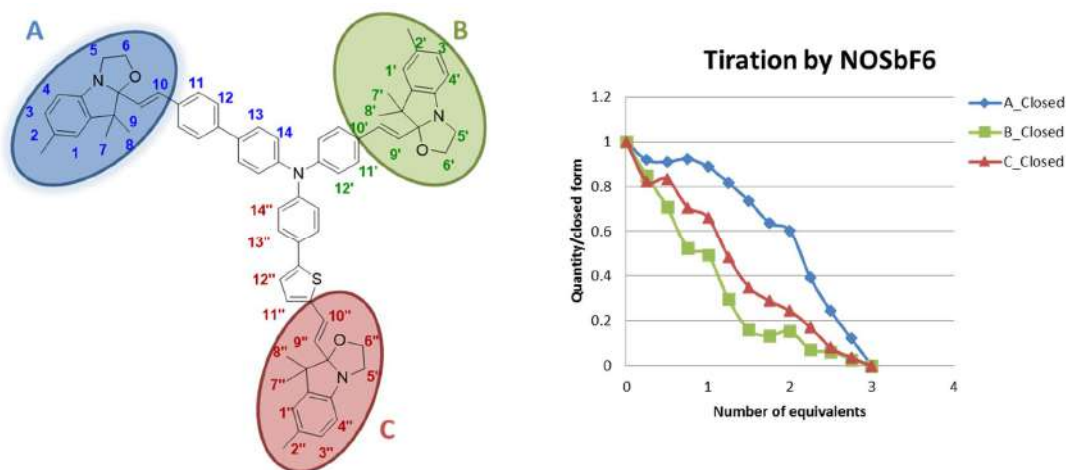


Figure 22.  $^1\text{H}$  NMR spectra upon titration of compound **29** (5 mM) by  $\text{NOSbF}_6$  in ACN at  $20^\circ\text{C}$

As under stimulation with acid, we can observe that the addition of  $\text{NOSbF}_6$  induces drastic changes on the NMR spectrum (Figure 22) but the generation of several new doublets at low field (8.1-8.5 ppm) and the multiplication of signals for the vinylic protons (6.0-6.5 ppm) suggests the formation of several isomers. As example, the addition of the oxidizing reagent until 0.5eq. induces the appearance of two new peaks at 8.2 and 8.4 ppm respectively assigned to the two protons  $10'$  and  $10''$  respectively translating, the preferential opening of the BOX units **B** and **C**. If the close vicinity of the different signals did not allow quantifying individually each isomer (*vide supra*), we have determined the relative proportion of the three different BOX (**ABC**) as function of their status (closed or open) upon the addition of the chemical oxidant (Figure 23).



**Figure 23.**  $^1\text{H}$  NMR quantification of the proportion of the three different BOX (**A****B****C**) in compound **29** (5mM in ACN) as function of their status (closed or open) upon the addition of a chemical oxidant ( $\text{NOSbF}_6$ ).

Surprisingly changing the nature of the stimulation did not allow to improve noticeably the opening differentiation between BOX **B** and **C**. In fact, after addition of 1 eq. of oxidant **51** and 44 % of **B** and **C** are open while in the same conditions HCl leads to 51 and 34% respectively. At the opposite, the discrimination between BOX **B** and **C** on one hand and BOX **A** on the other hand is more important. In fact, these preliminary results show that 1eq. of  $\text{NOSbF}_6$  lead to only to 11% of **A** opening (in comparison to 16% with acid). This higher discrimination seems not anymore observed at 2 eq. Indeed, we observe 39% of **A** opening while acid leads only to 19%. This behavior is easily explained by the more important reactivity of the system in redox media than in acidic conditions. In fact, the chemical oxidant leads quantitatively to corresponding open BOX quantity. As consequence, the full commutation of the system, **OOO** form, is reached after addition of only 3 eq. of  $\text{NOSbF}_6$  while 5.5 eq of acid were required to reach the same point.

We can conclude that, redox media as stimulation assure more efficient conversion but provide only a tiny improvement of selectivity between **C/B** vs **A** compared with acidochromic experiment. Nevertheless, this first investigation can be considered as a proof of concept that it is possible, by modifying the conjugated system linked to the BOX to promote the opening of

one species before another one. However, the close vicinity of different NMR signals corresponding to the 8 different isomers of compound **29** under its various states makes them difficult to quantify accurately. For this reason, the introduction of a fluorine atom on the indoline position 5 (compound **30**) could benefit to overcome this issue. In fact, the monitoring of the commutation of **30** by  $^{19}\text{F}$ -NMR (actually under progress) should lead to the complete quantification of each 8 different states allowing to confirm the preferential BOX opening sequence.

## V). Conclusion

In conclusion of this chapter, three series of multi-modal and multi-level molecular systems associating three BOX units to a central pi-conjugated core have been synthesized and investigated by the three different stimulations.

Initial work shows that, the possible triggers of compound **24** are only limited to two (photon and proton) of the three ways classically reported to induce BOX opening. Indeed, a direct stimulation by electron leads to an electropolymerization process through a C-C coupling on the position 5 of the BOX when it is not substituted.

At the opposite, studies performed on symmetrically TriBOX system using a triarylamine core **25-28** exhibit promising and analogous results. All three types of stimulation (proton, photon and electron) allow opening of BOX systems and in a sequential order.

In this later case it can be pointed out:

- That titration of **CCC**, **OCC**, **OOC** and **OOO** forms upon oxidation still have to be conducted to determine equilibria **C/O** constants.
- That such a derivative in terms of second order NLO could allow interesting properties. In fact, such system should allow to modulate the first hyperpolarizability over at least 3 different levels. Indeed, **CCC** and **OOO** states exhibiting a  $C_{3v}$

### **Chapter 3: Synthesis and characterization of new multi-level systems.**

---

symmetry they should be inactive except if conformational evolution occurs as in BiBOX-bithiophene compounds.

- Considering the recent demonstration to use BOX in order to modulate the two photons absorption phenomenon, the measurement of the two photons cross sections of the some of this molecular system have to be carried out as two forms (**OO** and **OOO**) present a promising quadrupolar structure.

Finally, a first non-symmetric triarylamine system bearing 3 different conjugated systems terminated by an identical BOX was synthesized and investigated. If its properties are globally analogous to those of symmetrical compounds, titration experiments conducted by our colleagues of Lille demonstrate unambiguously a preferential opening sequence under acidic and redox stimulation. If this selectivity is far to be sufficient for application, it can be considered as a proof of concept for a step forward in the exploitation of BOX properties.

As the two first chapters are focused on the properties of BOX covalently linked, the two next ones focus on a second strategy which consists in developing multi-responsive molecular systems based on coordination chemistry.

## VI). References

- [1] J. Andréasson and U. Pischel, *Chemical Society Reviews* **2010**, *39*, 174-188.
- [2] J. Andréasson and U. Pischel, *Chemical Society Reviews* **2015**, *44*, 1053-1069.
- [3] G. Szalóki and L. Sanguinet in *Properties and Applications of Indolinoxazolines as Photo-, Electro-, and Acidochromic Units*, Eds.: Y. Yokoyama and K. Nakatani), Springer Japan, Tokyo, **2017**, pp. 69-91.
- [4] G. r. Szalóki and L. Sanguinet, *The Journal of organic chemistry* **2015**, *80*, 3949-3956.
- [5] R. Bartnik, S. Lesniak, G. Mloston, T. Zielinski and K. Gebicki, *Chem. stosow* **1990**, *34*, 325-334.
- [6] R. Bartnik, G. Mloston and Z. Cebulska, *Chem. Stosow* **1990**, *34*, 343-352.
- [7] R. Hadji, G. Szalóki, O. Alévêque, E. Levillain and L. Sanguinet, *Journal of Electroanalytical Chemistry* **2015**, *749*, 1-9.
- [8] N. Sertova, J.-M. Nunzi, I. Petkov and T. Deligeorgiev, *Journal of Photochemistry and Photobiology A: Chemistry* **1998**, *112*, 187-190.
- [9] G. r. Szalóki, O. Alévêque, J.-L. Pozzo, R. Hadji, E. Levillain and L. Sanguinet, *The Journal of Physical Chemistry B* **2014**, *119*, 307-315.
- [10] L. Sanguinet, J. Berthet, G. Szalóki, O. Alévêque, J.-L. Pozzo and S. Delbaere, *Dyes and Pigments* **2017**, *137*, 490-498.
- [11] Y. Shirota, *Journal of Materials Chemistry* **2000**, *10*, 1-25.
- [12] Y. Shirota, *Journal of Materials Chemistry* **2005**, *15*, 75-93.
- [13] M. Thelakkat, *Macromolecular Materials and Engineering* **2002**, *287*, 442-461.
- [14] E. T. Seo, R. F. Nelson, J. M. Fritsch, L. S. Marcoux, D. W. Leedy and R. N. Adams, *Journal of the American Chemical Society* **1966**, *88*, 3498-3503.
- [15] R. Rybakiewicz, M. Zagorska and A. Pron, *Chemical Papers* **2017**, *71*, 243-268.
- [16] Y.-X. Wang and M.-k. Leung, *Macromolecules* **2011**, *44*, 8771-8779.
- [17] H. Kageyama, H. Ohishi, M. Tanaka, Y. Ohmori and Y. Shirota, *Advanced Functional Materials* **2009**, *19*, 3948-3955.
- [18] R. Nelson and R. Adams, *Journal of the American Chemical Society* **1968**, *90*, 3925-3930.
- [19] I. Tabakovic, Y. Kunugi, A. Canavesi and L. L. Miller, *Acta Chemica Scandinavica* **1998**, *52*, 131-136.
- [20] J. K. Kochi, *Accounts of Chemical Research* **1992**, *25*, 39-47.
- [21] J. Andréasson and U. Pischel, *Chemical Society Reviews* **2010**, *39*, 174-188.
- [22] C. Joachim and G. Rapenne, *ACS Nano* **2013**, *7*, 11-14.
- [23] G. Szaloki and L. Sanguinet, *Journal of Organic Chemistry* **2015**, *80*, 3949-3956.
- [24] N. Sertova, J. M. Nunzi, I. Petkov and T. Deligeorgiev, *Journal of Photochemistry and Photobiology A: Chemistry* **1998**, *112*, 187-190.
- [25] R. Bartnik, S. Lesniak, G. Mloston, T. Zielinski and K. Gebicki, *Chem. Stosow.* **1990**, *34*, 325-334.
- [26] R. Bartnik, G. Mloston and Z. Cebulska, *Chemia Stosowana* **1990**, *34*, 343-352.



---

**Chapter 4: Syntheses and  
characterizations of ligands  
incorporating BOX units.**

---



## I). Introduction

In the previous chapters, we have demonstrated that the connection of two or three BOX by using a linear conjugated system or a C3-symmetry node allow to observe in almost all cases a stepwise commutation of the corresponding molecular system especially when an electro-mediated process is involved. It may be hypothesized in both of these cases that this promising addressability behavior results from some interactions between BOX moieties. Indeed, BOX moieties are allowed to interact through bond or *a minima via* the influence of the electron-withdrawing indoleninium motif which *de facto* decreases the donor ability of the central node. The question about the possibility to induce similar behavior by using through space interactions between BOX systems remains. In fact, similar strategies, applied to famous DTE unit, lead generally to observe a loss of selectivity and their random closure under irradiation.<sup>[1]</sup>

In this context, we have decided to take advantage of coordination chemistry to place the different BOX units in a specific spatial arrangement around a metallic ion. As this manner to pile-up BOX systems assure an electronic insulation of systems while allowing through space proximity, this strategy opens also new prospects. Indeed, the connection of a photochromic moiety to a transition metal ion could also induce a perturbation of the excited-state properties of both components and thus generate new reactivity and interesting photochemical properties.<sup>[2]</sup>

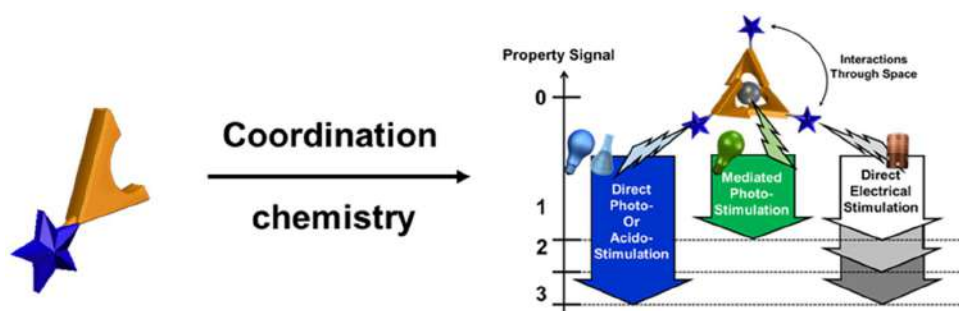
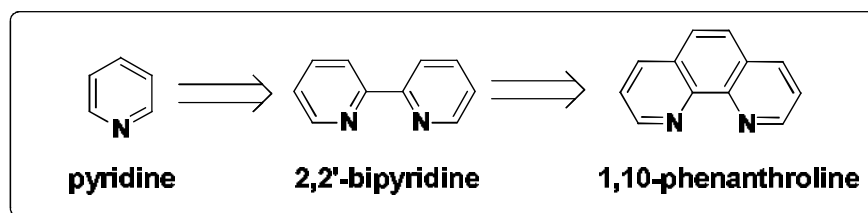


Figure 1. Schematic of a ligand substituted by a BOX and of the corresponding complex with a transition metal.

#### **Chapter 4: Syntheses and characterizations of ligands incorporating BOX units.**

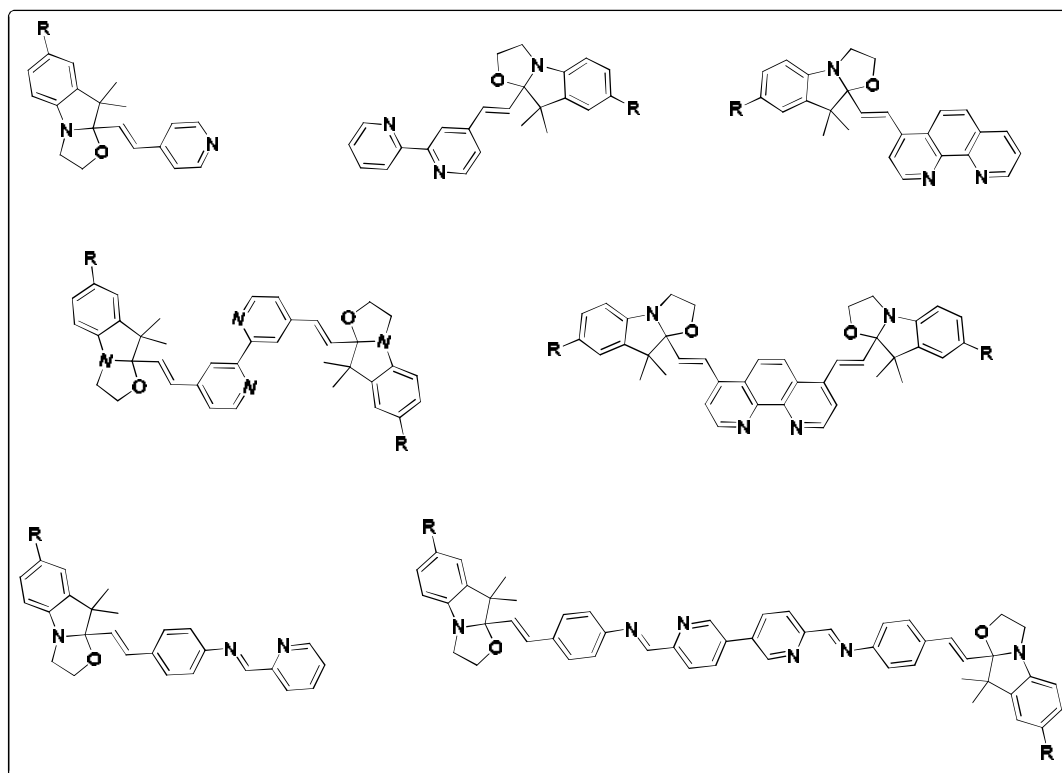
To the best of our knowledge, the development of molecular systems associating a BOX unit to a metal binding functionality is not reported in the literature. For this reason, this chapter is focused on the syntheses and characterization of a first series of isolated ligands bearing one or more BOX units. The preparation and studies of corresponding Zinc and Ruthenium complexes will be presented in the next chapter.

Concerning the metal binding functionality, the nitrogen-donor based ligands have been intensively studied in the context of their coordination ability to a variety of transition metal ions. In this context we have chosen to develop a library of organic aromatic heterocyclic ligands bearing one or several BOX units. Known to form stable complexes with numerous metal centers, their structure affects strongly the optical and electrochemical properties of resulting complex. In addition, the large possibilities of polypyridyl ligands functionalization by different groups have conducted to their use in a wide range of applications, which exploit their photophysical, photochemical and redox properties.<sup>[3]</sup> The simplest member of this family is the well-known pyridine motif<sup>[4]</sup> which is largely used as versatile building blocks for the preparation of polypyridyl ligands.<sup>[5]</sup> Among the numerous pyridine based ligands, bipyridines certainly represent the most important family especially the 2,2'-bipyridine (bpy). Resulting from the connection of two pyridine units through a single bond, this bidentate chelate is certainly the most used and studied nitrogen-donor based ligand due to its ability to form stable complexes with a large variety of metallic ions.<sup>[6]</sup> From the basic bipyridine structure, a lot of derivatives have been prepared upon functionalization with different groups. The synthetic approaches to bipyridine derivatives include the functionalization with substituent groups at the different positions of the aromatic rings as well as the incorporation of fused aromatic or aliphatic rings to lead as example to famous phenanthroline (scheme 1). Indeed, this important bipyridine derivatives presents a fused aromatic ring between the two pyridyl groups.<sup>[7, 8]</sup>



*Scheme 1. Molecular structure of the different aromatic nitrogen heterocycles.*

As consequence, the polypyridyl ligands represent logically the first molecular family to exploit in order to elaborate some BOX derivatives including some metal binding functionalities. In this context, the functionalization of various aromatic nitrogen heterocycles by one or more BOX units was undertaken. Differing by the nature of the heterocycle (pyridine, bipyridine, and phenanthroline), the nature and position of substituents and, finally, the number of grafted BOX units, a first library of multi-functional ligands have been prepared (scheme 2). Their syntheses are described in the following sections.

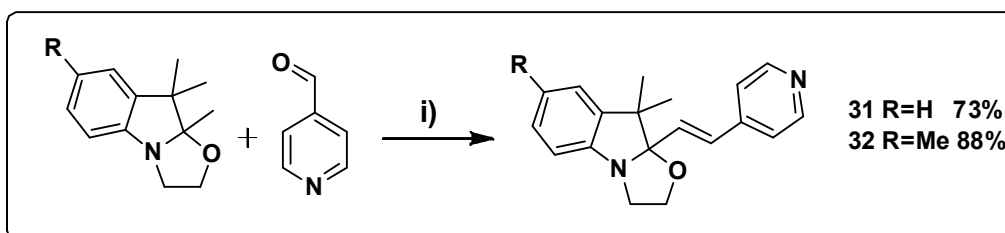


*Scheme 2. Different models of synthesized ligands bearing BOX units.*

## II). Synthesis

### A. Synthesis and characterization of pyridine ligand with one BOX unit.

To prepare the targeted molecules, a convergent synthesis strategy, laying on condensation between an aromatic aldehyde and the corresponding trimethylindolino-oxazolidine derivative as final step, has been adopted. If this condensation reaction was reported with numerous aromatic hydrocarbon bearing a large variety of substituent in various experimental conditions (protic and aprotic solvents, acid or basic catalysis, solvent-free), the used of heterocycle appears surprisingly limited to thiophene.<sup>[9, 10, 11]</sup> As example, the functionalization of an aromatic nitrogen heterocycle by a BOX unit is not something known from before. In this context, our first attempt was dedicated to the condensation of trimethylindolino-oxazolidine derivatives on cheap and commercially available 4-pyridinecarboxaldehyde using the silica mediated procedure which was successfully applied up to now (scheme 3).



*Scheme 3. Synthetic route to ligands 31 and 32, (i) silica gel, 100°C, 10 minutes.*

Differing from the substituent nature in the position 5 of the indoline heterocycle, the two ligands **31** and **32** were obtained with satisfactory yields of 73 and 88 % respectively. As usual, the structures of the compounds, especially the trans isomery of the ethylenic junction, were confirmed by NMR spectroscopy (proton and carbon), IR, mass spectrometry.

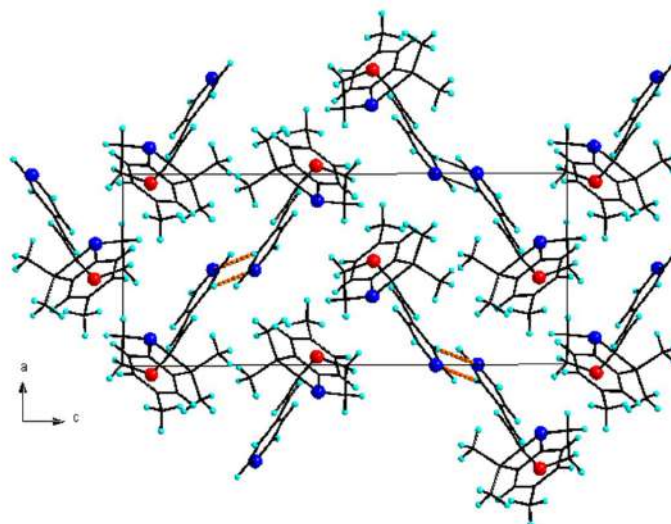
In addition, it was possible to obtain some single crystals suitable for X-ray diffraction studies by recrystallization of **31** and **32** in their closed form in ethanol. The crystallographic data are described in table 1.

(E)-9,9-dimethyl-9a-(2-(pyridin-4-yl)vinyl)-2,3,9,9a-tetrahydrooxazolo[3,2-a]indole (31)	
<b>Orthorhombic,</b> a = 8.7072(2) Å b = 9.0385(2) Å c = 20.4631(5) Å V = 1610.45(6) Å <sup>3</sup> Yellow crystals	<b>P 2<sub>1</sub>2<sub>1</sub>2<sub>1</sub></b> α = 90° β = 90° γ = 90° Z = 4
(E)-7,9,9-trimethyl-9a-(2-(pyridin-4-yl)vinyl)-2,3,9,9a-tetrahydrooxazolo[3,2-a]indole (32)	
<b>Orthorhombic,</b> a = 83310(10) Å b = 9.37090(10) Å c = 20.5380(3) Å V = 1700.01(4) Å <sup>3</sup> Yellow crystals	<b>P 2<sub>1</sub>2<sub>1</sub>2<sub>1</sub></b> α = 90° β = 90° γ = 90° Z = 4

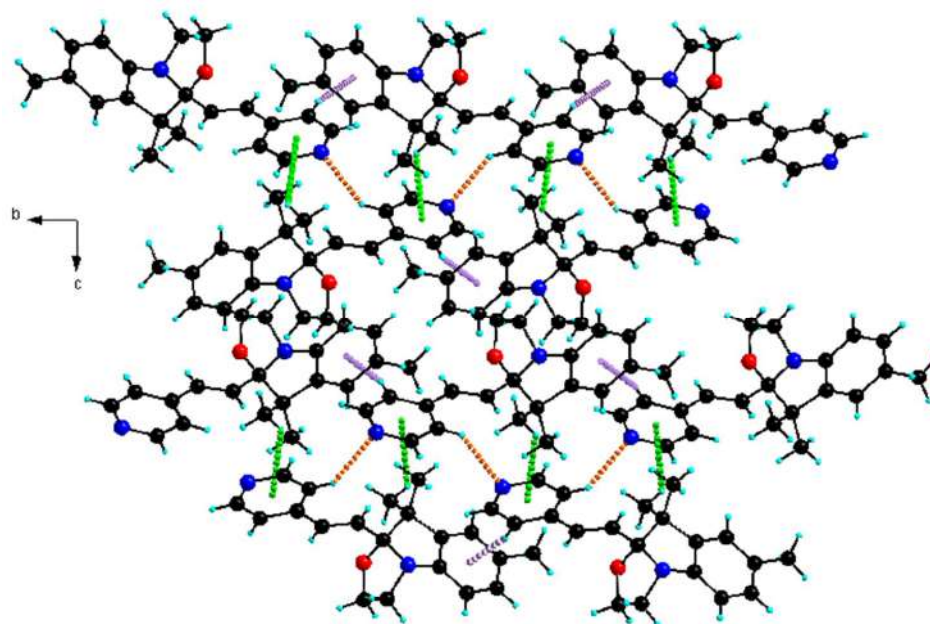
**Table 1.** Crystal structures of ligands **31** and **32**, main parameters and representation of the molecules.

Both ligands crystallize in the orthorhombic system space group P 2<sub>1</sub> 2<sub>1</sub> 2<sub>1</sub>, with one independent molecule in the unit cell. As previous prepared BOX derivatives, the obtained data highlight the almost orthogonality of the two aromatic systems and the trans configuration of the double C=C bond linking the BOX unit and the pyridine.

Furthermore, viewing along the crystallographic *a* axis of ligand **32** (ligand **31** behaves the same), each molecule interacts with the adjacent molecule by non-conventional hydrogen bonds C–H⋯N, (C2–H2⋯N1, 2.544(0) Å) (Figure 2). In the solid state, each ligand molecule interacts with two neighboring ones by hydrogen bonds, C–H⋯π (C4–H4⋯π (2.712 (0) Å), C13–H13B⋯π (2.853(0) Å)), from phenyl ring and from pyridine fragment respectively as represented in Figure 2. These interactions lead to the formation of 3D supramolecular layers which are parallel with the *bc* crystallographic plane (Figure 3).



**Figure 2.** Perspective view of ligand 32 in the *ac* plane: C–H···N contacts (orange dashed lines).



**Figure 3.** Crystal packing of ligand 32 showing the two types of interactions C–H···N hydrogen bonds (orange dashed lines), C–H··· $\pi$  interactions, from phenyl ring (purple dashed lines) and from pyridine fragment (green dashed lines).

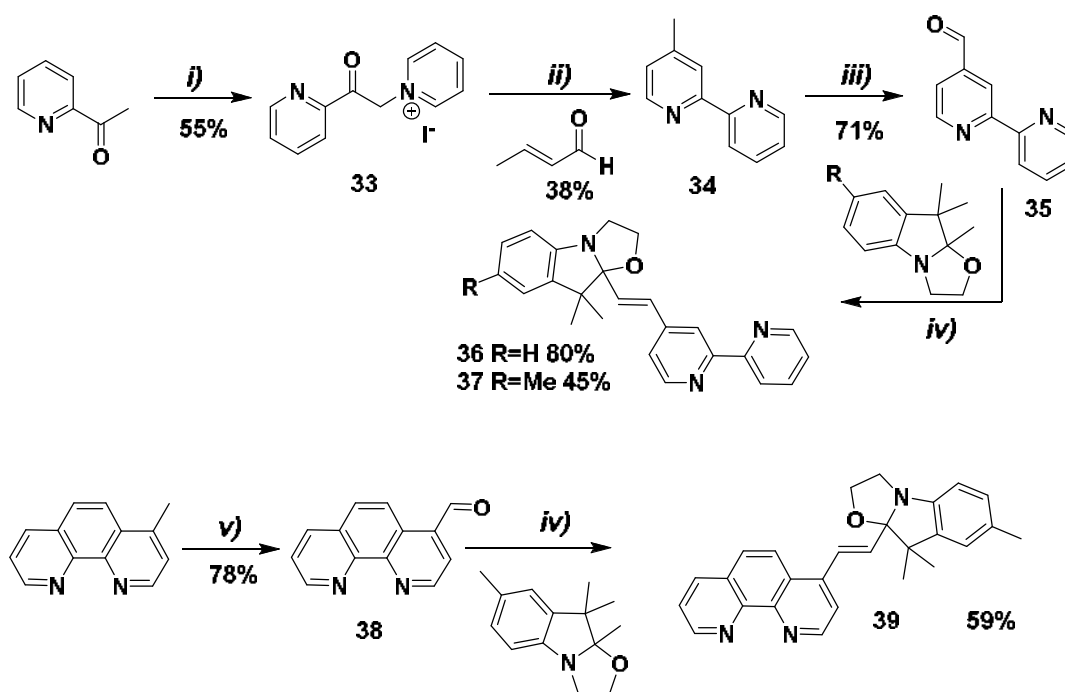
Through the preparation of derivatives **31-32**, we have then demonstrated that the silica mediated procedure is an easy and convenient manner to carry out the functionalization of nitrogen heterocycle by some BOX units without loss of effectiveness. In addition, both compounds present all the classical characteristics of BOX derivatives where both pi-conjugated systems are almost perpendicular and should behave independently. As

consequence, compound **31** and **32** can be considered as potential monodentate ligands. Driven by this success, we have pursued our effort in order to prepare some bidentate ligands based on bipyridine and phenanthroline which are known to lead to more robust complexes.

B. Synthesis and characterization of bidentate ligands.

B.1. Synthesis of bidentate ligands with one BOX unit.

To prepare this second series of ligands bearing one BOX unit, typical convergent strategy was applied as depicted on scheme 4. It consists in preparing in first place the corresponding N-heterocycle incorporating a carboxaldehyde function and then performing its condensation with various trimethylindolino-oxazolidine derivatives (which differ by the nature of the substituent in position 5) as final step.



**Scheme 4.** Synthetic route to ligands **36**, **37** and **39** i)  $I_2$ , pyridine; ii)  $NH_4OAc$ , Methanol. iii)  $SeO_2$ , diglyme; iv) silica gel,  $100^\circ C$ , 10 min; v)  $SeO_2$ , Dioxane/ $H_2O$ .

## Chapter 4: Syntheses and characterizations of ligands incorporating BOX units.

The syntheses of ligands **36** and **37** require first to prepare the 2,2'-bipyridin-4-carbaldehyde (**35**). Concerning the latter, we have successfully applied the procedure reported in 2004 by Maestri *et al* [12] which consists in 3 steps starting from 2-acetylpyridine. As the first step involves the synthesis of the 1-[2-oxo-2-(2-pyridinyl)ethyl]pyridinium iodide **33** using iodine and pyridine in 55% yield, a further reaction with crotonaldehyde and NH<sub>4</sub>OAc in methanol leads to the 4-methyl-2,2'-bipyridine **34** in 38% yield. After that, an oxidation reaction of compound **34** using selenium dioxide in diglyme allows to obtain compound **35** in 71% yield. Finally, its condensation under solvent-free silica method [11] with trimethylindolino-oxazolidine derivatives did not raise any particular problems and bidentate ligands **36** and **37** were obtained in satisfactory yields of 80 and 45% respectively.

The preparation of ligand **39** is more straightforward. Indeed, the oxidation of commercially available 4-methyl-1,10-phenanthroline by SeO<sub>2</sub> allows the introduction of the carboxaldehyde function (78%) which is involved in the second condensation step with tetramethylindolino-oxazolidine allowing to obtain the targeted compound in 59% yield.

If the structure of all compounds were confirmed by NMR spectroscopy (proton and carbon), IR and mass spectrometry, single crystals allowing X-ray structural determination were obtained in case of ligand **36** by recrystallization using ethanol.

(E)-9a-(2-([2,2'-bipyridin]-4-yl)vinyl)-9,9-dimethyl-2,3,9a-tetrahydrooxazolo[3,2-a]indole	
<b>Triclinic,</b>	<b>P -1</b>
a = 8.4181(4) Å	α = 63.202°
b = 11.4615(6) Å	β = 84.360°
c = 11.5844(6) Å	γ = 83.085°
V = 989.19(10) Å <sup>3</sup>	Z = 2
Yellow crystals	

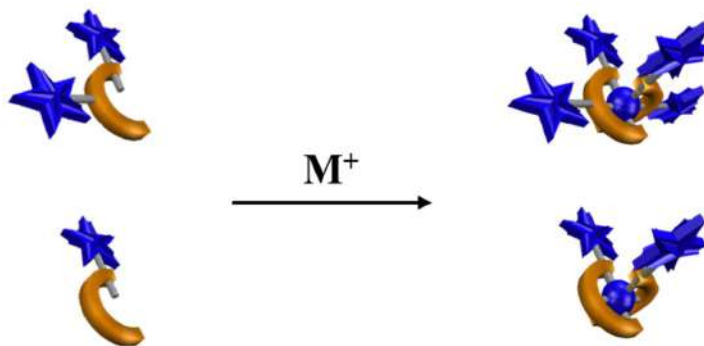
## Chapter 4: Syntheses and characterizations of ligands incorporating BOX units.

Ligand **36** crystallizes in the Triclinic system space group P-1, with one independent molecule in the unit cell (selected parameters of the X-ray diffraction data collection and refinement are gathered in table 2). Here again, the bipyridine ligand and the indolinooxazolidine unit are not coplanar and, as deduced in solution from NMR spectrum, the central ethylenic junction presents a trans configuration. In addition, it is worse to note that the bipyridine unit is planar and in an anti-conformation, (opposite position of nitrogen atoms N2 and N3).<sup>[13]</sup>

As seen in the two previous chapters, the connection of two BOX units by a pi-conjugated system conducts to enhance the number of metastable states in which a stepwise commutation is generally observed. Based on these promising results, a similar strategy has been envisioned here by the functionalization of one metal binding functionality (bipyridine or phenanthroline) by several BOX units.

### B.2. Synthesis of bidentate ligands with two BOX units.

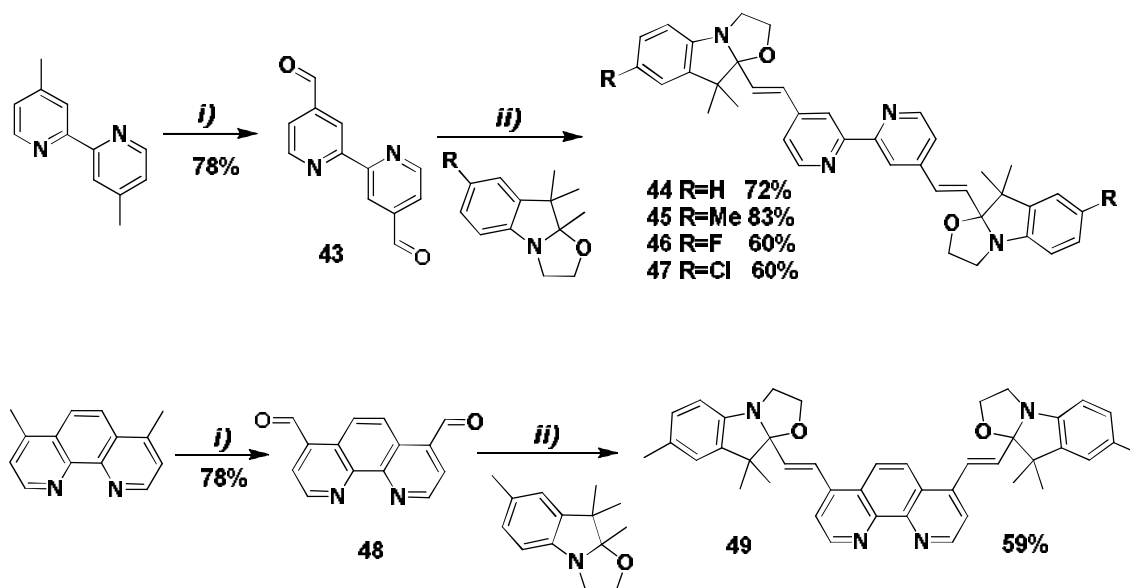
In order to control and increase the number of commutable switches around one metallic center, several strategies can be considered. The first one involves the selection of the number of ligands around this metal leading up to 3 BOX units and 4 possible metastable states. At the opposite, the second possibility consists in synthesizing ligands bearing several units.



*Figure 4 . Schematic representation of different complexes incorporating BOX units.*

## Chapter 4: Syntheses and characterizations of ligands incorporating BOX units.

In this context, we have focused our efforts on the preparation of some bidentate ligands based on bipyridine and phenanthroline heterocycles bearing two BOX units. As depicted on scheme 5, a similar strategy as the one used for BiBOX series was applied to prepare targeted ligands (**44-47, 49**).



*Scheme 5. Synthetic route to ligands 44-49 i) SeO<sub>2</sub>, Dioxane; ii) silica gel, 100°C, 10 min.*

In both cases (bipyridine/phenanthroline) the target ligands were prepared in two steps without particular difficulties. In first place, the bisaldehyde compounds (**43** and **48**) were prepared by an oxidation of corresponding dimethyl-heterocycles. Using the solvent-free conditions, the desired ligands (**44-47, 49**) were obtained with satisfactory yields ranging from 59 to 83%.

If the structure of all compounds, were confirmed by NMR spectroscopy (proton and carbon), IR and mass spectrometry, single crystals allowing X-ray structural determination were obtained in case of ligand **44** by recrystallization using ethanol. The latter crystallizes in the monoclinic system space group P2<sub>1</sub>/c, with one independent molecule in the unit cell. The crystal structure and selected parameters of the X-ray diffraction data collection and refinement are gathered in table 3.

4,4'-bis((E)-2-(9,9-dimethyl-2,3,9,9a-tetrahydrooxazolo[3,2-a]indol-9a-yl)vinyl)-2,2'-bipyridine (44)	
<b>Monoclinic,</b>	<b>P 21/c</b>
a = 11.2536(3) Å	$\alpha = 90^\circ$
b = 13.0614(4) Å	$\beta = 96.233^\circ$
c = 10.4320(3) Å	$\gamma = 90^\circ$
V = 1524.31(8) Å <sup>3</sup>	Z = 2
Yellow crystals	

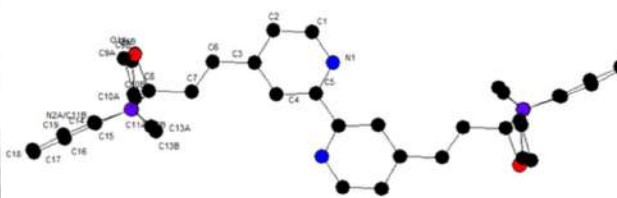


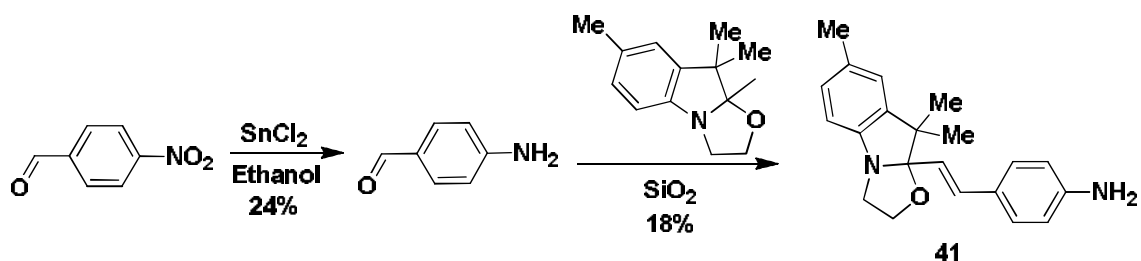
Table 3. Crystal structure of ligand 44, main parameters and representation of the molecule.

As in previous case, the bipyridine unit is planar and in anti-conformation, ethylenic spacers in trans configuration and lateral indolinoxazolidine moieties not coplanar with the central conjugated system.

Bipyridine and phenanthroline moieties are bidentate ligands bearing heterocyclic nitrogen atoms. It is possible to tune the complex force and geometry by using other sorts of ligands as for example, a pyrilyl-imide block.

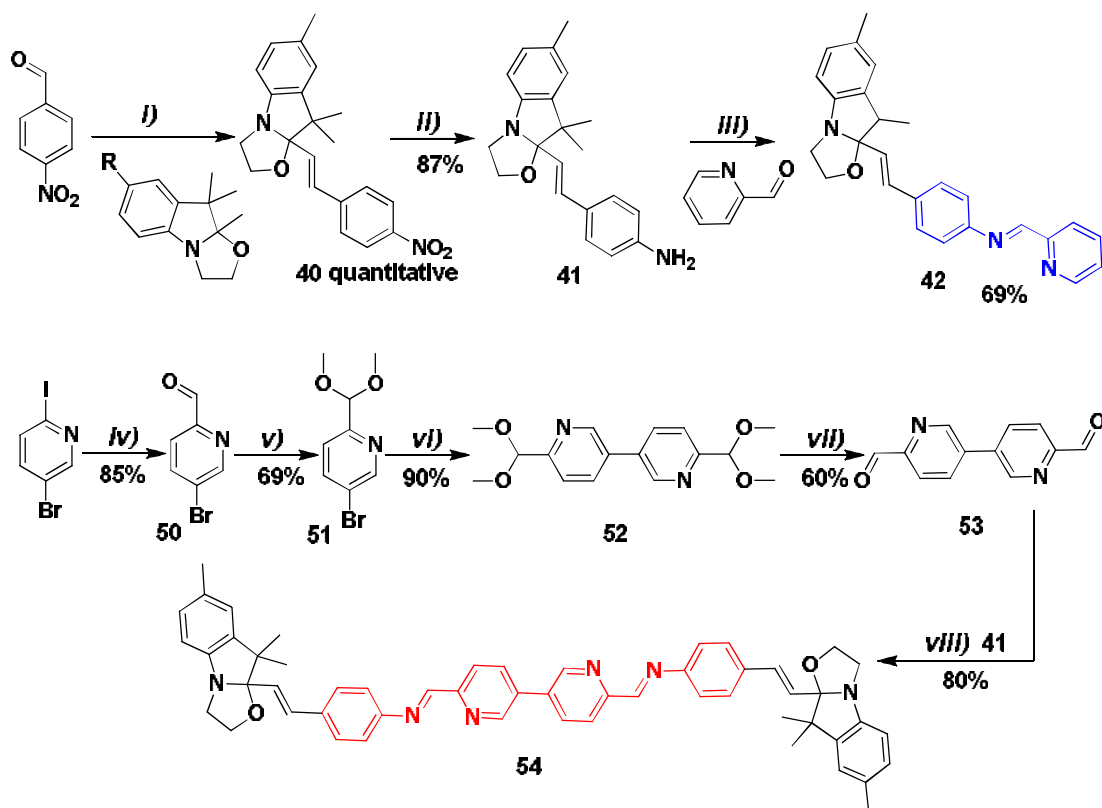
### B.3. Synthesis and characterization of Pyridyl-imine ligands.

Generally, the insertion of the suitable 2-pyrilyl-imide block is carried out through a condensation of the 2-formylpyridine with a partner bearing an amine function. Due to general lability of the imine bond in acidic conditions, the BOX unit have to be introduce in first place to lead to the intermediate **41**. Nevertheless, two synthesis pathways were explored to prepare this intermediate. The first one is the straight application of BOX derivative preparation based on the condensation of the trimethylindolino-oxazolidine with an aromatic aldehyde bearing appropriate functionality as described in scheme 6.



*Scheme 6. Synthetic route to compound 41.*

In this case, 4-aminobenzaldehyde was prepared by reduction of 4-nitrobenzaldehyde using  $\text{SnCl}_2$  in ethanol in 24% yield. This low yield is explained by the polymerization generated from the compound itself due to the presence of amine and aldehyde functions. After that, using the solvent free condition procedure under silica between BOX and 4-aminobenzaldehyde led to compound **41** in the low yield of 18% also due to the polymerization of 4-aminobenzaldehyde. As we can see, the targeted intermediate is only obtained with a poor overall yield (4%). To circumvent these issues of polymerization, a new synthesis approach was investigated where the generation of the problematic amine function should occur at the end (scheme 7). This second approach is much more effective. In fact, the intermediate **41** is obtained in a 87% overall yield thanks to a quantitative condensation reaction between trimethylindolino-oxazolidine and nitrobenzaldehyde followed by an efficient reduction of the nitro function into an amine.



**Scheme 7.** Synthetic route to ligands **42** and **54** i) silica gel, 100°C, 10 min. ii) SnCl<sub>2</sub>, ethanol. iii) DCM; iv) PrMgCl, DMF, THF; v) Methyl orthoformate, *p*-toluenesulfonic acid, MeOH; vi) Pd(PhCN)<sub>2</sub>Cl<sub>2</sub>, TDAE, DMF; vii) HCl, THF; viii) Acetonitrile.

The condensation between an aldehyde and an amine leading to an imine was described first by Hugo Schiff in 1864.<sup>[14]</sup> As consequence, pyridyl-imine ligands (**42** and **54**) were logically prepared according to a synthetic procedure which involves the condensation of 2-formylpyridine or 2,2'-bipyridine-5,5'-dicarboxyaldehyde with an appropriate amine **41** as shown in Scheme 7. Concerning the ligand **42**, the condensation of **41** with picolinaldehyde leads to target **42** in 69% yield without particular difficulties.

As for ligand based on bipyridine and phenantroline heterocycles, we have performed some attempts to introduce several BOX units on the same ligands. In this case, a new oligoiminobipyridine ligand incorporating two BOX units was prepared in order to form

double-stranded helical complexes with copper (I) and copper (II) ions as described in literature.<sup>[15]</sup>

Thus, the synthesis of ligand **54** was undergone in 5 steps starting from 5-bromo-2-iodopyridine. As the four first steps consist in reproducing the published synthesis of 2,2'-bipyridine-5,5'-dicarboxyaldehyde **53** <sup>[16]</sup> in an overall 32% yield, the last step of condensation with two equivalents of **41** leads to target **54** in 80% yield. The structures of the compounds were confirmed by NMR spectroscopy (proton and carbon), IR and mass spectrometry.

In summary, we have prepared a large library of different nitrogen aromatic heterocycle ligands functionalized by at least one BOX unit that are able to form some complexes based on Zn(II) and Ru(II) (see next chapter).

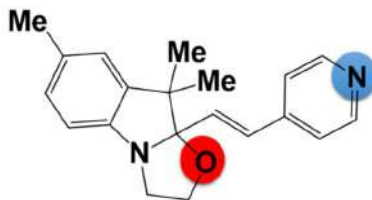
Before to go further, we have to verify that the presence on a metal binding functionality did not annihilate the commutation abilities of BOX unit. In such purpose, the response of chosen example of ligand under acido-, photo- and electro-stimulation were investigated and are described below.

### **III). Influence of the presence of a metal binding functionality on commutation abilities of BOX derivatives**

Before synthesizing and investigating properties of corresponding transition metal complexes, the multimodal commutabilities upon acid addition, photo- and redox-excitation of the prepared ligands have to be characterized. Indeed, the presence of a nitrogen heterocycle could strongly affect their behavior especially their acidochromic properties. Indeed, as upon opening, BOX systems capture a proton onto an oxygen atom, nitrogen heterocycle, which also presents some basic properties,<sup>[17]</sup> is susceptible to blur the commutability properties of the system.

## Chapter 4: Syntheses and characterizations of ligands incorporating BOX units.

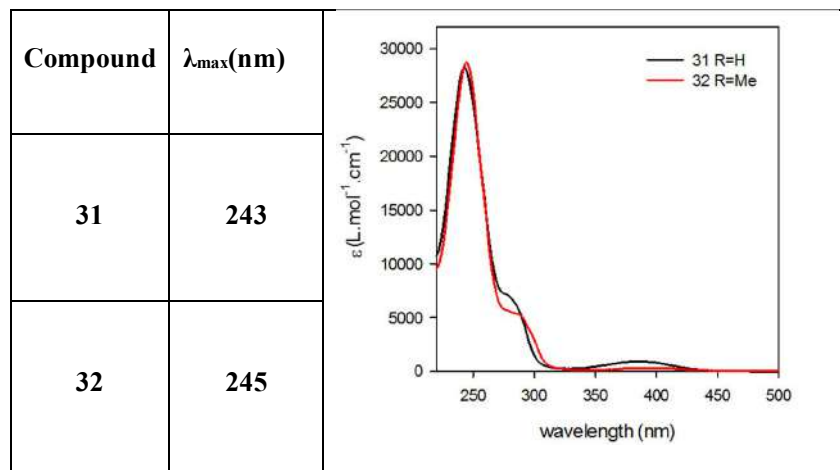
In this context, the compound **32** associating a BOX unit to a pyridine moiety acting as the weaker base ( $pK_a \sim 5,23$ ) of the series can be considered as a representative model and for this reason its commutation abilities were studied in details.



*Scheme 8. Schematic representation showing the two different sites evidenced by acid.*

### A. Acidochromic properties.

As mentioned previously, the UV-Visible spectroscopy represents certainly the most convenient technique to monitor the commutation of elaborated systems under stimulation. In this context, the closed form of ligands **31** and **32** are characterized by an absorption band centered at 245 nm without any significant effect of lateral substituents of BOX as shown on the table 4 below.



*Table 4. UV-Visible spectra of compounds 31 and 32 under their C form in ACN solution.*

In all cases, the stimulation of the system by addition of acid aliquots leads to a strong modification of the UV-Visible absorption spectra. As example, the variation of the UV-visible spectra of compound **32** as function of the added quantity of HCl is represented on figure 5.

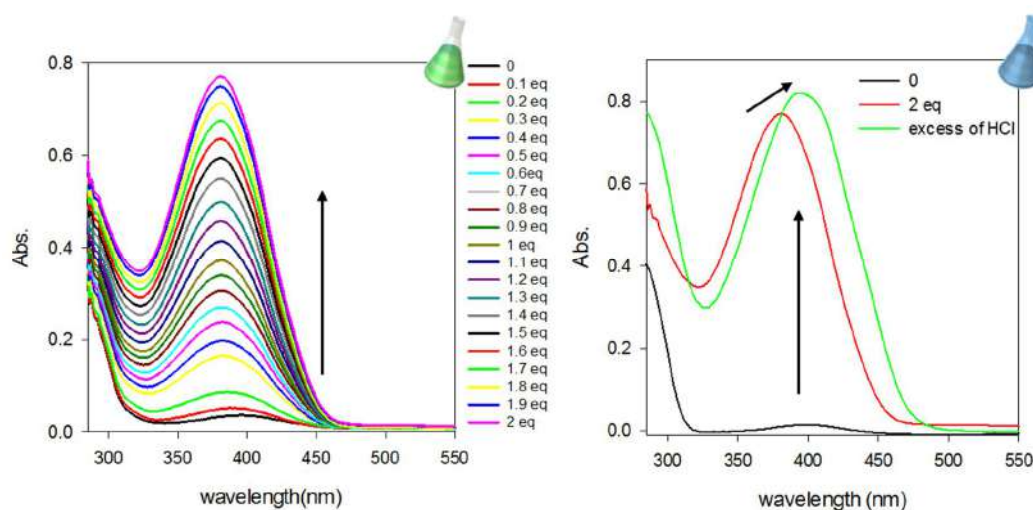
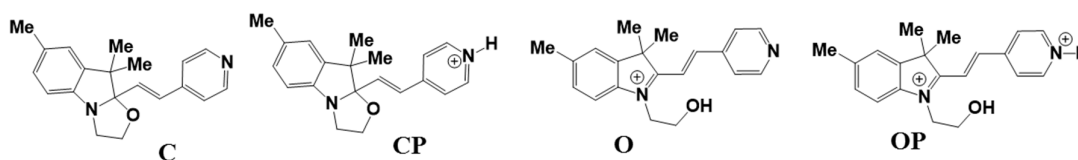


Figure 5. UV-Visible spectrum changes of a solution of ligand **32** in ACN (0.03mM) upon addition of HCl.

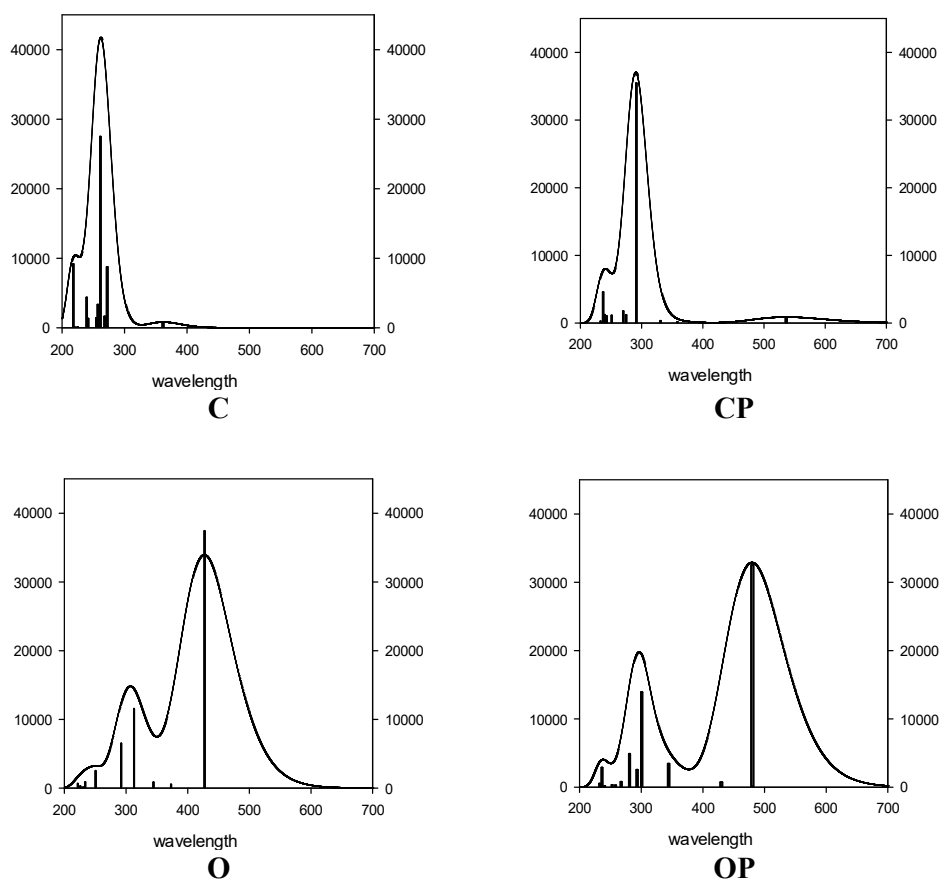
One can observe that the solution turns deep yellow upon acidification with hydrochloric acid. In fact, we notice the gradual formation and then increase of a unique intense band centered on 381nm (figure 5, left) upon the addition of HCl aliquots until 2 eq. without isosbestic point. This behavior suggests that both basic sites (BOX and pyridine) react with the acid without full control of processes suggesting that several species are generated. Indeed, four different species can be envisioned depending on the open/close status of the BOX and the protonation status of the pyridine moiety which will be referenced as **C**, **CP**, **O** and **OP** (Scheme 9).



Scheme 9. Four possible different forms of ligand **32**.

More important, the stationary state is reached only by adding an excess of acid leading to additional hyper- and bathochromic shifts of the visible absorption band (14 nm). This behavior seems indicating that an important quantity of acid is required to displace completely the system through the formation of the supposed **OP** state characterized by a maximum absorption wavelength of 395 nm.

In order to support this assumption, ab-initio quantum calculations were performed with the Gaussian 09 package of programs at a hybrid density functional theory (DFT) and time-dependent density functional theory (TD-DFT) levels carried out using the B3LYP-6.311 G(d) as basis for all 4 different forms.



**Figure 6.** UV-visible absorption spectra computed by B3LYP-6.311 G(d) methodology of **C**, **CP**, **O** and **OP** forms of ligand.

#### Chapter 4: Syntheses and characterizations of ligands incorporating BOX units.

Figure 6 shows the simulated spectra for all forms of ligand **32**. At first, the protonation of the pyridine (from **C** to **CP**) induces a poor variation of the absorption spectrum (bathochromic shift from 261 to 291 nm respectively). However, when these spectra are compared with the experimental data the absorption peak which corresponds to the **C** form fits very well showing a slight bathochromic shift (16nm). On the other hand, theoretical calculations predict that the opening of BOX will induce the strongest variation of the absorption spectra. In fact, simulated spectra of **O** and **OP** forms exhibit a maxima absorption wavelength of 427 nm and 480 nm respectively resulting from an enhancement of the conjugation. As consequence, the theoretical calculation fits well with the experimental results in which the yellow coloration can correspond to the formation of a mixture **O** and **OP** as the **CP** form should not induce strong variation of the visible spectra.

To confirm this assumption, proton NMR spectroscopy has been here used to unambiguously confirm the randomly generation of **CP**, **O**, **OP** forms upon acid stimulation. Solubility issues have unfortunately conducted to undergo these experiments in DMSO instead of acetonitrile. Under its closed form, compound **32** presents a simple proton NMR spectrum (figure 7) allowing an easy assignment of each signal.

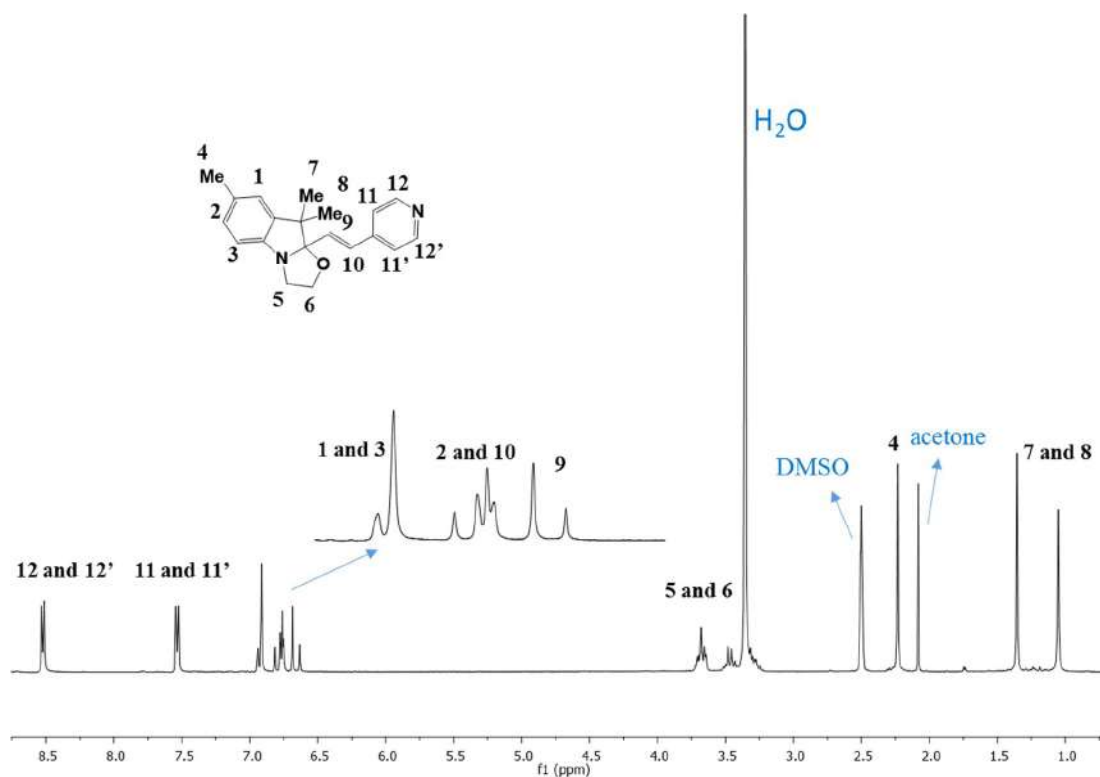


Figure 7.  $^1\text{H}$  NMR spectrum of ligand **32** in DMSO ( $(\text{CD}_3)_2\text{SO}$ ) at rt.

On this latter, we notice all the spectral characteristics of closed BOX derivatives:

- the two vinyl doublets (C=C linkage) at 6.66 and 6.79 ppm with a J coupling constant of 16 Hz confirming the trans isomery of the system,
- the three singlets at 1.05, 1.36 and 2.23 ppm assigned to the three methyl groups on the indoline part,
- a series of multiplets ranging from 3.2 to 3.78 ppm corresponding to the methylene groups adjacent to the nitrogen and oxygen atoms.

In addition to these classical indicators, the two doublets at 7.53 and 8.52 ppm with a J coupling constant of 5.9 Hz assigned to the pyridine unit are also useful.

As we can see on figure 8, the acidification of the media by adding some HCl aliquots conducts to observe a strong modification of the NMR spectra.

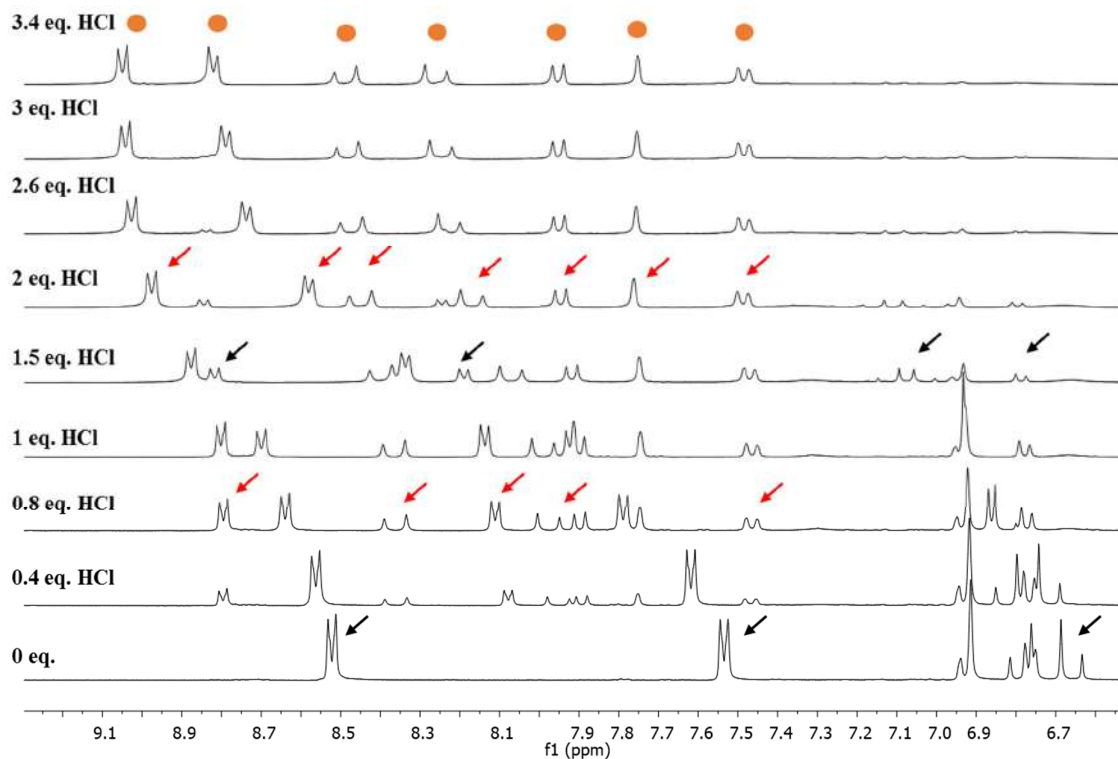
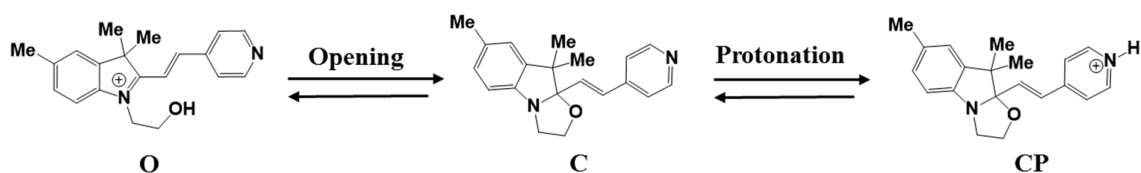


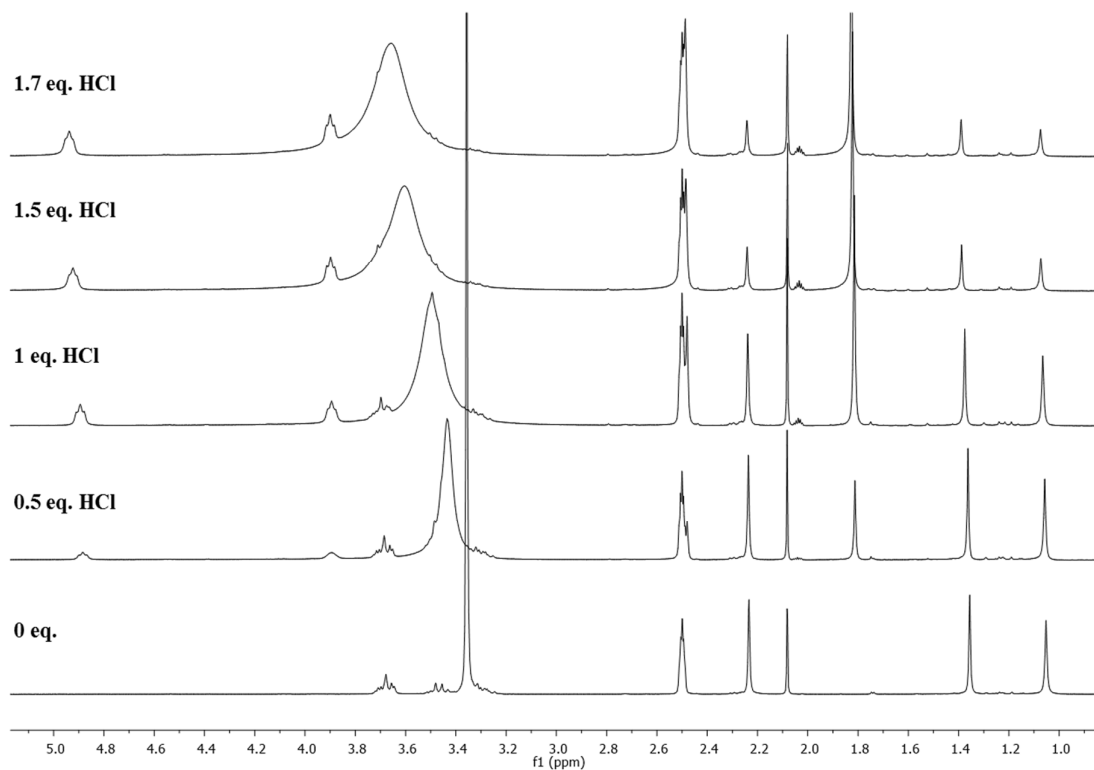
Figure 8.  $^1\text{H}$  NMR spectra upon titration of ligand **32** (14 mM) by HCl in DMSO- $d_6$  at 20°C up to 3.4 equivalents.

As expected, the characteristic peak-intensities of closed form (**C**) signals decrease with the addition of acid and a new set of signals is generated in agreement with the opening of BOX unit (red arrows). In complement, we notice that this HCl addition conducts also to observe a gradual displacement of the closed form peaks (black arrows) to higher chemical shifts. As example, both doublets assigned to pyridine protons initially at 8.52 and 7.53 ppm are strongly low field shifted to 8.70 and 7.92 ppm, respectively, after addition of one equivalent of HCl. We have to wait more than 1.5 equivalent to observe their stabilization. Already observed in the case of several pyridine derivatives,<sup>[18]</sup> such behavior translates a fast equilibrium at the NMR time scale between corresponding pyridine and pyridinium form. As consequence, the observed chemical shift is a function that depends on the ratio between both species (**C/CP**) and the chemical shift of each species. In this context, we can confirm that the addition of acid leads to the opening of oxazolidine ring (**O** form) and in the same time, the protonation of the pyridine moiety while the oxazolidine remains closed (**CP** form) (scheme10).



*Scheme 10.* The two different possibilities of ligand 32 (**O** and **CP**) upon addition of HCl (below 1.5 eq).

Naturally, these assumptions are confirmed by the observation of corresponding modification in the aliphatic range (figure 9).



*Figure 9.* Assigned aliphatic protons of the generated states of ligand 32 up to 1.7 equivalents of HCl.

Corresponding to a close oxazolidine ring (**C** and **CP**), the following signals decreases in intensity gradually:

- a set of unresolved multiplets between 3.3 and 3.73 ppm showing that a BOX function is in closed form

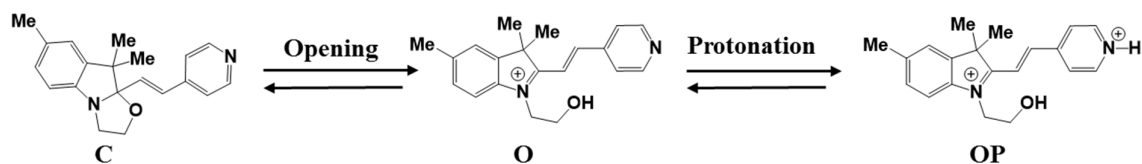
#### Chapter 4: Syntheses and characterizations of ligands incorporating BOX units.

- three singlets in the aliphatic region showing an integration for 3 protons each at 1.07, 1.38 and 2.24ppm

In agreement with the formation of an indoleninium (**O** form), we notice the appearance of the following new aliphatic signals:

- two triplets at 3.89 and 4.89 ppm corresponding on the pendant aliphatic chain,
- two singlets at 2.48 and 1.82 ppm in the aliphatic region integrating for 3 and 6 protons and corresponding to the methyl groups on the indoleninium in position 5 and 3 respectively.

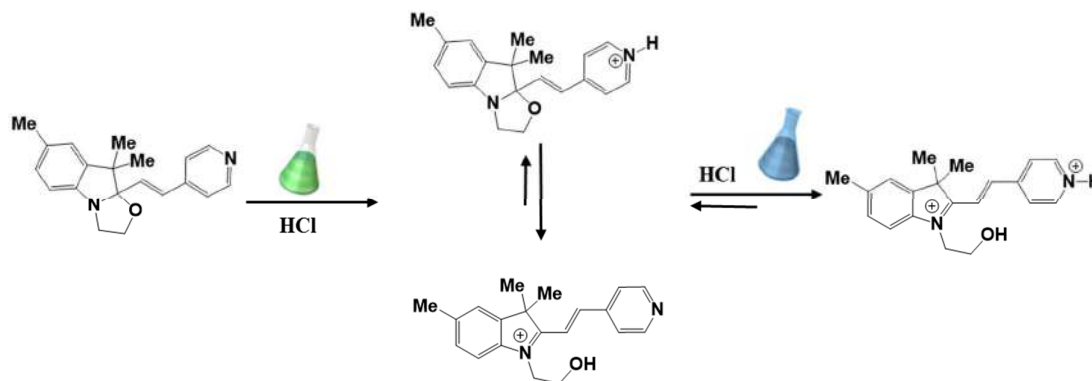
After 2.0 equivalents of HCl no trace of **C** or **CP** species can be detected anymore, suggesting that the equilibrium is fully displaced through the open form. Nevertheless, the signal of the open form starts to shift to lower field as soon as the quantity of acid reaches 1.0 equivalent. We can conclude that the pyridine/pyridinium equilibrium evidenced when the BOX is closed is still effective once the oxazolidine ring is opened but should exhibit a lower pKa value.



*Scheme 11 Displace of equilibrium from **O** to **OP** form upon further acidification.*

A stationary point is observed for 3.4 eq, allowing to conclude that the equilibria are fully displaced through the **OP** form (orange circles, figure 8) characterized by a pair of doublets at 8.79 and 9.04ppm with a vicinal coupling constant of 6.5 Hz. The two doublets at 8.25 and 8.48 ppm displaying a vicinal coupling constant of 16.6 Hz and assigned to the ethylenic protons confirm that neither the protonation of the pyridine moiety nor the oxazolidine ring opening influence the C-C double bond isomery.

To conclude, it was shown that the addressability of the different ligands by HCl leads to a complex mixture of **C**, **CP**, **O** and **OP** forms in equilibrium due to the competition of two acido-basic reactions. Nevertheless, it is possible to fully displace the equilibrium by introducing a large excess of acid and convert exclusively the initial compound to corresponding **OP** form (scheme 12).

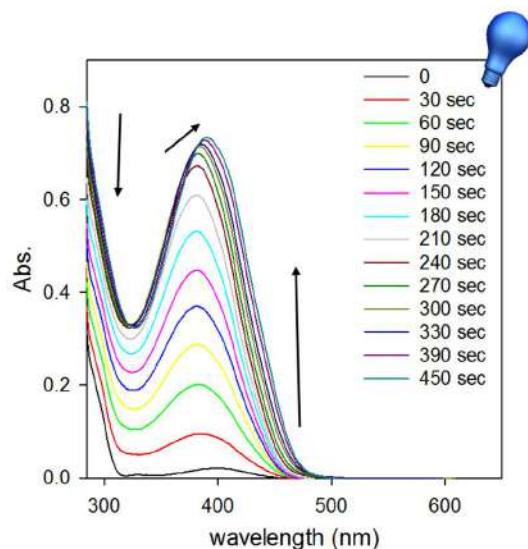


*Scheme 12. Different states generated upon stimulation by HCl.*

In chapter two on BiBOX series, we have demonstrated that the selectivity and the efficiency of the BOX addressability is strongly influenced by the nature of the stimulation. In this context, the possibilities to induce selectively the opening of the oxazolidine ring by irradiation or oxidation were explored.

### B. Photochromic properties.

As mentioned earlier, the oxazolidine ring opening can be photoinduced by an irradiation at 254 nm light in presence of chlorobenzene.<sup>[19]</sup> For this reason, the evolution of a solution of ligand **32** under its closed form submitted to successive periods of illumination was followed by UV-visible spectroscopy by recording spectrum between each period of irradiation (figures 10).

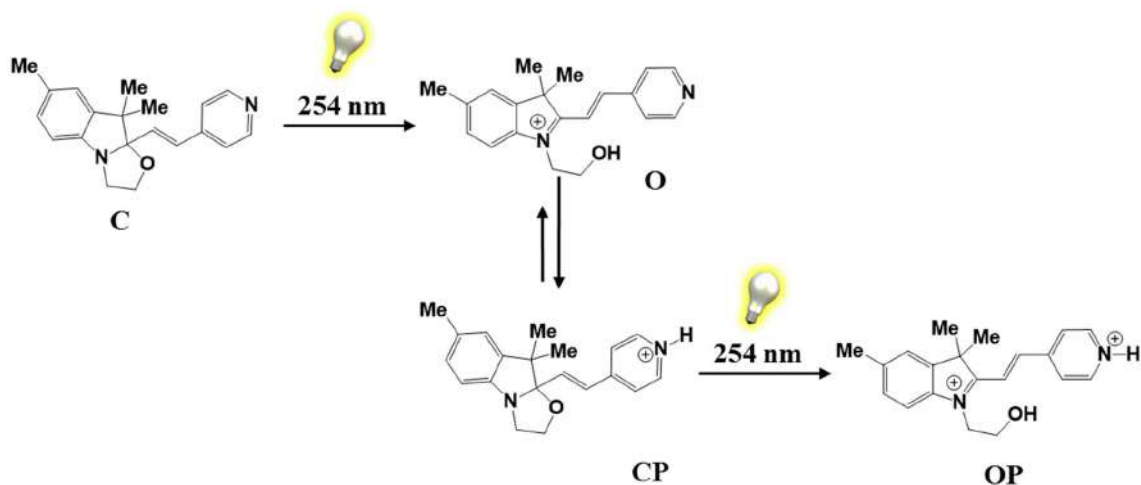


**Figure 10.** UV-Visible spectrum changes of a solution of ligand **32** in ACN (0.03mM) upon irradiation at 254 nm.

As we can observe, this UV irradiation leads to strong yellow coloration of the solution. Indeed, the appearance of a new broad absorption band centered at 381 nm is noticed up to 270 seconds of irradiation. Analogously to acidochromic experiments, maintaining the stimulation of the system lead to observe additional hyper- and bathochromic shifts of the visible absorption band (396 nm) and a photo-stationary state is reached after 450 seconds.

More important, an overlapping of the UV-visible spectra obtained by either irradiation or acidic titration confirm that both stimulations lead at the end to the same state (**OP**), and then, confirms the multi-modal switching abilities of ligand **32**.

At the first sight, the photo-generation of **OP** form under UV irradiation is not trivial. In order to explain this behavior, we have to consider a direct equilibrium between the **O** and the **CP** forms. In this context, the irradiation of the ligand **32** leads to its corresponding open form. Due to the mentioned tautomeric equilibrium between both forms, the concentration of **CP** forms starts to increase as function of irradiation time. Under this **CP** form, the system is likely to undergo another photoinduced oxazolidine ring opening leading to corresponding **OP** form as resumed on the scheme below.

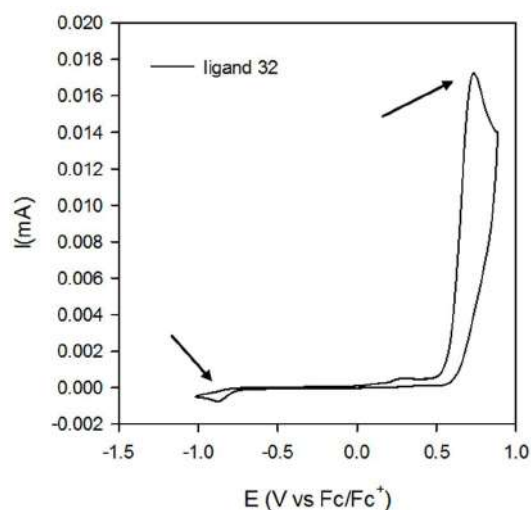


*Scheme 13. Different states generated upon irradiation at 254 nm.*

To verify the existence of a tautomeric equilibrium between **O** and **CP** forms, we have studied the electrochromic properties of the system which should lead to the same results.

### C. Electrochromic properties.

In this context, the electrochemical behavior of ligand **32** has been investigated by cyclic voltammetry (CV) and its voltamperogram is presented in figure 11.

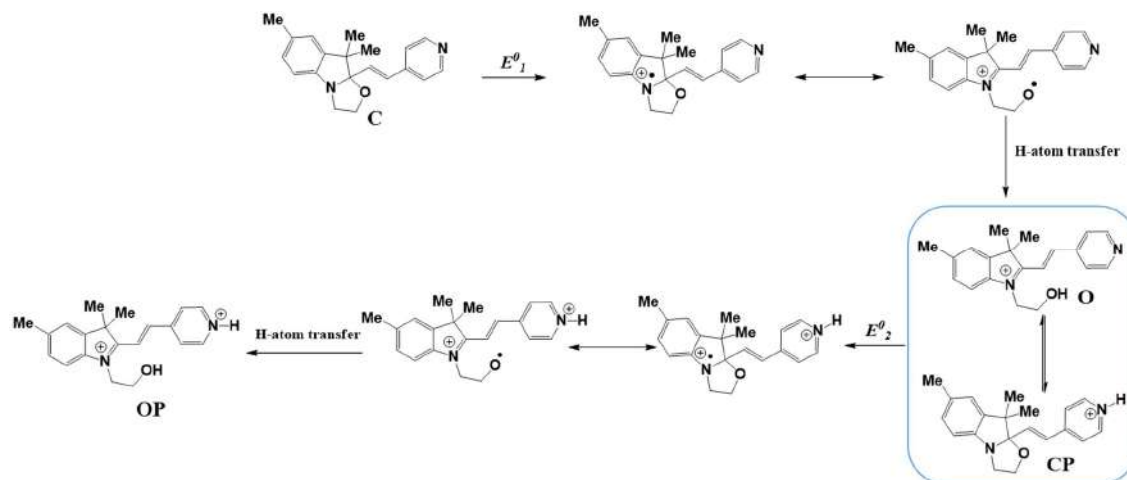


*Figure 11. Cyclic voltammetry of compound 32 at 100 mV/s (0.62 mM).*

## Chapter 4: Syntheses and characterizations of ligands incorporating BOX units.

As shown on Figure 11, the ligand **32** exhibits a non-reversible oxidation potential at 0.74V vs Fc/Fc<sup>+</sup>. The assignment of this electrochemical process to an oxidation mainly localized on the indoline unit leading to corresponding radical cation is in agreement with previous reported oxidation potential for isolated BOX.<sup>[20]</sup> More important, this oxidation generates a non-reversible reduction process (around -0.88 V) on the scan back. This typical electrochemical behavior indicates that the generated radical cation undergoes a chemical process leading to the opening of the oxazolidine ring. However, we have noticed a much more important difference of charge exchanged during the oxidation (BOX opening) and the reduction process (BOX closure) in comparison with other BOX derivatives studied during this thesis.

To explain this behavior, we have hypothesized that the electrochemical stimulation leads, as in the case of photo- and acido-stimulation, to the generation of the **OP** form according to the ECEC mechanism as presented on Scheme 14.

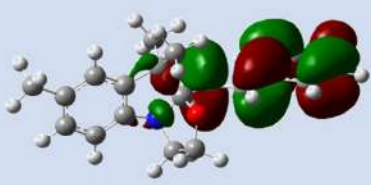
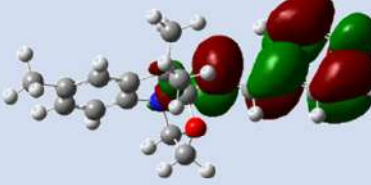
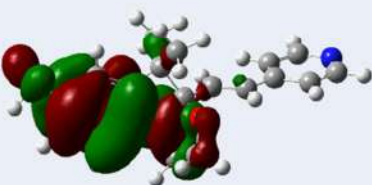
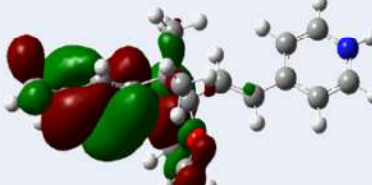


*Scheme 14. Proposed mechanism for the commutation of ligand **32** under stimulation with electrochemical potential.*

Indeed, the oxidation of the **C** form generates the corresponding radical cation which undergoes a chemical processing leading to the **O** form. Due to a tautomeric equilibrium, the **O** form is partially converted to **CP** form. Acting independently when the oxazolidine ring is

closed, the system is able to undergo an oxidation process at the same potential leading to the corresponding radical cation and at the end to the **OP** form.

This hypothesis is supported by performed theoretical calculations on the molecular system **32** under its **C** and **CP** forms. At first, in both forms the HOMO are localized on the BOX unit while LUMO are located on the pyridine, this can translate that the oxidation should happen directly on BOX. In addition, the variation of the HOMO energy level due to the generation of corresponding pyridinium acting as an electron withdrawing group, is quite limited. Indeed, the difference of HOMO energy between the two forms is 0.14eV which is much lower than in BiBOX and TriBOX systems. As we have observed this variation was not sufficient to observe in CV a clear differentiation of oxidation peaks between both states (**C** and **CP**) of the molecule.

	<b>C</b>	<b>CP</b>
<b>LUMO</b>	 -1.72eV	 -3.09eV
<b>HOMO</b>	 -5.76eV	 -5.90eV

*Table 5. DFT visualization of ligand 32 displaying the HOMO and LUMO under its **C** and **CP** forms.*

In order to verify this assumption, ligand **32** was investigated by using  $\text{NOSbF}_6$  as an oxidizing reagent. The electronic absorption spectra of the studied ligand are presented in figure 12.

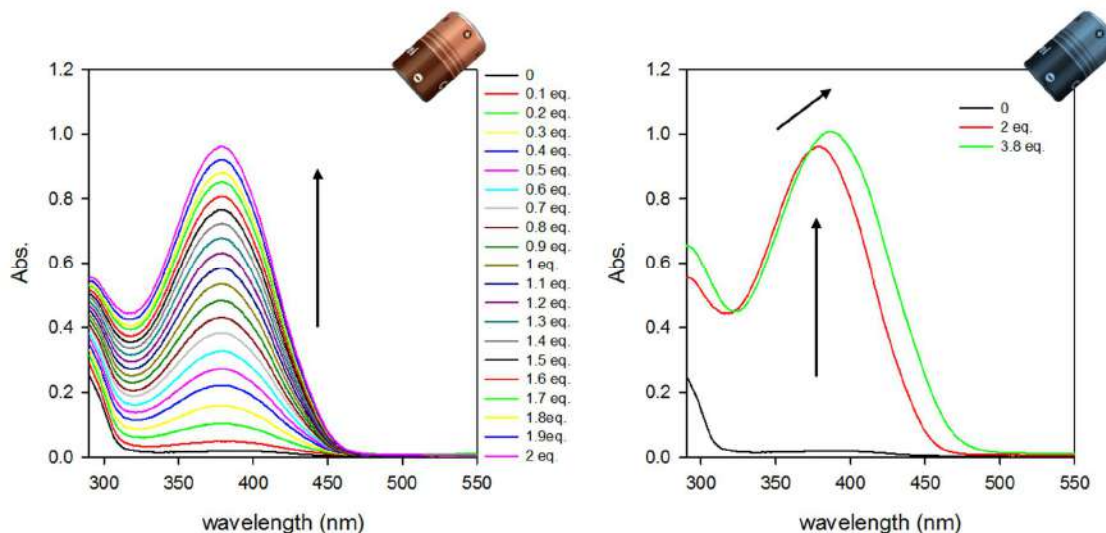


Figure 12. UV-Visible spectrum changes of a solution of ligand **32** in ACN (0.03mM) upon addition of HCl.

In this case and as expected, a drastic change of UV-Visible spectra upon the addition of  $\text{NOSbF}_6$  aliquots is observed (figure 12):

- generation of a broad absorption band centered at 381nm upon addition of oxidant up to 2 equivalents,
- generation of a bathochromic shift (from 381 to 396nm) upon further addition of  $\text{NOSbF}_6$ ,
- no isosbestic point observed.

Following these observations, the overlapping of the UV-visible spectra obtained by  $\text{NOSbF}_6$  or acidic titration can be noticed, then translating that both stimulation lead to the same commutation, and then, confirming the multi-modal switching abilities of these molecular systems.

#### **IV). Conclusion**

In this chapter, we have demonstrated that the functionalization of a nitrogen heterocycle by some BOX units did not raise any particular difficulties. As consequence, a large library of mono-; bi- and tetradentate ligands incorporating one or two BOX units were successfully prepared.

If the introduction of the different nitrogen heterocycle such as pyridine, bipyridine and phenanthroline as metal binding functionality did not perturb the synthesis, it conducts to the establishment of a tautomeric equilibrium between **O** and **CP** forms. As consequence, the stimulation of the different systems leads to a protonated open form (**OP**) whatever the nature of the stimulation.

Considering this **OP** form as a weak diacid specie unable to form some complex, it offers new prospects such as the controlled release of complexed cationic ions, or the cleavage of pH sensitive bond such as imine one under stimulation. If this latter part is still under progress, the formation of corresponding metal complexes by coordination chemistry and their stability under stimulation is detailed in the next chapter.



## V). References

- [1] A. Fihey, A. Perrier, W. R. Browne and D. Jacquemin, *Chemical Society Reviews* **2015**, *44*, 3719-3759.
- [2] E. C. Harvey, B. L. Feringa, J. G. Vos, W. R. Browne and M. T. Pryce, *Coordination Chemistry Reviews* **2015**, *282*, 77-86.
- [3] A. Coleman, C. Brennan, J. G. Vos and M. T. Pryce, *Coordination Chemistry Reviews* **2008**, *252*, 2585-2595.
- [4] G. D. Henry, *Tetrahedron* **2004**, *29*, 6043-6061.
- [5] F. Dumur, E. Dumas and C. Mayer, *Syst* **2007**, pp. 70-103.
- [6] C. Kaes, A. Katz and M. W. Hosseini, *Chemical reviews* **2000**, *100*, 3553-3590.
- [7] C. Luman and F. Castellano, *ChemInform* **2004**, *35*, no-no.
- [8] L. A. Summers in *The phenanthrolines*, Vol. 22 Elsevier, **1978**, pp. 1-69.
- [9] M. Hayami and S. Torikoshi in *Color-changing compounds*, Vol. DE2541666A1, **1976**.
- [10] G. Sevez in *Conception, synthèse et étude de nouveaux switches multimodulables*, Vol. Bordeaux 1, **2009**.
- [11] G. r. Szalóki and L. Sanguinet, *The Journal of organic chemistry* **2015**, *80*, 3949-3956.
- [12] P. D. Beer, F. Szemes, P. Passaniti and M. Maestri, *Inorganic chemistry* **2004**, *43*, 3965-3975.
- [13] V. M. Iyer, H. Stoeckli-Evans, A. D'Aléo, L. D. Cola and P. Belsler, *Acta Crystallographica Section C: Crystal Structure Communications* **2005**, *61*, o259-o261.
- [14] H. Schiff, *Ann. Chem. Suppl* **1864**, *3*, 343-349.
- [15] M. Shu, W. Sun, C. Duan, Y. Fu, W. Tang and W. Zhang, *Science in China Series B: Chemistry* **1999**, *42*, 501-510.
- [16] I. A. Riddell, T. K. Ronson, J. K. Clegg, C. S. Wood, R. A. Bilbeisi and J. R. Nitschke, *Journal of the American Chemical Society* **2014**, *136*, 9491-9498.
- [17] B. G. Tehan, E. J. Lloyd, M. G. Wong, W. R. Pitt, E. Gancia and D. T. Manallack, **2002**, *21*, 473-485.
- [18] C. S. Handloser, M. R. Chakrabarty and M. W. Mosher, *Journal of Chemical Education* **1973**, *50*, 510.
- [19] N. Sertova, J.-M. Nunzi, I. Petkov and T. Deligeorgiev, *Journal of Photochemistry and Photobiology A: Chemistry* **1998**, *112*, 187-190.
- [20] R. Hadji, G. Szaloki, O. Aleveque, E. Levillain and L. Sanguinet, *J. Electroanal. Chem.* **2015**, *749*, 1-9.



---

**Chapter 5: Elaboration of multi-level molecular systems based on coordination chemistry.**

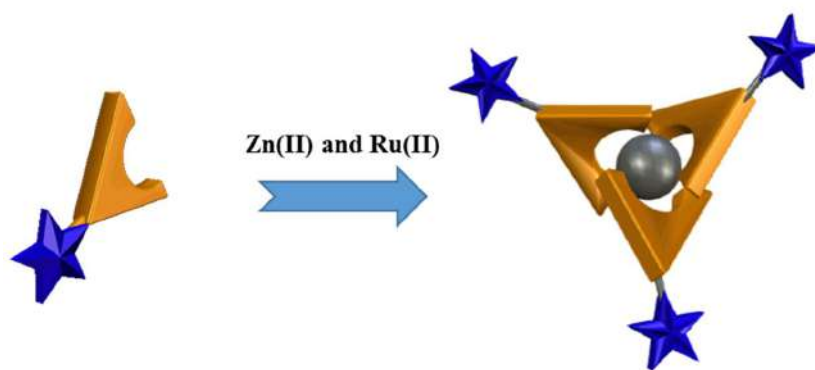
---



## I). Introduction

In our objective to elaborate multi-level molecular systems incorporating several BOX moieties, two main approaches were explored during this thesis. The first one has consisted in connecting BOX units around a pi-conjugated core in order to take advantage of through bonds interactions to assure their selective addressability (see chapter 2 and 3). The second one consists in taking advantage of coordination chemistry to place the different BOX units in a specific spatial arrangement around a metallic ion in order to promote through space interactions.

If the introduction of a transition metal ion in the close vicinity of a multimodal switchable unit such as BOX could open new prospects,<sup>[1]</sup> the elaboration of such complexes stays, to the best of our knowledge, unreported. In this context, we have prepared a library of ligands incorporating one or two BOX moieties (see chapter 4). As consequence, the present chapter reports our effort in the preparation and the preliminary characterizations of novel complexes bearing BOX as a switchable unit.



*Figure 1. Schematic representation of complexes with ligands incorporating a BOX unit.*

Among the large possibilities of useful transition metal ion in coordination chemistry, we have focused our efforts on the elaboration of complexes based on two of them (figure 1): Zn(II) and Ru(II), as their syntheses appear selective, relatively easy and well documented.

First, we report the synthesis and the characterization of a first series of complexes involving a zinc metal center and various ligands (31-42). Based on these preliminary results, we have pursued our efforts with two promising ligands (37 and 39) in order to elaborate corresponding Ru(II) complexes. The influence of those ligands on spectroscopic and photophysical properties of the Ru(II) polypyridyl complexes as well as their commutation abilities will be discussed.

## **II). Elaboration and characterization of multi-level molecular systems by coordination chemistry of Zn(II)**

Among the large variety of transition metal ions available, the choice to elaborate some Zn(II) complexes was motivated by numerous reasons<sup>[2]</sup> such as:

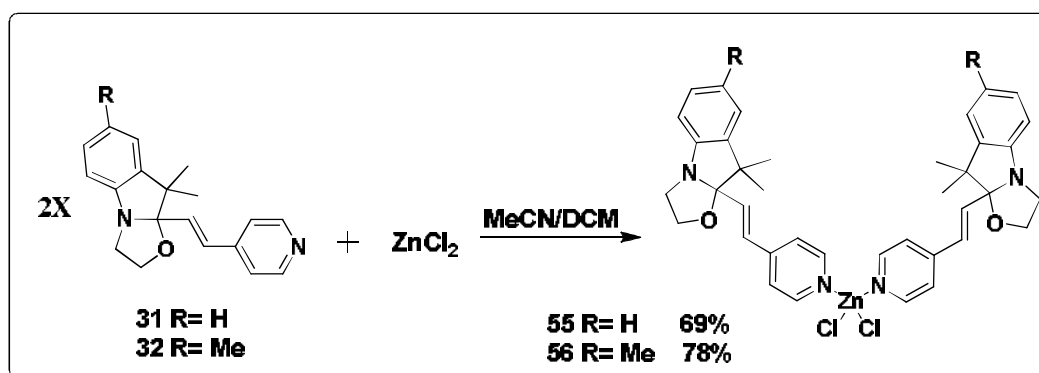
- an extensive and well documented coordination chemistry;
- a well-known propensity to form a large variety of complexes, especially with nitrogen, oxygen, sulfur, and halide donor ligands;
- a large range of coordination numbers varying from 2 to 8, such as example in  $\text{ZnEt}_2$  and  $[\text{Zn}(\text{NO}_3)_4]^{2-}$  respectively, leading to various geometries with a domination of tetrahedral and octahedral architectures;
- Zinc complexes have in recent years taken a considerable importance in the generation and self-assembly of a great range of 1-, 2-, and 3-D infinite structures;
- Zinc plays an essential role in biology, being a key constituent of at least 200 metalloproteins;
- Zn relative redox inactivity<sup>[3]</sup> is an asset to assure the observation of the electrocommutation of the BOX ligand as its diamagnetic properties<sup>[4]</sup> allow to monitor this commutation by NMR spectroscopy.

## Chapter 5: Elaboration of multi-level molecular systems based on coordination chemistry

Thus, herein, the syntheses and commutation behaviors of three kind of zinc complexes are described using N-heterocycles (pyridine, bipyridine or phenanthroline) bearing one or two BOX unit.

### A. Synthesis of Zinc complexes based on pyridine ligands.

The preparation of coordination compounds of pyridine and zinc salts was firstly reported by R. Varet in 1891.<sup>[5]</sup> Since this date, numerous studies were dedicated to their preparation and characterization such as example their formation constant.<sup>[6]</sup> In addition, the easy access to BOX based ligand **31** and **32** in which the metal binding functionality is a simple pyridine have driven us to perform our first attempts of coordination chemistry on them. As depicted on Scheme 1, classical experimental conditions used at the laboratory<sup>[7]</sup> allow the preparation of Zn(II)-pyridine complexes **55** and **56** in 69 and 78% yield respectively.

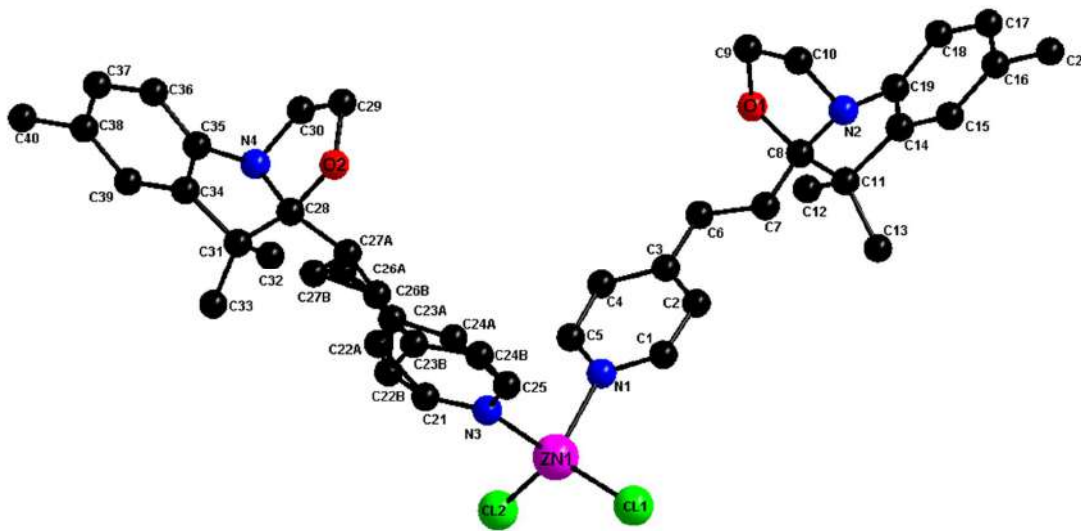


*Scheme 1. Synthesis of the Zinc (II) complexes with pyridine derived ligands.*

This one step procedure consists in mixing a solution of zinc chloride with appropriate ligand dissolved in DCM in a 2:1 ratio. The targeted complexes **55** and **56** referenced later by the formula  $\text{Zn}(\text{L})_2\text{Cl}_2$  and  $\text{Zn}(\text{L}')_2\text{Cl}_2$  respectively, are isolated by precipitation when diethyl ether is added. As usual, NMR spectroscopy (proton and carbon), IR and mass spectrometry were used to confirm the formation of complexes as well as the 2 to 1 ratio between ligand and Zinc.

## Chapter 5: Elaboration of multi-level molecular systems based on coordination chemistry

Fortunately in the case of **56**, it was possible to obtain some single crystals suitable for X-ray diffraction studies by the slow diffusion of latter dissolved in  $\text{CH}_3\text{CN}:\text{CH}_2\text{Cl}_2$  (1/1, v/v) into an ethylic ether layer. With selected parameters of the X-ray diffraction data collection and refinement (gathered in experimental section), it was possible to resolve the 3D structure of the complex presented below.



**Figure 2.** Crystal structure representation of zinc complex  $\text{Zn}(\text{L}')\cdot\text{Cl}_2$  with the atom-numbering scheme.

This complex crystallizes in a monoclinic system space group  $C2/c$ , with one independent molecule in the unit cell. The zinc ion is tetracoordinated leading to a classical tetrahedral geometry and selected bond lengths are resumed in Table 1. The distorted tetrahedral coordination sphere is formed by two pyridine nitrogen atoms and two chlorine atoms. As observed for free ligand, the indoline and pyridines moieties in each ligand are not coplanar and similar values of dihedral angle are measured ( $74.77(2)^\circ$  and  $69.41(2)^\circ$ ).

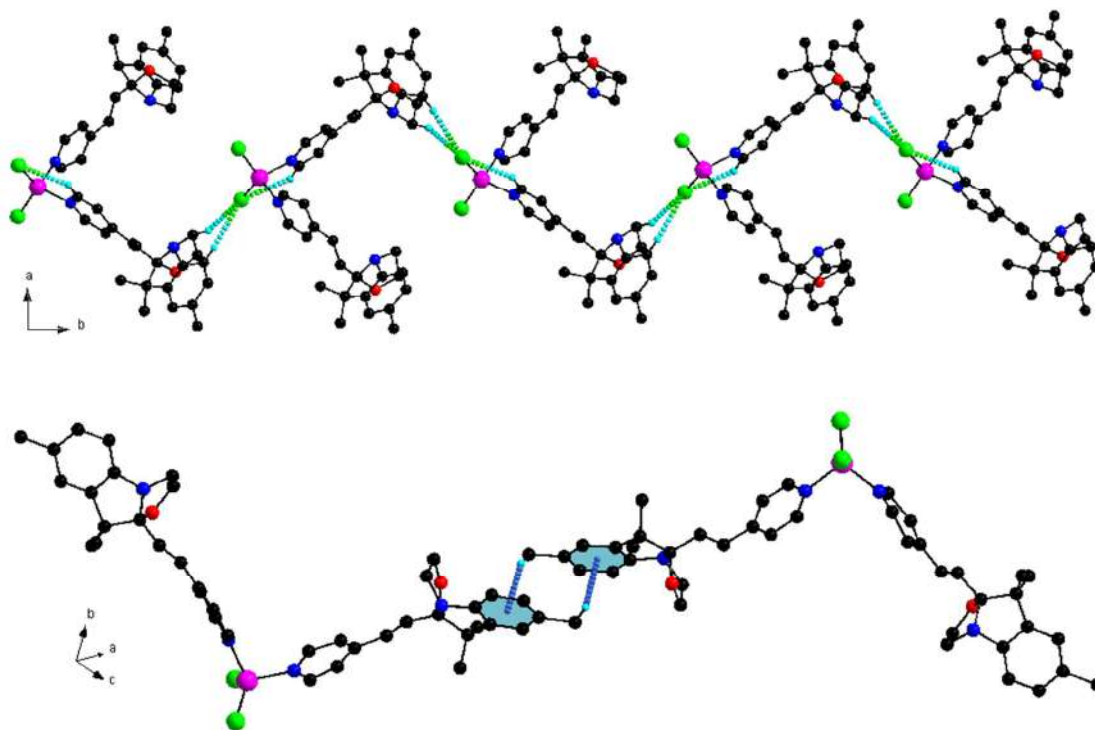
Furthermore, we can note that the geometry around Zn is affected by the presence of an intramolecular  $\text{H}\cdots\text{anion}$  interaction between the chlorine atom Cl1 coordinated to zinc and the hydrogen from pyridine ring (figure 3 top), as suggested by the C1–H1 $\cdots$ Cl1 distance of

## Chapter 5: Elaboration of multi-level molecular systems based on coordination chemistry

2.893(2) Å. As a consequence of this interaction, the Zn–Cl2 distance (2.222(2) Å) is significantly longer than Zn1–Cl1 (2.203(2) Å).

The angle formed by the zinc center and chlorine atoms equal to 123.79(8) ° what is higher than the angle formed between nitrogen atoms and the angles formed between nitrogen atom and chlorine atom N1–ZN1–N3, CL1–ZN1–N1, N3–ZN1–CL2 respectively are 99.10(6), 105.00(4), and 107.19(5)°.

In the crystal lattice, short intermolecular (figure 3 top) C–H···Cl contacts (C10–H10···Cl1= 2.691(2) Å) are established between chlorine atoms and hydrogen atoms from the oxazolidine rings from neighboring molecules resulting in a supramolecular chain parallel to the crystallographic *c* axis.



**Figure 3.** Perspective of the supramolecular chain generated by hydrogen bonding C–H···Cl (green-cyan dashed lines) in complex in the *ab* plane (top), and those reinforced by C–H··· $\pi$  (blue dashed line, bottom).

These supramolecular interactions are completed by C–H··· $\pi$  intermolecular interactions along the *a* axes between the indoline phenyl ring of one molecule and the hydrogen

**Chapter 5: Elaboration of multi-level molecular systems based on coordination chemistry**

---

atom from methyl group connected to the phenyl of the neighboring complex molecule (H40⋯centroid 2.819 (2) Å and H20B⋯centroid 2.640 (2) Å, (figure 3 bottom).

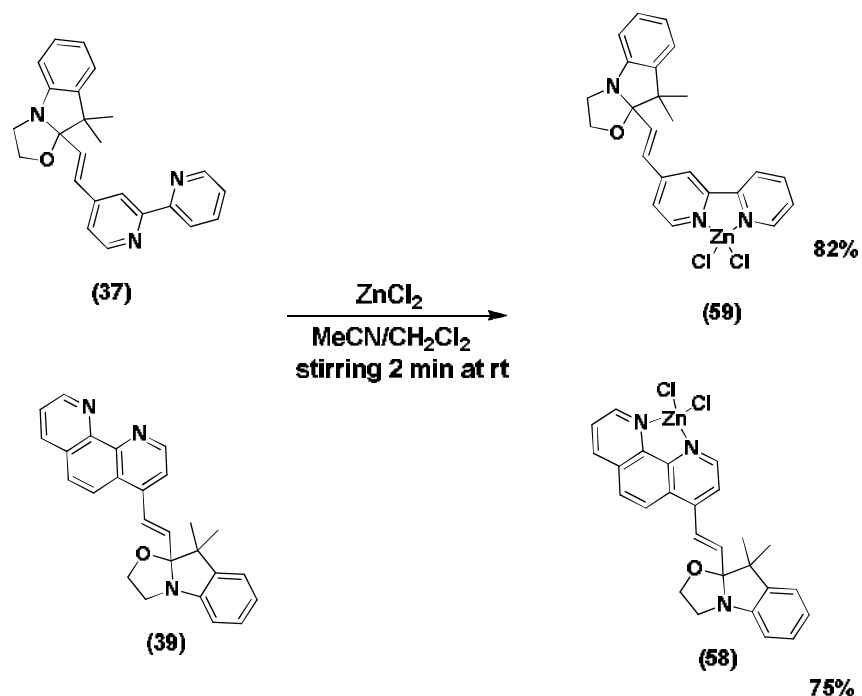
bond length (Å)			
C1—C2	1.348	C8—C11	1.533
C2—C3	1.387	C11—C12	1.536
C3—C4	1.360	C11—C13	1.517
C4—C5	1.373	C11—C14	1.522
C5—N1	1.331	C14—C15	1.391
C3—C6	1.472	C15—C16	1.374
C6—C7	1.321	C16—C20	1.522
C7—C8	1.501	C16—C17	1.365
C8—O1	1.449	C17—C18	1.414
O1—C9	1.428	C18—C19	1.390
C9—C10	1.513	ZN1—N1	2.048
N2—C8	1.468	ZN1—N3	2.046
ZN1—CL1	2.203	ZN1—CL2	2.222

*Table 1. Selected bond lengths (Å) in Zinc complex Zn(L')<sub>2</sub>Cl<sub>2</sub>.*

This preliminary result indicates that the metal binding functionality is not affected by the presence of the BOX unit. Indeed, the Box unit is not involved inside the coordination sphere of the metallic ion. It can then be presumed that the commutation abilities of the ligand will be preserved once the complexed formed. However, the known lability of pyridine zinc complexes in solution have driven us to expand our series of Zn complexes bearing some BOX units by using bidentate ligands such as bipyridine and phenanthroline based ones.<sup>[2]</sup>

## Chapter 5: Elaboration of multi-level molecular systems based on coordination chemistry

As consequence, the preparations of corresponding complexes were undertaken from ligands **36** and **39**. Analogous to **56** one, their preparation is resumed below (scheme 2).



*Scheme 2. Syntheses of the Zinc (II) complexes **58** and **59** with bipyridine and phenanthroline derived ligands.*

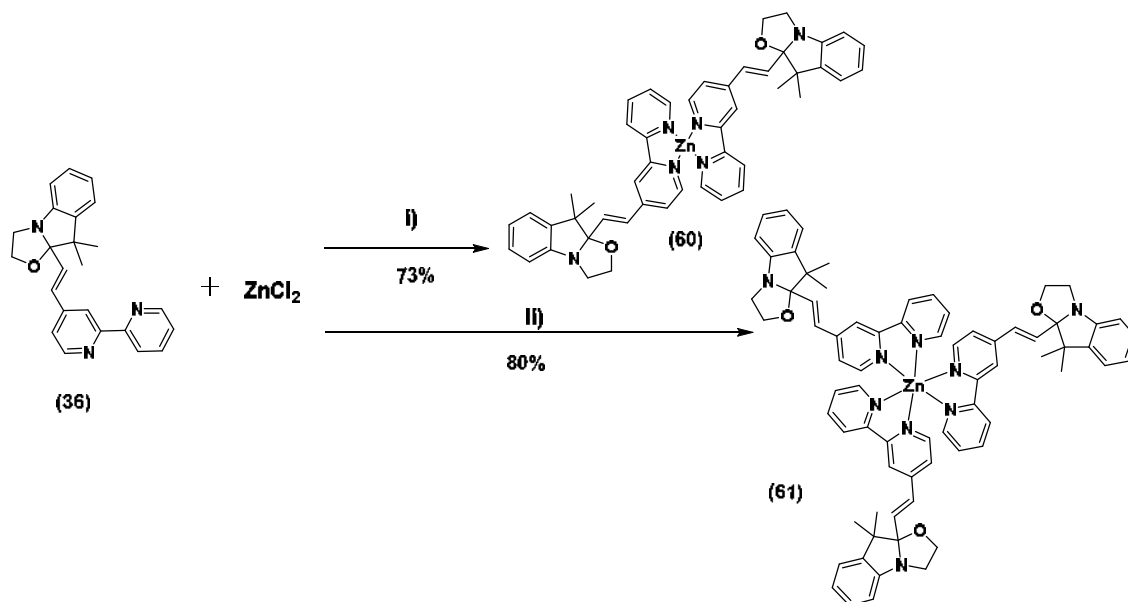
The structures of the two obtained complexes (**58** and **59**) were confirmed by NMR spectroscopy, IR and mass spectrometry.

Changing monodentate by bidentate ligand has certainly enhanced the stability of the generated complex but has also reduced the number of BOX units possibly arranged around the metal center, and as consequence, the number of reachable metastable states. To circumvent these issue two approaches were successfully explored.

The first one consists in changing the metal to ligand ratio, thanks to the large range of coordination numbers accessible for  $\text{Zn(II)}$ . As example, the control of bipyridine/ $\text{Zn}$  complexes stoichiometry is well documented and can be tuned from 1/1 up to 3/1 by playing on the experimental conditions.<sup>[8, 9]</sup>

## Chapter 5: Elaboration of multi-level molecular systems based on coordination chemistry

Following this approach, the novel complexes **60** and **61** were synthesized following a procedure inspired from that used for previous complexes. A mixture of ligand **36** and  $\text{ZnCl}_2$  were heated in  $\text{MeCN}/\text{CH}_2\text{Cl}_2$  at higher temperature ( $50\text{ }^\circ\text{C}$  for 3 hours) instead of stirring for two minutes at room temperature for  $\text{ZnL}_2\text{Cl}_2$  preparation. By applying these variations of experimental conditions to ligand **36** it was possible to extend the bipyridyl zinc complexes series to bis- and tris-bipyridyl ones as resumed on scheme 3.



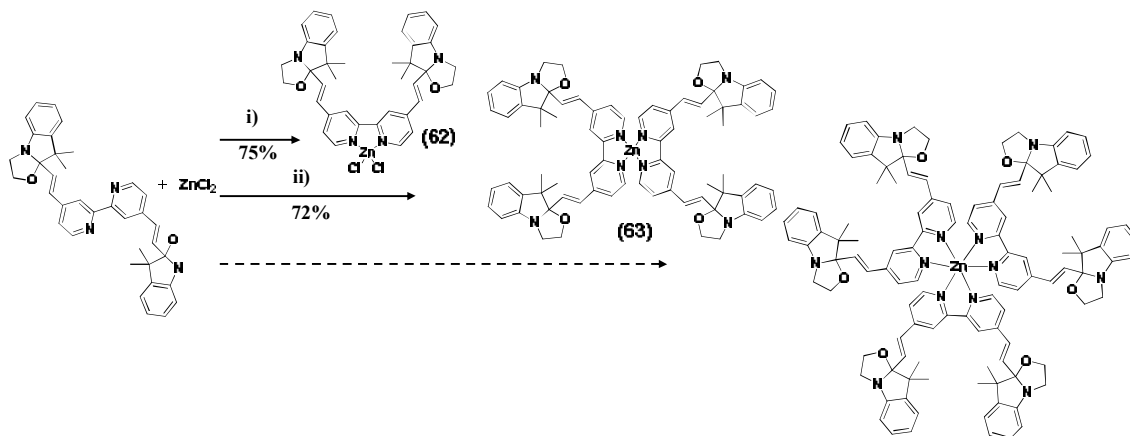
**Scheme 3.** Synthetic routes to complexes **60** and **61**. i) 2:1 (ligand: $\text{ZnCl}_2$ ),  $\text{MeCN}/\text{DCM}$ , stirred for 3 hrs. at  $50\text{ }^\circ\text{C}$ ; ii) 3:1 (ligand: $\text{ZnCl}_2$ ),  $\text{MeCN}/\text{DCM}$ , stirred for 3 hrs. at  $50\text{ }^\circ\text{C}$ .

In this context, if the structures and stoichiometry of complexes **36**, **60** and **61** were easily confirmed by NMR spectroscopy and mass spectrometry, we were unable to grow crystals of **60** and **61** of a sufficient quality to perform X-ray diffraction studies.

If this approach has successfully conducted to obtain some discrete molecular assemblies which are able to exhibit 2, 3 and 4 different metastable states respectively, the second strategy which consists in using ligand bearing two BOX units, could extend efficiently this number. By applying the same sequence of experimental conditions as mentioned above to

## Chapter 5: Elaboration of multi-level molecular systems based on coordination chemistry

BiBOX-bipyridyl ligand **44** (Scheme 4), the two new complexes **62** and **63**, able to exhibit 3 and 5 different metastable states were obtained. The synthesis of one additional complex based on coordinating three times ligand **44** (up to 7 possible metastable states) is still in progress.



**Scheme 4.** Synthetic route to complexes **62** and **63**. i) 1:1 (ligand:ZnCl<sub>2</sub>), MeCN/DCM, stirred for 2 min at rt; ii) 2:1 (ligand:ZnCl<sub>2</sub>), MeCN/DCM, stirred for 3 hrs at 50 °C.

Finally, the targeted molecular systems **62** and **63** were afforded as yellow solids in 75 and 72% yields respectively. Once again, their structures were confirmed by NMR spectroscopy, IR and mass spectrometry.

Fortunately in the case of **62**, it was possible to obtain some single crystals suitable for X-ray diffraction studies by the slow diffusion of latter dissolved in CH<sub>3</sub>CN:CH<sub>2</sub>Cl<sub>2</sub> (1/1, v/v) into an ethylic ether layer. With selected parameters of the X-ray diffraction data collection and refinement (gathered in experimental section), it was possible to resolve the 3D structure of the complex presented below (table 2).

## Chapter 5: Elaboration of multi-level molecular systems based on coordination chemistry

$Zn(H\text{-BOX})_2bPyCl_2$ ( <b>62</b> )	
<b>Monoclinic,</b> a = 14.4680(10) Å b = 14.0067(9) Å c = 16.3903(9) Å V = 3319.4(4) Å <sup>3</sup> Yellow crystals	<b>P2<sub>1</sub>/c</b> $\alpha = 90^\circ$ $\beta = 92.032^\circ$ $\gamma = 90^\circ$ Z = 4

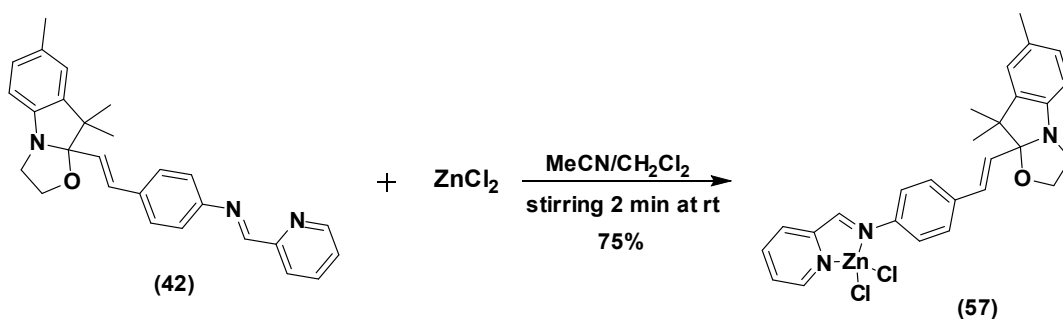
*Table 2.* Crystal structure of complex **62**, main parameters and representation of the molecule.

Complex **62** crystallizes in the Monoclinic system space group  $P2_1/c$ . As expected, the 3D structure confirms that bipyridine ligand and both indolinooxazolidine units are not coplanar. Once again, an important disorder at the BOX units is noticed. As for simple BOX-ligand series the different BOX units are not involved in the coordination sphere of the metal ion. As consequence, the commutation properties of the ligand should be preserved after its complexation.

As the continuation on the preparation of suitable complexes, are reported below the synthesis and X-ray characterization of an iminopyridine ligand based neutral Zn(II) complex.

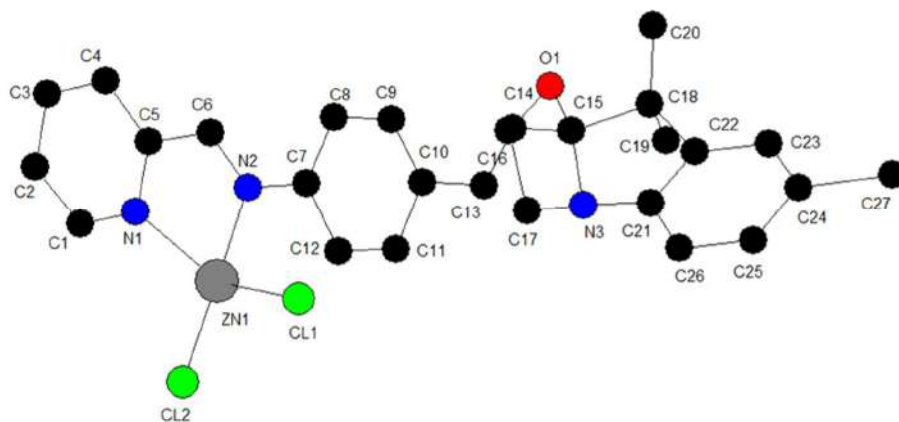
### B. Synthesis of Zinc complex **57** based on pyrilyl-imide ligand.

As part of our screening strategy, we have explored the possibility to tune the complex force and geometry by using another metal binding functionality than classical bipyridine and phenanthroline moieties. For this reason, we have described in chapter 4 the preparation of a pyrilyl-imide block functionalized by a BOX unit (**42**). Once the ligand in our hand, using similar experimental conditions as for pyridine ligands affords the obtainment of corresponding Zn(II)- pyrilyl-imide complex **57** in good yield (75%) as depicted in Scheme 5.



*Scheme 5. Synthesis of the Zinc (II) complex 57.*

If the formation of the complex was established by NMR spectroscopy (proton and carbon), IR, mass spectrometry, its structure was confirmed by X-ray diffraction. Indeed, suitable monocrystals of **57** were grown by the slow diffusion of **57** in CH<sub>3</sub>CN:CH<sub>2</sub>Cl<sub>2</sub> (1/1, v/v) into an ethylic ether layer. This complex crystallizes in the Triclinic space group P-1 and the resolved crystal structure is shown in Figure 4.



*Figure 4. Crystal structure of ZnL<sub>1</sub>Cl<sub>2</sub> complex (57).*

The tetracoordinated zinc(II) ion exhibits the expected tetrahedral geometry. The coordination sphere is formed by two chlorine atoms (Cl1, Cl2) and the two nitrogen atoms from the iminopyridyl motif of the chelating ligand **42**. The stereochemistry around the zinc(II) ion is slightly distorted as evidenced by the difference between the values of the angles formed by the metal center and the donor atoms.

## Chapter 5: Elaboration of multi-level molecular systems based on coordination chemistry

---

This distortion can be assigned to the small cavity size of ligand **42**, a common feature of iminopyridyl type ligands.<sup>[7]</sup> It results in a significantly narrow N-Zn-N angle (N1-Zn1-N2 81.236(335)°) in comparison with the other angles around the zinc atom.

In this part, we have synthesized and described the first examples of zinc(II) complexes coordinated to nitrogen aromatic heterocycle ligands bearing BOX. Notably, the BOX unit was not involved inside the coordination sphere of the metallic ion (independency between BOX on its closed form and metal binding functionality). Among that, and as previously mentioned, such kind of systems should exhibit acido-, photo- and electrochromic properties due to the possible commutation of each BOX units. For this reason, the addressability of the zinc(II) complexes under various stimulation is investigated and presented below.

### C. Commutation and abilities of Zinc complexes.

In order to study this first series of metal complexes, the complex **56** which involves two pyridyl ligands was chosen as model. As the commutation of the free ligand (see chapter 4), the behavior of complex **56** under acido-, photo- and electro- stimulations was monitored by spectroscopy (UV-Visible and NMR) and cyclic voltammetry. Noteworthy, observations and conclusions obtained for **56** can be generalized to the whole series of simple Zn based N-heterocycle complexes. In fact, behaving analogously to **56**, their studies will not be detailed here.

#### C.1. Acidochromic properties.

Before further investigations, it should be noted that the closed form of complex **56** is characterized in acetonitrile by a main absorption band, analogously to the free ligand, centered at 245 nm as shown in figure 6.

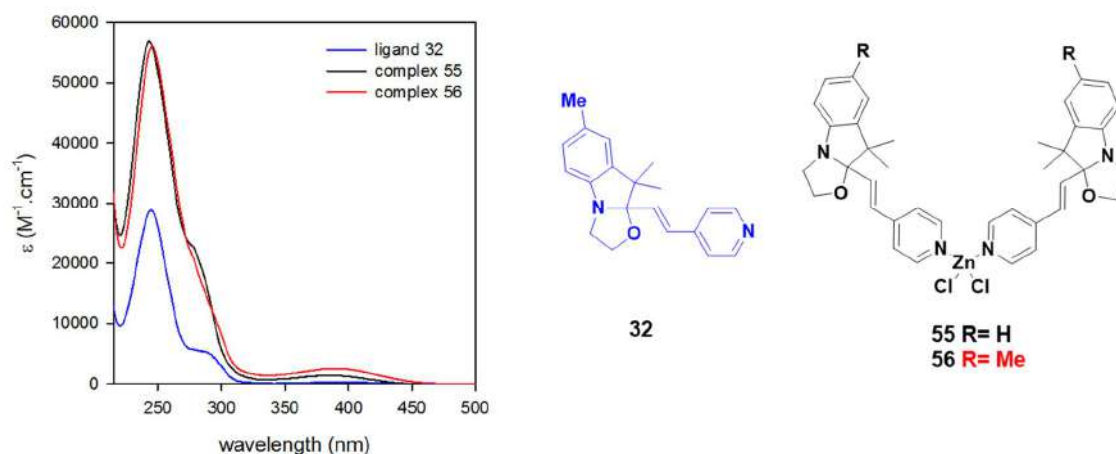
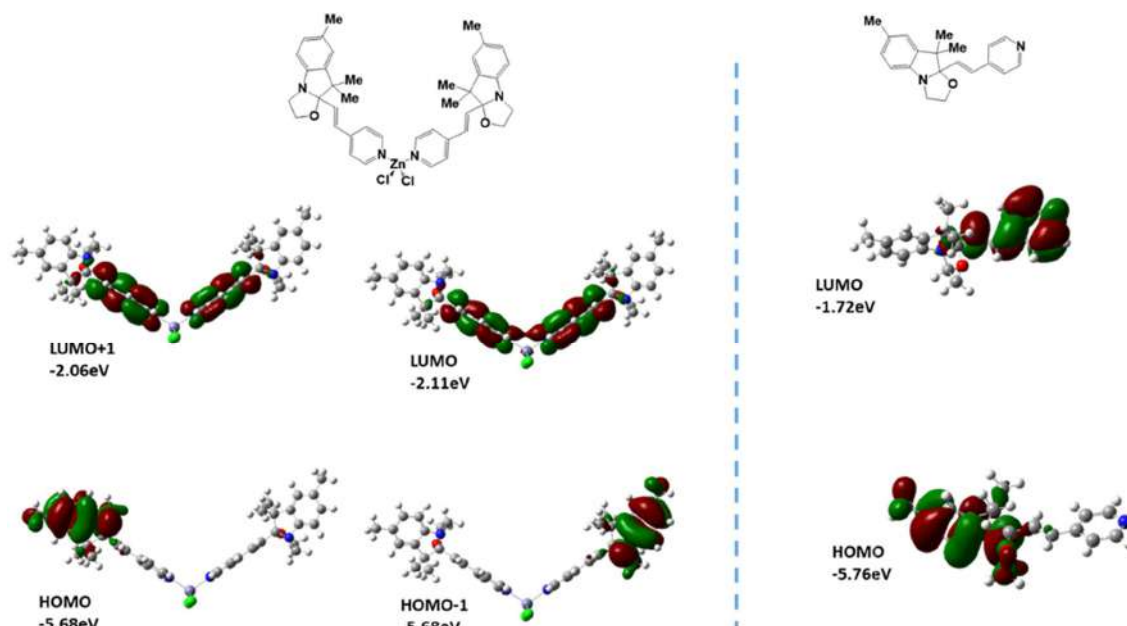


Figure 6. UV-Visible spectra of ligand **32** and complexes **55** and **56** under their closed form in ACN solution

As expected, free and complexed ligand only differs by an enhancement of the extinction coefficient at 245nm by an almost factor 2. More important, the shoulder observed at 286nm is more intense in the complex. In this context, we can conclude that this absorption corresponds to an Intra Ligand Charge Transfer. This assumption is perfectly supported by *ab initio* quantum calculations (B3LYP-6.311 G(d)) as basis. Indeed, **56** exhibits degenerated HOMO and LUMO orbitals similar in energy and localization to that observed for free ligand (figure 7).

## Chapter 5: Elaboration of multi-level molecular systems based on coordination chemistry

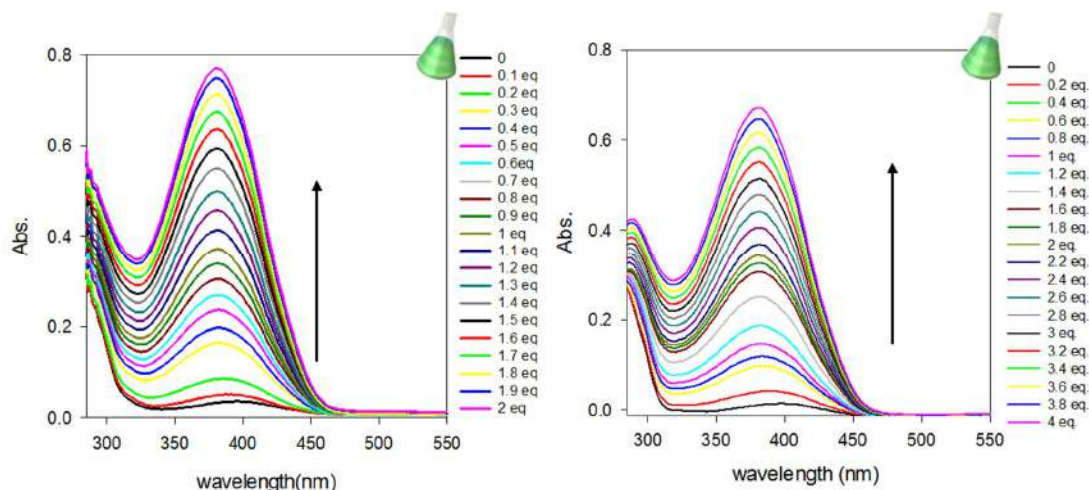


*Figure 7. Frontier orbitals of complex **56** and ligand **32** under their closed form.*

As previously discussed, among other methods, the oxazolidine ring opening can be induced using a source of  $H^+$ . Nevertheless, the previous chapter has demonstrated that the stimulation of free ligands by some acid leads, in all explored conditions, to the establishment of a tautomeric equilibrium between the open form (resulting from the box opening) and the protonated closed form (resulting from protonation of the pyridine). As the Zn-Ligand link is known to be relatively weak,<sup>[10]</sup> one may ask the question about the selectivity of the BOX opening when the complex is stimulated in same conditions as before. In order to solve this issue, an experiment, monitored upon UV-Visible spectroscopy, was undergone.

Figure 8 shows series of spectra obtained upon progressive addition of acid on solutions initially containing the ligand **32** (left, upon 2 eq.) and the complex **56** (right, upon 4 eq. as two ligands are involved) in their closed forms.

## Chapter 5: Elaboration of multi-level molecular systems based on coordination chemistry



**Figure 8.** UV-Visible spectrum changes of a solution of complex **56** in ACN (0.027mM) upon addition of HCl (right), compared to that with ligand **32** (0.03mM) (left).

As observed for free ligand, the solution of complex **56** turns deep yellow upon acidification with hydrochloric acid and leads exclusively to the formation of an intense broad band centered at 381 nm. If the appearance of this band unambiguously demonstrates the BOX opening, it is worth to note that, analogously to **32** which captures 2 eq. of acid before showing stabilized spectroscopic properties here also, an excess of acid is added before the new band stops growing. As, no isosbestic point is observed during this addition, it may be hypothesized that BOX opening and protonation (and thus complex dissociation) are concomitantly observed as in the case of free ligand. In order to confirm this behavioral analogy, a similar experiment was monitored by NMR.

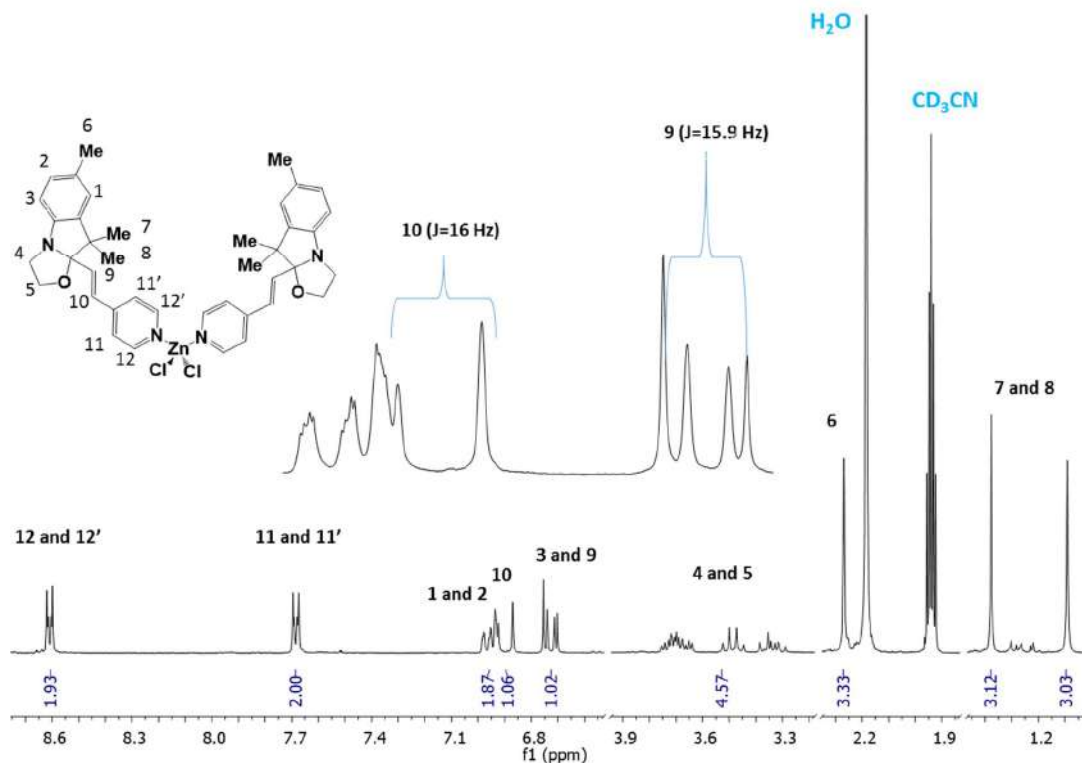


Figure 9.  $^1\text{H}$  NMR spectrum of complex **56** in  $\text{CD}_3\text{CN}$  at rt.

Initially, the proton NMR spectrum of **56** (in  $^3\text{d-ACN}$ ) looks relatively simple due to the symmetry of the compound (figure 9). This symmetry allows us the assignment of each signal and common characteristics of closed BOX derivatives are observed such as:

- two doublets at 6.73 and 6.90 ppm respectively are attributed to the protons 9-10 of the ethylenic junction. Exhibiting a vicinal coupling constant around 16 Hz, they confirm the trans isomery of the junction.
- three aromatic signals including two doublets and a singlet in the 6.7-7.0 region are characteristic of protons 1 to 3 of the indoline part.
- two doublets at 7.68 and 8.61 ppm with a coupling constant of 6.6 and 6.5 Hz respectively, are attributed to the protons of the pyridine bridge 11 and 12.
- a set of multiplets between 3.35 and 3.75 ppm integrating for 4 protons, with the presence of three singlets integrating for 3 protons each in the aliphatic region at 2.27,

## Chapter 5: Elaboration of multi-level molecular systems based on coordination chemistry

1.38 and 1.09 ppm, characteristics of methyls 6, 7 and 8, confirms definitively the closed status of oxazolidine rings.

Moreover, the NMR signature of **56** appears extremely similar to that of ligand **32**. Indeed, both spectra differ only by an extremely tiny positive chemical shift of the pyridine and ethylenic protons when the ligand is complexed. This can be explained by the break of conjugation between the BOX and pyridine which acts independently. Moreover, the small effect observed with the complexation suggests an analogous magnetic environment and thus a probably weak interaction between the zinc center and ligands.

The  $^1\text{H}$  NMR spectra (figure 10) recorded during acidification show a decrease of intensity of the signals of the initial closed form and the appearance of new resonances. Unfortunately, it is important to note that a precipitate appears as soon as the first aliquot of acid is added (in a similar way as with ligand **32** in  $\text{CD}_3\text{CN}$ ). As consequence, the observed variations in the NMR spectrum have to be regarded with wariness.

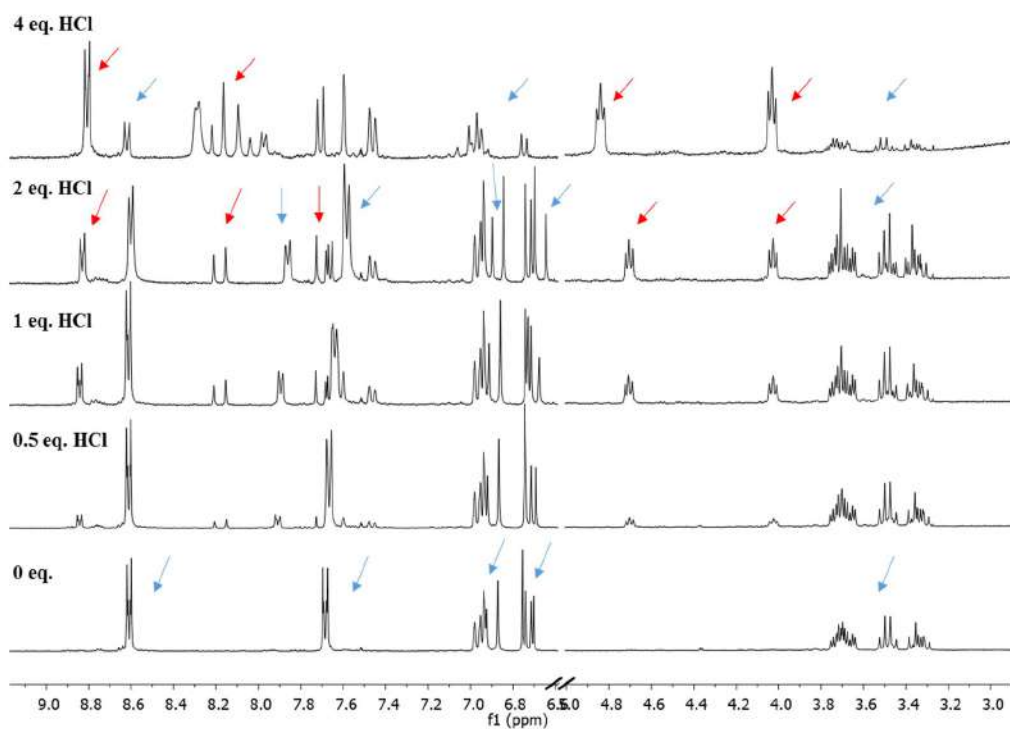
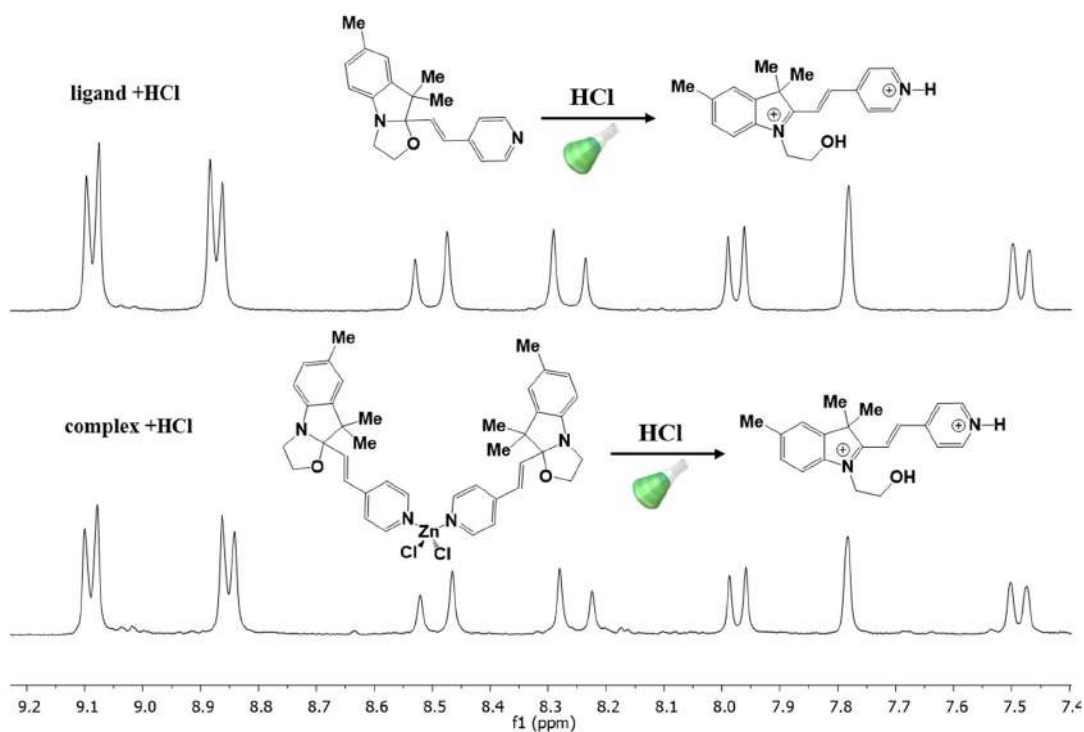


Figure 10.  $^1\text{H}$  NMR spectra upon titration of complex **56** (3 mM) by HCl in  $\text{CD}_3\text{CN}$  at  $20^\circ\text{C}$ .

## Chapter 5: Elaboration of multi-level molecular systems based on coordination chemistry

Nevertheless, despite this problem, the gradual decrease of signals attributed to **56** as well as signals characteristic of the opened form of the BOX are observed. Here again the continuous evolution of spectra upon addition of 4 eq. of acid indicates that both BOX and pyridine are protonated without demonstrating any selectivity or preferential order between phenomena and unit.

To confirm the nature of the final species, supposed as being the free **OP** species, NMR spectra both obtained in DMSO (due to solubility issues) of **32** and **56** upon addition of an excess of HCl respectively were recorder (Figure 11).



**Figure 11.** <sup>1</sup>H NMR spectra of ligand **32** and complex **56** upon adding an excess of HCl in DMSO-d<sub>6</sub> at 20°C.

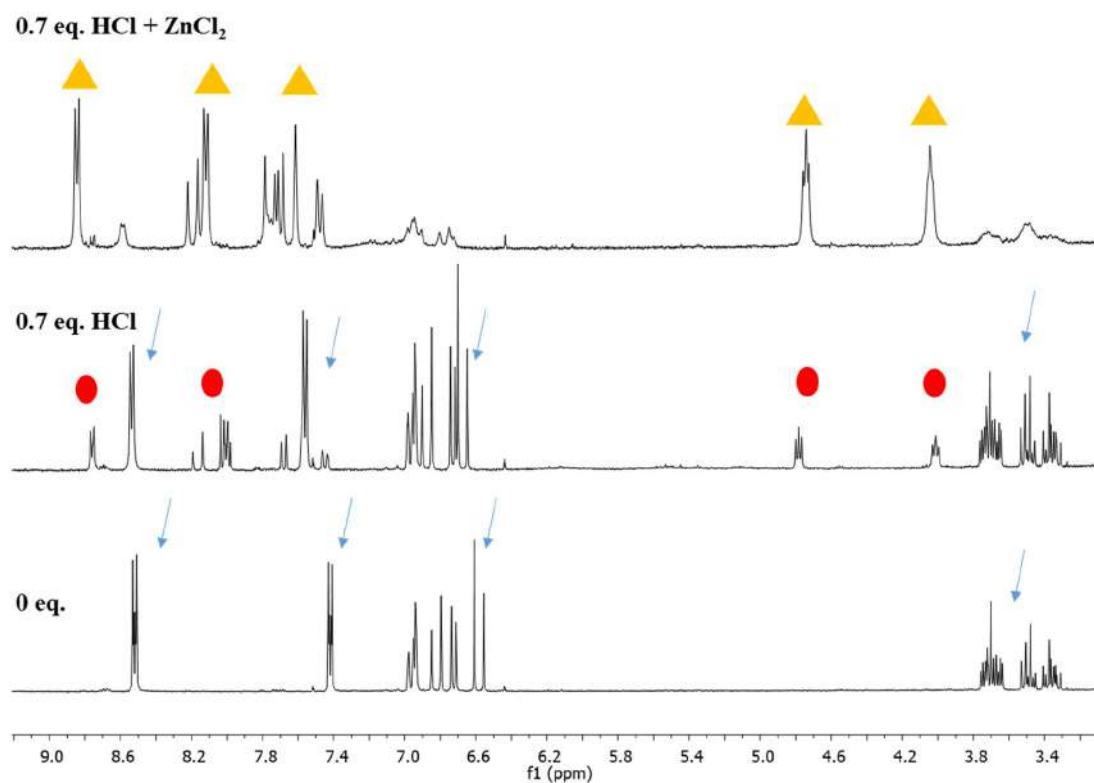
According to figure 11, an overlapping of the NMR spectrum of ligand **32** upon excess addition of HCl (presented in chapter 4) and complex **56** is noticed suggesting again that both complex and ligand lead at the end to the same free species in its open protonated form (**OP**).

## Chapter 5: Elaboration of multi-level molecular systems based on coordination chemistry

These experiments thus demonstrate, as the addition of a large excess of acid is necessary to obtain a stable NMR or UV-vis spectrum, that:

- the BOX are opened,
- the lability of Zn complex in solution leads to observe again the tautomeric equilibrium between **O** and **CP**, and at the end a fully conversion to **OP** form.

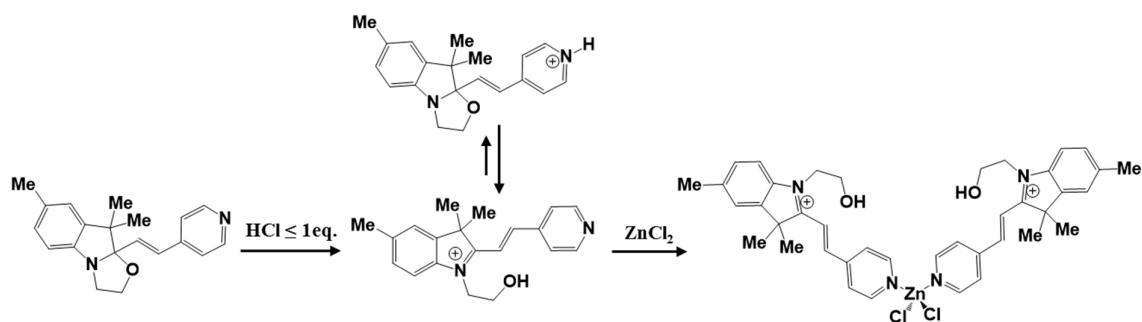
Moreover, further experiments are necessary to understand what happens during acidification and determine the course of events. A first approach, before answering these questions, consists in verifying if the complex substituted with opened BOX is stable enough to be formed. For this purpose, following preliminary experiment was undergone.



**Figure 12.**  $^1\text{H}$  NMR spectra of ligand 32 upon addition of 0.7 eq. of HCl (middle) and further addition of ZnCl<sub>2</sub> (top) in  $\text{CD}_3\text{CN}$ .

## Chapter 5: Elaboration of multi-level molecular systems based on coordination chemistry

As shown on figure 12, the addition of 0.7 equivalent of HCl to ligand **32** in deuterated acetonitrile leads, as described in chapter 4, to a decrease of intensity of the signals of the closed form with an increase in chemical shifts, the appearance of new resonances corresponds to the opening of BOX and in addition an observation of a precipitate. Furthermore, when  $\text{ZnCl}_2$  is added to the mixture, the precipitate is dissolved leading to the appearance of a new form. In particular, an increase of the chemical shifts that corresponds to the open form was observed, and this can be due to the change in magnetic equivalency in the ligand because the pyridyl group is coordinated to the metal center (scheme 6).



*Scheme 6. Generation of the open BOX coordinated to zinc.*

As a consequence, the stimulation of zinc complex by acid does not show any change vs free ligand alone and it's well investigated by UV-visible and NMR spectroscopy. On the other hand, a question can be asked. Does the other sources of stimulation lead to the same behavior?

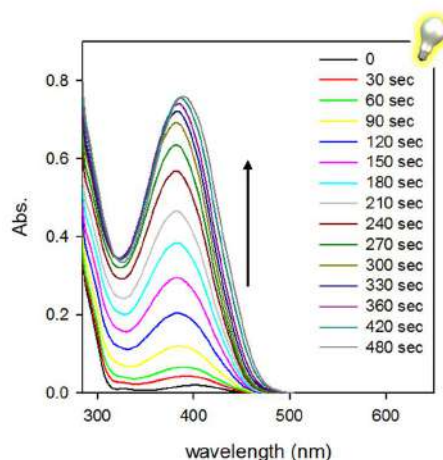
Thus, it has been shown here that, upon acidic stimulation, like in the case of the free ligand, the BOX is opened and the pyridine is protonated without preferential order. As consequence, stimulation by acid lead at the end to the complete complex dissociation. Nevertheless, a preliminary experiment demonstrates that a complex with an opened BOX can be generated. In these conditions, others stimulations of complexes which need less acidic conditions (but protic environments) may lead (or not) to a different behavior.

## Chapter 5: Elaboration of multi-level molecular systems based on coordination chemistry

### C.2. Release of Zinc ion under photo- or electro-stimulation.

In previous chapter, we have demonstrated that the stimulation of the free ligand **32** conducts to the **OP** form whatever the nature of the stimuli (proton, electron, or photon). In this context, the observation of a dissociation of the Zn(II) complex **56** is stimulated by some acid aliquots due to the formation of an **OP** form let us presume that photo- and electrostimulations of the complex will have the same effect.

In order to verify this assumption, a solution of complex **56** in presence of chlorobenzene as photosensitizer was irradiated at 254 nm, and the evolution of the system was monitored by UV-visible spectroscopy (figure 13).



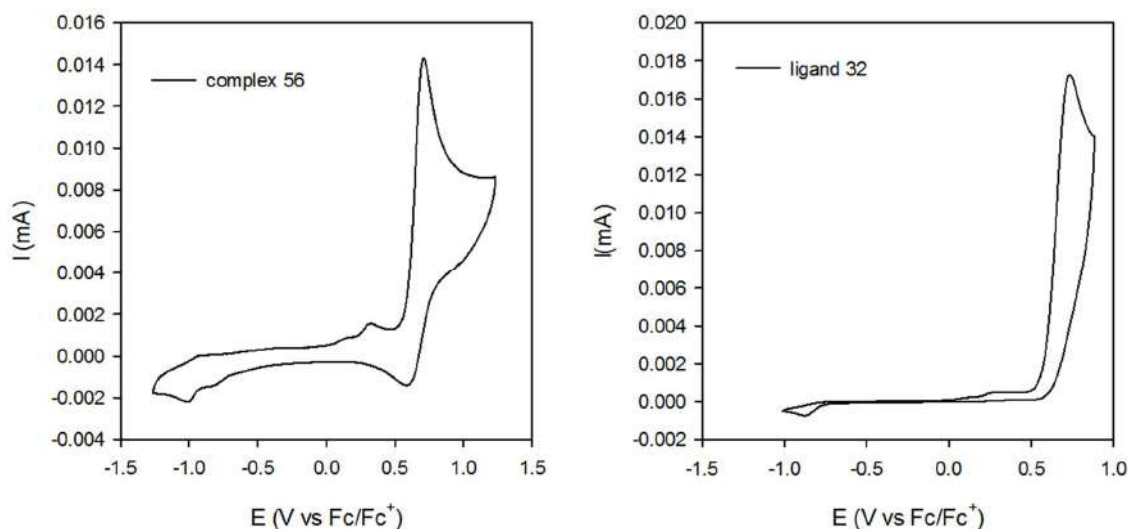
**Figure 13.** UV-Visible spectrum changes of a solution of complex **56** in ACN (0.027mM) upon irradiation at 254 nm.

As we can observe on figure 13, this UV irradiation leads to strong yellow coloration of the solution. Indeed, the appearance of a new broad absorption band centered at 381nm is noticed. In addition, maintaining the stimulation of the system leads to observe additional hyper- and bathochromic shifts of the visible absorption band (14 nm) and a photostationary state is reached after 480 seconds. More important, an overlapping of the UV-visible spectra

## Chapter 5: Elaboration of multi-level molecular systems based on coordination chemistry

obtained by either irradiation or acidic titration confirms that both stimulations lead at the end to the same state, and then, confirm the photoinduced Zn release.

Before to look at the possibility to obtain the same result under electrostimulation, the electrochemical behavior of the complex **56** was investigated by CV (figure 14) in order to confirm the redox inactivity of the Zn(II) ion in our experimental conditions (0.1 M TBAPF<sub>6</sub> as a supporting electrolyte in CH<sub>3</sub>CN, platinumium working electrode).



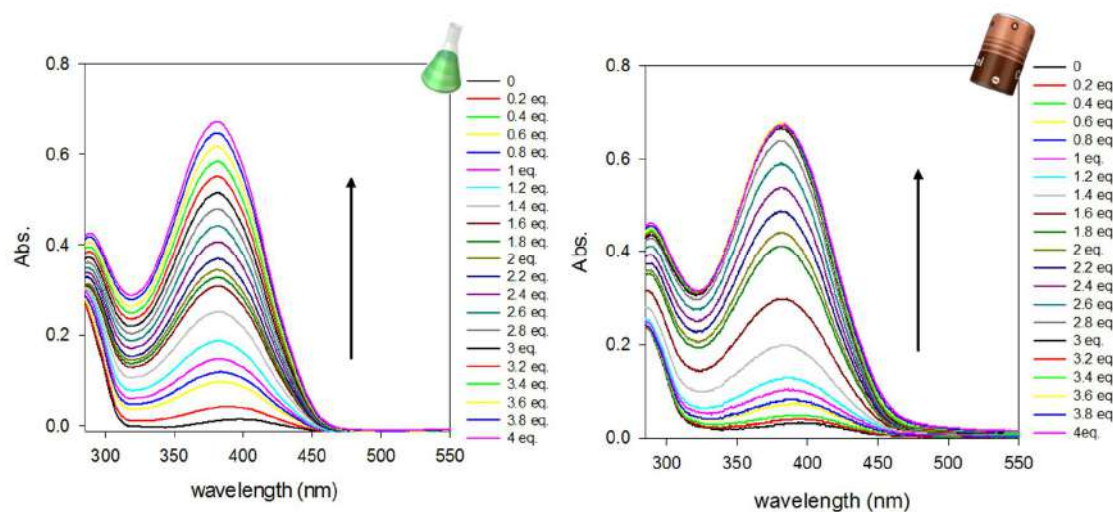
**Figure 14.** Cyclic voltammetry of complex **56** at 100 mV/s (0.57 mM) (left), compared to that of ligand **32** (0.62 mM) (right).

According to figure 14, the cyclic voltammetry shows that the complex **56** exhibits one pseudo non-reversible oxidation wave at almost the same potential as the free ligand (0.72 and 0.74 V respectively). This oxidation process can then be assigned to an oxidation mainly localized on the indoline moieties leading to corresponding radical cations in agreement with performed theoretical calculations (*vide supra*). More important, we did not notice any splitting of the oxidation peaks suggesting that both BOX units are oxidized at almost the same potential, and as consequence, opened simultaneously. In comparison to the free ligand, the observation of a full non-reversible oxidation process requires to decrease the scan rate. Based on these results, we can assume that the kinetic rate leading to the opening of the BOX was decreased

## Chapter 5: Elaboration of multi-level molecular systems based on coordination chemistry

with the complexation of the Zn which probably slows down the tautomeric equilibrium leading to the **OP** form.

To verify the **OP** formation and, as consequence, the Zn(II) decomplexation by electrostimulation of complex **56**, its titration using  $\text{NOSbF}_6$  as oxidant (0.87 V vs  $\text{Fc}/\text{Fc}^+$ ) was monitored by UV-Visible spectroscopy.<sup>[11]</sup>



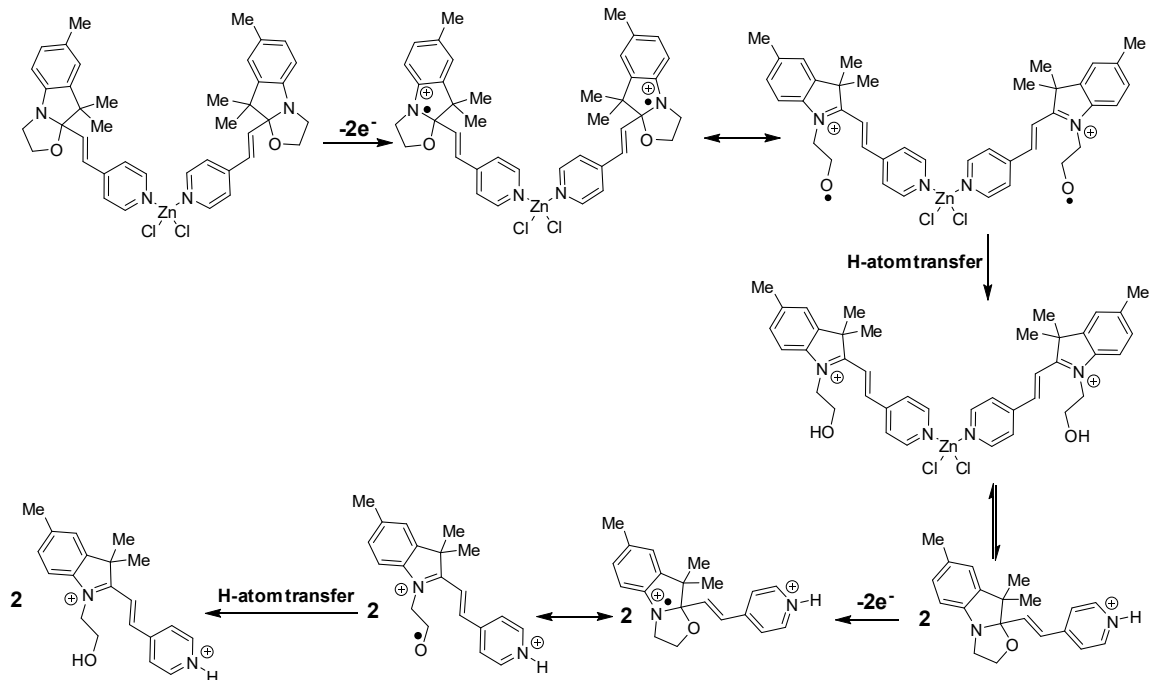
**Figure 15.** UV-Visible spectrum changes of a solution of complex **56** in ACN (0.027mM) upon addition of  $\text{NOSbF}_6$  (right) compared to that with acid (left).

As expected, the addition of oxidizing reagent to complex **56** leads to an analogous spectrum as the one obtained after stimulation with acid (figure 15) and free ligand **32**:

- generation of a broad absorption band centered at 381nm;
- no isosbestic point is observed during this addition, translating that the BOX opening and protonation (and thus complex dissociation) are concomitantly observed as in the case of acid;

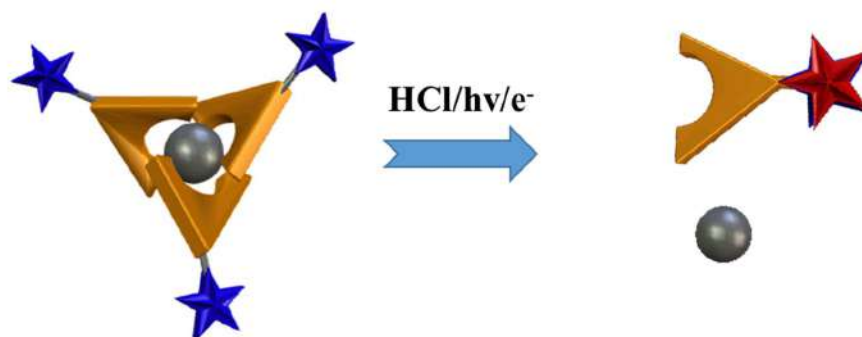
Moreover, we can propose that the electrochemical process could be described as a ECEC mechanism divided in three different states as presented on Scheme 7.

## Chapter 5: Elaboration of multi-level molecular systems based on coordination chemistry



*Scheme 7. Electrochemical oxidation of zinc complex 56.*

In summary, all synthesized ligands allow an easy synthesis and purification of corresponding Zn-complexes which have been fully characterized, sometimes by X-ray diffraction, what confirms their awaited tetrahedral geometry. The commutation properties of one complex (**56**) chosen as model have been detailed in this document and summarize what happen also with others.



*Figure 16. Schematic representation of Zinc complexes upon stimulating with different kind of stimulations.*

## Chapter 5: Elaboration of multi-level molecular systems based on coordination chemistry

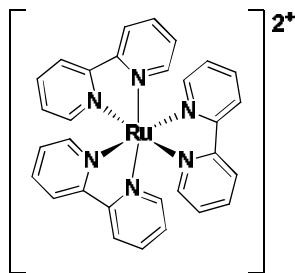
---

Indeed, whatever the stimulation (acid, light, oxidant), the formation of the **OP** form as well as the complex dissociation are observed. The absence of isosbestic point in UV-vis spectroscopy during the process excludes a step by step mechanism. As example, we could suggest that the BOX opening decrease the electronic density around the N-donor conducting to increase the lability of the complex in solution. At the opposite we can suggest a more direct mechanism where the direct protonation of the pyridine induces the dissociation due to a poor difference of pKa between the different species to exclude selectivity between N-protonation and BOX-opening.

In order to circumvent the issues due to the lability of the zinc complexes in solution, we have pursued our effort on the elaboration of multi-level molecular systems with the help of the ruthenium coordination chemistry. As consequence, the next section presents the elaboration and the characterization of a new series of ruthenium complexes, bearing one or more BOX unit.

### III). Elaboration and characterizations of multi-level molecular systems by coordination chemistry of Ru(II)

Ru(II) is a  $d^6$  transition metal well known<sup>[12]</sup> to form complexes with polypyridyl ligands possessing  $\sigma$  donor orbitals on nitrogens and  $\pi$  donor and  $\pi^*$  acceptor orbitals delocalized on the aromatic rings.<sup>[13]</sup> As shown in scheme 8,  $[\text{Ru}(\text{bpy})_3]^{2+}$  is one of the most widely studied ruthenium bipyridine complexes. Indeed, such kind of complexes is used for different applications such as molecular wires,<sup>[14, 15]</sup> sensors<sup>[16]</sup> and in solar energy research.<sup>[17, 18]</sup>



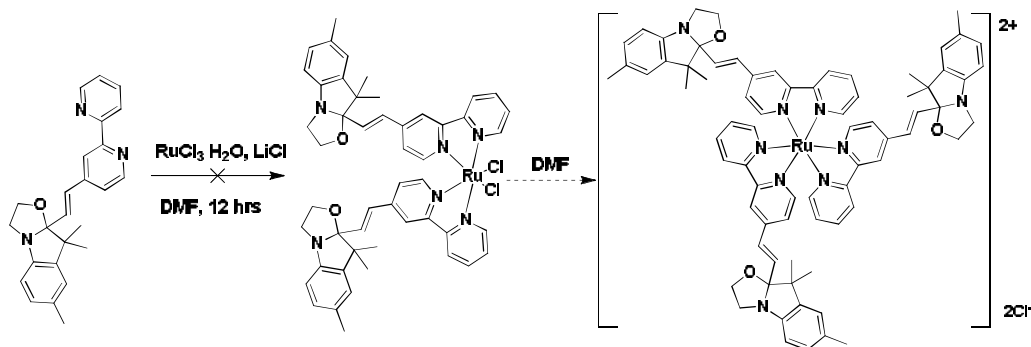
Scheme 8. Structure of  $[Ru(bpy)_3]^{2+}$ .

According to previous studies, it was possible to promote some commutation of photochromic compounds such as diarylethenes coupled to a ruthenium polypyridine chromophore.<sup>[19]</sup> As consequence, herein, we report our efforts concerning the syntheses and the characterizations of a second series of complexes bearing some BOX unit(s) by using the Ru(II) coordination chemistry. In this context, we have focused our interest on the use of elaborated bidentate ligand where the metal binding functionality is either a 2,2'-bipyridine or a phenanthroline moiety.

#### A. Synthesis of ruthenium complexes incorporating BOX unit(s).

In this section all approaches - unsuccessful and successful syntheses - are reported.

Our first approach have been focused on the synthesis of symmetrical and homoleptic Ru(II) complexes incorporating ligand **37**. In such purpose, all our attempts were based on classical preparation of homoleptic complex from ruthenium chloride precursor (scheme 9).



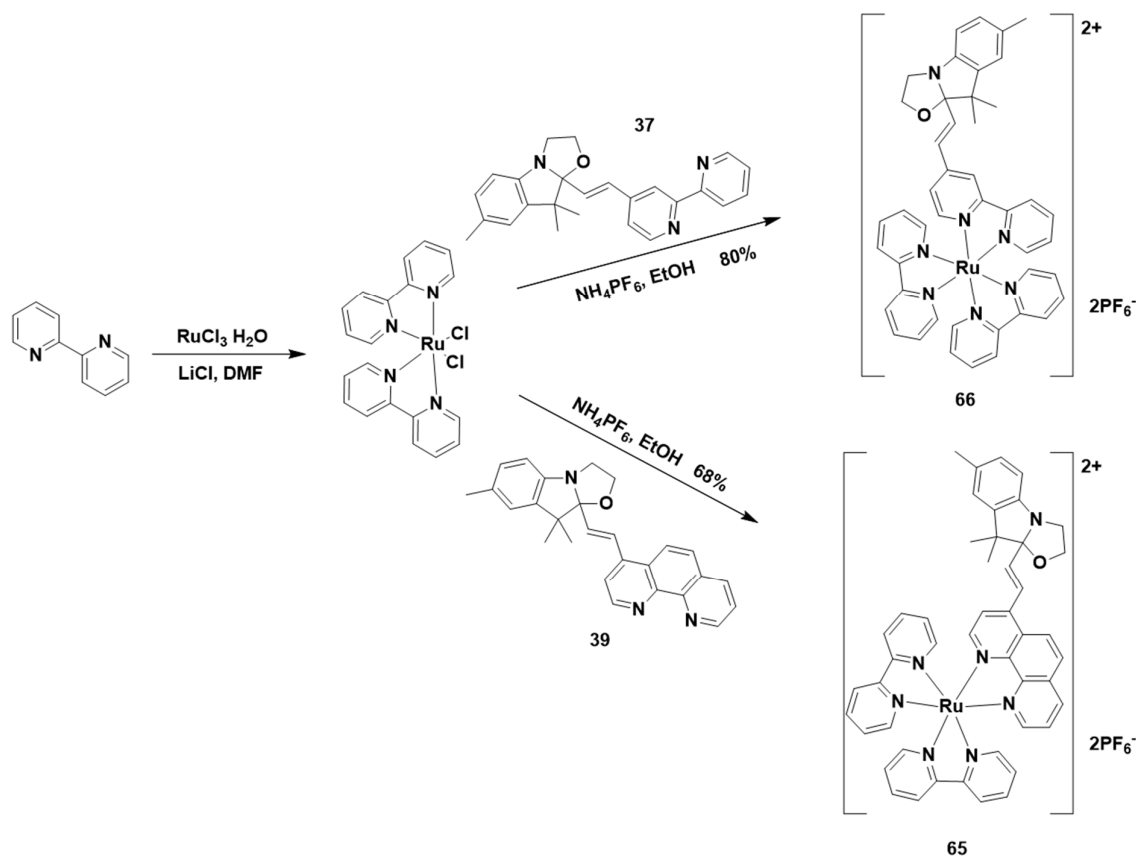
Scheme 9. Synthesis of homoleptic ruthenium complex based on ligand **37**.

## Chapter 5: Elaboration of multi-level molecular systems based on coordination chemistry

---

This chosen methodology which is based on the reported synthesis of  $[\text{Ru}(\text{bipy})_3]^{2+}$  where the three bipyridine ligands around the ruthenium are inserted in two successive steps.<sup>[20]</sup> The first one leading theoretically to the insertion of two ligands consists in mixing at reflux (12h) the  $\text{RuCl}_3$  precursor,  $\text{LiCl}$  and the ligand in dry DMF in a 2:1 ratio. Unfortunately, this first step leads to a black (totally) insoluble solid when using ligand **37** and similar experimental conditions. This problem prompts us to change slightly our approach by firstly introducing one or two ligands.

In order to introduce only one functionalized ligand, the most efficient and well-known procedure consists in a ligand exchange reaction on the cis-bis(2,2'-bipyridine)dichlororuthenium(II),  $[\text{Ru}(\text{bpy})_2\text{Cl}_2]$  complex by the targeted ligand.<sup>[21, 22]</sup> In this purpose, we have prepared this reactant from  $\text{RuCl}_3$  precursor according to the procedure reported by Meyer.<sup>[23]</sup> Generally, the ligand exchange reaction requires high temperature and polar solvent. In our case, performing the reaction in boiling alcohol appears as the most efficient way to introduce ligands **37** and **39** and allows the obtainment of corresponding complexes **65** and **66** in 68 and 80% yield respectively (scheme 10).

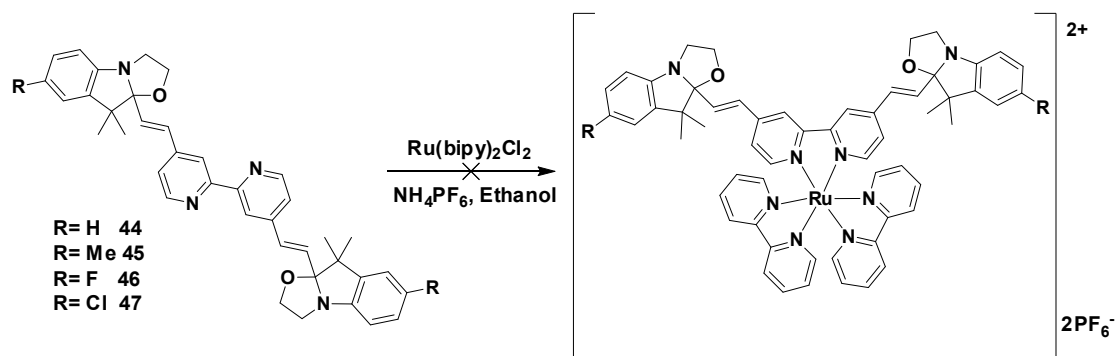


*Scheme 10.* Synthetic routes of bis-heteroleptic ruthenium complexes **65** and **66**.

Obtained as bright orange solid, the formation of both complexes was confirmed by NMR spectroscopy (proton and carbon), IR and mass spectrometry. Unfortunately, despite numerous attempts we were not able to obtain monocystals exhibiting enough quality for X-Ray diffraction studies.

The enhancement of the number of BOX units and, as consequence, the number of possible metastable states can be obtained by two approaches as in the case of Zinc complexes. The first consists in introducing one ligand bearing two BOX units such as ligands **44-47** (scheme 11).

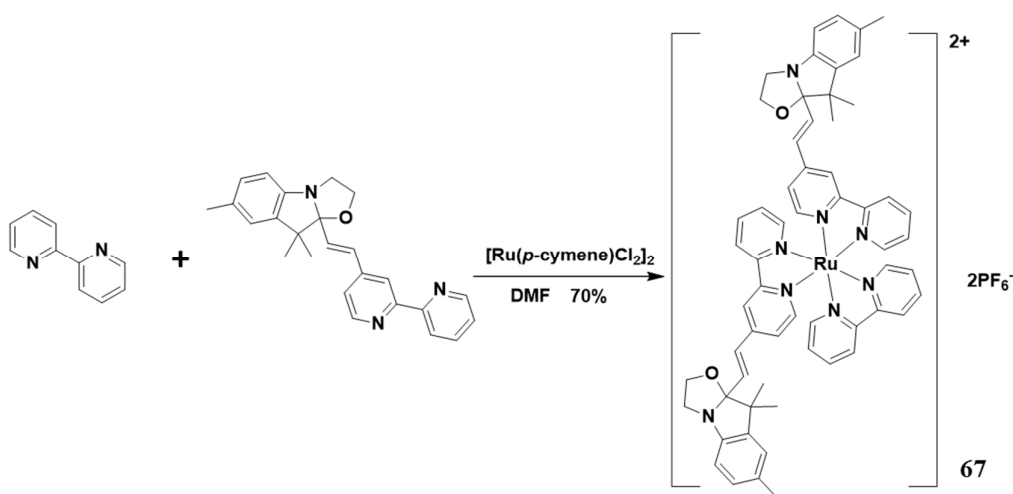
## Chapter 5: Elaboration of multi-level molecular systems based on coordination chemistry



*Scheme 11. Unsuccessful attempt by using biBOX-bipyridine ligand to obtain ruthenium complex.*

In this case, preliminary attempts have been performed using the same strategy than for complexes **65** and **66**. All these attempts lead to the formation of orange solid which presents some instability when dissolved in acetonitrile and avoiding their complete characterization.

A second approach consists in introducing two ligands bearing one BOX unit around the Ru(II). In this purpose, the richness of ruthenium coordination chemistry was helpful. Indeed, several routes were developed in order to functionalize 2 on 3 bipyridine ligands. Among them, the new method starting from  $[\text{Ru}(p\text{-cymene})\text{Cl}_2]_2$ <sup>[24]</sup> was successfully applied to ligand **37** (scheme 12) and allows the preparation of corresponding complex **67** in good yield (70%).



*Scheme 12. Synthetic routes of bis-heteroleptic ruthenium complex 67.*

## Chapter 5: Elaboration of multi-level molecular systems based on coordination chemistry

The complex was characterized by NMR spectroscopy (proton and carbon), IR and mass spectrometry.

To conclude, a first series of three heteroleptic complexes (**65**, **66** and **67**) have been synthesized allowing to dispose one or two BOX unit in the close vicinity of a Ru(II) ion. The syntheses of other compounds have to be investigated more deeply especially new routes to homoleptic systems allowing to enhance the number of BOX unit from 2 to 3.

Due to time consideration, we have preferred to focus our efforts on some preliminary studies concerning the commutation abilities of obtained compounds which are detailed in the next section.

### B. Commutation and abilities of ruthenium complexes.

As already underlined, to study the commutation properties of such systems, the UV-Visible spectroscopy represents a convenient investigation technique. Noteworthy, ruthenium(II) polypyridyl complexes have been studied extensively over last few decades for their rich optical and optoelectronic properties. [25, 26, 27] In this context, the spectroscopic properties of ruthenium polypyridyl complexes in UV-visible range are well documented. [28]

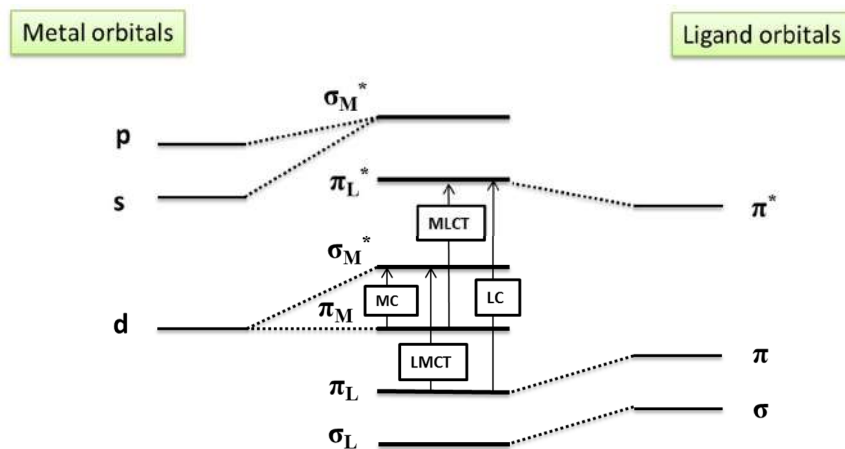


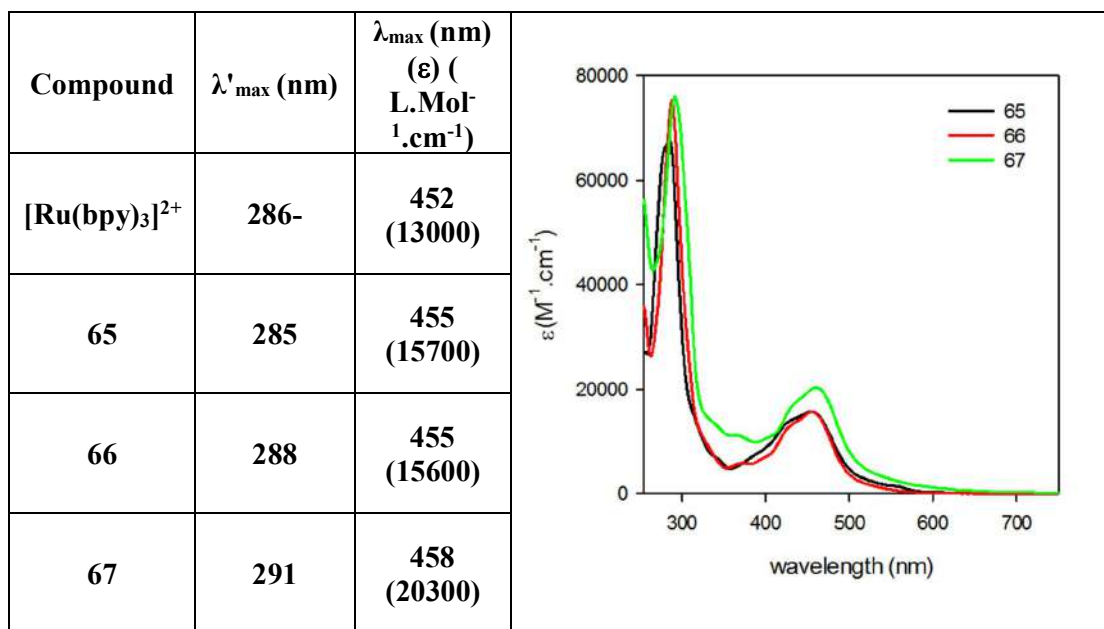
Figure 17. Molecular orbital diagram for an octahedral metal complex.<sup>[28]</sup>

## Chapter 5: Elaboration of multi-level molecular systems based on coordination chemistry

The four energetic transitions highlighted in figure 17 can be classified into 4 different categories: on one hand the metal (MC) and ligand (LC) centered transitions, and on the other hand the transitions involving a charge transfer character such as Metal to Ligand (MLCT) and Ligand to Metal (LMCT). To represent those on a diagram (figure 17), we have to consider that:

- the  $\sigma_L$  and  $\pi_L$  ligand orbitals are generally full for  $d^6$  complex ground states,
- the  $\pi_M$  orbitals are partially filled depending on the oxidation state of the metal,
- the remaining orbitals are usually empty.

In this context, it is possible to perform a rough assignment of the different bands observed on the UV-Visible spectra of our complexes (**65**, **66** and **67**) under their closed form (table 3).



**Table 3.** UV-Visible spectra of complexes **65**, **66** and **67** under their closed form in ACN solution ( $2.09 \times 10^{-5}$  and  $3.60 \times 10^{-5}$  and  $1.40 \times 10^{-5} M$  respectively).<sup>[29]</sup>

## Chapter 5: Elaboration of multi-level molecular systems based on coordination chemistry

---

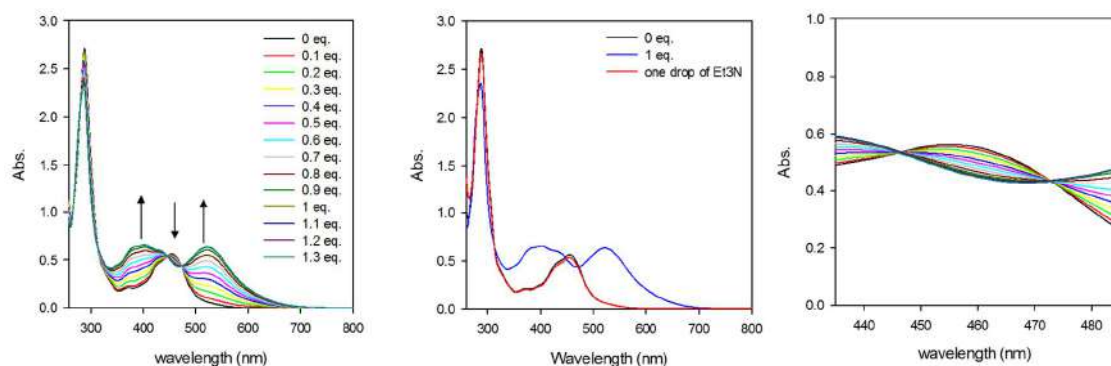
All prepared complexes exhibit similar absorption spectrum, a broad absorption bands in the visible region of spectrum (400-500 nm), and a more intense one at higher energy (260-320 nm). Based on studies on similar bipyridine ruthenium complexes,<sup>[30, 31]</sup> the latter can be reasonably assigned to some intraligand  $\pi \rightarrow \pi^*$  transitions. At the opposite, the nature of the visible absorption band is more difficult to determine. The observation of different shoulders on this band suggests the overlapping of different transitions such as MC transition involving the metal d-orbitals and MLCT transition as commonly observed in Ru(II) complexes coordinated to organic ligands, such as polypyridyl derivatives. However, it is important to keep in mind that, under their closed form the BOX units and the metal binding functionality have to be considered as independent (see chapter 4). Presenting higher energy level than bipyridine, charge transfer band from the BOX centered molecular orbital to empty metal orbitals have to be also considered. In this context, it is understandable to observe almost identical optical properties for complexes **66** and **67** (with, in this later case, an hyperchromic effect on the low energy band due to the addition of a second BOX moiety on the system). Changing the nature of the BOX ligand (**65** vs **66**) induces naturally a broadening of the band at higher energy which was assigned to the CT transitions in agreement with previous studies on Ru(bpy)<sub>2</sub>(L)<sup>2+</sup> complexes.<sup>[32]</sup> Presenting a variation of donor ability, the substitution of a bipyridyl by a phenanthroline unit leads to observe some variations on the visible band especially at the MLCT band level.<sup>[32]</sup>

Due to the lack of time, we have chosen to focus our effort on the commutation properties of complex **66**. Incorporating one BOX unit, this model compound should exhibit acido-, photo- and electro-chromic behaviors. Characterizations are provided in the next sections.

## Chapter 5: Elaboration of multi-level molecular systems based on coordination chemistry

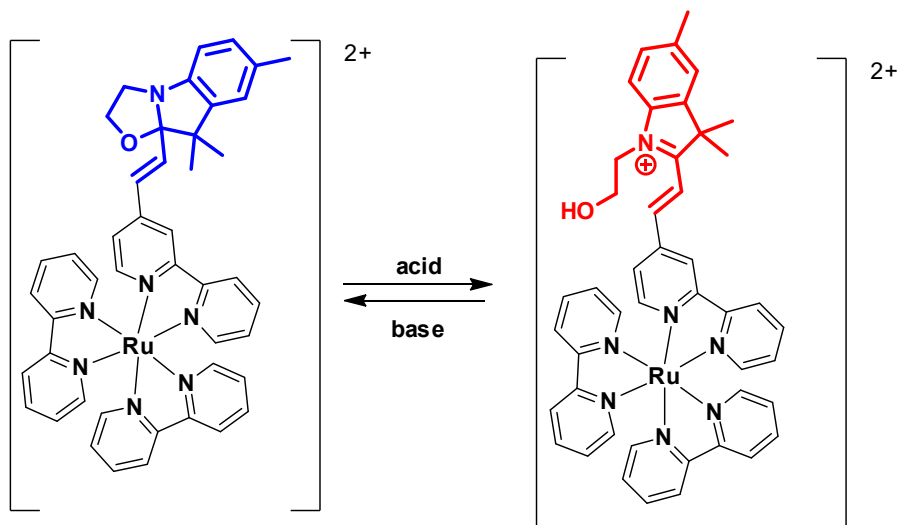
### B.1. Acidochromic properties.

For this reason, the variations of the UV-Visible absorption spectrum of **66** in acetonitrile have been recorded upon the addition of HCl aliquots (Figure 18).



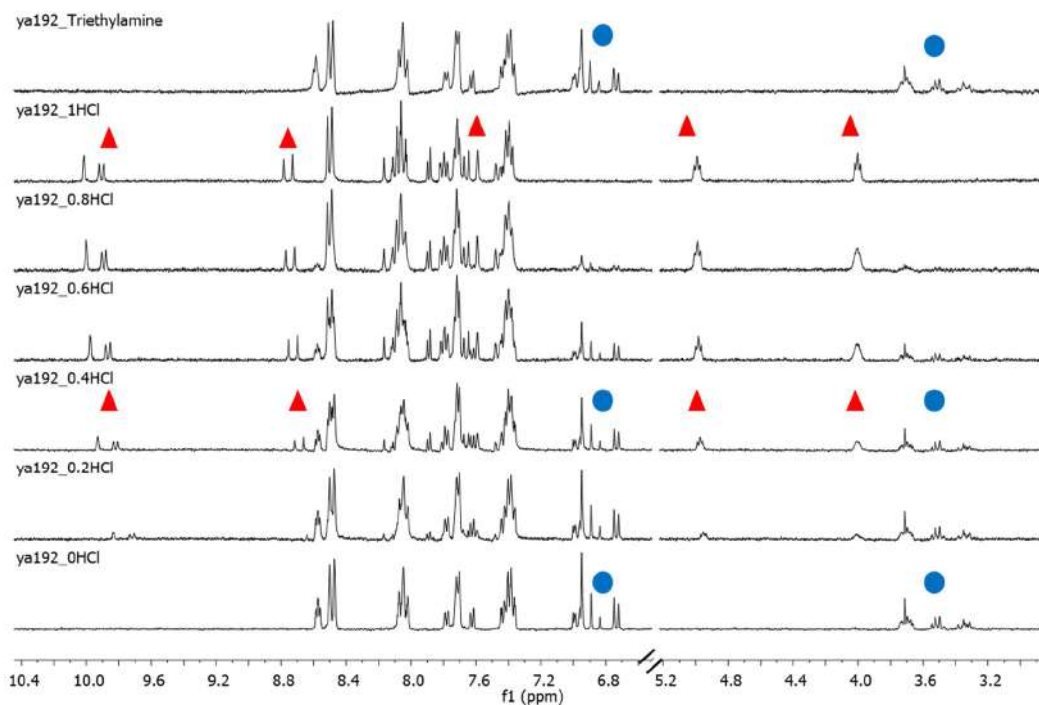
**Figure 18.** UV-Visible spectra changes of a solution of complex **66** in ACN ( $3.60 \times 10^{-5} M$ ) upon addition of HCl aliquots.

As expected, the addition of acid induces a solution coloration change from orange to crimson. Indeed, the initial main absorption band centered at 455nm is gradually replaced by two new bands centered at 402 and 522nm upon the addition of acid. More important, two isosbestic points at 446 and 472nm are detected up to one equivalent suggesting an equilibrium between two species. Starting from this, we can suggest that the addition of acid induces selectively and exclusively the opening of the oxazolidine ring without inducing the Ru(II) decomplexation (figure 18). This assumption is supported by two facts. First, adding an excess of acid does not affect the spectrum, and thus demonstrates the stability of the complex in acid conditions. Second, the media neutralization by addition of some base (such as  $NEt_3$ ) allows recovering the initial spectrum, including the supposed CT band.



**Scheme 13.** Representation of the two different states of the molecular system: **C** and **O**, depending on closed (**C**) or open (**O**) status of BOX units.

The selective addressability of the BOX unit under acidic stimulation was verified by NMR spectroscopy. In this context, the figure 19 represents the variation of the proton NMR spectrum of complex **66** upon the successive addition of HCl aliquots.



**Figure 19.** Monitoring of the titration of complex **66** (2.63 mM) in ACN by HCl at 20°C.

## Chapter 5: Elaboration of multi-level molecular systems based on coordination chemistry

---

Due to the lack of symmetry, an increase of the complexity of the NMR spectrum of complex **66** under its closed form in comparison to free ligand **37** is noticed and did not allow the complete assignment of each signal without more complete 2D NMR study. Nevertheless, it is possible to observe common features of closed BOX derivatives such as:

- the doublet assigned to an ethylenic proton at 6.9ppm. Exhibiting a vicinal coupling constant of 15.9 Hz, it confirms the trans isomery of the ethylenic junction between the bipyridine and the BOX unit.
- a series of multiplet ranging from 3.36 to 3.76 ppm, corresponding to the methylene groups of the oxazolidine ring. Associated to the detection of three singlets at 2.28, 1.41 and 1.12 ppm corresponding to the three nonequivalent methyl group, it confirms the closed status of the BOX unit.

Upon acid addition, the decrease of the proton peaks intensities of the initial state are observed and concomitant new resonances appear such as:

- two triplets at 4.00 and 4.50 ppm characteristic of the pendant alkyl chain of indoleninium moiety,
- two vinyl doublets at 8.15 and 8.76 ppm with a coupling constant of 16.4 and 16.6 Hz assigned to the protons of the ethylenic junction.

All of them confirm the gradual opening of the BOX opening during the acidic stimulation of **66**. In addition, the stable chemical shift of the different peaks upon the HCl addition as well as well as the subsequent restoration of the initial spectrum by treatment with  $\text{NEt}_3$  (figure 19) corroborate the stability of Ru(II) complex in these conditions.

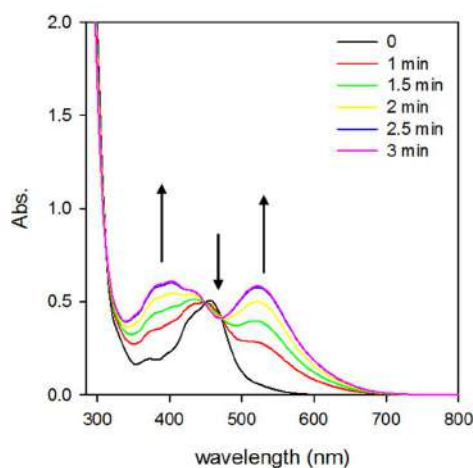
From these investigations, we have demonstrated that changing the metal ion (from Zinc to Ruthenium) leads to a better stability of the complex upon stimulating by acid and leads to the selective opening of the oxazolidine ring. Following that, it appears interesting to check if

## Chapter 5: Elaboration of multi-level molecular systems based on coordination chemistry

the use of a photoactive ruthenium complex has really an influence and can influence the photochromic properties of the system.

### B.2. Photochromic properties.

In this context, the response of the complex **66** under light stimulation was investigated. For this reason, the evolution of **66** in acetonitrile/chlorobenzene mixture (90/10) was submitted to successive periods of illumination at 254 nm and corresponding UV-visible spectrum was recorded between each period (figure 20).



**Figure 20.** UV-Visible spectrum changes of a solution of complex **66** in ACN/PhCl (90/10;  $3.25 \times 10^{-5}$  mM) upon UV light irradiation (254 nm).

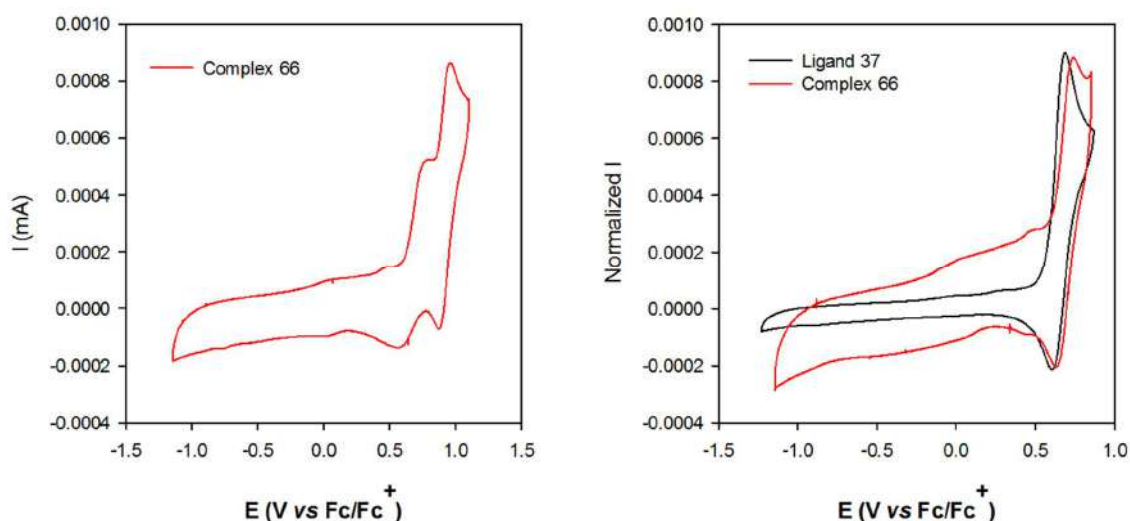
As expected, a coloration change of the solution was noticed as soon as we applied the irradiation and a photostationary point was reached after 2.5 minutes. The initial main absorption band centered at 455 nm is gradually replaced by two new bands centered at 402 and 522 nm as observed under acidic stimulation. In addition, the same isosbestic points are observed at 446 and 472 nm respectively. As consequence, we can conclude that the UV irradiation at 254 nm leads, as observed with acid, to the opening of the oxazolidine ring which generates the open form of the complex highlighting its multi-modal switching ability.

## Chapter 5: Elaboration of multi-level molecular systems based on coordination chemistry

In fact, it is important to note that the presence of the photoactive Ruthenium atom has no influence on the photochromic properties of the system due to the independence of both pi-conjugated system and BOX under its closed form. At the opposite, the photostimulation of the metallic center in the LMCT band may conduct to observe a similar commutation of the molecular system due to photoinduced electron transfer between metal and multimodal BOX unit. From that, it was interesting to look at other wavelengths in order to take advantage of the Ru photoactivity. These studies are actually under progress.

### B.3. Electrochromic properties.

If the photochromic properties of the BOX were not perturbed by the presence in its close vicinity of a Ru(II) cation, the electrochromic properties of our multimodal switching unit can be influenced. In fact, [Ru(Bipy)<sub>3</sub>] is known to be redox active, its CV presents one reversible oxidation wave at 0.85 V and three successive reductions ones at -1.76V; -1.92V and -2.16V respectively.<sup>[33, 34]</sup> For this reason, we have explored the electrochemical behavior of the heteroleptic complex **66** by cyclic voltammetry (figure 21).

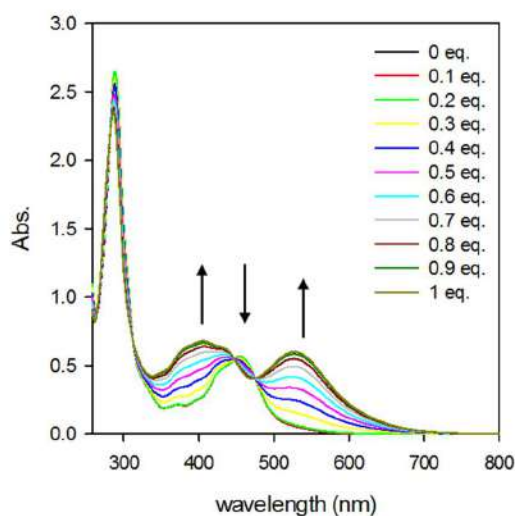


**Figure 21.** Cyclic voltammetry of complex **66** (left), compared CV of ligand **37** with the first oxidation of complex **66** in ACN (1.45 and 1.22 mM) with TBAPF<sub>6</sub> as electrolyte (0.1M) on Pt working electrode at 100mV.s<sup>-1</sup>.

## Chapter 5: Elaboration of multi-level molecular systems based on coordination chemistry

As one can observe, the complex **66** exhibits two successive oxidation processes at 0.69 V and 0.91 V. The first one was assigned to an oxidation mainly localized on the BOX unit and leading to the radical cation. This assignment was supported by the close value of oxidation potential measured for the free ligand **37** (figure 21). Nevertheless, a tiny anodic shift is observed which can be due to the electron withdrawing effect of coordination or some electrostatic repulsions. More important, the process is not perfectly reversible suggesting that the generated BOX radical cation is not stable in these experimental conditions and is involved in a chemical process such as the oxazolidine ring opening (*vide infra*). Concerning the second reversible oxidation process at 0.91 V, it can be reasonably assigned to the oxidation of the metal center from Ru<sup>2+</sup> to Ru<sup>3+</sup> in agreement with reported value for various Ru(bpy)<sub>2</sub>(L)<sup>2+</sup> complex ranging from 0.8 and 1.1 V.<sup>[35]</sup>

To confirm the opening of the oxazolidine ring during the first oxidation process, titration of complex **66** by NOSbF<sub>6</sub> as an oxidizing reagent was monitored by UV-Visible spectroscopy (figure 22).



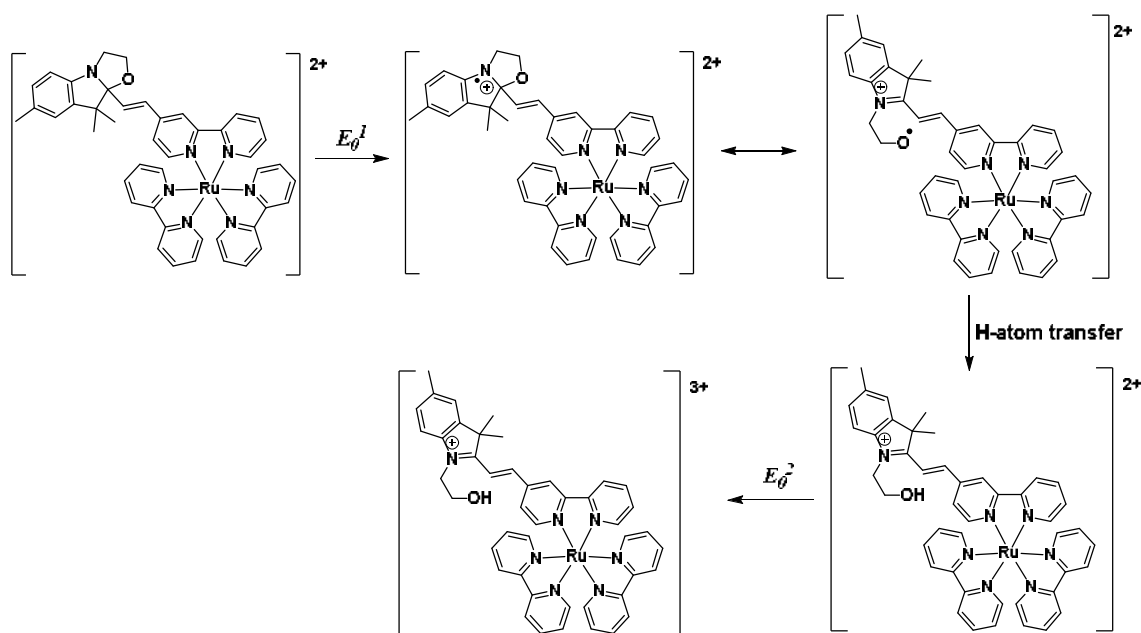
**Figure 22.** UV-Visible spectra changes of a solution of complex **66** in ACN ( $3.60 \times 10^{-5} M$ ) upon addition of NOSbF<sub>6</sub>.

## Chapter 5: Elaboration of multi-level molecular systems based on coordination chemistry

As expected, a drastic change of UV-Visible spectra upon the addition of  $\text{NOSbF}_6$  aliquots is observed (figure 22). As observed with other kinds of stimulation, we observe identical variation:

- decrease of the absorption band centered at 455nm,
- generation of two absorption bands centered at 402 and 522nm respectively,
- observation of two isosbestic points at 446 and 472nm translating an equilibrium between two species.

Associated with the perfect overlapping of the spectra obtained under electrochemical and acidic stimulation, we can assume that the oxidation conducts to the formation of the open form of the complex **66**. As consequence, this experiment confirms the trimodal (photon, electron proton) commutation ability of the complex.



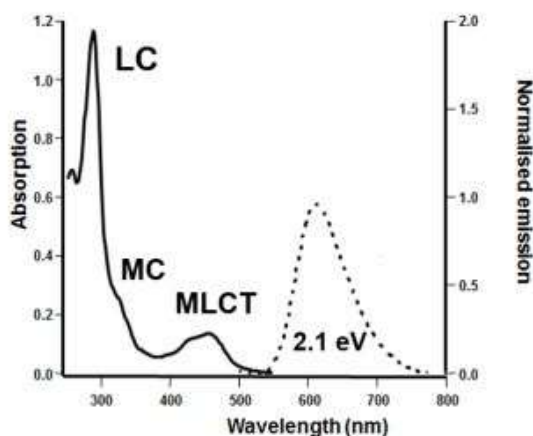
*Scheme 14. Electrochemical mechanism of complex 66.*

In summary, the chelation of ruthenium center with a ligand bearing a BOX moiety has been done. Corresponding complex has been fully characterized and shows reversible multimodal (acido- photo- and electro-) commutation properties. Particularly, the commutation

properties of one complex (**66**) chosen as model shows a highly stable ruthenium complexes opposite to what observed on Zinc(II) complexes.

C. Potential application of BOX complexes as multimodal switching luminophores.

As mentioned previously, ruthenium polypyridyl complexes are largely reported in the literature for their impressive photophysical characteristics.<sup>[28, 36, 37, 38]</sup> Indeed, the luminescence properties of  $[\text{Ru}(\text{bpy})_3]^{2+}$ , the most well-known of them, are largely studied and continue to be commonly used as a standard to explain similar processes occurring in other ruthenium(II) complexes.<sup>[38]</sup>



**Figure 23.** Absorbance and emission spectra of  $[\text{Ru}(\text{bpy})_3]^{2+}$  in acetonitrile solution.

Interestingly, the luminescence properties of ruthenium polypyridyls complexes are strongly influenced by the nature of the ligand and their substitution.<sup>[39]</sup> In this context, the elaboration of complexes bearing a multimodal switching unit such as BOX could present some benefit. Considered as almost independent under its closed form, its opening by using indifferently some photons, electrons or a proton leads to the formation of an indolenium moiety acting as a strong electron withdrawing group which is now fully conjugated with the

## Chapter 5: Elaboration of multi-level molecular systems based on coordination chemistry

metal binding functionality, and then, should strongly affect the luminescence properties of the compound.

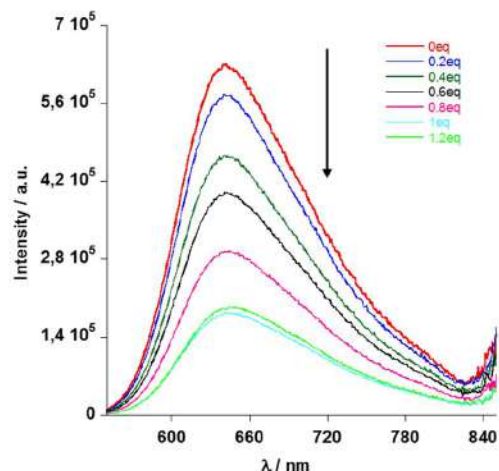
In order to explore the potentiality of complex **66** as multimodal switching luminophore, its luminescence properties were investigated (in collaboration with Dr J-L Fillaut's group from ISCR at Université de Rennes). As expected, the complex **66** under its closed form exhibits an intense luminescence (600-780nm) after excitation at 455nm in deaerated acetonitrile.

If the spectral characteristics of **66** are very similar to  $[\text{Ru}(\text{bpy})_3]^{2+}$ , the determination of the quantum yield let appear its enhancement by a factor 2 (table 4).

Complexes	$\lambda_{\text{max}}$ (nm)	$\epsilon(\text{M}^{-1} \cdot \text{cm}^{-1})$	$\lambda_{\text{em}}$ (nm)	Quantum yield $\phi$
$[\text{Ru}(\text{bpy})_3]^{2+}$	452	13 000	611	0.058
<b>66</b>	455	15 600	642	0.12

*Table 4. Collected photo-physical data for complex 66 under its closed form compared to  $[\text{Ru}(\text{bpy})_3]^{2+}$  in deoxygenated  $\text{CH}_3\text{CN}$  solution.*

As expected, the opening of the BOX unit leads to observe a drastic decrease of the luminescence. As example, the figure 24 shows the variation of the emission spectra of compound **66** upon the successive addition of HCl.



**Figure 24.** Overlaid emission spectra of complex **66** ( $5 \times 10^{-4}$  M) in acetonitrile upon addition of HCl.

As we can see, the emission band centered at 642 nm decreases gradually upon the addition of HCl and a stationary point is reached after one equivalent excluding possible quenching effect by chloride anion. Surprisingly, the extinction of the luminescence is only partial, and the opened form emits at almost the same wavelength than the closed one. Only a negligible shift of the maximum emission wavelength from 642 to 645 nm is observed. At this time no clear explanation to this behavior can be done. Nevertheless, performed DFT calculations using a hybrid basis (B3LYP/LANL2DZ) highlight the influence of the BOX status in the localization of the electronic density in LUMO as shown below.

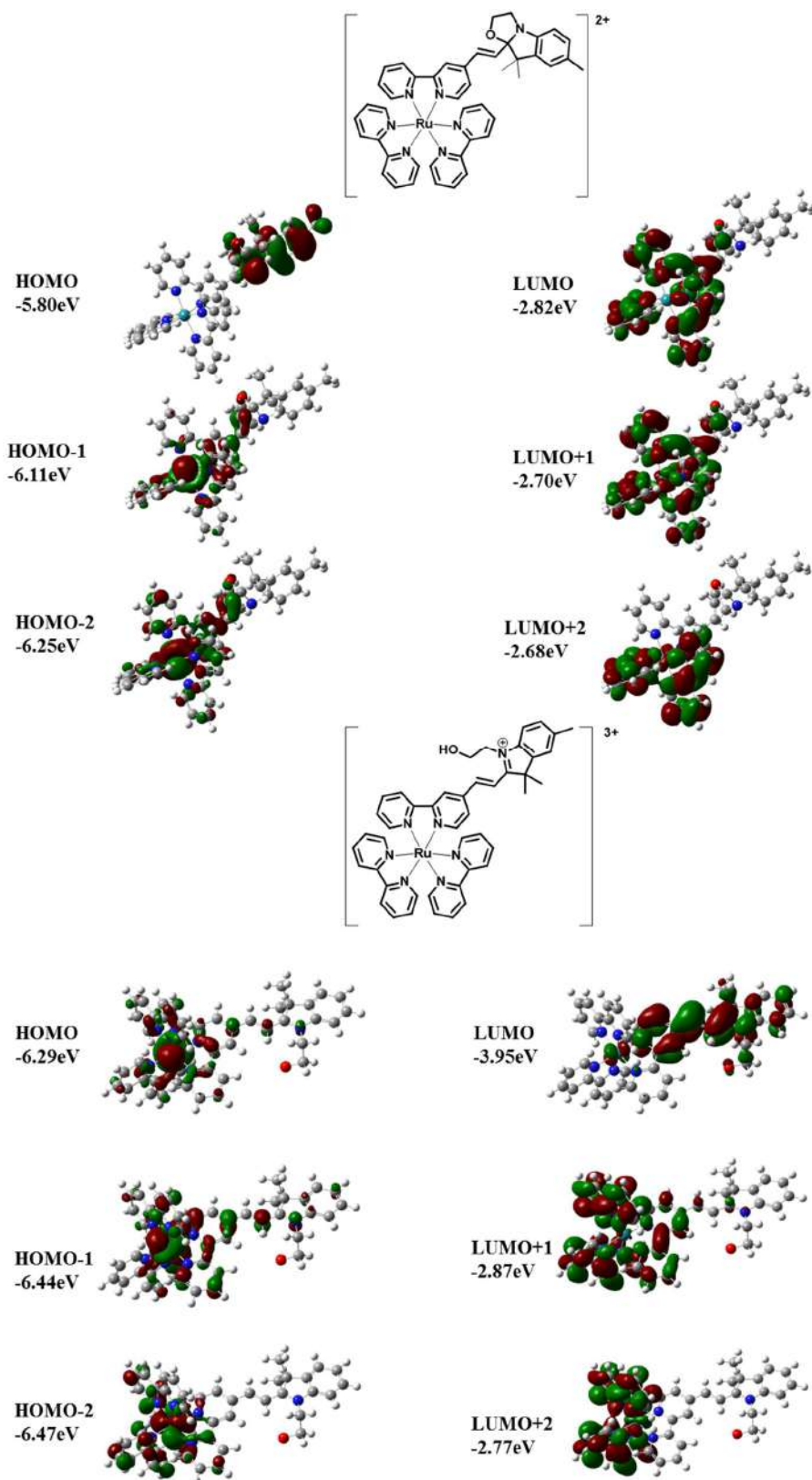


Figure 25. Frontier orbitals of complex 66 under its closed and opened form.

#### IV). Conclusion

Through this chapter, two new series of multi-modal and multi-level molecular systems based on Zinc and Ruthenium complexes have been described. The compounds have been characterized using a combination of analytical techniques including NMR spectroscopy, IR spectroscopy, mass spectrometry, elemental analysis and single crystal X-ray crystallography. Experimental characterizations of the different switching states of chosen Zinc and Ruthenium complexes have been carried out, as well as the study of the chemical, photochemical and electrochemical associated processes.

A first part of this work was mainly focused on zinc complex **56**, a credible model for zinc complexes which all behave the same. The investigations show that, whatever the kind of stimulation, a dissociation of the zinc complex is observed in addition to the multimodal switching of the BOX. This latter conclusion is supported by:

- NMR titration by HCl of complex **56** which shows a concomitant BOX opening and complex dissociation.
- An overlap of UV-visible spectra of species obtained from ligand or complex with all kinds of stimulation.
- The stimulation of the complex **56** by using UV light or chemical oxidant lead at the end to identical UV-Visible spectrum.

Nevertheless, preliminary experiments also allow hypothesize that Zn-complexes can be obtained from the opened form of the BOX what could lead to other experiments (for example in non protic solvents) starting from the latter.

Finally, a new series of ruthenium complexes bearing at least one BOX unit has been synthesized and investigated. In this case, starting from a heteroleptic complex presenting a unique BOX system, all experimental characterizations show that, upon stimulating, an opening

## Chapter 5: Elaboration of multi-level molecular systems based on coordination chemistry

---

of the oxazolidine ring is observed without any further dissociation. In addition to that, preliminary experiments have demonstrated that the luminescence properties of complex **66** can be modulated *via* the BOX-opening.

This new class of Ru-complexes appears promising and experiments from other synthesized systems including several BOX units have to be conducted. As example, the study of complex **67** where two ligands bears one BOX units will allow to conclude concerning possible through space interactions.



## II). References

- [1] E. C. Harvey, B. L. Feringa, J. G. Vos, W. R. Browne and M. T. Pryce, *Coordination Chemistry Reviews* **2015**, 282, 77-86.
- [2] J. Burgess and R. H. Prince in *Zinc: Inorganic & Coordination Chemistry* (Ed. L. John Wiley & Sons), **2006**.
- [3] S. Bang, Y.-M. Lee, S. Hong, K.-B. Cho, Y. Nishida, M. S. Seo, R. Sarangi, S. Fukuzumi and W. Nam, *Nature chemistry* **2014**, 6, 934.
- [4] A. Kochem in *Synthèse et caractérisation de complexes de coordination contenant des ligands rédox-actifs, Vol.* Université de Grenoble, **2012**.
- [5] R. Varet, *C. r. d. l'Acad. des sciences* **1897**, 124, 1155-1157.
- [6] C. J. Nyman, *Journal of the American Chemical Society* **1953**, 75, 3575-3576.
- [7] I. Guezguez, A. Ayadi, K. Ordon, K. Iliopoulos, D. G. Branzea, A. Migalska-Zalas, M. Makowska-Janusik, A. El-Ghayoury and B. Sahraoui, *The Journal of Physical Chemistry C* **2014**, 118, 7545-7553.
- [8] Y. J. Yadav, T. F. Mastropietro, E. I. Szerb, A. M. Talarico, S. Pirillo, D. Pucci, A. Crispini and M. Ghedini, *New Journal of Chemistry* **2013**, 37, 1486-1493.
- [9] E. B. Dianov, I. G. Pervova, E. A. Dvoskin and P. A. J. R. J. o. G. C. Slepukhin, **2018**, 88, 843-845.
- [10] M. S. Nair, P. T. Arasu, S. S. Mansoor, P. Shenbagavalli and M. Neelakantan, **1995**.
- [11] J. K. Kochi, *Accounts of Chemical Research* **1992**, 25, 39-47.
- [12] L. Spiccia, G. B. Deacon and C. M. Kepert, *Coordination Chemistry Reviews* **2004**, 248, 1329-1341.
- [13] E. Rajkumar, S. Rajagopal, P. Ramamurthy and M. Vairamani, *Inorganica Chimica Acta* **2009**, 362, 1629-1636.
- [14] F. Barigelletti and L. Flamigni, *Chemical Society Reviews* **2000**, 29, 1-12.
- [15] N. Robertson and C. A. McGowan, *Chemical Society Reviews* **2003**, 32, 96-103.
- [16] A. P. De Silva, H. N. Gunaratne, T. Gunlaugsson, A. J. Huxley, C. P. McCoy, J. T. Rademacher and T. E. Rice, *Chemical Reviews* **1997**, 97, 1515-1566.
- [17] E. A. Medlycott and G. S. Hanan, *Coordination chemistry reviews* **2006**, 250, 1763-1782.
- [18] L. Sun, *Chem. Soc. Rev* **2001**, 30, 36-49.
- [19] M. T. Indelli, S. Carli, M. Ghirotti, C. Chiorboli, M. Ravaglia, M. Garavelli and F. Scandola, *Journal of the American Chemical Society* **2008**, 130, 7286-7299.
- [20] W. Zhang, B. Li, H. Ma, L. Zhang, Y. Guan, Y. Zhang, X. Zhang, P. Jing and S. Yue, *ACS applied materials & interfaces* **2016**, 8, 21465-21471.
- [21] S. A. Cotton, *Chemistry of precious metals*, Springer Science & Business Media, **2012**, p.
- [22] E. A. Seddon and K. R. Seddon, *The chemistry of ruthenium*, Elsevier, **2013**, p.
- [23] B. Sullivan, D. Salmon and T. Meyer, *Inorganic Chemistry* **1978**, 17, 3334-3341.
- [24] D. A. Freedman, J. K. Evju, M. K. Pomije and K. R. Mann, *Inorganic chemistry* **2001**, 40, 5711-5715.
- [25] C. Houarner, E. Blart, P. Buvat and F. Odobel, *Photochemical & Photobiological Sciences* **2005**, 4, 200-204.
- [26] H. Rudmann, S. Shimada and M. F. Rubner, *Journal of the american chemical society* **2002**, 124, 4918-4921.
- [27] A. Wild, A. Winter, F. Schlütter and U. S. Schubert, *Chemical Society Reviews* **2011**, 40, 1459-1511.
- [28] V. Balzani, G. Bergamini, S. Campagna and F. Puntoriero in *Photochemistry and photophysics of coordination compounds: overview and general concepts*, Springer, **2007**, pp. 1-36.
- [29] N. Yoshikawa, H. Kimura, S. Yamabe, N. Kanehisa, T. Inoue and H. Takashima, *Journal of Molecular Structure* **2016**, 1117, 49-56.
- [30] A. O. Adeloye, *Molecules* **2011**, 16, 8353-8367.
- [31] J. R. Lakowicz, *Principles of fluorescence spectroscopy*, Springer Science & Business Media, **2013**, p.
- [32] N. Yoshikawa, H. Kimura, S. Yamabe, N. Kanehisa, T. Inoue and H. Takashima, *Journal of Molecular Structure* **2016**, 1117, 49-56.

## Chapter 5: Elaboration of multi-level molecular systems based on coordination chemistry

---

- [33] A. Juris, V. Balzani, F. Barigelletti, S. Campagna, P. Belser and A. von Zelewsky, *Coordination Chemistry Reviews* **1988**, *84*, 85-277.
- [34] S. Hohloch, D. Schweinfurth, M. G. Sommer, F. Weisser, N. Deibel, F. Ehret and B. Sarkar, *Dalton Transactions* **2014**, *43*, 4437-4450.
- [35] H. B. Ross, M. Boldaji, D. P. Rillema, C. B. Blanton and R. P. White, *Inorganic Chemistry* **1989**, *28*, 1013-1021.
- [36] F. Barigelletti, A. Juris, V. Balzani, P. Belser and A. Von Zelewsky, *Inorganic Chemistry* **1987**, *26*, 4115-4119.
- [37] A. Juris, V. Balzani, F. Barigelletti, S. Campagna, P. I. Belser and A. Von Zelewsky, *Coordination Chemistry Reviews* **1988**, *84*, 85-277.
- [38] D. P. Rillema, G. Allen, T. Meyer and D. Conrad, *Inorganic chemistry* **1983**, *22*, 1617-1622.
- [39] A. J. McConnell, M. H. Lim, E. D. Olmon, H. Song, E. E. Dervan and J. K. Barton, *Inorganic chemistry* **2012**, *51*, 12511-12520.

---

## **General conclusion**

---



The objective of this pH-D project was to demonstrate the feasibility and efficiency of (supra) molecular assemblies of multi-level and multi-modal switches based on the indolinooxazolidine (BOX) motif. Indeed, the association of several BOX units through covalent bond or *via* supramolecular chemistry may allow controlling upon various stimulations the reversible commutation between more than 2 discrete and discernable states potentially interesting for molecular (opto) electronics.

To reach this objective, several series of derivatives have been developed following two main methodologies. In the first approach, an organic core (thiophene based linear conjugated bridge or a triarylamine node) was used to covalently bond 2 or 3 BOX units. The second approach lays on the BOX association by coordination chemistry. In this context, a large library of ligands bearing one or two BOX moieties have been developed and some of those then associated with Zn or Ru metals to form corresponding complexes. Noteworthy, most syntheses have implied in last step the condensation of the BOX termination onto an aldehyde function. Taking advantage of a procedure recently developed has allowed decent to high yields despite the structural variety of synthons and the number (up to three) of functionalities concerned.

After syntheses, the commutation abilities of all compounds and complexes have been studied. After classical characterizations allowing their identification, *a minima* monitoring by UV-Visible spectroscopy as well as by NMR spectrometry have confirmed their multi-modal possibility to induce their commutation.

First characterizations conducted from simple BiBox-BiT systems (chapter 2) have demonstrated that all stimuli (acid, light and redox) allow from their closed **CC** form the reversible and step wise formation of partially **OC** and then fully **OO** opened forms. Noteworthy, the indirect redox stimulation which acts through the conjugated system which presents an oxidation potential lower than that of BOX appears more selective than others which directly stimulate the switching unit.

## General conclusion

---

If the quantity of oxidizing reagent allows controlling the BOX O open/C close ratio, this first example did not allow controlling the switching unit via an imposed potential. In order to better discriminate the redox phenomena, a longer and more rigid ETE conjugated system was inserted between BOX terminations. Indeed, the cyclic voltammetry of such system allows observing discriminate oxidations processes not seen with the shorter bithiophene spacer, further investigations . Conducted experiments suggest, here again

- A stepwise and multi-modal commutation of BOX systems
- An electromediated commutation of both BOX occurring at similar potential too close to permit their clear discrimination.

As the grafting of two BOX on a unique conjugated system did not allow potential controlled step wise commutation and as a step forward in order to increase the number of possible metastable states, compounds covalently linking 3 BOX units were considered. As a first series of derivatives constituted on a simple phenyl ring directly functionalized with BOX systems allowed the validation of the synthetic strategy, two series of symmetric triarylamine based derivatives were developed. Here again, the conducted analyses allowed demonstrating a step wise and multi-modal reversible commutation between, this time, four states from the full closed **CCC** one to the **OCC**, **OOC** and then finally **OOO** one. Thus, the strategy started from a linear conjugated system may be generalized to more extended conjugated systems but electronically dependent systems

Starting from this point and as a first try to control the sequence of the BOX-openings, a prototype of triarylamine unsymmetrically substituted with three different spacers terminated with the same BOX unit was synthesized. If, here again, as previously observed with symmetrical and linear systems, a stepwise and multimodal commutation of switching units is observed, a preferential opening sequence is also characterized. Indeed, NMR studies demonstrate that the opening ability of each BOX may be linked to its conjugation quality with

the central electron rich node. Noteworthy, the selectivity appears more marked when a redox stimulation is undergone. If these last results could be considered as perfectible due to the observed low selectivity between BOX units, it may be considered as a proof of concept as it paves the way to possible sequencing of the stimulation of identified BOX. Indeed, further experiments with more dissymmetrical (or other) structures will be necessary to extend and exploit this concept

Step-wise commutation between discrete states has interest if these last exhibit very discriminated physico-chemical properties especially optical ones. Indeed, optical reading is commonly admitted as an easy, rapid and non-destructive method. Nevertheless, UV-visible spectroscopic experiments, conducted from all synthesized compounds, demonstrate that all species presenting at least one opened BOX absorb in the same area with various and close intensities. In contrary, nonlinear optical properties of linear compounds appear contrasted. Indeed, as the symmetrical and non-polar **CC** form of BiBOX-Bithiophene system only exhibits very weak NLO activity, its polar **OC** and **OO** forms present high and contrasted first hyperpolarizabilities ( $\beta_{\text{HRS}}$ ). These measurements were inefficient from ETE based compounds due to their strong two photon absorption abilities which after full characterization may allow application in medical imagery. Noteworthy, NLO characterization of triphenylamine based derivatives is still in progress.

As this first “covalent approach” has unambiguously demonstrated through bond interactions between BOX moieties linked via conjugated systems, the possibility to exploit through space interactions still poses question. In this context, we envisioned the geneses of metal complexes liganded with species bearing some BOX moieties. In such architectures, the spatial arrangement between BOX moieties can be finely controlled and, moreover, original interactions between the metallic center and the switchable arms may also be awaited. Due to the large library of ligands synthesized, many structures were possible. Due to lack of time,

## General conclusion

---

only few of those were, successfully, synthesized and characterized. First of all, as many Zn complexes were prepared, it appears that, whatever the stimulation (acid, light and redox) the BOX opening is accompanied with a ligand N-protonation which leads at the end to zinc ion release. If this phenomenon needs further experiments to clear up its mechanism, one may note that this first series of complexes won't allow programmed studied. In contrary, if Ru complexes syntheses appear a little trickier, a first series of stimulation conducted on a complex system bearing one BOX unit, allowed demonstrating the complex stability as well as the reversible multimodal commutation of the switchable unit. Moreover, complementary spectroscopic experiments have also demonstrated the influence of the BOX status on the complex emission properties.

If the results obtained during this pH-D appear promising, they also pave the way to many further experiments. First, in short term,

- Complex bearing several BOX (on several or in the contrary on the same ligand) will be studied. Their step wise or in contrary all-in commutation will give insights about the possibility to promote through space interactions the differentiation between BOX units.
- The studies and exploitation of NLO properties of linear and trigonal species will be extended and deepened.

Results and experiences acquired during this work allow extending some studies but also developing new other ones.

The presence of two BOX on one conjugated system has first demonstrated their possible step wise commutation and the dissymetrization of triarylamine systems allowed the observation of a sort of selectivity depending on the electronic environment of the BOX. This idea has to be pushed further in order to develop systems in which it will be possible to

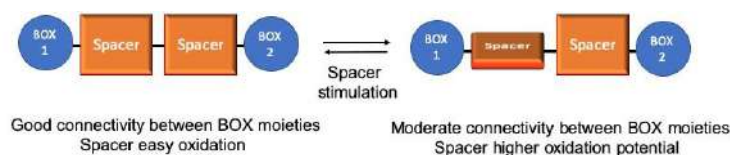
## General conclusion

---

selectively address one box or one other with possible different (non)linear optical properties. Playing on the donor ability of two different pi-conjugated systems and/or on the substitution of the grafted BOX units could represent complementary approaches.



Non direct stimulation of BOX systems *via* the oxidation of conjugated system may also allow to control the redox potential of the BOX opening by toning the spacer donor ability.



A huge work remains on this complex topic. In complement to the numerous possibilities which imply metal and ligand modifications, a shorter term and challenging topic may consist in exploiting MLCT transitions to develop a new mode of stimulation of BOX units. By analogy with the redox non direct stimulation, a light emission in the exciting band the metal may in these conditions allow the stimulation of BOX derivatives.



---

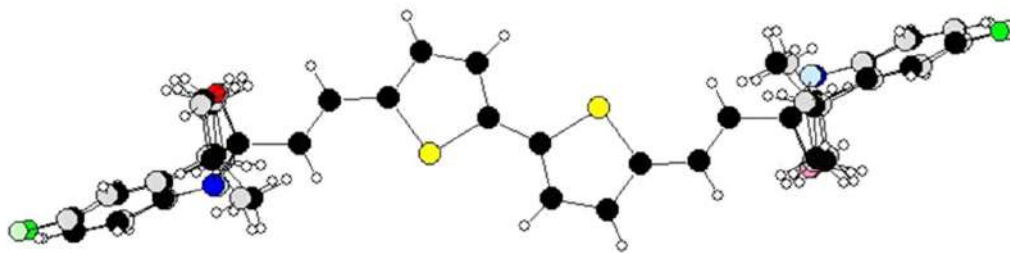
# **Appendix 1: Crystallographic Structures**

---



## Appendix 1: Crystallographic Structures

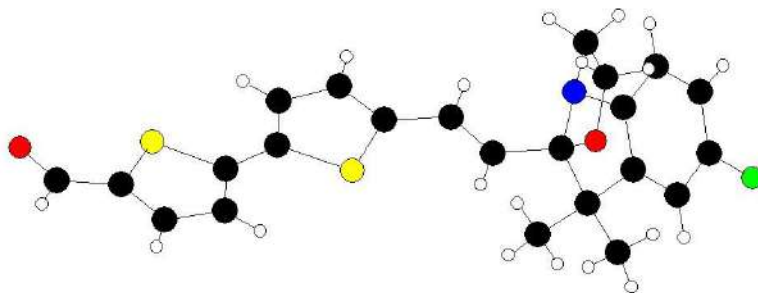
### 5,5'-bis((E)-2-(7-fluoro-9,9-dimethyl-2,3,9,9a-tetrahydrooxazolo[3,2-a]indol-9a-yl)vinyl)-2,2'-bithiophene (22)



Empirical formula	C <sub>36</sub> H <sub>34</sub> F <sub>2</sub> N <sub>2</sub> O <sub>2</sub> S <sub>2</sub>
Formula weight	628.77
Temperature	150.0(1) K
Wavelength	1.54184 Å
Crystal system, space group	Orthorhombic, P b a m
Unit cell dimensions	a = 17.5518(7) Å alpha = 90 deg. b = 15.6052(6) Å beta = 90 deg. c = 11.5200(3) Å gamma = 90 deg.
Volume	3155.32(19) Å <sup>3</sup>
Z, Calculated density	4, 1.324 Mg/m <sup>3</sup>
Absorption coefficient	1.920 mm <sup>-1</sup>
F(000)	1320
Crystal size	0.239 x 0.144 x 0.062 mm
Theta range for data collection	3.790 to 76.371 deg.
Limiting indices	-21 ≤ h ≤ 21, -13 ≤ k ≤ 19, -13 ≤ l ≤ 14
Reflections collected / unique	10673 / 3412 [R (int) = 0.0185]
Completeness to theta = 75.000	98.4 %
Absorption correction	Semi-empirical from equivalents
Max. and min. transmission	1.00000 and 0
Refinement method	Full-matrix least-squares on F <sup>2</sup>
Data / restraints / parameters	3412 / 24 / 353
Goodness-of-fit on F <sup>2</sup>	1.409
Final R indices [I > 2σ(I)]	R1 = 0.0993, wR2 = 0.3008 [2754 Fo]
R indices (all data)	R1 = 0.1093, wR2 = 0.3212
Largest diff. peak and hole	0.841 and -0.831 e.Å <sup>-3</sup>

## Appendix 1: Crystallographic Structures

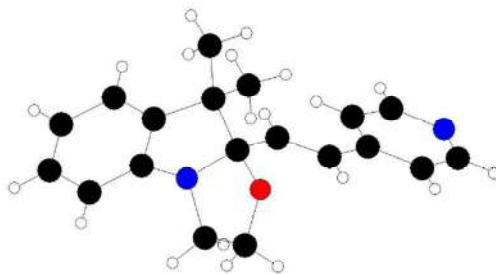
### (E)-5'-(2-(7-fluoro-9,9-dimethyl-2,3,9,9a-tetrahydrooxazolo[3,2-a]indol-9a-yl)vinyl)-[2,2'-bithiophene]-5-carbaldehyde



Empirical formula	C <sub>23</sub> H <sub>20</sub> FNO <sub>2</sub> S <sub>2</sub>
Formula weight	425.52
Temperature	150.0(1) K
Wavelength	1.54184 Å
Crystal system, space group	Monoclinic, P 2 <sub>1</sub> /c
Unit cell dimensions	a = 22.5829(12) Å    alpha = 90 deg. b = 11.0469(7) Å    beta = 100.297(7) deg. c = 8.0566(6) Å    gamma = 90 deg.
Volume	1977.5(2) Å <sup>3</sup>
Z, Calculated density	4, 1.429 Mg/m <sup>3</sup>
Absorption coefficient	2.690 mm <sup>-1</sup>
F (000)	888
Crystal size	0.099 x 0.034 x 0.015 mm
Theta range for data collection	3.979 to 72.948 deg.
Limiting indices	-27 ≤ h ≤ 20, -13 ≤ k ≤ 11, -9 ≤ l ≤ 9
Reflections collected / unique	8706 / 3806 [R (int) = 0.0569]
Completeness to theta = 72.948	98.1 %
Absorption correction	Semi-empirical from equivalents
Max. and min. transmission	1.00000 and 0.79895
Refinement method	Full-matrix least-squares on F <sup>2</sup>
Data / restraints / parameters	3806 / 0 / 265
Goodness-of-fit on F <sup>2</sup>	1.021
Final R indices [I > 2σ(I)]	R1 = 0.0476, wR2 = 0.0940 [2810 Fo]
R indices (all data)	R1 = 0.0722, wR2 = 0.1043
Largest diff. peak and hole	0.230 and -0.246 e.Å <sup>-3</sup>

## Appendix 1: Crystallographic Structures

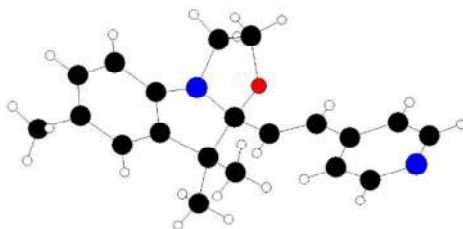
### (E)-9,9-dimethyl-9a-(2-(pyridin-4-yl)vinyl)-2,3,9,9a-tetrahydrooxazolo[3,2-a]indole (31)



Empirical formula	C <sub>19</sub> H <sub>20</sub> N <sub>2</sub> O
Formula weight	292.37
Temperature	150.0(1) K
Wavelength	1.54184 Å
Crystal system, space group	Orthorhombic, P 21 21 21
Unit cell dimensions	a = 8.7072(2) Å    alpha = 90 deg. b = 9.0385(2) Å    beta = 90 deg. c = 20.4631(5) Å    gamma = 90 deg.
Volume	1610.45(6) Å <sup>3</sup>
Z, Calculated density	4, 1.206 Mg/m <sup>3</sup>
Absorption coefficient	0.589 mm <sup>-1</sup>
F(000)	624
Crystal size	0.292 x 0.253 x 0.087 mm
Theta range for data collection	4.321 to 76.280 deg.
Limiting indices	-10 ≤ h ≤ 10, -11 ≤ k ≤ 10, -25 ≤ l ≤ 24
Reflections collected / unique	7944 / 3158 [R (int) = 0.0604]
Completeness to theta = 76.280	99.3 %
Absorption correction	Semi-empirical from equivalents
Max. and min. transmission	1.00000 and 0.85769
Refinement method	Full-matrix least-squares on F <sup>2</sup>
Data / restraints / parameters	3158 / 0 / 201
Goodness-of-fit on F <sup>2</sup>	1.062
Final R indices [I > 2σ(I)]	R1 = 0.0518, wR2 = 0.1386 [3019 Fo]
R indices (all data)	R1 = 0.0542, wR2 = 0.1413
Absolute structure parameter	0.3(4)
Largest diff. peak and hole	0.180 and -0.221 e.Å <sup>-3</sup>

## Appendix 1: Crystallographic Structures

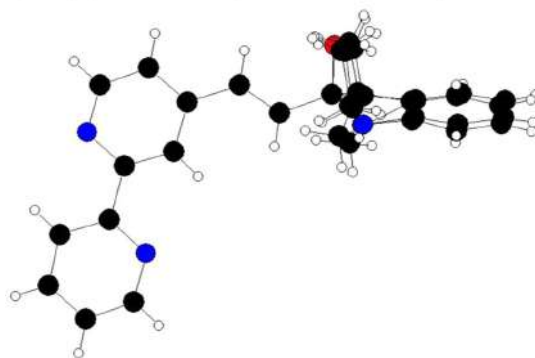
### (E)-7,9,9-trimethyl-9a-(2-(pyridin-4-yl)vinyl)-2,3,9a-tetrahydrooxazolo[3,2-a]indole (32)



Empirical formula	C <sub>20</sub> H <sub>22</sub> N <sub>2</sub> O
Formula weight	306.39
Temperature	150.0(3) K
Wavelength	1.54184 Å
Crystal system, space group	Orthorhombic, P 21 21 21
Unit cell dimensions	a = 8.83310(10) Å    alpha = 90 deg. b = 9.37090(10) Å    beta = 90 deg. c = 20.5380(3) Å    gamma = 90 deg.
Volume	1700.01(4) Å <sup>3</sup>
Z, Calculated density	4, 1.197 Mg/m <sup>3</sup>
Absorption coefficient	0.579 mm <sup>-1</sup>
F(000)	656
Crystal size	0.369 x 0.268 x 0.148 mm
Theta range for data collection	4.305 to 76.497 deg.
Limiting indices	-8 ≤ h ≤ 11, -11 ≤ k ≤ 10, -25 ≤ l ≤ 18
Reflections collected / unique	4701 / 2939 [R (int) = 0.0451]
Completeness to theta = 76.000	98.0 %
Absorption correction	Semi-empirical from equivalents
Max. and min. transmission	1.00000 and 0.85580
Refinement method	Full-matrix least-squares on F <sup>2</sup>
Data / restraints / parameters	2939 / 0 / 212
Goodness-of-fit on F <sup>2</sup>	1.062
Final R indices [I > 2σ(I)]	R1 = 0.0462, wR2 = 0.1259 [2872 F <sub>o</sub> ]
R indices (all data)	R1 = 0.0481, wR2 = 0.1308
Absolute structure parameter	0.1(4)
Extinction coefficient	0.0036(8)
Largest diff. peak and hole	0.211 and -0.194 e.Å <sup>-3</sup>

## Appendix 1: Crystallographic Structures

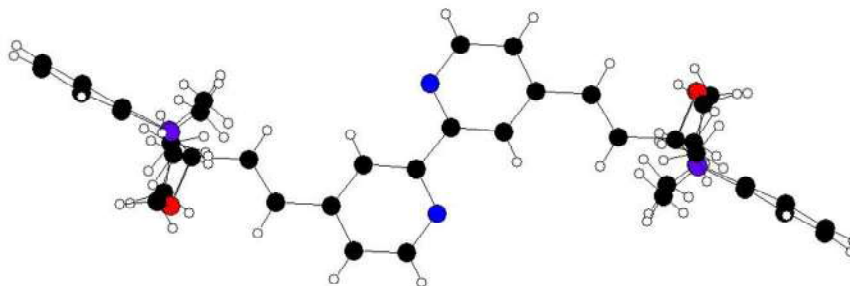
### (E)-9a-(2-([2,2'-bipyridin]-4-yl)vinyl)-9,9-dimethyl-2,3,9a-tetrahydrooxazolo[3,2-a]indole (36)



Empirical formula	C <sub>24</sub> H <sub>23</sub> N <sub>3</sub> O
Formula weight	369.45
Temperature	293(2) K
Wavelength	1.54184 Å
Crystal system, space group	Triclinic, P -1
Unit cell dimensions	a = 8.4181(4) Å    alpha = 63.202(5) deg. b = 11.4615(6) Å    beta = 84.360(4) deg. c = 11.5844(6) Å    gamma = 83.085(4) deg.
Volume	989.19(10) Å <sup>3</sup>
Z, Calculated density	2, 1.240 Mg/m <sup>3</sup>
Absorption coefficient	0.606 mm <sup>-1</sup>
F(000)	392
Crystal size	0.299 x 0.209 x 0.158 mm
Theta range for data collection	4.281 to 76.526 deg.
Limiting indices	-10 ≤ h ≤ 9, -14 ≤ k ≤ 12, -14 ≤ l ≤ 14
Reflections collected / unique	7410 / 4023 [R (int) = 0.0121]
Completeness to theta = 74.000	98.5 %
Absorption correction	Semi-empirical from equivalents
Max. and min. transmission	1.00000 and 0.87923
Refinement method	Full-matrix least-squares on F <sup>2</sup>
Data / restraints / parameters	4023 / 0 / 376
Goodness-of-fit on F <sup>2</sup>	1.092
Final R indices [I > 2σ(I)]	R1 = 0.0627, wR2 = 0.1633 [3612 Fo]
R indices (all data)	R1 = 0.0679, wR2 = 0.1678
Extinction coefficient	0.0053(8)
Largest diff. peak and hole	0.166 and -0.169 e.Å <sup>-3</sup>

## Appendix 1: Crystallographic Structures

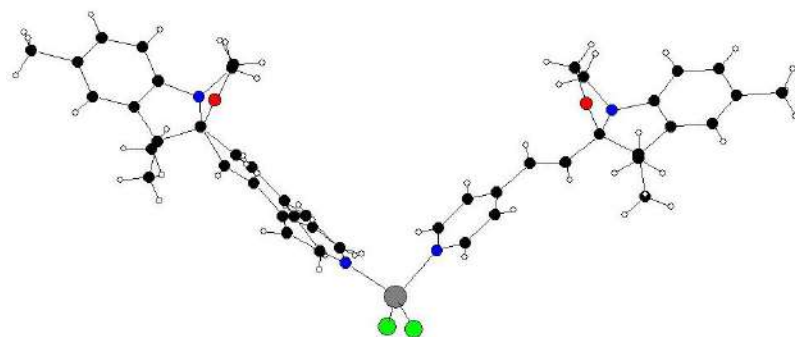
### 4,4'-bis((E)-2-(9,9-dimethyl-2,3,9a-tetrahydrooxazolo[3,2-a]indol-9a-yl)vinyl)-2,2'-bipyridine (44)



Empirical formula	$C_{38}H_{38}N_4O_2$
Formula weight	582.72
Temperature	150.0(1) K
Wavelength	1.54184 Å
Crystal system, space group	Monoclinic, P 21/c
Unit cell dimensions	a = 11.2536(3) Å    alpha = 90 deg. b = 13.0614(4) Å    beta = 96.233(3) deg. c = 10.4320(3) Å    gamma = 90 deg.
Volume	1524.31(8) Å <sup>3</sup>
Z, Calculated density	2, 1.270 Mg/m <sup>3</sup>
Absorption coefficient	0.622 mm <sup>-1</sup>
F(000)	620
Crystal size	0.216 x 0.157 x 0.062 mm
Theta range for data collection	3.951 to 73.468 deg.
Limiting indices	-13 ≤ h ≤ 12, -16 ≤ k ≤ 10, -12 ≤ l ≤ 9
Reflections collected / unique	6019 / 2972 [R (int) = 0.0154]
Completeness to theta = 73.468	97.0 %
Absorption correction	Semi-empirical from equivalents
Max. and min. transmission	1.00000 and 0.88872
Refinement method	Full-matrix least-squares on F <sup>2</sup>
Data / restraints / parameters	2972 / 7 / 229
Goodness-of-fit on F <sup>2</sup>	1.858
Final R indices [I > 2σ(I)]	R1 = 0.1168, wR2 = 0.3855 [2455 Fo]
R indices (all data)	R1 = 0.1280, wR2 = 0.4114
Largest diff. peak and hole	0.844 and -0.754 e.Å <sup>-3</sup>

## Appendix 1: Crystallographic Structures

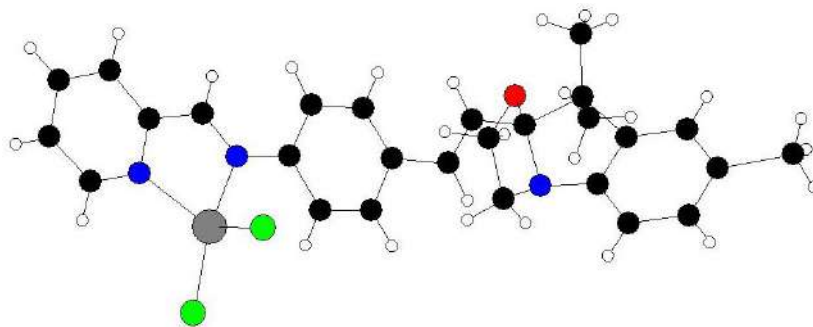
### Zn(L')<sub>2</sub>Cl<sub>2</sub> (56)



Empirical formula	C <sub>40</sub> H <sub>44</sub> Cl <sub>2</sub> N <sub>4</sub> O <sub>2</sub> Zn
Formula weight	749.06
Temperature	130.0(1) K
Wavelength	1.54184 Å
Crystal system, space group	Monoclinic, C 2/c
Unit cell dimensions	a = 31.867(4) Å    alpha = 90 deg. b = 7.5786(6) Å    beta = 93.636(7) deg. c = 32.783(3) Å    gamma = 90 deg.
Volume	7901.3(14) Å <sup>3</sup>
Z, Calculated density	8, 1.259 Mg/m <sup>3</sup>
Absorption coefficient	2.399 mm <sup>-1</sup>
F(000)	3136
Crystal size	0.126 x 0.063 x 0.035 mm
Theta range for data collection	2.701 to 75.777 deg.
Limiting indices	-39 ≤ h ≤ 39, -9 ≤ k ≤ 8, -40 ≤ l ≤ 40
Reflections collected / unique	15973 / 7945 [R (int) = 0.0496]
Completeness to theta = 74.000	98.3 %
Absorption correction	Semi-empirical from equivalents
Max. and min. transmission	1.00000 and 0.81935
Refinement method	Full-matrix least-squares on F <sup>2</sup>
Data / restraints / parameters	7945 / 0 / 482
Goodness-of-fit on F <sup>2</sup>	1.026
Final R indices [I > 2σ(I)]	R1 = 0.0938, wR2 = 0.2432 [5688 Fo]
R indices (all data)	R1 = 0.1202, wR2 = 0.2659
Largest diff. peak and hole	0.586 and -0.548 e.Å <sup>-3</sup>

## Appendix 1: Crystallographic Structures

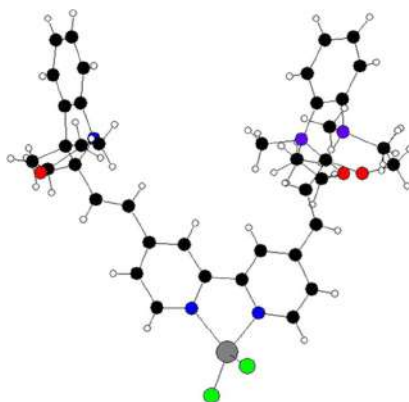
### ZnL<sub>1</sub>Cl<sub>2</sub> (57)



Empirical formula	C <sub>27</sub> H <sub>27</sub> Cl <sub>2</sub> N <sub>3</sub> OZn
Formula weight	545.78
Temperature	149.9(5) K
Wavelength	1.54184 Å
Crystal system, space group	Triclinic, P -1
Unit cell dimensions	a = 7.9133(16) Å    alpha = 90.723(15) deg. b = 9.4574(16) Å    beta = 100.719(19) deg. c = 19.213(4) Å    gamma = 109.877(18) deg.
Volume	1324.2(5) Å <sup>3</sup>
Z, Calculated density	2, 1.369 Mg/m <sup>3</sup>
Absorption coefficient	3.329 mm <sup>-1</sup>
F(000)	564
Crystal size	0.084 x 0.027 x 0.023 mm
Theta range for data collection	4.701 to 70.628 deg.
Limiting indices	-9 ≤ h ≤ 8, -11 ≤ k ≤ 11, -22 ≤ l ≤ 17
Reflections collected / unique	9114 / 4862 [R (int) = 0.1281]
Completeness to theta = 67.684	98.2 %
Absorption correction	Semi-empirical from equivalents
Max. and min. transmission	1.00000 and 0.51696
Refinement method	Full-matrix least-squares on F <sup>2</sup>
Data / restraints / parameters	4862 / 6 / 297
Goodness-of-fit on F <sup>2</sup>	1.001
Final R indices [I > 2σ(I)]	R1 = 0.1102, wR2 = 0.2583 [2154 Fo]
R indices (all data)	R1 = 0.1915, wR2 = 0.3283
Largest diff. peak and hole	0.738 and -0.782 e.Å <sup>-3</sup>

## Appendix 1: Crystallographic Structures

### Zn((H-BOX)<sub>2</sub>bPy)Cl<sub>2</sub> (62)



Empirical formula	C <sub>38</sub> H <sub>38</sub> Cl <sub>2</sub> N <sub>4</sub> O <sub>2</sub> Zn
Formula weight	718.99
Temperature	150.0(1) K
Wavelength	1.54184 Å
Crystal system, space group	Monoclinic, P 2 <sub>1</sub> /c
Unit cell dimensions	a = 14.4680(10) Å    α = 90 deg. b = 14.0067(9) Å    β = 92.032(5) deg. c = 16.3903(9) Å    γ = 90 deg.
Volume	3319.4(4) Å <sup>3</sup>
Z, Calculated density	4, 1.439 Mg/m <sup>3</sup>
Absorption coefficient	2.833 mm <sup>-1</sup>
F(000)	1496
Crystal size	0.245 x 0.189 x 0.051 mm
Theta range for data collection	3.056 to 72.353 deg.
Limiting indices	-17 ≤ h ≤ 15, -11 ≤ k ≤ 16, -20 ≤ l ≤ 14
Reflections collected / unique	11004 / 6242 [R (int) = 0.0217]
Completeness to theta = 68.000	98.2 %
Absorption correction	Semi-empirical from equivalents
Max. and min. transmission	1.00000 and 0.657
Refinement method	Full-matrix least-squares on F <sup>2</sup>
Data / restraints / parameters	6242 / 30 / 442
Goodness-of-fit on F <sup>2</sup>	1.235
Final R indices [I > 2σ(I)]	R1 = 0.1017, wR2 = 0.3015 [4178 Fo]
R indices (all data)	R1 = 0.1282, wR2 = 0.3302
Largest diff. peak and hole	0.969 and -0.498 e.Å <sup>-3</sup>



---

## **Appendix 2: Experimental Parts**

---



### General Informations

All reagents and chemicals from commercial sources were used without further purification. Solvents were dried and purified using standard techniques. Column chromatography was performed with analytical-grade solvents using Aldrich silica gel (technical grade, pore size 60 Å, 230-400 mesh particle size). Flexible plates ALUGRAM® Xtra SIL G UV254 from MACHEREY-NAGEL were used for TLC. Compounds were detected by UV irradiation (Bioblock Scientific) or staining with iodine, unless otherwise stated.

**NMR spectra** were recorded on a Bruker AVANCE III 300 ( $^1\text{H}$ , 300 MHz;  $^{13}\text{C}$ , 75 MHz) or a Bruker AVANCE DRX500 ( $^1\text{H}$ , 500 MHz;  $^{13}\text{C}$ , 125 MHz). Chemical shifts are given in parts per million (ppm) relative to TMS and coupling constants  $J$  in Hertz (Hz).

**Infrared spectra** were recorded on a Bruker spectrometer Vertex 70.

**High Resolution Mass Spectrometry (HRMS)** was performed with a JEOL JMS-700 B/E.

**Elemental analyses** were performed with a thermo-electron instrument (FLASH 2000, Thermo Scientific).

**UV-visible absorption spectra** were recorded at room temperature on a Perkin Elmer 950 spectrometer or a Shimadzu UV-1800 spectrometer.

**X-Ray Diffraction:** Single crystals of the compounds were mounted on glass fibre loops using a viscous hydrocarbon oil to coat the crystal and then transferred directly to cold nitrogen stream for data collection. Data collection were mostly performed at 150 K on an Agilent Supernova with  $\text{CuK}\alpha$  ( $\lambda = 1.54184 \text{ \AA}$ ). The structures were solved by direct methods with the SIR97 program and refined against all  $F_2$  values with the SHELXL-97 program using the WinGX graphical user interface.

**Electrochemical measurements** were performed using a Biologic SP-150 potentiostat with positive feedback compensation. Samples were dissolved in acetonitrile HPLC grade, purchased from Carlo Erba (HPLC grade). Tetrabutylammonium hexafluorophosphate (0.1 M as supporting electrolyte) was purchased from Sigma-Aldrich and recrystallized prior to use. Experiments were carried out under an inert atmosphere (Ar) using a glovebox, in a one-compartment cell equipped with platinum working

microelectrode ( $\varnothing = 2$  mm) and a platinum wire counter electrode. A silver wire immersed in 0.10 M  $\text{Bu}_4\text{NPF}_6/\text{CH}_3\text{CN}$  was used as pseudo-reference electrode and checked against ferrocene/ferrocenium couple ( $\text{Fc}/\text{Fc}^+$ ) before and after each experiment.

## Synthetic procedures

### Organic part

#### Synthesis of indolinooxazolidines:

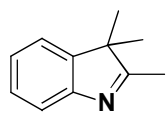
Indolinooxazolidine derivatives were synthesized according to a 3 step procedure described below<sup>[1]</sup>, in which indolenine derivatives were prepared first.

#### General procedure for synthesizing indolenine derivatives:

Phenylhydrazines (200 mmol) and 3-methylbutan-2-one (300 mmol, 1.5 eq.) were refluxed in (480 mL) of AcOH for 12 hours. Acetic acid was removed under reduced pressure, DCM was added in order to wash the system with  $\text{NaHCO}_3$  (2 times),  $\text{H}_2\text{O}$  (2 times), brine (1 time) and the combined organic layers were dried by  $\text{MgSO}_4$ . The solvent was evaporated under reduced pressure to afford a brown oil.

The purity of the indolenine derivatives was checked by proton NMR.

#### 2,3,3-trimethyl-3H-indole (1)

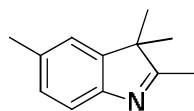


**$\text{C}_{11}\text{H}_{13}\text{N}$**   
 **$159.23 \text{ g}\cdot\text{mol}^{-1}$**

$^1\text{H NMR}$  (300 MHz,  $\text{CDCl}_3$ )  $\delta$  7.54 (d,  $J = 7.5$  Hz, 1H), 7.33 – 7.26 (m, 2H), 7.23 – 7.16 (m, 1H), 2.28 (s, 3H), 1.30 (s, 6H).

---

#### 2,3,3,5-tetramethyl-3H-indole (2)

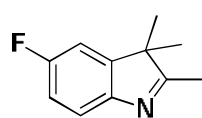


**$\text{C}_{12}\text{H}_{15}\text{N}$**   
 **$173.25 \text{ g}\cdot\text{mol}^{-1}$**

$^1\text{H NMR}$  (300 MHz,  $\text{CDCl}_3$ )  $\delta$  7.43 (d,  $J = 8.1$  Hz, 1H), 7.09 (d,  $J = 7.7$  Hz, 1H), 7.08 (s, 1H), 2.39 (s, 3H), 2.27 (s, 3H), 1.28 (s, 6H).

---

**5-fluoro-2,3,3-trimethyl-3H-indole (3)**

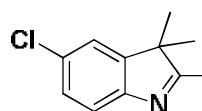


$^1\text{H NMR}$  (300 MHz,  $\text{CDCl}_3$ )  $\delta$  7.44 (dd,  $J = 9.2, 4.5$  Hz, 1H), 7.02 – 6.93 (m, 2H), 2.26 (s, 3H), 1.29 (s, 6H).

$\text{C}_{11}\text{H}_{12}\text{FN}$   
177.22  $\text{g}\cdot\text{mol}^{-1}$

---

**5-chloro-2,3,3-trimethylindolenine (4)**



$^1\text{H NMR}$  (300 MHz,  $\text{CDCl}_3$ )  $\delta$  7.34–7.39 (m, 1H), 7.15–7.24 (m, 2H), 2.19 (s, 3H), 1.21 (s, 6H).

$\text{C}_{11}\text{H}_{12}\text{ClN}$   
193.67  $\text{g}\cdot\text{mol}^{-1}$

---

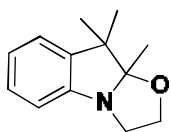
**General procedure for synthesizing indolinooxazoline derivatives:**

Indolinooxazolidines were prepared in two steps from indolenine derivatives.

**First step.** A solution of indolenine derivative (86.9 mmol) and 2-iodoethanol (130.4 mmol, 1.5 eq.) in toluene (135 mL) was refluxed for 12 hours. The solution was allowed to cool to room temperature and filtered. The product was washed with cold  $\text{Et}_2\text{O}$  (3 times) and acetone (3 times) consecutively and dried to afford the indoleninium iodide.

**Second step.** The crude material of indoleninium iodide was used in the following step without further purification. To a suspension of indoleninium iodide (70.5 mmol) in water (500 mL) a solution of NaOH in water (250 mL) was added and the resulting solution was stirred at room temperature for 30 min. The reaction mixture was extracted with  $\text{Et}_2\text{O}$  (3 times), washed with water (2 times), brine (1 time) and the combined organic layers were dried by  $\text{MgSO}_4$ . The solvent was evaporated to afford the indolinooxazoline as a brown solid (compounds were used without further purification).

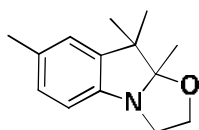
9,9,9a-trimethyl-2,3,9a-tetrahydrooxazolo[3,2-a]indole (5)



$^1\text{H NMR}$  (300 MHz,  $\text{CDCl}_3$ )  $\delta$  7.14 (td,  $J = 7.7, 1.2$  Hz, 1H), 7.08 (d,  $J = 7.4$  Hz, 1H), 6.93 (td,  $J = 7.4, 0.8$  Hz, 1H), 6.77 (d,  $J = 7.8$  Hz, 1H), 3.90 – 3.43 (m, 4H), 1.43 (s, 3H), 1.39 (s, 3H), 1.18 (s, 3H).

**$\text{C}_{13}\text{H}_{17}\text{NO}$**   
**203.28 g.mol $^{-1}$**

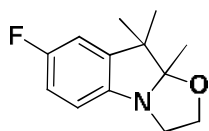
7,9,9,9a-tetramethyl-2,3,9,9a-tetrahydrooxazolo[3,2-a]indole (6)



$^1\text{H NMR}$  (300 MHz,  $\text{CDCl}_3$ ):  $\delta$  6.93 (d,  $J = 7.9$  Hz, 1H), 6.89 (s, 1H), 6.66 (d,  $J = 7.9$  Hz, 1H), 3.91-3.42 (m, 4H), 2.30 (s, 3H), 1.41 (s, 3H), 1.38 (s, 3H), 1.17 (s, 3H).

**$\text{C}_{14}\text{H}_{19}\text{NO}$**   
**217.31 g.mol $^{-1}$**

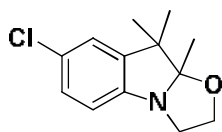
7-fluoro-9,9,9a-trimethyl-2,3,9,9a-tetrahydrooxazolo[3,2-a]indole (7)



$^1\text{H NMR}$  (300 MHz,  $\text{CDCl}_3$ )  $\delta$  6.81 (td,  $J = 8.8, 2.6$ , 1H), 6.77 (dd,  $J = 8.2, 2.5$ , 1H), 6.66 (dd,  $J = 8.4, 4.3$ , 1H), 3.79–3.88 (m, 1H), 3.45–3.70 (m, 3H), 1.40 (s, 3H), 1.37 (s, 3H), 1.17 (s, 3H).

**$\text{C}_{13}\text{H}_{16}\text{FNO}$**   
**221.27 g.mol $^{-1}$**

7-chloro-9,9,9a-trimethyl-2,3,9,9a-tetrahydrooxazolo[3,2-a]indole (8)

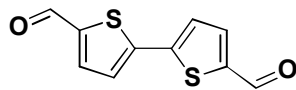


$^1\text{H NMR}$  (300 MHz,  $\text{CDCl}_3$ )  $\delta$  7.08 (dd,  $J = 8.3, 2.2$ , 1H), 7.02 (d,  $J = 2.0$ , 1H), 6.66 (d,  $J = 8.3$ , 1H), 3.79–3.88 (m, 1H), 3.45–3.70 (m, 3H), 1.40 (s, 3H), 1.36 (s, 3H), 1.17 (s, 3H).

**$\text{C}_{13}\text{H}_{16}\text{ClNO}$**   
**237.73 g.mol $^{-1}$**

Synthesis of aldehyde derivatives:

2,2'-bithiophene 5,5'-bis-dicarboxydialdehyde (9)



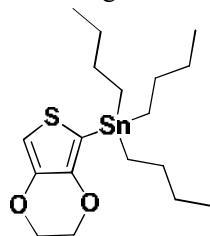
$C_{10}H_6O_2S_2$   
222.28 g.mol<sup>-1</sup>

2,2'-bithiophene 5,5'-bis-dicarboxydialdehyde was prepared according to already reported procedure<sup>[2]</sup> starting from bithiophene.

<sup>1</sup>H NMR (300 MHz, CDCl<sub>3</sub>) δ: 9.91 (s, 2H), 7.72 (d, J = 6.1 Hz, 2H), 7.42 (d, J = 3.9 Hz, 2H).

Tributyl(2,3-dihydrothieno[3,4-b][1,4]dioxin-5-yl)stannane (10)

Under argon atmosphere, EDOT (2 g, 14 mmol) was dissolved in dry THF (40 mL) and cooled to -78



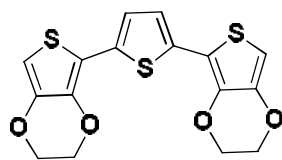
$C_{18}H_{32}O_2SSn$   
431.22 g.mol<sup>-1</sup>

°C. To this solution *n*-BuLi (1.6 M in hexane 8.75 mL, 14 mmol) was added dropwise. The resulting mixture was stirred for 15 min at -78 °C, then 100 min at room temperature. The solution was cooled again to -78 °C and a solution of tributyltin chloride (4.94 mL, 18.2 mmol) in dry THF (20 mL) was added dropwise over a period of 20 min. the mixture was allowed to warm to room temperature

and stirred at this temperature for another 19 h. The reaction mixture was poured into cold water and the aqueous layer was extracted with Et<sub>2</sub>O three times. The combined organic phases were dried over MgSO<sub>4</sub> and filtered over celite. The solvent and the residual starting material were removed under reduced pressure to afford yellow oil (6 g, 98%). The compound was used without further purification.

<sup>1</sup>H NMR (300 MHz, CDCl<sub>3</sub>) δ 6.58 (s, 1H), 4.16 (s, 4H), 0.86-1.64(m, 27H).

2,5-bis(2,3-dihydrothieno[3,4-b][1,4]dioxin-5-yl)thiophene (11)



$C_{18}H_{12}O_4S_3$   
364.46 g.mol<sup>-1</sup>

The synthesis of 2,5-bis(2,3-dihydrothieno[3,4-b][1,4]dioxin-5-yl)thiophene was done following the procedure described in Ref<sup>[3]</sup> with modification A mixture of 2, 5-dibromothiophene (1 g, 4.1 mmol), EDOT derivative (3.96 g, 9.1 mmol) and 7% of Pd(PPh<sub>3</sub>)<sub>4</sub> was dissolved in 30 mL

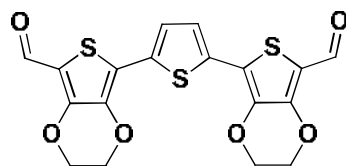
of DMF. The mixture was refluxed overnight, then poured into sat. aq. NH<sub>4</sub>Cl and extracted with DCM and the organic phase was washed with water. After being dried over anhydrous Na<sub>2</sub>SO<sub>4</sub>, the solvent

## Appendix 2: Experimental Parts

was evaporated, and the residue was purified by flash column chromatography on silica gel using a mixture of hexane/ethyl acetate (3/2) to afford a yellow solid (1.3 g, 86%).

$^1\text{H NMR}$  (300 MHz,  $\text{CDCl}_3$ )  $\delta$  7.12 (s, 1H), 6.21(s, 1H), 4.24-4.35(m, 4H).

### 7,7'-(thiophene-2,5-diyl)bis(2,3-dihydrothieno[3,4-b][1,4]dioxine-5-carbaldehyde) (12)



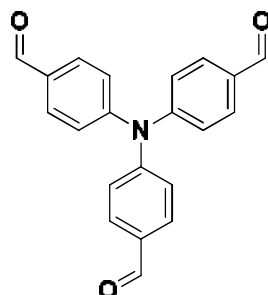
$\text{C}_{18}\text{H}_{12}\text{O}_6\text{S}_3$   
420.48  $\text{g}\cdot\text{mol}^{-1}$

To a solution of 2,5-bis(2,3-dihydrothieno[3,4-b][1,4]dioxin-5-yl)thiophene (0.5 g, 1.37 mmol) and anhydrous DMF (0.22 mL, 2.88 mmol) in anhydrous 1,2-dichloroethane (30 mL) at  $0^\circ\text{C}$ ,  $\text{POCl}_3$  (0.27 mL, 2.88 mmol) was added dropwise. The mixture was then refluxed for 18 h under argon atmosphere. After being cooled to room

temperature, the mixture was slowly poured into an aqueous solution of sodium acetate and then stirred for 2 h. The obtained precipitate was filtered and the solid was washed by ethanol to afford pure compound as an orange solid (500 mg, 87%).

$^1\text{H NMR}$  (300 MHz, DMSO)  $\delta$  9.85 (s, 1H), 7.50 (s, 1H), 4.52 (s, 4H). **IR**  $\nu$  ( $\text{cm}^{-1}$ ): 2923, 2852, 1727, 1636, 1450, 1122, 955  $\text{cm}^{-1}$ . No  $^{13}\text{C NMR}$  due to very low solubility.

### 4,4',4''-nitriлотрибензалdehyde (13)



$\text{C}_{21}\text{H}_{15}\text{NO}_3$   
329.35  $\text{g}\cdot\text{mol}^{-1}$

The synthesis of 4,4',4''-nitriлотрибензалdehyde was done following the procedure described in Ref <sup>[4]</sup> with modification. 2 g of triphenylamine were added to 8 mL of DMF under argon protection at  $0^\circ\text{C}$ . 7.5 mL of phosphorus oxychloride were added dropwise. After stirring for 1 h, the mixture was heated to  $105^\circ\text{C}$  for another 4 hours. Upon cooling to room temperature, ice water was poured into the mixture slowly while stirring. The mixture was left to stand for 3 hours to precipitate completely. The precipitate was collected

via filtration. Subsequently, the material was washed three times with 20 mL of a saturated  $\text{NaHCO}_3$  solution and once with a saturated  $\text{NaCl}$  solution. The crude product was purified by flash column chromatography on silica gel using a mixture of DCM/PE (1/2) to afford dialdehyde substituted triphenylamine as a yellow solid (1.72 g, 70%).

## Appendix 2: Experimental Parts

---

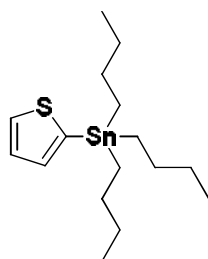
$^1\text{H NMR}$  (300 MHz, DMSO)  $\delta$  9.87 (s, 2H), 7.84 (d,  $J = 8.6$  Hz, 4H), 7.47 (dd,  $J = 7.5, 8.1$  Hz, 2H), 7.31 (t,  $J = 7.5$  Hz, 1H), 7.21 (d,  $J = 7.6$  Hz, 2H), 7.16 (d,  $J = 8.6$  Hz, 4H).

1.72 g of dialdehyde substituted triphenylamine was added to 7 mL of DMF under argon protection at 0 °C. 6.4 mL of phosphorus oxychloride was added dropwise. After stirring for 1 hour, the mixture was heated to 105 °C for 1 hour. Upon cooling to room temperature, ice water was added slowly while stirring. The mixture was left to stand for 3 hours to precipitate completely. The precipitate was collected *via* filtration. The product was then washed three times with 15 mL of a saturated  $\text{NaHCO}_3$  solution and once with a saturated  $\text{NaCl}$  solution. The crude product was purified by flash column chromatography on silica gel using a mixture of DCM/PE (1/1) to afford a bright yellow solid (640 mg, 34%).

$^1\text{H NMR}$  (300 MHz,  $\text{CDCl}_3$ )  $\delta$  9.95 (s, 1H), 7.84 (d,  $J = 8.3$  Hz, 2H), 7.25 (d,  $J = 8.0$  Hz, 2H).

---

### Tributyl(thiophen-2-yl)stannane (14)



$\text{C}_{16}\text{H}_{30}\text{SSn}$   
 $373.18 \text{ g}\cdot\text{mol}^{-1}$

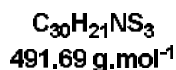
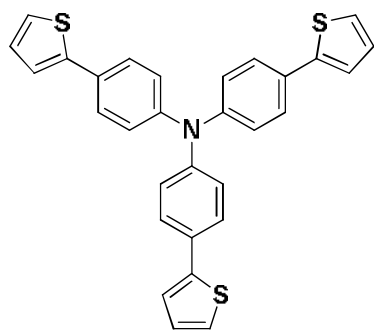
The synthesis of tributyl(thiophen-2-yl)stannane was done following the procedure described in Ref <sup>[5]</sup>. Thiophene (2 g, 23.8 mmol) was dissolved in 45 mL of anhydrous THF under argon. The solution was cooled down to -78°C and *n*-BuLi (1.6 M in hexane 16.4 mL, 26.2 mmol) was added dropwise over 1 hour. After being stirred at -78°C for 1 hour, tributyltin chloride (8.51 g, 26.2 mmol) was added dropwise within 30 min. After the addition the resulting mixture was stirred at -

-78°C for another 1 hour and was allowed to warm to room temperature. The mixture was then poured into 70 mL of water and extracted with diethyl ether. The solution was washed with saturated  $\text{NH}_4\text{Cl}$ , and the combined organic layer was dried over anhydrous  $\text{MgSO}_4$ . The solvent was evaporated, and crude product was purified by flash column chromatography on silica gel using petroleum ether to afford a yellow oil compound (8.2 g, 92%).

$^1\text{H NMR}$  (300 MHz,  $\text{CDCl}_3$ )  $\delta$  7.66 (dd,  $J = 4.7, 0.7$  Hz, 1H), 7.28 (dd,  $J = 4.6, 3.2$  Hz, 1H), 7.21 (dd,  $J = 3.2, 0.7$  Hz, 1H), 1.15-1.10 (m, 12H), 1.00-0.80 (m, 15H).

---

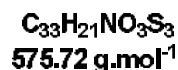
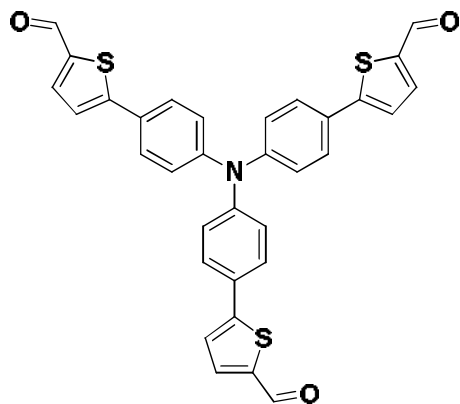
**Tris(4-(thiophen-2-yl)phenyl)amine (15)**



To a solution of tris(4-bromophenyl)amine (1.84 g, 3.84 mmol) in 75 mL of toluene, were added 2-tributylstannylthiophene (4.7 g, 12.7 mmol) and Pd(PPh<sub>3</sub>)<sub>4</sub> (0.23g). The mixture was refluxed 12 h under argon and then cooled to room temperature. The solution was washed with brine and dried over MgSO<sub>4</sub>. The solvent was evaporated, residue was rinsed with petroleum ether and filtered to afford a yellow solid (1.5 g, 92%).

<sup>1</sup>H NMR (300 MHz, CDCl<sub>3</sub>) δ 7.52 (d, *J* = 8.6 Hz, 2H), 7.25 (d, *J* = 3.9, 2H), 7.14 (d, *J* = 8.7 Hz, 2H), 7.07 (dd, *J* = 5.0, 3.6 Hz, 1H). <sup>13</sup>C NMR (75 MHz, CDCl<sub>3</sub>) δ 146.6, 144.2, 129.4, 128.2, 127, 124.5, 124.4, 122.6.

**5,5',5''-(nitrotris(benzene-4,1-diyl))tris(thiophene-2-carbaldehyde) (16)**

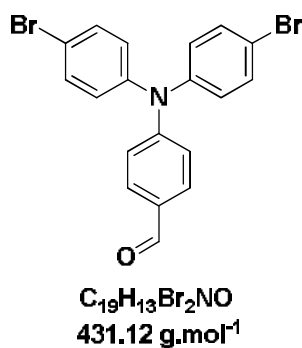


To a solution of tris[4-(2-thienyl)phenyl]amine (1.2 g, 2.45 mmol) and anhydrous DMF (0.94 mL, 12.2 mmol) in anhydrous 1,2-dichloroethane (60 mL) at 0 °C under a N<sub>2</sub> atmosphere POCl<sub>3</sub> (1.14 mL, 12.2 mmol) was added dropwise, and the mixture was refluxed for 18 h. After being cooled to room temperature, the mixture was poured into an aqueous solution of sodium acetate and then stirred for 2 h.

The organic phase was separated by decantation and the aqueous phase was extracted with CH<sub>2</sub>Cl<sub>2</sub> (2 times). The organic phases were combined and dried over MgSO<sub>4</sub>. The solvent was evaporated and crude product was purified by flash column chromatography on silica gel using DCM to afford an orange solid (1.26 g, 90%).

<sup>1</sup>H NMR (300 MHz, CDCl<sub>3</sub>) δ 9.89 (s, 1H), 7.74 (d, *J* = 4.0 Hz, 1H), 7.61 (d, *J* = 8.6 Hz, 2H), 7.36 (d, *J* = 4.0 Hz, 1H), 7.19 (d, *J* = 8.6 Hz, 2H). <sup>13</sup>C NMR (75 MHz, CDCl<sub>3</sub>) δ 182.7, 153.6, 147.5, 142.0, 137.6, 128.4, 127.6, 124.6, 123.6.

4-(bis(4-bromophenyl)amino)benzaldehyde (17)

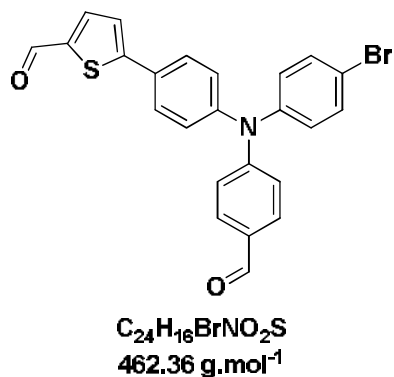


The synthesis of 4-(bis(4-bromophenyl)amino)benzaldehyde was done following the procedure described in Ref<sup>[6]</sup>. NBS (1.43 g, 8.06 mmol) was added to a solution of 4-(diphenylamino)benzaldehyde (1g, 3.66 mmol) in anhydrous THF (25 mL) and then stirred at 0°C for 4 hours. The solvent was evaporated under reduced pressure, the residue was dissolved in DCM and washed with H<sub>2</sub>O, saturated NaCl and the combined organic layers

were dried over MgSO<sub>4</sub>. The solvent was evaporated and crude product was purified by flash column chromatography on silica gel using a mixture of PE/DCM (4/1) to afford a yellow solid (1.48 g, 94%).

<sup>1</sup>H NMR (300 MHz, CDCl<sub>3</sub>) δ 9.84 (s, 1H), 7.71 (d, J = 8.8 Hz, 2H), 7.44 (d, J = 8.9 Hz, 4H), 7.08 – 6.97 (m, 6H).

5-(4-((4-bromophenyl)(4-formylphenyl)amino)phenyl)thiophene-2-carbaldehyde (18)

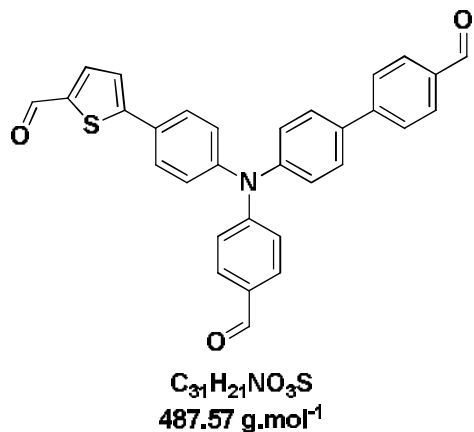


The solution of 4-(bis(4-bromophenyl)amino)benzaldehyde (0.2 g, 0.466 mmol), (5-formylthiophen-2-yl)boronic acid (0.22 g, 1.4 mmol) and 3 equivalent of K<sub>2</sub>CO<sub>3</sub> in 30 mL of mixture Dioxane/H<sub>2</sub>O (4/1) was bubbled by using argon for 30 min. 7% of Pd(dppf)Cl<sub>2</sub> was added and then the reaction mixture was refluxed for 12 hours. After concentration, the residue was dissolved in DCM and washed by H<sub>2</sub>O (2 times), the organic layers were

combined and dried over MgSO<sub>4</sub>. The solvent was evaporated and crude product was purified by flash column chromatography on silica gel using a mixture of PE/EtOAc (7/3) to afford a yellow solid (128 mg, 60%).

<sup>1</sup>H NMR (300 MHz, CDCl<sub>3</sub>) δ 9.87 (s, 1H), 9.85 (s, 1H), 7.74 (d, J = 8.7 Hz, 2H), 7.73 (d, J = 4.0 Hz, 1H), 7.61 (d, J = 8.7 Hz, 2H), 7.46 (d, J = 8.8 Hz, 2H), 7.36 (d, J = 4.0 Hz, 1H), 7.16 (d, J = 8.7 Hz, 2H), 7.11 (d, J = 8.7 Hz, 2H), 7.06 (d, J = 8.8 Hz, 2H). <sup>13</sup>C NMR (75 MHz, CDCl<sub>3</sub>) δ 190.5, 182.7, 153.3, 152.2, 147, 145, 142.3, 137.6, 133.1, 131.4, 130.6, 129.2, 127.8, 125.5, 123.9, 121.3, 118.4. HRMS (FAB+): m/z calcd. For C<sub>24</sub>H<sub>16</sub>NO<sub>2</sub>SBr: 461.0085[M+H]<sup>+</sup>; found: 461.0083.

5-(4-((4'-formyl-[1,1'-biphenyl]-4-yl)(4-formylphenyl)amino)phenyl)thiophene-2-carbaldehyde (19)



The solution of 5-(4-((4-bromophenyl)(4-formylphenyl)amino)phenyl)thiophene-2-carbaldehyde (0.15 g, 0.325 mmol), (4-formylphenyl)boronic acid (0.1 g, 0.65 mmol) and 3 equivalent of K<sub>2</sub>CO<sub>3</sub> in 30 mL of mixture Dioxane:H<sub>2</sub>O/ 4:1 was bubbled by using argon for 30 min. 7% of Pd(dppf)Cl<sub>2</sub> was added and then the reaction mixture was refluxed overnight. After concentration, the

residue was dissolved in DCM and washed by H<sub>2</sub>O (2 times), the organic layers were combined and dried over MgSO<sub>4</sub>. The solvent was evaporated and crude product was purified by flash column chromatography on silica gel using a mixture of PE/EtOAc (6/4) to afford a yellow solid (130 mg, 82%).

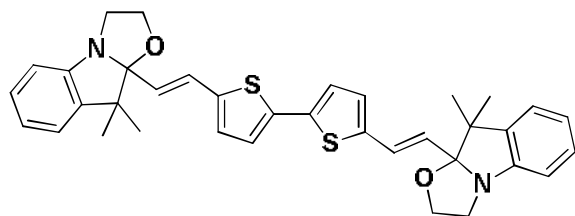
<sup>1</sup>H NMR (300 MHz, CDCl<sub>3</sub>) δ 10.04 (s, 1H), 9.87 (s, 2H), 7.95 (d, *J* = 8.2 Hz, 2H), 7.79 – 7.72 (m, 5H), 7.64 (dd, *J* = 8.6, 1.9 Hz, 4H), 7.38 (d, *J* = 4.0 Hz, 1H), 7.27 (d, *J* = 8.5 Hz, 2H), 7.23 (d, *J* = 8.6 Hz, 2H), 7.19 (d, *J* = 8.6 Hz, 2H). <sup>13</sup>C NMR (75 MHz, CDCl<sub>3</sub>) δ 191.8, 190.5, 182.7, 153.4, 152.3, 147.2, 146.3, 146.0, 142.2, 137.7, 136.3, 135.2, 131.4, 130.6, 130.4, 129.3, 128.8, 127.8, 127.3, 126.3, 125.7, 123.9, 121.6. HRMS (FAB+): *m/z* calcd. For C<sub>31</sub>H<sub>21</sub>NO<sub>3</sub>S: 487.1242[M+H]<sup>+</sup>; found: 487.1231.

Synthesis of multi-level systems:

General procedure for syntheses in the BT series:

For all functionalization of the bithiophene by BOX unit the following experimental procedure was used. A mixture of 2,2'-bithiophene-5,5'-bisdicarboxyalddehyde (1.35 mmol) and corresponding inolinoxazolidine (2.7 mmol) was dissolved in a little amount of acetonitrile. 1.35 g of technical grade silica were put in suspension and the solvent was removed under reduced pressure. The resulting reaction mixture was heated under stirring at 100°C during 10 min. After cooling down to room temperature, the crude material was directly purified by flash column chromatography using a mixture of DCM/ Methanol (98/2).

**5,5'-bis((E)-2-(9,9-dimethyl-2,3,9,9a-tetrahydrooxazolo[3,2-a]indol-9a-yl)vinyl)-2,2'-bithiophene (20)**

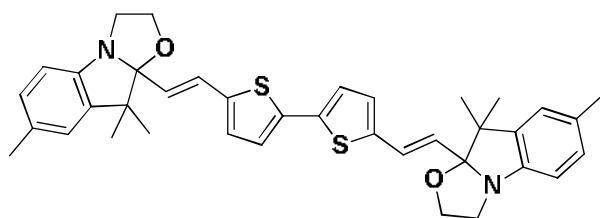


**C<sub>36</sub>H<sub>36</sub>N<sub>2</sub>O<sub>2</sub>S<sub>2</sub>**  
**592.81 g.mol<sup>-1</sup>**

(75 MHz, CDCl<sub>3</sub>) δ (ppm): 20.4, 28.4, 48.1, 50.2, 63.7, 109.6, 112.1, 121.8, 122.4, 124, 125.4, 126.1, 127.5, 127.7, 136.4, 139.7, 140.8, 150.4. **IR** ν (cm<sup>-1</sup>): 2969, 1739, 1365, 1216, 746 cm<sup>-1</sup>. **HRMS (FAB+):** m/z calcd. For C<sub>36</sub>H<sub>36</sub>N<sub>2</sub>O<sub>2</sub>S<sub>2</sub>: 592.2218[M+H]<sup>+</sup>; found: 593.2299. **Anal. Calc. (%) for C<sub>36</sub>H<sub>36</sub>N<sub>2</sub>O<sub>2</sub>S<sub>2</sub>:** C 72.94, H 6.12, S 10.82, N 4.73; found: C 72.79, H 6.35, S 10.41, N 4.58.

**Compound BOX-H:** Product was isolated as a yellow solid (496 mg, 62%). **m.p.:** 170-173°C. **<sup>1</sup>H NMR** (300 MHz, CDCl<sub>3</sub>) δ 7.17 (td, *J* = 7.7, 1.3 Hz, 1H), 7.09 (d, *J* = 7.4 Hz, 1H), 7.05 (d, *J* = 3.7 Hz, 1H), 6.98 – 6.91 (m, 3H), 6.80 (d, *J* = 7.7 Hz, 1H), 6.11 (d, *J* = 15.6 Hz, 1H), 3.83 – 3.42 (m, 4H), 1.45 (s, 3H), 1.18 (s, 3H). **<sup>13</sup>C NMR**

**5,5'-bis((E)-2-(7,9,9-trimethyl-2,3,9,9a-tetrahydrooxazolo[3,2-a]indol-9a-yl)vinyl)-2,2'-bithiophene (21)**

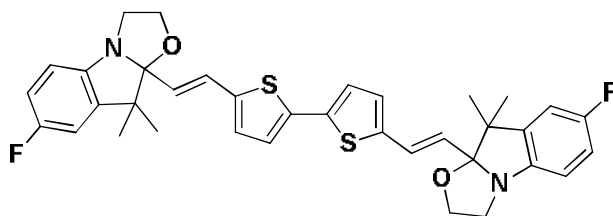


**C<sub>38</sub>H<sub>40</sub>N<sub>2</sub>O<sub>2</sub>S<sub>2</sub>**  
**620.87 g.mol<sup>-1</sup>**

20.3, 21.0, 28.4, 48.1, 50.3, 63.6, 109.9, 111.8, 123.5, 124.0, 125.4, 126.2, 127.4, 128.1, 131.2, 136.5, 139.8, 140.9, 148.1. **IR** ν (cm<sup>-1</sup>): 2969, 1739, 1363, 1215, 808 cm<sup>-1</sup>. **HRMS (FAB+):** m/z calcd. For C<sub>38</sub>H<sub>40</sub>N<sub>2</sub>O<sub>2</sub>S<sub>2</sub>: 620.2531[M+H]<sup>+</sup>; found: 621.2623. **Anal. Calc. (%) for C<sub>38</sub>H<sub>40</sub>N<sub>2</sub>O<sub>2</sub>S<sub>2</sub>:** C 73.51, H 6.49, S 10.33, N 4.51; found: C 72.45, H 6.43, S 10.25, N 4.45.

**Compound BOX-Me:** Product was isolated as a yellow solid (460 mg, 55%). **m.p.:** 232-235°C. **<sup>1</sup>H NMR** (300 MHz, CDCl<sub>3</sub>) δ 7.04 (d, *J* = 3.7 Hz, 1H), 7.00 – 6.87 (m, 4H), 6.70 (d, *J* = 7.9 Hz, 1H), 6.10 (d, *J* = 15.3 Hz, 1H), 3.82 – 3.40 (m, 4H), 2.31 (s, 3H), 1.42 (s, 3H), 1.16 (s, 3H). **<sup>13</sup>C NMR** (75 MHz, CDCl<sub>3</sub>) δ (ppm):

**5,5'-bis((E)-2-(7-fluoro-9,9-dimethyl-2,3,9,9a-tetrahydrooxazolo[3,2-a]indol-9a-yl)vinyl)-2,2'-bithiophene (22)**



**C<sub>36</sub>H<sub>34</sub>F<sub>2</sub>N<sub>2</sub>O<sub>2</sub>S<sub>2</sub>**  
**628.79 g.mol<sup>-1</sup>**

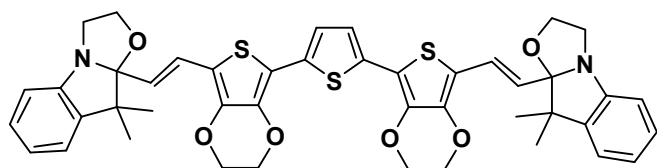
(75 MHz, CDCl<sub>3</sub>) δ (ppm): 20.4, 28.4, 48.1, 50.2, 63.7, 109.6, 112.1, 121.8, 122.4, 124, 125.4, 126.1, 127.5, 127.7, 136.4, 139.7, 140.8, 150.4. **IR** ν (cm<sup>-1</sup>): 2969, 1739, 1365, 1216, 746 cm<sup>-1</sup>. **HRMS (FAB+):** m/z calcd. For C<sub>36</sub>H<sub>34</sub>F<sub>2</sub>N<sub>2</sub>O<sub>2</sub>S<sub>2</sub>: 628.2418[M+H]<sup>+</sup>; found: 629.2499. **Anal. Calc. (%) for C<sub>36</sub>H<sub>34</sub>F<sub>2</sub>N<sub>2</sub>O<sub>2</sub>S<sub>2</sub>:** C 72.94, H 6.12, S 10.82, N 4.73; found: C 72.79, H 6.35, S 10.41, N 4.58.

**Compound BOX-F:** Product was isolated as a yellow solid (568 mg, 67%). **m.p.:** 200-204°C. **<sup>1</sup>H NMR** (300 MHz, CDCl<sub>3</sub>) δ 7.05 (d, *J* = 3.8 Hz, 1H), 6.98 – 6.90 (m, 2H), 6.85 (td, *J* = 8.8, 2.6 Hz, 1H), 6.79 (dd, *J* = 8.3, 2.5 Hz, 1H), 6.70 (dd, *J* = 8.5, 4.3 Hz, 1H), 6.08 (d, *J* = 15.7 Hz, 1H), 3.84 – 3.39 (m, 4H),

## Appendix 2: Experimental Parts

1.42 (s, 3H), 1.17 (s, 3H).  $^{13}\text{C}$  NMR (75 MHz,  $\text{CDCl}_3$ )  $\delta$  (ppm): 20.2, 28.3, 48.3, 50.5, 63.7, 109.7, 110.1, 110.2, 112.4, 112.5, 113.7, 114, 124.1, 125.6, 125.7, 127.6, 136.5, 140.7, 141.4, 141.5, 146.3, 157.4, 160.5.  $^{19}\text{F}$  NMR (282 MHz,  $\text{CDCl}_3$ )  $\delta$  -122.67. IR  $\nu$  ( $\text{cm}^{-1}$ ): 2968, 1739, 1480, 1365, 1204, 807  $\text{cm}^{-1}$ . HRMS (FAB+):  $m/z$  calcd. For  $\text{C}_{38}\text{H}_{40}\text{N}_2\text{O}_2\text{S}_2$ : 628.2030[M+H] $^+$ ; found: 629.2109. Anal. Calc. (%) for  $\text{C}_{36}\text{H}_{36}\text{N}_2\text{O}_2\text{S}_2$ : C 68.76, H 5.45, S 10.2, N 4.46; found: C 68.86, H 5.49, S 9.72, N 4.25. X-Ray structure: Orthorhombic, P b a m.

### 2,5-bis(7-((E)-2-(9,9-dimethyl-2,3,9,9a-tetrahydrooxazolo[3,2-a]indol-9a-yl)vinyl)-2,3-dihydrothieno[3,4-b][1,4]dioxin-5-yl)thiophene (23)



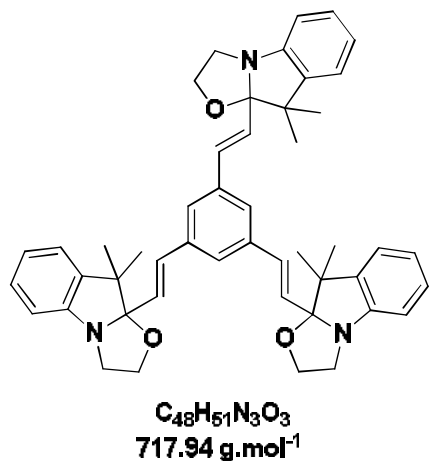
$\text{C}_{44}\text{H}_{42}\text{N}_2\text{O}_6\text{S}_3$   
 $791.01\text{g}\cdot\text{mol}^{-1}$

A mixture of **12** (100 mg, 0.238 mmol) and corresponding inolinoxazolidine (106 mg, 0.524 mmol) was dissolved in little amount of DCM. 0.8 g of technical grade silica were put in suspension and

the solvent was removed under reduced pressure. The resulting reaction mixture was heated under stirring at 100°C during 4 hours. After cool down to room temperature, the crude material was removed from silica by washing first with DCM followed by methanol. Solvent was slowly removed under reduced pressure until a precipitate was obtained. The precipitate was filtered and the solid was purified by flash column chromatography on silica gel using a mixture of  $\text{CHCl}_3/\text{MeOH}$  (9/1) to afford a yellow solid (120 mg, 63%).

$^1\text{H}$  NMR (300 MHz,  $\text{CDCl}_3$ )  $\delta$  7.16 (t,  $J = 7.1$  Hz, 1H), 7.13 (s, 1H), 7.07 (d,  $J = 6.2$  Hz, 1H), 6.92 (dd,  $J = 15.5, 9.3$  Hz, 2H), 6.79 (d,  $J = 7.7$  Hz, 1H), 6.03 (d,  $J = 15.7$  Hz, 1H), 4.42 – 4.26 (m, 4H), 3.84 – 3.42 (m, 4H), 1.43 (s, 3H), 1.16 (s, 3H).  $^{13}\text{C}$  NMR (75 MHz,  $\text{CDCl}_3$ )  $\delta$  150.6, 139.8, 139.5, 137.6, 133.3, 127.6, 123.6, 123.2, 122.4, 121.7, 121.4, 113, 112.1, 110.8, 109.9, 65.2, 64.7, 63.6, 50.3, 48, 28.5, 20.3. HRMS (FAB+):  $m/z$  calcd. For  $\text{C}_{44}\text{H}_{42}\text{N}_2\text{O}_6\text{S}_3$ : 790.2205[M+H] $^+$ ; found: 791.2279. Anal. Calc. (%) for  $\text{C}_{44}\text{H}_{42}\text{N}_2\text{O}_6\text{S}_3$ : C 66.81, H 5.35, S 12.16, N 3.54; found: C 66.62, H 5.46, S 12.29, N 3.63.

**1,3,5-tris((E)-2-(9,9-dimethyl-2,3,9,9a-tetrahydrooxazolo[3,2-a]indol-9a-yl)vinyl)benzene (24)**



A mixture of benzene-1,3,5-tricarbaldehyde (150 mg, 0.925 mmol) and corresponding inolinoxazolidine (660 mg, 3.24 mmol) was dissolved in a little amount of DCM. 1.35 g of technical grade silica were put in suspension and the solvent was removed under reduced pressure. The resulting reaction mixture was heated under stirring at 100°C during 3 hours. After cool down to room temperature, the crude material was removed from silica by washing first with DCM followed by

methanol. Solvent was slowly removed under reduced pressure until a precipitate was obtained. The precipitate was filtered and the solid was purified by flash column chromatography on silica gel using a mixture of Et<sub>2</sub>O/DCM (6/4) to afford a yellow solid (500 mg, 75%).

<sup>1</sup>H NMR (300 MHz, CDCl<sub>3</sub>) δ 7.45 (s, 1H), 7.18 (td, *J* = 7.6, 1.3 Hz, 1H), 7.09 (dd, *J* = 7.4, 1.0 Hz, 1H), 6.99 – 6.93 (m, 1H), 6.90 (d, *J* = 16.1 Hz, 1H), 6.81 (d, *J* = 7.7 Hz, 1H), 6.35 (d, *J* = 15.9 Hz, 1H), 3.87 – 3.43 (m, 4H), 1.47 (s, 3H), 1.19 (s, 3H). <sup>13</sup>C NMR (75 MHz, CDCl<sub>3</sub>) δ 150.6, 139.7, 137.3, 131.8, 127.6, 126.9, 124.6, 122.4, 121.8, 112.1, 109.9, 63.6, 50.2, 48, 28.5, 20.4. IR ν (cm<sup>-1</sup>): 2958, 1739, 1592, 1477, 1455, 1291, 746 cm<sup>-1</sup>. HRMS (FAB+): *m/z* calcd. For C<sub>48</sub>H<sub>51</sub>N<sub>3</sub>O<sub>3</sub>: 717.3930[M+H]<sup>+</sup>; found: 717.3929. Anal. Calc. (%) for C<sub>48</sub>H<sub>51</sub>N<sub>3</sub>O<sub>3</sub>: C 80.30, H 7.16, N 5.85; found: C 79.95, H 7.27, N 5.92.

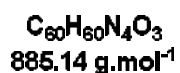
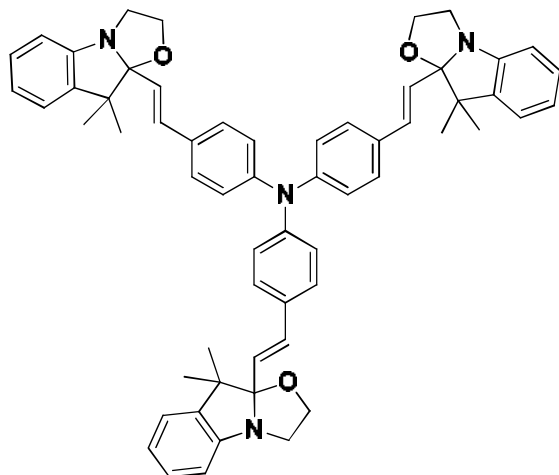
**General procedure for synthesizing Triphenylamine series:**

For all functionalization of the triphenylamine by BOX unit the following experimental procedure was used.

A mixture of 4,4',4''-nitriлотribenzaldehyde (0.608 mmol) and corresponding inolinoxazolidine (2.18mmol) was dissolved in a little amount of DCM. 1.35 g of technical grade silica were put in suspension and the solvent was removed under reduced pressure. The resulting reaction mixture was heated under stirring at 100°C during 7 hours. After cooling down to room temperature, the crude material was removed from silica by washing first with DCM followed by methanol. Solvent was slowly removed under reduced pressure until a precipitate was obtained. The precipitate was filtered and the

solid was purified by flash column chromatography on silica gel using a mixture of PE/EtOAc (6/4) neutralized by triethylamine in order to assure the full closed state.

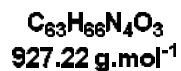
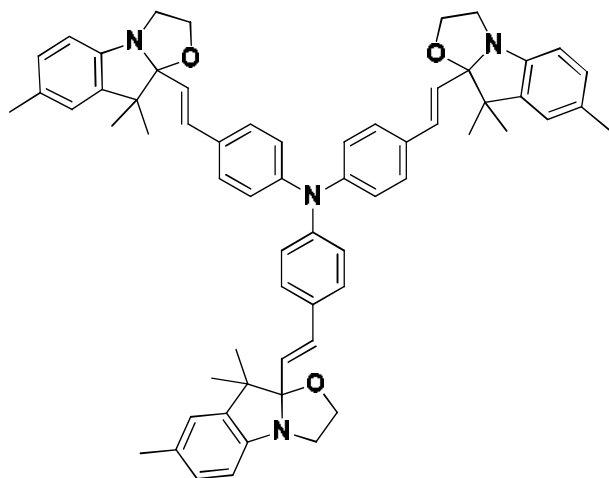
**Tris(4-((E)-2-(9,9-dimethyl-2,3,9,9a-tetrahydrooxazolo[3,2-a]indol-9a-yl)vinyl)phenyl)amine (25)**



**Compound BOX-H:** Product was isolated as a yellow solid (360 mg, 67%). **m.p.:** 137-138°C. <sup>1</sup>H NMR (300 MHz, CDCl<sub>3</sub>) δ 7.37 (d, *J* = 8.5 Hz, 2H), 7.18 (t, *J* = 7.5 Hz, 1H), 7.14 – 7.06 (m, 3H), 6.96 (t, *J* = 7.3 Hz, 1H), 6.83 (t, *J* = 10.9 Hz, 2H), 6.21 (d, *J* = 15.9 Hz, 1H), 3.89 – 3.37 (m, 4H), 1.46 (s, *J* = 6.1 Hz, 3H), 1.19 (s, *J* = 9.3 Hz, 3H). <sup>13</sup>C NMR (75 MHz, CDCl<sub>3</sub>) δ 150.6, 147, 139.8, 131.6, 131.4, 127.8, 127.6, 124.6, 124.2, 122.4, 121.7, 112, 110, 63.6, 50.2, 48, 28.5, 20.4. **IR** ν (cm<sup>-1</sup>): 2958, 1738, 1595, 1504, 1289, 1109, 745 cm<sup>-1</sup>. **HRMS (FAB+):** *m/z* calcd. For

C<sub>60</sub>H<sub>60</sub>N<sub>4</sub>O<sub>3</sub>: 884.4665[M+H]<sup>+</sup>; found: 885.4739. **Anal. Calc. (%) for C<sub>60</sub>H<sub>60</sub>N<sub>4</sub>O<sub>3</sub>:** C 81.42, H 6.83, N 6.33; found: C 81.33, H 6.59, N 6.25.

**Tris(4-((E)-2-(7,9,9-trimethyl-2,3,9,9a-tetrahydrooxazolo[3,2-a]indol-9a-yl)vinyl)phenyl)amine (26)**



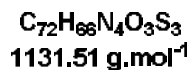
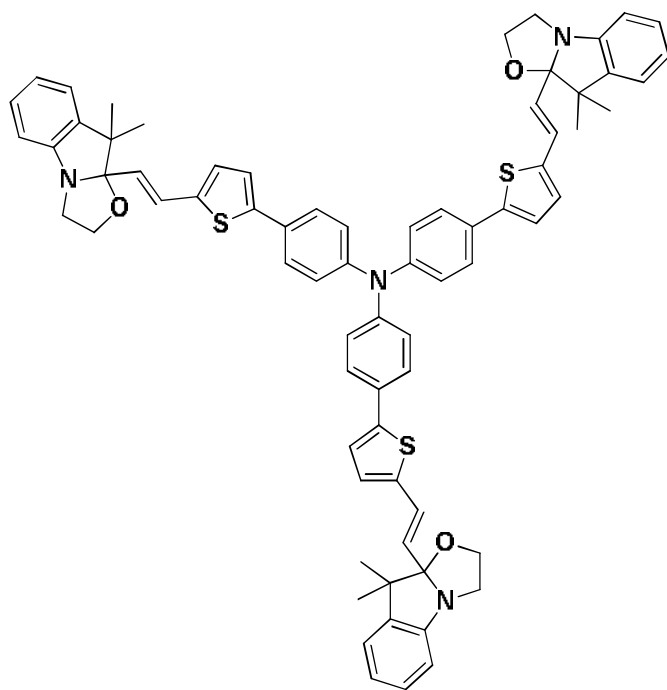
**Compound BOX-Me:** Product was isolated as a yellow solid (414 mg, 77%). **m.p.:** 145-146°C. <sup>1</sup>H NMR (300 MHz, CDCl<sub>3</sub>) δ 7.37 (d, *J* = 8.5 Hz, 2H), 7.10 (d, *J* = 8.4 Hz, 2H), 6.99 (d, *J* = 7.9 Hz, 1H), 6.92 (s, 1H), 6.85 (d, *J* = 15.9 Hz, 1H), 6.72 (d, *J* = 7.9 Hz, 1H), 6.22 (d, *J* = 15.9 Hz, 1H), 3.86 – 3.38 (m, 4H), 2.33 (s, *J* = 16.2 Hz, 3H), 1.46 (s, 3H), 1.19 (s, 3H). <sup>13</sup>C NMR (75 MHz, CDCl<sub>3</sub>) δ 148.3, 147, 139.9, 131.6, 131.4, 131.1, 128.1, 127.8, 124.7, 124.2, 123.2, 111.8, 110.3, 63.6, 50.3, 48, 28.5, 21.1, 20.3. **IR** ν (cm<sup>-1</sup>): 2958, 1737,

1597, 1504, 1278, 1106, 808 cm<sup>-1</sup>. **HRMS (FAB+):** *m/z* calcd. For C<sub>63</sub>H<sub>66</sub>N<sub>4</sub>O<sub>3</sub>: 926.5135[M+H]<sup>+</sup>; found: 926.5120. **Anal. Calc. (%) for C<sub>63</sub>H<sub>66</sub>N<sub>4</sub>O<sub>3</sub>:** C 81.61, H 7.17, N 6.04; found: C 81.39, H 5.84, N 6.19.

**General procedure for synthesizing (R-BOX-T-Ph)<sub>3</sub>N series:**

For all functionalization of the (R-BOX-T-Ph)<sub>3</sub>N unit the following experimental procedure was used. A mixture of 5,5',5''-(nitriлотris(benzene-4,1-diyl))tris(thiophene-2-carbaldehyde) (0.434 mmol) and corresponding inolinoxazolidine (1.74 mmol) was dissolved in little amount of DCM. 1.35 g of technical grade silica were put in suspension and the solvent was removed under reduced pressure. The resulting reaction mixture was heated under stirring at 100°C during 7 hours. After cooling down to room temperature, the crude material was removed from silica by washing first with DCM followed by methanol. Solvent was slowly removed under reduced pressure until a precipitate was obtained. The precipitate was filtered and the solid was purified by flash column chromatography on silica gel using Et<sub>2</sub>O neutralized by triethylamine in order to assure the full closed state.

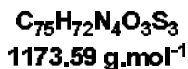
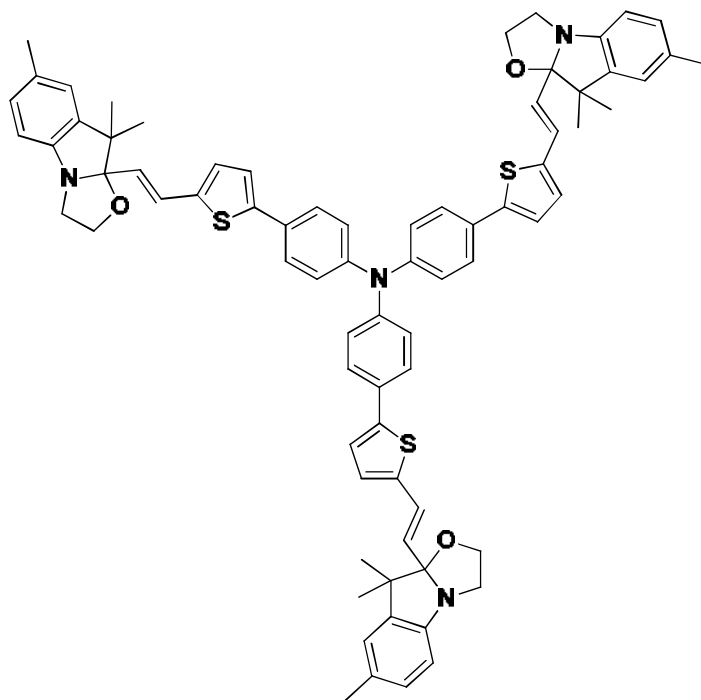
**Tris(4-(5-((E)-2-(9,9-dimethyl-2,3,9a-tetrahydrooxazolo[3,2-a]indol-9a-yl)vinyl)thiophen-2-yl)phenyl)amine (27)**



**Compound BOX-H:** Product was isolated as a yellow solid (300 mg, 61%). **m.p.:** 156-158°C. **<sup>1</sup>H NMR** (300 MHz, CDCl<sub>3</sub>) δ 7.51 (d, *J* = 8.6 Hz, 2H), 7.21 – 7.12 (m, 4H), 7.09 (d, *J* = 7.4 Hz, 1H), 7.02 – 6.92 (m, 3H), 6.81 (d, *J* = 7.8 Hz, 1H), 6.12 (d, *J* = 15.7 Hz, 1H), 3.89 – 3.41 (m, 5H), 1.45 (s, 3H), 1.22 – 1.15 (m, *J* = 6.5 Hz, 3H). **<sup>13</sup>C NMR** (125 MHz, CDCl<sub>3</sub>) δ 150.5, 146.5, 143.2, 140.6, 139.7, 129.2, 127.7, 127.6, 126.7, 125.7, 125.4, 124.4, 122.8, 122.4, 121.7, 112, 109.7, 63.6, 50.2, 48.1, 28.4, 20.4. **IR** ν (cm<sup>-1</sup>): 2958, 1598, 1537, 1504, 1477, 1320, 1290, 1111, 745 cm<sup>-1</sup>. **HRMS (FAB+):** *m/z* calcd. For C<sub>72</sub>H<sub>66</sub>N<sub>4</sub>O<sub>3</sub>S<sub>3</sub>: 1130.4297[M+H]<sup>+</sup>;

found: 1130.4294. **Anal. Calc. (%) for C<sub>72</sub>H<sub>66</sub>N<sub>4</sub>O<sub>3</sub>S<sub>3</sub>:** C 76.43, H 5.88, S 8.50, N 4.95; found: C 76.59, H 5.49, S 8.23, N 4.52.

Tris(4-(5-((E)-2-(7,9,9-trimethyl-2,3,9,9a-tetrahydrooxazolo[3,2-a]indol-9a-yl)vinyl)thiophen-2-yl)phenyl)amine (28)



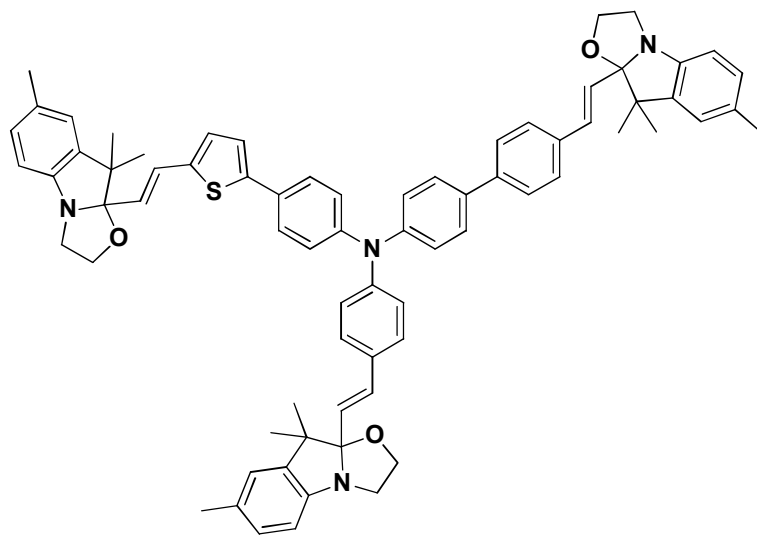
**Compound BOX-Me:** Product was isolated as a yellow solid (275 mg, 54%). **m.p.:** 153-155°C. <sup>1</sup>H NMR (300 MHz, CDCl<sub>3</sub>) δ 7.50 (d, *J* = 8.7 Hz, 2H), 7.13 (dd, *J* = 6.2, 2.5 Hz, 2H), 6.98 (d, *J* = 5.1 Hz, 2H), 6.95 (d, *J* = 6.7 Hz, 2H), 6.90 (s, 1H), 6.70 (d, *J* = 7.9 Hz, 1H), 6.12 (d, *J* = 15.7 Hz, 1H), 3.85 – 3.41 (m, 4H), 2.31 (s, 3H), 1.43 (s, 3H), 1.18 (s, 3H). <sup>13</sup>C NMR (75 MHz, CDCl<sub>3</sub>) δ 148.1, 146.5, 143.2, 140.6, 139.8, 131.2, 129.2, 128.1, 127.7, 126.7, 125.7, 125.5, 124.4, 123.2, 122.8, 111.8, 110, 63.6, 50.3, 48.1, 28.5, 21.1, 20.3. **IR** ν (cm<sup>-1</sup>): 2955, 1596, 1536, 1502, 1489, 1456 1320, 1280, 1107,

809, 792 cm<sup>-1</sup>. **HRMS (FAB+):** *m/z* calcd. For C<sub>75</sub>H<sub>72</sub>N<sub>4</sub>O<sub>3</sub>S<sub>3</sub>: 1172.4767[M+H]<sup>+</sup>; found: 1173.4837. **Anal. Calc. (%)** for C<sub>75</sub>H<sub>72</sub>N<sub>4</sub>O<sub>3</sub>S<sub>3</sub>: C 76.76, H 6.18, S 8.20, N 4.77; found: C 76.94, H 6.39, S 8.09, N 4.54.

**General procedure for the three different arms of TPA series:**

For all functionalization of the three **different arms of TPA** unit the following experimental procedure was used. A mixture of 5-(4-((4'-formyl-[1,1'-biphenyl]-4-yl)(4-formylphenyl)amino)phenyl)thiophene-2-carbaldehyde (0.267 mmol) and corresponding inolinoxazolidine (1.33 mmol) was dissolved in little amount of DCM. 1.35 g of technical grade silica were put in suspension and the solvent was removed under reduced pressure. The resulting reaction mixture was heated under stirring at 100°C during 6 hours. After cool down to room temperature, the crude material was removed from silica by washing first with DCM followed by methanol. Solvent was slowly removed under reduced pressure until a precipitate was obtained. The precipitate was filtered and the solid was purified by flash column chromatography on silica gel using a mixture of PE/EtOAc (7/4) which is neutralized by triethylamine in order to assure the full closed state.

4'-((E)-2-(7,9,9-trimethyl-2,3,9a-tetrahydrooxazolo[3,2-a]indol-9a-yl)vinyl)-N-(4-((E)-2-(7,9,9-trimethyl-2,3,9,9a-tetrahydrooxazolo[3,2-a]indol-9a-yl)vinyl)phenyl)-N-(4-(5-((E)-2-(7,9,9-trimethyl-2,3,9,9a-tetrahydrooxazolo[3,2-a]indol-9a-yl)vinyl)thiophen-2-yl)phenyl)-[1,1'-biphenyl]-4-amine (29)



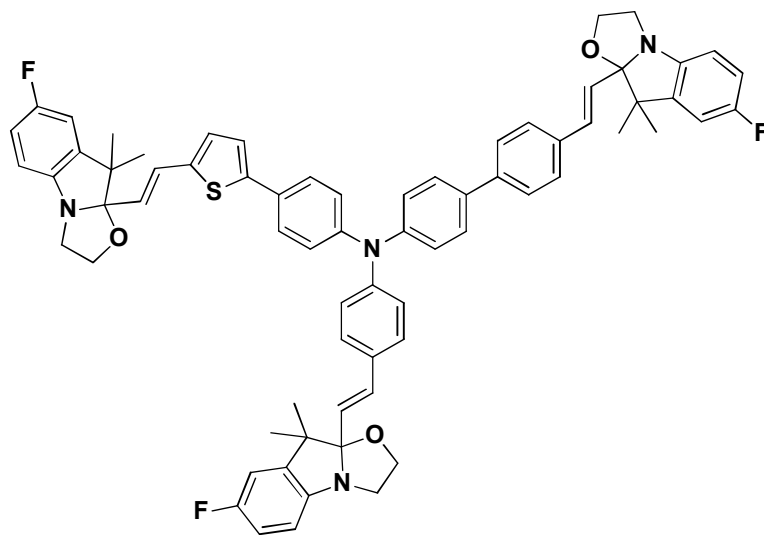
**C<sub>73</sub>H<sub>72</sub>N<sub>4</sub>O<sub>3</sub>S**  
**1085.44 g.mol<sup>-1</sup>**

**Compound BOX-Me:** Product was isolated as a yellow solid (197 mg, 69%). <sup>1</sup>H NMR (300 MHz, CDCl<sub>3</sub>) δ 7.51 (d, *J* = 8.5 Hz, 2H), 7.46 (s, 2H), 7.41 (d, *J* = 9.0 Hz, 4H), 7.32 (d, *J* = 8.6 Hz, 2H), 7.12 (d, *J* = 8.7 Hz, 2H), 7.09 – 7.03 (m, 5H), 6.94 – 6.86 (m, 6H), 6.82 (d, *J* = 7.2 Hz, 3H), 6.77 (d, *J* = 16.0 Hz, 1H), 6.68 – 6.60 (m, 3H), 6.26 (d, *J* = 15.9 Hz, 1H), 6.15 (d, *J* = 15.9 Hz, 1H), 6.04 (d, *J* = 15.7 Hz, 1H), 3.78 – 3.35 (m, 12H),

2.24 (s, 9H), 1.40 – 1.34 (m, 9H), 1.11 (s, 9H). IR ν (cm<sup>-1</sup>): 2969, 1739, 1490, 1366, 1215, 809 cm<sup>-1</sup>.

**HRMS (FAB<sup>+</sup>):** *m/z* calcd. For C<sub>73</sub>H<sub>72</sub>N<sub>4</sub>O<sub>3</sub>S: 1084.5325[M+H]<sup>+</sup>; found: 1084.5334. **Anal. Calc. (%)** for C<sub>73</sub>H<sub>72</sub>N<sub>4</sub>O<sub>3</sub>S: C 80.78, H 6.69, N 5.16; found: C 70.54, H 6.78, N 5.35. No <sup>13</sup>C NMR due to stability in chloroform and low solubility in acetonitrile.

4'-((E)-2-(7-fluoro-9,9-dimethyl-2,3,9,9a-tetrahydrooxazolo[3,2-a]indol-9a-yl)vinyl)-N-(4-((E)-2-(7-fluoro-9,9-dimethyl-2,3,9,9a-tetrahydrooxazolo[3,2-a]indol-9a-yl)vinyl)phenyl)-N-(4-(5-((E)-2-(7-fluoro-9,9-dimethyl-2,3,9,9a-tetrahydrooxazolo[3,2-a]indol-9a-yl)vinyl)thiophen-2-yl)phenyl)-[1,1'-biphenyl]-4-amine (30)



$C_{70}H_{63}F_3N_4O_3S$   
1097.33 g.mol<sup>-1</sup>

**Compound BOX-F:** Product was isolated as a yellow solid (129 mg, 44%). <sup>1</sup>H NMR (300 MHz, CDCl<sub>3</sub>) δ 7.54 (dt, *J* = 16.5, 8.7 Hz, 9H), 7.39 (d, *J* = 8.6 Hz, 2H), 7.20 (d, *J* = 8.7 Hz, 2H), 7.17 – 7.11 (m, 4H), 7.01 – 6.96 (m, 2H), 6.94 (s, 1H), 6.90 – 6.85 (m, 3H), 6.84 – 6.77 (m, 4H), 6.75 – 6.67 (m, 3H), 6.32 (d, *J* = 15.9 Hz, 1H), 6.20 (d, *J* = 15.9 Hz, 1H), 6.10 (d, *J* = 15.7 Hz, 1H), 3.89 – 3.40 (m, 12H), 1.44 (t, *J* = 2.7 Hz, 9H),

1.19 (s, 9H). <sup>13</sup>C NMR (75 MHz, CDCl<sub>3</sub>) δ 160.5, 157.4, 147.0, 146.9, 146.6, 146.5, 146.4, 146.4, 146.3, 146.3, 146.3, 143.4, 141.6, 141.6, 141.6, 141.6, 141.6, 141.5, 141.5, 141.5, 141.5, 140.3, 140.1, 135.8, 135.4, 135.1, 132.1, 131.8, 131.3, 128.9, 127.9, 127.8, 127.8, 127.3, 126.9, 126.7, 125.9, 125.6, 125.5, 125.5, 125, 124.6, 124.4, 124.3, 124.2, 122.7, 113.9, 113.6, 112.5, 112.4, 110.5, 110.5, 110.2, 110.1, 109.8, 65.9, 63.6, 50.5, 48.3, 48.3, 48.2, 48.2, 48.2, 48.2, 30.4, 29.7, 28.3, 20.2, 15.3. <sup>19</sup>F NMR (282 MHz, CDCl<sub>3</sub>) δ -122.73 (s), -122.77 (s), -122.79 (s). IR ν (cm<sup>-1</sup>): 2922, 2852, 1739, 1482, 1365, 1262, 809 cm<sup>-1</sup>. HRMS (FAB<sup>+</sup>): *m/z* calcd. For C<sub>73</sub>H<sub>72</sub>N<sub>4</sub>O<sub>3</sub>S: 1096.4573[M+H]<sup>+</sup>; found: 1097.4665. Anal. Calc. (%) for C<sub>70</sub>H<sub>63</sub>N<sub>4</sub>O<sub>3</sub>S: C 76.62, H 5.79, N 5.11; found: C 76.74, H 5.65, N 5.06.

### Coordination part

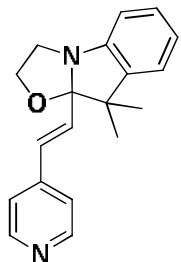
#### Synthesis of ligand bearing one BOX unit.

#### General procedure for synthesizing pyridine ligands

A mixture of 4-pyridinecarboxaldehyde (2.33 mmol) and corresponding inolinoxazolidine (2.8mmol) was dissolved in little amount of DCM. 1g of technical grade silica were put in suspension and the solvent was removed under reduced pressure. The resulting reaction mixture was heated under stirring at 100°C during 10 min. After cooling down to room temperature, the crude product was directly purified

by flash column chromatography on silica gel using a mixture of PE/EtOAc (3/7). The desired compounds were recrystallized in ethanol to afford yellow single crystals.

**(E)-9,9-dimethyl-9a-(2-(pyridin-4-yl)vinyl)-2,3,9a-tetrahydrooxazolo[3,2-a]indole (31)**

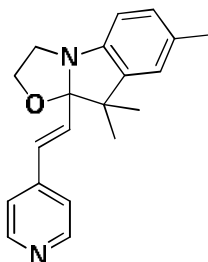


**C<sub>19</sub>H<sub>20</sub>N<sub>2</sub>O**  
**292.37 g.mol<sup>-1</sup>**

**Compound L<sub>1</sub>, BOX-H:** Product was isolated as a yellow solid (496 mg, 73%). **m.p.:** 115°C, <sup>1</sup>H NMR (300 MHz, CDCl<sub>3</sub>) δ 8.58 (dd, *J* = 4.5, 1.6 Hz, 2H), 7.31 (dd, *J* = 4.6, 1.5 Hz, 2H), 7.22 – 7.15 (m, 1H), 7.09 (dd, *J* = 7.4, 0.9 Hz, 1H), 6.96 (td, *J* = 7.4, 1.0 Hz, 1H), 6.83 (dd, *J* = 11.9, 6.6 Hz, 2H), 6.53 (d, *J* = 15.9 Hz, 1H), 3.85 – 3.37 (m, 4H), 1.46 (s, 3H), 1.17 (s, 3H). <sup>13</sup>C NMR (75 MHz, CDCl<sub>3</sub>) δ 150.3, 150.2, 143.8, 139.5, 131.5, 130.1, 127.8, 122.4, 122, 121.3, 112.1, 109.5, 63.8, 50.2, 48.2, 28.4, 20.5. **IR** ν (cm<sup>-1</sup>): 2962, 2889, 1595, 1476, 1454, 1292, 1149, 975, 750 cm<sup>-1</sup> **HRMS (FAB+): m/z calcd. For C<sub>19</sub>H<sub>20</sub>N<sub>2</sub>O: 292.1576[M+H]<sup>+</sup>; found: 292.1574. **Anal. calcd for C<sub>19</sub>H<sub>20</sub>N<sub>2</sub>O:** C, 78.05; H, 6.89; N, 9.58, found: C, 77.80; H, 6.75; N, 9.45. **X-Ray structure:****

Orthorhombic, P 21 21 21.

**(E)-7,9,9-trimethyl-9a-(2-(pyridin-4-yl)vinyl)-2,3,9a-tetrahydrooxazolo[3,2-a]indole (32)**

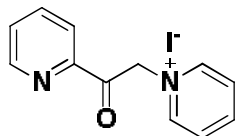


**C<sub>20</sub>H<sub>22</sub>N<sub>2</sub>O**  
**306.40 g.mol<sup>-1</sup>**

**Compound L<sub>1</sub>', BOX-Me:** Product was isolated as a yellow solid (627 mg, 88%). **m.p.:** 114-115°C. <sup>1</sup>H NMR (300 MHz, CDCl<sub>3</sub>) δ 8.57 (d, *J* = 6.0 Hz, 2H), 7.30 (d, *J* = 6.1 Hz, 2H), 6.99 (d, *J* = 7.9 Hz, 1H), 6.90 (s, 1H), 6.83 (d, *J* = 15.9 Hz, 1H), 6.71 (d, *J* = 7.9 Hz, 1H), 6.53 (d, *J* = 15.9 Hz, 1H), 3.83 – 3.34 (m, 4H), 2.32 (s, 3H), 1.45 (s, 3H), 1.16 (s, 3H). <sup>13</sup>C NMR (75 MHz, CDCl<sub>3</sub>) δ 150.3, 148, 143.8, 139.6, 131.6, 131.4, 130, 128.3, 123.2, 121.2, 111.9, 109.8, 63.7, 50.4, 48.2, 28.4, 21.1, 20.4. **IR** ν (cm<sup>-1</sup>): 2967, 2882, 1737, 1595, 1479, 1413 1284, 972, 815, 800 cm<sup>-1</sup>. **HRMS (FAB+): m/z calcd. For C<sub>20</sub>H<sub>22</sub>N<sub>2</sub>O: 306.1732[M+H]<sup>+</sup>; found: 306.1728. **Anal. calcd for C<sub>20</sub>H<sub>22</sub>N<sub>2</sub>O:** C, 78.40; H, 7.24; N, 9.14, found: C, 78.13; H, 7.04; N, 9.3. **X-Ray structure:****

Orthorhombic, P 21 21 21.

**1-(2-oxo-2-(pyridin-2-yl)ethyl)pyridin-1-ium iodide (33)**

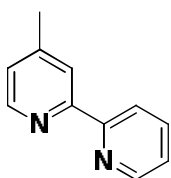


**C<sub>12</sub>H<sub>11</sub>IN<sub>2</sub>O**  
**326.13 g.mol<sup>-1</sup>**

The synthesis of 1-(2-oxo-2-(pyridin-2-yl)ethyl)pyridin-1-ium iodide was done following the procedure described in Ref [7]. A mixture of iodine (11.5 g, 91 mmol) and 2-acetylpyridine (5 g, 41 mmol) in pyridine (100 mL) was heated at 100°C under N<sub>2</sub>. The reaction mixture was stirred for 5 hours until 2-acetylpyridine total consumption, then cooled to room temperature and filtered. The residue was washed with Et<sub>2</sub>O and recrystallized in ethanol to afford a light yellow solid (7.5 g, 55%).

$^1\text{H NMR}$  (300 MHz, DMSO)  $\delta$  9.01 (dd,  $J = 6.7, 1.2$  Hz, 2H), 8.87 (ddd,  $J = 4.7, 1.6, 0.9$  Hz, 1H), 8.78 – 8.68 (m, 1H), 8.28 (dd,  $J = 7.7, 6.7$  Hz, 2H), 8.18 – 8.05 (m, 2H), 7.84 (ddd,  $J = 7.3, 4.7, 1.5$  Hz, 1H), 6.51 (s, 2H).

**4-methyl-2,2'-bipyridine (34)**

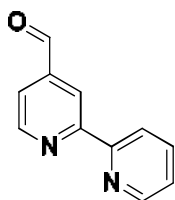


$\text{C}_{11}\text{H}_{10}\text{N}_2$   
**170.21 g.mol<sup>-1</sup>**

1-(2-oxo-2-(pyridin-2-yl) ethyl) pyridin-1-ium iodide (5 g, 15.3 mmol), ammonium acetate (5.91 g, 76.6 mmol) and crotonaldehyde (2.58 g, 36.8 mmol) were added to methanol (100 mL). The solution was refluxed overnight. The solvent was then evaporated in vacuum and the black oil extracted with DCM 3 times. The combined organic layers were washed with saturated brine and dried over  $\text{MgSO}_4$ . The solvent was evaporated and crude product was purified by flash column chromatography on  $\text{Al}_2\text{O}_3$  using a mixture of PE/acetone (9/1) to afford a white powder (1 g, 38%), **m.p** 65-66°C (lit. 62-64°C<sup>[8]</sup>).

$^1\text{H NMR}$  (300 MHz,  $\text{CDCl}_3$ )  $\delta$  8.67 (d,  $J = 4.7$  Hz, 1H), 8.53 (d,  $J = 5.0$  Hz, 1H), 8.38 (d,  $J = 8.0$  Hz, 1H), 8.22 (s, 1H), 7.81 (td,  $J = 7.9, 1.6$  Hz, 1H), 7.33 – 7.27 (m, 1H), 7.13 (d,  $J = 4.9$  Hz, 1H), 2.43 (s, 3H).

**[2,2'-bipyridine]-4-carbaldehyde (35)**



$\text{C}_{11}\text{H}_8\text{N}_2\text{O}$   
**184.19 g.mol<sup>-1</sup>**

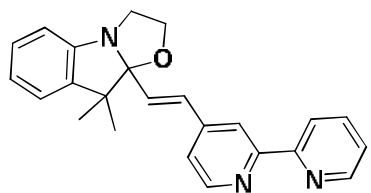
To a solution of 4-methyl-2,2'-bipyridine (0.4 g, 2.35 mmol) in diethylene glycol dimethyl ether (13 mL) was added selenium dioxide (0.57 g, 5.17 mmol), and the solution was mildly refluxed for 4.5 h. On cooling of the solution to 90-95°C, water (4 mL) was added and a black solid was formed, separated and washed two times with dioxane, the filtrate was evaporated to dryness. The white solid was dissolved in  $\text{CH}_2\text{Cl}_2$  (100 mL), and the solution vigorously stirred with a solution of  $\text{K}_2\text{CO}_3$  (5%, 2.5 mL) for 15 min; the water layer was separated and extracted with  $\text{CH}_2\text{Cl}_2$  (15 mL). The combined organic layers were dried over  $\text{MgSO}_4$ . The solvent was evaporated and crude product was crystallized from hexane (25 mL) to afford the pure aldehyde as a slight yellow powder (310 mg, 71%), (lit.<sup>[9]</sup>).

$^1\text{H NMR}$  (300 MHz,  $\text{CDCl}_3$ )  $\delta$  10.16 (s, 1H), 8.88 (d,  $J = 4.9$  Hz, 1H), 8.82 (s, 1H), 8.70 (dd,  $J = 4.8, 0.7$  Hz, 1H), 8.43 (d,  $J = 8.0$  Hz, 1H), 7.84 (td,  $J = 7.8, 1.8$  Hz, 1H), 7.70 (dd,  $J = 4.9, 1.5$  Hz, 1H), 7.35 (ddd,  $J = 7.5, 4.8, 1.1$  Hz, 1H).

**General procedure for preparing bipyridine ligands bearing one BOX unit:**

A mixture of [2,2'-bipyridine]-4-carbaldehyde (1.36 mmol) and corresponding indolinoxazolidine derivatives (1.77mmol) was dissolved in a little amount of DCM. 1g of technical grade silica were put in suspension and the solvent was removed under reduced pressure. The resulting reaction mixture was heated under stirring at 100°C during 10 min. After cooling down to room temperature, the crude material was purified by flash column chromatography on silica gel using a mixture of PE/EtOAc (7/3).

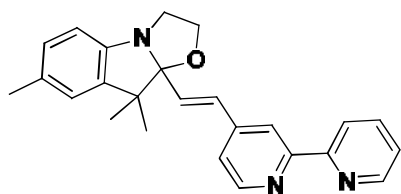
**(E)-9a-(2-((2,2'-bipyridin)-4-yl)vinyl)-9,9-dimethyl-2,3,9a-tetrahydrooxazolo[3,2-a]indole (36)**



**C<sub>24</sub>H<sub>23</sub>N<sub>3</sub>O**  
**369.46 g.mol<sup>-1</sup>**

**Compound BOX-H:** Recrystallized by ethanol to afford as a yellow crystal (402 mg, 80%). <sup>1</sup>H NMR (300 MHz, CDCl<sub>3</sub>) δ 8.70 (ddd, *J* = 4.8, 1.7, 0.9 Hz, 1H), 8.64 (d, *J* = 5.1 Hz, 1H), 8.46 (s, 1H), 8.40 (d, *J* = 8.0 Hz, 1H), 7.83 (td, *J* = 7.8, 1.8 Hz, 1H), 7.36 – 7.30 (m, 2H), 7.18 (td, *J* = 7.6, 1.3 Hz, 1H), 7.09 (dd, *J* = 7.4, 0.9 Hz, 1H), 6.99 – 6.91 (m, 2H), 6.81 (d, *J* = 7.8 Hz, 1H), 6.65 (d, *J* = 15.9 Hz, 1H), 3.84 – 3.39 (m, 4H), 1.47 (s, 3H), 1.18 (s, 3H). <sup>13</sup>C NMR (75 MHz, CDCl<sub>3</sub>) δ 156.7, 156.1, 150.4, 149.7, 149.2, 144.9, 139.6, 137, 131.6, 130.4, 127.7, 123.8, 122.4, 121.8, 121.3, 121.3, 118.7, 112.1, 63.7, 50.2, 48.1, 28.5, 20.5. **HRMS (FAB+):** *m/z* calcd. For C<sub>24</sub>H<sub>23</sub>N<sub>3</sub>O: 369.1841[M+H]<sup>+</sup>; found: 369.1728. **X-Ray structure:** Triclinic, P -1.

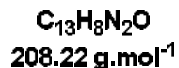
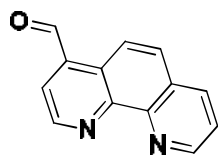
**(E)-9a-(2-((2,2'-bipyridin)-4-yl)vinyl)-7,9,9-trimethyl-2,3,9a-tetrahydrooxazolo[3,2-a]indole (37)**



**C<sub>25</sub>H<sub>25</sub>N<sub>3</sub>O**  
**383.49 g.mol<sup>-1</sup>**

**Compound BOX-Me:** Product was isolated as a yellow solid (234 mg, 45%). <sup>1</sup>H NMR (300 MHz, CDCl<sub>3</sub>) δ 8.70 (ddd, *J* = 4.8, 1.8, 0.9 Hz, 1H), 8.64 (d, *J* = 5.1 Hz, 1H), 8.46 (s, 1H), 8.43 – 8.38 (m, 1H), 7.87 – 7.79 (m, 1H), 7.36 – 7.29 (m, 2H), 7.01 – 6.89 (m, 3H), 6.71 (d, *J* = 7.9 Hz, 1H), 6.64 (d, *J* = 15.9 Hz, 1H), 3.81 – 3.38 (m, 4H), 2.32 (s, 3H), 1.45 (s, 3H), 1.18 (s, 3H). <sup>13</sup>C NMR (75 MHz, CDCl<sub>3</sub>) δ 156.7, 156.1, 149.7, 149.2, 148.1, 145, 139.6, 137, 131.7, 131.3, 130.3, 128.2, 123.8, 123.1, 121.3, 121.3, 118.7, 111.8, 109.9, 63.7, 50.4, 48.1, 28.5, 21, 20.4. **IR** ν (cm<sup>-1</sup>): 2963, 1582, 1490, 1459, 793 cm<sup>-1</sup>. **HRMS (FAB+):** *m/z* calcd. For C<sub>25</sub>H<sub>25</sub>N<sub>3</sub>O: 383.1998[M+H]<sup>+</sup>; found: 383.2077.

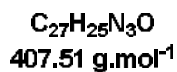
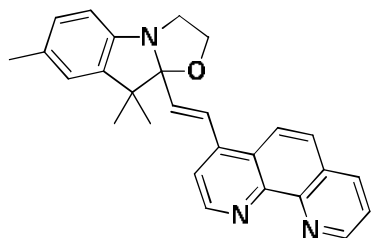
**1,10-phenanthroline-4-carbaldehyde (38)**



In a 200 mL two-necked round bottom flask containing, 4-methyl-1,10-phenanthroline (0.5 g, 2.57 mmol), a mixture 1,4-dioxane/water (24/1 mL) was added drop wise and stirred to get a homogenous mixture and the solution was bubbled with argon for 15 min while stirring. After addition of 1.02 g of SeO<sub>2</sub> (3.6 eq.), the mixture was refluxed under argon atmosphere for 16 hours. After the completion of the reaction (Monitored by TLC), the reaction mixture was washed with warm 1,4-dioxane for 2 to 3 minutes and filtered. The solvent was removed under reduced pressure. The residue was then dissolved in hot ethyl acetate, filtered and again washed with hot ethyl acetate. The ethyl acetate layer was washed with 1M Na<sub>2</sub>CO<sub>3</sub> (250mL) to remove additional carboxylic acid. The organic layer was dried with anhydrous Na<sub>2</sub>SO<sub>4</sub>, and solvent was evaporated to afford a white powder (420 mg, 78%).

<sup>1</sup>H NMR (300 MHz, CDCl<sub>3</sub>) δ 10.61 (s, 1H), 9.48 (d, *J* = 4.4 Hz, 1H), 9.25 (d, *J* = 3.9 Hz, 1H), 9.03 (d, *J* = 9.2 Hz, 1H), 8.39 – 8.24 (m, 1H), 8.01 (t, *J* = 6.8 Hz, 2H), 7.71 (dd, *J* = 8.0, 4.4 Hz, 1H).

**(E)-9a-(2-(1,10-phenanthrolin-4-yl)vinyl)-7,9,9-trimethyl-2,3,9a-tetrahydrooxazolo[3,2-a]indole (39)**



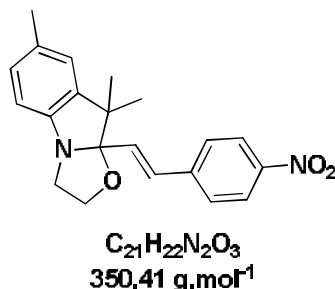
A mixture of 1,10-phenanthroline-4-carbaldehyde (0.2 g, 0.96 mmol) and corresponding inolinoxazolidine (0.27 g, 1.25 mmol) was dissolved in a little amount of DCM. 1g of technical grade silica were put in suspension and the solvent was removed under reduced pressure. The resulting reaction mixture was heated under stirring at 100 °C during 30 min. After cooling down to room temperature, the crude material was removed from silica by DCM and methanol. The solvent was evaporated and crude product was washed by petroleum ether to remove the excess of BOX and filter to afford a white solid (230 mg, 59%).

<sup>1</sup>H NMR (300 MHz, CDCl<sub>3</sub>) δ 9.13 (dd, *J* = 4.3, 1.7 Hz, 1H), 9.08 (d, *J* = 4.7 Hz, 1H), 8.18 (dd, *J* = 8.1, 1.7 Hz, 1H), 8.08 (d, *J* = 9.2 Hz, 1H), 7.75 (d, *J* = 9.2 Hz, 1H), 7.66 (d, *J* = 4.7 Hz, 1H), 7.61 (d, *J* = 16.0 Hz, 1H), 7.57 – 7.53 (m, 1H), 6.94 (ddd, *J* = 7.9, 1.7, 0.6 Hz, 1H), 6.86 (s, 1H), 6.68 (d, *J* = 7.9 Hz, 1H), 6.52 (d, *J* = 15.7 Hz, 1H), 3.84 – 3.41 (m, 4H), 2.26 (s, *J* = 3.8 Hz, 3H), 1.44 (s, 3H), 1.16 (s, 3H).

<sup>13</sup>C NMR (75 MHz, CDCl<sub>3</sub>) δ 150.5, 150, 148, 146.7, 146.5, 142.5, 139.5, 135.9, 134.1, 131.5, 128.3,

127.3, 126.4, 126.3, 123.2, 122.3, 119.9, 111.9, 110.1, 63.9, 50.5, 48.2, 28.6, 21, 20.5. **IR**  $\nu$  ( $\text{cm}^{-1}$ ): 2959, 2923, 1490, 1281, 1109, 976, 837, 811  $\text{cm}^{-1}$ . **HRMS (FAB+): m/z calcd. For  $\text{C}_{27}\text{H}_{25}\text{N}_3\text{O}$ :** 407.1998  $[\text{M}+\text{H}]^+$ ; found: 407.1994. **mp** 252-253  $^{\circ}\text{C}$ .

**(E)-7,9,9-trimethyl-9a-(4-nitrostyryl)-2,3,9a-tetrahydrooxazolo[3,2-a]indole (40)**

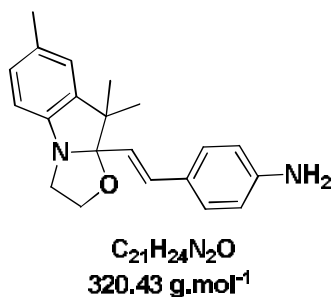


A mixture of 4-nitrobenzaldehyde (1 g, 6.62 mmol) and corresponding indolinoxazolidine (1.44 g, 6.62 mmol) were dissolved in little amount of DCM. 1g of technical grade silica were put in suspension and the solvent was removed under reduced pressure. The resulting reaction mixture was heated under stirring at 100 $^{\circ}\text{C}$  during 30 min.

After cooling down to room temperature, the crude material was removed from silica by methanol, DCM. The solvent was evaporated and crude product was washed by petroleum ether to remove the excess of BOX and filtered to afford a yellow solid with a quantitative yield.

**$^1\text{H NMR}$**  (300 MHz,  $\text{CDCl}_3$ )  $\delta$  8.21 (d,  $J = 8.8$  Hz, 2H), 7.57 (d,  $J = 8.8$  Hz, 2H), 6.95 (dd,  $J = 23.0, 6.9$  Hz, 3H), 6.72 (d,  $J = 7.9$  Hz, 1H), 6.49 (d,  $J = 15.9$  Hz, 1H), 3.87 – 3.38 (m, 4H), 2.32 (s, 3H), 1.45 (s, 3H), 1.17 (s, 3H). **IR**  $\nu$  ( $\text{cm}^{-1}$ ): 2968, 1739, 1509, 1487, 1463, 1368, 1216, 1106, 816  $\text{cm}^{-1}$ .

**(E)-4-(2-(7,9,9-trimethyl-2,3,9a-tetrahydrooxazolo[3,2-a]indol-9a-yl)vinyl)aniline (41)**

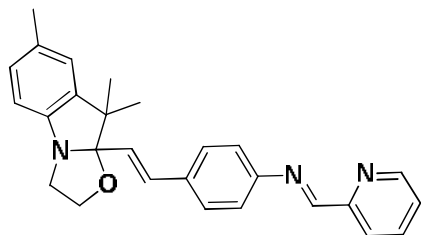


A mixture of (E)-7,9,9-trimethyl-9a-(4-nitrostyryl)-2,3,9a-tetrahydrooxazolo[3,2-a]indole (0.5 g, 1.43 mmol) and  $\text{SnCl}_2$  (1.35 g, 7.14 mmol) in 10 mL of ethanol was refluxed under argon for 7 hours. Solvent was evaporated under reduced pressure. The residue was dissolved in DCM and the solution was washed with NaOH in order to

close the BOX. The solvent was evaporated and product was afforded as a brown orange solid (400 mg, 87%).

**$^1\text{H NMR}$**  (300 MHz,  $\text{CDCl}_3$ )  $\delta$  7.27 (d,  $J = 8.1$  Hz, 2H), 6.97 (ddd,  $J = 7.9, 1.7, 0.7$  Hz, 1H), 6.89 (d,  $J = 1.7$  Hz, 1H), 6.76 (d,  $J = 15.9$  Hz, 1H), 6.70 (d,  $J = 7.9$  Hz, 1H), 6.66 (d,  $J = 8.5$  Hz, 2H), 6.07 (d,  $J = 15.9$  Hz, 1H), 3.86–3.40 (m, 4H), 2.31 (s, 3H), 1.42 (s, 3H), 1.15 (s, 3H).  **$^{13}\text{C NMR}$**  (75 MHz,  $\text{CDCl}_3$ )  $\delta$  148.3, 146.3, 140, 132, 131, 128, 128, 127.2, 123.2, 121.9, 115.1, 111.8, 110.4, 63.5, 50.2, 47.9, 29.7, 28.4, 21.1, 20.3. **IR**  $\nu$  ( $\text{cm}^{-1}$ ): 3356, 2917, 1739, 1608, 1588, 1518, 1489, 1465, 1280, 1199, 907, 728  $\text{cm}^{-1}$ .

(E)-N-(pyridin-2-ylmethylene)-4-((E)-2-(7,9,9-trimethyl-2,3,9a-tetrahydrooxazolo[3,2-a]indol-9a-yl)vinyl)aniline (42)



**C<sub>27</sub>H<sub>27</sub>N<sub>3</sub>O**  
**409.52 g.mol<sup>-1</sup>**

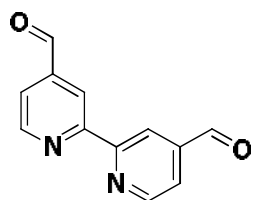
A solution of picolinaldehyde (0.22 g, 2.06 mmol) and (E)-4-(2-(7,9,9-trimethyl-2,3,9a-tetrahydrooxazolo[3,2-a]indol-9a-yl)vinyl)aniline (0.33 g, 1.03 mmol) in dichloromethane (15 mL) was stirred at room temperature during 24 hours. The solvent was evaporated and crude product washed by petroleum ether in order to remove the excess of starting material before

drying. The desired product was obtained as a yellow powder (290 mg, 69%).

<sup>1</sup>H NMR (300 MHz, CDCl<sub>3</sub>) δ 8.72 (d, *J* = 4.8 Hz, 1H), 8.63 (s, 1H), 8.21 (d, *J* = 8.0 Hz, 1H), 7.82 (t, *J* = 8.0 Hz, 1H), 7.51 (d, *J* = 8.4 Hz, 2H), 7.38 (dd, *J* = 6.3, 4.9 Hz, 1H), 7.30 (d, *J* = 8.4 Hz, 2H), 6.98 (d, *J* = 7.9 Hz, 1H), 6.93 – 6.86 (m, 2H), 6.71 (d, *J* = 7.9 Hz, 1H), 6.31 (d, *J* = 15.9 Hz, 1H), 3.85 – 3.41 (m, 4H), 2.32 (s, 3H), 1.45 (s, 3H), 1.18 (s, 3H). IR ν (cm<sup>-1</sup>): 2969, 1739, 1366, 1215 cm<sup>-1</sup>. No <sup>13</sup>C NMR due to the stability of imine bond.

Ligand synthesis bearing two BOX units.

[2, 2'-bipyridine]-4, 4'-dicarbaldehyde (43)



**C<sub>12</sub>H<sub>8</sub>N<sub>2</sub>O<sub>2</sub>**  
**212.20 g.mol<sup>-1</sup>**

In a 200mL two-necked round bottom flask containing, dimethyl bipyridine (1 g, 5.43 mmol), 150 mL of 1,4-dioxane was added drop wise and stirred to get a homogenous mixture. The solution was bubbled with argon for 15 min while stirring. 2.41 g of SeO<sub>2</sub> (4 eq.) were added and the mixture was refluxed under argon atmosphere for 44 hours. After the completion of the reaction (Monitored

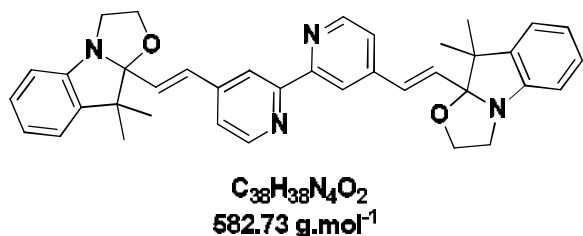
by TLC), the reaction mixture was washed with warm 1,4-dioxane for 2 to 3 minutes and filtered. 1,4-dioxane was removed under reduced pressure. The residue was then dissolved in hot distilled ethyl acetate, filtered and again washed with hot ethyl acetate. The ethyl acetate layer was washed with 1M Na<sub>2</sub>CO<sub>3</sub> (25 0mL) to remove additional carboxylic acid. The organic layer was dried with anhydrous Na<sub>2</sub>SO<sub>4</sub>. The solvent was evaporated and crude product was purified by flash column chromatography on Al<sub>2</sub>O<sub>3</sub> by using a mixture of PE/EtOAc (4/6) to afford a white powder (900 mg, 78%).

<sup>1</sup>H NMR (300 MHz, CDCl<sub>3</sub>) δ 10.21 (s, 1H), 8.96 (d, *J* = 4.9 Hz, 1H), 8.91 – 8.86 (m, 1H), 7.79 (dd, *J* = 4.9, 1.5 Hz, 1H). <sup>13</sup>C NMR (75 MHz, CDCl<sub>3</sub>) δ 192.3, 156.5, 150.9, 142.9, 125.5, 122.6, 120.1.

General procedure for preparing bipyridine ligands bearing Two BOX units:

A mixture of [2,2'-bipyridine]-4,4'-dicarbaldehyde (1.41 mmol) and corresponding inolinoxazolidine derivatives (3.25 mmol) was dissolved in a little amount of DCM. 1g of technical grade silica were put in suspension and the solvent was removed under reduced pressure. The resulting reaction mixture was heated under stirring at 100°C during 10 min. After cooling down to room temperature, the crude product was purified by flash column chromatography on Al<sub>2</sub>O<sub>3</sub> (PE/ EtOAc, 7/3) to afford the pure compound.

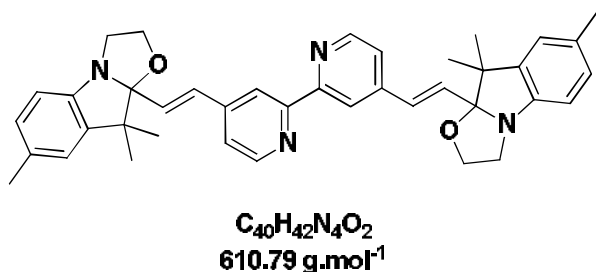
4,4'-bis((E)-2-(9,9-dimethyl-2,3,9,9a-tetrahydrooxazolo[3,2-a]indol-9a-yl)vinyl)-2,2'-bipyridine (44)



**Compound BOX-H:** Recrystallized by ethanol to afford as a yellow crystal (591 mg, 72%). **mp** 222-225 °C. **<sup>1</sup>H NMR** (300 MHz, CDCl<sub>3</sub>) δ 8.66 (d, *J* = 5.2 Hz, 1H), 8.47 (s, 1H), 7.35 (dd, *J* = 5.1, 1.6 Hz, 1H), 7.19 (td, *J* = 7.7, 1.3 Hz, 1H), 7.10 (d, *J* = 6.5 Hz, 1H), 6.96 (dd, *J* = 8.5, 7.6

Hz, 2H), 6.82 (d, *J* = 7.8 Hz, 1H), 6.66 (d, *J* = 15.9 Hz, 1H), 3.83 – 3.41 (m, 4H), 1.47 (s, 3H), 1.19 (s, 3H). **<sup>13</sup>C NMR** (76 MHz, CDCl<sub>3</sub>) δ 156.6, 150.4, 149.6, 145, 139.5, 131.7, 130.3, 127.7, 122.4, 121.9, 121.4, 118.8, 112.1, 109.6, 63.7, 50.2, 48.1, 28.5, 20.5. **IR** ν (cm<sup>-1</sup>): 2955, 1589, 1475, 1454, 1112, 1007, 977, 751 cm<sup>-1</sup>. **HRMS (FAB+):** *m/z* calcd. For C<sub>38</sub>H<sub>38</sub>N<sub>4</sub>O<sub>2</sub>: 582.2995[M+H]<sup>+</sup>; found: 582.2993. **X-Ray structure:** Monoclinic, P 21/c.

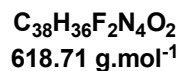
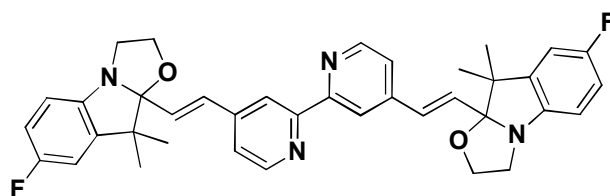
4,4'-bis((E)-2-(7,9,9-trimethyl-2,3,9,9a-tetrahydrooxazolo[3,2-a]indol-9a-yl)vinyl)-2,2'-bipyridine (45)



**Compound BOX-Me:** Product was isolated as a brown solid (714 mg, 83%). **mp** 252-253 °C. **<sup>1</sup>H NMR** (300 MHz, CDCl<sub>3</sub>) δ 8.65 (d, *J* = 5.1 Hz, 1H), 8.47 (s, 1H), 7.34 (dd, *J* = 5.1, 1.6 Hz, 1H), 6.97 (t, *J* = 11.3 Hz, 2H), 6.91 (s, 1H), 6.72 (d, *J* = 7.9 Hz, 1H), 6.65 (d, *J* = 15.9 Hz,

1H), 3.81 – 3.41 (m, 4H), 2.32 (s, 3H), 1.46 (s, 3H), 1.18 (s, 3H). **<sup>13</sup>C NMR** (76 MHz, CDCl<sub>3</sub>) δ 156.6, 149.6, 148.1, 145, 139.6, 131.8, 131.3, 130.3, 128.2, 123.1, 121.4, 118.8, 111.8, 109.9, 63.7, 50.4, 48.1, 28.5, 21, 20.4. **IR** ν (cm<sup>-1</sup>): 2958, 1739, 1590, 1489, 1459, 1106, 979, 809 cm<sup>-1</sup>. **HRMS (FAB+):** *m/z* calcd. For C<sub>40</sub>H<sub>42</sub>N<sub>4</sub>O<sub>2</sub>: 610.3308[M+H]<sup>+</sup>; found: 610.3297.

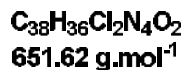
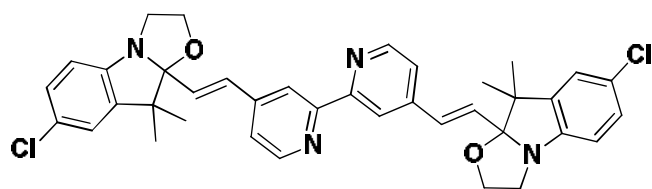
4,4'-bis((E)-2-(7-fluoro-9,9-dimethyl-2,3,9,9a-tetrahydrooxazolo[3,2-a]indol-9a-yl)vinyl)-2,2'-bipyridine (46)



**Compound BOX-F:** Product was isolated as a white solid (523 mg, 60%). mp 255-256 °C. <sup>1</sup>H NMR (300 MHz, CDCl<sub>3</sub>) δ 8.66 (d, *J* = 5.1 Hz, 1H), 8.47 (s, 1H), 7.34 (d, *J* = 5.1 Hz, 1H), 6.95 (d, *J* = 16.3 Hz, 1H), 6.86 (t, *J* = 8.8 Hz, 1H), 6.79 (d, *J* = 8.3 Hz, 1H), 6.71 (dd, *J* = 8.6, 4.2 Hz, 1H), 6.62 (d, *J* = 15.9 Hz, 1H),

3.65 (m, 4H), 1.44 (s, 3H), 1.18 (s, 3H). <sup>19</sup>F NMR (282 MHz, CDCl<sub>3</sub>) δ -122.58 (s). IR ν (cm<sup>-1</sup>): 2979, 2896, 1739, 1591, 1482, 1375, 1264, 1183, 1098, 980, 814 cm<sup>-1</sup>.

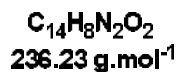
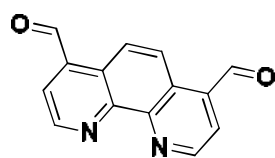
4,4'-bis((E)-2-(7-chloro-9,9-dimethyl-2,3,9,9a-tetrahydrooxazolo[3,2-a]indol-9a-yl)vinyl)-2,2'-bipyridine (47)



**Compound BOX-Cl:** Product was isolated as a white solid (551 mg, 60%). mp 249-251 °C. <sup>1</sup>H NMR (300 MHz, CDCl<sub>3</sub>) δ 8.70 (d, *J* = 5.1 Hz, 1H), 8.50 (s, 1H), 7.38 (dd, *J* = 5.1, 1.6 Hz, 1H), 7.17 (dd, *J* = 8.3, 2.1 Hz, 1H), 7.07 (d, *J* = 2.1 Hz, 1H), 6.98 (d, *J* = 15.9 Hz, 1H), 6.76 (d, *J* = 8.3 Hz,

1H), 6.65 (d, *J* = 15.9 Hz, 1H), 3.88 – 3.42 (m, 4H), 1.48 (s, 3H), 1.22 (s, 3H). IR ν (cm<sup>-1</sup>): 2969, 1739, 1590, 1458, 1374, 1112, 979, 816 cm<sup>-1</sup>.

1,10-phenanthroline-4,7-dicarbaldehyde (48)



In a 200 mL two-necked round bottom flask containing, 4,7-dimethyl-1,10-phenanthroline (1 g, 4.81 mmol), 100 mL of 1,4-dioxane was added drop wise and stirred to get a homogenous mixture. The latter was bubbled with argon for 15 min while stirring. 1.6 g of SeO<sub>2</sub> (3 equiv) were added and the mixture was refluxed under argon atmosphere for 16 hours. After the

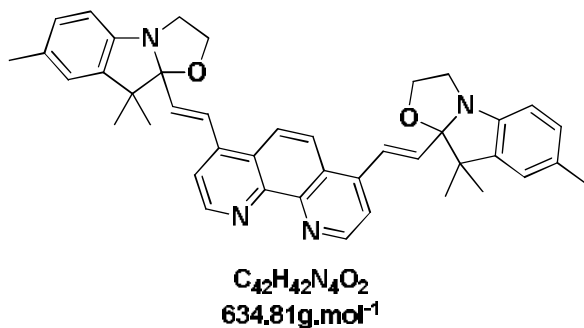
completion of the reaction (Monitored by TLC), the reaction mixture was washed with warm 1,4-dioxane for 2 to 3 minutes and filtered and 1,4-dioxane was removed under reduced pressure. The residue was then dissolved in hot distilled ethyl acetate, filtered and again washed with hot ethyl acetate. The ethyl acetate layer was washed with 1M Na<sub>2</sub>CO<sub>3</sub> (250mL) to remove additional carboxylic acid.

## Appendix 2: Experimental Parts

The organic layer was dried with anhydrous Na<sub>2</sub>SO<sub>4</sub>. The solvent was evaporated to afford a yellowish powder (730 mg 64%).

<sup>1</sup>H NMR (300 MHz, CDCl<sub>3</sub>) δ 10.63 (s, 1H), 9.53 (d, *J* = 4.4 Hz, 1H), 9.22 (s, 1H), 8.09 (d, *J* = 4.4 Hz, 1H).

### 4,7-bis((E)-2-(7,9,9-trimethyl-2,3,9,9a-tetrahydrooxazolo[3,2-a]indol-9a-yl)vinyl)-1,10-phenanthroline (49)

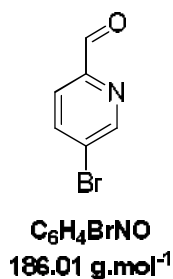


A mixture of 1,10-phenanthroline-4,7-dicarbaldehyde (0.2 g, 0.847 mmol) and corresponding inolinoxazolidine (0.4 g, 1.86 mmol) was dissolved in a little amount of DCM. 1g of technical grade silica were put in suspension and the solvent was removed under

reduced pressure. The resulting reaction mixture was heated under stirring at 100°C during 30 min. After cooling down to room temperature, the crude material was removed from silica by DCM and methanol. The solvent was evaporated and crude product was washed by petroleum ether to remove the excess of BOX and filtered to afford a white solid (320 mg 59%).

<sup>1</sup>H NMR (300 MHz, CDCl<sub>3</sub>) δ 9.16 (d, *J* = 4.6 Hz, 1H), 8.19 (s, 1H), 7.74 (d, *J* = 4.7 Hz, 1H), 7.69 (d, *J* = 15.8 Hz, 1H), 7.02 (d, *J* = 7.8 Hz, 1H), 6.94 (s, 1H), 6.76 (d, *J* = 7.9 Hz, 1H), 6.60 (d, *J* = 15.7 Hz, 1H), 3.93 – 3.50 (m, 4H), 2.34 (s, 3H), 1.51 (s, 3H), 1.24 (s, 3H). IR ν (cm<sup>-1</sup>): 2958, 1489, 1459, 1280, 1109, 1005, 810, 725 cm<sup>-1</sup>. HRMS (FAB<sup>+</sup>): *m/z* calcd. For C<sub>42</sub>H<sub>42</sub>N<sub>4</sub>O<sub>2</sub>: 634.3308[M+H]<sup>+</sup>; found: 634.3302. mp 257-259 °C.

### 5-bromopicolinaldehyde (50)

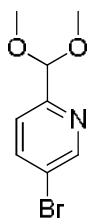


A solution of 2-iodo-5-bromopyridine (10.0 g, 35.2 mmol) in 100 mL of dry THF was cooled to 0 °C before adding PrMgCl (19.35 mL, 2 M soln. in diethyl ether). The reaction was stirred for 1 hour before dropwise addition of dry DMF (4.1 mL, 53.2 mmol) ensuring the temperature did not rise above 0 °C. After stirring for 30 minutes at same temperature, the reaction was allowed to warm to room temperature before quenching with HCl (16 mL, 2 M). The reaction was stirred for a further 30 minutes before the pH was adjusted to 7 by addition of NaOH. The desired product was then extracted into DCM three times. The

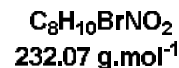
organic layer was dried with over  $\text{MgSO}_4$ . The solvent was evaporated to afford a white solid (5.46 g, 85 %). Compound was pure and used without further purification.

$^1\text{H NMR}$  (300 MHz,  $\text{CDCl}_3$ ):  $\delta$  10.04 (d,  $J = 0.8$  Hz, 1H), 8.85 (dd,  $J = 0.8, 2.2$  Hz, 1H), 8.02 (ddd,  $J = 0.8, 2.2, 8.3$  Hz, 1H), 7.85 (dd,  $J = 0.8, 8.2$  Hz, 1H).

### 5-bromo-2-(dimethoxymethyl) pyridine (51)

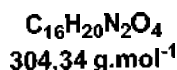
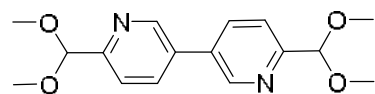


Methyl orthoformate (12.87 mL, 117.6 mmol), 5-bromopicolinaldehyde (5.47 g, 29.4 mmol) and *p*-toluenesulfonic acid (112 mg, 0.5 mmol) were refluxed in distilled MeOH (100 mL) during 4 hours. After that, MeOH was removed under vacuum and the residue dissolved in DCM. The organic layer was neutralized with saturated  $\text{NaHCO}_3$ , then extracted and dried over  $\text{MgSO}_4$ . The solvent was evaporated to afford an orange oil which was used without further purification (6.14 g, 90%).



$^1\text{H NMR}$  (300 MHz,  $\text{CDCl}_3$ ):  $\delta = 8.61$  (dd,  $J = 0.7, 2.4$  Hz, 1H), 7.79 (dd,  $J = 2.3, 8.4$  Hz, 1H), 7.40 (d,  $J = 8.4$  Hz, 1H), 5.28 (s, 1H), 3.33(s, 6H);  $^{13}\text{C NMR}$  (75 MHz,  $\text{CDCl}_3$ ):  $\delta$  155.8, 150.17, 139.2, 122.7, 120.5, 103.3, 53.6.

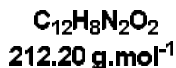
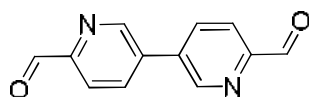
### 6,6'-bis(dimethoxymethyl)-3,3'-bipyridine (52)



This compound was synthesized according to a modified literature procedure<sup>[10]</sup>. To a stirred solution of 5-bromo-2-(dimethoxymethyl) pyridine (1.75 g, 7.54 mmol) and  $\text{Pd}(\text{PhCN})_2\text{Cl}_2$  (0.14 g, 0.38 mmol) in dry DMF (16 mL) under an inert atmosphere of argon was added TDAE (1.1 mL, 4.5  $\mu\text{mol}$ ) dropwise. The solution immediately turned dark brown, the reaction mixture was then heated at 50 °C during 3 days. After that DMF was removed under reduced pressure. The crude compound was purified by flash column chromatography on silica using a mixture of PE/EtOAc (6/4) to afford a yellow solid (0.69 g, 60%).

$^1\text{H NMR}$  (300 MHz,  $\text{CDCl}_3$ )  $\delta$  8.84 (d,  $J = 2.3$  Hz, 1H), 7.94 (dd,  $J = 8.1, 2.3$  Hz, 1H), 7.67 (d,  $J = 8.1$  Hz, 1H), 5.45 (s, 1H), 3.45 (s, 6H).  $^{13}\text{C NMR}$  (75 MHz,  $\text{CDCl}_3$ ):  $\delta$  157.2, 147.7, 135.2, 133.1, 121.5, 103.9, 53.9.

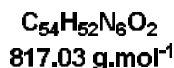
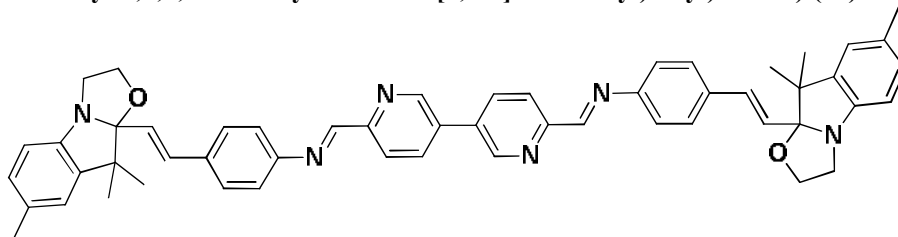
[3,3'-bipyridine]-6,6'-dicarbaldehyde (**53**)



2 M HCl (20 mL) was added to a solution of **52** (0.69 g, 2.2 mmol) in THF (10 mL). The reaction was sealed under an inert atmosphere of argon and stirred at room temperature during 24 hours. After monitoring by TLC (100% EtOAc), the reaction was neutralized by addition of saturated NaHCO<sub>3</sub>, allowing the formation of an off-white precipitate. The precipitate was dissolved in a mixture of CHCl<sub>3</sub>/isopropanol alcohol (3/1), the organic layer was separated and dried over MgSO<sub>4</sub>. The solvent was evaporated to afford a pale yellow powder (0.4 g, 86 %).

<sup>1</sup>H NMR (300 MHz, CDCl<sub>3</sub>) δ 10.16 (d, *J* = 0.5 Hz, 1H), 9.07 (dd, *J* = 1.9, 1.2 Hz, 1H), 8.18 – 8.10 (m, 2H). <sup>13</sup>C NMR (75 MHz, CDCl<sub>3</sub>): δ 193.2, 152.1, 144.6, 136.3, 133.7, 121.9.

(N,N'E,N,N'E)-N,N'-([3,3'-bipyridine]-6,6'-diylbis(methanylylidene))bis(4-((E)-2-(7,9,9-trimethyl-2,3,9,9a-tetrahydrooxazolo[3,2-a]indol-9a-yl)vinyl)aniline) (**54**)



A solution of [3,3'bipyridine]6,6'-dicarbaldehyde (0.024 g, 0.113 mmol) and (E)-4-(2-(7,9,9-trimethyl-2,3,9,9a-tetrahydrooxazolo[3,2-a]indol-9a-yl)vinyl)aniline **41** (0.075 g, 0.226 mmol) in acetonitrile (3 mL) was heated under reflux overnight. After cooling to room temperature, the solution was concentrated under reduced pressure, the crude was washed by diethyl ether in order to remove the excess of starting material before drying. The desired product was isolated as a yellow powder (74 mg, 80%).

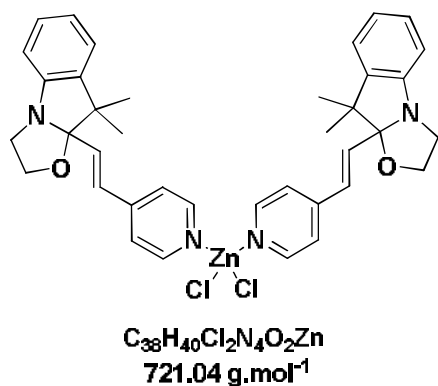
<sup>1</sup>H NMR (300 MHz, CDCl<sub>3</sub>) δ 9.02 (s, 1H), 8.70 (s, 1H), 8.37 (d, *J* = 8.2 Hz, 1H), 8.12 – 8.08 (m, 1H), 7.54 (d, *J* = 8.4 Hz, 2H), 7.34 (d, *J* = 8.4 Hz, 2H), 6.99 (d, *J* = 8.1 Hz, 1H), 6.95 – 6.87 (m, 2H), 6.72 (d, *J* = 8.0 Hz, 1H), 6.33 (d, *J* = 15.9 Hz, 1H), 3.85 – 3.42 (m, 4H), 2.32 (s, 3H), 1.45 (s, 3H), 1.19 (s, 3H). <sup>13</sup>C NMR (125 MHz, CDCl<sub>3</sub>) δ 159.6, 154.7, 150.4, 148.3, 148.3, 139.9, 135.2, 131.7, 131.3, 128.2, 127.9, 126.5, 123.3, 122.3, 121.8, 112, 110.3, 63.7, 50.4, 48.2, 29.8, 28.6, 21.20, 20.50. **HRMS (FAB+): m/z calcd. For C<sub>54</sub>H<sub>52</sub>N<sub>6</sub>O<sub>2</sub>: 816.4152[M+H]<sup>+</sup>; found: 817.4230.**

Complexes using zinc metal.

General procedure for Zinc Complexes with pyridine ligands

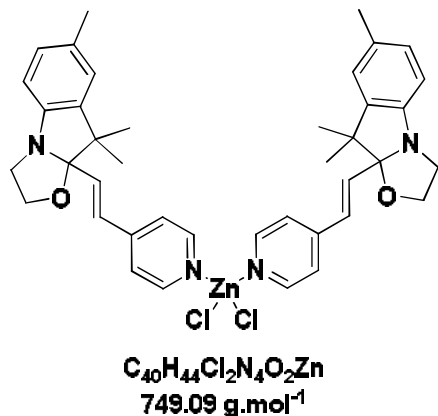
In a test tube, a solution of pyridine ligand (0.147 mmol, 2 eq.) in CH<sub>2</sub>Cl<sub>2</sub> (5 mL) was mixed with a solution of ZnCl<sub>2</sub> (0.073 mmol) in CH<sub>3</sub>CN (5 mL) and ultra-sonicated for 2 min. On top of the resulting solution a layer of diethyl ether was added to afford (when efficient) the formation of single crystals of complex after one week.

Zn(L)<sub>2</sub>Cl<sub>2</sub> (55)



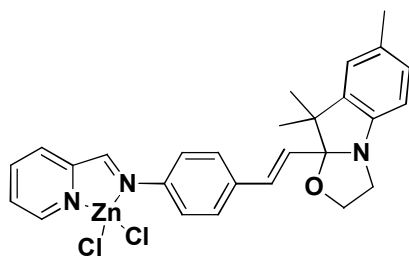
**Compound Zn(L)<sub>2</sub>Cl<sub>2</sub>, BOX-H:** Product was isolated as a yellow solid (69%). <sup>1</sup>H NMR (300 MHz, CD<sub>3</sub>CN) δ 8.66 (dd, *J* = 5.0, 1.5 Hz, 2H), 7.74 (dd, *J* = 5.0, 1.6 Hz, 2H), 7.24 – 7.17 (m, 1H), 7.15 (dd, *J* = 7.4, 0.8 Hz, 1H), 6.96 (ddd, *J* = 10.6, 3.5, 2.1 Hz, 2H), 6.89 (d, *J* = 7.8 Hz, 1H), 6.78 (d, *J* = 15.9 Hz, 1H), 3.82 – 3.36 (m, 4H), 1.44 (s, 3H), 1.15 (s, 3H). IR ν (cm<sup>-1</sup>): 2960, 1612, 1477, 1275, 749 cm<sup>-1</sup>. Anal. calcd for C<sub>38</sub>H<sub>40</sub>N<sub>4</sub>O<sub>2</sub>Cl<sub>2</sub>Zn: C, 63.30; H, 5.59; N, 7.77, found: C, 62.92; H, 5.44; N, 7.35.

Zn(L')<sub>2</sub>Cl<sub>2</sub> (56)



**Compound Zn(L')<sub>2</sub>Cl<sub>2</sub>, BOX-Me:** Product was isolated as yellow single crystals (78%). <sup>1</sup>H NMR (300 MHz, CD<sub>3</sub>CN) δ 8.61 (d, *J* = 6.5 Hz, 2H), 7.68 (d, *J* = 6.5 Hz, 2H), 6.97 (d, *J* = 7.9 Hz, 1H), 6.94 (s, 1H), 6.90 (d, *J* = 16.1 Hz, 1H), 6.73 (dd, *J* = 11.9, 4.0 Hz, 2H), 3.77 – 3.28 (m, 4H), 2.27 (s, 3H), 1.38 (s, 3H), 1.09 (s, 3H). <sup>13</sup>C NMR (75 MHz, CD<sub>3</sub>CN) δ 149.6, 149.3, 149, 140.5, 136.4, 132, 129.6, 129, 123.9, 112.8, 110.5, 64.4, 50.8, 48.8, 28.5, 20.9, 20.6. IR ν (cm<sup>-1</sup>): 2958, 1613, 1489, 811 cm<sup>-1</sup>. ESI-MS: *m/z* = 711.14 Zn(L'<sub>1</sub>)<sub>2</sub>Cl. Anal. calcd for C<sub>40</sub>H<sub>44</sub>N<sub>4</sub>O<sub>2</sub>Cl<sub>2</sub>Zn: C, 64.13; H, 5.92; N, 7.48, found: C, 62.15; H, 5.75; N, 7.14. X-Ray structure: Monoclinic, C 2/c

**ZnL<sub>1</sub>Cl<sub>2</sub> (57)**

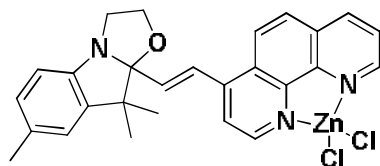


**C<sub>27</sub>H<sub>27</sub>Cl<sub>2</sub>N<sub>3</sub>OZn**  
**545.81 g.mol<sup>-1</sup>**

In a test tube, a solution of ligand (15 mg, 0.036 mmol) in CH<sub>2</sub>Cl<sub>2</sub> (5 mL) was mixed with a solution of ZnCl<sub>2</sub> (5 mg 0.036 mmol, 1 eq.) in CH<sub>3</sub>CN (5 mL) and ultra-sonicated for 2 min. On top of the resulting solution a layer of Et<sub>2</sub>O was added to afford the formation of single crystals of complex after one week (15 mg, 75%).

<sup>1</sup>H NMR (300 MHz, CDCl<sub>3</sub>) δ 8.84 (d, *J* = 4.8 Hz, 1H), 8.81 (s, 1H), 8.16 (t, *J* = 7.8 Hz, 1H), 8.03 (d, *J* = 7.8 Hz, 1H), 7.78 – 7.67 (m, 3H), 7.56 (d, *J* = 8.4 Hz, 2H), 6.99 (d, *J* = 6.7 Hz, 1H), 6.93 – 6.86 (m, 2H), 6.72 (d, *J* = 7.8 Hz, 1H), 6.39 (d, *J* = 15.9 Hz, 1H), 3.84 – 3.40 (m, 4H), 2.32 (s, 2H), 1.45 (s, 3H), 1.17 (s, 3H). IR ν (cm<sup>-1</sup>): 2970, 1738, 1365, 1205 cm<sup>-1</sup>. ESI-MS: *m/z* = 507.92 ZnLCl. Anal. calcd for C<sub>27</sub>H<sub>27</sub>N<sub>4</sub>OCl<sub>2</sub>Zn: C, 59.41; H, 4.99; N, 7.70, found: C, 59.56; H, 4.85; N, 7.76. X-Ray structure: Triclinic, P -1.

**Zn(Phenanthroline)Cl<sub>2</sub> (58)**

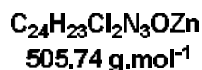
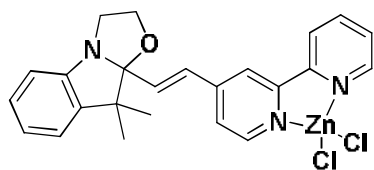


**C<sub>27</sub>H<sub>25</sub>Cl<sub>2</sub>N<sub>3</sub>OZn**  
**543.79 g.mol<sup>-1</sup>**

In a test tube, a solution of ligand (E)-9a-(2-(1,10-phenanthrolin-4-yl)vinyl)-7,9,9-trimethyl-2,3,9,9a-tetrahydrooxazolo[3,2-a]indole (30 mg, 0.073 mmol) in CH<sub>2</sub>Cl<sub>2</sub> (5 mL) was mixed with a solution of ZnCl<sub>2</sub> (10 mg 0.073 mmol, 1 eq.) in CH<sub>3</sub>CN (5 mL) and ultra-sonicated for 2 min. On top of the resulting solution a layer of Et<sub>2</sub>O

was added to afford the formation of powder of the complex after one week. Yield: (30 mg, 75%).

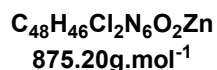
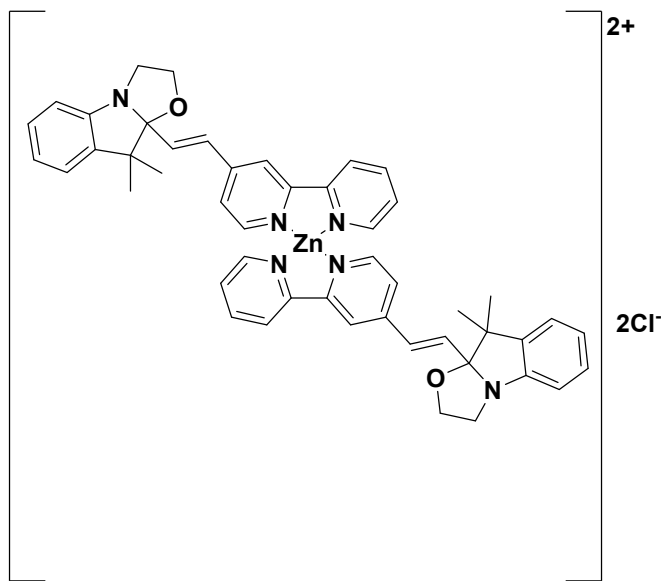
<sup>1</sup>H NMR (300 MHz, CD<sub>3</sub>CN) δ 9.09 (d, *J* = 21.1 Hz, 2H), 8.82 (d, *J* = 8.2 Hz, 1H), 8.44 (d, *J* = 9.3 Hz, 1H), 8.21 (t, *J* = 8.2 Hz, 2H), 8.09 (dd, *J* = 8.1, 4.9 Hz, 1H), 7.72 (d, *J* = 15.7 Hz, 1H), 7.00 (d, *J* = 10.8 Hz, 2H), 6.85 (d, *J* = 15.7 Hz, 1H), 6.79 (d, *J* = 7.8 Hz, 1H), 3.94 – 3.44 (m, 4H), 2.30 (s, 3H), 1.47 (s, 3H), 1.19 (s, 3H). IR ν (cm<sup>-1</sup>): 2959, 2921, 1620, 1587, 1519, 1488, 1426, 1108, 975 cm<sup>-1</sup>. Anal. calcd for C<sub>27</sub>H<sub>25</sub>N<sub>3</sub>OCl<sub>2</sub>Zn: C, 59.63; H, 4.63; N, 7.73, found: C, 59.49; H, 4.77; N, 7.69.

**Zn(H-BOX-biPy)Cl<sub>2</sub> (59)**


In a test tube, a solution of ligand (E)-9a-(2-([2,2'-bipyridin]-4-yl)vinyl)-9,9-dimethyl-2,3,9,9a-tetrahydrooxazolo[3,2-a]indole (27 mg, 0.073 mmol) in CH<sub>2</sub>Cl<sub>2</sub> (5 mL) was mixed with a solution of ZnCl<sub>2</sub> (10 mg 0.073 mmol, 1 eq.) in CH<sub>3</sub>CN (5 mL) and ultrasonicated for 2 min. On top of the resulting solution a layer of Et<sub>2</sub>O

was added to afford the formation of powder of the complex after one week (30 mg, 82%).

<sup>1</sup>H NMR (300 MHz, CD<sub>3</sub>CN) δ 8.72 (dd, *J* = 22.4, 4.3 Hz, 2H), 8.56 (d, *J* = 8.5 Hz, 2H), 8.30 (t, *J* = 7.3 Hz, 1H), 7.88 – 7.77 (m, 2H), 7.18 (t, *J* = 7.7 Hz, 1H), 7.13 (d, *J* = 7.0 Hz, 1H), 7.05 (d, *J* = 16.0 Hz, 1H), 6.96 (dd, *J* = 11.7, 4.3 Hz, 2H), 6.88 (d, *J* = 7.8 Hz, 1H), 3.83 – 3.37 (m, 4H), 1.45 (s, 3H), 1.16 (s, 3H). <sup>13</sup>C NMR (75 MHz, CD<sub>3</sub>CN) δ 150.4, 149.5, 149, 148.8, 148.6, 148.5, 141.7, 139.1, 136.3, 128.1, 127.5, 127.3, 124.6, 122.6, 122, 121.4, 120, 111.8, 109.1, 63.2, 49.5, 47.6, 27.3, 19.4. ESI-MS: *m/z* = 469.92 Zn(H-BOX-biPy)Cl. Anal. calcd for C<sub>24</sub>H<sub>23</sub>N<sub>3</sub>OCl<sub>2</sub>Zn: C, 57.00; H, 4.58; N, 8.31, found: C, 56.61; H, 4.78; N, 8.45.

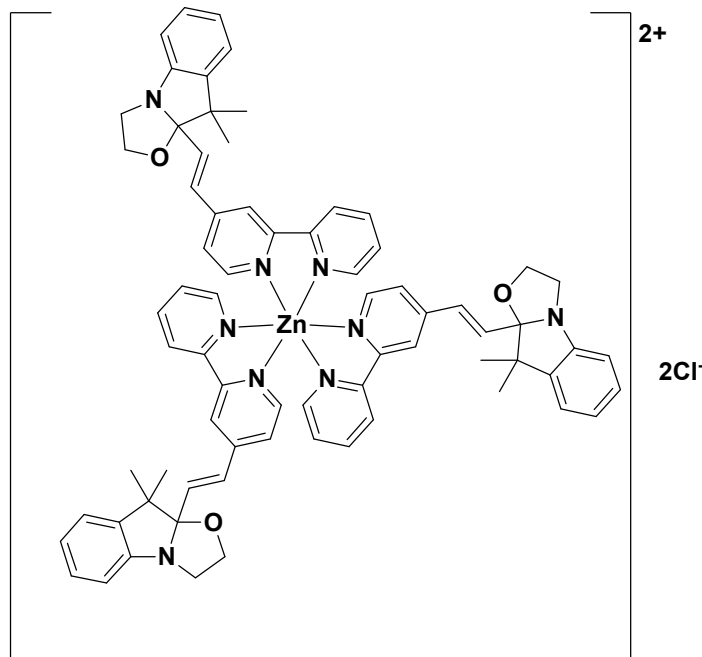
**[Zn(H-BOX-biPy)<sub>2</sub>]<sup>2+</sup>2Cl<sup>-</sup>(60)**


In a test tube, a solution of ligand (54 mg, 0.146 mmol, 2 eq.) in CH<sub>2</sub>Cl<sub>2</sub> (5 mL) was mixed with a solution of ZnCl<sub>2</sub> (10 mg 0.073 mmol) in CH<sub>3</sub>CN (5 mL) and ultrasonicated for 2 min. Furthermore, the mixture was heated for 3 hours at 50 °C. After cooling to room temperature, on top of the resulting solution a layer of Et<sub>2</sub>O was added to afford the formation of powder of the complex after one week (46 mg, 73%).

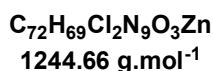
<sup>1</sup>H NMR (300 MHz, CD<sub>3</sub>CN) δ 8.66 (dd, *J* = 19.8, 3.3 Hz, 2H), 8.55 – 8.44 (m, 2H), 8.06 (t, *J* = 7.4 Hz, 1H), 7.63 (dd, *J* = 5.3, 1.4 Hz, 1H), 7.58 – 7.51 (m, 1H), 7.17 (td, *J* = 7.7, 1.3 Hz, 1H), 7.14 – 7.09 (m, 1H), 7.00 (d, *J* = 15.9 Hz, 1H), 6.93 (td, *J* = 7.4, 0.9 Hz, 1H), 6.86 (d, *J* = 7.8 Hz, 1H), 6.78 (d, *J* = 15.9

H<sub>z</sub>, 1H), 3.82 – 3.34 (m, 4H), 1.43 (s, 3H), 1.14 (s, 3H). **ESI-MS:**  $m/z = 400.99$  [**Zn(H-BOX-biPy)**]<sub>2</sub><sup>2+</sup>.  
**Anal. calcd for C<sub>48</sub>H<sub>46</sub>N<sub>6</sub>O<sub>2</sub>Cl<sub>2</sub>Zn:** C, 69.87; H, 5.30; N, 9.60, found: C, 69.92; H, 5.46; N, 9.43.

**[Zn(H-BOX-biPy)<sub>3</sub>]<sup>2+</sup>2Cl<sup>-</sup> (61)**



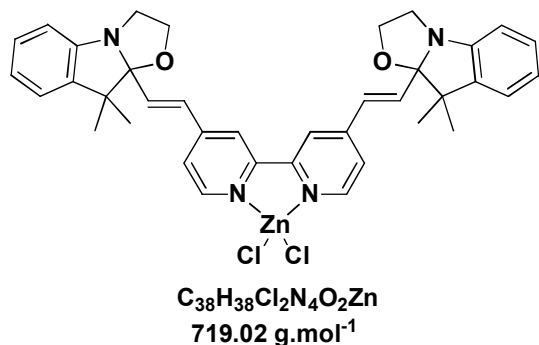
In a test tube, a solution of ligand (80.8 mg, 0.219 mmol, 3 eq.) in CH<sub>2</sub>Cl<sub>2</sub> (5 mL) was mixed with a solution of ZnCl<sub>2</sub> (10 mg 0.073 mmol) in CH<sub>3</sub>CN (5 mL) and ultra-sonicated for 2 min, the mixture was heated for 3 hours at 50 °C. On top of the resulting solution a layer of Et<sub>2</sub>O was added to afford the formation of powder of the complex which was filtered after one week (72 mg, 80%).



<sup>1</sup>H NMR (300 MHz, CD<sub>3</sub>CN) δ 8.72

(d,  $J = 4.5$  Hz, 1H), 8.65 (d,  $J = 5.2$  Hz, 1H), 8.50 (d,  $J = 10.4$  Hz, 2H), 8.16 – 8.06 (m, 1H), 7.69 (d,  $J = 5.1$  Hz, 1H), 7.65 – 7.56 (m, 1H), 7.17 (dd,  $J = 10.8, 4.4$  Hz, 1H), 7.12 (s, 1H), 7.02 (d,  $J = 15.9$  Hz, 1H), 6.94 (td,  $J = 7.4, 0.9$  Hz, 1H), 6.87 (d,  $J = 7.9$  Hz, 1H), 6.82 (d,  $J = 16.0$  Hz, 1H), 3.83 – 3.18 (m, 4H), 1.44 (s, 3H), 1.16 (s, 3H). **IR**  $\nu$  (cm<sup>-1</sup>): 2970, 1738, 1610, 1365, 1228 cm<sup>-1</sup>. **ESI-MS:**  $m/z = 586.57$  [**Zn(H-BOX-biPy)**]<sub>3</sub><sup>2+</sup>. **Anal. calcd for C<sub>72</sub>H<sub>69</sub>N<sub>9</sub>O<sub>3</sub>Cl<sub>2</sub>Zn:** C, 69.48; H, 5.59; N, 10.13, found: C, 69.56; H, 5.40; N, 10.29.

**Zn((H-BOX)<sub>2</sub>biPy)Cl<sub>2</sub> (62)**



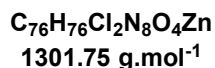
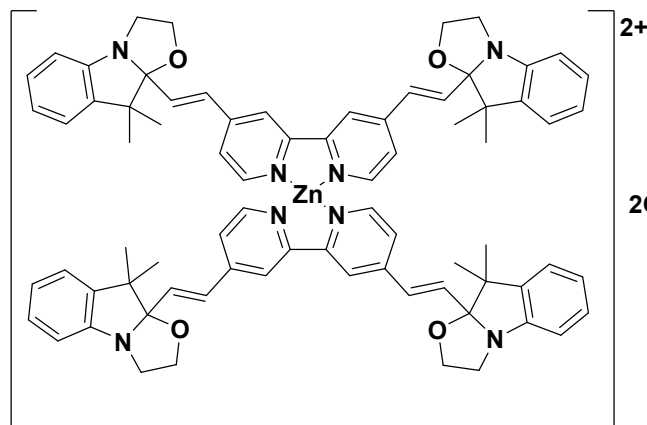
In a test tube, a solution of ligand (21 mg, 0.036 mmol) in CH<sub>2</sub>Cl<sub>2</sub> (5 mL) was mixed with a solution of ZnCl<sub>2</sub> (5 mg 0.036 mmol, 1 eq.) in CH<sub>3</sub>CN (5 mL) and ultra-sonicated for 2 min. On top of the resulting solution a layer of Et<sub>2</sub>O was added to afford the formation of single crystals of complex which was

filtered after one week (19 mg, 75%).

## Appendix 2: Experimental Parts

$^1\text{H NMR}$  (300 MHz,  $\text{CD}_3\text{CN}$ )  $\delta$  8.72 (d,  $J = 5.5$  Hz, 1H), 8.68 (s, 1H), 7.85 (s, 1H), 7.26 – 7.19 (m, 1H), 7.18 (d,  $J = 6.6$  Hz, 1H), 7.10 (d,  $J = 16.0$  Hz, 1H), 7.04 (s, 1H), 6.98 (t,  $J = 7.4$  Hz, 1H), 6.92 (d,  $J = 8.0$  Hz, 1H), 3.86 – 3.43 (m, 4H), 1.50 (s, 3H), 1.21 (s, 3H). **IR**  $\nu$  ( $\text{cm}^{-1}$ ): 2958, 2920, 2849, 1738, 1609, 1480, 1456, 1364, 1228, 1216, 1114, 747  $\text{cm}^{-1}$ . **ESI-MS**:  $m/z = 681.28$  **Zn((H-BOX) $_2$ biPy)Cl**. **Anal. calcd for  $\text{C}_{38}\text{H}_{38}\text{N}_4\text{O}_2\text{Cl}_2\text{Zn}$** : C, 63.48; H, 5.33; N, 7.79, found: C, 63.20; H, 5.62; N, 7.54. **X-Ray structure**: Monoclinic, P 21/c

### Zn[(H-BOX) $_2$ biPy] $_2^{2+}$ 2Cl $^-$ (63)



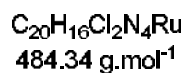
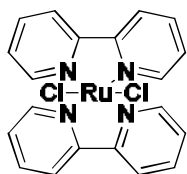
In a test tube, a solution of ligand (85 mg, 0.146 mmol, 2 eq.) in  $\text{CH}_2\text{Cl}_2$  (5 mL) was mixed with a solution of  $\text{ZnCl}_2$  (10 mg 0.073 mmol) in  $\text{CH}_3\text{CN}$  (5 mL) and ultra-sonicated for 2 min, the mixture was heated for 3 hours at 50 °C. On top of the resulting solution a layer of  $\text{Et}_2\text{O}$  was added to afford the formation of powder of the complex

which was filtered after one week (72 mg, 76%).

$^1\text{H NMR}$  (300 MHz,  $\text{CD}_3\text{CN}$ )  $\delta$  8.65 (d,  $J = 5.3$  Hz, 1H), 8.58 (s, 1H), 7.70 (s, 1H), 7.18 (t,  $J = 7.6$  Hz, 1H), 7.15 – 7.11 (m, 1H), 7.02 (d,  $J = 15.9$  Hz, 1H), 6.94 (td,  $J = 7.4, 1.0$  Hz, 1H), 6.90 – 6.81 (m, 2H), 3.82 – 3.39 (m, 6H), 1.44 (s, 3H), 1.16 (s, 3H). **IR**  $\nu$  ( $\text{cm}^{-1}$ ): 2969, 1737, 1607, 1477, 1365, 1229, 1020, 747  $\text{cm}^{-1}$ . **Anal. calcd for  $\text{C}_{76}\text{H}_{76}\text{N}_8\text{O}_4\text{Cl}_2\text{Zn}$** : C, 70.12; H, 5.88; N, 8.61, found: C, 70.43; H, 5.45; N, 8.23.

## Complexes using ruthenium metal

### Ru(biPy) $_2$ Cl $_2$ (64)

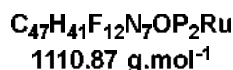
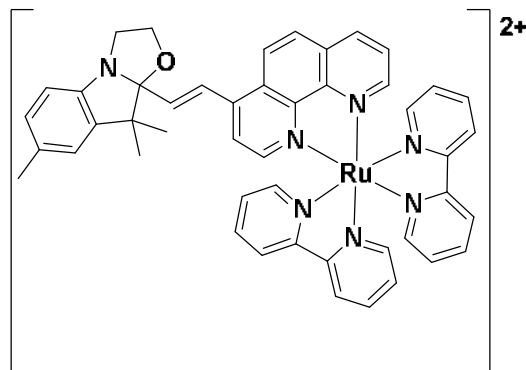


The following modification of the preparation of this complex developed by Meyer<sup>[11]</sup> was utilized. In a round bottomed flask,  $\text{RuCl}_3 \cdot 3\text{H}_2\text{O}$  (0.400 g, 1.91 mmol), bipyridine (0.506 g, 3.82 mmol, 2 eq.), and LiCl (0.0054 g, 0.128 mmol) were refluxed in dimethylformamide (5 mL) for 8 h under argon atmosphere. After it cooled to room temperature, 25 mL of acetone were added, and the resultant solution

## Appendix 2: Experimental Parts

was cooled at 0 °C overnight, to yield a red-violet solution and a red-black solid, which was filtered, washed three times with hexane and three times with diethyl ether to afford an orange solid (87%).

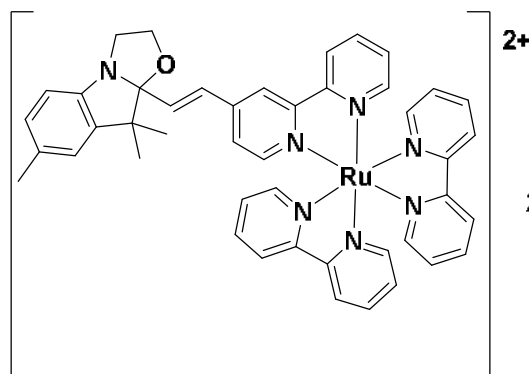
### [Ru(Phenanthroline)(biPy)<sub>2</sub>]<sup>2+</sup>2PF<sub>6</sub><sup>-</sup> (65)



**2+** Ru(bPy)<sub>2</sub>Cl<sub>2</sub> (50 mg, 0.1 mmol) and ligand (E)-9a-(2-(1,10-phenanthrolin-4-yl)vinyl)-7,9,9-trimethyl-2,3,9,9a-tetrahydrooxazolo[3,2-a]indole (38 mg, 0.092) were combined in 6 mL of ethanol under argon. The reaction mixture was refluxed overnight at 90°C. The solvent was evaporated to yield a dark orange solid and the crude was purified by flash column

chromatography on silica gel using a mixture of Acetone/water 8/2 to remove the excess of Ru(bPy)<sub>2</sub>Cl<sub>2</sub>, followed by Acetone/saturated aqueous NH<sub>4</sub>PF<sub>6</sub> 8/2 in order to isolate the desired product. Concentration under reduced pressure to remove acetone allowed obtaining a precipitate. The latter was filtered and washed several times by Et<sub>2</sub>O to afford a bright orange solid (70 mg, 68%).

**<sup>1</sup>H NMR** (300 MHz, CD<sub>3</sub>CN) δ 8.62 (d, *J* = 8.3 Hz, 1H), 8.55 – 8.46 (m, 5H), 8.26 (d, *J* = 8.8 Hz, 1H), 8.10 (t, *J* = 7.9 Hz, 3H), 7.99 (t, *J* = 6.3 Hz, 3H), 7.88 (d, *J* = 5.5 Hz, 1H), 7.84 (d, *J* = 5.3 Hz, 2H), 7.77 – 7.69 (m, 2H), 7.58 (d, *J* = 5.4 Hz, 1H), 7.52 (d, *J* = 5.7 Hz, 1H), 7.48 – 7.42 (m, 2H), 7.28 – 7.18 (m, 2H), 7.03 – 6.96 (m, 2H), 6.79 (s, 1H), 6.75 (d, *J* = 7.1 Hz, 1H), 3.69 (m, 4H), 2.29 (s, 3H), 1.45 (d, *J* = 3.0 Hz, 3H), 1.15 (s, 3H). **IR** ν (cm<sup>-1</sup>): 2970, 1739, 1365, 1216, 829, 760 cm<sup>-1</sup>. **Anal. calcd for C<sub>47</sub>H<sub>41</sub>N<sub>7</sub>OF<sub>12</sub>P<sub>2</sub>Ru**: C, 50.82; H, 3.72; N, 8.83, found: C, 50.77; H, 3.63; N, 8.92.

**[Ru(BOX-biPy)(biPy)<sub>2</sub>]<sup>2+</sup>PF<sub>6</sub><sup>-</sup> (66)**


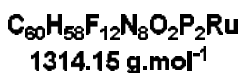
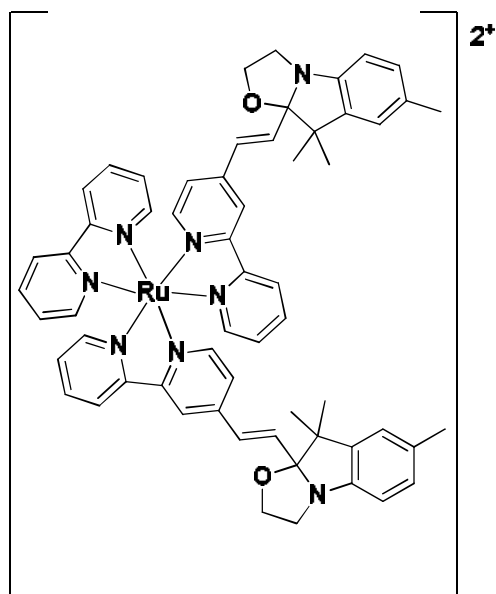
**C<sub>45</sub>H<sub>41</sub>F<sub>12</sub>N<sub>7</sub>OP<sub>2</sub>Ru**  
**1086.85 g.mol<sup>-1</sup>**

**2PF<sub>6</sub><sup>-</sup>**

Ru(bPy)<sub>2</sub>Cl<sub>2</sub> (50 mg, 0.1mmol) and ligand (E)-9a-(2-([2,2'-bipyridin]-4-yl)vinyl)-7,9,9-trimethyl-2,3,9,9a-tetrahydrooxazolo[3,2-a]indole (35 mg, 0.092 mmol) were combined in 6 mL of ethanol under argon. The reaction mixture was refluxed overnight at 90°C. The solvent was evaporated to yield a dark orange solid and the crude was purified by flash column

chromatography on silica using a mixture of Acetone/water 8/2 to remove the excess of Ru(bPy)<sub>2</sub>Cl<sub>2</sub>, followed by Acetone/saturated aqueous NH<sub>4</sub>PF<sub>6</sub> 8/2 in order to isolate the desired product. Concentration under reduced pressure to remove acetone led to a precipitate. The latter was filtered and washed several times by Et<sub>2</sub>O to afford a bright orange solid (80 mg, 80%).

<sup>1</sup>H NMR (300 MHz, CD<sub>3</sub>CN) δ 8.59 (d, *J* = 7.2 Hz, 2H), 8.50 (d, *J* = 8.1 Hz, 4H), 8.06 (t, *J* = 7.9 Hz, 5H), 7.79 (d, *J* = 5.5 Hz, 1H), 7.72 (d, *J* = 5.5 Hz, 4H), 7.63 (d, *J* = 6.2 Hz, 1H), 7.46 – 7.36 (m, 6H), 7.02 – 6.94 (m, 3H), 6.87 (d, *J* = 16.0 Hz, 1H), 6.74 (d, *J* = 7.9 Hz, 1H), 3.77 – 3.34 (m, 4H), 2.28 (s, 3H), 1.41 (s, 3H), 1.12 (s, 3H). <sup>13</sup>C NMR (75 MHz, CD<sub>3</sub>CN) δ 156.9, 156.8, 156.7, 156.7, 151.4, 151.3, 151.2, 148, 145.5, 139.2, 137.5, 135.3, 130.9, 127.8, 127.7, 127.3, 124.5, 124, 122.7, 121.3, 111.6, 109.4, 63.2, 49.7, 47.6, 27.3, 19.7, 19.4. IR ν (cm<sup>-1</sup>): 2961, 1739, 1464, 1256, 1018, 830, 760 cm<sup>-1</sup>. ESI-MS: *m/z* = 942.05 [Ru(BOX-biPy)(biPy)<sub>2</sub>]<sup>2+</sup>PF<sub>6</sub><sup>-</sup>, 512.03 [Ru(BOX-biPy)(biPy)<sub>2</sub>]<sup>2+</sup>. Anal. calcd for C<sub>45</sub>H<sub>41</sub>N<sub>7</sub>OF<sub>12</sub>P<sub>2</sub>Ru: C, 49.73; H, 3.80; N, 9.02, found: C, 49.52; H, 3.60; N, 8.92.

**[Ru(BOX-biPy)<sub>2</sub>(biPy)]<sup>2+</sup>PF<sub>6</sub><sup>-</sup> (67)**


Dichloro(*p*-cymene)ruthenium(II) dimer (40 mg, 0.065 mmol) and 2,2'-bipyridine (20 mg, 0.13 mmol) were combined and refluxed for 4 hours in the presence of 5 mL of DMF under argon atmosphere. After it cooled to room temperature, 2PF<sub>6</sub><sup>-</sup> (100 mg, 0.26 mmol) of (E)-9a-(2-([2,2'-bipyridin]-4-yl)vinyl)-7,9,9-trimethyl-2,3,9,9a-tetrahydrooxazolo[3,2-a]indole were added to the reaction mixture and the resultant solution was refluxed overnight. The solvent was evaporated to yield a dark orange solid and the crude was

purified by flash column chromatography on silica gel by using a mixture of Acetone/water 8/2 to remove the excess of starting material, followed by Acetone/saturated aqueous NH<sub>4</sub>PF<sub>6</sub> 8/2 in order to isolate the desired product. Concentration under reduced pressure to remove acetone led to precipitation. The precipitate was filtered and washed several times by Et<sub>2</sub>O to afford a bright orange solid (60 mg, 70%).

<sup>1</sup>H NMR (300 MHz, CD<sub>3</sub>CN) δ 8.62 (d, *J* = 6.6 Hz, 2H), 8.51 (d, *J* = 8.1 Hz, 1H), 8.06 (dd, *J* = 11.1, 4.6 Hz, 2H), 7.84 – 7.58 (m, 3H), 7.42 (dt, *J* = 11.6, 4.8 Hz, 3H), 6.98 (dd, *J* = 14.1, 3.7 Hz, 3H), 6.88 (d, *J* = 16.0 Hz, 1H), 6.74 (d, *J* = 7.9 Hz, 1H), 3.53 (m, 4H), 2.28 (s, 3H), 1.41 (s, 3H), 1.11 (s, 3H). <sup>13</sup>C NMR (125 MHz, CD<sub>3</sub>CN) δ 157.7, 157.7, 157.7, 157.6, 157.5, 152.3, 152.2, 152.1, 148.8, 146.3, 140.0, 138.4, 136.2, 131.8, 128.7, 128.6, 128.1, 125.3, 124.8, 123.6, 122.1, 112.5, 110.3, 64.1, 50.6, 48.5, 28.2, 20.5, 20.3. IR ν (cm<sup>-1</sup>): 2923, 1609, 1465, 1439 1281, 1109, 835, 763 cm<sup>-1</sup>. ESI-MS: *m/z* = 1169.13 [Ru(BOX-biPy)<sub>2</sub>(biPy)]<sup>2+</sup>PF<sub>6</sub><sup>-</sup>, 512,03 [Ru(BOX-biPy)<sub>2</sub>(biPy)]<sup>2+</sup>.

## Reference

- [1] G. r. Szalóki and L. Sanguinet, *The Journal of organic chemistry* **2015**, *80*, 3949-3956.
- [2] M. M. Bader, P.-T. T. Pham and E. H. Elandalousi, *Crystal Growth & Design* **2010**, *10*, 5027-5030.
- [3] I. Imae, H. Sagawa, T. Mashima, K. Komaguchi, Y. Ooyama and Y. Harima, *Open Journal of Polymer Chemistry* **2014**, *4*, 83.
- [4] Y.-X. Wang and M.-k. Leung, *Macromolecules* **2011**, *44*, 8771-8779.
- [5] C. Istanbuluoglu, S. Göker, G. Hizalan, S. O. Hacioglu, Y. A. Udum, E. D. Yildiz, A. Cirpan and L. Toppare, *New Journal of Chemistry* **2015**, *39*, 6623-6630.
- [6] H. Wang, W. Ding, G. Wang, C. Pan, M. Duan and G. Yu, *Journal of Applied Polymer Science* **2016**, *133*.
- [7] G. Koohmareh and Z. Souri, *Designed Monomers and Polymers* **2011**, *14*, 475-485.
- [8] E. C. Constable, E. Figgemeier, C. E. Housecroft, J. Olsson and Y. C. Zimmermann, *Dalton Transactions* **2004**, 1918-1927.
- [9] B. Imperiali, T. J. Prins and S. L. Fisher, *The Journal of Organic Chemistry* **1993**, *58*, 1613-1616.
- [10] M. Kuroboshi, Y. Waki and H. Tanaka, *Synlett* **2002**, *2002*, 0637-0639.
- [11] B. Sullivan, D. Salmon and T. Meyer, *Inorganic Chemistry* **1978**, *17*, 3334-3341.

## Elaboration de systèmes moléculaires multi-chromophoriques pour l'électronique moléculaire

**Mots clés :** Indolinoxazolidine, systèmes  $\pi$ -conjugués, commutateur moléculaire, acidochromiques, photochromiques, électrochromes, complexes, RMN, DFT, optique non linéaire

**Résumé :** Au cours des dernières décennies, de nombreux efforts se sont focalisés sur la synthèse, la modification et l'utilisation de systèmes moléculaires multi-adressables. Afin d'élaborer de tels systèmes capables de répondre à des stimulations de différentes natures (par exemple : photon, électron, proton, etc...) les deux principales stratégies consistaient à ce jour à connecter différents types d'unités stimulables soit par liaison covalente soit par dispersion au sein d'assemblages supramoléculaires. Au cours de cette thèse, nous nous sommes attachés à développer une nouvelle approche basée sur l'utilisation d'un unique switch multi-mode : les indolino-oxazolidine (BOX). En effet, cette unité est capable de commuter entre deux états métastables (ouvert et fermé) et ce de façon indifférenciée par application d'une stimulation lumineuse, électrochimique ou encore par variation du pH. En suivant une première stratégie, deux unités BOX ont été connectées via l'utilisation d'un simple système conjugué linéaire tels qu'une unité bithiophène et un

enchaînement EDOT-Thiophène-EDOT (ETE) comme espaceur. Nous avons démontré que ces systèmes multi-stimulables sont capables de commuter de façon pas à pas entre 3 états métastables différents et ce quel que soit la nature du stimulus. Afin de démontrer les nombreuses possibilités de cette approche et augmenter le nombre d'états métastables, 3 unités BOX ont été connectés par l'utilisation de systèmes conjugués plus élaborés permettant ainsi de conduire à des interrupteurs moléculaires capables de présenter jusqu'à 4 états différents. En complément de cette approche purement organique, une seconde stratégie a consisté à fonctionnaliser différents ligands azotés par au moins une entité BOX afin d'élaborer des systèmes plus complexes par chimie de coordination avec des ions métalliques de zinc et de ruthénium. Les ligands préparés ainsi que les complexes correspondants ont été pleinement caractérisés et leur adressabilité sous stimulation chimique, électrique et lumineuse étudiée.

## Development of multi-modal and multi-level molecular systems

**Keywords :** Indolinoxazolidine,  $\pi$ -conjugated systems, molecular switches, multi-modal, multi-level, acidochromic, photochromic, electrochromic, complexes, NMR, DFT, nonlinear optics

**Abstract:** Over the past decade many efforts have been focused on the synthesis, modification and application of multi-responsive molecular systems. Up to now, two main strategies have been conducted to elaborate such systems: either by connecting different molecular switches through covalent links or by mixing them within supramolecular assemblies to obtain multi-responsiveness through the combination of various stimulations (i.e., photon, electron, proton, etc...). In this thesis, we report a different approach based on the employment of identical indolinoxazolidine (BOX) unit as multi-modal switch. Indeed, the opening of the oxazolidine ring can be reversibly and selectively achieved either under UV irradiation, electrochemical stimulation or acidity changes. According to our first strategy, two BOX units were connected around a

simple linear aromatic plate forms, such as bithiophene and EDOT-Thiophene-EDOT unit as spacer. Interestingly, these systems are able to commute between 3 different metastable states in a stepwise manner with all kinds of stimulations. Going further, in order to promote the metastable states, it was possible to increase the number of BOX by connecting three of them on more elaborated pi systems which are potentially able to exhibit up to four discriminate metastable states. Complementary to that, a second strategy was to synthesize various nitrogen ligands functionalized by at least one BOX unit and their coordination chemistry with zinc and ruthenium metals. The response of the ligands as well as their corresponding complexes under photo, electro and acidic stimulation were also investigated and fully characterized.